Neuromethods 165

Springer Protocols

Marc Fakhoury *Editor*

The Brain Reward System

Humana Press

NEUROMETHODS

Series Editor
Wolfgang Walz
University of Saskatchewan
Saskatoon, SK, Canada

For further volumes:
http://www.springer.com/series/7657

Neuromethods publishes cutting-edge methods and protocols in all areas of neuroscience as well as translational neurological and mental research. Each volume in the series offers tested laboratory protocols, step-by-step methods for reproducible lab experiments and addresses methodological controversies and pitfalls in order to aid neuroscientists in experimentation. *Neuromethods* focuses on traditional and emerging topics with wide-ranging implications to brain function, such as electrophysiology, neuroimaging, behavioral analysis, genomics, neurodegeneration, translational research and clinical trials. *Neuromethods* provides investigators and trainees with highly useful compendiums of key strategies and approaches for successful research in animal and human brain function including translational "bench to bedside" approaches to mental and neurological diseases.

The Brain Reward System

Edited by

Marc Fakhoury

Department of Natural Sciences, School of Arts and Sciences, Lebanese American University, Beirut, Lebanon

Humana Press

Editor
Marc Fakhoury
Department of Natural Sciences
School of Arts and Sciences
Lebanese American University
Beirut, Lebanon

ISSN 0893-2336 ISSN 1940-6045 (electronic)
Neuromethods
ISBN 978-1-0716-1145-6 ISBN 978-1-0716-1146-3 (eBook)
https://doi.org/10.1007/978-1-0716-1146-3

This Humana imprint is published by the registered company Springer Science+Business Media, LLC, part of Springer Nature.
The registered company address is: 1 New York Plaza, New York, NY 10004, U.S.A.

Preface to the Series

Experimental life sciences have two basic foundations: concepts and tools. The *Neuromethods* series focuses on the tools and techniques unique to the investigation of the nervous system and excitable cells. It will not, however, shortchange the concept side of things as care has been taken to integrate these tools within the context of the concepts and questions under investigation. In this way, the series is unique in that it not only collects protocols but also includes theoretical background information and critiques which led to the methods and their development. Thus it gives the reader a better understanding of the origin of the techniques and their potential future development. The *Neuromethods* publishing program strikes a balance between recent and exciting developments like those concerning new animal models of disease, imaging, in vivo methods, and more established techniques, including, for example, immunocytochemistry and electrophysiological technologies. New trainees in neurosciences still need a sound footing in these older methods in order to apply a critical approach to their results.

Under the guidance of its founders, Alan Boulton and Glen Baker, the *Neuromethods* series has been a success since its first volume published through Humana Press in 1985. The series continues to flourish through many changes over the years. It is now published under the umbrella of Springer Protocols. While methods involving brain research have changed a lot since the series started, the publishing environment and technology have changed even more radically. Neuromethods has the distinct layout and style of the Springer Protocols program, designed specifically for readability and ease of reference in a laboratory setting.

The careful application of methods is potentially the most important step in the process of scientific inquiry. In the past, new methodologies led the way in developing new disciplines in the biological and medical sciences. For example, Physiology emerged out of Anatomy in the nineteenth century by harnessing new methods based on the newly discovered phenomenon of electricity. Nowadays, the relationships between disciplines and methods are more complex. Methods are now widely shared between disciplines and research areas. New developments in electronic publishing make it possible for scientists that encounter new methods to quickly find sources of information electronically. The design of individual volumes and chapters in this series takes this new access technology into account. Springer Protocols make it possible to download single protocols separately. In addition, Springer makes its print-on-demand technology available globally. A print copy can therefore be acquired quickly and for a competitive price anywhere in the world.

Saskatoon, SK, Canada ***Wolfgang Walz***

Preface

This volume of the series *Neuromethods* provides an overview of cutting-edge and well-established techniques used in neuroscience for better understanding the brain reward system with respect to neurotransmitters, brain structures, and connectivity. The study of the brain reward system is a burgeoning field that started in the early 1950s, when Olds and Milner discovered that rats would readily press a lever to obtain pulses of electrical stimulation in certain brain regions. The brain reward system can be activated by artificial rewards such as electrical stimulation or addictive drugs and by natural rewards such as food and sex. In the aftermath of Olds and Milner's discovery, numerous investigations were conducted to characterize the brain regions that are part of the reward system. The emerging picture resulting from these studies suggests that the brain reward system is comprised of two main pathways: (i) the medial forebrain bundle, which descends from the basal forebrain and courses through midbrain regions to terminate into the brainstem, and (ii) the dorsal diencephalic conduction system, which extends from the rostral part of the medial forebrain bundle, courses through the habenula, and terminates into midbrain regions.

The aim of this book is to equip readers with tested laboratory protocols to study the neural circuitry and biological processes implicated in reward and in neuropsychiatric disorders such as substance use disorder. The chapters have been designed to provide a comprehensive overview of neurochemical, behavioral, chemogenetic, neuroimaging, and electrophysiological techniques used for mapping the brain reward system. The first part of the book addresses classical techniques to study the brain reward system, which include the use of the curve shift paradigm in intracranial self-stimulation (Chapter 1), the use of stereotaxic surgery in rodents (Chapter 2), and the use of brain lesions (Chapter 3). The second part of the book focuses on neurochemical, behavioral, and chemogenetic techniques to study the brain reward system. In particular, it addresses the techniques of immunofluorescence for assessing adult hippocampal neurogenesis (Chapter 4), the technique of fast-scan voltammetry (Chapter 5), the use of carbon fiber probes for monitoring dopamine neuron activity (Chapter 6), the use of behavioral paradigms for studying anhedonia, aversion, and despair during inflammatory conditions (Chapter 7), the use of behavioral techniques for assessing pain sensitivity (Chapter 8), and the use of designer receptors exclusively activated by designer drugs (DREADDs) for investigating motivated behaviors (Chapter 9). The third part of the book highlights techniques used for assessing the rewarding potential of drugs of abuse. These include the technique of intracranial self-stimulation combined with drug injection (Chapter 10), the technique of drug self-administration (Chapter 11), the use of viral vectors (Chapter 12), and the technique of conditioned place preference (Chapter 13). Finally, the last part of the book introduces imaging and electrophysiological techniques for investigating the brain reward system, such as positron emission tomography (Chapter 14), in vivo electrophysiology (Chapter 15), fiber photometry (Chapter 16), and two-photon microscopy (Chapter 17).

This book, written by leading experts around the world, will be a valuable tool for researchers who seek to better understand current techniques employed in research for delineating the brain reward system. Special thanks go to all authors for their hard work and valuable contributions, and to the series editor, Wolfgang Walz, for his guidance and support.

Beirut, Lebanon ***Marc Fakhoury***

Contents

Preface to the Series . . . . . *v*
Preface . . . . . *vii*
Contributors . . . . . *xi*

PART I CLASSICAL TECHNIQUES TO STUDY THE BRAIN REWARD SYSTEM

1 Intracranial Self-Stimulation and the Curve-Shift Paradigm: A Putative Model to Study the Brain Reward System 3
Marc Fakhoury and Pierre-Paul Rompré

2 Stereotaxic Surgery in Rodents for Stimulation of the Brain Reward System 21
Brenda M. Geiger, Monika Irene, and Emmanuel N. Pothos

3 Characterizing the Neural Substrate of Reward with the Use of Specific Brain Lesions 51
Howard Casey Cromwell

PART II NEUROCHEMICAL BEHAVIORAL AND CHEMOGENETIC TECHNIQUES

4 Assessment of Adult Hippocampal Neurogenesis: Implication for Neurodegenerative Diseases and Neurological Disorders 77
Farah Chamaa, Batoul Darwish, Nayef E. Saadé, and Wassim Abou-Kheir

5 Fast-Scan Voltammetry for In Vivo Measurements of Neurochemical Dynamics 93
Carl J. Meunier and Leslie A. Sombers

6 Carbon Fiber Probes for Real-Time Monitoring of Dopamine 125
Helen N. Schwerdt, Ann M. Graybiel, and Michael J. Cima

7 Immune-to-Brain Signaling Effects on the Neural Substrate for Reward: Behavioral Models of Aversion, Anhedonia, and Despair 145
Anna Mathia Klawonn and Michael Fritz

8 Behavioral Tests for Assessing Pain and Nociception: Relationship with the Brain Reward System 169
Marc Fakhoury, Reem Habib Mohamad Ali Ahmad, Elie D. Al-Chaer, and Nada B. Lawand

9 Chemogenetic (DREADD) Exploration of Circuits Mediating Reward-Motivated Attention 181
Hrishikesh Pattabhiraman and Ryan D. Ward

PART III TECHNIQUES FOR ASSESSING THE EFFECT OF DRUG OF ABUSE

10 Intracranial Self-Stimulation: Using the Curve-Shift Paradigm to Assess the Abuse Potential of Drugs 199
Ritchy Hodebourg

11 Drug Self-Administration as a Model to Study the Reward System 209
Florence Allain and Anne-Noël Samaha

12 Viral Vectors for Studying Drug-Seeking Behavior 233
Arlene Martínez-Rivera, Caitlin E. Burgdorf, and Anjali M. Rajadhyaksha

13 Conditioned Place Preference Test for Assessing the Rewarding Effects of Drugs of Abuse 263
Todd Hillhouse and Adam Prus

Part IV Imaging and Electrophysiological Techniques

14 Positron Emission Tomography of the Reward System 281
Diego Romero-Miguel, Nicolás Lamanna-Rama, Marta Casquero-Veiga, Vanessa Gómez-Rangel, Manuel Desco, and María Luisa Soto-Montenegro

15 In Vivo Electrophysiology for Reward Anticipation and Processing 307
Laura A. Alba, Elizabeth Baker, and Katherine K. M. Stavropoulos

16 Fiber Photometry of Neural Activity in Specific Neural Circuit 327
Jinsong Yu, Yue Li, Mona N. Hussein, Zhongchao Wang, Jinxia Dai, and Gang Cao

17 Two-Photon Microscopy for Studying Reward Circuits of the Brain 339
Rafiq Huda, Leena Ali Ibrahim, and Bernard Bloem

Index *365*

Contributors

Wassim Abou-Kheir • *Department of Anatomy, Cell Biology and Physiological Sciences, American University of Beirut, Beirut, Lebanon*

Reem Habib Mohamad Ali Ahmad • *Department of Anatomy, Cell Biology and Physiological Sciences, Faculty of Medicine, American University of Beirut, Beirut, Lebanon*

Laura A. Alba • *Graduate School of Education, University of California, Riverside, CA, USA*

Elie D. Al-Chaer • *Department of Anatomy, Cell Biology & Physiological Sciences, Faculty of Medicine, American University of Beirut, Beirut, Lebanon*

Florence Allain • *Department of Pharmacology and Physiology, Faculty of Medicine, Groupe de recherché sur le Système Nerveux Central, Université de Montréal, Montréal, QC, Canada*

Elizabeth Baker • *Graduate School of Education, University of California, Riverside, CA, USA*

Bernard Bloem • *McGovern Institute for Brain Research, Massachusetts Institute of Technology, Cambridge, MA, USA*

Caitlin E. Burgdorf • *Division of Pediatric Neurology, Department of Pediatrics, Weill Cornell Medicine, New York, NY, USA*

Gang Cao • *State Key Laboratory of Agricultural Microbiology, Huazhong Agricultural University, Wuhan, China; College of Veterinary Medicine, Huazhong Agricultural University, Wuhan, China; Key Laboratory of Development of Veterinary Diagnostic Products, Ministry of Agriculture, College of Veterinary Medicine, Huazhong Agricultural University, Wuhan, China; Bio-Medical Center, Huazhong Agricultural University, Wuhan, China*

Marta Casquero-Veiga • *Instituto de Investigación Sanitaria Gregorio Marañón, Madrid, Spain; CIBER de Salud Mental (CIBERSAM), Madrid, Spain*

Farah Chamaa • *Department of Anatomy, Cell Biology and Physiological Sciences, American University of Beirut, Beirut, Lebanon*

Michael J. Cima • *Koch Institute for Integrative Cancer Research, Massachusetts Institute of Technology, Cambridge, MA, USA; Department of Materials Science, Massachusetts Institute of Technology, Cambridge, MA, USA*

Howard Casey Cromwell • *Department of Psychology and John Paul Scott Center for Neuroscience, Mind and Behavior, Bowling Green State University, Bowling Green, OH, USA*

Jinxia Dai • *State Key Laboratory of Agricultural Microbiology, Huazhong Agricultural University, Wuhan, China; College of Veterinary Medicine, Huazhong Agricultural University, Wuhan, China; Key Laboratory of Development of Veterinary Diagnostic Products, Ministry of Agriculture, College of Veterinary Medicine, Huazhong Agricultural University, Wuhan, China*

Batoul Darwish • *Department of Anatomy, Cell Biology and Physiological Sciences, American University of Beirut, Beirut, Lebanon*

Manuel Desco • *Instituto de Investigación Sanitaria Gregorio Marañón, Madrid, Spain; CIBER de Salud Mental (CIBERSAM), Madrid, Spain; Departamento de Bioingeniería*

e Ingeniería Aeroespacial, Universidad Carlos III de Madrid, Madrid, Spain; Centro Nacional de Investigaciones Cardiovasculares, Madrid, Spain

Marc Fakhoury • *Department of Natural Sciences, School of Arts and Sciences, Lebanese American University, Beirut, Lebanon*

Michael Fritz • *Department of Biomedical and Clinical Sciences, Linköping University, Linköping, Sweden*

Brenda M. Geiger • *Department of Biomedical and Nutritional Sciences, Zuckerberg College of Health Sciences, University of Massachusetts Lowell, Lowell, MA, USA*

Vanessa Gómez-Rangel • *Instituto de Investigación Sanitaria Gregorio Marañón, Madrid, Spain*

Ann M. Graybiel • *McGovern Institute for Brain Research and Department of Brain and Cognitive Sciences, Massachusetts Institute of Technology, Cambridge, MA, USA*

Todd Hillhouse • *Department of Psychology, University of Wisconsin Green Bay, Green Bay, WI, USA*

Ritchy Hodebourg • *Department of Neuroscience, Medical University of South Carolina, Charleston, SC, USA*

Rafiq Huda • *WM Keck Center for Collaborative Neuroscience, Department of Cell Biology and Neuroscience, Rutgers University—New Brunswick, Piscataway, NJ, USA*

Mona N. Hussein • *State Key Laboratory of Agricultural Microbiology, Huazhong Agricultural University, Wuhan, China; College of Veterinary Medicine, Huazhong Agricultural University, Wuhan, China; Histology and Cytology Department, Faculty of Veterinary Medicine, Benha University, Banha, Egypt*

Leena Ali Ibrahim • *Department of Neurobiology, Harvard Medical School, Boston, MA, USA*

Monika Irene • *Department of Biomedical and Nutritional Sciences, Zuckerberg College of Health Sciences, University of Massachusetts Lowell, Lowell, MA, USA*

Anna Mathia Klawonn • *Department of Psychiatry and Behavioral Sciences, Stanford University, Stanford, CA, USA*

Nicolás Lamanna-Rama • *Instituto de Investigación Sanitaria Gregorio Marañón, Madrid, Spain*

Nada B. Lawand • *Department of Anatomy, Cell Biology & Physiological Sciences, Faculty of Medicine, American University of Beirut, Beirut, Lebanon*

Yue Li • *State Key Laboratory of Agricultural Microbiology, Huazhong Agricultural University, Wuhan, China; College of Veterinary Medicine, Huazhong Agricultural University, Wuhan, China*

Arlene Martínez-Rivera • *Division of Pediatric Neurology, Department of Pediatrics, Weill Cornell Medicine, New York, NY, USA*

Carl J. Meunier • *Department of Chemistry, North Carolina State University, Raleigh, NC, USA*

Hrishikesh Pattabhiraman • *Department of Psychology, University of Otago, Dunedin, New Zealand*

Emmanuel N. Pothos • *Program in Pharmacology and Experimental Therapeutics & Pharmacology and Drug Development, Graduate School of Biomedical Sciences, Department of Immunology (Former Integrative Physiology and Pathobiology), Tufts University School of Medicine, Boston, MA, USA*

Adam Prus • *Department of Psychological Science, Northern Michigan University, Marquette, MI, USA*

Anjali M. Rajadhyaksha • *Division of Pediatric Neurology, Department of Pediatrics, Weill Cornell Medicine, New York, NY, USA; Feil Family Brain and Mind Research Institute, Weill Cornell Medical College, New York, NY, USA*

Diego Romero-Miguel • *Instituto de Investigación Sanitaria Gregorio Marañón, Madrid, Spain*

Pierre-Paul Rompré • *Faculty of Medicine, Department of Neurosciences, Université de Montréal, Montréal, QC, Canada*

Nayef E. Saadé • *Department of Anatomy, Cell Biology and Physiological Sciences, American University of Beirut, Beirut, Lebanon*

Anne-Noël Samaha • *Department of Pharmacology and Physiology, Faculty of Medicine, Groupe de recherché sur le Système Nerveux Central, Université de Montréal, Montréal, QC, Canada*

Helen N. Schwerdt • *McGovern Institute for Brain Research and Department of Brain and Cognitive Sciences, Massachusetts Institute of Technology, Cambridge, MA, USA; Koch Institute for Integrative Cancer Research, Massachusetts Institute of Technology, Cambridge, MA, USA*

Leslie A. Sombers • *Department of Chemistry, North Carolina State University, Raleigh, NC, USA*

María Luisa Soto-Montenegro • *Instituto de Investigación Sanitaria Gregorio Marañón, Madrid, Spain; CIBER de Salud Mental (CIBERSAM), Madrid, Spain; Laboratorio de Imagen, Medicina Experimental, Hospital General Universitario Gregorio Marañón, Madrid, Spain*

Katherine K. M. Stavropoulos • *Graduate School of Education, University of California, Riverside, CA, USA*

Zhongchao Wang • *State Key Laboratory of Agricultural Microbiology, Huazhong Agricultural University, Wuhan, China; College of Veterinary Medicine, Huazhong Agricultural University, Wuhan, China*

Ryan D. Ward • *Department of Psychology, University of Otago, Dunedin, New Zealand*

Jinsong Yu • *State Key Laboratory of Agricultural Microbiology, Huazhong Agricultural University, Wuhan, China; College of Veterinary Medicine, Huazhong Agricultural University, Wuhan, China*

Part I

Classical Techniques to Study the Brain Reward System

Chapter 1

Intracranial Self-Stimulation and the Curve-Shift Paradigm: A Putative Model to Study the Brain Reward System

Marc Fakhoury and Pierre-Paul Rompré

Abstract

Since its discovery in the early 1950s, intracranial self-stimulation (ICSS) has proved valuable in studying the brain reward circuitry. This behavior was serendipitously discovered by Olds and Milner at McGill University who noticed that laboratory animals would readily learn to self-administer pulses of electrical stimulation in septal regions of the brain. Till the present day, numerous laboratories worldwide are using ICSS to delineate brain regions and pathways that are involved in processing information related to reward. Such work could lead to improved understanding and new therapeutic strategies not only for psychiatric diseases such as depression and substance use disorder but also for schizophrenia and Parkinson's disease. This chapter provides a detailed description of the ICSS behavior in experimental animals and how it is used for studying the brain reward pathway.

Key words Intracranial self-stimulation, Drugs of abuse, Lesion, Rat, Reward

1 Introduction

1.1 Intracranial Self-Stimulation: Context and Discovery

Throughout their lives, humans learn different patterns of behavior to adapt to their environment and meet their vital needs. One of the most fundamental processes of learning is the ability to effectively associate different stimuli for acquiring or strengthening a behavior. In the early twentieth century, Ivan Pavlov, a Russian physiologist, introduced the notion of classical conditioning, in which subjects learn to associate a previously neutral stimulus to an unconditioned stimulus that reliably elicits a response [1]. In his experiments, he observed that dogs would normally salivate upon the presentation of food (the unconditioned stimulus). However, dogs would also drool whenever they saw the lab coats that were worn by the technicians who normally feed them, even when there was no food in sight. Pavlov, therefore, conducted an experiment in which a bell was rung every time food was presented to the animals. As predicted, the sound of the bell (the neutral stimulus) was able to trigger the salivation response in dogs. Pavlov concluded that

Marc Fakhoury (ed.), *The Brain Reward System*, Neuromethods, vol. 165, https://doi.org/10.1007/978-1-0716-1146-3_1,

any event or object that the animals learn to associate with a reward (in this case food) would trigger the same behavioral response obtained upon presentation of the reward itself. Pavlov's research on classical conditioning has set the ground for much of the subsequent research on conditioning and still serves as a historical backdrop for current learning theories. Influenced by Pavlov's experiments on classical conditioning, John B. Watson, an American psychologist, established the first basic principles of behaviorism, which are described in the article "Psychology as the behaviorist views it" [2]. In this article, Watson argued that psychology should be viewed as an objective experimental branch of science whose theoretical goal is the understanding of the behavior of humans or animals, rather than their consciousness or internal state. Watson's theory of behaviorism played a significant role in paving the way for the changes in psychological research that ensued. In 1938, Burrhus F. Skinner introduced the notion of operant conditioning based on the observation that animals would quickly learn to press a lever (the operant response) in order to receive food [3]. He coined the terms positive reinforcers for stimuli that increase the likelihood of the operant response to occur and punishers for stimuli that decrease the likelihood of the operant response to occur. Most of Skinner's ideas, however, are built upon Edward Thorndike's law of effect, which states that the behavioral responses that are followed by pleasant consequences are more likely to occur again in the same situation, while the behavioral responses that are followed by unpleasant consequences are less likely to be repeated [4]. Nonetheless, Skinner's theories on conditioning behavior differ from those of Thorndike insofar as they established a distinction between positive and negative reinforcers, the latter being defined by stimuli whose removal increases the likelihood of the operant response to occur. An example of negative reinforcement is when animals need to press a lever to avoid receiving aversive stimuli such as electrical foot shocks. Skinner also found that the way in which reinforcers are scheduled can significantly affect the rate of lever press (or operant response rate) and the rate at which the operant response is extinguished (or extinction rate) [5]. For instance, a continuous reinforcement, where food is delivered after every lever press, would produce a slow rate of responding and a relatively fast extinction rate, whereas a variable ratio reinforcement, where food is delivered after an unpredictable number of lever presses, will tend to sustain high rates of responding with relatively slow extinction rates [5].

Although research on classical and operant conditioning in the first half of the twentieth century has shaped our understanding of motivated behaviors, it failed to characterize its underlying neural basis. The first evidence showing that there exists a neural substrate underlying reward and motivated behaviors came from a study conducted by James Olds and Peter Milner in the early 1950s. In

their experiments, the electrode that was initially intended to be implanted into the reticular formation missed its target and ended up in the septal area. Their initial observation suggested that the electrical stimulation within this region was rewarding [6]. Then, they discovered that rats would also press the lever for stimulation of other brain areas, including the tegmentum, subthalamus, hypothalamus, and cingulate gyrus of the cortex [6]. This behavioral paradigm was termed intracranial self-stimulation (ICSS) on the basis that rats had to perform a specific response to receive a train of electrical pulses. The discovery that ICSS of certain brain areas could serve as a reinforcer spurred intense interest among psychologists and neuroscientists and led to a wide array of subsequent experiments on the neural substrate underlying brain stimulation reward. An urgent requirement at that time was to discover all the brain areas that could support ICSS and to determine whether this behavior could be reproduced in other species [7]. Following Olds and Milner's observations, the reinforcing properties of ICSS have been described in numerous brain regions [7] and several species, including monkeys [8], dogs [9], cats [10], chicks [11], and humans [12].

1.2 Anatomical Substrate of Brain Stimulation Reward

The discovery by Olds and Milner that rats would readily press a lever to obtain pulses of electrical stimulation in certain brain regions [6] ushered in a series of investigations aiming at determining the neuroanatomical substrate underlying brain stimulation reward. Shortly after this discovery, studies showed that electrical stimulation of forebrain and hypothalamic structures [13, 14] could also generate high response rates in an ICSS paradigm, which unequivocally pointed to the medial forebrain bundle (MFB) as a key neural pathway in the brain reward system. The MFB is a large tract of ascending and descending axons that span the entire length of the brain, passing through the basal forebrain and the lateral hypothalamus (LH) in a rostral–caudal direction. MFB fibers also course through midbrain regions including the ventral tegmental area (VTA), to terminate into several nuclei of the brainstem including the dorsal raphe (DR) nucleus [15], thus relaying information from one pole of the brain to the other. Another neural pathway of the brain reward system is the dorsal diencephalic conduction system (DDC), which is composed of the stria medullaris, the habenula, and the fasciculus retroflexus. The information received by the DDC travels from the anterior portion of the LH to the habenula through the SM and gets transmitted to midbrain regions via the FR [16, 17].

Following the identification of the MFB as a major substrate for ICSS, numerous brain mapping studies, where the anatomical site of the stimulation electrode is manipulated, were conducted to characterize the brain regions that could support ICSS. The emerging picture resulting from these studies suggests that operant

responding for ICSS could be obtained along brain regions known to send or receive MFB fibers, including the orbitofrontal cortex (OFC) [18], the medial prefrontal cortex (mPFC) [19], the caudate–putamen [19], the lateral preoptic area [20], the ventral pallidum [21], the amygdala [22], the pontine tegmentum [23], the median raphe (MR) [24], and the DR [23, 25]. ICSS has also been reported in the habenula [26, 27], the olfactory bulbs [28], the hippocampus [29, 30], the nucleus accumbens (NAc) [31], the VTA [32], and the cerebellum [33, 34]. To date, one of the most extensively studied substrates for brain stimulation reward is the LH owing to its critical role in energy homeostasis and motivated behaviors [35, 36].

The LH is a heterogeneous area of the MFB located posterior to the preoptic area and anterior to the VTA. It resides dorsoventrally between the zona incerta and the base of the brain, and mediolaterally between the optic tract and the fornix. Studies employing electrical or optogenetic stimulation of the LH have implicated this structure in feeding [37] and reward-seeking [6, 38] behaviors. Anatomically, the LH comprises several distinct nuclear subgroups that receive a wide array of internal and external information, making it well-suited to mediate functions across major output axes [35]. Afferents to the LH have been classically studied using injections of a retrograde tracer (i.e., transport of the dye occurs in the reverse direction, from the axon terminal back to the cell body), the results of which have demonstrated the existence of projections originating from the bed nucleus of the stria terminalis (BNST), the diagonal tract of Broca, the caudate–putamen, the NAc, the lateral septal nuclei, the lateral preoptic area, the amygdala, and the zona incerta [39, 40]. On the other hand, studies employing anterograde tracing techniques (i.e., transport of the dye occurs in the forward direction, from the cell body out to the axon terminal) showed that LH neurons project to distinct areas of the brain including the hypothalamic paraventricular nucleus, the lateral habenula, the VTA, the mesencephalic and pontine central gray, the lateral parabrachial nucleus, and the raphe nucleus [40, 41].

Numerous studies have also employed lesions along certain brain structures or pathways in order to evaluate their impact on the reinforcing properties of ICSS. The reasoning behind this technique is based on the assumption that the destruction of axons or cellular elements involved in brain stimulation reward should result in an attenuation of the reinforcing effects obtained from ICSS. Therefore, assessing the strength of the reinforcing effect of ICSS before and after a lesion could help characterize the underlying neural circuit of brain stimulation reward. A common finding is that electrolytic lesions or knife cuts along the MFB cause a rightward shift in response/frequency (R/F) curves obtained from LH [42, 43] or VTA [44] self-stimulation, indicating a

sustained attenuation of the rewarding effectiveness of ICSS. Lesions encompassing the habenula [45], the cortical and adjacent amygdaloid subnuclei [46], the lateral preoptic area [47], and the posterior mesencephalon (PM) [48] also cause a rightward shift in R/F curves for MFB self-stimulation. However, several other studies employing electrolytic lesions failed to observe decreases in the rewarding effectiveness of MFB stimulation. In particular, lesions at the amygdala [49], the dorsomedial hypothalamus [50], the parabrachial nucleus [51], the rostral LH [43], and the lateral PM [48] have not resulted in consistent and noticeable changes in the rewarding effectiveness of MFB stimulation. A hypothesis to account for these negative findings is that the neural network subserving ICSS is anatomically diffuse, collateralized, and highly heterogeneous [44, 52], and may be comprised of several pathways that are functionally interconnected. As such, the loss of reward-relevant neurons within one pathway would be compensated by the other, and vice versa, thereby enabling the integration and transmission of reward signals in the brain. Last but not the least, sites within the DDC, including the stria medularis and the habenula, have all been shown to support operant responding for ICSS [26, 53, 54], and electrolytic lesions in the DDC were shown to attenuate the rewarding effect of ICSS [55, 56], indicating that this pathway plays crucial roles in the modulation of reward and goal-directed behaviors.

2 Materials

2.1 Electrodes

For delivery of the rewarding electrical stimulation, both monopolar or bipolar electrodes can be used, although the former type is most frequently employed in rodents due to its smaller diameter, thereby allowing more precise targeting of specific brain areas [57]. Electrodes used in ICSS are typically made of stainless steel wires of approximately 100–250 μm diameter in size and connected to a male Amphenol connector. An Epoxylite solution is used to insulate the electrode, however, care must be taken to remove the insulation from the tip by cutting it with a blade. The electrode wire is also cut with a blade to achieve the desired length. Finally, all electrodes are cleaned with 100% alcohol and stored in vials until use.

2.2 Animals

Typically, any strain of rat could serve as experimental subjects. It is recommended, however, that adult animals be used (~300 g for rats) during electrode implantation since bone growth could result in the displacement of affixed electrodes. Prior to surgery, the animals must be kept in temperature (22 °C) and humidity (50%) controlled colony lit with a 12-h light–dark cycle and ad libitum access to food and water. All experiments must be carried out in

compliance with the national and institutional guidelines on animal care.

2.3 Surgical Equipment

The following equipment is necessary for the surgical implantation of electrodes in the brain of rodents: (i) stereotaxic apparatus, (ii) surgical microscope and light illumination system, (iii) isoflurane, (iv) analgesics (Ketoprofen; 5 mg/kg of body weight), (v) ophthalmic ointment, (vi) sterilized razor blades, (vii) betadine and alcohol, (viii) uninsulated stainless steel wire coupled to a male amphenol connector, (ix) micro drill, (x) miniature screws, (xi) dental cement, (xii) tweezers with fine tips, (xiii) shaver, and (xiv) electrodes. For intracranial drug injection, the following additional equipment is necessary: (i) injection cannula, (ii) guide cannula, (iii) polyethylene tubing, (iv) microsyringe, and (iv) microinfusion pump.

2.4 Behavioral Apparatus

ICSS training and testing are typically conducted in operant conditioning cages (28 cm wide × 29.4 cm deep × 68.6 cm high) made from polymer walls (back and sidewall) and one front Plexiglas wall to allow constant viewing of the animal (*see* Fig. 1a). Operant conditioning chambers are usually equipped with a nonretractable lever or a nose poke device located approximately 3 cm above the metal rod floor (*see* Fig. 1b) and are encased in sound-attenuating wooden boxes with appropriate light and ventilation systems. Depression of the lever or entry into the nose poke device by the experimental animal triggers the delivery of a single train of rectangular cathodal pulses into the desired region of the brain by a stimulator. The stimulators should have the capability to deliver trains of rectangular cathodal pulses over a wide range of current intensities and frequencies and have a separate output monitor with an oscilloscope. Finally, computer and software programs (e.g., Med Associates) should be used to automate the ICSS procedures.

3 Methods

3.1 Surgical Procedure for Electrode Implantation

For the surgical implantation of electrodes into the brain, animals are first anesthetized with isoflurane and oxygen (2.5–3.5% O_2, 0.6 L/min) and administered with an analgesic subcutaneously (e.g., Ketoprofen or Anaphen; 5 mg/kg of body weight). After being fixed to the stereotaxic apparatus, the head of the animal is shaved and an incision is made on his scalp. An uninsulated stainless steel wire coupled to a male Amphenol connector is then wrapped around four to five miniature screws inserted into the skull of the animal. This will serve as the anodal current path. The electrodes are then inserted into the desired region of the brain following specific coordinates expressed in reference to the bregma. Coordinates can be derived from the Paxinos and Watson atlas of the rat

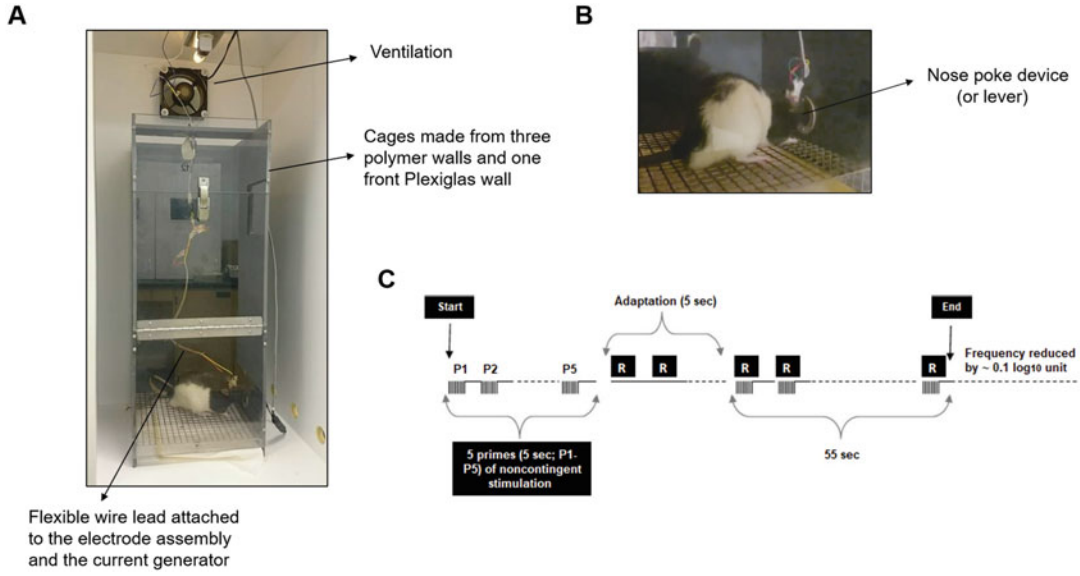

Fig. 1 ICSS apparatus and protocol in rats. (**a**) Operant self-stimulation chamber made of polymer walls and a front Plexiglas wall. Each lever press triggers the delivery of a short train of electrical pulses to a specific brain region through an implanted electrode. (**b**) Zoomed photograph of a self-stimulating rat using a nose poke device. (**c**) Schematic illustration of a single trial of ICSS. Each trial starts with the delivery of five trains of priming stimulation delivered over 5 s, followed by a 5 s adaptation period. The nose poke response or the number of lever presses of the animal is then recorded during discrete 55 s trials. After the 55 s of self-stimulation, the stimulation frequency is reduced by approximately 0.1-log unit and another trial is conducted. Several trials of different frequencies are performed so as to generate at the end of the entire session a plot of the response rate as a function of the pulse frequency

brain [58]. After implantation of the electrodes, dental cement is used to secure the electrode assembly to the skull, and the animal is given another dose of analgesic. At the end of the surgery, the animal should be strictly monitored for changes in body weight. The technique of stereotaxic surgery for the implantation of electrodes is described in more detail in Chapter 2 of the present book.

3.2 ICSS Testing and the Curve-Shift Paradigm

One week following surgery, rats are trained to self-administer a train of pulses using a fixed ratio (FR1) schedule of reinforcement. Initially, a low current intensity (i.e., 200–250 μA) and a low stimulation frequency (30–40 pulses per train) should be used to determine whether the electrical stimulation induces an approach response toward the lever or the hole. If the rat did not respond to the initial parameters of stimulation, the current intensity and stimulation frequency are progressively increased by 0.1–0.2 log unit until a consistent operant response is obtained. Once the response is learned, rats are allowed to self-stimulate continuously for 1 h at stimulation parameters that support consistent responding. Following this period of shaping, rats are tested in the curve-shift paradigm of ICSS.

In the curve-shift paradigm of ICSS, animals are tested during several trials (~12 trials) of varying stimulation frequencies (by 0.1 log unit) and a constant current intensity so as to maintain the population of neurons that is stimulated unchanged. After measuring operant responding of the animals at each of the 12 different trials (a "pass"), the procedure is repeated such that each rat is given four passes per day. Therefore, an entire session of ICSS typically consists of four passes, each lasting approximately 15 min and containing 12 trials with varying frequencies. The first pass usually serves as a warm-up and is excluded from data analysis. Although the parameters used for ICSS can greatly vary from one study to another, each trial typically begins with a 15 s inter-trial interval during which no electrical stimulation is provided, followed by the delivery of five trains of noncontingent priming stimulation, and a 5 s adaptation period (*see* Fig. 1c). The priming trains of stimulation are typically delivered at a rate of 1 prime per second and are used to signal the arrival of discrete 55 s trials during which the animals will be allowed to self-stimulate at constant stimulation parameters (*see* Fig. 1c). During the discrete 55 s trials of ICSS, each operant response triggers the delivery of a single 400 ms train of rectangular cathodal pulses of very short duration (0.1 ms) so as to induce only one action potential per stimulated fiber. Cathodal currents are used instead of anodal currents because they are more effective in triggering action potentials [59]. At the end of each trial, the frequency (i.e., the number of pulses per train of stimulation) is lowered by approximately 0.1-log units, and at the end of the entire session, a R/F curve illustrating the rate of responding (number of lever presses or nose poke response) versus the stimulation frequency is obtained. Moreover, when using stainless steel electrode, it is important that the electrodes be connected to the ground between the delivery of each pulse of train to avoid build-up of charge at the tip; building up of charge can be detrimental particularly with anodal stimulation. The delivery of each train of cathodal pulses is followed by a 600 ms period during which the pulse generator could not be triggered. The introduction of a fixed-interval delay after the delivery of each rewarding stimulation prevents the summation between two consecutive trains [60] and enables better control over reward density, thus ensuring that the amount of reward received by the animal does not depend on its speed of responding, but rather on the rewarding effectiveness of the stimulation [61].

3.3 Reward Thresholds and Maximum Response Rates: Two Measures of ICSS Rewarding Efficacy

The plot of the rate of responding of the animal for different pulse frequencies yields an R/F curve of quasi-sigmoidal shape characterized by a bottom portion (floor), a rising portion, and an upper limit (also called plateau). It is important to note that the plateau does reflect a reward saturation; it is rather due to the maximum capacity of the animal to produce the operant response. Theoretical examples of R/F curves generated under different experimental

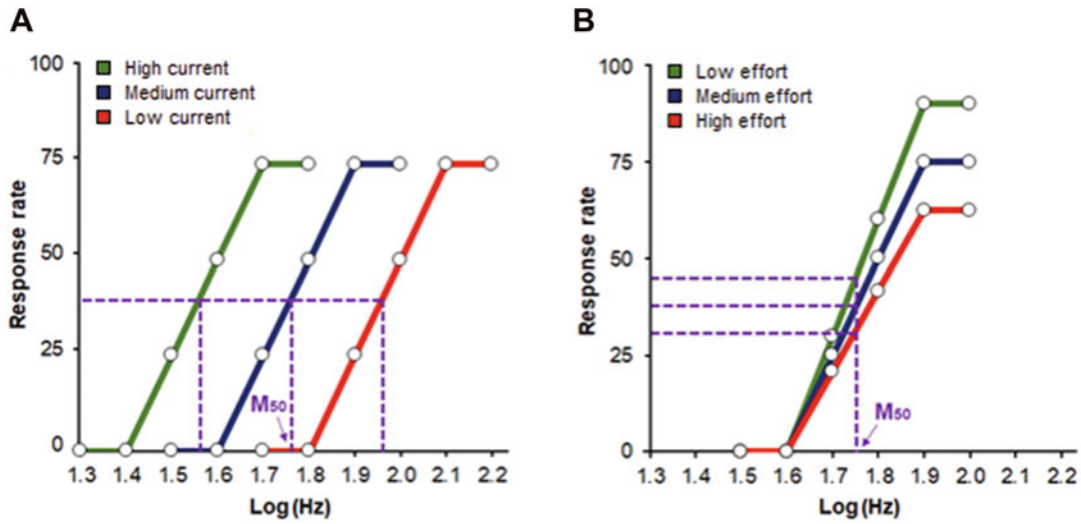

Fig. 2 Theoretical response/frequency curves. Schematic illustration of the theoretical functions that relate response rates to stimulation frequency under different current intensities (**a**) and effort requirements (**b**). The stimulation frequency that maintains half-maximal responding (M50 or reward threshold) is indicated by the pink arrow. Changes in the current intensity of the stimulation cause lateral displacement of the R/F curve (**a**) while changes in task difficulty cause a vertical displacement of the R/F curve (**b**)

conditions are illustrated in Fig. 2a, b. When the current intensities and pulse duration of the stimulation are constant, the magnitude of the reinforcing effect of ICSS is a function of the pulse frequency [62]; animals will respond at negligible rates at low frequencies, intermediate rates for moderate frequencies, and maximal or asymptotic rates at high frequencies (*see* Fig. 2a, b). The most intuitive measure of the reinforcing efficacy of the stimulation is the brain reward threshold, or M50, which corresponds to the pulse frequency sustaining a half-maximal rate of responding. Manipulations that increase or decrease the rewarding efficacy of ICSS shift the M50 toward lower or higher values, respectively, thereby causing lateral displacement of the R/F curve [63]. A decrease in the current intensity of the stimulation increases the M50, while the opposite effect is observed when the current intensity of the stimulation is increased (*see* Fig. 2a). An advantage of using the curve-shift paradigm is that the reward threshold that is derived from this method is remarkably stable over time (weeks and months), thus allowing for multiple testing of each experimental animal over a long period of time [64]. The curve-shift paradigm also enables experimenters to evaluate the capacity of the subject to self-stimulate. Manipulations that induce a change in the capacity of the animal to self-stimulate (such as increasing or decreasing the effort needed to perform the operant response) lead to upward or downward shifts in the maximum response rate [65]. Animals will typically have a higher rate of responding when the effort required

to self-stimulate is low, and a lower rate of responding when the effort required to self-stimulate is high (*see* Fig. 2b). When the reduction in the maximum response rate is proportional at each of the pulse frequency tested, the M50 remains unchanged (*see* Fig. 2b). It is important to note, however, that the curve shift paradigm does not necessarily enable a clear dissociation between reward threshold and maximum response rate since small lateral displacements of the R/F curve can be produced by strong increases in task difficulty [65–67]. The curve-shift paradigm is also insufficient inasmuch as it does not dissociate between the change in the subjective intensity and the cost of reward; this could be better addressed by the "reinforcement mountain" model, though this method is highly time-consuming [68].

3.4 Interpreting Results with the Curve-Shift Paradigm: Effect of Lesion and Drug Injection

The curve-shift paradigm in ICSS has been widely used to quantify the effect of lesions within specific areas of the brain [45, 56, 69] and to quantify the impact of given drug treatment on the reward-relevant circuitry [70], thus enabling a better understanding of the brain reward system with respect to structures and pathways.

3.4.1 ICSS to Evaluate the Rewarding Effect of Electrolytic/Neurotoxic Lesion

There are several strategies for making lesions of specific brain structures or pathways, and these include using neurotoxic and electrolytic lesions (*see* also Chapter 3). While neurotoxic lesions only target neurons, electrolytic lesions destroy fibers of passage as well. Work from our group [45, 56, 69] has recently focused on assessing the effect of electrolytic and neurotoxic lesions of the LHb, a region involved in negative reward processing, on the rewarding properties of ICSS at multiple sites including the lateral hypothalamus (LH) and the dorsal raphe (DR).

Effect of electrolytic lesions of the DDC on ICSS at the LH and DR: Previous work from our group has evaluated the role of the DDC in the rewarding effect induced by ICSS at the LH and DR through the use of electrolytic lesions. Rats were inserted with a lesion electrode (250 μm diameter rod coated with Epoxylite except for the dome-shaped tip) into the DDC (see surgical procedure described earlier) with coordinates taken from a rat brain atlas [55, 58]. Rats were also implanted with stimulation electrodes aimed at the LH and DR [55, 56]. At least 1 week following surgery, rats were trained to self-stimulate, and after at least 4 days of stable operant response (reward threshold ~20 pulses per train), an electrolytic lesion to the DDC was made by passing an anodal current (100 μA, 20–30 s) through the lesion electrode [55, 56]. Rats were then tested for ICSS the following days. The effect of the lesion on the rewarding properties of ICSS was evaluated by comparing the mean reward threshold and maximum response rate pre- and post-lesion. Using this approach, we showed

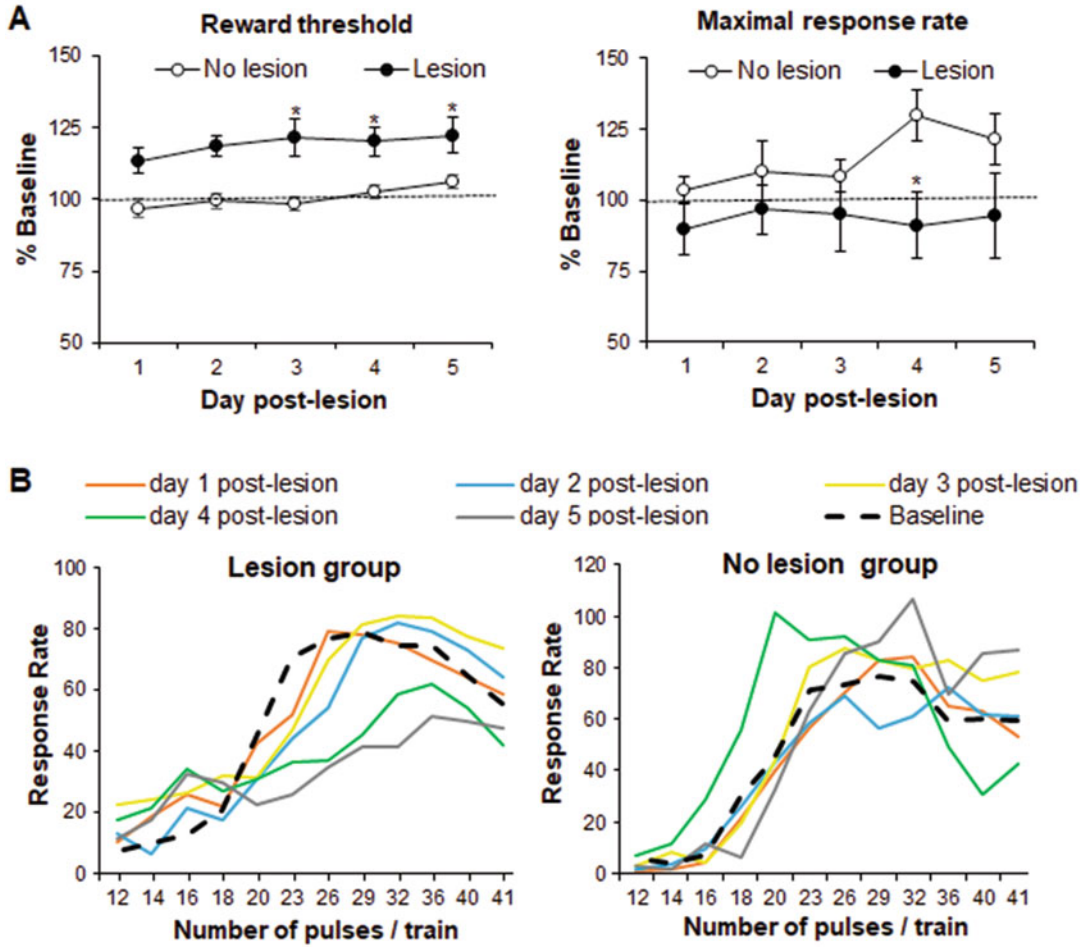

Fig. 3 Assessing the effect of electrolytic lesions at the DDC on the rewarding effect of ICSS at the LH. (**a**) Changes in reward threshold (left panel) and maximum response rate (right panel) following electrolytic lesions at the DDC. Data are expressed in percentage (%) of baseline, which consisted of the mean values obtained during the 3 days that preceded the lesion. Two groups of rats were included ($n = 7$/group): one that received an electrolytic lesion at the DDC, and another one that received no lesion. Both groups were trained and tested for LH self-stimulation in a similar manner. Error bars represent the standard error of the mean (SEM). Taken and adapted from [55]. (**b**) Representative R/F curves of an individual rat from the lesioned group (left panel) and the non-lesioned group (right panel). A clear displacement of the R/F curve to the right is observed following a lesion at the DDC (left panel), indicating that the manipulation decreased the rewarding efficacy of ICSS

that electrolytic lesions aimed at the DDC produce long-lasting increases in ICSS brain reward thresholds at the LH or DR with no or minimal changes in the maximal response rate, indicating that this manipulation decreases brain stimulation reward and that this effect is not due to changes in the motor capacity of rats to self-stimulate [55, 56] (*see* Fig. 3a).

Effect of neurotoxic lesions of the lateral habenula on ICSS at the LH and DR: Work from our group has also evaluated the role of

the lateral habenula in the rewarding and locomotor-stimulant effect of psychostimulants by using neurotoxic lesions in rats. Neurotoxic lesions were conducted under anesthesia with isoflurane (see surgical procedure described earlier), and consisted of injections of a neurotoxin (e.g., Ibotenic acid 0.25 μg/0.25 μL) directly into the lateral habenula via a cannula (30 ga) connected to a 5 μL Hamilton syringe via PE10 tubing [69]. The infusion was controlled by an infusion pump (Harvard Apparatus, MA, USA) and occurred over 1 min [69]. An additional minute was allowed at the end of each infusion in order to maximize drug diffusion. Rats were also implanted with stimulation electrodes aimed at the LH and DR as described in the previous paragraph. Using this methodological approach, Gifuni and colleagues showed that neurotoxic lesions of the lateral habenula significantly enhance the locomotor-stimulant effect of amphetamine but do not alter the reward-enhancing properties of amphetamine as assessed by ICSS at the LH or DR, suggesting that these dopamine-dependent behaviors (i.e., locomotor activity and ICSS) are differentially modulated by the lateral habenula [69].

3.4.2 ICSS to Evaluate the Rewarding Effect of Drugs

In clinical practice, drugs often produce therapeutic effects that help patients cope with their symptoms, however, these effects are often accompanied by adverse reactions that pose serious problems to the health of the afflicted individual. One such undesirable effect is drug abuse. Although the standard model for evaluating the abuse potential of a drug is the drug self-administration procedure (*see* also Chapter 11), ICSS has also been widely used to evaluate the rewarding effect of drugs and their potential for abuse [70] (*see* also Chapter 10). In typical experiments of ICSS for evaluating the rewarding or abuse potential of drugs, animals are tested for self-stimulation before and after drug administration, and changes in the rewarding efficacy of the stimulation are assessed through the curve-shift paradigm. Drugs can be administered through various routes, including intracranial, intravenous, intraperitoneal, oral, and subcutaneous. When rats are tested with the curve-shift paradigm, drug-induced increases in ICSS reward threshold are interpreted as a decrease in the rewarding efficacy of the stimulation, whereas drug-induced decreases in ICSS reward threshold are interpreted as an increase in the rewarding efficacy of the stimulation.

Effect of intracranial drug injection on the ICSS behavior (*see* also Chapter 10): Previous work from our group has evaluated the effect of injecting the glutamate NMDA receptor antagonist, PPPA, into the ventral midbrain (VM) on the rewarding properties of ICSS at the posterior mesencephalon (PM) [71]. Rats were

implanted with a stimulation electrode into the PM and two guide cannulae (HRS Scientific, model C315G) in each hemisphere, above the VM. Each cannula was closed with an obturator of the same length. Injection of PPPA was made by inserting an injection cannula directly into a guide cannula implanted into the desired region of the brain. Each injection cannula extended 2 mm beyond the guide cannula tip and was connected to a 5 mL Hamilton microsyringe via polyethylene tubing. A volume (0.5 µL) containing the desired drug solution (PPPA; 0.825 or 1.65 nmol) or the vehicle was delivered through the cannula over a 60 s period using a micro-infusion pump. The injection cannula was then left in place for an additional 60 s to allow for proper diffusion into the brain, after which animals were immediately tested for ICSS. Using this methodological approach, Bergeron and Rompré (2013) showed that injection of PPPA into the VM produces a dose and time dependent decrease in the ICSS reward threshold (*see* Fig. 4), suggesting that NMDA receptors located in the VM play an important role in brain stimulation reward.

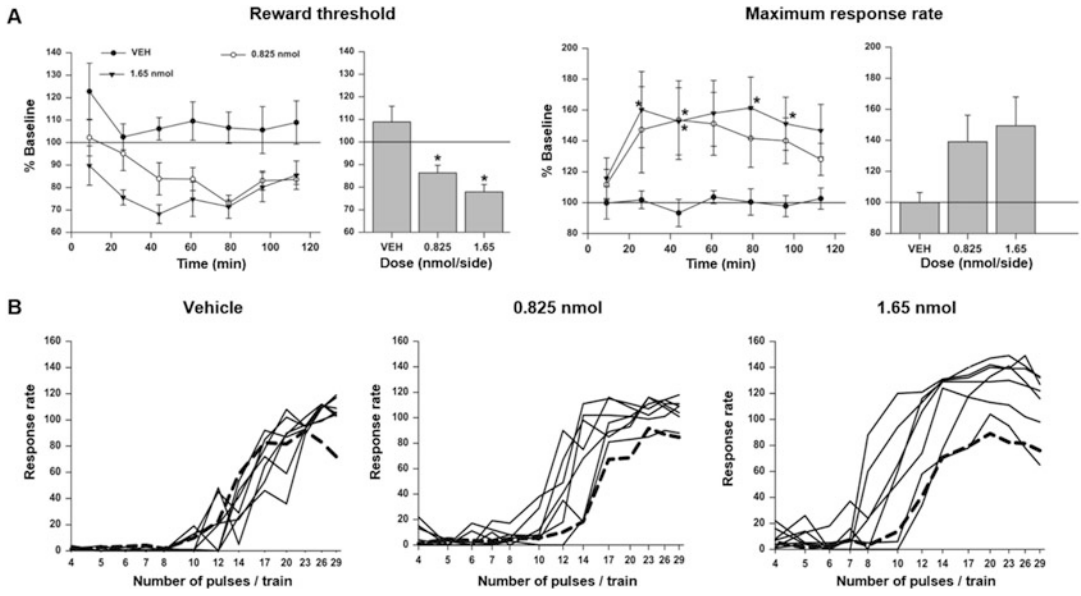

Fig. 4 Assessing the effect of intra-VM injection of the NMDA receptor antagonist, PPPA, on the rewarding effect of ICSS at the PM. (**a**) Changes in reward threshold (left panels) and maximum response rate (right panels) following injection of vehicle (VEH) and each of the two doses of PPPA (0.825 and 1.65 nmol). Data represent mean ± SEM ($n = 7$/group) and are expressed as % of baseline. Bar graphs illustrate the changes measured over the entire test session. Significant differences from the control group are indicated by * for $p < 0.05$. Taken and adapted from [71]. (**b**) Rate–frequency curves obtained from one tested animal prior to (dotted line) and for 2 h (line) after injection of vehicle (left panel) and two doses of PPPA (0.825 and 1.65 nmol). The x-axis represents the number of pulses per train on a log scale. Taken and adapted from [71]

4 Notes and Conclusion

Since its discovery and implementation, the ICSS paradigm has become a powerful tool to study the neural substrates underlying reward and goal-directed behaviors. A major strength of this paradigm is that the electrical stimulation directly activates the brain reward circuitry, bypassing sensory systems and natural physiological processes like satiation. The ICSS procedure also provides quantitative measurements of brain stimulation reward that are robust and stable over long periods of time, thus allowing the experimenter to perform multiple tests or longitudinal studies on the same subjects [64]. Another advantage of ICSS is that the stimulation can be delivered to the desired regions of the brain with extremely high temporal accuracy. This can be achieved by controlling external parameters such as the pulse frequency and duration of the stimulation. However, studies employing ICSS with the use of electrical stimulation have been plagued with a lack of anatomical specificity. The main issue is that the electrical stimulation of the brain does not allow the distinction between reward-relevant neural elements and those that do not play a role in reward, thus making the identification of the neural substrate for brain stimulation reward extremely challenging [72]. The recently developed technique of optogenetics, which is discussed in subsequent chapters, can circumvent this problem by using light to achieve gain- or loss-of-function within specific neurons or pathways, thus enabling a more precise delineation of the neural substrate of behavior [73, 74]. Nevertheless, despite its technical limitations, ICSS with electrical stimulation is still widely used in rodents for the identification of the neuroanatomical substrates of reward and has proven valuable in the study of the reinforcing effects of drugs of abuse.

Acknowledgments

Research described in the present chapter was conducted in the Department of Neuroscience of the Université de Montréal and supported by the Natural Sciences and Engineering Research Council of Canada (NSERC).

References

1. Pavlov I (1927) Conditioned reflexes: an investigation of the physiological activity of the cerebral cortex. Translated and edited by G. V. Anrep. Oxford University Press, London, p 142
2. Watson J (1913) Psychology as the behaviorist views it. Psychol Rev 20:158–177
3. Skinner B (1938) The behavior of organisms: an experimental analysis. Appleton Century-Crofts, New York

4. Thorndike E (1911) Animal intelligence. Macmillan, New York
5. Fesrter C, Skinner B (1957) Schedules of reinforcement. Appleton-Century-Crofts, New York
6. Olds J, Milner P (1954) Positive reinforcement produced by electrical stimulation of septal area and other regions of rat brain. J Comp Physiol Psychol 47(6):419–427. https://doi.org/10.1037/h0058775
7. Milner PM (1991) Brain-stimulation reward: a review. Can J Psychol 45(1):1–36. https://doi.org/10.1037/h0084275
8. Bursten B, Delgado JM (1958) Positive reinforcement induced by intracerebral stimulation in the monkey. J Comp Physiol Psychol 51(1):6–10. https://doi.org/10.1037/h0048182
9. Sadowski B (1972) Intracranial self-stimulation patterns in dogs. Physiol Behav 8(2):189–193. https://doi.org/10.1016/0031-9384(72)90359-9
10. Wilkinson HA, Peele TL (1963) Intracranial self-stimulation in cats. J Comp Neurol 121:425–440. https://doi.org/10.1002/cne.901210310
11. Andrew RJ (1967) Intracranial self-stimulation in the chick. Nature 213(5078):847–848. https://doi.org/10.1038/213847a0
12. Bishop MP, Elder ST, Heath RG (1963) Intracranial self-stimulation in man. Science 140(3565):394–396. https://doi.org/10.1126/science.140.3565.394
13. Olds J (1956) A preliminary mapping of electrical reinforcing effects in the rat brain. J Comp Physiol Psychol 49(3):281–285. https://doi.org/10.1037/h0041287
14. Olds J (1956) Runway and maze behavior controlled by basomedial forebrain stimulation in the rat. J Comp Physiol Psychol 49(5):507–512. https://doi.org/10.1037/h0047544
15. Nieuwenhuys R, Geeraedts LM, Veening JG (1982) The medial forebrain bundle of the rat. I General introduction. J Comp Neurol 206(1):49–81. https://doi.org/10.1002/cne.902060106
16. Sutherland RJ (1982) The dorsal diencephalic conduction system: a review of the anatomy and functions of the habenular complex. Neurosci Biobehav Rev 6(1):1–13. https://doi.org/10.1016/0149-7634(82)90003-3
17. Beretta CA et al (2012) Habenula circuit development: past, present, and future. Front Neurosci 6:51. https://doi.org/10.3389/fnins.2012.00051
18. Mora F, Avrith DB, Rolls ET (1980) An electrophysiological and behavioural study of self-stimulation in the orbitofrontal cortex of the rhesus monkey. Brain Res Bull 5(2):111–115. https://doi.org/10.1016/0361-9230(80)90181-1
19. Bielajew C, Trzcinska M (1998) Activation of reward-relevant neurons in the caudate-putamen influences the development of medial prefrontal cortex self-stimulation: a moveable electrode mapping study. Acta Neurobiol Exp (Wars) 58(3):189–198
20. Bushnik T, Bielajew C, Konkle AT (2000) The substrate for brain-stimulation reward in the lateral preoptic area. I Anatomical mapping of its boundaries. Brain Res 881(2):103–111. https://doi.org/10.1016/s0006-8993(00)02564-6
21. Panagis G et al (1995) Ventral pallidum self-stimulation: a moveable electrode mapping study. Behav Brain Res 68(2):165–172. https://doi.org/10.1016/0166-4328(94)00169-g
22. Kane F, Coulombe D, Miliaressis E (1991) Amygdaloid self-stimulation: a movable electrode mapping study. Behav Neurosci 105(6):926–932. https://doi.org/10.1037//0735-7044.105.6.926
23. Rompre PP, Boye S (1989) Localization of reward-relevant neurons in the pontine tegmentum: a moveable electrode mapping study. Brain Res 496(1–2):295–302. https://doi.org/10.1016/0006-8993(89)91076-7
24. Rompre PP, Miliaressis E (1985) Pontine and mesencephalic substrates of self-stimulation. Brain Res 359(1–2):246–259. https://doi.org/10.1016/0006-8993(85)91435-0
25. Corbett D, Wise RA (1979) Intracranial self-stimulation in relation to the ascending noradrenergic fiber systems of the pontine tegmentum and caudal midbrain: a moveable electrode mapping study. Brain Res 177(3):423–436. https://doi.org/10.1016/0006-8993(79)90461-x
26. Sutherland RJ, Nakajima S (1981) Self-stimulation of the habenular complex in the rat. J Comp Physiol Psychol 95(5):781–791. https://doi.org/10.1037/h0077833
27. Nakajima S (1984) Serotonergic mediation of habenular self-stimulation in the rat. Pharmacol Biochem Behav 20(6):859–862. https://doi.org/10.1016/0091-3057(84)90007-8
28. Phillips AG (1970) Enhancement and inhibition of olfactory bulb self-stimulation by odours. Physiol Behav 5(10):1127–1131. https://doi.org/10.1016/0031-9384(70)90200-3

29. Ursin R, Ursin H, Olds J (1966) Self-stimulation of hippocampus in rats. J Comp Physiol Psychol 61(3):353–359. https://doi.org/10.1037/h0023253
30. Phillips AG, Van Der Kooy D, Fibiger HC (1977) Maintenance of intracranial self-stimulation in hippocampus and olfactory bulb following regional depletion of noradrenaline. Neurosci Lett 4(2):77–84. https://doi.org/10.1016/0304-3940(77)90148-3
31. Mogenson GJ et al (1979) Self-stimulation of the nucleus accumbens and ventral tegmental area of Tsai attenuated by microinjections of spiroperidol into the nucleus accumbens. Brain Res 171(2):247–259. https://doi.org/10.1016/0006-8993(79)90331-7
32. Fibiger HC et al (1987) The role of dopamine in intracranial self-stimulation of the ventral tegmental area. J Neurosci 7(12):3888–3896
33. Ball GG, Micco DJ Jr, Berntson GG (1974) Cerebellar stimulation in the rat: complex stimulation-bound oral behaviors and self-stimulation. Physiol Behav 13(1):123–127. https://doi.org/10.1016/0031-9384(74)90313-8
34. Corbett D, Fox E, Milner PM (1982) Fiber pathways associated with cerebellar self-stimulation in the rat: a retrograde and anterograde tracing study. Behav Brain Res 6(2):167–184. https://doi.org/10.1016/0166-4328(82)90012-2
35. Berthoud H, Münzberg H (2011) The lateral hypothalamus as integrator of metabolic and environmental needs: from electrical self-stimulation to opto-genetics. Physiol Behav 104(1):29–39
36. Stuber GD, Wise RA (2016) Lateral hypothalamic circuits for feeding and reward. Nat Neurosci 19(2):198–205. https://doi.org/10.1038/nn.4220
37. Delgado JM, Anand BK (1953) Increase of food intake induced by electrical stimulation of the lateral hypothalamus. Am J Phys 172(1):162–168. https://doi.org/10.1152/ajplegacy.1952.172.1.162
38. Kempadoo KA et al (2013) Hypothalamic neurotensin projections promote reward by enhancing glutamate transmission in the VTA. J Neurosci 33(18):7618–7626. https://doi.org/10.1523/JNEUROSCI.2588-12.2013
39. Barone FC et al (1981) Afferent connections to the lateral hypothalamus: a horseradish peroxidase study in the rat. Brain Res Bull 7(1):75–88. https://doi.org/10.1016/0361-9230(81)90101-5
40. Kita H, Oomura Y (1982) An HRP study of the afferent connections to rat lateral hypothalamic region. Brain Res Bull 8(1):63–71. https://doi.org/10.1016/0361-9230(82)90028-4
41. Larsen PJ, Hay-Schmidt A, Mikkelsen JD (1994) Efferent connections from the lateral hypothalamic region and the lateral preoptic area to the hypothalamic paraventricular nucleus of the rat. J Comp Neurol 342(2):299–319. https://doi.org/10.1002/cne.903420211
42. Janas JD, Stellar JR (1987) Effects of knife-cut lesions of the medial forebrain bundle in self-stimulating rats. Behav Neurosci 101(6):832–845. https://doi.org/10.1037//0735-7044.101.6.832
43. Gallistel CR et al (1996) Destruction of the medial forebrain bundle caudal to the site of stimulation reduces rewarding efficacy but destruction rostrally does not. Behav Neurosci 110(4):766–790. https://doi.org/10.1037//0735-7044.110.4.766
44. Simmons JM, Ackermann RF, Gallistel CR (1998) Medial forebrain bundle lesions fail to structurally and functionally disconnect the ventral tegmental area from many ipsilateral forebrain nuclei: implications for the neural substrate of brain stimulation reward. J Neurosci 18(20):8515–8533
45. Morissette MC, Boye SM (2008) Electrolytic lesions of the habenula attenuate brain stimulation reward. Behav Brain Res 187(1):17–26. https://doi.org/10.1016/j.bbr.2007.08.021
46. Bielajew C, Miguelez M, Shiao R (2002) Electrolytic lesions of the cortical and adjacent nuclei in the amygdala differentially influence thresholds for rewarding medial forebrain bundle stimulation. Behav Neurosci 116(4):660–671
47. Waraczynski MA (1988) Basal forebrain knife cuts and medial forebrain bundle self-stimulation. Brain Res 438(1–2):8–22. https://doi.org/10.1016/0006-8993(88)91319-4
48. Boye SM (2005) Mesencephalic substrate of reward: lesion effects. Behav Brain Res 156(1):31–43. https://doi.org/10.1016/j.bbr.2004.05.005
49. Waraczynski M, Ton MN, Shizgal P (1990) Failure of amygdaloid lesions to increase the threshold for self-stimulation of the lateral

hypothalamus and ventral tegmental area. Behav Brain Res 40(2):159–168. https://doi.org/10.1016/0166-4328(90)90007-2

50. Waraczynski M, Conover K, Shizgal P (1992) Rewarding effectiveness of caudal MFB stimulation is unaltered following DMH lesions. Physiol Behav 52(2):211–218
51. Waraczynski M, Shizgal P (1995) Self-stimulation of the MFB following parabrachial lesions. Physiol Behav 58(3):559–566. https://doi.org/10.1016/0031-9384(95)00092-w
52. Lorens SA (1966) Effect of lesions in the central nervous system on lateral hypothalamic self-stimulation in the rat. J Comp Physiol Psychol 62(2):256–262. https://doi.org/10.1037/h0023658
53. Blander A, Wise RA (1989) Anatomical mapping of brain stimulation reward sites in the anterior hypothalamic area: special attention to the stria medullaris. Brain Res 483 (1):12–16. https://doi.org/10.1016/0006-8993(89)90029-2
54. Vachon MP, Miliaressis E (1992) Dorsal diencephalic self-stimulation: a movable electrode mapping study. Behav Neurosci 106 (6):981–991. https://doi.org/10.1037//0735-7044.106.6.981
55. Fakhoury M et al (2016) Effect of electrolytic lesions of the dorsal diencephalic conduction system on the distribution of Fos-like immunoreactivity induced by rewarding electrical stimulation. Neuroscience 334:214–225. https://doi.org/10.1016/j.neuroscience.2016.08.002
56. Fakhoury M, Rompre PP, Boye SM (2016) Role of the dorsal diencephalic conduction system in the brain reward circuitry. Behav Brain Res 296:431–441. https://doi.org/10.1016/j.bbr.2015.10.038
57. Carlezon WA Jr, Chartoff EH (2007) Intracranial self-stimulation (ICSS) in rodents to study the neurobiology of motivation. Nat Protoc 2 (11):2987–2995. https://doi.org/10.1038/nprot.2007.441
58. Paxinos G, Watson C (2013) The rat brain in stereotaxic coordinates, 7th edn. Academic Press, San Diego
59. Ranck JB Jr (1975) Which elements are excited in electrical stimulation of mammalian central nervous system: a review. Brain Res 98 (3):417–440. https://doi.org/10.1016/0006-8993(75)90364-9
60. Fouriezos G (1995) Temporal integration in self-stimulation: a paradox lost? Behav Neurosci 109(5):965–971. https://doi.org/10.1037//0735-7044.109.5.965
61. Boye SM, Rompre PP (1996) Effect of pimozide on self-stimulation threshold under a continuous and fixed-interval schedule of reinforcement. Behav Brain Res 78 (2):243–245. https://doi.org/10.1016/0166-4328(95)00239-1
62. Gallistel CR, Shizgal P, Yeomans JS (1981) A portrait of the substrate for self-stimulation. Psychol Rev 88(3):228–273
63. Edmonds DE, Gallistel CR (1974) Parametric analysis of brain stimulation reward in the rat: III. Effect of performance variables on the reward summation function. J Comp Physiol Psychol 87(5):876–883. https://doi.org/10.1037/h0037217
64. Stoker A, Markou A (2011) The intracranial self-stimulation procedure provides quantitative measures of brain reward function. In: Gould TJ (ed) Mood and anxiety related phenotypes in mice, Neuromethods, vol 63. Humana Press, New York
65. Miliaressis E et al (1986) The curve-shift paradigm in self-stimulation. Physiol Behav 37 (1):85–91. https://doi.org/10.1016/0031-9384(86)90388-4
66. Frank R, Williams H (1985) Both response effort and current intensity affect self-stimulation train duration thresholds. Pharmacol Biochem Behav 22(4):527–530
67. Fouriezos G, Bielajew C, Pagotto W (1990) Task difficulty increases thresholds of rewarding brain stimulation. Behav Brain Res 37 (1):1–7
68. Arvanitogiannis A, Shizgal P (2008) The reinforcement mountain: allocation of behavior as a function of the rate and intensity of rewarding brain stimulation. Behav Neurosci 122 (5):1126–1138
69. Gifuni AJ et al (2012) Lesions of the lateral habenula dissociate the reward-enhancing and locomotor-stimulant effects of amphetamine. Neuropharmacology 63(6):945–957. https://doi.org/10.1016/j.neuropharm.2012.07.032
70. Negus SS, Miller LL (2014) Intracranial self-stimulation to evaluate abuse potential of drugs. Pharmacol Rev 66(3):869–917. https://doi.org/10.1124/pr.112.007419
71. Bergeron S, Rompre PP (2013) Blockade of ventral midbrain NMDA receptors enhances brain stimulation reward: a preferential role

for GluN2A subunits. Eur Neuropsychopharmacol 23(11):1623–1635. https://doi.org/10.1016/j.euroneuro.2012.12.005

72. Murray B, Shizgal P (1996) Behavioral measures of conduction velocity and refractory period for reward-relevant axons in the anterior LH and VTA. Physiol Behav 59 (4–5):643–652. https://doi.org/10.1016/0031-9384(96)80249-6
73. Bernstein JG, Boyden ES (2011) Optogenetic tools for analyzing the neural circuits of behavior. Trends Cogn Sci 15(12):592–600. https://doi.org/10.1016/j.tics.2011.10.003
74. Yizhar O et al (2011) Optogenetics in neural systems. Neuron 71(1):9–34. https://doi.org/10.1016/j.neuron.2011.06.004

Chapter 2

Stereotaxic Surgery in Rodents for Stimulation of the Brain Reward System

Brenda M. Geiger, Monika Irene, and Emmanuel N. Pothos

Abstract

The use of stereotaxic surgery to implant devices like microdialysis probes or stimulating electrodes in specific regions of the central nervous system (CNS) is critical for our understanding of the neurobiology of reward and aversion in rodents. Here we review the different methodological approaches to the study of brain reward systems and outline the procedure for stereotaxic implantation of devices in reward-associated CNS sites in mice and rats. We also discuss applications that take advantage of our ability to target precisely defined regions in the CNS. Applications addressed include response to drugs and natural rewards (food), drug self-administration, electrical self-stimulation, delivery of viral constructs to alter gene expression, optogenetics to evaluate reward and avoidance behaviors, fiber photometry to measure transient calcium signaling, and real-time electrochemical detection through amperometry and fast-scan cyclic voltammetry. Using the knowledge gained by these experiments, we can move forward with new treatments for disorders related to disruptions in the reward systems of the CNS.

Key words Amperometry, Brain microdialysis, Electrical self-stimulation, Fiber photometry, Nucleus accumbens, Optogenetics, Prefrontal cortex, Stereotactic, Striatum, Voltammetry

1 Introduction

Stereotaxic surgery has proven to be a valuable and elegant tool for understanding the neurobiology of reward and aversion in rodents. This chapter explores the use of stereotaxic surgery in a variety of experimental frameworks and settings, all of which help us understand the role of different central nervous system (CNS) regions in the three-dimensional plane in the behavioral responses to rewarding and aversive stimuli, either external or internal.

1.1 What are Reward and Aversion?

Reward and aversion are two neurochemical responses that in principle lead to opposing behaviors. A rewarding stimulus will induce feelings of pleasure and lead to behaviors of approach and consumption. These behaviors will be reinforced as the rewarding stimuli occur over time [1]. In comparison, aversive stimuli cause

Marc Fakhoury (ed.), *The Brain Reward System*, Neuromethods, vol. 165, https://doi.org/10.1007/978-1-0716-1146-3_2,

negative emotions and experiences like anxiety, pain, or fear and lead to behaviors of avoidance. Sometimes, even one exposure or repeated exposures to these stimuli significantly reduce the likelihood that the behavior would occur again. Taken together, humans and animals are much more likely to obtain reward and avoid punishment so these neurochemical responses help to drive decision-making and motivate our learning [2].

When considering the reward response, it is often separated into several different psychobehavioral components. These components include liking, wanting, and learning. Liking is the basic reaction to the reward stimulus. Wanting is related to the motivation to seek the rewarding stimulus through the process of incentive salience. Learning is related to the associations or cognitive representations that relate to the rewarding stimulus. Each of these psychological components has distinct neural mechanisms [3, 4]. This chapter discusses ways in which stereotaxic implants can be used in rodents to help us understand the neurological responses to rewarding stimuli in the brain.

1.2 Dopamine's Role in Reward and Aversion

It is well known that midbrain dopamine neurons are activated in response to a rewarding stimulus. For example, in response to food, increased dopamine release and turnover have been shown in the nucleus accumbens, dorsal striatum, and medial prefrontal cortex through stereotaxic placement of neurotransmitter collectors or sensors such as microdialysis probes [1, 5–8]. Furthermore, dopamine in these areas is known to increase with exposure to food-associated stimuli and motor activity related to attainment of food [9–11].

It has also been shown that dopamine neurons are activated in cases where the stimulus has been aversive or non-rewarding [12]. Other studies have shown that dopamine neurons fall into two categories. Most dopamine neurons are excited by rewarding stimuli and inhibited by aversive stimuli and a second population of neurons is excited by both rewarding and aversive stimuli [13–15]. Furthermore, mesolimbic dopamine release is typically inhibited by aversive stimuli or aversive states such as opiate withdrawal [16, 17].

While dopamine is one of the primary neurotransmitters that has been associated with reward-seeking behavior, it is not the only reward transmitter and dopaminergic neurons are not always the final common path for reward [2, 18]. The endogenous opioid system also provides a mechanism for reward responses through interactions of the hypothalamus and striatum [19]. For example, the actions of the widely distributed mu opioid receptors are important in the brain responses to the rewarding stimuli from palatable high-fat food [20, 21]. The more these receptors are stimulated, the higher the intake of palatable foods [22]. There is also plasticity in this pathway, as repeated exposure to high-fat and high-

carbohydrate diets result in decreased levels and release of the endogenous opioid enkephalin [23, 24].

Activation of certain glutamate neurons has also been shown to be involved in reward-related responses. Glutamate neurons that are the afferent inputs to reward-responding dopamine neurons may initiate many of the dopamine-mediated reward responses when activated. This function is supported by the observation that when dopamine neurons respond to reward signals by burst firing it is in response to glutamatergic inputs [25, 26]. Finally, the dorsal raphe nucleus contains neurons with serotonin (5-hydroxytryptamine; 5-HT), glutamate, GABA, and dopamine phenotypes. Further pharmacological studies in these populations indicate that serotonin might also be involved in modulating reward- or punishment-related behaviors. Recent optogenetic stimulations demonstrate that transient activation of dorsal raphe nucleus neurons produces strong reinforcement signals that are carried out primarily by glutamate. Moreover, activation of the serotonin neurons in this brain region enhances reward expectations [27].

1.3 Challenges for Measuring Reward Responses in Humans

Understanding the circuits and molecular mechanisms that underlie a complex decision-making process is challenging in a highly complex organism with a large nervous system. In humans, where invasive techniques involving device implantation in the brain that carries a high likelihood to severely injure the subject are typically not allowed with some notable exceptions as in the case of brain radiotherapy, Parkinson's disease or mental disorder treatment [28–30], we must rely on less invasive imaging techniques to evaluate reward mechanisms. These techniques typically employ labeled compounds to measure glucose metabolism/oxygen consumption and therefore activity in the various areas of the brain and deduce functional connections between regions of interest that are activated at the same time. However, it is still technically challenging to directly link these responses to the specific neurotransmitters responsible for the activity. Instead, one can use other inferences from what we know about the neuronal populations of different brain regions to hypothesize which neurotransmitters are most likely involved. Pharmacological manipulation of the reward pathways in humans is often not possible as many of the drugs used to manipulate these systems are habit-forming, so conducting experiments on humans using these drugs is not considered ethical.

1.4 Use of Non-murine Animal Models to Measure Reward Responses

While mice and rats are by far the most common animal models used to measure reward and aversive responses in order to better understand the neurobiology behind these behaviors, it is important to note that other species have also been employed for this purpose and often without the benefit of brain stereotaxic surgery as local injections into the CNS without coordinates or bath

exposure to pharmacological agents are often adequate to produce the desired effects. However, stereotaxic instruments can be used for intracerebral injections in fish [31]. For instance, the balance between aversion and reward has been evaluated in zebrafish (*Danio rerio*) because the dopaminergic pathways in this species are similar to the dopaminergic systems in mammals, including all of the same receptors except for the D5 receptor [32–35]. A key difference is that the majority of zebrafish dopamine neurons are located across the *diencephalon* with ascending projections to the telencephalon, while the midbrain is the main center of dopaminergic domains in mammals. However, some of the zebrafish dopamine neurons appear to be functionally equivalent to the mammalian dopamine system [36, 37]. Several neurobehavioral abnormalities associated with dysfunction of the dopaminergic system have been reported in zebrafish [38–40]. Additionally, behavioral alterations as a result of acute exposure to dopaminergic drugs have been observed in this species [34, 41]. The zebrafish model is also gaining momentum in the field of learning and memory [42–44]. A number of studies revealed robust cognitive abilities of zebrafish in a range of learning tasks such as visual choice discrimination learning [44], shuttle box learning [45], place conditioning [46], active avoidance learning [47], spatial memory tasks [48], and plus-maze nonspatial and spatial associative learning paradigms [49–51].

Caenorhabditis elegans (C. elegans) is another model organism that has been used to advance our understanding in this area. In an assay to map the important events that go into the decision to cross an aversive barrier to get to the source of an attractive food-related cue, it was found that worms avoid aversive stimuli while approaching food as they must balance the drive for food with the threat of hyperosmolarity-induced desiccation and death [52]. Based on this study, it appears that the internal physiological state modulates decision-making circuits and thereby reshapes the behavioral output [52]. Furthermore, in addition to other previously reported factors, the internal physiological state, including hunger, reshapes threat–reward decision-making by modifying this neural circuit [52–54].

Higher level organisms have also been used to evaluate behaviors associated with rewarding and aversive stimuli, including nonhuman primates, this time typically with the benefit of targeting brain regions with stereotaxic coordinates. Many of these studies have focused on understanding decision-making and preference between two different tasks with different rewards associated with them. One elegant study was able to link the role of dopamine in macaque monkeys to reward-predicting choices, as monkeys were more likely to choose objects that were associated with optogenetic activation of dopamine neurons than identical objects that were not linked to dopamine neuron activation [55]. A number of studies in

nonhuman primates look at social reward compared to individual reward and the likelihood of choosing self-reward versus social reward. In general, it has been shown that striatal neurons activate differently depending on whether the reward is advantageous or not to the monkey tested. Tasks linked with social rewards can be learned, but food reward tasks are more readily learned, and in the amygdala, release of the prosocial peptide oxytocin enhances the natural tendency of monkeys to make prosocial decisions [56–58]. A number of other studies have also been carried out in primates that try to elucidate the role of reward value, difficulty to obtain reward, and natural versus drug reward in the learning of reward-related behaviors and the brain regions that control these behaviors. Techniques like fMRI or FDG-PET are used in several of those studies to try to visualize areas of the brain that react differently to distinct stimuli. However, there are limitations to these approaches as they only show activity and not necessarily the specific neuron type that is activated in a given brain region [59–64].

In the remainder of this chapter, we discuss the basics of stereotaxic implantation of guide cannulas and various types of probes, including microdialysis probes, optogenetic probes, or stimulating electrodes in rodents and how these can be used to better understand the neurochemistry involved in coding of reward and aversive stimuli in the rodent brain.

2 Materials

To surgically implant a probe or guide cannula into a rodent, one would need the following infrastructure and supplies in place at a minimum:

- Approval of all preoperative, surgical, and postoperative procedures by the appropriate Institutional Animal Care and Use Committee (IACUC) or equivalent body for investigators outside the United States.
- Ongoing consultation with the veterinarian and animal care personnel of the institution's animal facility.
- A laboratory animal facility compliant with all applicable federal, state, and/or international standards.
- A species-appropriate stereotaxic apparatus.
- A cocktail of anesthetic agents as approved by the IACUC committee of the institution or the designated committee or process of the institution if located outside the United States.
- Devices for providing and monitoring thermoregulation (heating pad, (rectal) thermometer).
- Eye lubricant.

- Shaving tools for removing fur in the area to be dissected.
- Dissecting tools (scalpel and blade, hemostats).
- Sterilizing procedures (iodine, microbead sterilizer).
- Cotton swabs to maintain dissected area as dry as possible.
- Pencil or equivalent marker to mark skull holes for cannulas and screws.
- Guide cannulas and microdialysis, optogenetic or electrode probes (or equivalent per experimental needs), custom made or commercially available.
- Sterile needles to gently puncture meninges and facilitate cannula insertion.
- At least six skull screws to anchor the headcap with the cannulas.
- Hand drill with appropriate size drill bits to accommodate the diameter of the cannulas installed.
- Dental cement for the headcap.
- Anchor for a swivel if sampling from the freely moving animal is desired after recovery from surgery.
- Sutures or wound clips to be removed 7–14 days post-surgery.
- Local (usually bacitracin) and systemic antibiotic as approved by IACUC to prevent infections.
- Monitoring of the animal until it sufficiently recovers from anesthesia.
- Daily monitoring of the animal for at least the first week post-op for infections and treatment with appropriate analgesics. Since opioids directly affect reward systems, it is best to use alternative pain management as per IACUC approval. Typical alternatives may include acetaminophen, meloxicam, and bupivacaine (the latter being administered prior to incision).
- A ductless hood or workstation with active airflow and use of gloves, single-use aprons, hair cups, and face masks would constitute an optimized environment to perform the surgery and ensure sterile technique is observed to the best extent possible.

3 Methods

In this section, we discuss the procedures used to surgically implant probes or cannula into specific brain regions of rodents. We first give an overview of the surgical parameters that are typically used. We also discuss how to place the cannula via stereotaxic coordinates and some of the common methods used for sample acquisition and analysis.

3.1 Stereotaxic Surgical Procedure

3.1.1 Anesthesia and Preparation of Rodents for Surgery

To surgically implant a probe or cannula into the brain of a rodent according to our protocol, young adult (12–15 week old) C57BL/6 J mice or Sprague Dawley rats or equivalent are anesthetized with a mixture of ketamine (60 mg/kg for rats; 100 mg/kg for mice) and xylazine (10 mg/kg for either species) via intraperitoneal injection or with inhaled isoflurane via a nose cone on the stereotaxic apparatus. Because of how the animal is eventually placed on the stereotaxic instrument, it can be difficult to get a good seal on the nose cone and therefore difficult to use inhaled isoflurane. Toe pinch withdrawal reflex is usually used to demonstrate sedation [65, 66]. To ensure thermoregulation throughout the surgery, the animal is placed on a heating pad and body temperature is monitored using a rectal thermometer.

Once the sedation fully takes effect, the animal head is shaved, and the exposed skin is sterilized using iodine prior to incision. The animal is fixed to the stereotaxic apparatus by placing one ear bar into the ear canal and holding the animal steady while sliding the other ear bar to the opposite ear until the ear bars are properly positioned and the head is immobilized. The mouth is secured with the anterior incisor bar and the head is secured leveled. To ensure this, a ruler is held vertically with reference to the stereotaxic platform, and the head is positioned so that there is a 90° angle between the ruler and the middle of the animal's scalp [67]. Some stereotaxic instruments can digitally confirm level positioning.

3.1.2 Surgical Procedure for Guide Cannula Placement

Following proper positioning of the animal on the stereotaxic apparatus, an anterior–posterior incision (2 cm long for rats, 1 cm long for mice) is made on the scalp from the back of the eyes to the lambda with a sterile scalpel. Sterilized hemostats are used to keep the incision open and to provide full exposure of the skull. The pericranial tissues on the skull surface are removed using cotton swabs. The guide cannula is mounted and positioned over the bregma. The anterior, posterior, and lateral coordinates are taken and then known coordinates can be used to determine the correct location for the probe with respect to the bregma [67]. For example, to place a probe into the nucleus accumbens of a rat, the stereotaxic coordinates are 10 mm anterior to interaural zero, 1.2 mm lateral to the midsagittal sinus, and 4 mm ventral to the level skull surface. The probe dialysis fiber extends another 4 mm ventral to reach the target site [68].

The guide cannula is positioned to the desired coordinate by adding to or subtracting from the bregma coordinates, then the cannula is brought down to the surface of the skull. This is the ventral coordinate where the drilling will take place. A pencil or equivalent marker is used to mark this precise position. Using a drill for rodent surgery (e.g., from Fine Science Tools, Inc.), a small hole is made through the skull, making sure that the hole is large enough for insertion of the cannula without the cannula touching the sides

of the hole. A sterile needle is used to gently break the meninges and allow for cannula insertion. Six other holes for skull screws are made using a hand drill: two anterior, two posterior, and two lateral to the cannula hole. After ensuring that the screws are sterilized, they are securely tightened onto the skull [67].

3.1.3 Stereotaxic Placement of Guide Cannula

To place the guide cannula, it is first sterilized and then mounted on a holder and placed to the ventral coordinate designated by the appropriate stereotaxic atlas for a specific brain region. Dopamine is a critical neurotransmitter in reward and aversive responses and stereotaxic experiments often target the regions of the brain innervated with dopamine terminals and/or cell bodies. The latter are to a very large extent concentrated in either the ventral tegmental area (VTA) or the substantia nigra pars compacta (SNpc). The dopaminergic projections originating in the SNpc primarily project to the dorsal striatum forming the nigrostriatal pathway. Mesolimbic/mesoaccumbens and mesocortical dopaminergic pathways are dopaminergic projections from the cell bodies in the VTA to the nucleus accumbens shell and core and the prefrontal cortex, respectively. In addition to the dopamine input from the VTA, the dopamine projections in the nucleus accumbens also receive glutamate input from the prefrontal cortex, amygdala, and hippocampus. Serotonin inputs from the dorsal raphe nucleus to the nucleus accumbens have also been identified, in addition to serotonin and GABA (medium spiny) interneurons. This wide variety of input to the dopaminergic projections in the nucleus accumbens makes this area of the brain central to the midbrain reward response [2, 69, 70]. In addition to the midbrain regions, the lateral habenula (LHb) may also be a target for stereotaxic implants to study reward- and aversion-related behaviors in rodents. It has been hypothesized that this region could mediate the negative motivational value signals to the dopamine and serotonin systems through mechanisms like suppression of motor behavior in the absence of reward or the presence of an adverse stimulus [2, 71, 72]. Table 1 lists the stereotaxic coordinates used for some of the more common brain sites used to assess reward and aversion in rodents.

3.1.4 Securing of the Guide Cannula and Anchor Screw

To secure the guide cannula and an anchor screw, which will help ensure that stress on the cannula by any swivel attached to the animal is reduced during any procedures that follow with awake animals, liquid dental cement is used to make a skull cap. To do this, the anchor screw is held with tweezers medially behind the posterior skull screws and with its flat head on the surface of the skull until the cement cures. Liquid dental cement is used to cover the entire exposed skull surface, including the guide cannula and the screws after the skull is dried and incised skin has been pushed on the side. Before cement cures completely, the skin is gently

Table 1
Common stereotaxic coordinates for distinct brain reward-associated sites

Brain site	Mouse coordinates	Rat coordinates	References
Nucleus accumbens	Shell AP = 1.35–1.5 ML = 1.44–2.5 DV = 4.0–4.2	Shell AP = 1.3–1.8 ML = 0.8–2.3 DV = 2.0–8.2	[73–82]
		Core AP = 1.3 ML = 1.3–1.8 DV = 2.0–6.2	[76–80, 83, 84]
	AP = 1.5–1.6 ML = 0.5–1.5 DV = 2.9–4.8	AP = 1.6–1.7 ML = 0.8–2.45 DV = 4.4–6.7	[85–91]
Ventral tegmental area	AP = −3.0 ML = +0.45 DV = −4.4	AP = 5.2–5.8 ML = 0.6–1.0 DV = 7.3–8.3	[80, 89, 92–94]
Substantia nigra pars compacta	AP = 1.0 ML = 2.5 DV = −3.0	AP = 4.2–5.2 ML = 1.9–2.5 DV = 7.0–7.6	[95–97]
Dorsomedial striatum		AP = +1.0 ML = +1.2	[98]
Dorsolateral striatum		AP = +1.0 ML = +2.4	[98]
Dorsal striatum	AP = +1.15 ML = +1.40 DV = −1.60		[90]
Ventral midbrain		AP = −5.5 ML = +3.2 DV = −6.5	[99]
Basolateral amygdala		AP = −3.2 ML = +4.9 DV = −8.5, −8.1	[100]
Central nucleus of amygdala	AP = +1.45 ML = +2.75 DV = −4.7		[101]
Dorsolateral septum	AP = +0.5 ML = +0.3 DV = −2.6		[102]
Ventral pallidum		AP = −0.12 ML = +2.4 DV = −8.2	[75]
Prefrontal cortex	AP = +1.8 ML = +0.75 DV = +2.7		[103]

(continued)

Table 1
(continued)

Brain site	Mouse coordinates	Rat coordinates	References
Caudate–putamen	AP = 0.0–1.5 ML = 0.5–2.2 DV = 2.5–3.3		[82, 85]
Laterodorsal tegmental nucleus		AP = 8.3–8.7 ML = 1.13 DV = 6.4–7.0	[104]
Dorsal raphe		AP = −7.8 ML = +0 DV = −7.0	[105]
Lateral hypothalamus		AP = −2.5 ML = +1.7 DV = −8.6	[105, 106]
Arcuate nucleus	AP = −1.7 ML = 0.3 DV = −5.6	AP = 2.8 ML = 0.4 DV = −9.5	[107, 108]
Medial forebrain bundle	AP = 1.0–1.2 ML = 1.0 DV = 5.0–5.2	AP = −3.8 ML = +1.7 DV = −8.6	[105, 109–112]
Lateral parabrachial subnucleus		AP = −0.16 ML = +2.5 DV = +3.0	[113]

separated from the cement cap. It is essential to then smooth the cement cap with a spatula into an elliptical shape with no rough edges to avoid irritation of the animal's skin. After the cement dries completely, the hemostats are removed and an antibiotic ointment (typically bacitracin) is applied around the cement cap. The animal is removed from the stereotaxic frame and monitored until it regains consciousness. An injection of 1 mL saline subcutaneous before the animal is placed to its cage helps prevent dehydration while systemic injection of antibiotics and daily monitoring in the week after surgery are essential to address any wound infections [67].

3.1.5 Confirmation of Probe Placement

Upon completion of the experiment, placement of the probe in the target site must be verified. This is particularly important if the strain, age, or gender used are different than the ones that the stereotaxic brain atlases were derived from. For example, the atlas most commonly used for stereotaxic coordinates in the rat uses the brain of an adult male Wistar rat [114]. While this brain is overall similar to the brains of rats of different strains, there may be deviations in the distances between skull markings. Additionally, the

skulls of female or juvenile rats are in slightly different positions than the model rat used for the atlas [114, 115]. Therefore, verification of placement following the procedure is important. Following completion of all studies, the animal is deeply anesthetized and then perfused with saline and paraformaldehyde through the heart. The brain is extracted following careful removal of the skull cap with any cannulas, injectors, and probes. A cut is made at the location of the hole where the probe entered the brain and the location of the probe is identified by histological examination of the probe tract. Only results from animals whose probe tract was correctly placed should be included in the data analysis.

In some cases, probe placement may be tested during the implantation surgery. For example, when placing a bipolar stimulation electrode in the VTA, brief stimulation bursts can be administered to ensure that the electrode was placed in a location that evokes whisker movement [116].

3.2 Sample Analysis

The greatest advantage of the stereotaxic placement of devices like microdialysis probes is the combined precision of anatomical selectivity with sampling from a specific brain region and high chemical resolution, with samples being analyzed for a range of neurotransmitters and metabolites, particularly monoamine neurotransmitters which are all oxidizable molecules that can be detected electrochemically. Depending on the type of experiment carried out, sample analysis will vary following stereotaxic implantation. For example, if the study involves assessing changes in neurochemical levels in microdialysates, samples may be analyzed via high-performance liquid chromatography (HPLC) [117, 118]. A variation on this approach involves quantitative no net flux microdialysis whereby changes in neurotransmitter uptake and basal neurotransmitter dynamics can be assessed with precision along with steady-state concentrations of brain glucose, effects of reverse-infused drugs, or screening of blood–brain barrier penetration of compounds in the brain and other tissues [187–191].

In a study where the microdialysis probe or other device has delivered a fluorescent viral construct in the brain, sample analysis may involve imaging of a brain slice at the end of the experiment or another method of fluorescence detection in vivo (e.g., [119]).

3.2.1 HPLC Analysis of Neurotransmitters and Metabolites

Microdialysis samples usually contain dopamine and other neurotransmitters in the picogram range. In order to assess dopamine levels at a concentration this low, HPLC coupled with electrochemical detection is typically used. To measure dopamine using HPLC-EC, volumes ranging from 5 to 25 μL from the microdialysate are injected into an appropriate HPLC-EC system (i.e., with an amperometric or coulometric detector). The HPLC instrument typically incorporates a liquid chromatography column with a specific packing material (silica, polymer, cellulose, or others) and separation

mode (i.e., reverse phase, normal phase, ion exchange, etc.) to isolate chemicals to be detected, mobile phase containing a phosphate buffer or equivalent, an average flow rate of 1.0 mL/min and setting of the oxidation potential around 400 mV or higher for catecholamines. Such conditions allow for the successful separation of dopamine and the dopamine metabolites, dihydroxyphenylacetic acid (DOPAC), and homovanillic acid (HVA), which were quantified based on their peak amplitudes relative to a standard [117, 118], while with minor modifications of the mobile phase, separation of neurotransmitters like norepinephrine and serotonin is also feasible.

3.2.2 Fluorescent Visualization

In experiments where gene expression is altered, the impacted brain region can be verified through fluorescence microscopy. The brains are sliced coronally at the injection site and visualization of the proteins can be done using a TSC SPE confocal microscope (or equivalent). The detected signal can be of either GFP or similar fluorescent protein that is introduced as part of a viral construct or a fluorescent antibody, like Alexa-546-conjugated mouse antibody [120].

4 Applications using Stereotaxic Implants

The ability to implant a probe, electrode, or other device into specific brain regions allows for the successful completion of a wide variety of experimental procedures. These experiments are summarized in Table 2 and range from measuring brain neurotransmitter responses to injection of drugs or food intake, self-administration of drugs of misuse and instrumental learning responses or validation of viral construct delivery, optogenetics, fiber photometry, and real-time neurotransmitter exocytosis through amperometry or fast-scan cyclic voltammetry. The rest of this chapter discusses these approaches and how stereotaxic probes or cannulas were used to show specific brain responses to reward or aversion.

4.1 Response to Drugs and Food

One application where stereotaxic surgery has been extensively utilized to assess the reward response to food and drugs in reward coding sites like the nucleus accumbens is in vivo brain microdialysis. In one example, guide cannulas for microdialysis probes were implanted in the nucleus accumbens of Sprague–Dawley rats that had been fed either a normal diet or a cafeteria-style diet, which induced obesity in these rats as described above. During week 14 of the study (after the animals had sufficient time to recover from the surgery), animals were placed individually in microdialysis cages and microdialysis probes were inserted into the guide cannula and

Table 2
Applications using stereotaxic surgical procedures

Experimental technique using stereotaxic implantation	Application(s)	Example reference(s)
Microdialysis	Evaluate responses to drugs and food	[117, 118, 121–126]
Reverse/no net flux microdialysis	Evaluate responses to drugs and food	[127–132]
Direct dosing of drugs to brain regions	Understand drug self-administration and reward-related behaviors	[133]
Detection of neuronal activity	Understand drug self-administration and reward-related behaviors	[134]
Electrical self-stimulation	Mapping of reward pathways Misuse potential of drugs Adaptation of reward pathways	[105, 106, 109–113, 135–147]
Viral construct delivery	Genetic manipulation of specific neurons	[73–75, 85–89, 92, 102, 103, 148, 149]
Optogenetic activation of ion channels	Evaluation of tonic neuronal signaling Mapping of reward pathways Investigation of molecular mechanisms associated with reward responses	[93, 150–162]
Fiber photometry	Measure transient calcium signaling to measure neuronal activity	[163–168]
Fast scan cyclic voltammetry and amperometry	Detect phasic dopamine signaling	[76–78, 81, 83, 84, 94, 169–175]

perfused with Ringer's solution. After allowing about 12 h for the system to equilibrate, samples were collected for 30 min at a time. Baseline samples were collected for at least 2 h and then the animals were challenged with either a meal or a systemic amphetamine injection. Interestingly, in this experiment, there were significant increases in dopamine levels following the food and drug challenges in the rats that had been fed a normal chow diet, but only a more highly palatable cafeteria diet induced a response in obese animals, indicating that dopamine at least in part responds to the relative palatability of the rewarding stimuli [117, 118]. Several other studies that have used microdialysis to observe reward responses to food or drug administration have also shown an increase in levels of extracellular dopamine in the nucleus accumbens following consummatory reward. These types of studies have also shown that treatment with drugs, like the aldehyde dehydrogenase 2 inhibitor, GS 455534, may be a good candidate for treatment of the reward-related binge eating disorder as it modifies the amount of dopamine released in a rat that was trained to binge on sugar [121–126].

Reverse microdialysis can also be used to determine changes in responses to food or drugs. In these studies, a dialysate-like

Ringer's solution is used to establish a stable baseline reading for the molecule of interest. In studies of reward, basal extracellular dopamine levels are routinely measured. Following establishment of the baseline, a drug can be infused through the probe and changes in dopamine levels can be measured as a percentage of the baseline. In a study that investigated the effect of the adenosine analog, COA-Cl (6-amino-2-chloro-9-[trans-trans-2,3- bis (hydroxymethyl)cyclobutyl]purine) on dopamine release in the dorsal striatum, use of reverse microdialysis showed a dose-dependent increase in dopamine in the striatum, indicating a direct effect of the drug on activation of the dopamine-releasing striatal neurons [127].

4.2 Drug Self-Administration and Electrical Self-Stimulation

Microdialysis following stereotaxic implantation of guide cannulas to the midbrain dopamine cell body or terminal regions is useful not only in assessing the response of the reward systems to food or drug administration but also in assessing the neurobiological changes in these brain regions following self-administration of drugs, particularly drugs of misuse. In some cases, the drugs themselves are directly administered to the brain region of interest as was the case in a study that looked at the effects of neuropeptide Y receptor activity on ethanol self-administration. Rats were trained to administer ethanol directly into the VTA for 4 days. On days 5 and 6, neuropeptide Y signaling was blocked and a corresponding decrease in lever pressing for ethanol occurred, indicating that neuropeptide Y plays a role in reward responses to ethanol [133]. In other studies, rats are trained to self-administer psychostimulants or opioids and changes to the neural activity of the reward system can be assessed using implanted probes. One such study showed that up to 1 month following cocaine self-administration, the rats exposed to cocaine had reduced reward-related neuronal firing during delays for reward than the control animals [134]. A recent elegant study that modified the pharmacokinetics of cocaine used a stereotaxic injection of adenoviral cocaine hydrolase to increase cocaine metabolism. This accelerated hydrolysis of cocaine resulted in a reduction in cocaine infusions by the exposed animals [176].

In addition to using substances to activate the reward pathways in the brain, the reward pathways can be activated using electrical stimulation of specific brain regions. In these experiments, animals are trained to lever press to receive an electrical stimulation from an electrode stereotaxically placed in the brain, to specifically activate the neurons or fibers of passage in that brain region. In this way, early work demonstrated the importance of dopamine pathways in reward behaviors and the differing roles of the lateral hypothalamus and nucleus accumbens in behaviors associated with reward [135, 136]. Another similar study used response to electrical self-stimulation in the medial forebrain bundle to demonstrate the

heterogeneity of neuronal response to rewarding stimuli [137]. Electrical self-stimulation is also a tool researchers use to determine the misuse potential of new stimulants, efficacy of drugs to alter the reward pathways, adaptation of the pathways with changing stimuli, and the molecular mechanisms that are altered through learning of this behavior [106, 109–111, 138–144]. Electrical self-stimulation alone or in combination with optogenetic techniques, which we will discuss in more detail later, can also be used to refine our understanding of the complex pathways related to reward and feeding in the midbrain regions [105, 112, 113, 145–147].

4.3 Delivery of Viral Constructs to Alter Gene Expression

With the advent of genetic manipulation techniques, one can now transfect specific subpopulations of neurons with viral constructs by delivering them through stereotaxically placed guide cannulas. In one such experiment, this technique has allowed investigators to determine the specific effects of cocaine on dopamine clearance through the dopamine transporter (DAT) in the various brain regions associated with reward. In one experiment, DAT was reintroduced to specific brain regions using viral constructs in mice lacking DAT globally to assess its function when active in those specific regions [85]. Epigenetic changes in the reward regions of the brain have also been assessed by delivering viral constructs that target histone acetylation and demethylation processes via zinc finger proteins. In one case, acetylation resulted in transcriptional activation of the CDK5 locus, which increased reward-related behaviors like cocaine-induced locomotor behavior. Demethylation, on the other hand, resulted in attenuated reward-related behaviors [86]. Other studies have altered the expression of numerous other genes coding for proteins and peptides that have been known to influence reward and aversive behaviors to assess their specific roles in these behaviors [73, 74, 87, 88, 92, 102, 103, 148]. Viral constructs can also be used in studies involving Designer Receptors Exclusively Activated by Designer Drugs (DREADDs). They have demonstrated the specific roles of various parts of the nucleus accumbens in reward-related behaviors, including the effect of anorexia nervosa on these pathways [75, 89, 149]. Viral constructs are also used in optogenetic studies and photo fluorometry experiments that are discussed in more detail later in this chapter.

4.4 Use of Optogenetics to Evaluate Reward

In optogenetic studies of reward and avoidance, neurons are modified to express ion channels that are sensitive to light, usually channelrhodopsin-2 (ChR2). Light is then used to control the cells so that the neurons may be modulated in awake and freely moving animals. These approaches can be employed for gain or loss-of-function studies in very specific cell populations in the brain [150–152]. The use of this cutting-edge technology has provided

new insight into the complex neural pathways that are involved in reward and avoidance behaviors. In one experiment to evaluate the effect of tonic dopamine on reward-related behaviors, ChR2 was preferentially expressed on tyrosine hydroxylase (TH+) neurons, which are specifically dopamine-expressing neurons that project from the VTA. The expression of ChR2 was accomplished using a series of viral constructs including one that expresses Cre in TH+ cells and a second one containing the ChR2 gene that would only be expressed in Cre-containing cells. These viral constructs were then injected into an optic fluid cannula that had been inserted into the VTA using stereotaxic surgery. Four weeks after viral transfection, ChR2 levels were sufficient for stimulation of dopamine release. The optical laser was inserted into the cannula and set to 473 nm. The VTA or nucleus accumbens were then exposed to 3000 light pulses over 10 min. To determine the effect on reward-related behaviors, the number of sucrose licking bouts was measured throughout the duration of the stimulation and for an additional 20 min. Data from both the nucleus accumbens and the VTA showed that increased tonic dopamine resulted in reduced licking bouts for sucrose, indicating that higher tonic dopamine codes for reward and results in less reward-consuming behavior. Such tools allow to elegantly increase tonic dopamine signaling in a controlled manner in a freely moving animal and monitor the associated reward-related responses [93]. Other studies using optogenetics have shown better resolution of known pathways associated with reward responses, better resolution of behavioral responses to reward, and even new molecular mechanisms associated with reward response [153–155]. This technique has also been utilized to better understand the role of GABAergic and glutamatergic inputs into the VTA from various brain regions and their influence on both reward and avoidance behaviors [156–162]. Finally, optogenetics has proven especially useful because it allows us to selectively activate pathways without electrical stimulation that can cause interference with neuronal depolarization events [158]. It should be mentioned though that optogenetics has so far been optimized for acute manipulations of dopamine neuronal activation and it is not currently used as extensively for selective inhibition of dopamine neurons or for chronic changes in basal dopamine release. For such purposes, reverse microdialysis of pharmacological agents locally in the brain or studies correlating systemic or local drug injections, dopamine neurochemistry, and behavior on a long-term basis still constitute a more advantageous approach.

4.5 Fiber Photometry Calcium Imaging

Calcium is a key transient molecule in active neurons that initiates neurotransmitter exocytosis once it enters terminals through voltage-dependent calcium channels. Therefore, tracking calcium levels throughout a task in real time is advantageous for

understanding the complex neural networks that make up the reward response. Fiber photometry calcium imaging allows researchers to introduce a genetically modified calcium signaling molecule that they can visualize in specific neuronal populations as those neurons are activated. In a recent study using this technique, de Jong et al. were able to show that neurons in different areas of the nucleus accumbens respond differently to aversive and rewarding stimuli [163]. This technique has proven extremely valuable in studies trying to understand the neural networks involved in aversive and fear responses in a number of regions of the brain including the lateral habenula, the dorsal raphe nucleus, and the VTA [164–166]. Fiber photometry has also allowed researchers to differentiate the roles of specific neuron types that might be in the same brain regions. For example, several studies have looked at the different roles of serotonin and dopamine neurons in Pavlovian conditioning and stress responses as well as in response to drugs of misuse [167, 168]. The resolution of time, location, and neuronal type using this technique has provided valuable insight into specific roles of different dopamine receptors in stress-induced susceptibility to depression, the role of dopamine signaling in fear extinction, the mechanisms of coding responses to novelty as well as reward prediction in areas like the dorsal striatum, and the modulatory roles of neuropeptides in reward and aversive responses [177–181].

4.6 Rapid Electrochemical Detection Tools

Methods used to measure released amines as part of neuronal exocytosis were originally optimized for single cells that feature or model the secretory apparatus of neurons including adrenal chromaffin cells and pheochromocytoma 12 cells [182]. They also became available for recording from primary dissociated midbrain dopamine neurons [118].

Fast-scan cyclic voltammetry (FSCV) enables the in vivo or ex vivo measurement of extracellular fluctuations in multiple electrochemical species, primarily neurotransmitters. The technique can sample millisecond (phasic) concentration changes of the neurotransmitter dopamine in awake and behaving rodents. Resolving the real-time dopamine signal requires simultaneous understanding of the synchronized activity of dopamine cell subpopulations and identification of the downstream functional effect of dopamine release, often necessitating the combined use of computational modeling and FSCV [76]. Phasic dopamine signaling is implicated in reinforcement, goal-directed behavior, and locomotion, and FSCV has been used to investigate how rapid changes in striatal dopamine concentration contribute to this repertoire of reward-related behaviors [77]. Carbon fiber amperometry can be used in brain slices or in vivo similarly to FSCV but with even faster time resolution for dopamine release in response to a stimulus. Both FSCV and amperometry remain on the cutting edge of real-time electrochemical detection with the advent of different types of glass

or fused silica microelectrodes that can be stereotaxically implanted [169] although their use has been reported for some time now by select groups [28, 117, 183–185].

Interestingly, measurements of dopamine release in different terminal regions using FSCV can be coupled with optogenetic stimulation of the cell bodies in the VTA [94]. Differences in dopamine release versus reuptake in distinct terminal fields may be implicated in region-specific responses to drugs of misuse and contrasting roles in mediating reward-related behavior. Other versions of this technique feature wireless FSCV for monitoring the dopamine signal in the ventral striatum with an electrical stimulator that induces biphasic current to excite dopaminergic neurons in awake freely moving rats [170]. The FSCV unit and the electrical stimulator are isolated with the latter being controlled by an infrared controller to reduce artifacts. Deep brain stimulation (DBS) can also be combined with FSCV in freely moving rodents [171]. Animals can be implanted with a stimulating electrode in the MFB to target fibers of passage from the VTA and an FSCV microelectrode in terminal regions to detect dopamine during the onset of stimulation.

A further advantage of rapid electrochemical detection approaches lies in the comparison of dopamine release dynamics in precisely defined subregions of reward-related pathways to cues exclusively signaling the availability of different reward magnitudes [78]. For example, one could assess how phasic dopamine release correlates with the price to obtain a given reward and how can signals like dopamine change the magnitude of the behavioral response to the price of reward. In one example, it was determined that the concentration of accumbens dopamine as measured by FSCV was time-matched to a range of prices for animals to obtain sucrose presentation and decreased with price [83].

In terms of behavioral economics, debate is ongoing as to whether learning or incentive salience is signaled by dopamine transients identified through rapid electrochemical detection techniques and thus altered in (e.g.) substance use disorders. Drugs of misuse can result in pathological overlearning of drug-predictive cues, while at the same time can also attribute incentive salience to drug-predictive cues. Different doses of d-amphetamine, even therapeutic ones such as those used to treat attention-deficit hyperactivity disorder, cocaine, or distinct food rewards may enhance the ventral striatal dopamine transients that are critical for reward-related learning and amplify Pavlovian type of conditioning [186–188]. Furthermore, mesolimbic dopamine is phasically released during appetitive behaviors, though there is substantive disagreement about the specific purpose of these dopamine signals. Prediction error models suggest a role of learning, while incentive salience models argue that the dopamine signal attributes reward value to specific stimuli and thereby induces motivated behavior [79, 189].

FSCV has been routinely employed to determine how changes in the operant requirement affect dopamine release coupled to self-administration of different types of reward [172]. It remains fundamental for our understanding of the neurobiology of reward, particularly in the effort to establish whether phasic dopamine changes are linked to drug-motivated behaviors. During alcohol-seeking behavior dependent on a variable-interval schedule of reinforcement, robust phasic dopamine release in the dorsolateral striatum but inconsistent dopamine release in the dorsomedial striatum was reported after reinforced lever presses, thus providing proof of principle that tools like FSCV, when combined with stereotaxic implantation of microelectrodes can yield not only excellent time resolution but also outstanding anatomical resolution [186]. Such advantages can be further amplified at the level of chemical resolution and drug–neurotransmitter interactions through the use of FSCV to explore, for instance, peptide receptor (e.g., GLP-1R) modulation of dynamic dopamine release in distinct brain subregions during administration of drugs or natural rewards [80]. Similarly, selective serotonin receptor ligand effects on dopamine phasic signaling have proved insightful on the role of serotonin in motivated behaviors [90] while blockade of ventral midbrain *N*-methyl-D-aspartate (NMDA) receptors potentiates brain stimulation reward, likely through a reduction in inhibitory drive of dopamine neurons under the control of glutamate [99]. However, disruption of accumbens muscarinic acetylcholine receptor activity blunts, whereas blockade of nicotinic receptors amplifies cue-induced invigoration of reward seeking as determined by the combined use of FSCV with local pharmacological manipulation of acetylcholine receptors [84]. Notably, utilizing intracranial self-stimulation and FSCV, it was concluded that cocaine-induced increases in brain stimulation reward and evoked dopamine release in the accumbens core were potentiated when cocaine was administered in less than 1 h after a kappa opioid receptor agonists, but attenuated when administered 24 h after such drugs [173].

FSCV can also provide new insights on the mechanism of action of drugs of misuse. Amphetamine (AMPH) is historically assumed by some investigators to increase dopamine by an action potential-independent, non-exocytotic type of release called "efflux", involving reversal of dopamine transporter function and driven by vesicular dopamine depletion. Growing evidence suggests that AMPH also acts by an action potential-dependent mechanism. FSCV has been used to consider the action potential dependence of AMPH-induced elevations in central dopamine. AMPH increased the frequency, amplitude, and duration of transients, in addition to dopamine elevations of slower kinetics [81]. Eugeroic drugs like modafinil have also exhibited unexpected effects on phasic dopamine signaling in the striatum in addition to their role in dopamine clearance through the DAT transporter [174]. One should be

advised however to approach FSCV findings with anesthetized animals (typically under isoflurane or urethane) with caution as anesthetics may impact on brain reward systems.

Finally, technology is rapidly evolving toward the use of sensors that can detect non-oxidizable neurotransmitter signals in vivo so that substantially more insights can be gained on the function of non-monoamine neurotransmitters in central reward processing. Examples of such tools include genetically encoded fluorescent reporters for gamma-aminobutyric acid (GABA), glutamate [190, 191], and are mostly optimized at the level of single cells, brain slices and fluorescent, confocal, and 2-photon microscopy for now. Stereotaxically implanted carbon fiber nanocomposite sensors and ceramic-based microbiosensor arrays have reached the milestone of allowing ascorbate and glutamate measurements in the brain of anesthetized rats with very high spatial, temporal, and chemical resolution [175]. It remains to be decided how stereotaxic implantation of devices versus imaging tools will comparatively contribute to the field of the neurobiology of reward in the near future. However, one can readily notice the advantages of the complementarity of such approaches and the tested experimental hypotheses as determinants of the tools adopted.

5 Conclusions

Stereotaxic implantation of devices like probes, electrodes, injection cannulas, and other types of sensors to the reward centers of the rodent brain can provide insightful information related to the neurobiology of reward- and aversion-related behaviors. Experiments using microdialysis or real-time electrochemical detection of phasic neurotransmitter release, particularly those in the freely moving animal, contribute to the understanding of the association between pharmacology, neurotransmitter release, and behavior and can provide precise assessment of dopamine release versus clearance in the living brain. Cutting-edge experiments involving genetic manipulations of various genes specifically in the nucleus accumbens and other reward regions of the brain, combined with measurements of neurotransmitter exocytosis in real time through carbon fiber electrodes have elucidated the specific role of these proteins in mediating reward- or aversion-related behaviors. With this knowledge, we will be able to more effectively understand and subsequently treat disorders related to aberrations in reward systems like obesity, diabetes, eating disorders, substance use disorders, mood/psychotic disorders, and Parkinson's disease.

Acknowledgments

The original research work of the authors cited in this chapter was funded by NIH/NIDA (F31 DA023760; BMG), NIH/NIDDK (R01 DK065872 and ARRA 3R01DK065872-04S1; ENP) as well as an Award of Excellence in Biomedical Research by the Smith Family Foundation (ENP). Fondly dedicated to late Prof. Bartley G. Hoebel who extensively contributed to our understanding of the neurobiology of reward.

References

1. Schultz W (2010) Dopamine signals for reward value and risk: basic and recent data. Behav Brain Funct 6:24. https://doi.org/10.1186/1744-9081-6-24
2. Hu H (2016) Reward and Aversion. Annu Rev Neurosci 39:297–324. https://doi.org/10.1146/annurev-neuro-070815-014106
3. Berridge KC, Kringelbach ML (2015) Pleasure systems in the brain. Neuron 86 (3):646–664. https://doi.org/10.1016/j.neuron.2015.02.018
4. Berridge KC, Robinson TE (2003) Parsing reward. Trends Neurosci 26(9):507–513. https://doi.org/10.1016/S0166-2236(03)00233-9
5. Hernandez L, Hoebel BG (1990) Feeding can enhance dopamine turnover in the prefrontal cortex. Brain Res Bull 25(6):975–979
6. Hernandez L, Hoebel BG (1988) Food reward and cocaine increase extracellular dopamine in the nucleus accumbens as measured by microdialysis. Life Sci 42 (18):1705–1712
7. Yoshida M et al (1992) Eating and drinking cause increased dopamine release in the nucleus accumbens and ventral tegmental area in the rat: measurement by in vivo microdialysis. Neurosci Lett 139(1):73–76
8. Mark GP et al (1992) Effects of feeding and drinking on acetylcholine release in the nucleus accumbens, striatum, and hippocampus of freely behaving rats. J Neurochem 58 (6):2269–2274
9. Salamone JD et al (1991) Haloperidol and nucleus accumbens dopamine depletion suppress lever pressing for food but increase free food consumption in a novel food choice procedure. Psychopharmacology 104 (4):515–521
10. Bradberry CW et al (1991) Individual differences in behavioral measures: correlations with nucleus accumbens dopamine measured by microdialysis. Pharmacol Biochem Behav 39(4):877–882
11. Mogenson GJ, Wu M (1982) Neuropharmacological and electrophysiological evidence implicating the mesolimbic dopamine system in feeding responses elicited by electrical stimulation of the medial forebrain bundle. Brain Res 253(1–2):243–251
12. Bromberg-Martin ES, Matsumoto M, Hikosaka O (2010) Dopamine in motivational control: rewarding, aversive, and alerting. Neuron 68(5):815–834. https://doi.org/10.1016/j.neuron.2010.11.022
13. Matsumoto M, Hikosaka O (2009) Two types of dopamine neuron distinctly convey positive and negative motivational signals. Nature 459(7248):837–841. https://doi.org/10.1038/nature08028
14. Eshel N et al (2015) Arithmetic and local circuitry underlying dopamine prediction errors. Nature 525(7568):243–246. https://doi.org/10.1038/nature14855
15. Cohen JY et al (2012) Neuron-type-specific signals for reward and punishment in the ventral tegmental area. Nature 482 (7383):85–88. https://doi.org/10.1038/nature10754
16. Umberg EN, Pothos EN (2011) Neurobiology of aversive states. Physiol Behav 104 (1):69–75. https://doi.org/10.1016/j.physbeh.2011.04.045
17. Pothos E et al (1991) Dopamine microdialysis in the nucleus accumbens during acute and chronic morphine, naloxone-precipitated withdrawal and clonidine treatment. Brain Res 566(1–2):348–350. https://doi.org/10.1016/0006-8993(91)91724-f
18. Wise RA, Rompre PP (1989) Brain dopamine and reward. Annu Rev Psychol 40:191–225. https://doi.org/10.1146/annurev.ps.40.020189.001203

19. Kelley AE, Baldo BA, Pratt WE (2005) A proposed hypothalamic-thalamic-striatal axis for the integration of energy balance, arousal, and food reward. J Comp Neurol 493 (1):72–85. https://doi.org/10.1002/cne.20769
20. Wassum KM et al (2009) Distinct opioid circuits determine the palatability and the desirability of rewarding events. Proc Natl Acad Sci U S A 106(30):12512–12517. https://doi.org/10.1073/pnas.0905874106
21. Will MJ, Franzblau EB, Kelley AE (2004) The amygdala is critical for opioid-mediated binge eating of fat. Neuroreport 15 (12):1857–1860
22. Zhang M, Gosnell BA, Kelley AE (1998) Intake of high-fat food is selectively enhanced by mu opioid receptor stimulation within the nucleus accumbens. J Pharmacol Exp Ther 285(2):908–914
23. Kelley AE et al (2003) Restricted daily consumption of a highly palatable food (chocolate Ensure(R)) alters striatal enkephalin gene expression. Eur J Neurosci 18(9):2592–2598
24. Smith SL, Harrold JA, Williams G (2002) Diet-induced obesity increases mu opioid receptor binding in specific regions of the rat brain. Brain Res 953(1–2):215–222
25. Qi J et al (2014) A glutamatergic reward input from the dorsal raphe to ventral tegmental area dopamine neurons. Nat Commun 5:5390. https://doi.org/10.1038/ncomms6390
26. Schultz W, Apicella P, Ljungberg T (1993) Responses of monkey dopamine neurons to reward and conditioned stimuli during successive steps of learning a delayed response task. J Neurosci 13(3):900–913
27. Luo M, Zhou J, Liu Z (2015) Reward processing by the dorsal raphe nucleus: 5-HT and beyond. Learn Mem 22(9):452–460. https://doi.org/10.1101/lm.037317.114
28. Coenen VA et al (2019) Frontal white matter architecture predicts efficacy of deep brain stimulation in major depression. Transl Psychiatry 9(1):197. https://doi.org/10.1038/s41398-019-0540-4
29. Mirzadeh Z et al (2016) Parkinson's disease outcomes after intraoperative CT-guided "asleep" deep brain stimulation in the globus pallidus internus. J Neurosurg 124 (4):902–907. https://doi.org/10.3171/2015.4.JNS1550
30. Shaffie A et al (2018) A generalized deep learning-based diagnostic system for early diagnosis of various types of pulmonary nodules. Technol Cancer Res Treat 17:1533033818798800. https://doi.org/10.1177/1533033818798800
31. Barbosa ACB et al (2012) Rapid method for acute intracerebroventricular injection in adult zebrafish. In: Kaleuff A, Stewart A (eds) Zebrafish protocols for neurobehavioral research. neuromethods, vol 66. Humana Press, c/o Springer Science+Business Media, New York
32. Maximino C, Herculano AM (2010) A review of monoaminergic neuropsychopharmacology in zebrafish. Zebrafish 7(4):359–378. https://doi.org/10.1089/zeb.2010.0669
33. Li P et al (2007) Cloning and spatial and temporal expression of the zebrafish dopamine D1 receptor. Dev Dyn 236 (5):1339–1346. https://doi.org/10.1002/dvdy.21130
34. Boehmler W et al (2007) D4 Dopamine receptor genes of zebrafish and effects of the antipsychotic clozapine on larval swimming behaviour. Genes Brain Behav 6 (2):155–166. https://doi.org/10.1111/j.1601-183X.2006.00243.x
35. Boehmler W et al (2004) Evolution and expression of D2 and D3 dopamine receptor genes in zebrafish. Dev Dyn 230(3):481–493. https://doi.org/10.1002/dvdy.20075
36. Yamamoto K, Vernier P (2011) The evolution of dopamine systems in chordates. Front Neuroanat 5:21. https://doi.org/10.3389/fnana.2011.00021
37. Tay TL et al (2011) Comprehensive catecholaminergic projectome analysis reveals single-neuron integration of zebrafish ascending and descending dopaminergic systems. Nat Commun 2:171. https://doi.org/10.1038/ncomms1171
38. Powers CM et al (2011) Silver exposure in developing zebrafish produces persistent synaptic and behavioral changes. Neurotoxicol Teratol 33(2):329–332. https://doi.org/10.1016/j.ntt.2010.10.006
39. Chatterjee D, Gerlai R (2009) High precision liquid chromatography analysis of dopaminergic and serotoninergic responses to acute alcohol exposure in zebrafish. Behav Brain Res 200(1):208–213. https://doi.org/10.1016/j.bbr.2009.01.016
40. Anichtchik OV et al (2004) Neurochemical and behavioural changes in zebrafish Danio rerio after systemic administration of 6-hydroxydopamine and 1-methyl-4-phenyl-1,2,3,6-tetrahydropyridine. J Neurochem 88 (2):443–453. https://doi.org/10.1111/j.1471-4159.2004.02190.x

41. Scerbina T, Chatterjee D, Gerlai R (2012) Dopamine receptor antagonism disrupts social preference in zebrafish: a strain comparison study. Amino Acids 43(5):2059–2072. https://doi.org/10.1007/s00726-012-1284-0
42. Gomez-Laplaza LM, Gerlai R (2010) Latent learning in zebrafish (Danio rerio). Behav Brain Res 208(2):509–515. https://doi.org/10.1016/j.bbr.2009.12.031
43. Gerlai R (2011) Associative learning in zebrafish (Danio rerio). Methods Cell Biol 101:249–270. https://doi.org/10.1016/B978-0-12-387036-0.00012-8
44. Colwill RM et al (2005) Visual discrimination learning in zebrafish (Danio rerio). Behav Process 70(1):19–31. https://doi.org/10.1016/j.beproc.2005.03.001
45. Pather S, Gerlai R (2009) Shuttle box learning in zebrafish (Danio rerio). Behav Brain Res 196(2):323–327. https://doi.org/10.1016/j.bbr.2008.09.013
46. Zala SM, Maattanen I (2013) Social learning of an associative foraging task in zebrafish. Naturwissenschaften 100(5):469–472. https://doi.org/10.1007/s00114-013-1017-6
47. Aoki R, Tsuboi T, Okamoto H (2015) Y-maze avoidance: an automated and rapid associative learning paradigm in zebrafish. Neurosci Res 91:69–72. https://doi.org/10.1016/j.neures.2014.10.012
48. Luchiari AC, Salajan DC, Gerlai R (2015) Acute and chronic alcohol administration: effects on performance of zebrafish in a latent learning task. Behav Brain Res 282:76–83. https://doi.org/10.1016/j.bbr.2014.12.013
49. Fernandes Y et al (2014) Embryonic alcohol exposure impairs associative learning performance in adult zebrafish. Behav Brain Res 265:181–187. https://doi.org/10.1016/j.bbr.2014.02.035
50. Sison M, Gerlai R (2010) Associative learning in zebrafish (Danio rerio) in the plus maze. Behav Brain Res 207(1):99–104. https://doi.org/10.1016/j.bbr.2009.09.043
51. Grossman L et al (2011) Effects of piracetam on behavior and memory in adult zebrafish. Brain Res Bull 85(1–2):58–63. https://doi.org/10.1016/j.brainresbull.2011.02.008
52. Ghosh DD et al (2016) Neural architecture of hunger-dependent multisensory decision making in C. elegans. Neuron 92(5):1049–1062. https://doi.org/10.1016/j.neuron.2016.10.030
53. Ezcurra M et al (2016) Neuropeptidergic signaling and active feeding state inhibit nociception in Caenorhabditis elegans. J Neurosci 36(11):3157–3169. https://doi.org/10.1523/JNEUROSCI.1128-15.2016
54. Bendesky A et al (2011) Catecholamine receptor polymorphisms affect decision-making in C. elegans. Nature 472(7343):313–318. https://doi.org/10.1038/nature09821
55. Stauffer WR et al (2016) Dopamine neuron-specific optogenetic stimulation in rhesus macaques. Cell 166(6):1564–1571. e1566. https://doi.org/10.1016/j.cell.2016.08.024
56. Baez-Mendoza R, van Coeverden CR, Schultz W (2016) A neuronal reward inequity signal in primate striatum. J Neurophysiol 115(1):68–79. https://doi.org/10.1152/jn.00321.2015
57. Freeman SM, Rebout N, Bales KL (2018) Effect of reward type on object discrimination learning in socially monogamous coppery titi monkeys (Callicebus cupreus). Am J Primatol 80(6):e22868. https://doi.org/10.1002/ajp.22868
58. Chang SW et al (2015) Neural mechanisms of social decision-making in the primate amygdala. Proc Natl Acad Sci U S A 112(52):16012–16017. https://doi.org/10.1073/pnas.1514761112
59. Toda K et al (2012) Differential encoding of factors influencing predicted reward value in monkey rostral anterior cingulate cortex. PLoS One 7(1):e30190. https://doi.org/10.1371/journal.pone.0030190
60. Murray EA, Rudebeck PH (2018) Specializations for reward-guided decision-making in the primate ventral prefrontal cortex. Nat Rev Neurosci 19(7):404–417. https://doi.org/10.1038/s41583-018-0013-4
61. Opris I, Hampson RE, Deadwyler SA (2009) The encoding of cocaine vs. natural rewards in the striatum of nonhuman primates: categories with different activations. Neuroscience 163(1):40–54. https://doi.org/10.1016/j.neuroscience.2009.06.002
62. Nakamura K et al (2012) Differential reward coding in the subdivisions of the primate caudate during an oculomotor task. J Neurosci 32(45):15963–15982. https://doi.org/10.1523/JNEUROSCI.1518-12.2012
63. Hampson RE et al (2011) Effects of cocaine rewards on neural representations of cognitive demand in nonhuman primates. Psychopharmacology 213(1):105–118. https://doi.org/10.1007/s00213-010-2017-2

64. Arsenault JT et al (2013) Dopaminergic reward signals selectively decrease fMRI activity in primate visual cortex. Neuron 77 (6):1174–1186. https://doi.org/10.1016/j.neuron.2013.01.008
65. Walantus W, Elias L, Kriegstein A (2007) In utero intraventricular injection and electroporation of E16 rat embryos. J Vis Exp 6:236. https://doi.org/10.3791/236
66. Szot GL, Koudria P, Bluestone JA (2007) Transplantation of pancreatic islets into the kidney capsule of diabetic mice. J Vis Exp 9:404. https://doi.org/10.3791/404
67. Geiger BM et al (2008) Survivable stereotaxic surgery in rodents. J Vis Exp 20:880. https://doi.org/10.3791/880
68. Paxinos G, Watson C (2007) The rat brain in stereotaxic coordinates. Academic Press, Amsterdam
69. Smits SM, Burbach JP, Smidt MP (2006) Developmental origin and fate of mesodiencephalic dopamine neurons. Prog Neurobiol 78(1):1–16. https://doi.org/10.1016/j.pneurobio.2005.12.003
70. Carlezon WA Jr, Thomas MJ (2009) Biological substrates of reward and aversion: a nucleus accumbens activity hypothesis. Neuropharmacology 56(Suppl 1):122–132
71. Proulx CD, Hikosaka O, Malinow R (2014) Reward processing by the lateral habenula in normal and depressive behaviors. Nat Neurosci 17(9):1146–1152. https://doi.org/10.1038/nn.3779
72. Hikosaka O (2010) The habenula: from stress evasion to value-based decision-making. Nat Rev Neurosci 11(7):503–513. https://doi.org/10.1038/nrn2866
73. Brunzell DH et al (2009) Nucleus accumbens CREB activity is necessary for nicotine conditioned place preference. Neuropsychopharmacology 34(8):1993–2001. https://doi.org/10.1038/npp.2009.11
74. Neumaier JF et al (2002) Elevated expression of 5-HT1B receptors in nucleus accumbens afferents sensitizes animals to cocaine. J Neurosci 22(24):10856–10863
75. Smedley EB, DiLeo A, Smith KS (2019) Circuit directionality for motivation: Lateral accumbens-pallidum, but not pallidum-accumbens, connections regulate motivational attraction to reward cues. Neurobiol Learn Mem 162:23–35. https://doi.org/10.1016/j.nlm.2019.05.001
76. Dreyer JK et al (2016) Functionally distinct dopamine signals in nucleus accumbens core and shell in the freely moving rat. J Neurosci 36(1):98–112. https://doi.org/10.1523/JNEUROSCI.2326-15.2016
77. Fortin SM et al (2015) Sampling phasic dopamine signaling with fast-scan cyclic voltammetry in awake, behaving rats. Curr Protoc Neurosci 70:7.25.1–7.25.20. https://doi.org/10.1002/0471142301.ns0725s70
78. Sackett DA, Saddoris MP, Carelli RM (2017) Nucleus accumbens shell dopamine preferentially tracks information related to outcome value of reward. eNeuro 4(3): ENEURO.0058-17.2017. https://doi.org/10.1523/ENEURO.0058-17.2017
79. Saddoris MP et al (2015) Differential dopamine release dynamics in the nucleus accumbens core and shell reveal complementary signals for error prediction and incentive motivation. J Neurosci 35 (33):11572–11582. https://doi.org/10.1523/JNEUROSCI.2344-15.2015
80. Fortin SM, Roitman MF (2017) Central GLP-1 receptor activation modulates cocaine-evoked phasic dopamine signaling in the nucleus accumbens core. Physiol Behav 176:17–25. https://doi.org/10.1016/j.physbeh.2017.03.019
81. Covey DP et al (2016) Amphetamine elevates nucleus accumbens dopamine via an action potential-dependent mechanism that is modulated by endocannabinoids. Eur J Neurosci 43(12):1661–1673. https://doi.org/10.1111/ejn.13248
82. Pomeranz LE et al (2017) Gene expression profiling with cre-conditional pseudorabies virus reveals a subset of midbrain neurons that participate in reward circuitry. J Neurosci 37(15):4128–4144. https://doi.org/10.1523/JNEUROSCI.3193-16.2017
83. Schelp SA et al (2017) A transient dopamine signal encodes subjective value and causally influences demand in an economic context. Proc Natl Acad Sci U S A 114(52): E11303–E11312. https://doi.org/10.1073/pnas.1706969114
84. Collins AL et al (2016) Nucleus accumbens acetylcholine receptors modulate dopamine and motivation. Neuropsychopharmacology 41(12):2830–2838. https://doi.org/10.1038/npp.2016.81
85. O'Neill B et al (2014) Behavior of knock-in mice with a cocaine-insensitive dopamine transporter after virogenetic restoration of cocaine sensitivity in the striatum. Neuropharmacology 79:626–633. https://doi.org/10.1016/j.neuropharm.2013.12.023
86. Heller EA et al (2016) Targeted epigenetic remodeling of the Cdk5 gene in nucleus

accumbens regulates cocaine- and stress-evoked behavior. J Neurosci 36 (17):4690–4697. https://doi.org/10.1523/JNEUROSCI.0013-16.2016

87. Werner CT et al (2018) E3 ubiquitin-protein ligase SMURF1 in the nucleus accumbens mediates cocaine seeking. Biol Psychiatry 84 (12):881–892. https://doi.org/10.1016/j.biopsych.2018.07.013
88. Ferguson D et al (2015) SIRT1-FOXO3a regulate cocaine actions in the nucleus accumbens. J Neurosci 35(7):3100–3111. https://doi.org/10.1523/JNEUROSCI.4012-14.2015
89. Foldi CJ, Milton LK, Oldfield BJ (2017) The role of mesolimbic reward neurocircuitry in prevention and rescue of the activity-based anorexia (ABA) phenotype in rats. Neuropsychopharmacology 42(12):2292–2300. https://doi.org/10.1038/npp.2017.63
90. Bailey MR et al (2018) An interaction between serotonin receptor signaling and dopamine enhances goal-directed vigor and persistence in mice. J Neurosci 38 (9):2149–2162. https://doi.org/10.1523/JNEUROSCI.2088-17.2018
91. Kim HD et al (2016) SIRT1 mediates depression-like behaviors in the nucleus accumbens. J Neurosci 36(32):8441–8452. https://doi.org/10.1523/JNEUROSCI.0212-16.2016
92. Chen NA et al (2014) Knockdown of CRF1 receptors in the ventral tegmental area attenuates cue- and acute food deprivation stress-induced cocaine seeking in mice. J Neurosci 34(35):11560–11570. https://doi.org/10.1523/JNEUROSCI.4763-12.2014
93. Mikhailova MA et al (2016) Optogenetically-induced tonic dopamine release from VTA-nucleus accumbens projections inhibits reward consummatory behaviors. Neuroscience 333:54–64. https://doi.org/10.1016/j.neuroscience.2016.07.006
94. Wakabayashi KT et al (2016) Application of fast-scan cyclic voltammetry for the in vivo characterization of optically evoked dopamine in the olfactory tubercle of the rat brain. Analyst 141(12):3746–3755. https://doi.org/10.1039/c6an00196c
95. Singh S et al (2018) Axin-2 knockdown promote mitochondrial biogenesis and dopaminergic neurogenesis by regulating Wnt/beta-catenin signaling in rat model of Parkinson's disease. Free Radic Biol Med 129:73–87. https://doi.org/10.1016/j.freeradbiomed.2018.08.033
96. Voronkov DN et al (2019) Immunohistochemical assessment of the compensatory responses in rat olfactory bulbs after 6-hydroxydopamine-induced lesion of the substantia nigra. Bull Exp Biol Med 166(6):811–815. https://doi.org/10.1007/s10517-019-04446-8
97. Ramalingam M, Huh YJ, Lee YI (2019) The Impairments of alpha-synuclein and mechanistic target of rapamycin in rotenone-induced SH-SY5Y cells and mice model of Parkinson's disease. Front Neurosci 13:1028. https://doi.org/10.3389/fnins.2019.01028
98. Shnitko TA, Robinson DL (2015) Regional variation in phasic dopamine release during alcohol and sucrose self-administration in rats. ACS Chem Neurosci 6(1):147–154. https://doi.org/10.1021/cn500251j
99. Hernandez G et al (2016) Ventral midbrain NMDA receptor blockade: from enhanced reward and dopamine inactivation. Front Behav Neurosci 10:161. https://doi.org/10.3389/fnbeh.2016.00161
100. Orsini CA et al (2017) Optogenetic inhibition reveals distinct roles for basolateral amygdala activity at discrete time points during risky decision making. J Neurosci 37 (48):11537–11548. https://doi.org/10.1523/JNEUROSCI.2344-17.2017
101. Mahoney CE et al (2017) GABAergic neurons of the central amygdala promote cataplexy. J Neurosci 37(15):3995–4006. https://doi.org/10.1523/JNEUROSCI.4065-15.2017
102. Harasta AE et al (2015) Septal glucagon-like peptide 1 receptor expression determines suppression of cocaine-induced behavior. Neuropsychopharmacology 40(8):1969–1978. https://doi.org/10.1038/npp.2015.47
103. Cates HM et al (2019) A novel role for E2F3b in regulating cocaine action in the prefrontal cortex. Neuropsychopharmacology 44(4):776–784. https://doi.org/10.1038/s41386-018-0296-1
104. Steidl S et al (2017) Operant responding for optogenetic excitation of LDTg inputs to the VTA requires D1 and D2 dopamine receptor activation in the NAcc. Behav Brain Res 333:161–170. https://doi.org/10.1016/j.bbr.2017.06.045
105. Fakhoury M, Rompre PP, Boye SM (2016) Role of the dorsal diencephalic conduction system in the brain reward circuitry. Behav Brain Res 296:431–441. https://doi.org/10.1016/j.bbr.2015.10.038

106. Fakhoury M et al (2016) Effect of electrolytic lesions of the dorsal diencephalic conduction system on the distribution of Fos-like immunoreactivity induced by rewarding electrical stimulation. Neuroscience 334:214–225. https://doi.org/10.1016/j.neuroscience.2016.08.002
107. Bian J et al (2013) Lentiviral vector-mediated knockdown of Lrb in the arcuate nucleus promotes diet-induced obesity in rats. J Mol Endocrinol 51(1):27–35. https://doi.org/10.1530/JME-12-0212
108. Gaspar JM et al (2018) Downregulation of HIF complex in the hypothalamus exacerbates diet-induced obesity. Brain Behav Immun 73:550–561. https://doi.org/10.1016/j.bbi.2018.06.020
109. Fish EW et al (2014) Different contributions of dopamine D1 and D2 receptor activity to alcohol potentiation of brain stimulation reward in C57BL/6J and DBA/2J mice. J Pharmacol Exp Ther 350(2):322–329. https://doi.org/10.1124/jpet.114.216135
110. Robinson JE et al (2012) Mephedrone (4-methylmethcathinone) and intracranial self-stimulation in C57BL/6J mice: comparison to cocaine. Behav Brain Res 234(1):76–81. https://doi.org/10.1016/j.bbr.2012.06.012
111. Fish EW et al (2010) Alcohol, cocaine, and brain stimulation-reward in C57Bl6/J and DBA2/J mice. Alcohol Clin Exp Res 34(1):81–89. https://doi.org/10.1111/j.1530-0277.2009.01069.x
112. Kolodziej A et al (2014) SPECT-imaging of activity-dependent changes in regional cerebral blood flow induced by electrical and optogenetic self-stimulation in mice. NeuroImage 103:171–180. https://doi.org/10.1016/j.neuroimage.2014.09.023
113. Simon MJ, Molina F, Puerto A (2009) Conditioned place preference but not rewarding self-stimulation after electrical activation of the external lateral parabrachial nucleus. Behav Brain Res 205(2):443–449. https://doi.org/10.1016/j.bbr.2009.07.028
114. Paxinos G, Watson C (2014) Paxino's and Watson's: The rat brain in stereotaxic coordinates. Seventh edition. edn. Elsevier/AP, Academic Press is an imprint of Elsevier, Amsterdam; Boston
115. Paxinos G et al (1985) Bregma, lambda and the interaural midpoint in stereotaxic surgery with rats of different sex, strain and weight. J Neurosci Methods 13(2):139–143
116. Brocka M et al (2018) Contributions of dopaminergic and non-dopaminergic neurons to VTA-stimulation induced neurovascular responses in brain reward circuits. NeuroImage 177:88–97. https://doi.org/10.1016/j.neuroimage.2018.04.059
117. Geiger BM et al (2009) Deficits of mesolimbic dopamine neurotransmission in rat dietary obesity. Neuroscience 159(4):1193–1199. https://doi.org/10.1016/j.neuroscience.2009.02.007
118. Pothos EN, Sulzer D, Hoebel BG (1998) Plasticity of quantal size in ventral midbrain dopamine neurons: possible implications for the neurochemistry of feeding and reward. Appetite 31(3):405. https://doi.org/10.1006/appe.1998.0210
119. Cederfjall E, Sahin G, Kirik D, Bjorklund T (2012) Design of a single AAV vector for coexpression of TH and GCH1 to establish continuous DOPA synthesis in a rat model of Parkinson's disease. Mol Ther 20:1315–1326
120. Tokuoka H et al (2011) Compensatory regulation of dopamine after ablation of the tyrosine hydroxylase gene in the nigrostriatal projection. J Biol Chem 286(50):43549–43558. https://doi.org/10.1074/jbc.M111.284729
121. Bocarsly ME et al (2014) GS 455534 selectively suppresses binge eating of palatable food and attenuates dopamine release in the accumbens of sugar-bingeing rats. Behav Pharmacol 25(2):147–157. https://doi.org/10.1097/FBP.0000000000000029
122. Rada P et al (2010) Opioids in the hypothalamus control dopamine and acetylcholine levels in the nucleus accumbens. Brain Res 1312:1–9. https://doi.org/10.1016/j.brainres.2009.11.055
123. Avena N, Rada P, Hoebel B (2008) Evidence for sugar addiction: Behavioral and neurochemical effects of intermittent, excessive sugar intake. Neurosci Biobehav Rev 32(1):20–39
124. Avena NM et al (2008) After daily bingeing on a sucrose solution, food deprivation induces anxiety and accumbens dopamine/acetylcholine imbalance. Physiol Behav 94(3):309–315. https://doi.org/10.1016/j.physbeh.2008.01.008
125. Avena NM et al (2006) Sucrose sham feeding on a binge schedule releases accumbens dopamine repeatedly and eliminates the acetylcholine satiety response. Neuroscience 139(3):813–820. https://doi.org/10.1016/j.neuroscience.2005.12.037
126. Rada P, Avena NM, Hoebel BG (2005) Daily bingeing on sugar repeatedly releases

dopamine in the accumbens shell. Neuroscience 134(3):737–744

127. Jamal M et al (2019) COA-Cl induces dopamine release and tyrosine hydroxylase phosphorylation: In vivo reverse microdialysis and in vitro analysis. Brain Res 1706:68–74. https://doi.org/10.1016/j.brainres.2018.10.026
128. Chefer VI et al (2006) Quantitative no-net-flux microdialysis permits detection of increases and decreases in dopamine uptake in mouse nucleus accumbens. J Neurosci Methods 155(2):187–193. https://doi.org/10.1016/j.jneumeth.2005.12.018
129. Cremers TI et al (2009) Quantitative microdialysis using modified ultraslow microdialysis: direct rapid and reliable determination of free brain concentrations with the MetaQuant technique. J Neurosci Methods 178(2):249–254. https://doi.org/10.1016/j.jneumeth.2008.12.010
130. de Vries MG et al (2003) Extracellular glucose in rat ventromedial hypothalamus during acute and recurrent hypoglycemia. Diabetes 52(11):2767–2773. https://doi.org/10.2337/diabetes.52.11.2767
131. Justice JB, Jr (1993) Quantitative microdialysis of neurotransmitters. J Neurosci Methods 48(3):263–276. https://doi.org/10.1016/0165-0270(93)90097-b
132. Unger EL et al (2014) Low brain iron effects and reversibility on striatal dopamine dynamics. Exp Neurol 261:462–468. https://doi.org/10.1016/j.expneurol.2014.06.023
133. Borkar CD et al (2016) Neuropeptide Y system in accumbens shell mediates ethanol self-administration in posterior ventral tegmental area. Addict Biol 21(4):766–775. https://doi.org/10.1111/adb.12254
134. Burton AC et al (2018) Previous cocaine self-administration disrupts reward expectancy encoding in ventral striatum. Neuropsychopharmacology 43(12):2350–2360. https://doi.org/10.1038/s41386-018-0058-0
135. Mogenson GJ et al (1979) Self-stimulation of the nucleus accumbens and ventral tegmental area of Tsai attenuated by microinjections of spiroperidol into the nucleus accumbens. Brain Res 171(2):247–259. https://doi.org/10.1016/0006-8993(79)90331-7
136. Jenkins OF, Atrens DM, Jackson DM (1983) Self-stimulation of the nucleus accumbens and some comparisons with hypothalamic self-stimulation. Pharmacol Biochem Behav 18(4):585–591. https://doi.org/10.1016/0091-3057(83)90285-x
137. Sasaki K et al (1984) The effects of feeding and rewarding brain stimulation on lateral hypothalamic unit activity in freely moving rats. Brain Res 322(2):201–211. https://doi.org/10.1016/0006-8993(84)90110-0
138. Farakhor S, Shalchyan V, Daliri MR (2019) Adaptation effects of medial forebrain bundle micro-electrical stimulation. Bioengineered 10(1):78–86. https://doi.org/10.1080/21655979.2019.1599628
139. Katsidoni V, Kastellakis A, Panagis G (2013) Biphasic effects of Delta9-tetrahydrocannabinol on brain stimulation reward and motor activity. Int J Neuropsychopharmacol 16(10):2273–2284. https://doi.org/10.1017/S1461145713000709
140. Garcia R, Zafra MA, Puerto A (2015) Rewarding effects of electrical stimulation of the insular cortex: decayed effectiveness after repeated tests and subsequent increase in vertical behavioral activity and conditioned place aversion after naloxone administration. Neurobiol Learn Mem 118:64–73. https://doi.org/10.1016/j.nlm.2014.11.008
141. Grim TW et al (2015) Effects of acute and repeated dosing of the synthetic cannabinoid CP55,940 on intracranial self-stimulation in mice. Drug Alcohol Depend 150:31–37. https://doi.org/10.1016/j.drugalcdep.2015.01.022
142. van Wolfswinkel L, Seifert WF, van Ree JM (1988) Catecholamines and endogenous opioids in ventral tegmental self-stimulation reward. Pharmacol Biochem Behav 30(3):589–595. https://doi.org/10.1016/0091-3057(88)90070-6
143. Marcangione C, Rompre PP (2008) Topographical Fos induction within the ventral midbrain and projection sites following self-stimulation of the posterior mesencephalon. Neuroscience 154(4):1227–1241. https://doi.org/10.1016/j.neuroscience.2008.05.014
144. Fish EW et al (2014) Effects of the neuroactive steroid allopregnanolone on intracranial self-stimulation in C57BL/6J mice. Psychopharmacology 231(17):3415–3423. https://doi.org/10.1007/s00213-014-3600-8
145. Gigante ED et al (2016) Optogenetic activation of a lateral hypothalamic-ventral tegmental drive-reward pathway. PLoS One 11(7):e0158885. https://doi.org/10.1371/journal.pone.0158885
146. Touzani K, Velley L (1998) Electrical self-stimulation in the central amygdaloid nucleus after ibotenic acid lesion of the lateral hypothalamus. Behav Brain Res 90(2):115–124. https://doi.org/10.1016/s0166-4328(97)00090-9
147. Garcia R, Simon MJ, Puerto A (2013) Conditioned place preference induced by

electrical stimulation of the insular cortex: effects of naloxone. Exp Brain Res 226 (2):165–174. https://doi.org/10.1007/s00221-013-3422-7

148. Bahi A, Dreyer JL (2008) Overexpression of plasminogen activators in the nucleus accumbens enhances cocaine-, amphetamine- and morphine-induced reward and behavioral sensitization. Genes Brain Behav 7 (2):244–256. https://doi.org/10.1111/j.1601-183X.2007.00346.x
149. Runegaard AH et al (2018) Locomotor- and Reward-enhancing effects of cocaine are differentially regulated by chemogenetic stimulation of gi-signaling in dopaminergic neurons. eNeuro 5(3):ENEURO.0345-17.2018. https://doi.org/10.1523/ENEURO.0345-17.2018
150. Towne C, Thompson KR (2016) Overview on research and clinical applications of optogenetics. Curr Protoc Pharmacol 75:11.19.11–11.19.21. https://doi.org/10.1002/cpph.13
151. Deisseroth K (2011) Optogenetics. Nat Methods 8(1):26–29. https://doi.org/10.1038/nmeth.f.324
152. Deisseroth K et al (2006) Next-generation optical technologies for illuminating genetically targeted brain circuits. J Neurosci 26 (41):10380–10386. https://doi.org/10.1523/JNEUROSCI.3863-06.2006
153. Berrios J et al (2016) Loss of UBE3A from TH-expressing neurons suppresses GABA co-release and enhances VTA-NAc optical self-stimulation. Nat Commun 7:10702. https://doi.org/10.1038/ncomms10702
154. Han X et al (2017) Role of dopamine projections from ventral tegmental area to nucleus accumbens and medial prefrontal cortex in reinforcement behaviors assessed using optogenetic manipulation. Metab Brain Dis 32 (5):1491–1502. https://doi.org/10.1007/s11011-017-0023-3
155. van Zessen R et al (2012) Activation of VTA GABA neurons disrupts reward consumption. Neuron 73(6):1184–1194. https://doi.org/10.1016/j.neuron.2012.02.016
156. Wolfman SL et al (2018) Nicotine aversion is mediated by GABAergic interpeduncular nucleus inputs to laterodorsal tegmentum. Nat Commun 9(1):2710. https://doi.org/10.1038/s41467-018-04654-2
157. Shabel SJ et al (2012) Input to the lateral habenula from the basal ganglia is excitatory, aversive, and suppressed by serotonin. Neuron 74(3):475–481. https://doi.org/10.1016/j.neuron.2012.02.037
158. Lammel S et al (2012) Input-specific control of reward and aversion in the ventral tegmental area. Nature 491(7423):212–217. https://doi.org/10.1038/nature11527
159. Stamatakis AM et al (2013) A unique population of ventral tegmental area neurons inhibits the lateral habenula to promote reward. Neuron 80(4):1039–1053. https://doi.org/10.1016/j.neuron.2013.08.023
160. Sharpe MJ et al (2017) Lateral hypothalamic GABAergic neurons encode reward predictions that are relayed to the ventral tegmental area to regulate learning. Curr Biol 27 (14):2089–2100. e2085. https://doi.org/10.1016/j.cub.2017.06.024
161. Barbano MF et al (2016) Feeding and reward are differentially induced by activating GABAergic lateral hypothalamic projections to VTA. J Neurosci 36(10):2975–2985. https://doi.org/10.1523/JNEUROSCI.3799-15.2016
162. Steidl S et al (2017) Optogenetic excitation in the ventral tegmental area of glutamatergic or cholinergic inputs from the laterodorsal tegmental area drives reward. Eur J Neurosci 45 (4):559–571. https://doi.org/10.1111/ejn.13436
163. de Jong JW et al (2019) A neural circuit mechanism for encoding aversive stimuli in the mesolimbic dopamine system. Neuron 101(1):133–151. e137. https://doi.org/10.1016/j.neuron.2018.11.005
164. Wang D et al (2017) Learning shapes the aversion and reward responses of lateral habenula neurons. elife 6:e23045. https://doi.org/10.7554/eLife.23045
165. Li Y et al (2016) Serotonin neurons in the dorsal raphe nucleus encode reward signals. Nat Commun 7:10503. https://doi.org/10.1038/ncomms10503
166. Moriya S et al (2018) Acute aversive stimuli rapidly increase the activity of ventral tegmental area dopamine neurons in awake mice. Neuroscience 386:16–23. https://doi.org/10.1016/j.neuroscience.2018.06.027
167. Zhong W et al (2017) Learning and stress shape the reward response patterns of serotonin neurons. J Neurosci 37(37):8863–8875. https://doi.org/10.1523/JNEUROSCI.1181-17.2017
168. Wei C et al (2018) Response dynamics of midbrain dopamine neurons and serotonin neurons to heroin, nicotine, cocaine, and MDMA. Cell Discov 4:60. https://doi.org/10.1038/s41421-018-0060-z
169. Rodeberg NT et al (2017) Hitchhiker's guide to voltammetry: acute and chronic electrodes

for in vivo fast-scan cyclic voltammetry. ACS Chem Neurosci 8(2):221–234. https://doi.org/10.1021/acschemneuro.6b00393

170. Colon-Gonzalez F et al (2013) Obesity pharmacotherapy: what is next? Mol Asp Med 34 (1):71–83. https://doi.org/10.1016/j.mam.2012.10.005
171. Klanker M et al (2017) Deep brain stimulation of the medial forebrain bundle elevates striatal dopamine concentration without affecting spontaneous or reward-induced phasic release. Neuroscience 364:82–92. https://doi.org/10.1016/j.neuroscience.2017.09.012
172. Oliva I, Wanat MJ (2019) Operant costs modulate dopamine release to self-administered cocaine. J Neurosci 39 (7):1249–1260. https://doi.org/10.1523/JNEUROSCI.1721-18.2018
173. Chartoff EH et al (2016) Relative timing between kappa opioid receptor activation and cocaine determines the impact on reward and dopamine release. Neuropsychopharmacology 41(4):989–1002. https://doi.org/10.1038/npp.2015.226
174. Bobak MJ et al (2016) Modafinil activates phasic dopamine signaling in dorsal and ventral striata. J Pharmacol Exp Ther 359 (3):460–470. https://doi.org/10.1124/jpet.116.236000
175. Ferreira NR et al (2018) Simultaneous measurements of ascorbate and glutamate in vivo in the rat brain using carbon fiber nanocomposite sensors and microbiosensor arrays. Bioelectrochemistry 121:142–150. https://doi.org/10.1016/j.bioelechem.2018.01.009
176. Zlebnik NE et al (2014) Long-term reduction of cocaine self-administration in rats treated with adenoviral vector-delivered cocaine hydrolase: evidence for enzymatic activity. Neuropsychopharmacology 39 (6):1538–1546. https://doi.org/10.1038/npp.2014.3
177. Muir J et al (2018) In vivo fiber photometry reveals signature of future stress susceptibility in nucleus accumbens. Neuropsychopharmacology 43(2):255–263. https://doi.org/10.1038/npp.2017.122
178. Salinas-Hernandez XI et al (2018) Dopamine neurons drive fear extinction learning by signaling the omission of expected aversive outcomes. Elife 7:e38818. https://doi.org/10.7554/eLife.38818
179. Menegas W et al (2017) Opposite initialization to novel cues in dopamine signaling in ventral and posterior striatum in mice. elife 6: e21886. https://doi.org/10.7554/eLife.21886
180. Parker KE et al (2019) A paranigral VTA nociceptin circuit that constrains motivation for reward. Cell 178(3):653–671. e619. https://doi.org/10.1016/j.cell.2019.06.034
181. Itoga CA et al (2019) New viral-genetic mapping uncovers an enrichment of corticotropin-releasing hormone-expressing neuronal inputs to the nucleus accumbens from stress-related brain regions. J Comp Neurol 527(15):2474–2487. https://doi.org/10.1002/cne.24676
182. Clark RA, Ewing AG (1997) Quantitative measurements of released amines from individual exocytosis events. Mol Neurobiol 15 (1):1–16. https://doi.org/10.1007/BF02740612
183. Benoit-Marand M, Jaber M, Gonon F (2000) Release and elimination of dopamine in vivo in mice lacking the dopamine transporter: functional consequences. Eur J Neurosci 12 (8):2985–2992. https://doi.org/10.1046/j.1460-9568.2000.00155.x
184. Sulzer D, Pothos EN (2000) Regulation of quantal size by presynaptic mechanisms. Rev Neurosci 11(2–3):159–212. https://doi.org/10.1515/revneuro.2000.11.2-3.159
185. Geiger BM et al (2008) Evidence for defective mesolimbic dopamine exocytosis in obesity-prone rats. FASEB J 22(8):2740–2746. https://doi.org/10.1096/fj.08-110759
186. Schuweiler DR et al (2018) Effects of an acute therapeutic or rewarding dose of amphetamine on acquisition of Pavlovian autoshaping and ventral striatal dopamine signaling. Behav Brain Res 336:191–203. https://doi.org/10.1016/j.bbr.2017.09.003
187. Hart AS, Clark JJ, Phillips PEM (2015) Dynamic shaping of dopamine signals during probabilistic Pavlovian conditioning. Neurobiol Learn Mem 117:84–92. https://doi.org/10.1016/j.nlm.2014.07.010
188. Aitken TJ, Greenfield VY, Wassum KM (2016) Nucleus accumbens core dopamine signaling tracks the need-based motivational value of food-paired cues. J Neurochem 136 (5):1026–1036. https://doi.org/10.1111/jnc.13494
189. Sunsay C, Rebec GV (2014) Extinction and reinstatement of phasic dopamine signals in the nucleus accumbens core during Pavlovian conditioning. Behav Neurosci 128 (5):579–587. https://doi.org/10.1037/bne0000012

190. Jing M et al (2018) A genetically encoded fluorescent acetylcholine indicator for in vitro and in vivo studies. Nat Biotechnol 36(8):726–737. https://doi.org/10.1038/nbt.4184

191. Marvin JS et al (2019) A genetically encoded fluorescent sensor for in vivo imaging of GABA. Nat Methods 16(8):763–770. https://doi.org/10.1038/s41592-019-0471-2

Chapter 3

Characterizing the Neural Substrate of Reward with the Use of Specific Brain Lesions

Howard Casey Cromwell

Abstract

Examining the effects of brain lesions has been a key part of neuroscience since the earliest observations and research. Work using animal models with methods that aim to destruct targeted brain regions has been an essential strategy to reveal and understand localized brain function. This review is focused on experimental lesions and work using the rodent model examining the neural substrates of reward processing. This seemingly focused area is actually broad-based with literature using diverse means to produce experimental lesions and a host of behavioral methods to evaluate reward processing. This chapter mainly focuses on experimental lesions using neurochemical means including chemostimulation techniques with N-methyl-D-aspartate (NMDA), quinolinic, quisqualate, or kainic acid. Other means of lesion making will be briefly discussed. The chapter briefly describes general methods used to examine reward processing that measures operant responding, Pavlovian conditioning, and unconditioned responses (e.g., seeking and taste reactions) and provides the advantages of the lesion approach that include: (1) determination of cause/effect relationships, (2) revealing dissociations in functional neuroanatomy, and (3) producing work that can translate well to human neuroscience and neurological disorders. The chapter also highlights problems including: (1) incomplete/inaccurate lesion mapping, (2) confounds related to lesion timing and recovery periods, and (3) false dissociations that appear real but may underlie more complex functional neuroanatomy relationships. Finally, the chapter offers future directions by describing innovative methods that laboratories are developing to produce greater precision lesions in terms of neural connectivity and chemical phenotype targets (see related chapters in this book). Overall, the lesion method has been crucial to progress in revealing the true functional nature of the reward process.

Key words Basal ganglia, Excitotoxins, Motivation, Nucleus accumbens, Reinforcement, Stereology

1 Introduction: The Reward Process and the Lesion Approach

1.1 Reward: A Simple Process Becomes Highly Complex

Rewards can be defined principally as those outcomes, events, stimuli that an animal approaches and utilizes, consumes, or stores. A comparable version of this definition has been mentioned in well-known works in behavioral neuroscience [1–3]. The straightforward nature of this definition lures scientists into a belief that the overall process underlying the formation of a reward representation is straightforward and simple. Studying the effects of lesions, more

Marc Fakhoury (ed.), *The Brain Reward System*, Neuromethods, vol. 165, https://doi.org/10.1007/978-1-0716-1146-3_3,

than other methods, has revealed a complex, multicomponent means in creating and utilizing reward representations. One complex issue includes the information encoded or used to form or alter reward representations. Diverse sensory input that includes unconditioned stimuli and natural rewards to learned reward outcomes and their associative cues, contexts, and related stimuli are linked to the reward process. Norman White differentiated reward from reinforcement based upon influences on behavior and intrinsic representations [4]. Reward according to his analysis is linked to internal representations (i.e., memories) and core motivational/emotional states while reinforcement (and reinforcers) describes the effect of an outcome on altering behavioral dynamics [5]. He emphasizes that reward is only one of the several diverse factors that influence the reinforcement process. Studies using lesions have been important in showing that this is the case [6–8].

The idea that multiple memory stores are associated to reward processing is important. It provides a level of complexity that enables neuroscience methods to understand and track the dynamic properties of the reward process. It involves distinct components of discriminating and comparing values allowing a formation of both dynamic and stable preferences contributing to choice behavior [9]. Contemporary behavioral neuroscience focuses on reward valuation as a dynamic process and has used a wide array of behavioral methods to track reward updating and relative valuation [10, 11]. The reward process can be dissociated into two main phases, the appetitive and consummatory [1]. This classic distinction provides a way to parcel behavior into anticipatory, flexible responses that precede more stereotyped actions essential upon reward acquisition. Appetitive behaviors are measured in diverse ways from basic exploration and seeking highly organized operant and instrumental responses that can involve complex action sequences. Consummatory phase is typically measured as licking rates, taste reactions, amount of food consumed, or copulatory acts. Utilizing specific behavioral measures and not others (e.g., interresponse times vs. rate of response [12]) could lead to a substantial difference in terms of how post-lesion alterations are found and interpreted.

Lesion studies have provided results supporting division of psychological functions into distinct subfunctions in ways that sometimes seem paradoxical and suboptimal. Lesions to key structures, such as the mesolimbic system, result in deficits that affect one aspect of reward processing while sparing others. One of the most well-published effects in this realm is the separation of "liking" from "wanting" and vice versa [13]. Lesions that moderately lower dopamine levels and spare motoric abilities influence reward "wanting" without altering reward "liking" [14, 15]. The finding was surprising for the pioneering group because the motive for the work was to pin down the role of dopamine in hedonics.

Instead, the finding removed dopamine from hedonic processing within the consummatory phase [16]. Another example is recent work suggesting the components that form reward discriminations, preferences, or updated values can be "fractionated" [9]. Lesions to the striatum impact components of relative valuation while sparing more basic abilities of basic discrimination [17]. The ability to update reward value should involve memory retrieval of past reward value, a comparison process, and a linkage among previous reward representation and current reward values for all comparable alternatives. In contrast, reward discrimination can involve solely immediate value processing for each alternative. Alternatives are compared and new preference hierarchies created with each experience of outcome sampling. In some ways, a stable preference is an absolute value that could allow a more complex relative valuation to occur.

Finally, it is clear that lesion work is only as effective as the behavioral means to explore reward processing. Krakauer and colleagues [18] provided an elegant review emphasizing that neuroscience methods including the lesion approach are only as good as the measures of behavior examined, and each part of the study design must be carefully thought out, planned in ways to avoid confounds and reveal accurate levels of motivation, emotion, and cognitive abilities in the subjects. Crucial elements of the behavioral design include the general order of experience, the length and type of training, and the validity of the dependent measures to reveal reward influence.

1.2 The Lesion Approach and Functional Heterogeneity

Turning something off can alter, reduce, or abolish an operation. Taking a critical part out of an automotive engine could leave the vehicle "dead" or merely cause the air-conditioning to circulate warm air. Expert mechanics work at discovering the particular broken piece and restore complete functionality. Reverse engineering intentionally breaks/removes single parts to observe the damage inflicted. Causal attribution links the broken part to the missing/altered operation. Lesion methods simulate this approach by removing/destroying/inhibiting individual brain regions and examining alterations in specific behavioral or physiological functions. This chapter focuses mainly on standard lesion methods using excitotoxic chemicals targeting glutamate system including quinolinic, quisqualate, and kainic acids and N-methyl-D-aspartate (NMDA) as substrates. These chemostimulation methods have been well established for the last 50 years and remain a standard approach in the field. Other strategies include electrolytic, aspiration, cryoprobe (e.g., freezing), and chemogenetic approaches. Early work in the field often used electrolytic or aspiration methods. Both of these approaches can efficiently target and destroy select brain regions, yet the disadvantage comes in terms of general damage to all cell types (e.g., neurons and glial cells) as well as

destroying axon fibers passing through the region. The excitotoxic method enabled researchers to target neurons and spare other cell types and fibers of passage. The method was groundbreaking in providing a way that is effective in removing neurons from small subregions without directly influencing other regions [19, 20]. The mechanism is typically via binding to excitatory amino acid receptors on neuronal dendrites. Overstimulation leads to cell death acting through diverse ionotropic and metabotropic glutamate receptors [21]. The necrotic process is acute (<24 h) although there can be longer term effects locally and more globally. The mechanism of neuronal death can vary depending upon the toxin [22, 23]. NMDA receptor effects typically involve uncontrolled entry of Ca^{2+} into the neurons and without proper clearance, the overstimulation, including proteases and phospholipases, damages the cell's integrity. These excitotoxic-based methods are relatively straightforward and the toxins can be easily obtained (see Cambridge Research Biochemicals; Sigma, Saint Louis, MO). Methods can vary leading to differences in the diffusion of the excitotoxin, neuronal selectivity in terms of damage and fiber damage. Diverse excitotoxins do have distinct mechanisms including binding to distinct receptors. One example was work by Robbins, Everett, and colleagues [24] who utilized ibotenate (0.4 μL; 0.06 M in phosphate buffer) to target the parvocellular neurons of the substantia innominata, whereas quisqualate (0.5 μL; 0.12 M in phosphate buffer) was used to target magnocellular cholinergic neurons. The effect is relative as both toxins do affect both cell types but do so with varying efficacy. Saporin is another neurotoxin used to target selective neuronal populations with success [25]. Modern methods typically spare axons of passage using these chemotoxic approaches. There is some evidence to suggest that in certain locations and at relatively high doses/multiple injections, there is loss of myelin and local breakdown of the blood–brain barrier [26, 27]. For work targeting the striatum or prefrontal cortex, groups find similar extent of cellular neurotoxicity using quisqualate, ibotenate, or quinolinic acid [28]. These neurotoxins have all been shown to be effective at significantly reducing neuron numbers in the different striatal and pallidal subregions including the nucleus accumbens [29]. There is evidence to show that cholinergic neurons are relatively spared when using certain toxins rather than others [30, 31]. If the target is midbrain dopamine cells, unique neurotoxins selective for catecholamine neurons can be used (i.e., 6-hydroxy-dopamine) [32].

The lesion method overall has been exceptionally valuable in behavioral neuroscience (*see* Fig. 1). Foundational work uncovered competing or interactive systems involved in primary motivational systems. One of the best examples of early work is the research on hypothalamic systems of hunger and satiety [33]. The dual center hypothesis of hypothalamic function was based upon lesions to the

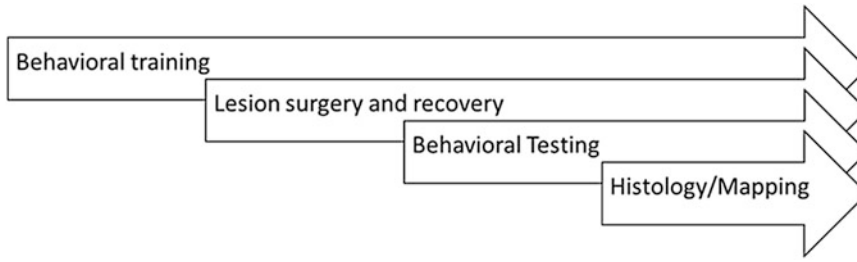

Fig. 1 General procedural design with major stages of a lesion study. This is an example design that would fit most lesion study protocols. The timing in between the main stages and the duration of each stage varies. Performing the lesion surgery following behavioral training enables one to examine post-training expression of reward function. Studies do perform lesions prior to training when examining the learning process (e.g., reward conditioning). As highlighted, recovery time post-lesion can make a difference in terms of deficits obtained. Post-lesion compensation can lead to transient impairments or compensatory mechanisms (behavioral and neural). The final step of histology and lesion mapping involved sectioning, staining, and viewing the tissue. Light microscopy is sufficient and neuron staining allowing cell counting is a method used by many research groups

lateral and ventromedial hypothalamus and remains a strong influence on the field of motivation [34, 35]. One of our earliest studies was devoted to examining hypothalamic regions of hunger and mapping lesions targeting hypothalamus as well as proximal areas of the ventral pallidum and substantia innominata [36, 37]. This previous work used a stereological approach to track lesion damage and uncovered a neural hotspot located outside the hypothalamus and inside the ventromedial ventral pallidum related to hunger and hedonic responses to taste. The early work using lesions laid the foundation for a large set of studies exploring specific functions for subregions in many diverse brain regions.

Reward function has been examined using the lesion approach as well. The basal ganglia have been a main target when examining reward processing [38–40]. Other regions of the brain are also primary targets including the prefrontal cortical subareas, hippocampus, and amygdala, which have been studied extensively using lesions. These regions are interconnected and damage to one brain area can lead to significant changes in multiple regions. This "cascade of damage" throughout a circuit has not been a focus of lesion work, yet some methods explicitly examine the circuit involved following a lesion and how recovery could vary depending upon the primary target site of damage.

The striatum provides one of the best examples of functional heterogeneity in terms of different subregions involved in different aspects of reward processing. Lesion work has identified subregions and specific functional attributes. The dorsomedial striatum has been found to be involved in cognitive functions of memory and associative learning [41–43], while the dorsolateral subregion has been mainly found to be involved in habit formation, sensorimotor

operations, and motor sequencing [44, 45]. The ventrolateral striatum has been found to play a key role in contextually modulated choice, stereotyped movements, and motor learning [46, 47]. The ventromedial striatum that includes all of the nucleus accumbens has been found to be the main "hotspot" for reward processing with subdivisions (core vs. shell) that parse reward functions into wanting and liking, approach and avoidance, hedonic attribution, and reward updating [48–51]. The conglomeration of striatal subregions combined provides the host of necessary operations to enable learning and expression of motivation in adaptive ways. Lesion methods in conjunction with neuroanatomical findings have provided the bulk of our present knowledge dividing the striatum into these compartmentalized subregions, each one with a key function isolable yet heavily dependent upon its neighbor.

2 Materials Required to Make Lesions and Examine Reward Processing

2.1 Animals

Rats or mice purchased from general distributors (e.g., Envigo, Harlan) or obtained from another source (Research Institute colony) should be ordered and allowed to habituate/acclimate to the facilities for 7 days prior to experimental use. Sex, age, and/or weight of animal are determined by experimental question and this chapter focuses on adult rat model. Modified stereotaxic equipment can be used to produce lesions in young animals or mice. Following the acclimation period, animals are housed individually so that they can be monitored in terms of food and water intake and for postsurgical recovery. Many studies utilize food restriction during behavioral training or testing. Food restriction prior to surgery is not necessary in the rodent model.

2.2 Solutions

Each neurotoxin is dissolved in phosphate-buffered saline (PBS). Using a 0.1 M phosphate buffer of pH 7.4 by adding 0.1 M sodium dihydrogen orthophosphate (monobasic) to 0.1 M disodium hydrogen orthophosphate (dibasic) until the pH reaches 7.4. Concentration of excitotoxin can be used up to 160 mM. Kainate must be used at much lower concentration (3 mM) compared to the other toxins. Exact doses and volume can vary. Often the buffer is not sufficient and the pH must be adjusted by adding small amounts of concentrated (2 M) NaOH until the pH returns to ~7. Other vehicles (e.g., saline) could be used but several of the excitotoxins are insoluble in fluctuating pH. Excitotoxin solution can be stored frozen for extended periods. Divide into stock solutions to avoid refreezing. Histological solutions include cresyl violet, ethanol, and xylene for tissue staining and for lesion mapping. Xylenes were standard but are now being replaced by more environmentally friendly alternatives such as **naphthenic solvents or D-limonenes (e.g., Histoclear). PBS for vehicle or solution and**

immunohistochemistry requires ordering appropriate kits and related materials. Resultant solutions and chemicals have high levels of toxicity so use caution in preparation and handling. Gloves, laboratory coats, and eye protection should be used at all times. Sterilize water and/or resultant solutions to be used in infusion pump tubing or to be injected by microsyringe.

2.3 Surgical Supplies

A stereotaxic apparatus and a stereotaxic atlas (a map of the typical brain and skull for the species) are necessary in order to perform the neurosurgery. The stereotaxic atlas of the rat brain is used to calculate the coordinates of the tissue to be lesioned. Stereotaxic procedures are also used in human neurosurgery—using radiographic rather than skull landmarks—to produce therapeutic brain lesions in deep regions of the brain that are inaccessible for visually guided dissection. Specific surgical tools include sterile gloves, drape, cotton tips, and instruments. Instruments include scalpel (blade # 10), hemostats [4–6], and dental drill bit. A Dremel moto-tool is the most effective tool to drill the craniotomies. Wound clips or suture material will be necessary and forceps can be used as extra clamps. Hot bead sterilizer and/or an autoclave can be used for instrument/gauze/cotton tip sterilization.

2.4 Testing Apparatus

Reward processing can be examined in a wide variety of ways, yet there are several methods that are standard to the field. Operant responding using lever press or nosepoke is often used when the aim is to examine the appetitive phase and motivation of the animal to acquire a particular outcome (e.g., food/sugar pellet or solution). These operant or instrumental tasks allow the animal to express motivation and time output to the reward as well as other behaviors. A standard for conditioned preference is conditioned place preference that can be used for natural or drug rewards. There are a plethora of choice tasks that involve different reward parameters including effort, magnitude, probability, and delay. These tasks are designed to incorporate risk and examine decision-making involved in reward acquisition.

3 Methods Used to Make Lesions

3.1 Surgery

Typical procedure: Prior to surgery (30 min prior to anesthesia), inject animal subcutaneously with Metacam (Boehringer Ingelheim Vetmedica, Inc., St. Joseph, MO, USA) (5 mg/mL) and Buprenex (Reckitt Benckiser Healthcare (UK) Ltd., Hull, England) (3 mg/mL). These prophylactic doses will aid anesthesia throughout surgery and after. Animals can be anesthetized with a variety of agents including pentobarbital (begin at 5 mg/kg and continue administration until the animal is unresponsive to pain) or inhalant (e.g., isoflurane using a small animal anesthesia system and placed in a

stereotaxic device). If pentobarbital is used, typically inject atropine to prevent respiratory failure (0.4 mg/kg, s.c.). Atropine appears safe in conjunction with inhalant anesthesia as well [52]. Anesthesia can effect excitotoxicity in particular using ketamine/xylazine can alter the neurotoxicity when using certain excitotoxins and specifically NMDA at neurotoxic doses. Inhalants work particularly well in combination with anticonvulsants and retain neurotoxic effects. Prior to making the initial incision, lidocaine (5 mg/kg transdermal) can be injected into the incision site for local anesthesia.

Prior to placing the rat in the stereotaxic frame, have the microinjection materials ready including the needle, and pump set at the appropriate rate with filled sterile water. Shave the animals head from the line of eyes to the ears and place the animal's teeth over the bite bar. Place the rat's body on a heating pad. Monitoring oxygen (oximeter) and temperature (rectal thermometer) is strongly advised. Move one ear into the earbar at a time and while holding the head steady place the opposite earbar into place. If right-handed, it is easier to begin with the right side. The pinnae should look equal and lie flat on the ear bars. The head should not move or wobble. Tighten the nose bar gently. This does not have to be tight. Check vitals regularly and monitor the level of anesthesia. Veterinary ophthalmic ointment should be placed onto each eye to protect from drying. Wipe the target shaved region with 2% chlorhexidine solution and iodine and ethanol. Repeat two to three times. Use iodine/povidone (10%) and the area is now disinfected and ready for incision.

Use the scalpel blade to make an incision along the longitudinal midline (2–3 cm). Pull the fascia to the edges using the cotton tips and use four curved hemostats to clamp the fascia (not the skin) and produce a surgical window. Sham animals received injections of PBS. Locate bregma (the frontal intersection of the three main plates of the skull). Level the skull by reading both bregma and lambda points from the skull. Lambda is the posterior point of intersect. These two points should be within 0.1 mm reading of one another. If the skull needs leveling, loosen the nose bar and raise or lower the bite plate and then remeasure.

Prefigured coordinates are used from the standard rat stereotaxic atlas [53]. Example anterior dorsolateral striatum: anterior–posterior (AP) +1.0 mm anterior to bregma, lateral (L) ±1.7 mm lateral to bregma and ventral (V) −4.5 mm below the skull. Major target regions for reward processing include nucleus accumbens, dorsal striatum, basolateral and central amygdala, and medial prefrontal cortex. Move needle to position calculated based on these coordinates. Mark the location on the skull. In addition, drill a hole ~2 mm in diameter in the location using Dremel moto-tool with sterile drill bit attached. Be careful, because when the drill breaks through bone it can damage dura and underlying brain tissue. Ream the hole to increase the size and absorb blood with sterile

cotton swab. Swing/place needle back into position and lower needle to the correct dorsal–ventral coordinate.

Microinjection of the 0.1–1.0 μL volume is the typical method of delivering the toxin into the brain. Three main methods are utilized: (1) injecting via a stainless steel cannula (30 gauge) already mounted onto a stereotaxic frame. This cannula is connected to a 5–10 μL syringe mounted on an infusion pump via polyethylene tubing. The infusion can be set to infuse at the desired rate: 0.5 μL/min is a standard rate. Slower rates typically allow for diffusion away from the needle and greater range of toxic dose, (2) injecting via a glass micropipette that has a fine tip and is fixed to the cannula. This method has been used to create smaller, more targeted lesions, and usually with one or limited injections, and (3) injecting using direct insertion of a stereotaxically mounted syringe. For example, a 1.0 μL Hamilton microsyringe can be used to insert sub-microliter volumes. One cautionary note with this technique is to be careful when lowering the needle to avoid nonspecific tissue or vascular damage. Multiple injections are used to produce a larger more complete lesion. In most cases, small amounts of toxin (0.05–0.1 μL at 0.1 μL/min) are injected at multiple sites within the brain structure. Injection numbers typically range from 2 to 13 depending upon the brain region and the intent to target a larger area of the structure. Few groups have used microiontophoresis to effectively control administration of neurotoxins for lesions [54, 55]. This technique would be appropriate to limit toxin movement and create small regions of damage. Regardless of the microinjection procedure, the cannulae should be left in situ for 1–5 min following the injection period. This is crucial in order to allow for the toxin to diffuse away from the needle and to reduce any fluid that might include neurotoxin drawn up the cannula/needle track.

When done infusing unilateral or bilateral microinjections, wipe away remaining blood and remove clamps from fascia. Incisions can be closed using sutures or wound clips. Using the forceps to hold two sides of the wound together, apply wound clips and staple along incision length. Use forceps to secure the clips (three to six clips). Use providine swab on skin and return the animal to home cage. Monitor until motility is observed. Inhalants anesthesia recovery can be faster (<1 h) while pentobarbital and other injectables can take longer (1–2 h).

3.2 Sequelae and Recovery

During surgery, possible problems include hemorrhage and seizure/convulsions. To avoid bleeding, aiming the lesion sites off the main intersection points of the cranium bone fissures can help. The neurovasculature tends to (but not always) follow these bone fissures along the latitude and longitude of the skull. Cauterizing can be completed but typically only for skull vasculature. Other sites are handled with light pressure, gauze, and other means to reduce the hemorrhage at the site of origin.

Seizures and convulsions can be prevented by administering pretreatment of benzodiazepine (e.g., 10 mg/kg of diazepam dissolved in propylene glycol and administered s.c.). It is very important that one monitors anesthesia closely as pre-administration of these compounds can contribute to anesthetic effect. Kainic acid has the greatest potential as an excitoxin to induce convulsions and seizures (24-h duration) while other neurotoxins (Quinolinic, quisqualic acids, or NMDA) lead to more acute seizures (3 h) without pretreatment. With pretreatment, these effects can be removed without causing an effect on the lesion.

Animals are typically given 7 days to recover from surgery. For 2 days following surgery, they received a dose of Metacam every 24 h and Buprenex every 12 h. Animals also received one dose per day (orally) of Doxycycline (Pfizer Labs, New York, NY) (5 mg/mL) for 3 weeks post-surgery. Animals have to be carefully monitored and possibly provided different diets following surgery or even tube fed. Lesions that damage midbrain and hindbrain regions require extensive postsurgical recovery care. For example, extensive lesions to midbrain dopamine cells require special feeding regimens that can include gastric intubations to allow the animals to recover. If body weight drops significantly after surgery, rats should be intubated with a liquid diet (sweetened condensed milk, water, and vitamins).

3.3 Analyzing Behavior

Typically the lesion approach involves a between-group design with animals that receive lesions compared to animals injected with the vehicle solution as controls. Dependent measures are compared using parametric statistics that typically include analysis of variance and pairwise *t*-tests. For example, latencies to bar press as a dependent measure can be compared between lesion and control groups to assess subjects' valuation of certain reward outcomes (e.g., sucrose solution). If the experimental question includes "lesion to area X alters reward valuation" then the prediction is that animals with lesions will show significantly reduced lever pressing and slower lever pressing latencies. One major problem with analyzing behavior after lesions is that other effects can occur that influence behavior but not directly influence reward processing. For example, motoric function could be compromised leading to a reduction in operant responding without directly altering the reward valuation of the organism. A number of methods are used to attempt to pinpoint effects of lesions in terms of reward processing: (1) use a battery of tests including basic motor and sensorimotor tests so that general motoric functions can be evaluated in all groups, (2) use a motor equivalent in the testing session so that the animals responding can still be observed yet lacking in direction or intensity as expected. One strategy is to use a response that does not provide reward or less reward and predict that the lesion will lead to equal levels of responding, yet the responses are now less selective in

terms of weighted toward the optimal outcome. (3) Perform a lesion control group possibly targeting a motor function more directly to compare a group with predicted motoric deficits. This final strategy would increase animal usage, yet in some studies, this lesion control can provide a possible "double dissociation" between neural regions with one group showing a deficit with one function and sparing of another while another lesion group demonstrates the opposite effect. This type of double dissociation is a strong test for localization and independence of neural substrates for diverse operations.

3.4 Histological Procedures

Animals are sacrificed under deep anesthesia by perfusing these solutions through the heart: (1) 50–100 mL of saline (0.9% sodium chloride in water) and (2) 300–400 mL of fixative containing paraformaldehyde and 0.1–1.0% glutaraldehyde in 0.1 M PBS (25°, pH 7.4). Remove the brains and store in 0.1 M PBS for 2–24 h (at 4°).

Block brain tissue leaving entire striatum or structure of interest. Obtain histological sections at 15–40 μm thick through the anterior–posterior extent of region of interest. Track order of tissue for mounting or storage. Using a sliding freezing microtome or cryostat, glutaraldehyde is omitted from the fixative and tissue needs to be cryoprotected by storing with sucrose in 0.1 M PBS (10–30% sucrose) at 4 °C until the brain sinks in solution.

Alternate slices can be saved for light microscopy analysis using cresyl violet staining, to label neuron cell bodies, and for glial fibrillary acidic protein immunoreactivity (GFAP-IR) staining, to label astrocytes. *Cresyl violet*: Slices are mounted directly onto gelatin-coated slides for Nissl staining. The slides are sequentially dipped in xylene and ethanol baths (70%, 95%, and 100%) for cleaning and defatting. After being dipped in cresyl violet, the slides are taken through the final set of alcohols and xylenes before coverslipping using permount. *GFAP-IR*: Slices are rinsed in three consecutive washes (PBS with 1% bovine serum albumin and 0.03% Triton X-100), transferred to 1.5 mL centrifuge tubes containing rabbit anti-GFAP (primary, diluted 1:500; Dako, Carpinteria, CA), and placed on a roto-torque to turn slowly for 20–24 h at 58 °C. The slices should be rinsed again, rotated for 1 h in peroxidase conjugated to goat anti-rabbit IgG (secondary, diluted 1:100; Dako), re-rinsed, and bathed in freshly prepared 3,3-diaminobenzidine tetrahydrochloride before mounting.

3.5 Lesion Mapping

3.5.1 Volumetric Analysis and Imaging of Lesion Area

One factor to take into account is regional shrinkage caused by the lesion. Larger regions or whole structures can be measured (e.g., horizontal and vertical distances of striatum) in both controls and animals with lesions. Shrinkage estimates for lesion groups and/or individual animals aid in determining accurate densities for neurons and volumes of lesions during mapping of damaged or targeted

area. Different methods include performing a volumetric analysis by marking out or drawing silhouettes using a drawing tube fitted to a microscope. Searching for the "bald spot" in a cresyl violet–stained section and using the needle track to aid in localizing the area. Surface area of the lesion can be computed using image analysis software (e.g., Image J) and then total lesion volume as an integral of section surface areas in which lesion was located (*see* Fig. 2; corrected or uncorrected for tissue shrinkage).

3.5.2 Quantitative Assessment of Lesions Using Stereological Lesion Analysis

There are diverse ways to quantify lesions. Cell counting is often used but one must be careful to use a technique that does not bias counts within regions, between brain areas or among subjects. We developed a modified fractionator procedure used to assess lesion size and it is carried out in three stages [37]. *Stage 1. Normal reference maps.* First, to obtain accurate normal baseline neuron averages, the striatopallidal region can be divided into fractions. We used 251 fractions to examine striatal and pallidal regions (*see* Fig. 3). The normal neuronal density of each fraction in control animals can be estimated by completing an exhaustive neuronal count on a "core sample" whose position is randomly chosen within the fraction. The microscope can be set at a high magnification (e.g., 400×), and all neurons within the core sample were counted using a computerized image-analysis system (JAVA, Jandel). Neuronal density varied in normal animals from 12 neurons per core sample in the globus pallidus to 154 neurons per core sample in certain fractions from the ventrolateral neostriatum; however, neuronal density never differed by >25% between different rats for the same fraction. This consistency in fraction neuronal number across animals allowed us to set a criterion for the detection of lesions. It meant that decrements in neuronal density significantly beyond 25% of the normal value for that fraction (e.g., by 50% or more) denoted pathological neuron loss. *Stage 2a. Lesion center identification.* "Moderate neuron loss" is judged to exist if a fraction lost at least 50% of its neurons. "Severe neuron loss" is judged to exist if the fraction had lost at least 80% of its neurons. Fractions that had the most severe neuron loss are labeled as the center of the lesion. *Stage 2b. Lesion border mapping.* Once the center of the lesion is located, eight radial arms emanating from the center along the major compass points (45°, 90°, 180°, etc.) are drawn using a video image analysis system (e.g., ImageJ). Core sample counts are taken along each line at 250 μm steps (see above) until the neuron density rises above 50% of the normal level for that fraction, which was labeled as the border of the lesion. *Stage 3. Subtraction of noncrucial sites of damage.* To identify a crucial site responsible for a deficit in reward processing, a composite map of total shared damage is first made. This is accomplished by adding the mapped lesions of each subject together, producing a large composite "group lesion." This site was *sufficient* to produce

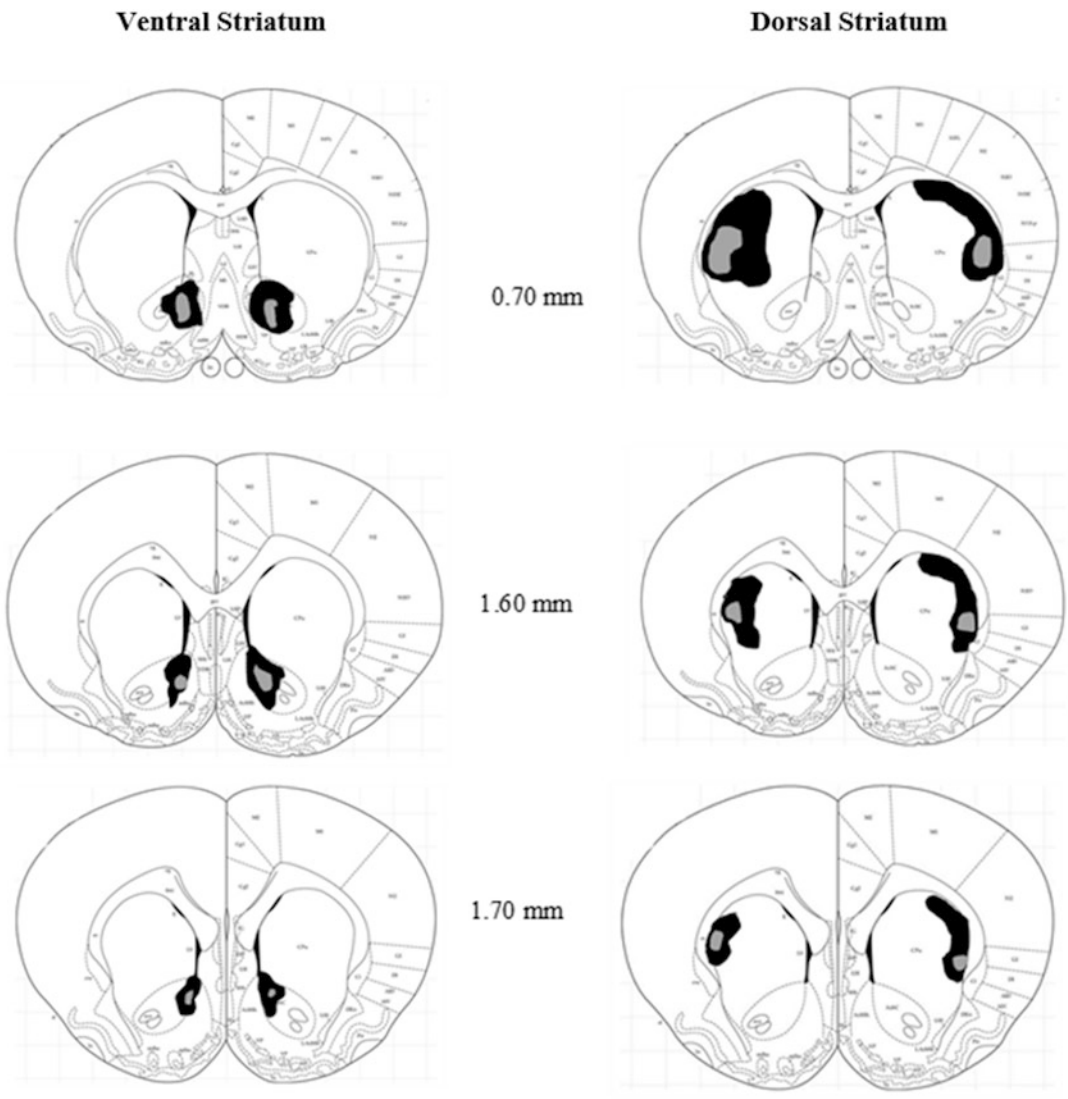

Fig. 2 Lesion analysis using qualitative observations. Various zones of damage determined by performing light microscopy analysis using cresyl violet stained sections. This volumetric analysis basically using a drawing tube to map areas of damage is noted by changes in cell density. Areas that had light staining relative to matched control sections were included for each subject. Maps of regions of cell loss were made for each section and these composite maps created. The numbers in the midline refer to millimeters from bregma in the anterior–posterior plane. This figure is modified from [17]

the deficit. Then areas in which only some of the symptomatic rats, but not others, had damage should be subtracted. These unshared areas, by definition, are undamaged in some symptomatic rats and thus are not strictly *necessary* for the behavioral deficit. The remaining composite lesion reveals a "crucial site" for producing deficits in reward processing following the lesion (*see* Figs. 4 and 5).

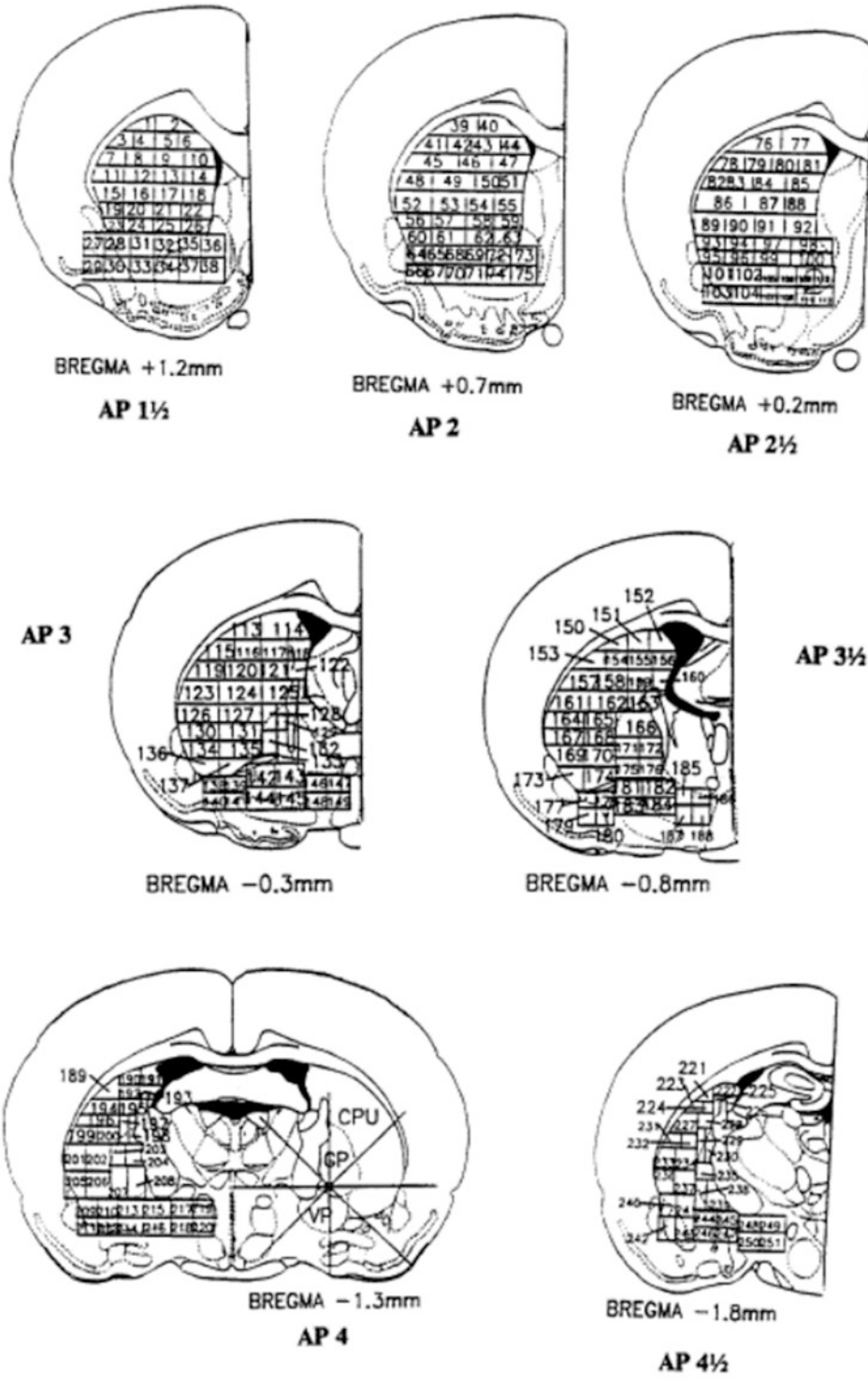

Fig. 3 Quantitative assessment of neuron loss divided brain region of striatopallidal area into different subregions. Map of fraction assignment within the striatopallidal system used for a modified fractionator

4 Notes and Conclusions

4.1 Value of the Lesion Approach

The lesion approach holds tremendous value when completed accurately and it can provide a way to connect brain regions to particular functions. Other methods including turning the brain on via stimulation (e.g., optogenetics) and monitoring activity (e.g., electrophysiology or Ca^{2+} imaging) are powerful and extremely useful but these techniques provide information on activity as a correlate linked to the functional process. These other methods provide great spatial and temporal precision, yet cannot identify the causal nature of the brain region activity to that particular function. The most effective approach to understand reward function is to combine diverse methods along with the lesion approach (*see* Fig. 6). Current use of transient inactivation or inhibition (via optogenetics) has been a key direction in the field. The standard lesion approach has advanced our understanding of neuroscience of reward function and contemporary work continues to challenge its basic tenets [56, 57]. For instance, dopamine as a key chemical mediator of hedonics has been replaced by dopamine acting as "craving agent" mediating sensitization process. Different nodes perform different key functions and specific neural subregions and neurochemicals are identified and linked to precise operations. Brain lesions producing clear deficits or obvious sparing provide a foundation to explore further functional neuroanatomy of brain circuits and determine more precisely neurochemical and neurophysiological substrates.

Interpreting results from lesion work is not trivial and functional dissociations can be due to more complex neural relationships. Tim Shallice presented an interesting view of dissociations and lesions from his own studies in neuropsychology [58]. Seemingly, functional dissociations could instead be differences in the degree of functional reliance on one subsystem versus another. Moreover, the two sites could function in a similar way yet the lesions did not target the overlapping region that could affect both regions. Lesion effects could vary from one site to another not solely based on the destruction of the inherent neural population but also because of changes to the interconnected circuit. These results would appear as a pure double dissociation but reflect more complicated functional neuroanatomy. Key psychological processes that involve emotion and motivation could overlap as a set of brain hotspots that operate in a dual manner. At one time point, a brain

Fig. 3 (continued) approach to lesion mapping. Neuronal densities can be calculated separately from core samples for each fraction. Baseline neuronal densities ranged from 12 neurons for fractions in the globus pallidus to >150 neurons in the ventrolateral neostriatum per core sample. For any given numbered fraction, however, neuronal density varied across different control rats by <25%. Modified from [44]

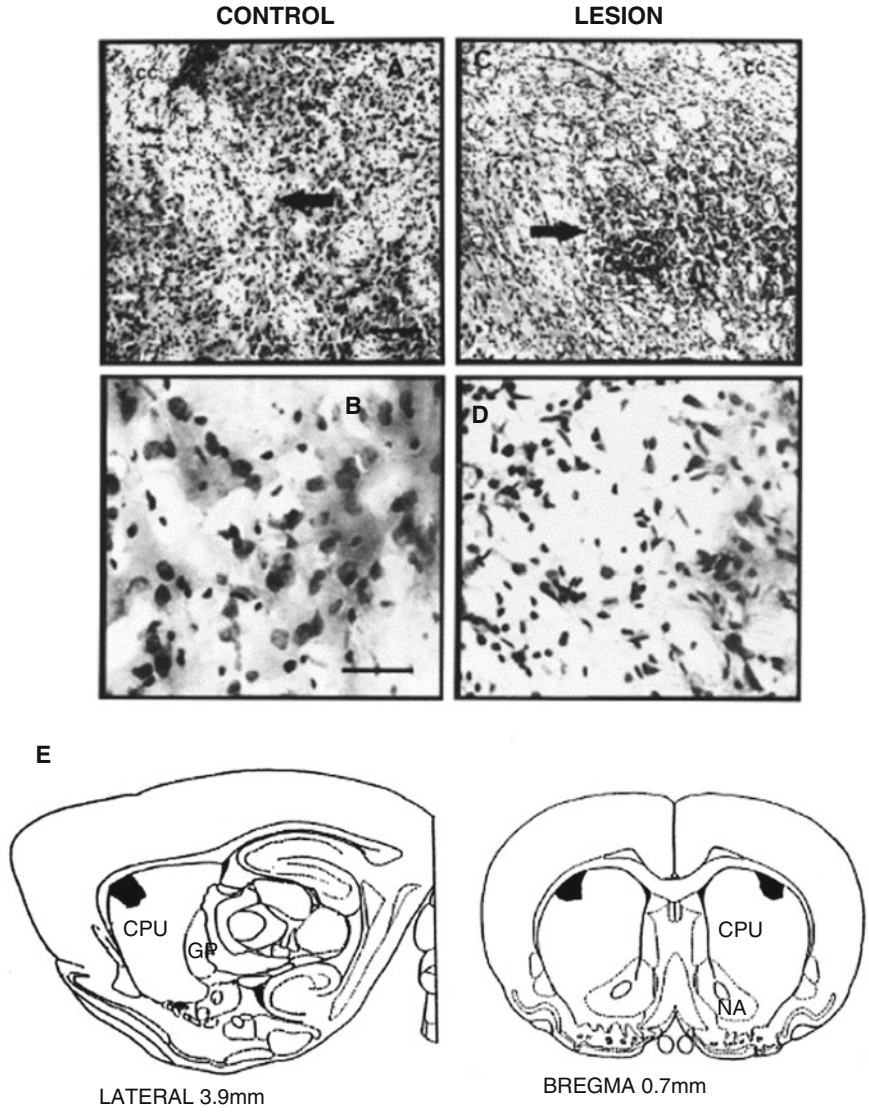

Fig. 4 Crucial lesion site and photomicrographs of lesions within the dorsolateral neostriatum. Photomicrographs show: (**a)** low magnification (10×) of the anterior dorsolateral neostriatum of a vehicle-injected control rat (*arrow* points to location of vehicle microinjection; *cc* denotes corpus callosum). (**b**) High magnification (40×) of the same anterior dorsolateral neostriatal region in vehicle-injected control rat. Note lack of neuronal death. (**c**) Low magnification of anterior dorsolateral neostriatum in rat that received an excitotoxin lesion and had impaired grooming syntax. (*Arrow* points to center of excitotoxin lesion; *cc* denotes corpus callosum). (**d**) High magnification of dorsolateral neostriatum after an excitotoxin lesion that impaired grooming syntax. Note paucity of neurons compared with those in **b**. Scale bars: **a** and **c**, 140 mm; **b** and **d**, 40 mm. (**e**) Map of the crucial "grooming syntax site." Atlas view shows boundaries of the lesion site, identified by the modified fractionator procedure. Figure modified from [44]

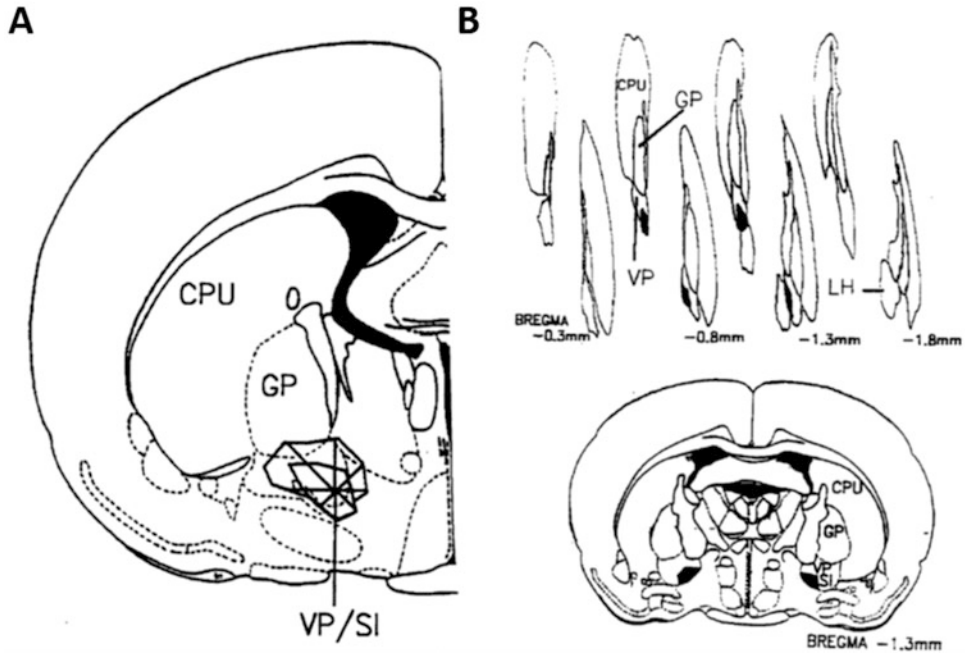

Fig. 5 Different views of the lesion using the coronal section from the stereotaxic atlas of the rat brain. (**a**) One AP section with the core damage region and the cellular damage emanating away from core in the major compass directions. (**b**) On top is the three-dimensional representation of the lesion with the core site mapped from front to back. Below is the single site with the greatest damage contained by all animals. Figure was modified from [36]

area performs key operations involved in affective states while at another involved in primary motivational states. The different operations can be merged or dissociated depending upon the type or intensity of intrinsic and extrinsic activity. Interpreting lesion outcomes is more complicated as research highlights multilevel systems in which brain subregions operate at several levels and damage can cause diverse effects depending upon the neural population and connections involved [58].

4.2 Notes on Method: Straying from the Typical Method

Cautionary notes include taking care to monitor the pH of the solution prior to use. Certain toxins do not dissolve properly if the pH is not within the range of 7–8 and the lower the pH, the less effective the solution will be in making the lesion in terms of actual damage (transporting the toxin) and in terms of creating nonspecific damage via acidosis-induced tissue reactions.

It is important to note that certain anesthetics could affect the excitotoxin and reduce or influence the degree of neuronal damage [59]. Inhalant anesthesia (isoflurane) has been found to have little impact on the local neuronal damage. Barbiturate anesthesia has been shown to reduce the lesion effect and other compounds have mixed results depending upon the dose and volume of injection.

Fig. 6 Diverse methods to understand processing of reward information. Lesion methods fit into "turning the brain off" and combine with other approaches that either turn the brain on (stimulation techniques) or monitor activity (e.g., CA^{2+} and optical imaging). Of course, new techniques transiently inactivate cell groups (inhibition used in optogenetics and DREAD). These techniques advance information gathering to new, sophisticated levels. Negative results from these means to TURN ON or MONITOR may not mean the brain structure is not necessary, but instead mean that specific connections or cell groups are not necessary or completely uninvolved

The microinjection method must be monitored. Air pockets in tubing have to be removed and needles can become impacted or clogged by tissue or blood. The patency of fluid flow should be checked often. Finally, do test animals after varying recovery time following the lesion. This could impact the behavioral results as differing recovery time could enable those that recover longer have differences in adaptive changes to the lesion compared to those tested sooner post-surgery. All animals should be tested at the same period to reduce this confound. This becomes difficult as cohorts of animals can be large and testing procedures require strict timing and durations. In some cases, the recovery of individuals is complicated and requires more time due to health reasons. Often times, these animals are excluded from the study for this reason. The different compounds provided following surgery have not been examined in much detail in terms of influencing behavioral results. Postoperative medicines and analgesics could alter aspects of brain function and indirectly change the lesion sequelae and related reward processing. For example, antibiotics provided post-surgery either routine or after an infection could alter the microbiome [60]. This exposure could change the way the gut–brain axis operates and plays a role in subsequent behavioral findings when testing the reward process [61]. Lesion mapping is not trivial and the methods provided can be time-consuming (stereological approach estimating cell numbers of fractions of a brain structure) and lead to

overestimating the importance of a crucial site involved in a reward function [62–64]. When pairing glial fibrillary acidic protein IHC with the lesion mapping of Nissl stained sections, reactive gliosis can be seen as relatively larger spheres that encompass the crucial site [65, 66]. Overlapping the sites of astrocyte reaction to the lesion provides a larger zone of damage and extends the crucial site into a larger domain.

4.3 Problems and Limitations of the Approach

There are problems inherent in every approach and lesion methods are no exception. One important problem is nontarget or remote lesions or brain damage occurring outside of the target area. This could occur either because the injection site was missed and another brain site was directly impacted by the surgery or because the initial target stimulation and damage led to remote damage. The nontarget direct damage arises mainly from the surgical procedures and use of the stereotaxic to guide the injection needle. This misdirection of microinjection could occur with any method that utilizes this approach. In any neurosurgical implantation/injection procedure, the stereotaxic guidance is of the utmost importance to carefully check and recheck coordinates and ensure target accuracy. This includes all facets from placing animals accurately in the earbars, to recording the coordinates, measuring the location for the injection, and ensuring that the skull is flat for proper depth in the dorsoventral plane. These aspects all work together to produce an accurate lesion of the target region.

Remote damage is a second major problem that could be more pervasive than what researchers realize. Typically, the procedures that include lesion mapping do not check for damage outside of a small proximal zone around the target region. Remote damage could be occurring in connected regions unchecked. This remote damage is not accounted for by spread of the neurotoxin but could arise because of overstimulation of a pathway that leads to damage in an interconnected site. If seizures are not well controlled, remote site damage could be due to brain injury (i.e., anoxia) during the seizure activity. Some brain regions such as the hippocampus seem to be more vulnerable to remote damage and research has found evidence that this damage is related to a history of seizure-like neural activity [67]. Lesions lead to diverse compensatory changes both locally and globally [68, 69].

Within-subject design is a rare feature in lesion work. Between-group design with animal lesion group compared to vehicle-injected sham control animals is common. Differences in pre-lesion behavior and variability between the groups can lead to spurious results. Another possible confound is variability of behavioral compensation following the brain lesion [70]. This could be related to the extent of the lesion or pre-lesion characteristics of the animal subject. How the brain adapts or changes after a lesion is a separate and typically independent area of research removed from

basic science of the study of reward process. Yet, the two could intermix in studies that want to examine how reward processing is defective and how brain changes could occur to ameliorate or compensate for lost functions or subfunctions.

4.4 Future Directions in Lesion Making

The future directions include more precise and sophisticated ways to make lesions and target specific connections and cell types [71]. In order to convert a standard lesion study to a within-subject model, other methods that include transient inactivation and chemogenetic manipulations could be used. These manipulation procedures can both increase and decrease brain activity to determine bidirectional effects of brain–behavior relationships. The specificity of new methods that target specific neuron subtypes and receptor populations is growing tremendously [72]. The advances are allowing for new insights into how select populations of neurons are working to process reward information [73]. In some cases, newer methods or other methods find conflicting results when compared to findings from lesion studies. Electrophysiology of the striatum has found neural activity related to reward processing and relative reward valuation in all subregions of the caudate nucleus and putamen in the primate model [74–77]. In the rat model, neurophysiology of single units has also obtained relative reward processing units and similarity across subregions in paradigms that test reward functions using instrumental responding [11, 78]. Functional homogeneity is infrequent in lesion studies, while heterogeneity is the norm [37, 44]. One method (electrophysiology) captures a signal widely broadcast while another method (lesion) can pinpoint the localization of function. Future directions should attempt to discover how these different methods can be used together to unravel the complex nature of brain function as it encodes and utilizes reward representations.

4.5 Reward Process Revisited

Combining diverse behavioral neuroscience methods is the best approach toward understanding how rewards are represented in the brain and how they influence behavior. Not surprisingly, different methods can provide very different pictures for brain localization of function. Examining reward is examining a process with diverse steps and components. Rewards are mainly external objects, outcomes, and events. They include complex things like conspecifics and interactive, multistep actions. As a process, rewards can have innate value and can involve innate actions themselves. They can depend heavily on context or the availability of other options or rewards. What is rewarding changes and what is a reward can be diverse in scope. Reward can be the behavior itself, the outcome, or the context experienced. Recently, we found that variety context effects influence behavior within a session as animals are exposed to different strings or bundles of more or less variety [79]. These types of influences are difficult to tease apart and examine. The lesion

approach would be searching for neural ensembles that encode variety as a reward [77]. As stated earlier, the behavioral paradigms need to catch up in many ways to the sophisticated neuroscience methods. The lesion method enables the researcher to utilize behavioral paradigms that can allow the organism to forage, perform "free" operants, and socially interact, yet the limitations that involve extent and precision of damage and the impact of recovery detracts from the approach [17]. Also the movement into examining real-time activity in diverse ways and manipulating smaller subregions more precisely overshadow and reduce the information gained from the standard lesion procedure. The classic approach is highly useful when combined with other approaches and provides a solid, first step toward understanding the role of brain circuitry in the myriad of functions involved in processing of reward information.

References

1. Craig W (1918) Appetites and aversions as constituents of instinct. Biol Bull 34:91–107
2. Panksepp J (1998) Affective neuroscience. Oxford University, Oxford, UK
3. Schultz W (2019) Recent advances in understanding the role of phasic dopamine activity. F1000Res 8: F1000 faculty Rev-1680. https://doi.org/10.12688/f1000research.19793.1. eCollection 2019
4. White NM (2011) Reward: what is it? How can it be inferred from behavior? In: Gottfried JA (ed) Neurobiology of sensation and reward. CRC Press/Taylor & Francis, Boca Raton, FL
5. Ferster CB (1953) The use of the free operant in the analysis of behavior. Psychol Bull 50 (4):263–274
6. Balleine BW, Killcross AS, Dickinson A (2003) The effect of lesions of the basolateral amygdala on instrumental conditioning. J Neurosci 23(2):666–675
7. Ouachikh O, Dieb W, Durif F et al (2013) Differential behavioral reinforcement effects of dopamine receptor agonists in the rat with bilateral lesion of the posterior ventral tegmental area. Behav Brain Res 252:24–31. https://doi.org/10.1016/j.bbr.2013.05.042
8. Skelin I, Hakstol R, VanOyen J et al (2014) Lesions of dorsal striatum eliminate lose-switch responding but not mixed-response strategies in rats. Eur J Neurosci 39(10):1655–1663. https://doi.org/10.1111/ejn.12518
9. Ricker JM, Hatch JD, Powers DD et al (2016) Fractionating choice: a study on reward discrimination, preference, and relative valuation in the rat (Rattus norvegicus). J Comp Psychol 130(2):174–186. https://doi.org/10.1037/com0000034
10. Webber ES, Chambers NE, Kostek JA et al (2015) Relative reward effects on operant behavior: incentive contrast, induction and variety effects. Behav Process 116:87–99. https://doi.org/10.1016/j.beproc.2015.05.003
11. Webber ES, Mankin DE, Cromwell HC (2016) Striatal activity and reward relativity: neural signals encoding dynamic outcome valuation. eNeuro 3(5):ENEURO.0022-16.2016. https://doi.org/10.1523/ENEURO.0022-16.2016
12. Lindsley O (1996) The four free-operant freedoms. Behav Anal 19(2):199–210. https://doi.org/10.1007/BF03393164
13. Berridge KC, Robinson TE (2016) Liking, wanting, and the incentive-sensitization theory of addiction. Am Psychol 71(8):670–679
14. Robinson TE, Berridge KC (1993) The neural basis of drug craving: an incentive-sensitization theory of addiction. Brain Res Brain Res Rev 18(3):247–291
15. Berridge KC, Robinson TE (1998) What is the role of dopamine in reward: hedonic impact, reward learning, or incentive salience? Brain Res Brain Res Rev 28(3):309–369
16. Berridge KC, Robinson TE (2003) Parsing reward. Trends Neurosci 26(9):507–513
17. Ricker JM, Kopchock RJ 3rd, Drown RM et al (2016) Effects of striatal lesions on components of choice: reward discrimination,

preference, and relative valuation. Behav Brain Res 315:130–140. https://doi.org/10.1016/j.bbr.2016.08.031

18. Krakauer JW, Ghazanfar AA, Gomez-Marin A et al (2017) Neuroscience needs behavior: correcting a reductionist Bias. Neuron 93 (3):480–490
19. Olney JW (1969) Brain lesions, obesity, and other disturbances in mice treated with monosodium glutamate. Science 164 (3880):719–721. https://doi.org/10.1126/science.164.3880.719
20. Winn P, Tarbuck A, Dunnett SB (1984) Ibotenic acid lesions of the lateral hypothalamus: comparison with the electrolytic lesion syndrome. Neuroscience 12(1):225–240
21. Winn P, Stone TW, Latimer M et al (1991) A comparison of excitotoxic lesions of the basal forebrain by kainate, quinolinate, ibotenate, N-methyl-D-aspartate or quisqualate, and the effects on toxicity of 2-amino-5-phosphonovaleric acid and kynurenic acid in the rat. Br J Pharmacol 102(4):904–908. https://doi.org/10.1111/j.1476-5381.1991.tb12274.x
22. Rothman SM, Olney JW (1986) Glutamate and the pathophysiology of hypoxic--ischemic brain damage. Ann Neurol 19(2):105–111. https://doi.org/10.1002/ana.410190202
23. Rothman SM, Olney JW (1995) Excitotoxicity and the NMDA receptor--still lethal after eight years. Trends Neurosci 18(2):57–58
24. Robbins TW, Everitt BJ, Marston HM et al (1989) Comparative effects of ibotenic acid- and quisqualic acid-induced lesions of the substantia innominata on attentional function in the rat: further implications for the role of the cholinergic neurons of the nucleus basalis in cognitive processes. Behav Brain Res 35 (3):221–240
25. Pappas BA, Sherren N (2003) Neonatal 192 IgG-saporin lesion of forebrain cholinergic neurons: focus on the life span? Neurosci Biobehav Rev 27(4):365–376
26. Coffey PJ, Perry VH, Allen Y et al (1988) Ibotenic acid induced demyelination in the central nervous system: a consequence of a local inflammatory response. Neurosci Lett 84 (2):178–184
27. Coffey PJ, Perry VH, Rawlins JN (1990) An investigation into the early stages of the inflammatory response following ibotenic acid-induced neuronal degeneration. Neuroscience 35(1):121–132
28. Tambasco N, Romoli M, Calabresi P (2018) Selective basal ganglia vulnerability to energy deprivation: experimental and clinical evidences. Prog Neurobiol 169:55–75
29. Roberts RC, Ahn A, Swartz KJ et al (1993) Intrastriatal injections of quinolinic acid or kainic acid: differential patterns of cell survival and the effects of data analysis on outcome. Exp Neurol 124(2):274–282
30. Beal MF, Ferrante RJ, Swartz KJ et al (1991) Chronic quinolinic acid lesions in rats closely resemble Huntington's disease. J Neurosci 11 (6):1649–1659
31. Vecsei L, Beal MF (1991) Comparative behavioral and neurochemical studies with striatal kainic acid- or quinolinic acid-lesioned rats. Pharmacol Biochem Behav 39(2):473–478
32. Tronci E, Francardo V (2018) Animal models of L-DOPA-induced dyskinesia: the 6-OHDA-lesioned rat and mouse. J Neural Transm (Vienna) 125(8):1137–1144. https://doi.org/10.1007/s00702-017-1825-5
33. Stellar E, Corbit JD (1973) Neural control of motivated behavior. Neurosci Res Program Bull 11(4):296–410
34. Elmquist JK, Elias CF, Saper CB (1999) From lesions to leptin: hypothalamic control of food intake and body weight. Neuron 22 (2):221–232
35. Ho C, Berridge KC (2014) Excessive disgust caused by brain lesions or temporary inactivations: mapping hotspots of the nucleus accumbens and ventral pallidum. Eur J Neurosci 40 (10):3556–3572. https://doi.org/10.1111/ejn.12720
36. Cromwell HC, Berridge KC (1993) Where does damage lead to enhanced food aversion: the ventral pallidum/substantia innominata or lateral hypothalamus? Brain Res 624 (1-2):1–10
37. Cromwell HC, Berridge KC (1994) Mapping of globus pallidus and ventral pallidum lesions that produce hyperkinetic treading. Brain Res 668(1-2):16–29
38. Berridge KC, Cromwell HC (1990) Motivational-sensorimotor interaction controls aphagia and exaggerated treading after striatopallidal lesions. Behav Neurosci 104 (5):778–795
39. Mogenson GJ, Jones DL, Yim CY (1980) From motivation to action: functional interface between the limbic system and the motor system. Prog Neurobiol 14(2-3):69–97
40. Berridge KC (2004) Motivation concepts in behavioral neuroscience. Physiol Behav 81 (2):179–209. https://doi.org/10.1016/j.physbeh.2004.02.004
41. Grospe GM, Baker PM, Ragozzino ME (2018) Cognitive flexibility deficits following 6-OHDA lesions of the rat dorsomedial striatum. Neuroscience 374:80–90

42. Pooters T, Gantois I, Vermaercke B et al (2016) Inability to acquire spatial information and deploy spatial search strategies in mice with lesions in dorsomedial striatum. Behav Brain Res 298(Pt B):134–141. https://doi.org/10.1016/j.bbr.2015.11.001
43. Tait DS, Phillips JM, Blackwell AD et al (2017) Effects of lesions of the subthalamic nucleus/zona incerta area and dorsomedial striatum on attentional set-shifting in the rat. Neuroscience 345:287–296
44. Cromwell HC, Berridge KC (1996) Implementation of action sequences by a neostriatal site: a lesion mapping study of grooming syntax. J Neurosci 16(10):3444–3458
45. Hawes SL, Evans RC, Unruh BA et al (2015) Multimodal plasticity in dorsal striatum while learning a lateralized navigation task. J Neurosci 35(29):10535–10549. https://doi.org/10.1523/JNEUROSCI.4415-14.2015
46. Pisa M (1988) Motor somatotopy in the striatum of rat: manipulation, biting and gait. Behav Brain Res 27(1):21–35
47. Thapa R, Gruber AJ (2018) Lesions of ventrolateral striatum eliminate lose-shift but not win-stay behaviour in rats. Neurobiol Learn Mem 155:446–451
48. Burgdorf J, Wood PL, Kroes RA et al (2007) Neurobiology of 50-kHz ultrasonic vocalizations in rats: electrode mapping, lesion, and pharmacology studies. Behav Brain Res 182(2):274–283
49. Maldonado-Irizarry CS, Kelley AE (1995) Excitotoxic lesions of the core and shell subregions of the nucleus accumbens differentially disrupt body weight regulation and motor activity in rat. Brain Res Bull 38(6):551–559
50. Richard JM, Castro DC, Difeliceantonio AG et al (2013) Mapping brain circuits of reward and motivation: in the footsteps of Ann Kelley. Neurosci Biobehav Rev 37(9 Pt A):1919–1931. https://doi.org/10.1016/j.neubiorev.2012.12.008
51. Sato C, Hoshino M, Ikumi N et al (2014) Contribution of nucleus accumbens core (AcbC) to behavior control during a learned resting period: introduction of a novel task and lesion experiments. PLoS One 9(4):e95941. https://doi.org/10.1371/journal.pone.0095941
52. Brock KA (2001) Preanaesthetic use of atropine in small animals. Aust Vet J 79(1):24–25. https://doi.org/10.1111/j.1751-0813.2001.tb10632.x
53. Paxinos G, Watson C (2007) The rat brain in stereotaxic coordinates, 6th edn. Academic Press, New York, NY
54. Hernadi I, Karadi Z, Vigh J et al (2000) Alterations of conditioned taste aversion after microiontophoretically applied neurotoxins in the medial prefrontal cortex of the rat. Brain Res Bull 53(6):751–758
55. Berta B, Peczely L, Kertes E et al (2018) Iontophoretic microlesions with kainate or 6-hydroxidopamine in ventromedial prefrontal cortex result in deficit in conditioned taste avoidance to palatable tastants. Brain Res Bull 143:106–115
56. Murray EA, Rudebeck PH (2018) Specializations for reward-guided decision-making in the primate ventral prefrontal cortex. Nat Rev Neurosci 19(7):404–417. https://doi.org/10.1038/s41583-018-0013-4
57. Noonan MP, Kolling N, Walton ME et al (2012) Re-evaluating the role of the orbitofrontal cortex in reward and reinforcement. Eur J Neurosci 35(7):997–1010. https://doi.org/10.1111/j.1460-9568.2012.08023.x
58. Shallice T (1988) From neuropsychology to mental structure. Cambridge University Press, Cambridge, UK
59. Karmarkar SW, Bottum KM, Tischkau SA (2010) Considerations for the use of anesthetics in neurotoxicity studies. Comp Med 60(4):256–262
60. Krezalek MA, Alverdy JC (2016) The role of the microbiota in surgical recovery. Curr Opin Clin Nutr Metab Care 19(5):347–352. https://doi.org/10.1097/MCO.0000000000000299
61. Gonzalez-Arancibia C, Urrutia-Pinones J, Illanes-Gonzalez J et al (2019) Do your gut microbes affect your brain dopamine? Psychopharmacology 236(5):1611–1622. https://doi.org/10.1007/s00213-019-05265-5
62. Deniz OG, Altun G, Kaplan AA et al (2018) A concise review of optical, physical and isotropic fractionator techniques in neuroscience studies, including recent developments. J Neurosci Methods 310:45–53
63. Napper RMA (2018) Total number is important: using the disector method in design-based stereology to understand the structure of the rodent brain. Front Neuroanat 12:16. https://doi.org/10.3389/fnana.2018.00016
64. Yurt KK, Kivrak EG, Altun G et al (2018) A brief update on physical and optical disector applications and sectioning-staining methods in neuroscience. J Chem Neuroanat 93:16–29
65. Ceresoli G, Fuller MS, Schwarcz R (1996) Excitotoxic lesions of the rat striatum: different responses of kynurenine pathway enzymes during ontogeny. Brain Res Dev Brain Res 92(1):61–69

66. Guncova I, Latr I, Mazurova Y (2011) The neurodegenerative process in a neurotoxic rat model and in patients with Huntington's disease: histopathological parallels and differences. Acta Histochem 113(8):783–792. https://doi.org/10.1016/j.acthis.2010.11.007
67. Schwarcz R, Kohler C (1983) Differential vulnerability of central neurons of the rat to quinolinic acid. Neurosci Lett 38(1):85–90
68. Cruz-Aguado R, Francis-Turner L, Diaz CM et al (2000) Quinolinic acid lesion induces changes in rat striatal glutathione metabolism. Neurochem Int 37(1):53–60
69. Andersson K, Schwarcz R, Fuxe K (1980) Compensatory bilateral changes in dopamine turnover after striatal kainate lesion. Nature 283(5742):94–96. https://doi.org/10.1038/283094a0
70. Schwarting RK, Busse S (2017) Behavioral facilitation after hippocampal lesion: a review. Behav Brain Res 317:401–414
71. Mahler SV, Vazey EM, Beckley JT et al (2014) Designer receptors show role for ventral pallidum input to ventral tegmental area in cocaine seeking. Nat Neurosci 17(4):577–585. https://doi.org/10.1038/nn.3664
72. Campbell EJ, Marchant NJ (2018) The use of chemogenetics in behavioural neuroscience: receptor variants, targeting approaches and caveats. Br J Pharmacol 175(7):994–1003. https://doi.org/10.1111/bph.14146
73. Sternson SM, Roth BL (2014) Chemogenetic tools to interrogate brain functions. Annu Rev Neurosci 37:387–407. https://doi.org/10.1146/annurev-neuro-071013-014048
74. Cromwell HC, Hassani OK, Schultz W (2005) Relative reward processing in primate striatum. Exp Brain Res 162(4):520–525. https://doi.org/10.1007/s00221-005-2223-z
75. Cromwell HC, Schultz W (2003) Effects of expectations for different reward magnitudes on neuronal activity in primate striatum. J Neurophysiol 89(5):2823–2838. https://doi.org/10.1152/jn.01014.2002
76. Hassani OK, Cromwell HC, Schultz W (2001) Influence of expectation of different rewards on behavior-related neuronal activity in the striatum. J Neurophysiol 85(6):2477–2489
77. Cromwell HC, Tremblay L, Schultz W (2018) Neural encoding of choice during a delayed response task in primate striatum and orbitofrontal cortex. Exp Brain Res 236(6):1679–1688. https://doi.org/10.1007/s00221-018-5253-z
78. Cromwell HC, Klein A, Mears RP (2007) Single unit and population responses during inhibitory gating of striatal activity in freely moving rats. Neuroscience 146(1):69–85
79. Halverstadt BA, Cromwell HC (2019) An investigation of variety effects during operant responding in the rat utilizing different reward flavors. Appetite 134:50–58

Part II

Neurochemical, Behavioral, and Chemogenetic Techniques

Chapter 4

Assessment of Adult Hippocampal Neurogenesis: Implication for Neurodegenerative Diseases and Neurological Disorders

Farah Chamaa, Batoul Darwish, Nayef E. Saadé, and Wassim Abou-Kheir

Abstract

Adult neurogenesis is a lifelong developmental process primarily described as the division of neural stem cells in order to generate new neurons. These stem cells predominantly reside in two well-defined areas of the mammalian brain: the subventricular zone (SVZ) along the lateral ventricles and the subgranular zone of the dentate gyrus (DG) in the hippocampus. Given the importance of this process in understanding structural and functional neuronal plasticity as well as its implications in neurodegenerative diseases and psychiatric disorders, several studies investigate adult neurogenesis. Here, we describe how to assess neurogenesis in the DG of adult rats. This chapter will mainly explain the steps needed to quantify proliferating stem/progenitor cells and the cells that ultimately differentiate into neurons.

Key words Adult neurogenesis, Stem/progenitor cells, Dentate gyrus, Hippocampus

1 Introduction: Adult Neurogenesis

Adult neurogenesis, the persistent birth of new neurons in the adult brain, was initially observed in the subgranular zone (SGZ) of the dentate gyrus (DG) in the hippocampus [1, 2], and later on in the subventricular zone (SVZ) lining the lateral ventricles [3–6]. These two areas house multipotent self-renewing stem/progenitor cells (NSPCs) and they provide a desirable microenvironment for generating new functional neurons [7–9]. Adult neurogenesis in the hippocampus emerges in the SGZ, principally considered the germinal layer with a stem cell-containing niche [1, 10, 11]. This thin layer provides a unique milieu that is permissive for the proliferation and differentiation of radial glia-like type 1 stem cells to generate newly integrated as well as functional granule cells [12] (*see* Fig. 1). The process starts with the activation of type 1 cells to produce non-radial proliferating transit-amplifying cells (TAPs) needed for the amplification of the neurogenic pool. In turn, these type-2 cells

Marc Fakhoury (ed.), *The Brain Reward System*, Neuromethods, vol. 165, https://doi.org/10.1007/978-1-0716-1146-3_4,

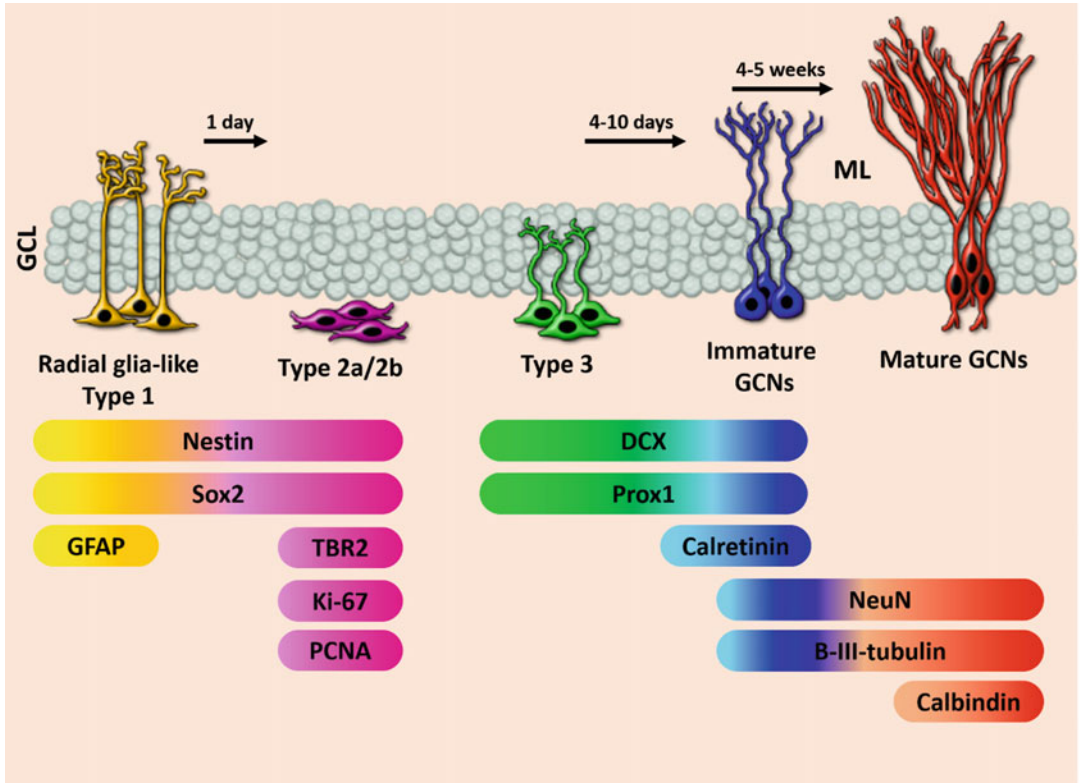

Fig. 1 Maturation of Neural Stem Cells in the DG. Radial glia-like type 1 cells express Nestin, Sox-2, and GFAP. They produce type-2 cells that loose GFAP and gain the expression of TBR2, Ki-67, and PCNA. These cells differentiate into type 3 and immature neurons that migrate short distances into the granule cell layer (GCL) and start expressing DCX and Prox1. Immature granule cell neurons (GCNs) express calretinin. Around 4–5 weeks of maturation are needed for cells to become functional dentate granule cell neurons expressing NeuN, B-III-tubulin, and Calbindin. The migration process is accompanied by the branching out of processes into the molecular layer (ML)

differentiate into immature neurons that migrate short distances into the granule cell layer (GCL). During maturation, the granule cells express distinct markers that help in the classification of the different developmental stages [13]. Radial glia-like type 1 cell send apical processes through the GCL to branch out into the molecular layer (ML) and they usually express markers such as Nestin, Sox2, and GFAP. These stem cells do not undergo frequent divisions, but whenever they do, they undergo an asymmetrical division to produce two types of cells; a self-renewed neural stem cell and an intermediate progenitor cell (IPC) [14]. IPCs are the type 2 cells that have short processes and undergo rapid proliferation. They usually express TBR2 in addition to Nestin and Sox2. As these cells proliferate, they generate type 3 cells that lose TBR2 expression and gain the immature neuronal markers, namely DCX and Prox1. Here is where they become committed to the neuronal lineage

and they start developing a short vertical process. Once differentiated into mature granule cells GCs, they express the neuronal markers NeuN and Calbindin where these mature cells extend their axons into the CA3 region of the hippocampus and branch their dendrites into the molecular layer (*see* Fig. 1). The whole maturation process needs around 4–5 weeks for cells to become functional dentate granule cell neurons [9, 15]. Such a process is highly regulated and systematically affected by each step, starting from the cellular activity and ending in the connectivity within preexisting networks [16–20]. Throughout this process, 50% or even more of the cells do not reach maturation [21–24]. They undergo active apoptosis and are selectively eliminated during the first few weeks [25, 26]. The rest of the cells, however, develop synapses and form interconnections that increase their chances of survival [27, 28]. Therefore, this process creates a kind of balance between apoptosis and survival, and it is properly controlled by the milieu of neuronal activity and by cognitive experiences [29]. The newly integrated neurons play an active role in influencing hippocampal functions of learning and memory as well as spatio-motor performances. Adding new neurons might provide a neural pool for accommodating new experiences, enduring anxiety or stress, and possibly preventing neurodegeneration [30, 31].

Neurodegenerative diseases such as Parkinson's disease (PD), Alzheimer's disease (AD), and Huntington's diseases (HD) are highly associated with alterations in adult neurogenesis. This was reported by multiple studies based on different animal models showing that neurodegenerative diseases may induce impairments in adult neurogenesis through alterations in the fate of stem cells or through modulation of synaptic plasticity and brain morphology [32–34]. Moreover, some of the early symptoms of neurodegenerative diseases frequently include depression, anxiety, and cognitive dysfunctions; collectively linked to the hippocampus [35–37]. This is in addition to the neurogenesis-related dysfunctions in mood and psychiatric disorders, where postmortem examination of the brains of schizophrenic patients showed lower numbers of proliferating stem cells in the hippocampus [38]. It has also been shown that neurogenesis is decreased with stress or depression, and increased with antidepressant treatment [39]. Interestingly, different lines of evidence showed that neurogenesis, enhanced through exercise or by genetic and pharmacological manipulation, reduces anxiety and depressant-like behavior [40, 41]. Further work and studies are still needed to clarify the connection between neurogenesis and neurodegenerative diseases as well as psychiatric disorders. Hence, thorough and controlled research in animal models is important as it reveals how neurogenesis gets impacted by psychiatric disorders or neurodegenerative diseases and how different treatments might reverse that.

1.1 Methods to Study Adult Neurogenesis

Joseph Altman reported the first observation of adult neurogenesis in rats in the 1960s. However, the experimental evidence provided at the time was not vigorous enough especially that this was a new concept and seemed improbable. Altman used tritiated thymidine (3HT) as a marker for cellular proliferation and detected neurogenesis by autoradiography [42]. He then used electron microscopy to prove that the cells labeled with 3HT are new neurons, and thereby confirmed the existence of neurogenesis in rodents [43, 44]. Evidence of neurogenesis in songbirds was then reported [45], and thereafter, more studies were conducted that further supported the existence of neurogenesis in different animal models. Bromodeoxyuridine (BrdU) was then discovered as a synthetic thymidine analog that is nonradioactive and can be administered either orally or intraperitoneally [46]. During cellular division, BrdU is incorporated into newly synthesized DNA and can be detected by a specific antibody. It can be used in conjugation with other cellular markers in order to confirm the neuronal identity of proliferating cells. BrdU was primarily used in human cancer research for the estimation of tumor growth [47]. It was identified in the adult human brain after investigation of post mortem brain samples of cancer patients who received BrdU for therapeutic purposes [10]. This was the first report to provide affirmative evidence of adult neurogenesis in the human brain. Further evidences were reported by other studies, which identified protein markers for the different stages of neurogenesis [48, 49]. All of those studies used immunohistochemistry to identify neurogenesis markers in postmortem brains. Electron microscopy has also been used to look for the detailed shape of newly born neurons [50]. A different methodology for the detection of neurogenesis relied on measuring the concentration of radioactive carbon (^{14}C) which is present in the environment and gets incorporated into the DNA of dividing cells [51]. Moreover, its concentration is accurately estimated and can be used to study the retrospective birth dating of neuronal cells in the brain. Accordingly, this carbon dating method showed that there is a steady dynamics of neurogenesis during adulthood in the human brain [52]. Additional reports either supported this evidence [48, 53, 54] or criticized it as being false signals for neurogenesis [50]. This discrepancy highlights the fact that the concept of neurogenesis, in humans at least, is uncertain, and more robust evidence is still required. The sparsity of human postmortem tissues and high variability in the results of postmortem studies are major limitations for studying neurogenesis in humans. Such variability can be attributed to the quality of the tissues at the time of staining, sample processing, the duration and latency for tissue fixation, and confounding factors such as the age of the deceased person and having neurodegenerative diseases or epilepsy [55]. Thus, until more advanced techniques are available for studying neurogenesis in humans, studies on animals remain crucial and are the basis that

provided important insight on the dynamics of neurogenesis and its regulation in response to many factors.

2 Materials

2.1 Animals

We used adult male or female Sprague Dawley rats weighing 250–300 g. All animals were housed in a controlled environment with a 12 h light/dark cycle, at a constant temperature of 23 ± 2 °C, along with standard rodent chow and water provided ad libitum. For the sake of studying the proliferation of stem/progenitor cells, animals were sacrificed 1 day after BrdU injection. To study neurogenesis, animals were sacrificed 4 weeks after BrdU injection.

2.2 BrdU Preparation

BrdU powder (Sigma-Aldrich, B5002) was weighed and dissolved in 0.9% warm sterile saline. Each rat received 3 BrdU injections (66 mg/Kg/300 μL per intraperitoneal injection). Therefore, each rat received a total concentration of 200 mg/kg of BrdU.

3 Methods

3.1 Perfusion and Brain Removal

Either 1 day (for proliferation) or 4 weeks (for neurogenesis) after BrdU injection, rats were deeply anesthetized and perfused transcardially with 200 mL of 0.9% saline followed by the same volume of 4% formalin. The chest cavity was opened to expose the heart and a perfusion cannula was introduced into the left ventricle. Once cleared, formaldehyde (4%) was allowed to flow in. The skull was exposed through a midline incision and opened with a bone cutter. The brain was carefully removed and placed in a 50 mL tube containing 4% paraformaldehyde.

3.2 Tissue Preparation for Stereology

Brains were fixed overnight in 4% paraformaldehyde at room temperature and then transferred to 30% sucrose solution in 0.1 M PBS and stored at 4 °C until full impregnation (typically 3 days). For unbiased cell stereology, systemic-random sampling of brain sections was completed following the Fractionator principle [56, 57] (*see* Fig. 2). In brief, 40 μm coronal sections were cut serially using a freezing microtome, from the rostral to the caudal extent of the DG at the following rostro-caudal coordinates covering the whole hippocampal formation (−2.12 to −6.3 mm relative to bregma). To highlight the topographic correspondence of BrdU distribution, the DG region was divided into three areas as follows: rostral ranging from −2.12 to −3.7 mm relative to bregma, intermediate ranging from −3.7 to −4.9 and caudal ranging from −4.9 to −6.3 [58]. Sections were serially collected in 24 well plates as six sets containing seven rostral, five intermediate, and six caudal sections

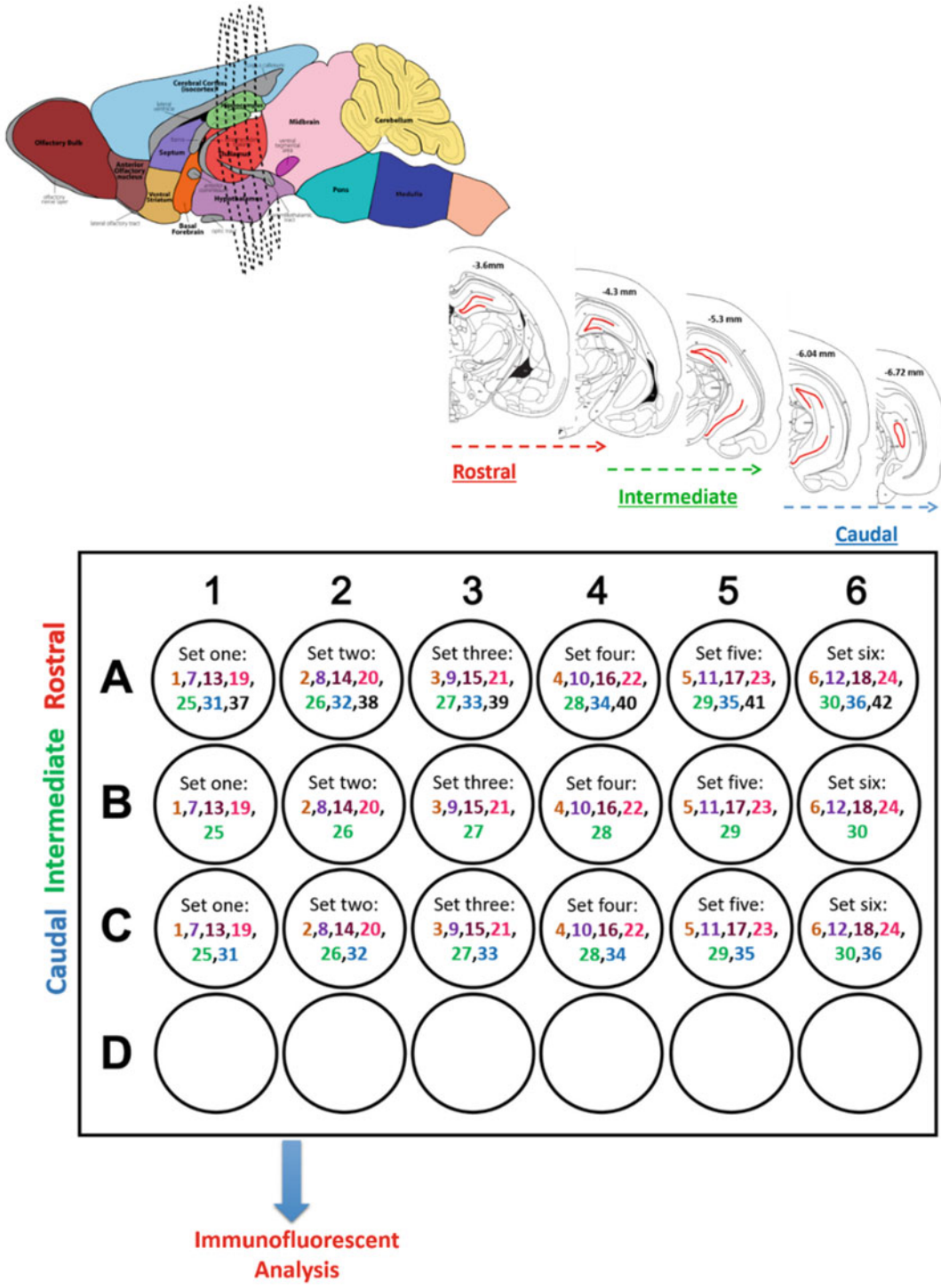

Fig. 2 Schematic diagram of the Fractionator Method. Free-floating coronal sections are distributed in a 24 well plate. The first section will be placed in the first well, and the following sections will follow in the adjacent wells reaching the sixth slice in well number 6. The seventh slice will be placed back with the first section in well number 1 and this procedure continues all through until the whole hippocampus is covered. This will provide a representative collection of sections encompassing the whole hippocampus whereby each section is 240 μm apart from the next one in the same well/set

per set, where each section is 240 μm apart from the next and each set represents the whole region of interest (*see* Fig. 2). Within the cutting procedure, a needle was used to pierce the right side of the brain. Piercing helps in identifying the right and left sides of the brain sections. All sections were collected and stored in 0.1 M PBS solution containing sodium azide (15 mM).

3.3 BrdU Detection by Immunofluorescence

For immunofluorescence and each rat, we chose one of the six collected sets of sections. Therefore, the final number of sections stained were around seven rostral sections, five intermediate sections, and six caudal sections (a total of 18–20 sections per rat). These free-floating sections were washed three times (5 min each) with 0.1 M PBS in a 24-well plate. For BrdU detection, DNA was denatured by incubating the sections in 2 N HCl for 30 min at 37 °C. Sections were then rinsed with 0.1 M PBS for 5 min and washed with 0.1 M Sodium Borate (pH 8.5) for 10 min at RT. Tissues were washed 2× with 0.1 M PBS and transferred to the blocking and permeabilization solution (10% NGS, 10% BSA, 0.1% Triton-X diluted in PBS) for 1 h at 4 °C. In order to minimize nonspecific cross labeling between different primary antibodies, we opted to sequentially stain the sections. Therefore, sections were incubated overnight at 4 °C with primary antibody rat monoclonal anti-BrdU (1:100; BioRad) diluted in PBS with 3% NGS, 3% BSA, 0.1% Triton-X. The next day, sections were washed three times with 0.1 M PBS and incubated in the dark with fluorochrome-conjugated secondary antibody Alexa Fluor-568 anti-rat (1:200; Molecular Probes, Invitrogen) diluted in PBS with 3% NGS, 3% BSA and 0.1% Triton-X for 2 h at room temperature on a shaker. Sections were then washed three times (5 min each) with 0.1 M PBS and incubated with mouse monoclonal anti-NeuN (1:500; Millipore) at 4 °C overnight diluted in the same solute. The next day the sections were washed three times and incubated in the dark, for 2 h at RT on a shaker, with the fluorochrome-conjugated secondary antibody Alexa Fluor-488 anti-mouse (1:250; Molecular Probes, Invitrogen) diluted also in the same solution as before. Hoechst stain (1:10,000 in PBS; Molecular Probes, Invitrogen) was added to the sections during the last 10 min of the final incubation. After that, the sections were washed with PBS and mounted onto slides with Fluoro-Gel without DAPI (Electron Microscopy Sciences, USA) and covered with a thin glass coverslip. The images were acquired by Zeiss LSM 710 confocal microscope using the 40× oil objective as Z-stack and tile scan [59]. This showed the BrdU+ cells in the SGZ distributed along the dentate gyrus (*see* Fig. 3) [59].

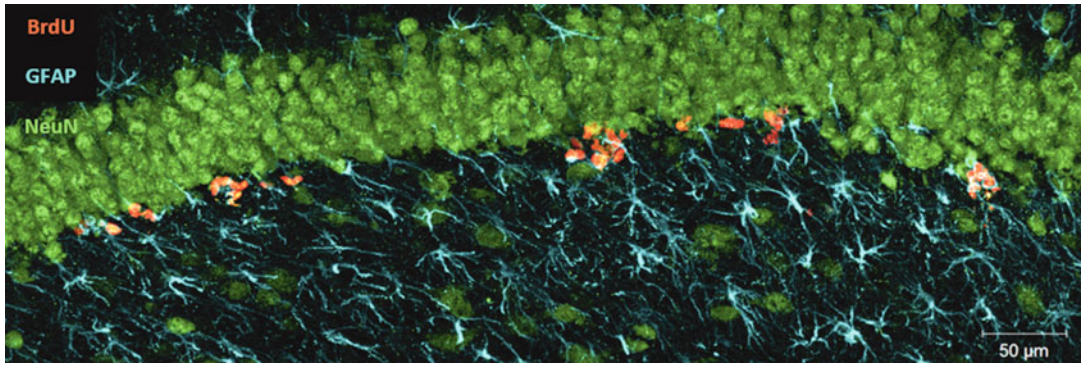

Fig. 3 Immunostaining of BrdU-positive cells in the DG. Tile scan image of one arm of the dentate gyrus showing proliferating BrdU-labeled cells in the SGZ. Some of these cells are co-labeled with GFAP

3.4 Identification of Different Developmental Stages

In order to identify the different developmental stages, double immunofluorescence staining was performed for the evaluation of the co-localization of BrdU with another cellular marker. To look for stem/progenitor cells during the early developmental stages, we injected BrdU 1–3 days before the rat sacrifice. After a sacrifice and tissue collection as explained earlier, we labeled radial type I neural stem cells by using an antibody against the glial fibrillary acidic protein marker (GFAP, 1:500, Abcam) along with BrdU (*see* Fig. 4) [60]. Moreover, stem/progenitor cell proliferation was identified by co-labeling of BrdU with the proliferation markers PCNA (1:100, Abcam) or Ki-67 (1:500, Abcam) (*see* Fig. 5) [61]. To identify cells at later developmental stages (immature granule cells), we gave BrdU injection 5–7 days before sacrifice and stained the sections with DCX and BrdU (*see* Fig. 6) [61]. Finally, to label new mature neurons, we injected BrdU 3–4 weeks before sacrifice and then stained the sections with BrdU and NeuN (*see* Fig. 7).

3.5 Cell Counting

For the cell count, BrdU+ cells were counted in every set using a 40× oil objective on a confocal microscope. We multiplied the total number of positive cells, counted in each rat, by 6 (the total number of sets per rat). This gave a rough representation of the total number of BrdU+ cells in each rat (refer to formulas below)

- Formula 1: Total number of BrdU+ in rostral DG = number of BrdU+ cells counted in one set (7 sections) × 6 (number of sets).
- Formula 2: Total number of BrdU+ in intermediate DG = number of BrdU+ cells counted in one set (5 sections) × 6 (number of sets).
- Formula 3: Total number of BrdU+ in caudal DG = number of BrdU+ cells counted in one set (6 sections) × 6 (number of sets).

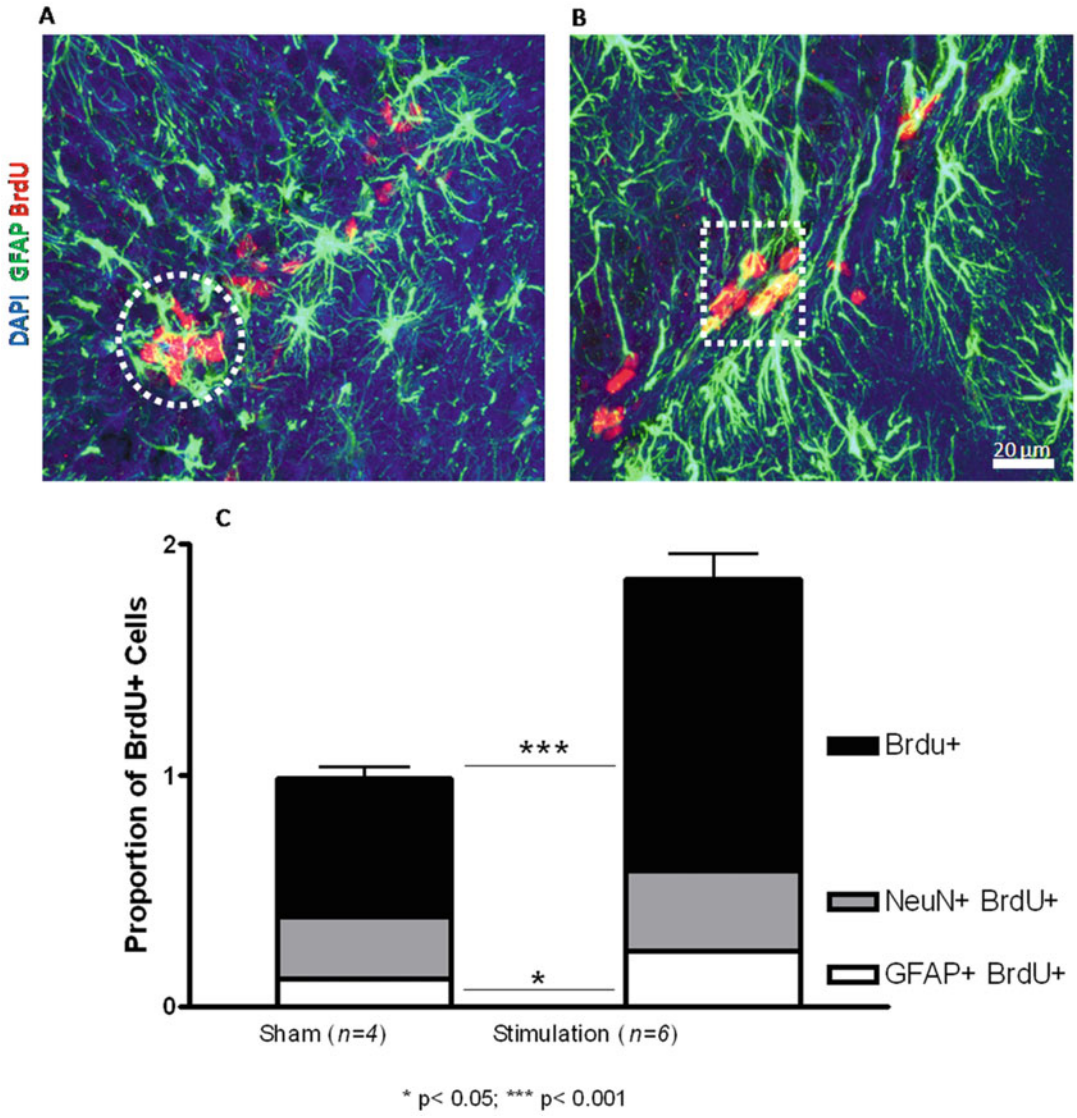

Fig. 4 Immunostaining of neural stem/progenitor cells. Images acquired by confocal microscopy to show cells in the SGZ expressing BrdU (red) alone or co-labeled with GFAP (green). The double-labeled cells represented stem/progenitor cells and were assembled either in clusters (white circle, **a**) or chains (white square, **b**). The images were acquired as serial Z-stack under 40× oil objective and maximal intensity projection was applied [60]

- To calculate the final number of BrdU+ cells in the whole DG of each rat:

Total number of BrdU+ in DG = Formula 1 + Formula 2 + Formula 3.

3.6 Microscopic Analysis

Microscopic analysis was performed using Zeiss LSM 710 confocal microscope and images were acquired using the 40× oil objective as Z-stack to show the BrdU+ cells distributed within the 40 µm

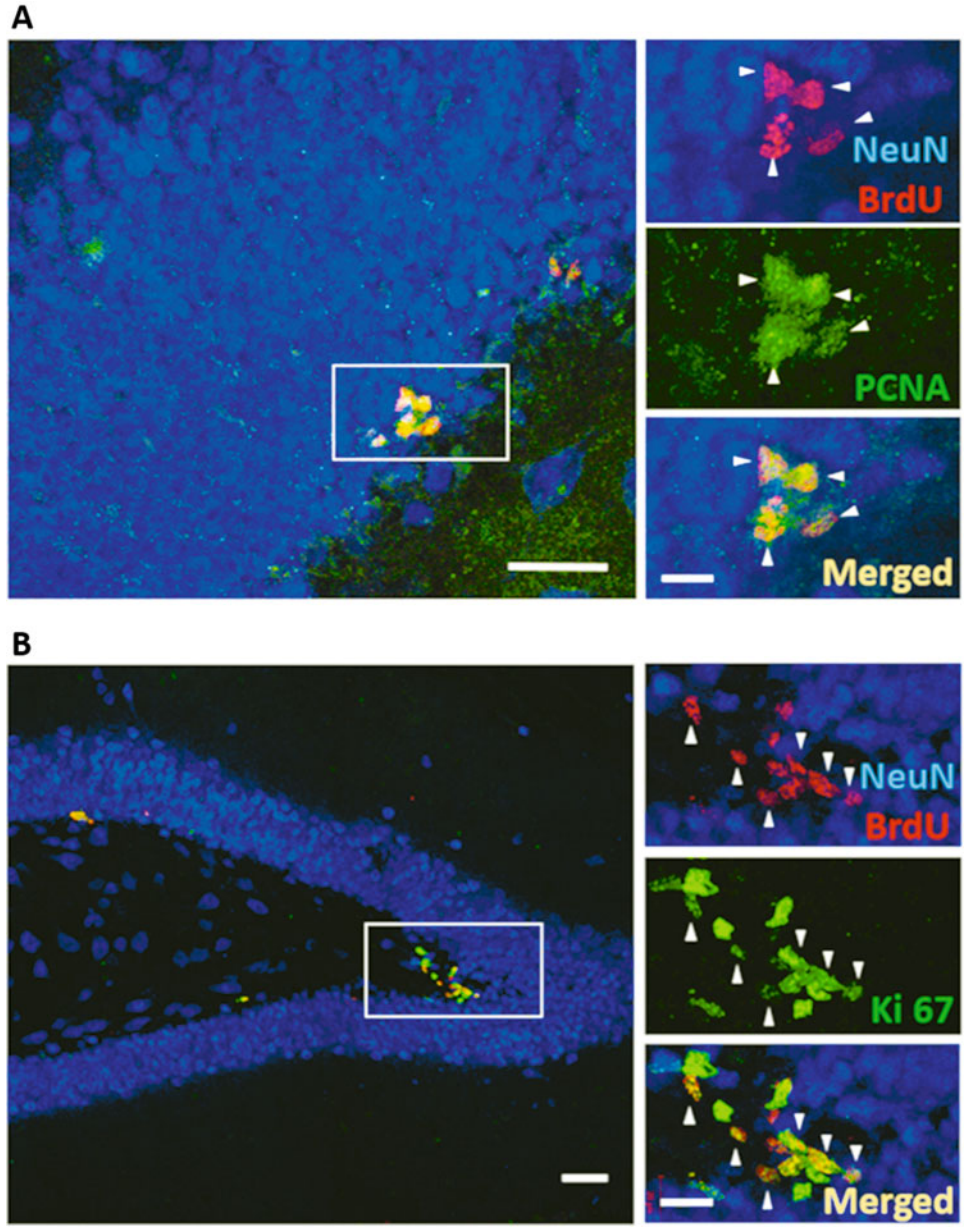

Fig. 5 Immunostaining of proliferating stem/progenitor cells. Images showing the co-localization of BrdU-labeled cells with the proliferation markers PCNA (**a**) and Ki 67 (**b**). The white arrowheads in the zoomed-in images to the right indicate co-labeling of BrdU stem/progenitor cells with the proliferating markers. Scale bars: 50 μm in enlarged images and 20 μm in the insets [61]

section and as tile scan to show the dentate gyrus of each region. The images were analyzed using the Zeiss ZEN 2009 image-analysis software and they were processed with maximal intensity projection. For the purpose of consistency, BrdU+ cells were counted by a single-blinded researcher, and images were acquired

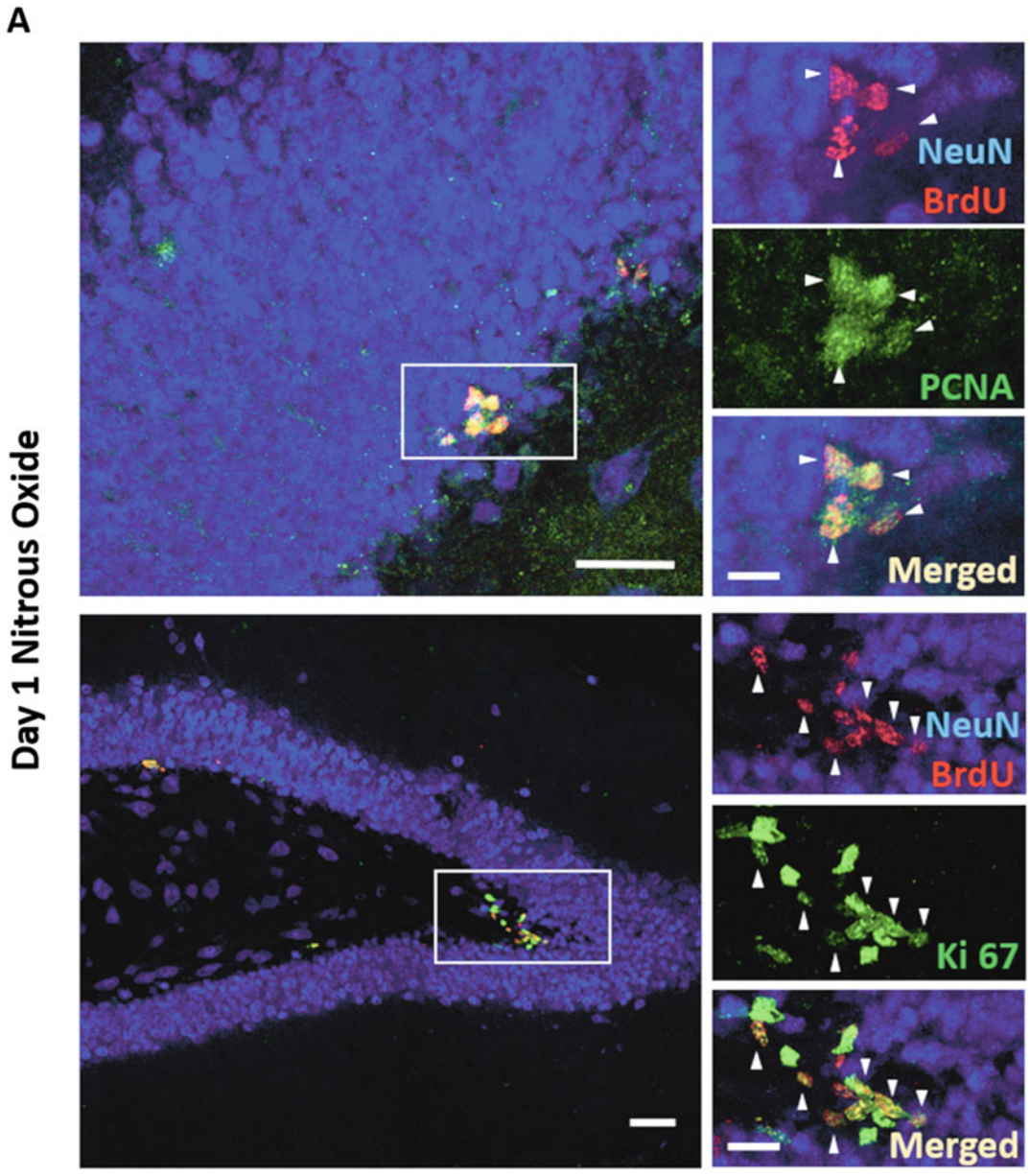

Fig. 6 Immunostaining of immature granule cells. The image shows BrdU-positive cells co-labeled with the neuronal lineage marker DCX. Co-localization is marked by white arrowheads in the right zoomed-in images. Scale bars: 50 μm in enlarged images and 20 μm in the insets [61]

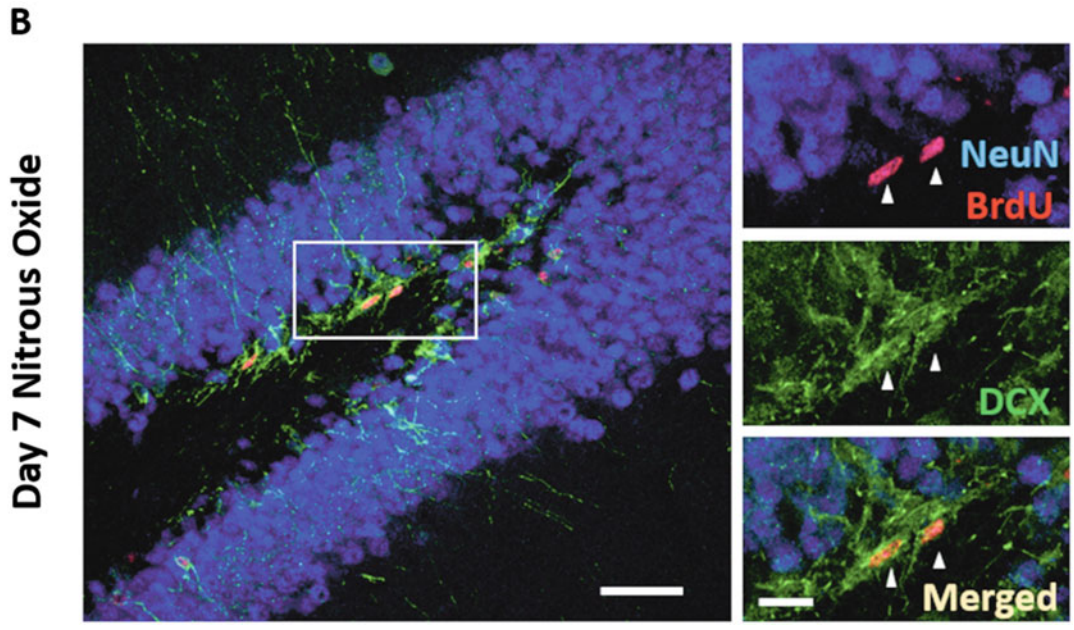

Fig. 6 (continued)

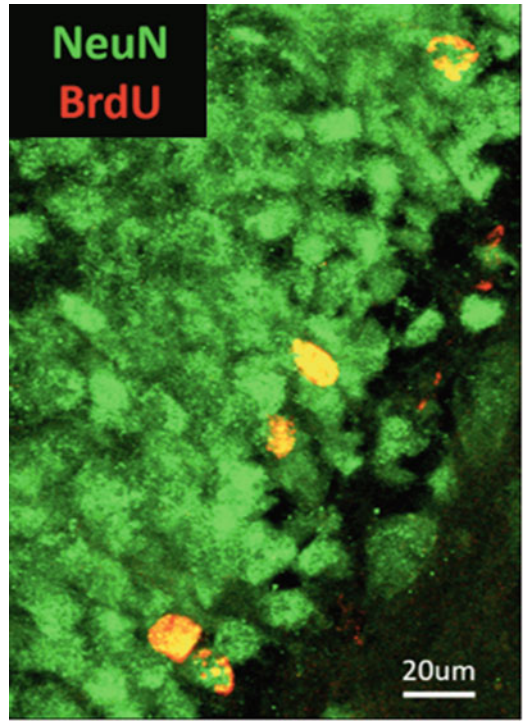

Fig. 7 Immunostaining of mature granule cells. The image shows BrdU-positive cells co-labeled with the mature neuronal marker NeuN

under the same laser and microscopic parameters. For the co-localization of BrdU with the different markers, Z-stack images were obtained with maximal intensity projection.

4 Conclusions

In the last two decades, neurogenesis has been established as a cellular mechanism in the adult mammalian brain. Technological advancement in the field served to add more knowledge on the process of neurogenesis and its dynamic regulation in response to many factors. However, most studies on neurogenesis have been conducted in rodents, birds, zebrafish, and monkeys. Identifying neurogenesis and pinpointing newly born neurons in humans has always been a challenge and there are a limited number of studies in humans that confirm its existence. Thus, molecular techniques for investigating neural stem cells in humans need to be optimized and controlled to minimize such variables. Additional techniques such as bioinformatics, high specificity neuroimaging, 3D organoid models, and the use of induced pluripotent stem cells can all help add further knowledge and advancement to this field.

Recently, the entire concept of neurogenic capacity in humans has been debated and put for questioning as new evidence suggested otherwise [50, 55, 62]. However, studies continue to reveal new findings and challenge each other [50, 53]. Recently, it was shown that neurogenesis is abundant in healthy individuals [63] and it persists not only in adults but also in Alzheimer's disease patients [64]. Whether or not neurogenesis exists in humans and to what extent it can salvage and repair any damage is still debatable but evidence in the literature, and with the help of technological improvements, are worth building on as they suggest beneficial and promising roles for neurogenesis.

Understanding how neurogenesis is regulated and finding ways or drugs to boost it has become a very interesting and important goal for many researchers in the context of neurodegenerative and neuropsychiatric disorders. Alterations in neurogenesis might offer explanations to certain mood and memory changes seen in depressed patients or patients with other psychiatric disorders. In fact, antidepressant drugs such as fluoxetine that have been shown to boost neurogenesis in rodents are thought to exert their beneficial effects through such mechanisms of action. As for neurodegenerative diseases, cell replacement therapy and boosting the neurogenic potential are being thoroughly investigated in animal models. Investigating neurogenesis in animal models allows us to answer questions of how neurogenesis can be manipulated, damaged, restored, and whether cell therapy such as pluripotent stem cell injection is a safe and/or beneficial option in the hostile environment of degenerating brains.

In conclusion, there are many limitations and discrepancies in methods for tracking neurogenesis in humans and it remains to be a challenge and a major drawback. We still need to learn more about human neurogenesis as it is very crucial and requires precise, controlled, and reproducible techniques and methods to probe for. However, continuing research in animal models will give valuable indispensable knowledge on how neurogenesis works and how it can be regulated.

References

1. Altman J, Das GD (1965) Autoradiographic and histological evidence of postnatal hippocampal neurogenesis in rats. J Comp Neurol 124(3):319–335
2. Kaplan MS, Hinds JW (1977) Neurogenesis in the adult rat: electron microscopic analysis of light radioautographs. Science (New York, NY) 197(4308):1092–1094
3. Altman J (1969) Autoradiographic and histological studies of postnatal neurogenesis. IV. Cell proliferation and migration in the anterior forebrain, with special reference to persisting neurogenesis in the olfactory bulb. J Comp Neurol 137(4):433–457. https://doi.org/10.1002/cne.901370404
4. Doetsch F, Garcia-Verdugo JM, Alvarez-Buylla A (1997) Cellular composition and three-dimensional organization of the subventricular germinal zone in the adult mammalian brain. J Neurosci 17(13):5046–5061
5. Kornack DR, Rakic P (2001) Cell proliferation without neurogenesis in adult primate neocortex. Science (New York, NY) 294 (5549):2127–2130. https://doi.org/10.1126/science.1065467
6. Kornack DR, Rakic P (2001) The generation, migration, and differentiation of olfactory neurons in the adult primate brain. Proc Natl Acad Sci U S A 98(8):4752–4757. https://doi.org/10.1073/pnas.081074998
7. Bonaguidi MA et al (2011) In vivo clonal analysis reveals self-renewing and multipotent adult neural stem cell characteristics. Cell 145 (7):1142–1155. https://doi.org/10.1016/j.cell.2011.05.024
8. Doetsch F et al (1999) Subventricular zone astrocytes are neural stem cells in the adult mammalian brain. Cell 97(6):703–716
9. Zhao C, Deng W, Gage FH (2008) Mechanisms and functional implications of adult neurogenesis. Cell 132(4):645–660. https://doi.org/10.1016/j.cell.2008.01.033
10. Eriksson PS et al (1998) Neurogenesis in the adult human hippocampus. Nat Med 4 (11):1313–1317. https://doi.org/10.1038/3305
11. Gould E et al (1998) Proliferation of granule cell precursors in the dentate gyrus of adult monkeys is diminished by stress. Proc Natl Acad Sci U S A 95(6):3168–3171
12. Kempermann G et al (2004) Milestones of neuronal development in the adult hippocampus. Trends Neurosci 27(8):447–452. https://doi.org/10.1016/j.tins.2004.05.013
13. Kronenberg G et al (2003) Subpopulations of proliferating cells of the adult hippocampus respond differently to physiologic neurogenic stimuli. J Comp Neurol 467(4):455–463. https://doi.org/10.1002/cne.10945
14. Bonaguidi MA et al (2012) A unifying hypothesis on mammalian neural stem cell properties in the adult hippocampus. Curr Opin Neurobiol 22(5):754–761. https://doi.org/10.1016/j.conb.2012.03.013
15. Lucassen PJ et al (2010) Regulation of adult neurogenesis by stress, sleep disruption, exercise and inflammation: implications for depression and antidepressant action. Eur Neuropsychopharmacol 20(1):1–17. https://doi.org/10.1016/j.euroneuro.2009.08.003
16. Deng W, Aimone JB, Gage FH (2010) New neurons and new memories: how does adult hippocampal neurogenesis affect learning and memory? Nat Rev Neurosci 11(5):339–350. https://doi.org/10.1038/nrn2822
17. Kelsch W, Sim S, Lois C (2010) Watching synaptogenesis in the adult brain. Annu Rev Neurosci 33:131–149. https://doi.org/10.1146/annurev-neuro-060909-153252
18. Toni N et al (2008) Neurons born in the adult dentate gyrus form functional synapses with target cells. Nat Neurosci 11(8):901–907. https://doi.org/10.1038/nn.2156
19. Toni N, Sultan S (2011) Synapse formation on adult-born hippocampal neurons. Eur J Neurosci 33(6):1062–1068. https://doi.org/10.1111/j.1460-9568.2011.07604.x

20. Zhao C et al (2006) Distinct morphological stages of dentate granule neuron maturation in the adult mouse hippocampus. J Neurosci 26(1):3–11. https://doi.org/10.1523/JNEUROSCI.3648-05.2006
21. Cameron HA et al (1993) Differentiation of newly born neurons and glia in the dentate gyrus of the adult rat. Neuroscience 56 (2):337–344
22. Biebl M et al (2000) Analysis of neurogenesis and programmed cell death reveals a self-renewing capacity in the adult rat brain. Neurosci Lett 291(1):17–20
23. Kempermann G et al (2003) Early determination and long-term persistence of adult-generated new neurons in the hippocampus of mice. Development 130(2):391–399
24. Hattiangady B, Shetty AK (2008) Aging does not alter the number or phenotype of putative stem/progenitor cells in the neurogenic region of the hippocampus. Neurobiol Aging 29 (1):129–147. https://doi.org/10.1016/j.neurobiolaging.2006.09.015
25. Sun W et al (2004) Programmed cell death of adult-generated hippocampal neurons is mediated by the proapoptotic gene Bax. J Neurosci 24(49):11205–11213. https://doi.org/10.1523/jneurosci.1436-04.2004
26. Sierra A et al (2010) Microglia shape adult hippocampal neurogenesis through apoptosis-coupled phagocytosis. Cell Stem Cell 7 (4):483–495. https://doi.org/10.1016/j.stem.2010.08.014
27. Kempermann G, Kuhn HG, Gage FH (1997) More hippocampal neurons in adult mice living in an enriched environment. Nature 386 (6624):493–495. https://doi.org/10.1038/386493a0
28. Gould E et al (1999) Learning enhances adult neurogenesis in the hippocampal formation. Nat Neurosci 2(3):260–265. https://doi.org/10.1038/6365
29. Dupret D et al (2007) Spatial learning depends on both the addition and removal of new hippocampal neurons. PLoS Biol 5(8):e214. https://doi.org/10.1371/journal.pbio.0050214
30. Kempermann G, Song H, Gage FH (2015) Neurogenesis in the adult Hippocampus. Cold Spring Harb Perspect Biol 7(9): a018812. https://doi.org/10.1101/cshperspect.a018812
31. von Bohlen Und Halbach O (2007) Immunohistological markers for staging neurogenesis in adult hippocampus. Cell Tissue Res 329 (3):409–420. https://doi.org/10.1007/s00441-007-0432-4
32. Hoglinger GU et al (2004) Dopamine depletion impairs precursor cell proliferation in Parkinson disease. Nat Neurosci 7(7):726–735. https://doi.org/10.1038/nn1265
33. Mu Y, Gage FH (2011) Adult hippocampal neurogenesis and its role in Alzheimer's disease. Mol Neurodegener 6:85. https://doi.org/10.1186/1750-1326-6-85
34. Phillips W, Morton AJ, Barker RA (2005) Abnormalities of neurogenesis in the R6/2 mouse model of Huntington's disease are attributable to the in vivo microenvironment. J Neurosci 25(50):11564–11576. https://doi.org/10.1523/jneurosci.3796-05.2005
35. Simuni T, Sethi K (2008) Nonmotor manifestations of Parkinson's disease. Ann Neurol 64 (Suppl 2):S65–S80. https://doi.org/10.1002/ana.21472
36. Stout JC et al (2011) Neurocognitive signs in prodromal Huntington disease. Neuropsychology 25(1):1–14. https://doi.org/10.1037/a0020937
37. Hinnell C et al (2012) Nonmotor versus motor symptoms: how much do they matter to health status in Parkinson's disease? Mov Disord 27 (2):236–241. https://doi.org/10.1002/mds.23961
38. Allen KM, Fung SJ, Weickert CS (2016) Cell proliferation is reduced in the hippocampus in schizophrenia. Aust N Z J Psychiatry 50 (5):473–480. https://doi.org/10.1177/0004867415589793
39. Mahar I et al (2014) Stress, serotonin, and hippocampal neurogenesis in relation to depression and antidepressant effects. Neurosci Biobehav Rev 38:173–192. https://doi.org/10.1016/j.neubiorev.2013.11.009
40. Wu MV, Hen R (2014) Functional dissociation of adult-born neurons along the dorsoventral axis of the dentate gyrus. Hippocampus 24 (7):751–761. https://doi.org/10.1002/hipo.22265
41. Hill AS, Sahay A, Hen R (2015) Increasing adult hippocampal neurogenesis is sufficient to reduce anxiety and depression-like behaviors. Neuropsychopharmacology 40 (10):2368–2378. https://doi.org/10.1038/npp.2015.85
42. Altman J (1962) Are new neurons formed in the brains of adult mammals? Science (New York, NY) 135(3509):1127–1128
43. Kaplan MS (1981) Neurogenesis in the 3-month-old rat visual cortex. J Comp Neurol 195(2):323–338. https://doi.org/10.1002/cne.901950211
44. Kaplan MS, McNelly NA, Hinds JW (1985) Population dynamics of adult-formed granule

neurons of the rat olfactory bulb. J Comp Neurol 239(1):117–125. https://doi.org/10.1002/cne.902390110

45. Nottebohm F (1985) Neuronal replacement in adulthood. Ann N Y Acad Sci 457:143–161. https://doi.org/10.1111/j.1749-6632.1985.tb20803.x
46. Gratzner HG (1982) Monoclonal antibody to 5-bromo- and 5-iododeoxyuridine: a new reagent for detection of DNA replication. Science (New York, NY) 218(4571):474–475
47. Waldman FM, Dolbeare F, Gray J (1988) Clinical applications of the bromodeoxyuridine/DNA assay. Cytometry Suppl 3:65–72
48. Moreno-Jimenez EP et al (2019) Adult hippocampal neurogenesis is abundant in neurologically healthy subjects and drops sharply in patients with Alzheimer's disease. Nat Med 25(4):554–560. https://doi.org/10.1038/s41591-019-0375-9
49. Knoth R et al (2010) Murine features of neurogenesis in the human hippocampus across the lifespan from 0 to 100 years. PLoS One 5(1):e8809. https://doi.org/10.1371/journal.pone.0008809
50. Sorrells SF et al (2018) Human hippocampal neurogenesis drops sharply in children to undetectable levels in adults. Nature 555(7696):377–381. https://doi.org/10.1038/nature25975
51. Spalding KL et al (2005) Retrospective birth dating of cells in humans. Cell 122(1):133–143. https://doi.org/10.1016/j.cell.2005.04.028
52. Spalding KL et al (2013) Dynamics of hippocampal neurogenesis in adult humans. Cell 153(6):1219–1227. https://doi.org/10.1016/j.cell.2013.05.002
53. Boldrini M et al (2018) Human hippocampal neurogenesis persists throughout aging. Cell stem cell 22(4):589–599.e585. https://doi.org/10.1016/j.stem.2018.03.015
54. Gage FH (2002) Neurogenesis in the adult brain. J Neurosci 22(3):612–613
55. Kempermann G et al (2018) Human adult neurogenesis: evidence and remaining questions. Cell Stem Cell 23(1):25–30. https://doi.org/10.1016/j.stem.2018.04.004
56. Gundersen HJ et al (1999) The efficiency of systematic sampling in stereology—reconsidered. J Microsc 193(Pt 3):199–211
57. Chamaa F et al (2018) Intracerebroventricular injections of endotoxin (ET) reduces hippocampal neurogenesis. J Neuroimmunol 315:58–67. https://doi.org/10.1016/j.jneuroim.2017.12.013
58. Paxinos G, Watson C (1998) The rat brain in stereotaxic coordinates. Academic Press, San Diego
59. Darwish B et al (2019) Intranigral injection of endotoxin suppresses proliferation of hippocampal progenitor cells. Front Neurosci 13:687. https://doi.org/10.3389/fnins.2019.00687
60. Chamaa F et al (2016) Thalamic stimulation in awake rats induces neurogenesis in the hippocampal formation. Brain Stimul 9(1):101–108. https://doi.org/10.1016/j.brs.2015.09.006
61. Chamaa F et al (2018) Nitrous oxide induces prominent cell proliferation in adult rat hippocampal dentate gyrus. Front Cell Neurosci 12:135. https://doi.org/10.3389/fncel.2018.00135
62. Dennis CV et al (2016) Human adult neurogenesis across the ages: an immunohistochemical study. Neuropathol Appl Neurobiol 42(7):621–638. https://doi.org/10.1111/nan.12337
63. Moreno-Jiménez EP et al (2019) Adult hippocampal neurogenesis is abundant in neurologically healthy subjects and drops sharply in patients with Alzheimer's disease. Nat Med 25(4):554–560. https://doi.org/10.1038/s41591-019-0375-9
64. Tobin MK et al (2019) Human hippocampal neurogenesis persists in aged adults and Alzheimer's disease patients. Cell Stem Cell 24(6):974–982.e973. https://doi.org/10.1016/j.stem.2019.05.003

Chapter 5

Fast-Scan Voltammetry for In Vivo Measurements of Neurochemical Dynamics

Carl J. Meunier and Leslie A. Sombers

Abstract

Background-subtracted fast-scan cyclic voltammetry (FSCV) is an electrochemical method that enables the monitoring of neurochemical dynamics in brain tissue with sub-second resolution. FSCV provides information regarding the magnitude and the time course of neurochemical release and reuptake, with additional qualitative information that can permit analyte identification. When performed in awake animals, this voltammetric approach can provide remarkable information regarding the molecular mechanisms that underlie goal-directed behavior and associative learning. In addition, FSCV can be used to quantify the impact of pharmacological agents on neurotransmitter kinetics. This chapter contains an explicit description of how to make these measurements in animals (rats) as well as critical considerations when interpreting FSCV data.

Key words Dopamine, Carbon-fiber microelectrode, Electrochemistry, Tutorial, Guidelines

1 Introduction

Electrochemical measurements permit in situ detection of neurochemicals with high sampling rates (μs–ms) when coupled with microelectrodes [1, 2]. These probes offer high spatial resolution and exact minimal tissue damage [3]. Electrochemical methods used in vivo generally involve the measurement of current flow in response to the application of a controlled potential and can be divided into two groups: voltammetric and amperometric methods. FSCV is well suited for in vivo studies as it affords the best balance of temporal resolution, sensitivity, and chemical selectivity. For example, FSCV has been used to monitor dopamine (DA) transients associated with reinforcement learning [4–9] as well as action initiation [10]. FSCV has also been used to monitor serotonin dynamics following treatment with selective serotonin reuptake inhibitors (SSRIs) [11–13]. One study revealed that SSRIs potentiated serotonin release in pair-housed animals, but not in those that were socially isolated [14]. Furthermore, FSCV

Marc Fakhoury (ed.), *The Brain Reward System*, Neuromethods, vol. 165, https://doi.org/10.1007/978-1-0716-1146-3_5,

can be paired with other techniques such as microinjection, iontophoresis, and electrophysiology to collect complementary information regarding specific neurotransmitter function(s) [5, 15–17].

1.1 Use of FSCV in Analyte Detection

Carbon-fiber microelectrodes are commonly used for neurochemical measurements, as carbon offers an inherent resistance to biofouling relative to other common electrode materials, such as gold and platinum [18–22]. The carbon fiber (5–10 μm diameter) is typically insulated using a borosilicate–glass or fused-silica capillary and the protruding carbon fiber is cut to a defined length (typically 75–125 μm) [1, 23]. These cylindrically shaped carbon-fiber microelectrodes are >40× smaller in each dimension than a typical microdialysis probe, permitting stereotaxic implantation with significantly less tissue damage [3]. The high aspect ratio and surface roughness provide a large surface area for sensing that is well suited to probe brain regions that have gradations in the density of neuronal terminals over micron-scale dimensions [24, 25]. Currents generated during in vivo measurements are typically on the order of 10s–100s of nanoamperes (nA). This magnitude of current does not result in significant polarization of the reference electrode (Ag/AgCl) [26]. Thus, relatively reliable measurements can be made without implantation of an auxiliary (counter) electrode.

In FSCV, a dynamic potential waveform is applied to drive electrons into, and out of, molecules that are located in the vicinity of the working electrode (*see* Fig. 1). Molecules that are capable of heterogeneous electron transfer have molecular orbitals that either contain, or are devoid of, electrons. As the potential is scanned through the waveform, the energy level of the carbon-fiber microelectrode shifts with respect to that of the molecular orbitals of the analyte, and an electron has a probability to be extracted from, or injected into, that molecular orbital. This is termed "oxidation" and "reduction," respectively. The movement of charge is measured in the form of current (charge/time), which is plotted versus applied potential, resulting in a cyclic voltammogram (CV). Importantly, the positions of these energy levels are specific to a given molecule. Thus, the kinetics associated with the heterogeneous electron transfer results in CVs that can be used as a "signature" for a particular analyte, allowing for putative identification.

DA is the neurotransmitter that is most often monitored using FSCV. Its characteristic CV (*see* Fig. 1) is used to distinguish it from a number of interferents, such as ascorbic acid and shifts in pH. Advances in electrode materials [27–30], voltammetric strategies [31–34], and data analysis strategies [35–38] have increased the number of neurochemicals targeted using FSCV. Currently, FSCV is used to monitor catecholamines (DA, norepinephrine, epinephrine) [39–41], indolamines (serotonin and melatonin) [34, 42, 43], hydrogen peroxide [44, 45], oxygen [46, 47], peptides [32], and purines (adenosine and guanosine) in vivo [31, 33,

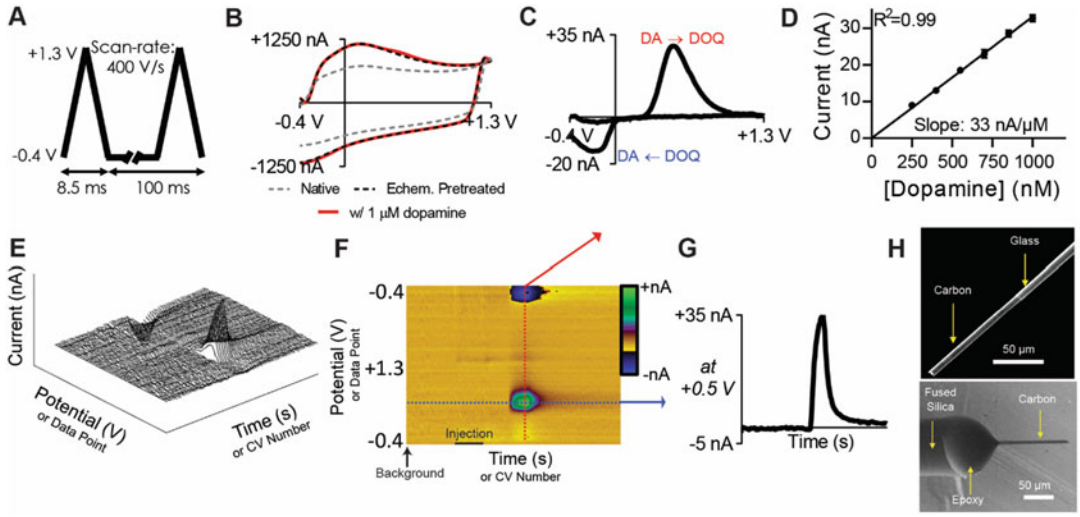

Fig. 1 Introduction to FSCV. (**a**) Typical FSCV potential waveform applied to a carbon fiber working electrode. (**b**) This generates a predominately non-faradaic background current (gray) that grows with repeated waveform application (black). The red trace is an example of the signal in the presence of DA. (**c**) The background can be subtracted to reveal a cyclic voltammogram for the oxidation of DA to dopamine-o-quinone (DOQ) and subsequent reduction of DOQ to DA. (**d**) The amplitude of the current is directly related to DA concentration. (**e**) Cyclic voltammograms can be converted to linear voltammograms and plotted in three dimensions. (**f**) This information can be plotted in 2-D to quickly visualize large amounts of data, current is plotted in false color. A vertical line through the color plot can be used to reconstruct cyclic voltammograms for analyte identification. (**g**) A horizontal line through the color plot can be used to report on current at an analyte's redox potential over time; i.e., chemical dynamics. (**h**) Representative scanning electron micrographs of carbon-fiber microelectrodes insulated in borosilicate glass (top) and fused silica (bottom)

48]. Although CVs serve to putatively identify a given analyte, selectivity is always a concern. For example, the CVs for DA and norepinephrine are virtually indistinguishable, and epinephrine can only be distinguished from these by a second peak that is evident only at more positive potentials (+1.4 V) [49]. Therefore, positive identification of a specific species must be electrochemically, anatomically, physiologically, and pharmacologically verified [50]. For example, to validate DA measurements using FSCV:

1. The in vivo signal should be consistent with a CV recorded using a standard collected in vitro.
2. The signal must have been collected in an anatomical region known to contain DA terminals.
3. Stimulation of cell bodies should illicit time-locked DA release.
4. Pharmacological manipulation should modulate the amount and/or kinetics of release and/or reuptake in a predictable manner, consistent with the literature.

When voltammetry is used to identify a molecule that has not been previously characterized using FSCV, an independent strategy should be used to validate the measurement (whenever possible) [50].

2 Materials

2.1 Electrode Fabrication

1. Carbon fiber: T-650, polyacrylonitrile-based fibers are commonly used (Cytec Industries, Woodland Park, NJ).
2. Borosilicate-glass capillary (1.0 mm O.D., 0.5 mm I.D.; A-M Systems, Sequim, WA), typically used for measurements in anesthetized animals or tissue slices.
3. Fused-silica tubing (164.7 μm O.D., 98.6 μm I.D.; Polymicro Technologies, Phoenix, AZ), typically used for experiments in awake animals.
4. Vertical electrode puller: PE-21 (Narishige, Tokyo, Japan).
5. Vacuum pump.
6. Stereo microscope.
7. Glass microscope slide.
8. Surgical scalpel.
9. Rubber/silicone putty.
10. Silver paint: Silver Print II (GC Electronics, Rockford, IL).
11. Silver wire: 0.5 mm diameter for Ag/AgCl reference electrode (Sigma-Aldrich, St. Louis, IL).
12. Insulated steel wire leads (Squires Electronics, Inc., Cornelius, OR).
13. Gold connectors: PCB socket (Newark Electronics, Chicago, IL).
14. Fast-hardening epoxy (McMaster Carr, Atlanta, GA).
15. Conductive silver epoxy (MG Chemical, Thief River Falls, MN).
16. Liquid electrical tape (GC Electronics, Rockford, IL).

2.2 Surgery

1. Anesthetic: ketamine/xylazine, urethane, or isoflurane (general anesthesia). Also bupivacaine (0.25%; local anesthetic).
   (a) Use of isoflurane requires additional equipment including an isoflurane vaporizer, oxygen gas, induction chamber, and an anesthesia mask that is compatible with the stereotaxic instrument.
2. Heating pad(s).
3. Stereotaxic instrument: such as Model 900 Small-Animal Stereotaxic Instrument (David Kopf Instruments, Tujunga, CA).

4. Guide cannula for reference electrode (BASi, West Lafayette, IN).
5. Surgical anchor screws (Gexpro, Indianapolis, IN).
6. Cranioplastic grip cement (Dentsply International, Inc., Milford, DE).
7. Surgical tools and materials: scissors, tweezers, gauze, cotton swabs, Betadine®, Virkon™, screwdriver.
8. Dremmel® rotary tool and small diameter drill bit (consistent with surgical screws).

2.3 Electrochemistry

1. Multifunction input/output data acquisition card: PCIe-6363 (National Instruments, Austin, TX).
2. Software for data collection and analysis: such as High Definition Cyclic Voltammetry (University of North Carolina at Chapel Hill, Department of Chemistry, Electronics Facility) or Fast Scan Cyclic Voltammetry Software (Pinnacle Technology Inc., Lawrence, KS).
3. Potentiostat. One of the following systems is appropriate: Universal Electrochemistry Instrument (UEI, UNC-Chapel Hill, Department of Chemistry, Electronics Facility), WaveNeuro FSCV System (Pine Research Instrumentation, Durham, NC), or Fast-Scan Cyclic Voltammetry System (Pinnacle Technology Inc., Lawrence, KS).
4. Headstage: miniaturized current-to-voltage converter. Can be purchased from UNC-Chapel Hill (Department of Chemistry, Electronics Facility) or Pine Research Instrumentation.
5. Commutator: 25 channels (Crist Instruments, Hagerstown, MD). Allows electrical connectivity to a freely moving animal.
6. Screened behavior chamber, grounded: custom made for in vivo experiments (Med Associates, Inc., St. Albans, VT). Screening serves as a Faraday cage.

2.4 Electrode Calibration

1. Buffered electrolyte: phosphate-buffered saline, TRIS-buffered saline, or artificial cerebral spinal fluid.
2. Grounded Faraday cage: custom-built in house.
3. Flow-injection apparatus: six-port, two-position high-performance liquid chromatography valve, air actuator, and digital valve interface (VICI, Houston, TX).
4. Custom molded flow chamber.
5. Micromanipulator, for electrode placement.
6. Analyte standards: prepared fresh or from frozen aliquots. For example, dopamine HCl: 5 mM in 0.1 M perchloric acid, stored at −20 °C. Dilutions made in buffer.

7. A commercial flow cell that uses a gravity-feed system is available from Pine Research Instrumentation (Durham, NC).

3 Methods

3.1 Electrochemistry, Instrumentation, and Software

3.1.1 Introduction

When a potential waveform is applied to a carbon-fiber microelectrode, two sources of current are generated: (1) Non-faradaic current (or charging current) results from the movement of charged species in close vicinity to the electrode/solution interface and (2) faradaic current is generated through the transfer of electrons into, and out of, specific molecules at the electrode surface. The non-faradaic current results largely from rapid charging of the electrochemical double layer at the electrode surface. It increases linearly with the scan rate and is the dominant source of current generated using FSCV. By contrast, faradaic current is generated: (1) with each waveform application, as redox-active functional groups on the carbon surface are oxidized and reduced [51, 52] and (2) through the oxidation and reduction of solution-phase analytes at the electrode surface. The overall current profile is specific to a given electrode. In the absence of a chemical change at the electrode surface, the signal is stable over tens of seconds. This "background" signal can be subtracted from a signal recorded in the presence of an electroactive neurochemical to reveal a characteristic CV (*see* Fig. 1). The overall shape of the voltammogram reveals information about analyte identity, reversibility, and electron transfer kinetics, and the magnitude of the peaks is indicative of the concentration of the analyte at the electrode surface [26]. It should be noted that background subtraction limits FSCV to monitoring analyte *fluctuations*, or changes in the absolute concentration, when in vivo. Basal levels of neurotransmitters that are stable over tens of seconds are subtracted in the background signal.

Carbon-fiber microelectrodes typically generate hundreds of nanoamperes to single-digit microamperes of background current with each scan, dependent on the surface area of the electrode. By contrast, the faradaic current generated in response to fluctuating neurochemicals encountered in vivo is generally on the order of hundreds of picoamperes to tens of nanoamperes. The large difference in the scale of the background signal as compared to that generated in oxidation or reduction of a species of interest requires the use of specialized instrumentation to reduce contamination of the resultant signal by noise. In addition, all measurements are performed in a grounded Faraday cage, this serves as the ground for the entire system. Instrumentation used for FSCV is often custom-made; however, some commercial systems are available (as described in the Methods). High-definition cyclic voltammetry (HDCV) is probably the software that is most often used to control waveform output and to process the collected signals, in

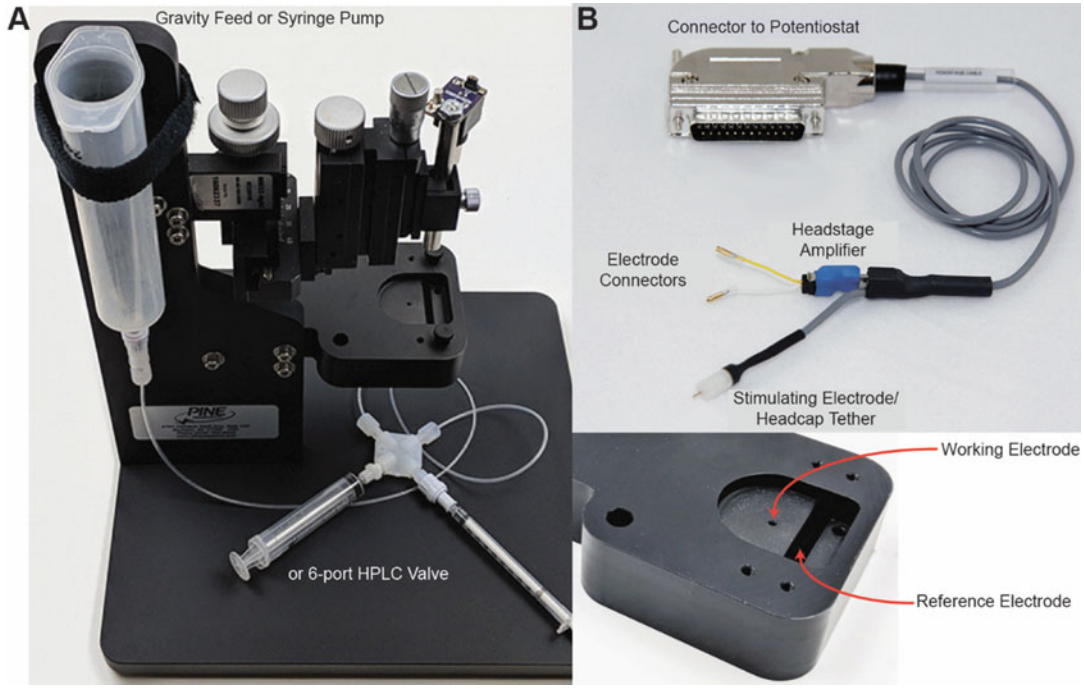

Fig. 2 (**a**) A typical flow cell used for electrode calibration. (**b**) Headstage used to connect the potentiostat to the electrodes. The same headstage is used to tether the animal during freely moving measurements. Tethering strategies can differ. Images: copyright Pine Research Instrumentation 2019, photos used with permission

conjunction with data acquisition cards that are used to interface the software with the hardware [53]. Briefly, the instrumentation generally consists of an analog low-pass filter and a head-amp module, and the "headstage" consists of relevant electrode leads as well as an op-amp that serves as a current–voltage converter (Fig. 2) [54]. The computer-generated potential waveform contains digitization noise that is smoothed using a low-pass filter prior to reaching the microelectrode. The current generated at the microelectrode is converted to an output voltage via a current-to-voltage converter, which amplifies the signal with minimal low-pass filtering. The data acquisition cards are responsible for digital-to-analog and analog-to-digital conversion to and from the headstage, respectively. The gain of the current-to-voltage amplifier is set to convert the output voltage to current based on the size of the electrode.

3.1.2 Waveform Selection and Data Interpretation

The potential waveform used for FSCV has a direct impact on the sensitivity and chemical selectivity of the measurement. For example, DA measurements are commonly made using a waveform that scans from −0.4 to +1.3 V and back (vs. Ag/Ag/Cl), using a scan rate of 400 V s^{-1}, and a waveform application frequency of 10 Hz.

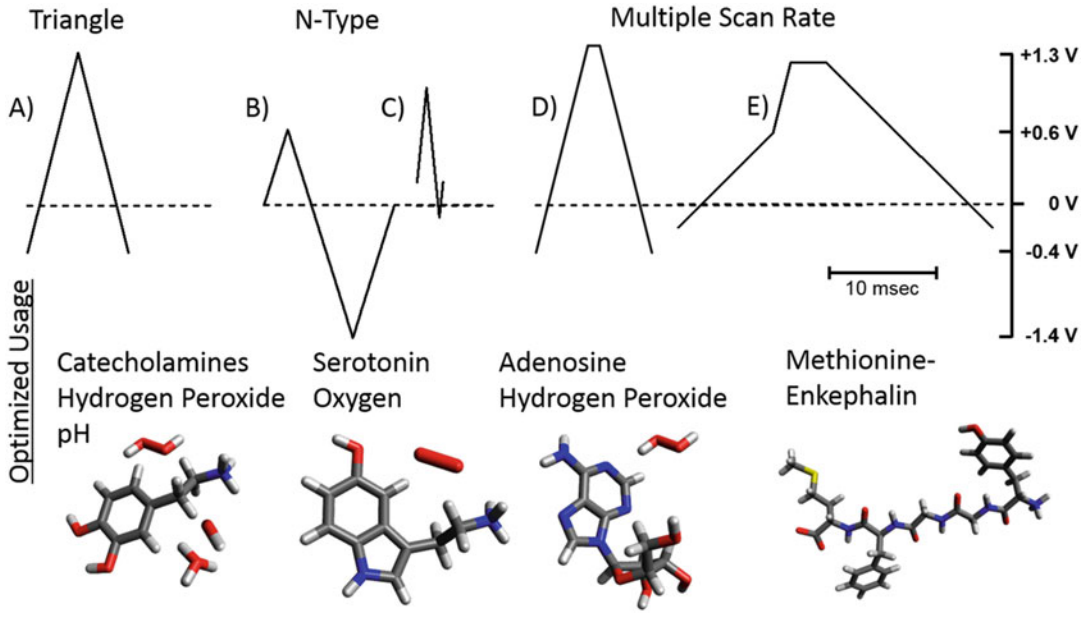

Fig. 3 The FSCV potential waveform can be optimized for the detection of different molecules. Reprinted with permission from Roberts, J.G.; Sombers, L.A. Fast-Scan Cyclic Voltammetry: Chemical Sensing in the Brain and Beyond. Analytical Chemistry. 2018, 90, 490–504. Copyright 2018 American Chemical Society

The voltammetric scan is completed in ~10 ms and the electrode is held at −0.4 V in the time between waveform applications, facilitating the pre-concentration (adsorption) of positively charged DA at the electrode surface [55]. Application of more extreme oxidation potentials improves the detection of many analytes through the generation of oxygen-containing functionalities on the carbon surface, which can facilitate adsorption [28, 56]. Sufficiently positive potentials have even been shown to etch the carbon, providing a renewed sensor surface with each voltammetric scan [22]. The wavelimits, scan rates, and waveform application frequency all impact measurement sensitivity, chemical selectivity, temporal resolution, and data density. For these reasons, the waveform can be customized to enable detection of a number of analytes that cannot be reliably detected using the standard triangular waveform, such as serotonin, oxygen, and neuropeptides [14, 32, 47]. The waveform should be selected based on the chemical nature of the analyte (*see* Fig. 3), the presence of potential interferents, and the lifetime of the targeted species in the extracellular space.

Conventional FSCV measurements are made with a high sampling rate (tens to hundreds of kilohertz), and the waveform is repeated every ~100 ms. To quickly interpret real-time recordings, data are displayed in the form of a color plot (*see* Fig. 1) in which time (or CV number) is plotted on the x-axis, potential (or data point within a CV) is plotted on the y-axis, and current is plotted in

false color. Color plots allow data that are collected over tens of seconds to be quickly visualized. It is important to realize that the time point at which the background is subtracted can be moved, changing the reference point. A vertical slice of the color plot returns a CV that can be used for analyte identification, and a horizontal slice returns information about chemical dynamics in the form of current versus time. The current collected at a specific potential can be converted to concentration through sensor calibration. In this way, information regarding the fluctuations of one or more analytes can be interpreted using voltammograms as chemical identifiers.

3.1.3 Stimulated Neurochemical Release

A variety of strategies can be used to depolarize neurons and induce neurotransmitter release from terminals. Perhaps the most straightforward approach is to use direct electrical stimulation. For this, a calibrated biphasic stimulus isolator delivers a waveform to the stimulating electrode, resulting in the controlled injection of current. The stimulating waveform is typically a biphasic square wave with a defined frequency, amplitude, pulse width, and number of pulses, depending on the experimental goals. For instance, a typical electrical stimulation of the rat midbrain consists of a series of 60–120, biphasic pulses (125–150 μA) with a 2 ms pulse width, applied at 60 Hz [57]. The stimulating waveform can be software controlled or delivered using a digitally triggered waveform generator. To avoid disturbance of electrochemical recordings, the stimulus is only delivered in the time between potential sweeps (for FSCV). Additional approaches for cellular depolarization include optical stimulation via optogenetics, chemogenetic stimulation via designer receptors that are exclusively activated by designer drugs (DREADDs), and local microinfusion of a chemical stimulus.

3.2 Electrode Fabrication

Carbon-fiber microelectrodes are typically insulated with either borosilicate–glass or fused-silica capillary (*see* Fig. 1h). Glass insulated carbon-fiber microelectrodes are easy to produce; however, they are relatively fragile and thus they are most commonly used for measurements in tissue slices or anesthetized animals. Microelectrodes that are insulated with silica capillary take longer to fabricate, but are more robust. These sensors can be used to reliably monitor neurotransmission during behavioral studies, sometimes lasting months [23].

3.2.1 Borosilicate–Glass Carbon-Fiber Microelectrode

1. Connect a vacuum pump to a Büchner (vacuum) flask held in place using a ring stand. Place a single-holed, rubber stopper in the flask, and attach a long plastic tube with a small inner diameter.
2. Place a single carbon fiber on a flat, clean, high-contrast surface that is well illuminated. Using one hand, pinch one end of a

borosilicate glass capillary in the plastic tubing. With the other hand, press one end of the carbon fiber against the surface. Carefully aspirate the fiber through the glass capillary so that the fiber extends from both ends.

3. Place the filled capillary in a vertical capillary puller. Heat softens the glass and gravity pulls the capillary to create two individual segments of glass, each with a taper that forms a seal around the carbon fiber. Cut the fiber with a scissor to make two separate electrodes.
4. Cover a microscope slide with transparent tape and affix a notched piece of putty at one end. The putty serves as a platform to gently lower the taper/seal of the electrode onto the slide. Inspect individual electrodes to ensure a tight glass seal is formed around the carbon fiber.
5. Cut the exposed carbon fiber to length (~100 μm is standard) with a scalpel under a magnification of 10×. Verify the integrity of the seal and the length of the exposed carbon under 40× magnification. Discard the electrode if defects are observed.
6. Solder a gold pin to one end of a steel wire lead. Then, establish electrical connection with the carbon fiber. This can be accomplished by:
   (a) Coat a steel wire lead with conductive silver paint and carefully insert it into the back of the glass capillary. Slight rotation of the wire ensures connectivity with the carbon fiber.
   (b) Backfill the glass capillary with a solution of 4 M potassium acetate and 150 mM potassium chloride. Then insert a wire lead to establish electrical connection.
7. Affix the lead to the glass capillary using small-diameter heat-shrink tubing.

3.2.2 Fused-Silica Carbon-Fiber Microelectrode

1. Cut fused-silica tubing using a pristine scalpel on a sheet of paper folded so that cut sections do not become lost. The length of the tubing segments will be tailored to the desired depth of the implant. To ensure clean cuts, replace the scalpel blade frequently.
2. Lower the silica tubing slowly, and at an angle, into a shallow glass dish containing 70% isopropyl alcohol (IPA). The goal is to remove any air bubbles from the tube. This may take ~20–30 min.
3. Place precut carbon fibers (~2 cm longer than tubing) into the 70% IPA bath. Using a boom microscope for visualization, use tweezers to hold the tubing, and using a cotton swab, float the carbon fiber into the tubing until it extends out of both ends equally.

4. Remove from the IPA bath and allow the outside of the tubing to dry. Using a microscope, note the more cleanly cut end of the tube. Affix filled tubing to a piece of folded tape (L- or V-shaped) placed on a small paper, in a manner that suspends the tubing in air. Fix paper to a container to prevent movement. Allow the IPA to completely evaporate overnight.
5. Take an individual piece of paper with attached tubing and visualize under a boom microscope. Place a drop of two-part hardening epoxy resin on the end of a small needle (26 gauge) and slowly raise the epoxy drop from below to deposit a small bead of epoxy at the clean-cut end of the tubing. This will serve as the electrode seal. Allow the epoxy to dry overnight.
   (a) An ideal seal will be dome-shaped, with no epoxy on the exposed carbon fiber, and minimal to no epoxy left on the shaft of the silica tubing.
   (b) If epoxy is evident on the extended carbon fiber, slowly pull the other end of the fiber to pull the epoxy into the dome.
   (c) Tip: If there are issues obtaining domed epoxy seals, try allowing the epoxy to thicken prior to application.
6. Apply a bead of conductive silver epoxy to the opposite end of the capillary (the other end of the carbon fiber should be evident here). Place a gold pin into the bead of silver epoxy, parallel to the shaft of the tubing. Allow this to dry overnight or cure in the oven at 100 °C for 1 h.
7. Apply two-part hardening epoxy resin with a toothpick to seal the silver epoxy segment. Allow this to dry overnight or cure at 100 °C for 30 min.
8. Coat the silver/epoxy/gold pin connector assembly with liquid electrical tape using a toothpick. Ensure that this coating also interfaces with the fused-silica tubing. Allow this to dry.
9. Cut the exposed carbon fiber to the desired length under a microscope as described in Subheading 3.2.1.
   (a) Alternatively, the electrode can be cut to the desired length between **steps 5** and **6**.

3.2.3 Ag/AgCl Reference Electrode

1. Cut a piece of silver wire to approximately 10 mm and solder it into a gold pin connector.
2. Cover the solder with a quick-dry epoxy, so that soldering material does not ultimately come into contact with tissue.
3. On the day of surgery, the reference electrode is chloridized using 0.1 M HCl and a 9 V battery. Connect the positive terminal to the gold pin on the silver wire and connect a wire or paper clip to the negative terminal. Submerge both wires

into 0.1 M HCl for ~10 s or until the surface of the silver wire turns slightly white.

(a) Alternatively, the reference wire can be chloridized by soaking the exposed silver in Clorox bleach for 2–4 h.

3.2.4 Microelectrode Pretreatment and Viability Assessment

Prior to use in an animal, electrode viability is confirmed in a buffered electrolyte. Electrodes can also be subjected to pretreatments such as flame-etching [58], laser activation [59, 60], and electrochemical conditioning [61, 62]. Such pretreatments can substantially improve sensitivity to a number of analytes. Due to the relative ease of electrochemical conditioning, this method will be briefly described. It can be carried out on the benchtop or in the tissue preparation immediately prior to recording; benchtop characterization permits evaluation of electrode viability prior to implantation.

1. Place a chloridized silver electrode into a beaker containing a buffered electrolyte. Lower the exposed carbon tip of the microelectrode into the buffered electrolyte. Connect the headstage leads (from the potentiostat) to the appropriate electrodes.
2. All potentiometric conditioning generally involves applying potentials $\geq$+ 1.0 V. Perhaps the most common approach is to apply an FSCV waveform scanning from −0.4 to +1.4 V at 400 V s^{-1} using a waveform application frequency of 60 Hz, for ~30 min. Over this time, the background signal should grow substantially, indicative of increasing electrode capacitance. The background signal should ultimately stabilize.
3. Decrease the waveform application frequency to 10 Hz and cycle on the waveform for an additional 5–10 min.
4. Verify electrode integrity. Make a 30–60 s recording using a 10 Hz application frequency. Analyze the recording for excessive noise, glitches, and electrode drift (changes in the background signal over time).
   (a) Assess noise by inspecting CVs and the current-versus-time traces. There may be differences in noise levels associated with different instruments, headstages, and gain. Periodic noise is evident as regular striations in the color plot. Acceptable noise levels are dependent on the amplitude of the signal of interest. Limit of detection is often defined to be 3–5× the standard deviation of the noise.
   (b) Glitches appear as large spikes in current. These are usually indicative of poor electrical connection to the carbon fiber or the reference electrode.
   (c) Drift is indicative of electrode instability and can be evaluated by inspecting color plots and current-versus-time

traces (across all potentials) for changes in current over time. If there is excessive drift (>1–2 nA for a 100-μm carbon-fiber microelectrode over a 30 sec period), further conditioning may stabilize the electrode. Alternatively, drift may indicate an imperfect seal about the carbon fiber. This issue is not remediated with additional conditioning.

3.3 Electrode Implantation in Rat Brain Tissue

FSCV has been used to study neurochemical dynamics in a range of animal models including rats [4, 5, 43, 63], mice [12–14], voles [64], birds [65], fruit flies (*drosophila*) [66, 67], pigs [68], nonhuman primates [69, 70], and even in humans [71]. The following section will describe implantation of a microelectrode in rat striatum to monitor DA release. These methods can serve as the framework for studies targeted at monitoring naturally occurring and stimulated neurotransmission in other brain regions and pathways. Note that all procedures should be approved by the appropriate Institutional Animal Care and Use Committee prior to adoption in the laboratory.

1. Sterilize working area and stereotaxic instrument prior to the procedure. Ensure that all surgical tools are clean and free of debris, then sterilize using an autoclave or bead sterilizer. Make sure other materials (swabs, gauze, etc.) are also sterile.
2. Anesthetize the rat using an approved procedure. Check for reflexes and shave the top of the head using a set of electric trimmers. Then, secure the animal in a stereotaxic frame. Apply eye lubricant and rest the animal on a heating pad to maintain body temperature.
3. Remove any loose hairs around the shaved site. Clean the shaved site by alternating application of 70% isopropyl alcohol and Betadine®, using a new gauze each time. Repeat three times.
4. Locally anesthetize the scalp with a subcutaneous injection of 0.25% bupivacaine (~0.3 mL). Make an incision (~15–20 mm) on the top of the head, parallel with the animal's spine. Carefully retract and cut away the skin to expose the skull (~20 × 15 mm, Fig. 4). Removal of conjunctive tissue and cleaning of the skull is facilitated by using 2–3% hydrogen peroxide and a cotton swab.
5. At this point, both bregma and lambda should be clearly visible (*see* Fig. 4). Use the stereotaxic apparatus to level the head until the difference in the dorsoventral (DV) coordinates at bregma and lambda is <0.2 mm. Make note of bregma coordinates. These will serve as a reference point for all implants.
6. Mark the skull above desired implantation sites using a rat atlas. For example, a location that is +1.2 mm anterior–posterior (AP) and + 1.4 mm medial–lateral (ML) relative to bregma

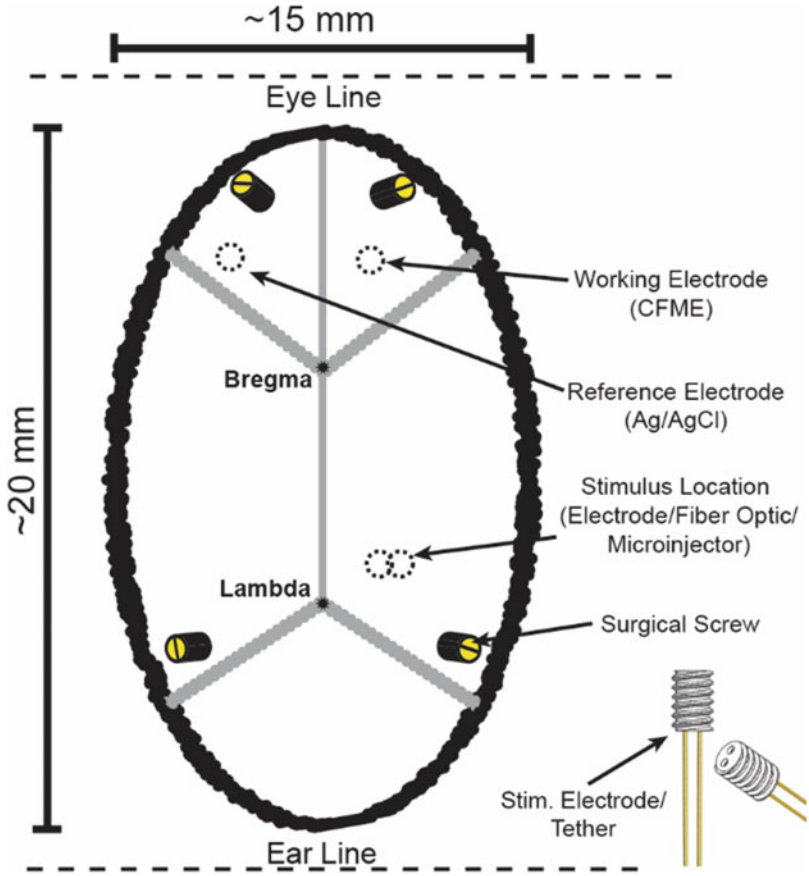

Fig. 4 A graphical representation of the exposed rat skull during surgery. Example markings for placement of electrodes and surgical screws are highlighted. Stimulating electrode/tether image: copyright Plastics One 2019

can be used to position the working electrode above the nucleus accumbens of a rat (~300 g). Mark a spot contralateral to the working electrode for placement of the reference electrode. If incorporating a stimulating electrode (or optrode, injection needle, etc.) into the experimental design, this position can also be marked (e.g., −5.2 mm AP and + 1.0 mm ML for the ventral tegmental area). *See* Fig. 4.

7. Use a rotary tool (Dremmel®) and a small-gauge drill bit to carefully drill through the skull at the marked locations. Drill additional holes for surgical screws:
   (a) Anesthetized preparation: Drill a hole at ~45° near the reference electrode and partially insert surgical screw. *See* Fig. 4.
   (b) Survival surgery: Drill four holes at ~45° at the corners of the exposed skull and insert surgical screws. *See* Fig. 4.

8. Use the stereotaxic instrument to slowly lower electrodes. Prior to each implantation, use a sterile needle to clear dura mater. Prior to the application of cement, ensure the skull is clean and dry.
   (a) Anesthetized preparation: Lower the reference electrode into brain tissue and secure in place using cranioplastic cement. The cement should cover both the reference electrode and the adjacent surgical screw.
   (b) Survival surgery: Mount the reference electrode in a locking intracerebral guide cannula. Lower the guide cannula/reference electrode assembly and affix to the skull and the closest surgical screw using cranioplastic cement. This allows a fresh reference electrode to be carefully inserted for electrochemical measurements and then removed from the guide cannula and replaced with a stylet while the rat is in the home cage.
   (c) If using a stimulating electrode or optrode, it is slowly lowered to target depth and can be cemented in place.
   (d) Lower the microelectrode to just above the hole. Connect the working (microelectrode) and reference electrodes (once cement has hardened) to the headstage and apply waveform. Continue to lower the microelectrode until electrical connection is established (as determined by observing the background current using an oscilloscope). Then slowly lower the microelectrode to just above target depth (−7.0 mm DV for ventral striatum).
9. If this is a survival surgery, affix the electrodes to the skull and complete the domed cement "headcap" by filling in gaps between electrodes with cement, covering all surgical screws and exposed skull area. Allow to harden. Remove the animal from stereotaxic instrument and place in a clean cage on top of a heating pad until recovery. Once fully awake, offer soft food and freshwater along with a fruit-flavored analgesic (acetaminophen 0.1–0.3 g/kg). Monitor the animal's implantation/headcap site, weight, and behavior daily for abnormalities. Generally, animals recover within 1–2 days.
10. Additional Notes.
    (a) *See* Subheading 3.4.1 for additional process that can be incorporated into the procedure for freely moving surgeries.
    (b) If a stimulating electrode is not to be implanted, the stimulation wires can be cut, and the threaded connector can be placed in the cranioplastic cement to provide a tether.

(c) Breathing rate and hydration should be monitored throughout the surgery.

3.4 Voltammetric Measurements

3.4.1 Anesthetized Preparation

1. Immediately following surgery, place the stereotaxic instrument inside a grounded Faraday cage.
2. Connect the working and reference electrodes to the headstage. Connect the stimulating electrode, as appropriate.
3. Condition the carbon-fiber microelectrode on the FSCV waveform to allow it to stabilize in the recording environment. A typical triangular waveform (−0.4 V to 1.3 V) can be applied at 60 Hz for ~15 min, followed by another 5–10 min at 10 Hz.
4. If using a stimulating electrode, cell bodies in the midbrain can be depolarized and recordings at the working electrode can be monitored for time-locked DA release at the terminals. Stimulations are generally spaced in ~5 min increments to allow adequate replenishment of vesicular stores.
5. If no (or low-) amplitude DA release is observed, lower the working electrode (0.1 mm increments) and repeat stimulation. Alternatively, stimulating electrode placement can be similarly adjusted (if not cemented in place).
6. The overall procedure is dependent on the experimental goals. Generally, this will involve monitoring stimulated or phasic neurochemical release before and after some pharmacological manipulation.
   (a) During the survival surgery, a procedure similar to that described in steps 4–5 can be used to position the working electrode prior to affixing in place with cranioplastic cement.
   (b) Specific anesthetics can directly influence dopaminergic systems [72–74].
   (c) Breathing rate (breath/s) and hydration should be continually monitored.

3.4.2 Freely-Moving Preparation

Three to five days after surgery, the animal can be prepared for the experiment (if fully recovered). However, many experimenters allow for up to 3 weeks of recovery time before making measurements. During this time, the animal can begin various behavioral trainings/assessments.

1. Behavior chamber should be placed inside a grounded Faraday cage and appropriate connections with instrumentation, lights, and cameras are established.
2. Test electrical connectivity and noise through the headstage and commutator using a dummy circuit (resistor and capacitor in series), prior to experimentation. The headstage cable should be just long enough to allow the animal to explore the

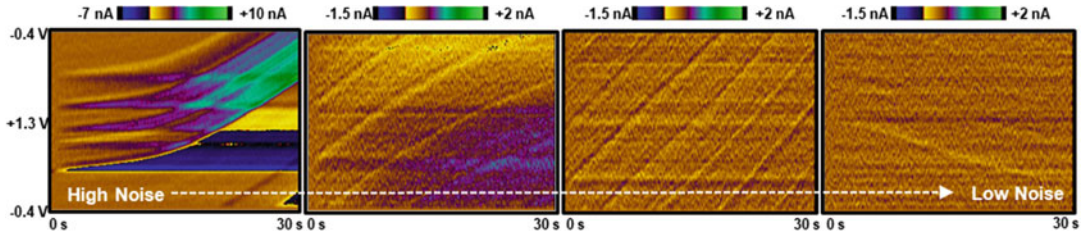

Fig. 5 Representative FSCV recordings with different levels of noise. The left color plot was recorded outside a Faraday cage using an ungrounded potentiostat. The right color plot was recorded in a grounded Faraday cage with a potentiostat sharing the same ground

entirety of the behavior chamber and noise should be minimal (<~0.3 nA). It is important that test recordings are free of noise prior to attaching an electrode, as noise will increase when an electrode is connected. There should be no evidence of any pattern or striping in the color plots (*see* Fig. 5). If noise is detected, disconnect all nonessential components to the system (lights, behavioral lines, etc.) and test again. Components can be added, one at a time, until the problem is identified.

3. On experiment day, tether the animal in the behavioral chamber. Connect the working and reference electrodes to the headstage.
4. Condition the carbon-fiber microelectrode on the desired waveform for ~15 min at 60 Hz, and then for ~10 min at 10 Hz, until the electrode is stable, as determined by inspection of the background current. During this time, the animal acclimates to the behavioral chamber.
5. Proceed with FSCV recordings, behavioral tests, pharmacological manipulations, etc. *See* Fig. 6. for representative data from a recording in the nucleus accumbens. This file includes an electrical stimulation of the ventral tegmental area (12 biphasic, 175 μA pulses at a frequency of 60 Hz with a pulse width of 2 ms).

3.5 Post-Experiment

3.5.1 Verification of Electrode Placement

The tip of the carbon-fiber microelectrode is too small to leave an observable mark in the tissue. Therefore, an electrical lesion can be created at the carbon-fiber tip by applying a high current in an anesthetized animal [23]. However, this process renders the electrode useless for calibration. The rat is transcardially perfused (0.9% saline and 10% formalin), then decapitated and the brain removed for histology.

3.5.2 Electrode Post-Calibration

Whenever possible, the electrode should be carefully removed from the preparation for calibration. The electrode is rinsed in water and calibrated for physiological concentrations (ideally ≥3) of the

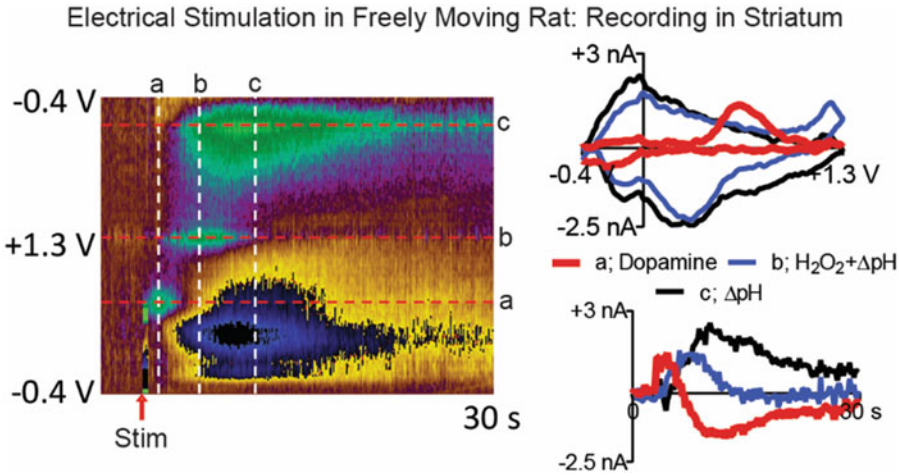

Fig. 6 Example of a DA release event (**a**) recorded in the nucleus accumbens of a freely moving rat in response to electrical stimulation of the ventral tegmental area. In this example, H_2O_2 (**b**) is also recorded along with a change in pH (**c**), due to a hemodynamic response to the stimulation. Voltammograms (top right panel) are extracted from the color plot (vertical lines) to identify chemical changes. Current-versus-time traces (bottom right panel) are extracted (horizontal lines) to reveal neurochemical dynamics. Current can be converted to concentration using the appropriate calibration factor for a given electrode

analytes of interest using a flow-injection apparatus (*see* Fig. 2). This system is composed of a simple electrochemical cell and a sample loop that is used to reproducibly inject a small bolus of analyte onto the electrode surface. A syringe pump (or gravity feed) provides a constant flow (0.5–3 mL/min) of buffer through the cell. A six-port HPLC value and a digitally controlled pneumatic actuator control analyte injections. The reference electrode is submerged in the buffer, the working electrode is slowly lowered into the center of the cell using a micromanipulator, and both are connected to a headstage that is identical that that used for in vivo measurements (ideally, the same headstage). The same waveform is applied to the microelectrode and samples are introduced to the electrode surface under software control. Each concentration is sampled at least in triplicate and the averaged peak current is plotted against concentration. A linear regression is used to relate collected current to analyte concentration.

3.6 Data Analysis

High-Definition Cyclic Voltammetry (HDCV) software can be used for data analysis and visualization as well as to export data as ".txt" files. MATLAB (Mathworks, Inc., Natick, MA) or R (R Core Team; www.r-project.org/) can also be used for data visualization, processing, and quantitative analysis. Principal component regression (PCR; Fig. 7) is the most common multivariate statistical analysis approach used to assess complex FSCV data. It is used to separate intensity-based data into relevant vector components and noise. A training set is constructed that contains cyclic

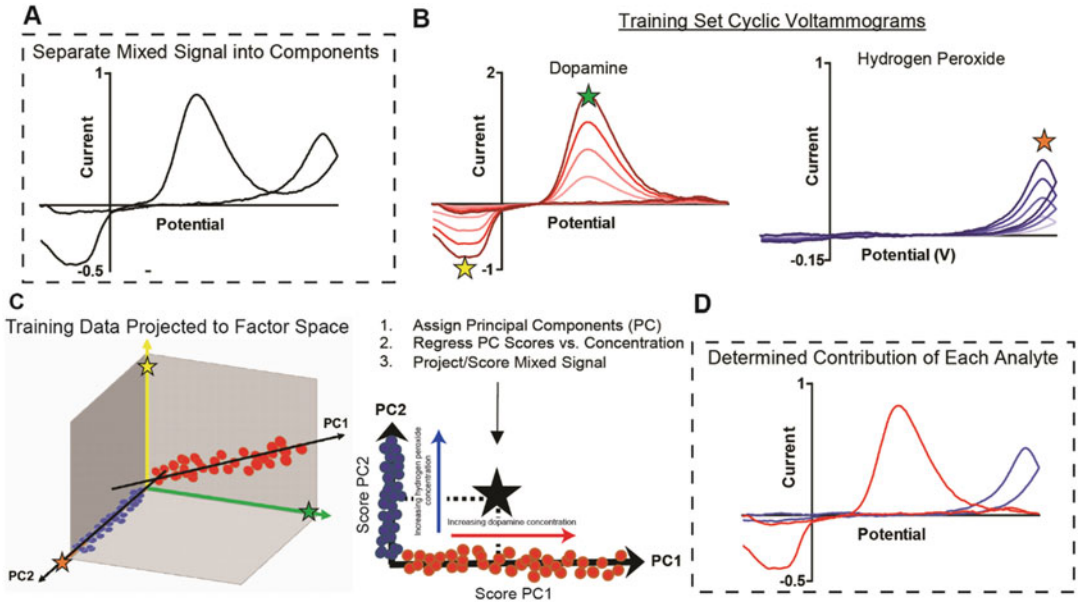

Fig. 7 Principal component regression. (**a**) A representative CV with contributions from both DA and hydrogen peroxide. (**b**) The training set data for these analytes must exhibit the correct shape (and peak position) and encompass the magnitude of the signals measured in vivo. (**c**) Projection of the training data onto factor space. Vectors, or principal components, are assigned to the largest sources of variance, with each orthogonal to the next. The scores of the principal components inherent to each training CV are regressed against analyte concentration. The mixed signal is then projected onto the principal component space. (**d**) Mixed-signal PC scores are used to quantify the contribution of each individual analyte

voltammograms for the major species observed in a recording, at ~5 physiological concentrations each. Principal components describing major sources of variance in the data (from both analyte and interferent signals) are selected, allowing species with sufficiently unique sources of variance to be discriminated from other analytes and interferents, and for noise to be discarded. Then, unknown cyclic voltammograms recorded in vivo are projected onto the principal components to determine unknown concentrations. A well-detailed explanation of the use and validation of PCR in analysis of FSCV data can be found elsewhere [35, 75].

3.7 Additional Experimental Options

3.7.1 Electrophysiology

FSCV can be combined with other measurements, such as electrophysiological measurements of cell activity, to provide additional information on the system under study [15, 54]. For instance, a switch can be incorporated into the headstage to disconnect the microelectrode from the potential waveform between sweeps. Thus, the electrode "floats," adopting the potential of the recording microenvironment in which it resides. This method allows specific molecular dynamics to be correlated with local neuronal activity.

3.7.2 Optogenetics and DREADDs

Advances in biotechnology have enabled a range of optogenetic and chemogenetic tools for investigation of brain function. Optogenetic approaches employ a virus to genetically modify a specific set of neurons to express light-sensitive ion channels (typically rhodopsins) [76, 77]. An implanted optical fiber can then be used to selectively activate or inhibit the specific subsets of neurons. However, penetration of light in tissue is limited, and use of high-intensity light can result in artifacts (photoelectric effects) or local heating of tissue (photothermal effects) [78]. Chemogenetic approaches are similar, in that a virus can be used to selectively target specific neuronal subsets in a given brain region. The targeted cells are genetically modified to express designer G-protein coupled receptors that are selectively activated or inhibited by non-endogenous designer drugs (DREADDS) [79–81]. The most common designer drug is probably clozapine N-oxide (CNO), which can be systemically or locally administered.

3.7.3 Microelectrode Arrays and Wireless Headcaps

Recent advances in instrumentation and microelectrode technologies have enabled microelectrode arrays to be incorporated into voltammetric experiments, simultaneously providing chemical information at multiple recording sites [82]. For example, arrays of polymer-insulated carbon-fiber microelectrodes have been used to monitor DA dynamics at multiple recording sites in rat striatum over months, with minimal tissue damage [69].

Most experiments in awake animals employ a tethered wire connection, which can significantly limit the options for behavioral challenges and can introduce electrical artifacts in response to vigorous movement of electrical connections. However, wireless integrated circuits can be used to create miniaturized potentiostat devices mounted directly on the animal itself [83, 84]. This advance promises to facilitate investigation of social interactions and more natural movement. However, limitations in wireless data transfer rates, especially in studies incorporating multiple electrodes, have limited widespread use. Advances in real-time data compression strategies (prior to transfer) will increase utilization of this technology [85].

3.7.4 Electrode Materials and Membrane Coatings

A significant amount of work has been done to characterize carbon-based materials for in vivo studies. Materials such as diamond [86], carbon nanotubes [28, 87], nanofibers [88], and nanotube yarns [27, 60] have all been utilized as sensors and can offer improved performance in specific experimental situations. It is becoming more common to exploit nanoscale electrode materials for in vivo studies as the smaller size domain can enhance mass transfer and electron transfer kinetics to benefit sensitivity and selectivity [27–29, 87].

It is also common to coat the sensor surface with chemically selective polymer membranes to enhance sensitivity, selectivity, or

stability. For instance, Nafion is a perfluorinated ion-exchange polymer that is often used, sometimes with polyethylenedioxythiophene (PEDOT), on the microelectrode surface to enhance sensitivity to DA and to decrease sensitivity to ascorbic acid [89, 90]. Nanoparticles and carbon nanomaterials can be incorporated into these membranes to further enhance electrode performance [87, 91]. In addition, chitosan hydrogels have been used to entrap various oxidase enzymes at the carbon electrode surface [92, 93]. This has allowed for indirect detection of non-electroactive molecules, such as glucose and lactate, by way of voltammetric measurements of hydrogen peroxide; e.g., glucose oxidase produces gluconic acid and hydrogen peroxide in the presence of glucose. With this approach, it is possible to simultaneously record both electroactive and non-electroactive species at the same recording site [94].

3.8 Critical Considerations and Alternative Methods

3.8.1 Calibration and Principal Component Regression for In Vivo Recordings

When making FSCV measurements, it is necessary to calibrate each electrode for accurate quantification of neurochemical events. Individual electrode performance is variable and dependent on the chemical nature of the electrode at the microscopic level as well as the nature of the insulating seal that defines the sensor size at the macroscopic level. Acutely implanted sensors can be removed and post-calibrated in a flow cell. This approach has been demonstrated to be effective; however, it does not account for possible matrix effects. Analyte(s), macromolecules, small organic molecules, and even spectator ions can interact with the carbon surface through potential-specific reactions to affect performance. The use of permanently implanted sensors presents additional analytical challenges, as electrodes can become significantly fouled [22, 95], can be encapsulated in response to the implantation (gliosis) [3], and are difficult to remove for calibration. Thus, electrode performance is assumed to be constant for the entirety of the experiment, which can last months.

Overall, these issues complicate the construction of appropriate training sets for multivariate analysis, typically achieved using principal component regression (PCR). A training set for DA can be collected in vivo using stimulated release or using DA transients that are reliably evoked by introduction of an unexpected reward stimulus (e.g., introduction of a sugar pellet) [96]. However, ensuring that a chemically independent signal is obtained in vivo is difficult. Alternatively, it is common to use data recorded at an electrode in another animal or collected ex vivo in a flow cell to serve as training data for PCR [7, 75, 97]. This approach, although in direct contrast to proper quantitative technique, has proved effective if significant care is taken in analysis. However, it is important to note that the analyte-specific voltammograms and scaling factors that lie at the core of PCR are dependent on the chemical nature of the recording environment. CVs recorded in vivo often

differ in overall shape compared to those for the same analyte recorded at another time in the living brain or when compared to CVs recorded in a benchtop flow cell. If there is significant mismatch between the training CVs and the CVs inherent to the unknown data set, model validation will fail. Misidentification of analyte contributions will lead to misestimation of chemical dynamics [98]. To combat this, it has become standard to apply a potential offset (~200 mV) to the waveform during in vivo measurements in order to artificially shift CVs such that they appear more like those recorded in vitro [23, 75, 99]. However, it is in this author's opinion that this approach should be avoided, as application of a potential offset shifts the applied waveform, which necessarily influences the electrochemistry.

There have been recent advances in electrode calibration strategies for in vivo measurements. It has been shown that the shape and magnitude of the background signal serve as predictors of both electrode sensitivity and the overall cyclic voltammogram shape for multiple analytes [61, 100]. Another study has demonstrated that exposing the sensor to a buffer containing bovine serum albumin before pre-calibration gives similar results as conventional post-calibration strategies that follow implantation [101].

3.8.2 Background Subtraction and Electrochemical Drift

FSCV is inherently a differential technique because the background current is subtracted to reveal faradaic contributions to the current that result from the oxidation or reduction of chemical species present in the vicinity of the electrode. Recently, an approach termed fast-scan controlled-adsorption voltammetry (FSCAV) has allowed direct determination of basal levels of neurotransmitter by manipulation of analyte adsorption on the electrode surface [102, 103]. FSCAV functions by applying a triangular FSCV waveform at a high frequency (~100 Hz) to thoroughly electrolyze species adsorbed on the electrode surface. This is followed by a seconds-long period at an electrostatically advantageous potential to adsorb analyte to the clean surface. Finally, there is a period of typical FSCV measurements to quantify the adsorbed material. The first CVs collected after the controlled-adsorption period contain information related to the basal levels of neurotransmitter in the vicinity of the electrode. This technique is applicable to species that adsorb to the sensor surface, such as DA and serotonin, with low nanomolar limits of detection. One drawback, however, is that it offers significantly less temporal resolution than FSCV.

In typical FSCV measurements, the background signal is only stable for ~60 s. Following this period, significant and diverse background subtraction artifacts, termed electrochemical drift, complicate data interpretation. Thus, in a continuous recording, the reference (background) must be repositioned in ~60 s increments to analyze the entirety of the recording. Assessment of more

gradual changes in analyte concentration occurring over several minutes cannot be reliably evaluated.

A number of strategies have been developed to address the limited time window and the differential nature of FSCV measurements. A charge-balanced waveform can be paired with background subtraction to permit the evaluation of more gradual changes in analyte concentration over an hour, albeit with a significant decrease in temporal resolution [104]. Another study has incorporated a small potential step to sample the impedance state of the sensor prior to the application of each triangular waveform. When combined with a convolution-based approach to data analysis, this strategy allows prediction and removal of non-faradaic contributions to electrode drift [36]. This method is particularly effective for removal of drift attributed to rapid changes in local ionic composition. A third method involves the use of a paired voltammetric waveform in which a smaller triangular sweep is used to sample the contribution of electrode drift to the signal immediately prior to each full voltammetric sweep. Partial-least-squares regression is used to predict and subtract the drift contribution recorded in each potential sweep [37]. This method provides a simple manner to evaluate both rapid and gradual molecular fluctuations in ~10–30 min in vivo recordings while maintaining temporal resolution.

3.8.3 Time-Consuming Data Analysis

The complex and seemingly random nature of the phasic neurochemical events monitored during in vivo studies can result in a significant amount of time spent in data analysis, particularly in light of the issues discussed in Subheadings 3.8.1 and 3.8.2. The general complexity of the signal necessitates appropriate background subtraction and careful construction and validation of training sets during data analysis. This can introduce human bias and error when analyzing data. An exciting step has been made toward automation of data analysis [105]. In this work, an algorithm was constructed using MATLAB to evaluate extended (>10 min) recordings of adenosine transients in live rats. The script was used to adjust the background position in a controlled and non-biased manner based on well-defined criteria. This approach was used to successfully identify transient neurochemical events with a high degree of accuracy, as compared to the traditional approach to data analysis by way of a human analyst. In this case, the human analysts spent >10 h evaluating the recording, whereas the algorithm was used to achieve similar results in <1 h. Significant expansion of these methods will be vital for increasing the throughput of FSCV analysis and for expanding from single-channel recordings to microelectrode arrays.

3.8.4 Data Density and Analog/Digital Filtering

During a typical in vivo FSCV experiment, it is common to make both short measurements (~1–2 min) and continuous recordings (10 min to >hour), but the longer recordings are analyzed as a series of short segments for background subtraction purposes, as described above. The default sampling rate and waveform application rate in HDCV software are 100 kHz and 10 Hz, respectively. Thus, the amount of recorded data becomes quite significant and requires adequate storage. It has been demonstrated that reduced sampling and waveform application rates can provide adequate temporal and electrochemical resolution for monitoring subsecond chemical dynamics in many experimental paradigms [106, 107].

It is common to use an analog filter to smooth the digitized waveform output. This is often a low-pass filter with a 2 kHz cutoff frequency (but is dependent on the scan rate of the applied waveform). It is also common to digitally filter the recorded current response. For example, the default filter setting in HDCV employs a fourth-order low-pass Bessel filter with a 2-kHz cutoff frequency. Fourier transforms can also be used to filter data sets [53]. When used carefully, filtering can greatly enhance the quality of the recording and ease data analysis. However, it is imperative that the effects of analog and digital filtering be critically assessed in advance and that filter settings remain consistent for every recording included in the experimental data set. This is because filtering can directly impact the apparent shape of a CV, the position of redox potentials, and current magnitude (*see* Fig. 8). These issues are exacerbated when lower sampling rates and/or faster scan rates are employed.

3.8.5 Systems Driven at the Reference Versus the Working Electrode

In a two-electrode setup, such as that which is commonly used in FSCV, the potentiostat can be used to directly drive either the reference or the working electrode to achieve the same potential difference across the system. In a reference-driven system, an inverse waveform is applied at the reference electrode to achieve the target potential at the working electrode. Alternatively, the potential can be directly controlled at the working electrode. Both methods result in identical measurements. However, it is imperative to consider future needs before purchasing an instrument of either type. For example, waveforms are selected based on the analyte(s) targeted. A reference-driven system will not be capable of individually addressing more than one working electrode at a time.

3.8.6 Electrical/Optical Stimulation Using HDCV

HDCV software can be used to design and control the delivery of customizable pulse sequences for optical and electrical stimulation. It is important to note that the pulsed waveform is gated so as not to interfere with the electrochemical measurement; i.e., the pulse train can only be applied between voltammetric sweeps. The user must be cognizant of this, to ensure delivery of the desired

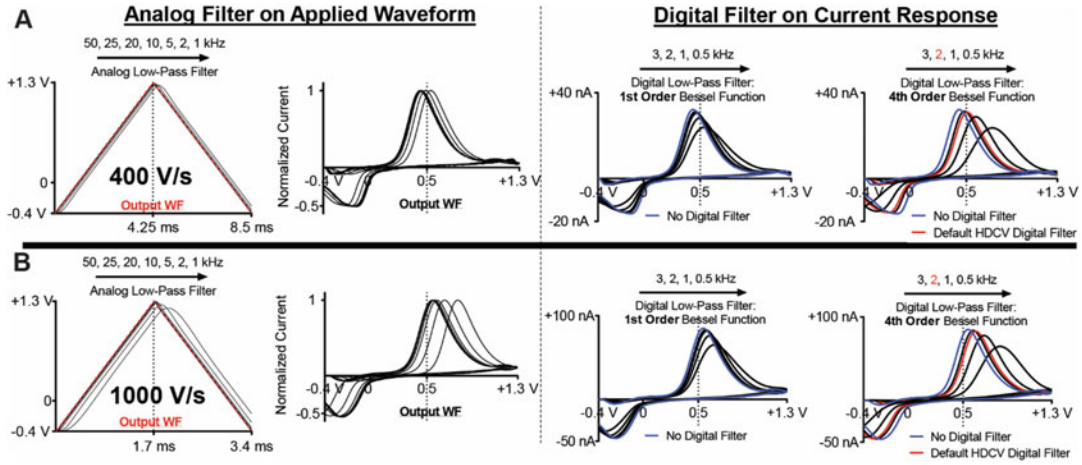

Fig. 8 (Left) Effects of low-pass analog filtering on the applied waveform and CVs for DA. (Right) Effects of digital low-pass filtering on the DA voltammograms. The trace in red represents the standard setting in HDCV and the blue trace represents no digital filtering. These data are displayed for a triangular waveform applied at 400 V s^{-1} (**a**) and 1000 V s^{-1} (**b**)

stimulation pulse train. For example, a 60 Hz stimulation consisting of 60 biphasic pulses, each 2 ms in duration, should presumably be delivered over the course of 1 s. However, the true stimulus delivered is dependent on the manner in which the stimulation pulses are "gated" relative to the applied waveform (*see* Fig. 9). In this case, if the "stim delay" time is 20 ms, then the true stimulus will more closely approximate a 10 Hz application of five 60 Hz pulses over 1 s, and only 50 total pulses will be delivered.

4 Conclusions

FSCV is a powerful electroanalytical method that provides the means to monitor rapid (sub-second), low-level (nano−/micromolar) molecular species in real time. When paired with carbon-based microelectrodes, reliable measurements can be made at single cells, in live tissue slices, and in intact animal subjects over the course of seconds, hours, weeks, or months. FSCV has provided remarkable insight into the molecular mechanisms that underlie specific aspects of goal-directed behavior and associative learning, when appropriate behavioral and pharmacological paradigms have been utilized. Advances in pharmacology and genetic methods to reliably manipulate brain circuitry have enhanced the power of these studies. Recent advances in sensor materials and data analysis paradigms have expanded the detectable pool of analytes and enabled simultaneous monitoring of multiple species, both electroactive and non-electroactive, at a single recording site. Additionally, new methods have allowed for evaluation of more gradual changes

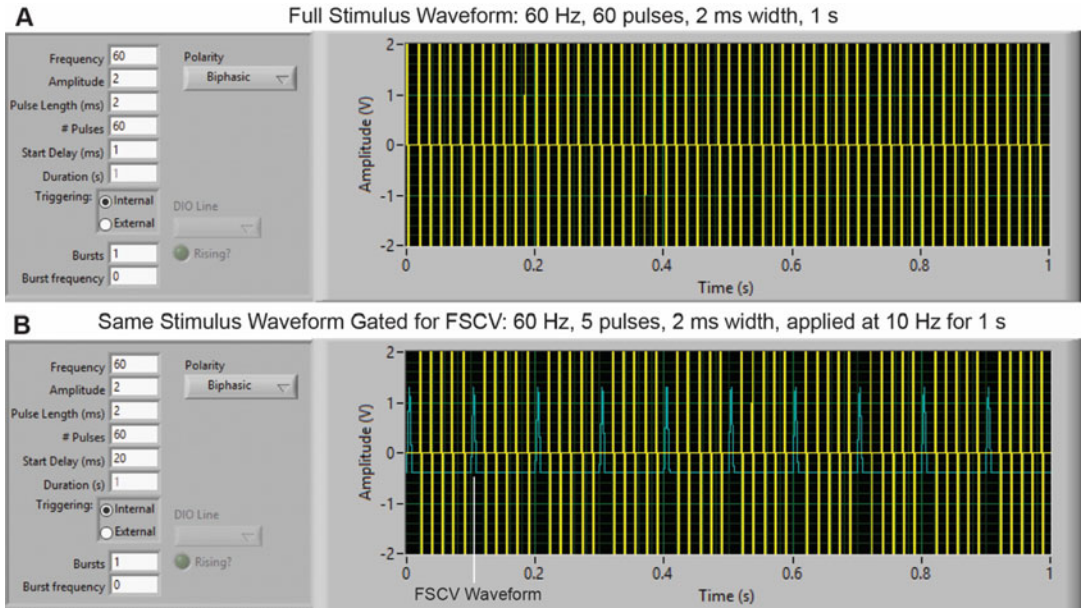

Fig. 9 Stimulation pulses are "gated" to prevent overlap with application of the voltammetric waveform. This can inadvertently result in stimulation parameters that differ from the assumed output. (**a**) Full stimulus waveform: 60 Hz, 60 pulses, 2 ms width, 1 s. (**b**) Same stimulus waveform gated for FSCV: 60 Hz, 5 pulses, 2 ms width, applied at 10 Hz for 1 s

in analyte concentration, expanding the scope of FSCV studies. Miniaturization of the instrumentation is enabling new behavioral studies, and the incorporation of microelectrode arrays is enabling regional mapping of molecular dynamics, on a broad spatial scale. Continued advances in semiautomated algorithms and multivariate strategies for high-throughput data analysis will empower researchers to draw more impactful conclusions from FSCV recordings.

Acknowledgments

Research in the Sombers laboratory on these topics has been funded by grants from the National Institutes of Health, the National Science Foundation, and NCSU Department of Chemistry. C.J.M. is supported by an NSF Graduate Research Fellowship (DGE-1252376). In addition, we gratefully acknowledge our colleagues and coworkers, past and present, for many of the studies cited in this review.

References

1. Michael AC, Borland LM (eds) (2006) Electrochemical methods for neuroscience. CRC Press, Boca Raton, FL
2. Bucher ES, Wightman RM (2015) Electrochemical analysis of neurotransmitters. Annu Rev Anal Chem 8:239–261

3. Peters JL, Miner LH, Michael AC, Sesack SR (2004) Ultrastructure at carbon fiber microelectrode implantation sites after acute voltammetric measurements in the striatum of anesthetized rats. J Neurosci Methods 137:9–23
4. Day JJ, Roitman MF, Wightman RM, Carelli RM (2007) Associative learning mediates dynamic shifts in dopamine signaling in the nucleus accumbens. Nat Neurosci 10:1020–1028
5. Stuber GD, Klanker M, de Ridder B et al (2008) Reward-predictive cues enhance excitatory synaptic strength onto midbrain dopamine neurons. Science 321:1690–1692
6. Gan JO, Walton ME, Phillips PEM (2010) Dissociable cost and benefit encoding of future rewards by mesolimbic dopamine. Nat Neurosci 13:25–27
7. Howe MW, Tierney PL, Sandberg SG, Phillips PEM, Graybiel AM (2013) Prolonged dopamine signalling in striatum signals proximity and value of distant rewards. Nature 500:575–579
8. Flagel SB, Clark JJ, Robinson TE, Mayo L, Czuj A, Willuhn I, Akers CA, Clinton SM, Phillips PEM, Akil H (2011) A selective role for dopamine in stimulus–reward learning. Nature 469:53–57
9. Owesson-White CA, Cheer JF, Beyene M, Carelli RM, Wightman RM (2008) Dynamic changes in accumbens dopamine correlate with learning during intracranial self-stimulation. Proc Natl Acad Sci U S A 105:11957–11962
10. Syed EC, Grima LL, Magill PJ, Bogacz R, Brown P, Walton ME (2016) Action initiation shapes mesolimbic dopamine encoding of future rewards. Nat Neurosci 19:34–36
11. Wood KM, Zeqja A, Nijhout HF, Reed MC, Best J, Hashemi P (2014) Voltammetric and mathematical evidence for dual transport mediation of serotonin clearance in vivo. J Neurochem 130:351–359
12. Saylor RA, Hersey M, West A, Buchanan AM, Berger SN, Nijhout HFm Reed MC, Best J, Hashemi P (2019) In vivo serotonin dynamics in male and female mice: determining effects of acute escitalopram using fast scan cyclic voltammetry. Front Neurosci 13:362
13. Dankoski EC, Carroll S, Wightman RM (2016) Acute selective serotonin reuptake inhibitors regulate the dorsal raphe nucleus causing amplification of terminal serotonin release. J Neurochem 136:1131–1141
14. Dankoski EC, Agster KL, Fox ME, Moy SS, Wightman RM (2014) Facilitation of serotonin signaling by SSRIs is attenuated by social isolation. Neuropsychopharmacology 39:2928–2937
15. Kirkpatrick DC, McKinney CJ, Manis PB, Wightman RM (2016) Expanding neurochemical investigations with multi-modal recording: simultaneous fast-scan cyclic voltammetry, iontophoresis, and patch clamp measurements. Analyst 141:4902–4911
16. Belle AM, Owesson-White C, Herr NR, Carelli RM, Wightman RM (2013) Controlled iontophoresis coupled with fast-scan cyclic voltammetry/electrophysiology in awake, freely moving animals. ACS Chem Neurosci 4:761–771
17. Gómez-A A, Shnitko TA, Barefoot HM, Brightbill EL, Sombers LA, Nicola SM, Robinson DL (2019) Local μ-opioid receptor antagonism blunts evoked phasic dopamine release in the nucleus accumbens of rats. ACS Chem Neurosci 10:1935–1940
18. Duwensee H, Vázquez-Alvarez T, Flechsig GU, Wang J (2009) Thermally induced electrode protection against biofouling. Talanta 77:1757–1760
19. Kuhlmann J, Dzugan LC, Heineman WR (2012) Comparison of the effects of biofouling on voltammetric and potentiometric measurements. Electroanalysis 24:1732–1738
20. Patel J, Radhakrishnan L, Zhao B, Uppalapati B, Daniels RC, Ward KR, Collinson MM (2013) Electrochemical properties of nanostructured porous gold electrodes in biofouling solutions. Anal Chem 85:11610–11618
21. Harreither W, Trouillon R, Poulin P, Neri W, Ewing AG, Safina G (2013) Carbon nanotube fiber microelectrodes show a higher resistance to dopamine fouling. Anal Chem 85:7447–7453
22. Takmakov P, Zachek MK, Keithley RB, Walsh PL, Donley C, McCarty GS, Wightman RM (2010) Carbon microelectrodes with a renewable surface. Anal Chem 82:2020–2028
23. Clark JJ, Sandberg SG, Wanat MJ, Gan JO, Horne EA, Hart AS, Akers CA, Parker JG, Willuhn I, Martinez V, Evans SB, Stella N, Phillips PEM (2010) Chronic microsensors for longitudinal, subsecond dopamine detection in behaving animals. Nat Methods 7:126–129
24. Park J, Aragona BJ, Kile BM, Carelli RM, Wightman RM (2010) In vivo voltammetric monitoring of catecholamine release in subterritories of the nucleus accumbens shell. Neuroscience 169:132–142

25. Arbuthnott GW, Wickens J (2007) Space, time and dopamine. Trends Neurosci 30:62–69
26. Bard AJ, Faulkner LR (2001) Electrochemical methods: fundamentals and applications, 2nd edn. John Wiley, New York
27. Schmidt AC, Wang X, Zhu Y, Sombers LA (2013) Carbon nanotube yarn electrodes for enhanced detection of neurotransmitter dynamics in live brain tissue. ACS Nano 7:7864–7873
28. Jacobs CB, Vickrey TL, Venton BJ (2011) Functional groups modulate the sensitivity and electron transfer kinetics of neurochemicals at carbon nanotube modified microelectrodes. Analyst 136:3557–3565
29. Puthongkham P, Yang C, Venton BJ (2018) Carbon nanohorn-modified carbon fiber microelectrodes for dopamine detection. Electroanalysis 30:1073–1081
30. Unwin PR, Güell AG, Zhang G (2016) Nanoscale electrochemistry of sp2 carbon materials: from graphite and graphene to carbon nanotubes. Acc Chem Res 49:2041–2048
31. Cryan MT, Ross AE (2019) Scalene waveform for codetection of guanosine and adenosine using fast-scan cyclic voltammetry. Anal Chem 91:5987–5993
32. Calhoun SE, Meunier CJ, Lee CA, McCarty GS, Sombers LA (2018) Characterization of a multiple-scan-rate voltammetric waveform for real-time detection of met-enkephalin. ACS Chem Neurosci 10:2022–2032
33. Ross AE, Venton BJ (2014) Sawhorse waveform voltammetry for selective detection of adenosine, ATP, and hydrogen peroxide. Anal Chem 86:7486–7493
34. Jackson BP, Dietz SM, Wightman RM (1995) Fast-scan cyclic voltammetry of 5-hydroxytryptamine. Anal Chem 67:1115–1120
35. Keithley RB, Carelli RM, Wightman RM (2010) Rank estimation and the multivariate analysis of in vivo fast-scan cyclic voltammetric data. Anal Chem 82:5541–5551
36. Johnson JA, Hobbs CN, Wightman RM (2017) Removal of differential capacitive interferences in fast-scan cyclic voltammetry. Anal Chem 89:6166–6174
37. Meunier CJ, McCarty GS, Sombers LA (2019) Drift subtraction for fast-scan cyclic voltammetry using double-waveform partial-least-squares regression. Anal Chem 91:7319–7327
38. Johnson JA, Gray JH, Rodeberg NT, Wightman RM (2017) Multivariate curve resolution for signal isolation from fast-scan cyclic voltammetric data. Anal Chem 89:10547–10555
39. Root DH, Hoffman AF, Good CH, Zhang S, Gigante E, Lupica CR, Morales M (2015) Norepinephrine activates dopamine D4 receptors in the rat lateral Habenula. J Neurosci 35:3460–3469
40. Wolf K, Zarkua G, Chan SA, Sridhar A, Smith C (2016) Spatial and activity-dependent catecholamine release in rat adrenal medulla under native neuronal stimulation. Physiol Rep 4:e12898
41. Park JW, Bhimani RV, Park JW (2017) Noradrenergic modulation of dopamine transmission evoked by electrical stimulation of the locus coeruleus in the rat brain. ACS Chem Neurosci 8:1913–1924
42. Hensley AL, Colley AR, Ross AE (2018) Real-time detection of melatonin using fast-scan cyclic voltammetry. Anal Chem 90:8642–8650
43. Hashemi P, Dankoski EC, Petrovic J, Keithley RB, Wightman RM (2009) Voltammetric detection of 5-hydroxytryptamine release in the rat brain. Anal Chem 81:9462–9471
44. Sanford AL, Morton SW, Whitehouse KL, Oara HM, Lugo-Morales LZ, Roberts JG, Sombers LA (2010) Voltammetric detection of hydrogen peroxide at carbon fiber microelectrodes. Anal Chem 82:5205–5210
45. Spanos M, Gras-Najjar J, Letchworth JM, Sanford AL, Toups JV, Sombers LA (2013) Quantitation of hydrogen peroxide fluctuations and their modulation of dopamine dynamics in the rat dorsal striatum using fast-scan cyclic voltammetry. ACS Chem Neurosci 4:782–789
46. Dengler AK, Wightman RM, McCarty GS (2015) Microfabricated collector-generator electrode sensor for measuring absolute pH and oxygen concentrations. Anal Chem 87:10556–10564
47. Zachek MK, Takmakov P, Moody B, Wightman RM, McCarty GS (2009) Simultaneous decoupled detection of dopamine and oxygen using Pyrolyzed carbon microarrays and fast-scan cyclic voltammetry. Anal Chem 81:6258–6265
48. Ross AE, Venton BJ (2015) Adenosine transiently modulates stimulated dopamine release in the caudate–putamen via A1 receptors. J Neurochem 132:51–60
49. Pihel K, Schroeder TJ, Wightman RM (1994) Rapid and selective cyclic voltammetric measurements of epinephrine and norepinephrine as a method to measure secretion from single

bovine adrenal medullary cells. Anal Chem 66:4532–4537

50. Phillips PEM, Wightman RM (2003) Critical guidelines for validation of the selectivity of in-vivo chemical microsensors. TrAC Trends Anal Chem 22:509–514
51. McCreery RL (2008) Advanced carbon electrode materials for molecular electrochemistry. Chem Rev 108:2646–2687
52. Takmakov P, Zachek MK, Keithley RB, Bucher ES, McCarty GS (2010) Characterization of local pH changes in brain using fast-scan cyclic voltammetry with carbon microelectrodes. Anal Chem 82:9892–9900
53. Bucher ES, Brooks K, Verber MD, Keithley RB, Owesson-White C, Carroll S, Takmakov P, McKinney CJ, Wightman RM (2013) Flexible software platform for fast-scan cyclic voltammetry data acquisition and analysis. Anal Chem 85:10344–10353
54. Takmakov P, McKinney CJ, Carelli RM, Wightman RM (2011) Instrumentation for fast-scan cyclic voltammetry combined with electrophysiology for behavioral experiments in freely moving animals. Rev Sci Instrum 82:074302
55. Bath BD, Michael DJ, Trafton BJ, Joseph JD, Runnels PL, Wightman RM (2000) Subsecond adsorption and desorption of dopamine at carbon-fiber microelectrodes. Anal Chem 72:5994–6002
56. Roberts JG, Moody BP, McCarty GS, Sombers LA (2010) Specific oxygen-containing functional groups on the carbon surface underlie an enhanced sensitivity to dopamine at electrochemically pretreated carbon Fiber microelectrodes. Langmuir 26:9116–9122
57. Trevathan JK, Yousefi A, Park HO, Bartoletta JJ, Ludwig KA, Lee KH, Lujan JL (2017) Computational modeling of neurotransmitter release evoked by electrical stimulation: nonlinear approaches to predicting stimulation-evoked dopamine release. ACS Chem Neurosci 8:394–410
58. Strand AM, Venton BJ (2008) Flame etching enhances the sensitivity of carbon-fiber microelectrodes. Anal Chem 80:3708–3715
59. Poon M, McCreery RL (1986) In situ laser activation of glassy carbon electrodes. Anal Chem 58:2745–2750
60. Yang C, Trikantzopoulos E, Nguyen MD, Jacobs CB, Wang Y, Mahjouri-Samani M, Ivanov IN, Venton BJ (2016) Laser treated carbon nanotube yarn microelectrodes for rapid and sensitive detection of dopamine in vivo. ACS Sens 1:508–515
61. Roberts JG, Toups JV, Eyualem E, McCarty GS, Sombers LA (2013) In situ electrode calibration strategy for voltammetric measurements in vivo. Anal Chem 85:11568–11575
62. Feng JX, Brazell M, Renner K, Kasser R, Adams RN (1987) Electrochemical pretreatment of carbon fibers for in vivo electrochemistry: effects on sensitivity and response time. Anal Chem 59:1863–1867
63. Spanos M, Xie X, Gras-Najjar J, White SC, Sombers LA (2019) NMDA receptor-dependent cholinergic modulation of mesolimbic dopamine cell bodies: neurochemical and behavioral studies. ACS Chem Neurosci 10:1497–1505
64. Resendez SL, Keyes PC, Day JJ, Hambro C, Austin CJ, Maina FK, Eidson LN, Porter-Stransky KA, Nevarez N, McLean JW, Kuhnmuench MA, Murphy AZ, Matthews TA, Aragona BJ (2016) Dopamine and opioid systems interact within the nucleus accumbens to maintain monogamous pair bonds. elife 5:e15325
65. Xiao L, Chattree G, Oscos FG, Coa M, Wanat MJ, Roberts TF (2018) A basal ganglia circuit sufficient to guide birdsong learning. Neuron 98:208–221.e5
66. Rees HR, Anderson SE, Privman E, Bau HH, Venton BJ (2015) Carbon Nanopipette electrodes for dopamine detection in Drosophila. Anal Chem 87:3849–3855
67. Makos MA, Kim Y-C, Han KA, Heien ML, Ewing AG (2009) In vivo electrochemical measurements of exogenously applied dopamine in Drosophila melanogaster. Anal Chem 81:1848–1854
68. Shon Y-M, Lee KH, Goerss SJ, Kim IY, Kimble C, Van Gompel JJ, Bennet K, Blaha CD, Chang SY (2010) High frequency stimulation of the subthalamic nucleus evokes striatal dopamine release in a large animal model of human DBS neurosurgery. Neurosci Lett 475:136–140
69. Schwerdt HN, Shimazu H, Amemori K-I, Amemori S, Tierney PL, Gibson DJ, Hong S, Yoshida T, Langer R, Cima MJ, Graybiel AM (2017) Long-term dopamine neurochemical monitoring in primates. Proc Natl Acad Sci U S A 114:13260–13265
70. Ariansen J, Heien MLAV, Hermans A, Phillips PEM, Hernadi I, Bermudez MA, Shultz W, Wightman RM (2012) Monitoring extracellular pH, oxygen, and dopamine during reward delivery in the striatum of primates. Front Behav Neurosci 6:36
71. Kishida KT, Saez I, Lohrenz T, Witcher MR, Laxton AW, Tatter SB, White JP, Ellis TL,

Phillips PEM, Montague PR (2016) Subsecond dopamine fluctuations in human striatum encode superposed error signals about actual and counterfactual reward. Proc Natl Acad Sci U S A 113:200–205

72. Votaw J, Byas-Smith M, Hua J, Voll R, Martarello L, Levey AI, Bowman D, Goodman M (2003) Interaction of isoflurane with the dopamine transporter. Anesthesiology 98:404–411
73. Brodnik ZD, España RA (2015) Dopamine uptake dynamics are preserved under isoflurane anesthesia. Neurosci Lett 606:129–134
74. Adachi YU, Yamada S, Satomoto M, Higuchi H, Watanabe K, Kazama T (2005) Isoflurane anesthesia induces biphasic effect on dopamine release in the rat striatum. Brain Res Bull 67:176–181
75. Rodeberg NT, Sandberg SG, Johnson JA, Phillips PEM, Wightman RM (2017) Hitchhiker's guide to voltammetry: acute and chronic electrodes for in vivo fast-scan cyclic voltammetry. ACS Chem Neurosci 8:221–234
76. Deisseroth K (2011) Optogenetics. Nat Methods 8:26–29
77. Adamantidis AR, Tsai H-C, Boutrel B, Zhang F, Stuber GD, Budygin EA, Tourino C, Bonci A, Deisseroth K, de Lecea L (2011) Optogenetic interrogation of dopaminergic modulation of the multiple phases of reward-seeking behavior. J Neurosci 31:10829–10835
78. Kozai TD, Vazquez AL (2015) Photoelectric artefact from optogenetics and imaging on microelectrodes and bioelectronics: new challenges and opportunities. J Mater Chem B 3:4965–4978
79. Armbruster BN, Li X, Pausch MH, Herlitze S, Roth BL (2007) Evolving the lock to fit the key to create a family of G protein-coupled receptors potently activated by an inert ligand. Proc Natl Acad Sci U S A 104:5163–5168
80. Calipari ES, Juarez B, Morel C, Walker DM, Cahill ME, Ribeiro E, Roman-Ortiz C, Ramakrishnan C, Deisseroth K, Han M-H, Nestler EJ (2017) Dopaminergic dynamics underlying sex-specific cocaine reward. Nat Commun 8:13877
81. Roth BL (2016) DREADDs for neuroscientists. Neuron 89:683–694
82. Zachek MK, Takmakov P, Park J, Wightman RM, McCarty GS (2010) Simultaneous monitoring of dopamine concentration at spatially different brain locations in vivo. Biosens Bioelectron 25:1179–1185
83. Dorta-Quiñones CI, Wang XY, Dokania RK, Gailey A, Lindau M, Apsel AB (2016) A wireless FSCV monitoring IC with analog background subtraction and UWB telemetry. IEEE Trans Biomed Circuits Syst 10:289–299
84. Roham M, Daberkow DP, Ramsson ES, Covey DP, Pakdeeronachit S, Garris PA, Mohseni P (2008) A wireless IC for wide-range neurochemical monitoring using amperometry and fast-scan cyclic voltammetry. IEEE Trans Biomed Circuits Syst 2:3–9
85. Zamani H, Bahrami HR, Chalwadi P, Garris PA, Mohseni P (2017) C–FSCV: compressive fast-scan cyclic voltammetry for brain dopamine recording. IEEE Trans Neural Syst Rehabil Eng 26:51–59
86. Bennet KE, Tomshine JR, Min H-K, Manciu FS, Marsh MP, Paek SB, Settell ML, Nicolai EN, Blaha CD, Kouzani AZ, Chang S-Y, Lee KH (2016) A diamond-based electrode for detection of neurochemicals in the human brain. Front Hum Neurosci 10:102
87. Ross AE, Venton BJ (2012) Nafion–CNT coated carbon-fiber microelectrodes for enhanced detection of adenosine. Analyst 137:3045–3051
88. Zhang DA, Rand E, Marsh M, Andrews RJ, Lee KH, Meyyappan M, Koehne JE (2013) Carbon nanofiber electrode for neurochemical monitoring. Mol Neurobiol 48:380–385
89. Brazell MP, Kasser RJ, Renner KJ, Feng J, Moghaddam B, Adams RN (1987) Electrocoating carbon fiber microelectrodes with Nafion improves selectivity for electroactive neurotransmitters. J Neurosci Methods 22:167–172
90. Vreeland RF, Atcherley CW, Russell WS, Xie JY, Lu D, Laude ND, Porreca F, Heien ML (2015) Biocompatible PEDOT:Nafion composite electrode coatings for selective detection of neurotransmitters in vivo. Anal Chem 87:2600–2607
91. Taylor IM, Robbins EM, Catt KA, Cody PA, Happe CL, Cui XT (2017) Enhanced dopamine detection sensitivity by PEDOT/graphene oxide coating on in vivo carbon fiber electrodes. 2D Mater Biosens Bioelectron 89:400–410
92. Smith SK, Lugo-Morales LZ, Tang C, Gosrani SP, Lee CA, Roberts JG, Morton SW, McCarty GS, Khan SA, Sombers LA (2018) Quantitative comparison of enzyme immobilization strategies for glucose biosensing in real-time using fast-scan cyclic voltammetry coupled with carbon-Fiber microelectrodes. ChemPhysChem 19:1197–1204

93. Smith SK, Gosrani SP, Lee CA, McCarty GS, Sombers LA (2018) Carbon-fiber microbiosensor for monitoring rapid lactate fluctuations in brain tissue using fast-scan cyclic voltammetry. Anal Chem 90:12994–12999
94. Smith SK, Lee CA, Dausch ME, Horman BM, Patisaul HB, McCarty GS, Sombers LA (2017) Simultaneous voltammetric measurements of glucose and dopamine demonstrate the coupling of glucose availability with increased metabolic demand in the rat striatum. ACS Chem Neurosci 8:272–280
95. Logman MJ, Budygin EA, Gainetdinov RR, Wightman RM (2000) Quantitation of in vivo measurements with carbon fiber microelectrodes. J Neurosci Methods 95:95–102
96. Rodeberg NT, Johnson JA, Cameron CM, Saddoris MP, Carelli RM, Wightman RM (2015) Construction of training sets for valid calibration of in vivo cyclic voltammetric data by principal component analysis. Anal Chem 87:11484–11491
97. Willuhn I, Burgeno LM, Groblewski PA, Phillips PE (2014) Excessive cocaine use results from decreased phasic dopamine signaling in the striatum. Nat Neurosci 17:704–709
98. Johnson JA, Rodeberg NT, Wightman RM (2016) Failure of standard training sets in the analysis of fast-scan cyclic voltammetry data. ACS Chem Neurosci 7:349–359
99. Heien MLAV, Khan AS, Ariansen JL, Cheer JF, Phillips PEM, Wassum KM, Wightman RM (2005) Real-time measurement of dopamine fluctuations after cocaine in the brain of behaving rats. Proc Natl Acad Sci U S A 102:10023–10028
100. Meunier CJ, Roberts JG, McCarty GS, Sombers LA (2017) Background signal as an in situ predictor of dopamine oxidation potential: improving interpretation of fast-scan cyclic voltammetry data. ACS Chem Neurosci 8:411–419
101. Liu X, Zhang M, Xiao T, Hao J, Li R, Mao L (2016) Protein pretreatment of microelectrodes enables in vivo electrochemical measurements with easy precalibration and interference-free from proteins. Anal Chem 88:7238–7244
102. Abdalla A, Atcherley CW, Pathirathna P, Samaranayake S, Qiang B, Peña E, Morgan SL, Heien ML, Hashemi P (2017) In vivo ambient serotonin measurements at carbon-fiber microelectrodes. Anal Chem 89:9703–9711
103. Atcherley CW, Laude ND, Parent KL, Heien ML (2013) Fast-scan controlled-adsorption voltammetry for the quantification of absolute concentrations and adsorption dynamics. Langmuir 29:14885–14892
104. Oh Y, Park C, Kim DH, Shin H, Kang YM, DeWaele M, Lee J, Min H-K, Blaha CD, Bennet KE, Kim IY, Lee KH, Jang DP (2016) Monitoring in vivo changes in tonic extracellular dopamine level by charge-balancing multiple waveform fast-scan cyclic voltammetry. Anal Chem 88:10962–10970
105. Borman RP, Wang Y, Nguyen MD, Ganesana M, Lee ST, Venton BJ (2017) Automated algorithm for detection of transient adenosine release. ACS Chem Neurosci 8:386–393
106. Lee CA, Qi L, Amos A, Blanton K, McCarty GS, Sombers LA (2018) Reducing data density in fast-scan cyclic voltammetry measurements of dopamine dynamics. J Electrochem Soc 165:G3042–G3050
107. Amos AN, Roberts JG, Qi L, Sombers LA, McCarty GS (2014) Reducing the sampling rate of biochemical measurements using fast-scan cyclic voltammetry for in vivo applications. IEEE Sensors J 14:2975–2980

Chapter 6

Carbon Fiber Probes for Real-Time Monitoring of Dopamine

Helen N. Schwerdt, Ann M. Graybiel, and Michael J. Cima

Abstract

Dopamine governs key behavioral processes including motivation, learning, and habit formation. Neurochemical monitoring of dopamine is necessary to identify its role in normal and pathologic conditions and in order to identify targets for treatment and to improve diagnosis. Recent advances have made it possible to record subsecond dopamine release over extended time frames (>months), opening up the possibility to evaluate dopamine's role over behavioral adaptation, learning, neurodegeneration, and other behavioral processes that take longer than a few hours. Key innovations that we have introduced involve miniaturizing implanted probe dimensions to the size of individual neurons in order to avert inflammatory responses that can restrict chronic viability and sensitivity as well as limit the feasibility of introducing multiple probes into the brain. The purpose of this chapter is to describe methods to fabricate these sensors and to implement them in rodents for the recording of dopamine release over extended periods of time.

Key words Striatum, Basal ganglia, Voltammetry, Microinvasive implant, Neurochemical, Implantable sensors, Microelectrodes, Dopamine, Chronic neural recording, Cellular-scale probes

1 Introduction

Dopamine, the major neurotransmitter in the circuit that undergoes degeneration in Parkinson's disease (PD), regulates critical behaviors related to movement, mood, and learning. Dopamine dysregulation is centrally implicated not only in PD, but also in Huntington's disease, major mood disorders, and a range of neuropsychiatric disorders. Dopamine is thought to be produced heterogeneously and episodically throughout the brain. Special tools are required to assess quantitatively normal dopamine physiology on spatial and temporal scales relevant to a behaving animal. Dopamine is mostly found in the striatum, a central hub of the basal ganglia, where it is released from axons projecting from the midbrain substantia nigra pars compacta (SNpc) and ventral tegmental area (VTA). The axons and their cell bodies of the SNpc dopamine-containing neurons progressively degenerate in PD. Striatal dopamine operates synaptically, but also, significantly, by spilling out of the synapse and diffusing up to several microns away to bind to

Marc Fakhoury (ed.), *The Brain Reward System*, Neuromethods, vol. 165, https://doi.org/10.1007/978-1-0716-1146-3_6,

extrasynaptic receptors [1] (*see* Fig. 1b). This dopamine overflow occurs in the extracellular space ranging tens of nanometers in between the micrometer scale (e.g., 10–50 μm diameter) striatal neurons that express these dopamine receptors. Sensors used to monitor dopamine overflow directly should thus conform to these small cellular geometries to minimize direct interference with the normal neuronal circuitry.

Techniques including electrochemical recording [2–5] and, more recently, fluorescent activity indicators [6, 7] have been established to monitor local changes in dopamine neurochemical concentration. Both methods offer temporal resolution (milliseconds) to capture the rapid dopamine release and uptake dynamics [2–5]. The latter technique operates by measuring changes in fluorescence due to dopamine binding at genetically engineered dopamine receptors that have been introduced onto the cells. These fluorescent reporters offer an advantage for ease of visualizing wide field dynamics in the brain, as discussed further below. The sensors reported here utilize fast scan cyclic voltammetry (FSCV) to monitor changes in electrochemical dopamine redox current without the need for exogenous molecules or genetic modification. FSCV affords the ability to distinguish redox-sensitive neurotransmitters based on their potential specific electrode reactions. Current is measured from an implanted probe that usually comprises a carbon fiber (CF) interface on which dopamine and other electroactive molecules adsorb and transfer electrons through voltage-dependent electrochemical reactions (*see* Fig. 1). The CF provides an optimal interface for electrochemically based dopamine detection due to its highly adsorptive properties, electrical conductivity, small size, and biocompatibility [8]. Dopamine reduces and oxidizes to generate current at its redox potentials of −0.2 and 0.6 V. A triangular voltage ramp from −0.4 to 1.3 V is applied to the implanted CF every 100 ms to sample chemical changes at a rate of 10 Hz during FSCV. The voltage-dependent current changes recorded from the implanted CF can be displayed in a color plot where the voltage-dependent current changes from each scan are concatenated across time. The redox current is directly proportional to the dopamine concentration change and can be used to estimate relative changes in vivo dopamine concentration. Principal component analysis (PCA) is used when other sources of current including pH and/or background drift due to changes in the electrical properties of the CF interface over the course of FSCV operation may interfere with the ability to extract accurately dopamine redox current. The measured current is usually background subtracted in order to remove the larger capacitive current contributions due to the charging and discharging of the capacitive interface across the CF–tissue interface and to isolate the faradaic current contributions from chemical redox. This background subtraction and the background drift inherent to FSCV operation

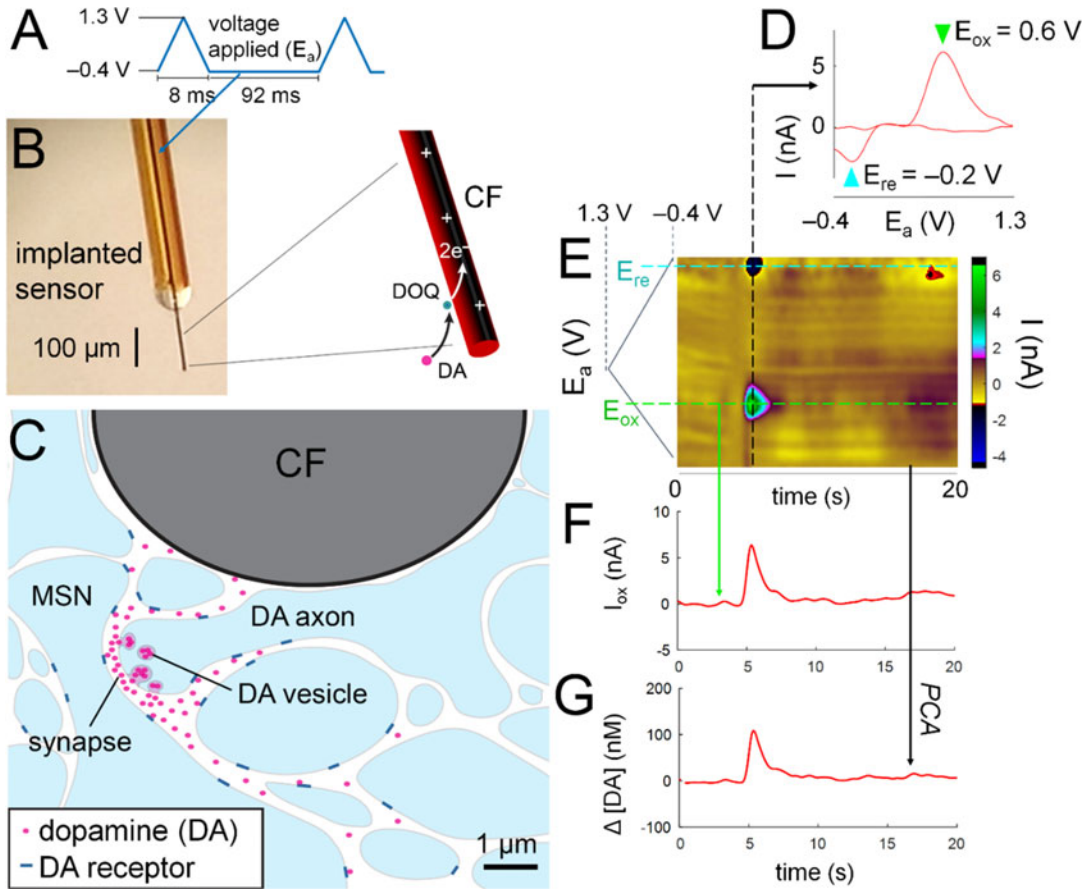

Fig. 1 Monitoring subsecond dopamine neurochemical changes with FSCV. (**a**) Voltage waveforms applied in FSCV to measure dopamine. The voltage ramps (E_a) from −0.4 to 1.3 V are applied every 100 ms at a scan rate of 400 V/s and the voltage is held at −0.4 V in between these voltage scans. (**b**) Photo of the implanted CF sensor on which these voltages are applied (left) and a close-up of the exposed CF sensing interface on which dopamine (DA) oxidizes to dopamine-o-quinone (DOQ) at its oxidation potential (E_{ox}) of 0.6 V (right). During the oxidation process, electrons are transferred to the CF and these current changes are amplified and converted to voltages from the FSCV circuits to which the CF connects externally. (**c**) Illustration of dopamine release and overflow out of the synapse to diffuse and bind to extrasynaptic receptors and the CF interface. The DA axon contains vesicles storing DA that undergo exocytosis to release DA into the synapse with the striatal medium spiny neuron (MSN). Released DA is rapidly transmitted out of the synapse to bind to receptors on the MSN as well as on other nearby neuronal processes and the DA axon itself. Some of this dopamine may also diffuse to an implanted CF sensing interface to be measured by FSCV. (**d**) A cyclic voltammogram (current versus voltage trace) showing the current peaks at the E_{ox} and reduction voltage (E_{re}) of dopamine. (**e**) FSCV color plot where current is shown in a nonlinear color scale (scale on right), E_a on the y-axis, and time on the x-axis. Visible current changes are seen along the redox potentials of dopamine, at 5 s, when the MFB dopamine axons were stimulated to controllably evoke striatal dopamine. (**f**) Oxidation current (current measured at 0.6 V) of dopamine as a function of time, which is directly proportional to dopamine concentration. (**g**) PCA computed dopamine concentration changes

restrict the ability to monitor absolute tonic dopamine concentrations. New approaches to manipulate voltage application parameters and/or digitally process recorded current may, however, enable measurement of absolute concentrations [9–11].

These CF probes in combination with FSCV recording have enabled a critical understanding of dopamine neurochemical operations and their function in behavior and pathological conditions [3–5, 12–17]. Recent experiments demonstrate that these chemicals operate in a more spatially variable manner than initially thought [18–21] (*see* Fig. 2). Mapping these site specific operations could be crucial to resolving the neural mechanisms of specific behavioral functions, for example, how select motor sequences or reward associations are processed by the brain. Dopamine is known to mediate goal-directed learning, habit formation, and other behavioral processes that can evolve over the course of weeks, months, and/or years. Ongoing work has, therefore, focused on sustaining the chemical recording operations over longer chronic (>days) timescales as well as to increase the channel capacity to monitor chemical activity from a larger number of brain sites [4, 22–24]. The methods described here attempt to support these two key functions as has been described in a condensed form previously [18, 22].

Implanted sensors physically disturb the brain regions in which they are placed, and their capacity to monitor neural activity over time suffers as well. The insertion of such devices creates a physical tract, compresses and/or damages neighboring cells and vasculature, and induces a host of inflammatory processes that result in the formation of a scar [25–27]. The indwelling device can further perpetuate recurring inflammation due to its mechanical mismatch with the surrounding brain tissue and the constant natural movement of the brain. The size of the implanted device has been shown to directly correlate with the amount of induced glial scarring and neuro-inflammation. This inflammatory response and damage can extend hundreds of microns away from the implanted object. All of these induced changes may impede the ability to monitor normal neurochemical activity and the scar that forms around the sensing interface obstructs diffusion of targeted chemicals thus degrading the probe's effective chemical sensitivity. The dimensions of the implanted devices should, therefore, be as small as possible to preserve the viability of the surrounding neural circuitry and to acquire longitudinally stable and sensitive measurements. The CF as supplied from the manufacturer (Good Fellow Corp) in diameters of 5 or 7 μm provides an inherently small geometry on par with the dimensions of single neuronal cell bodies (10 μm). A 50–200 μm length of CF is typically used for electrochemical sensing operations. The remainder of the CF is threaded, sealed, and insulated through glass or silica capillary that provides a structurally rigid shaft facilitating insertion into the brain [4, 23]. The

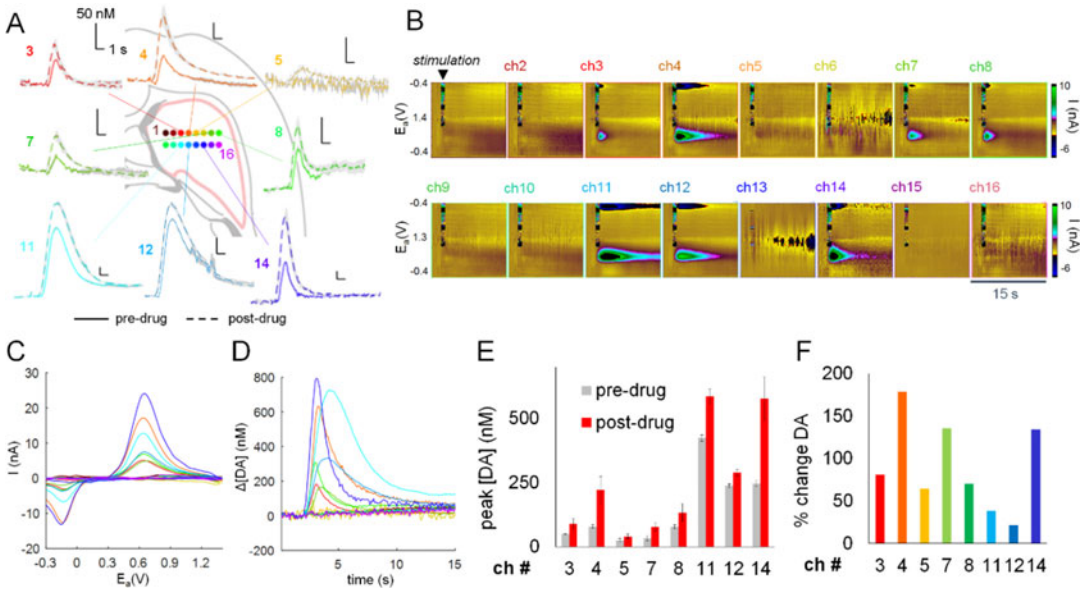

Fig. 2 Spatially heterogeneous changes in striatal dopamine signaling as measured from 16 implanted probes (two arrays) from the rat striatum. (**a**) PCA computed dopamine concentration changes as a function of time from all sites (estimated locations in striatum shown in the horizontal brain section in the center) that showed stimulation evoked dopamine release. Solid traces are the average of three trials before the raclopride drug administration and dashed traces are the average of 4 trials postdrug. MFB stimulation was applied at 60 Hz, 48 pulses, and 250 μA for all trials. Scale bars are 50 nM (vertical) and 1 s (horizontal) for all traces. (**b**) Background subtracted current in the form of color plots (each channel is shown on a separate plot). Stimulation (60 Hz, 48 pulses, and 300 μA) to the MFB was applied at 2 s (artifact seen as spurious current changes in all plots). (**c**) CV plots overlain for all channel data in **b** as taken directly after stimulation, demonstrating selective current changes at dopamine redox potentials (−0.2 and 0.6 V). (**d**) Dopamine (DA) concentration change vs. time overlain for the data in **b**. (**e**) Measured peak amplitudes in stimulation evoked DA for all 8 channels that had displayed dopamine. All of these sites displayed a significant increase in stimulation evoked DA after the raclopride. (**f**) Percent increase in DA for the measurements shown in **e**. Error bars and gray shading are ± standard error (SE). **a–e** reproduced with modifications from [18] with permission from the Royal Society of Chemistry

opposite end of the CF is conductively attached to an electronic connector for interfacing with FSCV circuitry to provide the recording functions. This silica or glass threaded CF sensor, usually termed the CF microelectrode (CFM), has been implemented for widespread use in recording dopamine in vitro and in vivo in freely behaving animals. The CFM shaft has a nominal diameter of around 100 μm as circumscribed by the insulating shaft. This shaft directly adjoins the protruding exposed CF sensing interface and has been shown to induce inflammatory responses extending 100 s of microns, directly encompassing the range of the sensing CF [22]. Parylene has been used as an alternative to these capillaries as it can be conformally deposited onto the bare CF at thicknesses of less than a micron. This thin coating thus helps retain the

cellular-scale footprint of the original CF (7 μm diameter) and would help reduce induced inflammatory response as implanted into the brain. These parylene-encapsulated CF probes or micro-invasive probes (μIPs) are described in this chapter.

Emerging evidence of the spatially heterogeneous characteristics of dopamine signaling has encouraged the development of multichannel sensing or optical imaging methods that would allow monitoring of dopamine activity from multiple sites at the same time [18–20, 28, 29]. The standard CFM sensor has limited practical capability for arraying due to its labor-intensive fabrication procedures as well as the diameter of each probe, which would make arrays of such sensors prohibitively damaging to its inserted brain tissue environment. We developed batch microfabrication techniques to create arrays with increased yield and reproducibility [18]. This batch fabrication procedure minimizes overall manufacturing time for multiple (>50) μIP sensors. The smaller, cellular-scale, diameters of the individual μIPs make it possible to insert them in manifold into the brain without inducing significant trauma [22]. More recently developed dopamine selective fluorescent indicators allow imaging and mapping the dynamics of dopamine release over a wide field with subcellular resolution [6, 7]. This technique involves implantation of an optical fiber (>100 μm) or a lens (>2 mm) to measure changes in fluorescence as detected from a single targeted brain site or as imaged over a larger plane, respectively. Imaging dopamine from subcortical structures, such as the striatum, thus requires cavitation of overlying brain tissue, which may be overly destructive in certain applications. Further investigations may be needed to characterize the performance of such sensors over chronic timescales for longitudinal recording applications.

Here, we describe methods to fabricate and implement arrayed μIP dopamine sensors for monitoring dopamine release in the rodent brain chronically. The μIPs have been shown to be capable of recording dopamine with long-term stability, a function necessary to longitudinally assess dopamine changes during the evolution of behavior and neural circuitry. These sensors are small enough to enable arrayed implantation without significant trauma. This improvement introduces the capability to characterize the spatially heterogeneous dopamine operations. The arrayed approach further enhances the probability of acquiring functional measurements of dopamine in vivo as the probability of inserting a probe into an active region of dopamine release in the striatum is about 50%. Recent advancements in FSCV and neurochemical sensing have further augmented the functions of these CF probes to be used for recording other electroactive [30, 31] and non-electroactive chemicals [32], as well as electrical neuronal activity (i.e., spikes and local field potentials) in the brain.

2 Materials

Probe fabrication materials and equipment.

Materials for probe fabrication include:

- 7 μm diameter carbon fiber (CF) (Goodfellow, C 005722) (cut to lengths of ~10 mm and stored in glass vials filled with isopropanol)
- Custom-built printed circuit boards (PCBs) (investigators may make their own layouts or may use those available at https://github.com/hschwerdt/multifscv).
- Electrical sockets (Mill-Max, 853-93-100).
- Silver epoxy (Epo-tek, H20S).
- Photoresist (AZ Electronics, AZ P4330) (if lift-off procedures are used).
- A174 parylene adhesion promoter (Sigma-Aldrich, 440,159).
- Butane torch (e.g., Weller, Portasol P2KC) (if flame etching procedures are used instead of liftoff).
- Razor blades.
- V-groove optic fiber mounts to be used as micromolds (P-M Optics, PGVG-2082205).
- 100-mm glass wafer (University Wafer, 1631) or any large glass or heat-resistant and chemically compatible flat substrate to mount individual arrays
- Parylene deposition system (Specialty Coating Systems, PDS 2010 Labcoater).
- Parylene-C dimer (Specialty Coating Systems, Para-Coat Technologies, Curtiss-Wright).
- Polyethylene glycol (PEG) (4000–8000 g/mol) (Sigma-Aldrich).
- Sterile mineral oil (Fresenius USA, Muri-Lube, 63323025410).
- Insulated silver (Ag) wires (A-M Systems, 787000 and 786000).
- Fast curing structural epoxy (Devcon, 14250).
- Double-sided polyimide tape (Ted Pella, 16087-12).
- Tweezers with fine tips (tip width $\leq$ 50 μm) (World Precision Instruments, 14095, or Electron Microscopy Sciences, 78325-5SA).
- Microprobe (Electron Microscopy Sciences, 62,091-01) or thin tungsten wire (A-M Systems, 797500, 797550, or 797600).

Solutions for in vitro characterization of probes:

- Dopamine hydrochloride (Sigma-Aldrich, H8502).

- Physiological saline, phosphate-buffered saline (PBS), or artificial cerebrospinal fluid (aCSF).

Surgical supplies and animals:

- Sprague-Dawley rats.
- Bone screws (Stoelting, 51457) or similar 0-80 stainless steel screws.
- Drill bit (1.35 mm) (Stoelting, 514555).
- Stereotaxic instrument (Stoelting, 51600, 51449).
- Stainless steel wire (A-M Systems, 792900).
- Acrylic cement (Ortho-Jet, 0206).
- Wire speculum or any other device to retract skin (World Precision Instruments, 500368).
- Pt/Ir microelectrodes (FHC, 30046, or Microprobes, PI20030.01A3) (if stimulation is to be used).
- Stimulus isolator (WPI, A365) (if stimulation is to be used).
- Raclopride (Sigma-Aldrich, R-121) (if pharmacology is to be used).
- Cocaine (Sigma-Aldrich, C5776) (if pharmacology is to be used).

2.1 Recording Equipment

FSCV dopamine-recording instrumentation can be purchased directly from Scott Ng-Evans at the University of Washington, Collin J. McKinney at the Electronics Design Facility at the University of North Carolina at Chapel Hill, Pine Research, and Pinnacle Technology. These systems usually provide up to four channels of recording. Sixteen channel recording systems can be created directly by users with a guide (available online at https://github.com/hschwerdt/multifscv). The circuit layouts for headstage current to voltage transducers and amplifiers as well as the adapter board to relay signals in and out of the headstages to a data acquisition card for computer control and monitoring are provided on this site and can be directly sent to PCB manufacturers (e.g., PCBway, or Advanced Circuits) to construct the boards. Each recording channel consists of the current to voltage transducer, an operational amplifier, and feedback resistor and capacitor, as has also been described in detail as incorporated with additional electrophysiological recording functions [33]. PCB manufacturers usually also provide assembly services, if needed, to integrate all the circuit components onto the boards. The software for FSCV recording is programmed in Matlab and is also available for download on this site.

3 Methods

Fabricating arrays of subcellular probes for chronically stable neurochemical monitoring.

Arrays of subcellular probes are fabricated as a batch on a large glass wafer or any appropriate substrate (should be ~100 mm diameter to fit at least ten arrays, resistant to heat, and compatible with the chemicals used in this procedure). The fabrication procedure is as follows:

1. Arrange and tape in a row multiple (8–14) PCBs onto a glass wafer with polyimide tape (*see* Fig. 3a).
2. Fix micromolds onto the wafer with epoxy with trenches aligned to the PCB conductive traces (CF bonding pads). The base of the trenches should match the height of the PCB traces so that subsequently placed CF's lay flat as mounted onto both substrates (*see* Fig. 3b).
3. Mount individually 10-mm long CF's into trenches with at least 1 mm of CF extending onto the PCB trace (*see* Fig. 3C and D). A bundle of CF's are placed in a white weighing dish filled with isopropanol and ultrafine tipped tweezers are used to pick up an individual CF from the solution under microscope visualization that is then transported carefully to the trench (*see* **Note 1**).
4. Apply a drop of silver epoxy with a microprobe or thin tungsten wire onto the PCB pad and overlying CF (*see* Fig. 3e).
5. Cure silver epoxy at 100 °C for 45 min in an oven or with a glass wafer on top of a hot plate set to 120 °C for 2 h or until completely dry.
   (a) The effective temperature at which the silver epoxy is cured on a hot plate depends on its height above the hot plate as well as the heat distribution of the hot plate. A dummy PCB can be mounted onto the glass wafer and applied with a trace of silver epoxy that can then be tested for curing on the hot plate.
6. The CF attachment to the PCB can be further reinforced by applying a thin layer of nonconductive structural epoxy over the CF-epoxied pads.
7. Carefully detach the CF-PCB assembly from the glass substrate. Move and remount the boards 4–8 mm away from the glass micromolds while maintaining alignment as much as possible of the CFs to the micromold trenches (*see* Fig. 3f). The separation distance should be $\geq$2 mm than the targeted implant length if flame-etching procedures are to be used.

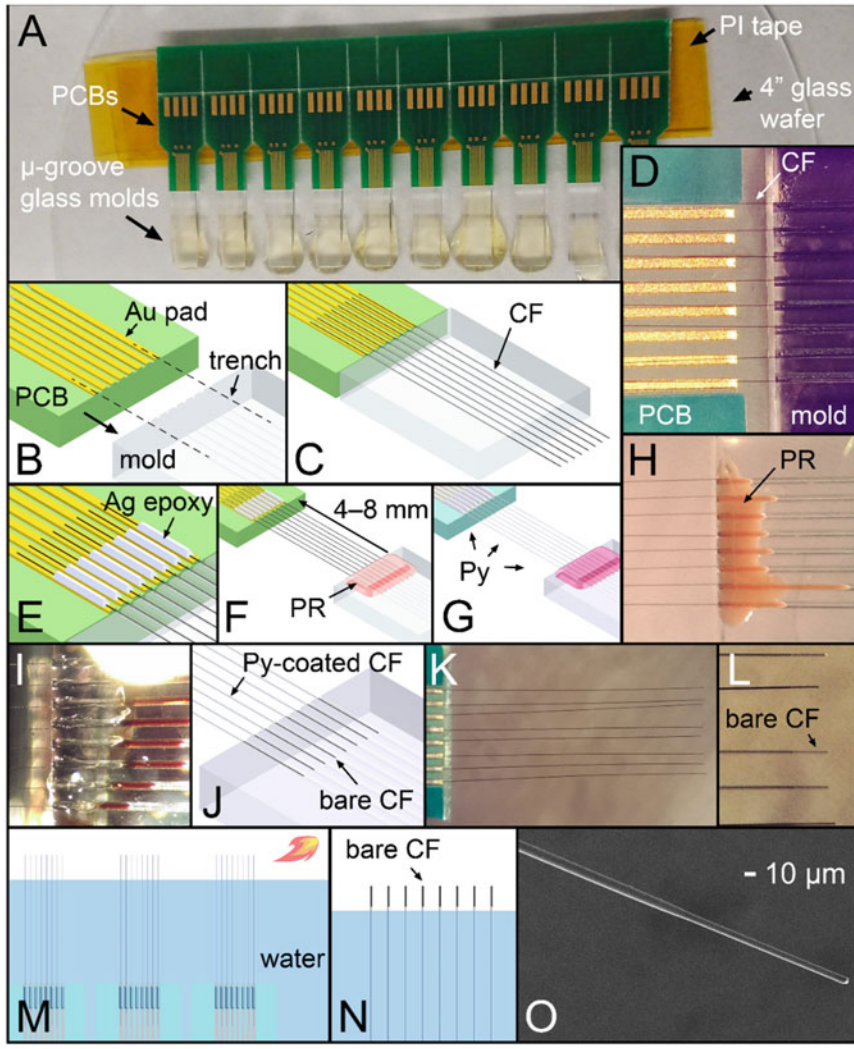

Fig. 3 Fabrication of arrayed sensors. (**a**) PCBs mounted on polyimide (PI) tape and aligned to microgroove glass molds on a glass wafer. (**b**) PCB gold (Au) pads aligned to individual microgroove trenches. (**c**) CFs placed on pads and into aligned mold trenches. (**d**) Photo of mounted CFs on PCB and mold. (**e**) Silver (Ag) epoxy applied to individual pads to create conductive bonds between CFs and pads. (**f**) PCBs extended 4–8 mm from glass molds and photoresist (PR) (for liftoff) or structural epoxy (for patterning) applied to tips of CFs on molds for masking and anchoring of tips. (**g**) Parylene (Py) conformally deposited onto the batch of CF-integrated PCBs following adhesion promotor treatment. (**h**) Photo of PR masked CF tips. (**i–l**) Lift-off procedures to expose CF sensing tips. (**i**) Photo of scraped Py-coated PR mask and dissolution of PR with acetone. (**j**) CFs exposed at tips held on the mold after PR dissolution. (**k**) Photo of the array with exposed CF tips after trimming exposed CF to 50–200 μm lengths. (**l**) Close up photo showing trimmed CF sensing tips. (**m–o**) Alternative procedure to expose CF tips by thermal patterning. (**m**) Py-coated CFs are cut away from the mold onto which the tips are epoxied and placed in a bath of water with 1–3 mm of the tips exposed in the air. A butane torch is used to produce a flame that is applied across all of the Py-coated CFs above the water to etch the tips and expose the underlying CFs. (**n**) Bare CFs after flame etching. (**o**) Scanning electron micrograph (SEM) of the flame etched Py-coated CF probe. **o** reproduced with modifications from [18] with permission from the Royal Society of Chemistry

8. Fix the tips of the CF to the micromold with sacrificial photoresist (for liftoff procedures) or structural epoxy (for flame-etching procedures) (*see* Fig. 3f). Sacrificial photoresist is used to temporarily protect the tips of the CFs from subsequent parylene encapsulation. The photoresist is dissolved at the end of the procedure to unmask the bare CFs that are the molecular electrochemical sensing interfaces.
9. Prepare parylene adhesion promotor solution (usually requires overnight activation) that consists of A174 silane, isopropanol, and distilled water at a volumetric ratio of 1:100:100. This can be left in a closed beaker with a gentle magnetic stirring overnight in a fume hood. Parylene deposition must follow within 48 h of preparing this solution for nominal adhesion (*see* **Note 2**).
10. Immerse the wafer with all arrays into isopropanol for 15–30 min, followed by the adhesion promotion solution for 15–30 min. Air-dry the wafer for 30 min and then soak the wafer again in isopropanol for 5 min followed by air drying for 30 min until all liquids are completely evaporated. Additionally, heating (~100 °C) in an oven or hot plate may be used to help ensure complete evaporation of liquids on the substrate.
11. Mask connector pins that will be connected to mill-max connectors to connect to FSCV circuits with polyimide tape so that they are not insulated by subsequent parylene deposition.
12. Place wafer in the parylene deposition chamber and deposit parylene at the targeted thickness (0.5–2 μm has been shown to be effective) as determined based on the weight of the loaded dimer and the deposition rate of the chamber (*see* Fig. 3g and h).
13. Expose CF sensing tips by liftoff or thermal patterning.
    (a) Liftoff (tips masked with photoresist): Gently score the parylene atop photoresist masked areas with a razor blade and immerse in acetone until photoresist has been completely dissolved followed by rinsing in isopropanol (*see* Fig. 3i–l).
    (b) Etching (tips anchored with structural epoxy): Cut all the fibers with small scissors where they are anchored to the micromolds and detach the boards from the glass wafer. Immerse the PCBs in water so that only 1–3 mm of the CF tip is exposed in the air (*see* Fig. 3m). Use a butane torch to create a flame that is then directed at the exposed CF tips until all of the CFs that had been exposed above the water are no longer visible (*see* Fig. 3n).
14. Trim exposed CF tips to lengths of 50–200 μm with a razor blade under the microscope.

15. Solder mill-max connectors to the PCBs for interfacing with FSCV circuits.
16. Test the CF sensors in vitro to determine operational probes (background current >100 nA, noise <0.1 nA, dopamine sensitivity of 2–50 nA/μM). CFs can be retrimmed as needed if the background current is too high and close to saturating the input of the headstage amplifiers (>1500 nA). This in vitro testing is typically performed in a flow cell to generate initial dopamine sensitivity calibration curves for the fabricated sensors as well as to generate "standards" or CV templates of expected chemical compounds that the probe would detect in vivo (e.g., dopamine, pH) (*see* **Note 3**).
17. Apply molten PEG (heated to 50–80 °C on a hot plate) to PCB-CF assemblies on a mineral oil coated micromold. Carefully detach the PCB-CF assembly from the micromold, after the PEG has cooled to room temperature and hardened (*see* **Note 4**).

3.1 Reference Electrode Construction

An Ag/AgCl pseudo-reference electrode is typically used for all FSCV based measurements of dopamine. A thin insulated Ag wire is exposed 1–3 mm (length that will be implanted into the brain or secured in the supradural layers) at the tip by scraping its insulation with a razor blade. The other end is also bared and crimped to a mill-max pin for subsequent connection to the reference input on a headstage amplifier. The exposed Ag is chloridized to form an AgCl surface either by electroplating or oxidation in a concentrated chloride solution. Electroplating is done by placing the Ag wire and a return wire (stainless steel or any other bare metal) into 1 M HCl solution under a fume hood. A power supply (1–9 V) or D size battery is connected to the Ag wire (positive terminal) and the return electrode is connected to the negative terminal. Hydrogen evolution during the electroplating process will cause bubbles to form and when these bubbles no longer appear to be forming (15–30 s) the power can be turned off and the Ag/AgCl wire is left to try in the air, followed by rinsing in water. The Ag wire can also be chloridized by immersing it in a concentrated chlorine solution overnight. The AgCl surface should appear black in color once successfully formed.

3.2 Multisite Monitoring of Dopamine Release In Vivo

The arrayed probes can be implanted into the striatum of the rat to measure dopamine release from multiple sites. This implantation requires surgical procedures to expose the surface of the brain for introducing probes into the striatum as well as pharmacological and/or electrical stimulation protocols to determine probes that have been inserted in an area of active dopamine release.

1. Anesthetize (1.5–2.0% isofluorane, 1 L/min oxygen) rat and administer preoperative analgesics (e.g., Meloxicam, 2 mg/kg subcutaneously).
2. Create a sterile field after shaving the hair on top of the animal's head and mounting the animal on the stereotaxic.
3. Create an incision on the skin overlying the calvarium and retract the skin with a self-retaining retractor.
4. Create a window with a drill to expose the underlying dura mater surface centered around coordinates of anteroposterior (AP) 0.5 mm and mediolateral (ML) 3 mm relative to bregma and the sagittal suture, respectively, on one or both hemispheres (for two arrays). The window should be sufficiently large to accommodate the width of the arrays with an additional ±0.5–1 mm of clearance. Also, create a hole through the bone, for inserting the reference electrode at a single point away from the window, and also at 2 or 3 points to insert bone screws for anchoring of subsequent acrylic cement (*see* **Note 5** on additional uses for bone screws) (*see* Fig. 4a).
5. Thread bone screws through holes created for these screws using a screwdriver (*see* Fig. 4a).
6. Remove the dura mater in the hole created for the reference electrode using a 32 G needle to incise the dura mater and a fine-tipped tweezer to peel away this membrane to expose a small area of the brain. Slowly insert the reference electrode 1–3 mm deep into the brain (the exposed length of the Ag/AgCl) using the stereotaxic micromanipulator arm to manually control the insertion rate (~100–1000 μm/min). Secure the reference electrode by applying a thin layer of cement around the wire and on top of the bone after drying the area with gauze or cotton-tipped applicators. Detach the rest of the reference wire from the micromanipulator arm after the cement has dried.
7. Remove the dura mater in the window created for probe arrays in the same manner as described in the previous step. The array can be connected to the headstage amplifier during this step to allow FSCV monitoring of background current during the lowering procedure, and then mounted to the micromanipulator. Position the tip of the PEG coated array above the window and lower the PEG until it sits above the brain surface (*see* Fig. 4b and f). Apply a small amount of saline at the base of the PEG to expose the tips of the CF (if these are not already exposed) that will be inserted into the brain immediately after PEG dissolution. Manually lower the probes incrementally as the CFs are exposed from the PEG that is being dissolved at the tips that have been immersed in fresh saline applied atop the brain (*see* Fig. 4c, d and g). An absorbent sponge or cotton tip

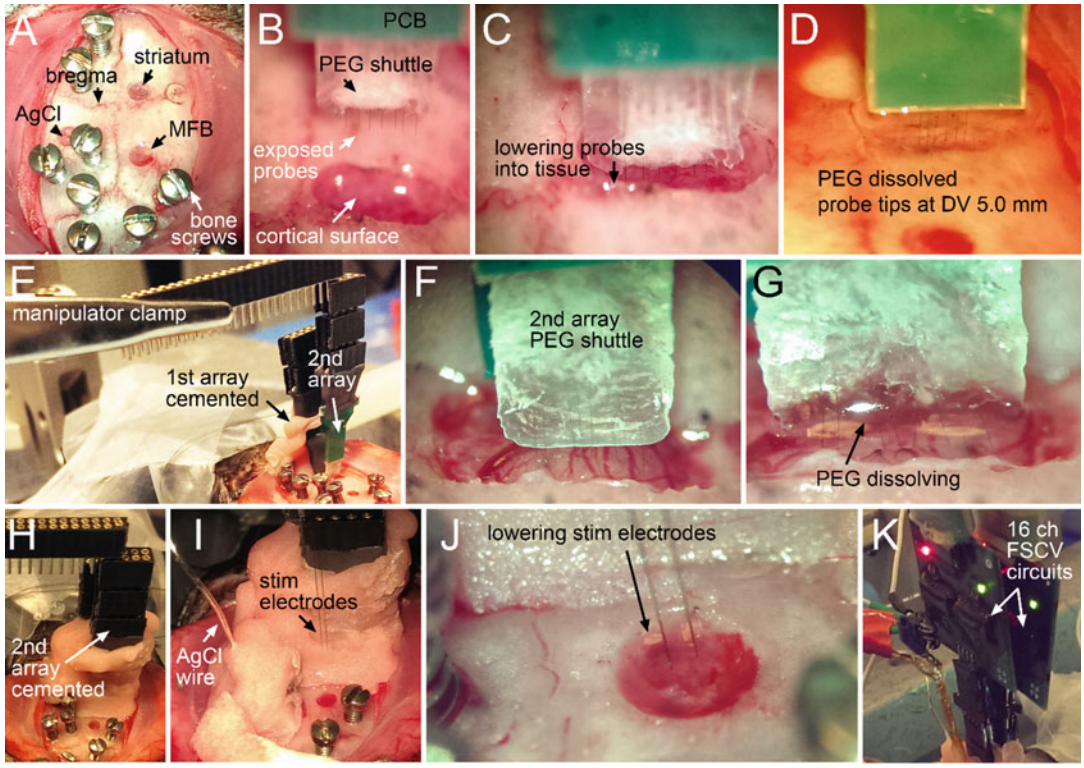

Fig. 4 Array implantation process to record dopamine in vivo. (**a**) Craniotomies for the striatal target for array implantation, the reference Ag/AgCl wire, and the MFB stimulation electrodes made by drilling the bone at the targeted stereotaxic coordinates. Bone screws are installed in the periphery for securing subsequent cement and implant devices as well as for electrical grounding. (**b**) Array positioned above striatal target. The PEG encapsulated probes are within the margins of the exposed brain tissue. The dura mater has been removed in order to expose the cortical surface and ease the penetration of probes. (**c**) 1–2 mm of the exposed probes lowered into the brain with the rigid PEG shuttle remaining above the tissue. (**d**) PEG dissolved by saline. The saline is applied onto the PEG slowly to dissolve the base of the shuttle and expose embedded probes as they are incrementally lowered until the probes have reached their targeted DV depth. (**e**) The first array secured to a bone and anterior bone screws with cement and a second array being lowered into the brain tissue. (**f**) ~1 mm of the exposed probes of the second array lowered into the brain. (**g**) PEG dissolution in saline during array lowering. (**h**) Second array secured with cement while ensuring that the access hole in the more posterior location remains accessible for the stimulation electrodes. (**i**) Stimulation electrodes positioned above the cranial window after removing the dura mater. The Ag/AgCl reference electrode has been implanted and secured with cement. (**j**) Stimulation electrodes incrementally lowered while recording stimulation evoked changes in current during FSCV recording at the implanted CF arrays. (**k**) 2 FSCV circuit boards connected to the two implanted arrays for concurrent recording from 16 striatal sites

and/or aspirating tube is used to remove saturated saline before reapplying fresh saline during the dissolution process. This step should be done under a microscope to allow visualization of probes during their insertion into the brain. Usually ~1 mm of a PEG-bared and, either free hanging or brain inserted, CF probe can be advanced in the brain without

deflection, but this largely depends on the angle of insertion (i.e., whether the insertion force is applied along the axis of the probe or at an angle) and the mechanical characteristics of the tissue into which it is being inserted. Therefore, it is important to lower the probes immediately after ~1 mm of the probes have been unattached from the dissolved PEG and before more PEG is dissolved from the tip. Also, the insertion should be slow enough that the undissolved rigid PEG shuttle does not penetrate the tissue. The targeted depth of the probe tips can span between 4 and 7 mm dorsoventral (DV) in the striatum. Record the background current at the targeted depth to ensure that the probes display the needed electrical current properties for dopamine recording. The PCB is then secured to the bone with cement, which is also applied around neighboring bone screws and bone (*see* Fig. 4e and h). Repeat this step if a second array is to be implanted (*see* Fig. 4e–h).

8. Measure stimulation evoked and/or pharmacologically induced dopamine from implanted probes. The capacity of inserted probes to detect dopamine is dictated by the noise and background current levels, as measured in the previous step. Nevertheless, the probability that probes have been inserted in an area of active dopamine release within the striatum is usually about 50%. Electrical stimulation of the dopamine containing neurons in the midbrain (SNpc/VTA) or the axonal fibers (medial forebrain bundle, MFB) and/or pharmacological manipulation of the dopamine receptors is usually performed in order to initially characterize dopamine release around the inserted probes and determine probes that would detect dopamine.
   (a) Electrical stimulation of the dopamine neurons or axons to trigger striatal dopamine release: A pair of stimulation electrodes spaced ~500 μm apart is slowly lowered into the MFB (AP −4.1 mm, ML +1.7 mm) and stimulation is applied across these electrodes beginning at a depth of DV 6.0 mm and at increments of 0.1–0.25 mm up to DV 8.7 mm until dopamine increases are triggered at the striatal probes as observed during concurrent FSCV recording (*see* Fig. 4i and j). Current-controlled electrical stimulation parameters can range 24–72 biphasic pulses (2 ms per pulse) with an amplitude of 100–300 μA and frequency of 60 Hz, as controlled by a stimulus isolator that is triggered by the software. The stimulation should be applied at minimum intervals of 2–5 min to avoid depleting terminal dopamine release (this can be observed to occur if the amplitude of stimulation evoked dopamine decreases for each subsequent stimulation). The main challenge with this approach is that the striatal probes may not always be located at the terminals of the fibers

in which stimulation is being applied, and the fibers may easily be missed during stimulation electrode insertion. If dopamine release is not observed to be evoked after testing stimulation at a full range of depth for an individual track, the electrodes may be removed slowly, reinserted into a different AP/ML coordinate targeting the MFB or SNc/VTA, and the same procedures repeated. The stimulating electrodes are fixed in place, with a silicone sealant and cement, once dopamine signals are observed to be evoked.

(b) Pharmacological manipulation to induce endogenous dopamine transients: Both raclopride (1–3 mg/kg) and cocaine (3–15 mg/kg) as prepared in a saline vehicle are administered to the animal via intraperitoneal (I.P.) injection during concurrent FSCV recording. Raclopride or cocaine by itself also has been found to produce spontaneous increases in dopamine transients (i.e., frequent fluctuations in dopamine concentration), but we have found that the combination of the two drugs greatly enhances the reproducibility and probability of successfully observing these dopamine signals. Dopamine transients should be observed in the recorded FSCV current 3–15 min following administration. Failure to observe these dopamine transients could be caused by the insertion of probe arrays outside of the striatum or failure to introduce drugs into the peritoneal cavity. Injections into one of the abdominal organs can easily occur inadvertently during I.P. administration and reduce the amount of drug that enters the bloodstream. Drug administrations may be reattempted, and usually, these are at a lower dose or with a single drug (cocaine is usually preferred as it is more effective) to prevent potential overdose. The lethal dose, 50% (LD50) of cocaine is ~50 mg/kg I.P. [34].

9. Complete surgical experiments.

(a) Acute recording: Apply electrolytic lesions at targeted probes by applying a DC cathodal current of 15 μA for 5 s, if the animal is to be euthanized directly after the recording experiment. These lesions can be used to identify recorded striatal sites if immunohistochemical methods will be used to cut and stain the brain tissue. Euthanize and perfuse the brain ~60 min after lesioning.

(b) Chronic recording: Apply cement to any exposed bone and bone screws while ensuring that connectors to the reference electrode and probes remain accessible. Recover animal, administer postoperative analgesics and any other required medications, return to the cage, and monitor until full recovery.

4 Notes

1. Transferring a CF to a dry glass substrate is difficult because the CF tends to readily adhere to structures including the tweezer that is holding it through electrostatic forces. Applying a small pool of isopropanol onto the mold helps facilitate the transfer of the CF from the tweezer to the glass trench by liquid bridging and surface tension.
2. Parylene depositions systems are also available with the ability to vapor deposit the adhesion promotor in the same chamber as the parylene deposition. This would obviate the need for liquid adhesion promotor procedures.
3. Various flow cell constructions have been described for use in testing and calibrating dopamine CF sensors. The flow cell consists of a channel for fluid flow in which the sensors and the reference electrode can be immersed and the ability to switch the fluid source from the saline or aCSF buffer to the analyte of interest (i.e., dopamine at a specific concentration prepared in the same buffer). Devices under test are connected to the headstage amplifier and immersed in a physiological saline environment. FSCV scans should be applied at 60 Hz for a period of 5 min, followed by scanning at 10 Hz for a period of 15–30 min or until the recorded current has stabilized ($<$1 nA change in current within a 30 s period), before dopamine or other targeted analytes are introduced to the sensor in the flow cell or readings are taken for background current and noise levels. Standards of both dopamine and pH are usually made from CVs measured in the flow cell, and these are used to estimate, based on principal component analysis [35, 36], chemically specific concentration changes in vivo. The most important measurements obtained during in vitro testing are the amplitude of the background current (maximum of the absolute current) that determines the overall sensitivity as well as the noise level (root mean squared of the background subtracted current for $\pm$5 scans around the time point of background subtraction at the oxidation potential) that determines the limit of detection. These two parameters primarily determine performance in dopamine monitoring in subsequent in vivo experiments. The reproducibility of the dopamine sensitivity (change in oxidation current for different concentrations of dopamine normalized to the background current) should be obtained for a cohort of fabricated probes to ascertain the relationship between background current and dopamine sensitivity. Probes may be tested purely in physiological saline or aCSF in a beaker to acquire key background current and noise level measurements once the reproducibility of

dopamine sensitivity has been ascertained for the fabricated sensors to expedite these tests. Background current levels can be used to then estimate the dopamine sensitivity based on measured calibration curves. It should be noted that these calibrations can only be used to roughly estimate the in vivo concentration changes detected by an implanted probe, in which the environment cannot always be accurately emulated in a flow cell.

4. The solidified PEG will often adhere to the glass mold. The PEG–PCB assembly should be carefully removed together. A tweezer or microprobe can be used to hinge and separate the PEG from the substrate below carefully to assess ease of separation and the PEG's adhesion. The PEG can be reheated on the hot plate or dissolved in water if it cannot be easily removed from the mold and this step can be repeated.
5. Electronic noise in the form of high-frequency current changes can arise in the surgical room environment, even if it was not present during in vitro testing, and degrade the ability to sufficiently detect dopamine. Potential solutions to minimize noise and shield the animal and the recording instrumentation from this noise includes connecting the metal stereotaxic to the instrumentation ground with an alligator clip terminated cable, connecting the surgery table (if this is conductive) to the ground, and disconnecting probable sources of noise including fluorescent light bulbs, motorized systems, or other electronics generating large voltages. Additionally, the bone screws installed during surgery could be connected to the ground to shield the surface of the brain. A stainless steel wire is wound around the bone screws and connected to a mill-max pin or another connector that can then be routed to the instrumentation ground. Grounding the stainless steel implanted components will shift the reference potential as the instrumentation ground is also connected to the reference input and the open circuit potentials (i.e., electrode potentials) of stainless steel and Ag/AgCl are different. Thus, the DC offset (0.1–0.2 V) applied to the FSCV scans may need to be modified until a proper background current curve is achieved. A good description of how to identify visually the proper background current curves can be found here [37].

Acknowledgments

The authors thank Dr. D. Hu (Massachusetts Institute of Technology) for help with surgical procedures. This work is supported by the National Institute of Biomedical Imaging and Bioengineering (R01 EB016101 to A.M.G. and M.J.C.), the National Institute of

Neurological Disorders and Stroke (R01 NS025529 to A.M.G., F32 NS093897 and K99 NS107639 to H.N.S), the Army Research Office (W911NF-16-1-0474), the Saks Kavanaugh Foundation, the Nancy Lurie Marks Family Foundation, and Dr. Tenley Albright (to A.M.G.).

References

1. Rice ME, Cragg SJ (2008) Dopamine spillover after quantal release: rethinking dopamine transmission in the nigrostriatal pathway. Brain Res Rev 58:303–313
2. Gonon F et al (1981) Voltammetry in the striatum of chronic freely moving rats: Detection of catechols and ascorbic acid. Brain Res 223:69–80
3. Stamford JA, Kruk ZL, Millar J (1988) Stimulated limbic and striatal dopamine release measured by fast cyclic voltammetry: anatomical, electrochemical and pharmacological characterisation. Brain Res 454:282–288
4. Clark JJ et al (2010) Chronic microsensors for longitudinal, subsecond dopamine detection in behaving animals. Nat Methods 7:126–129
5. Garris PA et al (2002) Real-time measurement of electrically evoked extracellular dopamine in the striatum of freely moving rats. J Neurochem 68:152–161
6. Patriarchi T et al (2018) Ultrafast neuronal imaging of dopamine dynamics with designed genetically encoded sensors. Science 360 (6396):eaat4422. https://doi.org/10.1126/science.aat4422
7. Sun F et al (2018) A genetically encoded fluorescent sensor enables rapid and specific detection of dopamine in flies, fish, and mice. Cell 174:481–496.e19
8. McCreery RL (2008) Advanced carbon electrode materials for molecular electrochemistry. Chem Rev 108:2646–2687
9. Burrell MH et al (2015) A novel electrochemical approach for prolonged measurement of absolute levels of extracellular dopamine in brain slices. ACS Chem Neurosci 6:1802–1812
10. Kishida KT et al (2016) Subsecond dopamine fluctuations in human striatum encode superposed error signals about actual and counterfactual reward. Proc Natl Acad Sci U S A 113:200–205
11. Oh Y et al (2018) Tracking tonic dopamine levels in vivo using multiple cyclic square wave voltammetry. Biosens Bioelectron 121:174–182
12. Wightman RM et al (2007) Dopamine release is heterogeneous within microenvironments of the rat nucleus accumbens. Eur J Neurosci 26:2046–2054
13. Threlfell S et al (2012) Striatal dopamine release is triggered by synchronized activity in cholinergic interneurons. Neuron 75:58–64
14. Howe MW et al (2013) Prolonged dopamine signalling in striatum signals proximity and value of distant rewards. Nature 500:575–579
15. Hernandez LF et al (2013) Selective effects of dopamine depletion and L-DOPA therapy on learning-related firing dynamics of striatal neurons. J Neurosci 33:4782–4795
16. Robinson DL, Wightman RM (2004) Nomifensine amplifies subsecond dopamine signals in the ventral striatum of freely-moving rats. J Neurochem 90:894–903
17. Williams GV, Millar J (1990) Concentration-dependent actions of stimulated dopamine release on neuronal activity in rat striatum. Neuroscience 39:1–16
18. Schwerdt HN et al (2017) Subcellular probes for neurochemical recording from multiple brain sites. Lab Chip 17:1104–1115
19. Fox ME et al (2016) Cross-hemispheric dopamine projections have functional significance. Proc Natl Acad Sci U S A 113:6985–6990
20. Cragg SJ, Hille CJ, Greenfield SA (2000) Dopamine release and uptake dynamics within nonhuman primate striatum in vitro. J Neurosci 20:8209–8217
21. Taylor IM et al (2015) Kinetic diversity of dopamine transmission in the dorsal striatum. J Neurochem 133:522–531
22. Schwerdt HN et al (2018) Cellular-scale probes enable stable chronic subsecond monitoring of dopamine neurochemicals in a rodent model. Commun Biol 144:1–11
23. Schwerdt HN et al (2017) Long-term dopamine neurochemical monitoring in primates. Proc Natl Acad Sci 114:13260–13265
24. Zachek MK et al (2010) Microfabricated FSCV-compatible microelectrode array for real-time monitoring of heterogeneous dopamine release. Analyst 135:1556–1563

25. Kozai TDY et al (2015) Brain tissue responses to neural implants impact signal sensitivity and intervention strategies. ACS Chem Neurosci 6:48–67
26. Spencer KC (2017) A three dimensional in vitro glial scar model to investigate the local strain effects from micromotion around neural implants. Lab Chip 17:795–804
27. Spencer KC et al (2017) Characterization of mechanically matched hydrogel coatings to improve the biocompatibility of neural implants. Sci Rep 7:1952
28. Lee RS (2019) Reward prediction error does not explain movement selectivity in DMS-projecting dopamine neurons. elife 8: e42992. https://doi.org/10.7554/eLife.42992
29. Engelhard B et al (2019) Specialized coding of sensory, motor and cognitive variables in VTA dopamine neurons. Nature 570:509–513
30. Schmidt AC et al (2014) Multiple scan rate voltammetry for selective quantification of real-time enkephalin dynamics. Anal Chem 86:7806–7812
31. Hashemi P et al (2012) Brain dopamine and serotonin differ in regulation and its consequences. Proc Natl Acad Sci U S A 109:11510–11515
32. Asri R et al (2016) Detection of evoked acetylcholine release in mouse brain slices. Analyst 141:6416–6421
33. Takmakov P et al (2011) Instrumentation for fast-scan cyclic voltammetry combined with electrophysiology for behavioral experiments in freely moving animals. Rev Sci Instrum 82:074302
34. Glantz JC, Woods JR (1994) Cocaine LD50 in long-evans rats is not altered by pregnancy or progesterone. Neurotoxicol Teratol 16:297–301
35. Heien MLAV, Johnson MA, Wightman RM (2004) Resolving neurotransmitters detected by fast-scan cyclic voltammetry. Anal Chem 76:5697–5704
36. Keithley RB, Wightman RM (2011) Assessing principal component regression prediction of neurochemicals detected with fast-scan cyclic voltammetry. ACS Chem Neurosci 2:514–525
37. Fortin SM et al (2015) Sampling phasic dopamine signaling with fast-scan cyclic voltammetry in awake behaving rats. Curr Protoc Neurosci 70:7.25.1–7.25.20

Chapter 7

Immune-to-Brain Signaling Effects on the Neural Substrate for Reward: Behavioral Models of Aversion, Anhedonia, and Despair

Anna Mathia Klawonn and Michael Fritz

Abstract

The role of immune-to-brain signaling in regulating mood and motivational states has received increasing interest, as clinical studies have uncovered a link between systemic inflammation and treatment-resistant major depressive disorder. With these findings, a need for relevant preclinical rodent models has arisen for investigating the role of systemic inflammation and immune-to-brain signaling on motivated behaviors. Here we describe some of the behavioral paradigms currently employed for examining inflammation-induced negative effect and malaise; more specifically we give examples of how the proinflammatory stimulus *Escherichia coli* lipopolysaccharide (LPS) can be combined with behavioral paradigms for anhedonia, aversion, and despair. We aim to provide the reader with guidance on how to prepare and conduct experiments exploring the effects of LPS induced systemic inflammation on affective behaviors.

Key words Anhedonia, Aversion, Conditioned place aversion, Depression, Despair, Forced swim test, Immune-to-brain signaling, Lipopolysaccharide, Sucrose preference test, Systemic inflammation

1 Introduction

1.1 Systemic Inflammation and Affective State

The innate immune system is pivotal for our survival, as it is the body's immediate defense against pathogens. White blood cells, leukocytes, are specialized in recognizing and initiating responses against invading bacteria and viruses. When specialized leukocytes, such as macrophages, identify an intruding pathogen they release various signaling molecules including the pro-inflammatory cytokines tumor-necrosis factor-α (TNF-α), interleukin-1-β (IL-1β), interleukin 6 (IL-6), and interferon-γ (IFN-γ). These cytokines are key mediators of the acute phase of systemic inflammation by signaling to the brain [1]. This phase is characterized by a variety of physiological symptoms, collectively described as "the sickness syndrome." Essentially, the sickness syndrome is an anhedonic state comprising decreased interest in eating and drinking, general inactivity, social withdrawal, as well as fever and hyperalgesia, and

Marc Fakhoury (ed.), *The Brain Reward System*, Neuromethods, vol. 165, https://doi.org/10.1007/978-1-0716-1146-3_7,

hypothalamic–pituitary–adrenal (HPA) axis activation. Interestingly, several of the key symptoms of sickness syndrome are also present during Major Depressive Disorder (MDD) [2, 3].

The pro-inflammatory signaling molecules mediating the sickness syndrome, in both the brain and periphery, are tightly linked with the development and treatment outcome of MDD and other affective disorders [4–6]. These include the previously mentioned cytokines TNFα, IL1β, IL6, and IFNγ; prostaglandins; and the chemokine CCL2 [7]. Furthermore, patients with inflammatory diseases have an increased risk of comorbidity with MDD and anxiety [8–10]. The noteworthy link between clinical MDD and systemic inflammation has made the development of preclinical rodent models in motivation and affect pivotal for uncovering new potential treatment targets—But how to measure the consequences of inflammation on motivation and mood in a mouse or a rat?

1.2 How to Measure Motivation and Mood in Rodents?

Mice and rats share a high level of biological equivalence with human beings, corresponding to 90% of their DNA being homologous with ours [11]. In line with this, the biological foundations for motivation and effect are broadly analogous between rodents and us. The mesolimbic dopamine system encodes reward and motivation in the same manner in rodents as in primates and humans [12–16], and structures such as the nucleus accumbens, hypothalamic nuclei, central and basolateral amygdala, and medial prefrontal cortex (mPFC) are heavily involved in regulating reward and mood in both rodents and human beings [17]. This makes rodents suited model animals for investigating new potential treatment targets against anhedonia and negative affective state. However, you can't ask a mouse or a rat how it is feeling.

Therefore, efforts have been made to develop behavioral affective assays, with a high level of face validity and translatability. The following subsections will go through the theory of some of the most central assays we use to measure core symptoms relevant for motivation and depression, such as aversion, anhedonia, and despair.

1.3 Pavlovian Place Conditioning

The famous physiologist Ivan Petrovich Pavlov was the first to describe the associative learning process through which neutral stimuli become meaningful (salient) predictors of either pleasant or unpleasant outcomes; this process was termed Pavlovian conditioning. Pavlov used experimental dogs for studying the physiology of digestion. One day, he noted that when the technician, who would normally feed the dogs, entered the laboratory most dogs started to salivate, even in the absence of food. This meant that the technician through repeated pairing with food had become a salient predictor of the food itself.

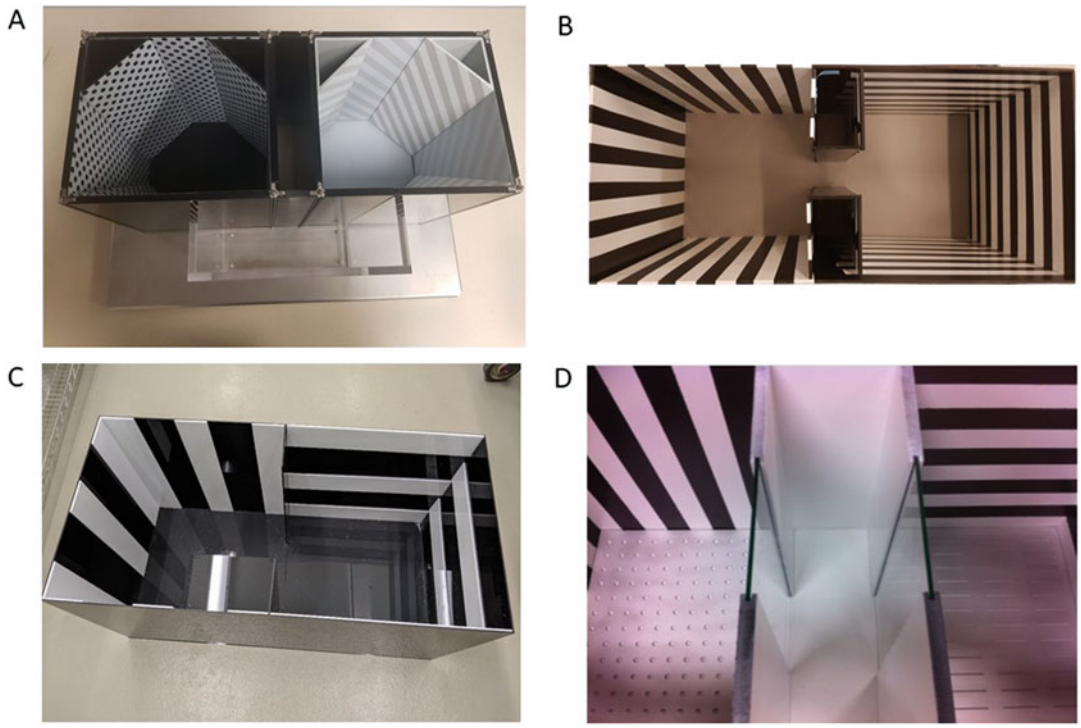

Fig. 1 Example of pictures of commercially available Spatial Place Preference Boxes versus homemade conditioning boxes. (**a**) A commercially available mouse Spatial Place Preference Box from Panlab Harvard Apparatus®. (**b**) A self-built two-chamber version for mice made of TAP Plastics® pieces. (**c** and **d**) Versions of self-built conditioning boxes suited for rats in a two-chamber (**c**) and a three-chamber variant (**d**)

Pavlovian conditioning is common to both animals and human beings. This type of learning is continually occurring in our everyday lives; it helps us predict outcomes of situations by evaluating present predictors (such as visual, tactile, olfactory, and auditory cues) and thereby guides us to respond behaviorally by pursuing the things we enjoy and avoiding what we dislike. In simple terms, conditioning occurs through the repeated pairing of a neutral conditioned stimulus (CS) and a rewarding or aversive unconditioned stimulus (US). When the association has been formed between the two, the CS will elicit a conditioned response (CR). In Pavlov's original case the CR was the salivation of his dogs, which also naturally (unconditioned) would be stimulated by the representation of food (the US). Conditioning will occur if the US and CS are presented simultaneously, or if the CS precedes the US by a short interval [18].

Rodent place conditioning is based on the same Pavlovian learning principles; it most often utilizes place conditioning boxes that have easily distinguishable compartments, such as two visually and tactilely different chambers, connected by a corridor with doors (*see* Subheading 2 and Fig. 1). In this way, the CS is the

environmental cues of the specific compartment, which after repeated pairings with an US will elicit either approach or avoidance behavior, depending on the nature of that US. When using an US with either appetitive or aversive properties, the specific paradigm is referred to as conditioned place preference (CPP) or conditioned place aversion (CPA), respectively [19]. Following the repeated CS–US pairings, the rodent will be given the choice to spend time in either of the chambers, when the experimenter has opened the doors between the two compartments. The choice to spend more time in a rewarding chamber versus decreasing time spent in an aversive chamber is the CR elicited by the animal. Developing place preference or avoidance behavior is the clearest answer a rodent can give us to the question: "Do you like or dislike the chamber where you experienced this particular thing?" Supporting this notion is that place-conditioning studies with human subjects have found that time spent in the conditioning room is proportional to the subjective feelings toward the US [20].

Several considerations should be made on both experimental design and conduct when planning a place conditioning experiment. It is often the case that a conditioning box caries a natural bias in its design, that is, the rodents will prefer one compartment over the other. This is revealed during an initial pretest where the animal is allowed to explore all compartments of the box. In our studies of inflammation-induced place aversion, we utilized a so-called biased place conditioning procedure to overcome any natural bias. In a biased protocol, the aversive US is paired with the most preferred chamber during the pretest, thereby preventing reinforcement of preexisting place aversion. This method has been shown to produce reliable conditioned place responses comparable with other paradigms [21] and prevents already existing bias to become a confounding variable.

It is also important to consider the pharmacokinetics of the US. Pavlovian conditioning relies on that the time between CS and US is brief, hence it is important that the rodent experiences the desired effect of the US when in the conditioning chamber. Another relevant point is to set proper criteria for ensuring that the test results reflect actual choice behavior, as a false positive result could be a consequence of inactivity. One way of ensuring exploration is to set a minimum number of crossings between chambers that have to be achieved by the rodent during test sessions. Practical considerations for conditioned place apparatus design and experimental conduct are described in the Subheadings 2, 3, and 4.

1.4 Anhedonia and Self-Care

We are naturally prone to pursue things that are rewarding for us, such as good company, caloric food, and drink [22]. In the same way, rodents will consume more sweet solutions when given the free choice between a sucrose drink and water [23]. These types of reward behaviors are sensitive to changes in affective state, as

anhedonia, the inability to feel pleasure from innately rewarding activities, is one of the core symptoms in MDD [24]. The most common way of investigating anhedonia preclinically in rodents is by the sucrose preference test (SPT). The SPT originated in the field of dietary metabolism several decades ago [25] and was subsequently used to evaluate reward deficits after chronic defeat stress [26]. The test is typically based on a two-bottle choice paradigm (water vs. sucrose solution) and has been published using various methods and protocols of different durations. Most common to these studies is a design with three phases: adaptation, baseline, and testing phase [27]. Typically, a reduction in sucrose preference ratio between experimental and control animals is considered symptomatic of anhedonia in rodents. This measure is preferably used over the actual sucrose consumption, as there can be great variations between the drinking days of individual animals [28]. Also, including the water bottle in the experimental design is absolutely pivotal, as any changes in sucrose drinking should reflect a changed interest in reward, not just fluctuations in overall liquid consumption [28]. An advantage with SPT is its high face validity, as effects of antidepressants are primarily measurable after the induction of deficits (caused by stimuli such as stress or inflammation) and long-term treatment. Essentially, SSRIs exhibit similar pharmacokinetics in the SPT as observed in patients with MDD [29].

1.5 A Despair Model: The Forced Swim Test

In 1977, Roger D. Porsolt and colleagues designed a behavioral test with the aim to achieve the two criteria of resembling depressive illness and being selectively sensitive to clinically effective antidepressant treatments [30, 31]. In this test, rodents are forced to swim when placed in a cylinder with water from which there is no escape. Though the test is relatively short (e.g., 6 min), most animals will express an early phase of vigorous swimming followed by inactivity, where they eventually become passive and only move to keep the head above water. This immobility behavior is interpreted as despair, that is, the loss of hope, and has been demonstrated to be sensitive to many types of antidepressant pharmacotherapy [30–32]. In this manner, a rodent that gives up swimming and spends a longer time being immobile is interpreted as displaying depression-like behavior, while antidepressant interventions will reinforce an active strategy toward survival and escape. The test was suitably named the forced swim test (FST) and the Porsolt test.

When employing the FST, it is important that the experimental treatment does not cause changes in normal locomotor activity, which can become a confounding factor in the analysis of the test results. To ensure validity, a separate experiment should be conducted in locomotion arena or home cage to explore any locomotor effects of the experimental conduct [29]. Furthermore, variables such as water level and water temperature can affect the behavioral

readout of the FST. For instance, studies have found that rodents exhibit more active swimming behavior in deeper water [33].

In recent years the FST has received criticism, as the pharmacokinetics of standard antidepressants are very different in the test rodents in comparison to that in depressed patients. Selective serotonin reuptake inhibitors (SSRIs) show efficacy after only 1 day in the FST, while it often takes weeks to months before similar effects are observed in depressed patients [29, 34, 35]. Hence, the results of the FST should always be evaluated with complementary behavioral data on affective states, such as measures of anhedonia and aversion.

1.6 Models of Systemic Inflammation

There exist a variety of inflammatory agents that can be used for studying innate immune reactivity on mood and reward, such as the viral mimetic Polyinosinic: polycytidylic acid (which is structurally similar to double-stranded RNA from virus), the Bacillus Calmette–Guerin (which is the current primary tuberculosis vaccine), or systemic injections of the pro-inflammatory cytokine IL-1β (which briefly elicits all symptoms of the acute phase of inflammation) [2, 3, 36]. However most commonly used for preclinical studies is Lipopolysaccharide (LPS), which is a typical component of the outer membrane of gram-negative bacteria. In particular, the active fragment of endotoxin produced by *Escherichia coli* (*E. coli*) bacteria has been used in several animal and human studies to produce systemic inflammation, in the absence of actual infection [37, 38].

When *E. coli* LPS is administered systemically, the innate immune system responds by inducing symptoms of the acute phase response [39, 40]. Intraperitoneal injections (i.p.) of LPS generate a pro-inflammatory cytokine profile similar to that observed in both humans and rodents during infections, and which is also characteristic of several chronic inflammatory diseases [40–44]. For our studies of inflammatory aversion, a low-grade systemic inflammation model was employed [36, 45, 46] based on acute injections of 10 μg/kg LPS i.p. from K-235 *E. coli*. At this dose, mice display mild symptoms of the sickness syndrome including elevated body temperature, anorexia, and inactivity [36, 47]. Place conditioning paradigms are particularly suited for this inflammatory model, as acute phase symptoms are absent when the LPS is not administered, such as on test days. However, the low inflammatory model is incompatible with despair tests (based on mobility) and anhedonia assays, as the dose is administered acutely and hence directly affect locomotion and food intake [36].

Many animal models used for investigating inflammation-induced negative affective state and anhedonia are based on administrations of high doses of LPS (500–2500 μg/kg) [42, 48]. It is worthwhile noting that these high concentrations of LPS may cause septic shock in rodents, and therefore are dissimilar to the inflammation levels occurring during common infections and chronic

inflammatory diseases in human beings. Hence the low dose of LPS (10 μg/kg i.p.) may represent an advantage, as it is more comparable to normal inflammatory conditions and is similar to doses used in studies showing that endotoxins rapidly cause a depressed mood in healthy human subjects [13, 49]. However, high doses of LPS are well suited for preclinical investigations of despair behavior and anhedonia, as 24 h after the acute LPS injection the sickness symptoms resolve, while the rodents exhibit a persistent anhedonic and depressed phenotype [3].

2 Materials

We use C57BL/6 J mice or Fischer 344 rats for all behavioral experiments, as these strains have been reported to exhibit appropriate inflammatory responses and affective behaviors [50, 51]. It is very important that rats and mice are housed separately, and that species-specific experiments are done in distinct experimental rooms, as rats have specialized odors that cause fear behavior in mice without prior associative conditioning [52]. We recommend using group sizes of $n = 8–10$ for the behavioral experiments in order to achieve significant differences between vehicle and inflammation groups. We use *E. Coli* Endotoxin Lipopolysaccharide (LPS) serotype 055:B5 in aqueous solution (Sigma–Aldrich) and store it according to manufacturer directions (e.g., 4 °C). We always prepare the experimental LPS solutions fresh on the day of the experiment, by making a dilution with physiological saline to a concentration of 10 μg/kg for CPA and 830 μg/kg for SPT and FST. The i.p. injection volumes used in our studies are 100 μL per 25 g mouse weight versus 100 μL per 250 g rat weight. When stored appropriately the original LPS stock, from the manufacturer, should be stable for up to 6 months, however, older stocks may lose potency.

2.1 Materials for the Conditioned Place Aversion Paradigm

For conditioned place aversion, a two- or three-chambered place conditioning box with both visible and/or tactile cues for either rat or mouse can be utilized. In our studies, we use the three-chambered Spatial Place Preference Box from Panlab, Harvard Apparatus (*see* Fig. 1a).

However, place conditioning boxes can be either commercially purchased or constructed by the experimenter by using premeasured and cut acrylic plastic or similar, in combination with specific acrylic glue or superglue. There exist many companies offering precut and colored plastics, which limits expenses compared to purchasing a commercial place conditioning box (for examples of homemade two- and three-chambered boxes *see* Fig. 1b–d). When constructing a CPA box, black plastic for the walls of the box and gray plastic for the flooring can be recommended, as a darker box

will make exploration easier for both mice and rats. Rodents are typically nocturnal and easy prey for predators, which means they tend to avoid bright spaces [53].

In the case that the place preference tests are video recorded and scored using a contrast-based tracking program such as Ethovision (Noldus®) or Viewer (Biobserve), consideration to the color of flooring is of particular importance; a white rodent can be difficult to track on a white/gray floor and a black rodent will be problematic to track on a black floor. Hence, when using contrast-based tracking, flooring should be selected to contrast the color of the experimental mouse or rat strain. Avoid to the largest extent possible bright white flooring, as it can cause "Open field test" like the approach–avoidance conflict in rodents [54, 55]. Alternatively, the CPA tests can be manually scored using video recordings off-line or during the experiment in real time. We recommend a standard high definition camera for recording the CPA tests from above, such as Logitech HD Pro Webcam C920, 1080p Camera (Logitech®). Blinding of the experimenter, on genotype or treatment, is absolutely pivotal in order to avoid bias during manual scoring! We scored all CPA tests manually using two stopwatches per experimenter (standard stopwatch from a sports shop), and hence were blinded on either treatment or alternatively on genotype when using transgenic mice in our LPS CPA studies [36, 45, 46].

The two box chambers can be combined with tactical cues, such as transparent graded plastic flooring, and visual cues to make them easily distinguishable for the rodent. For example, white electrical tape is convenient for making horizontal versus vertical stripes as visual cues in the individual chambers. Choosing electrical tape for decorating the CPP box is convenient as this type of tape is made of thick plastic, which makes the surfaces of the box easier to clean (*see* Fig. 1b). But visual cues can be made of various materials, as long as they make noticeable differences between the two chambers, without causing extensive bias toward one chamber over the other. In terms of cleaning, commercial CPP boxes often offer an advantage, as they are likely to have smooth surfaces and are made of multiple segments (i.e., floors, walls, etc.) that can be separated and washed.

For making your own place conditioning box for mice we suggest the following measures: Overall exterior 46 cm (w) × 20 cm (d) × 25 cm (h), with each of the two chambers being square (i.e., 20 cm (w) × 20 cm (d)) and separated by walls forming a small corridor measuring 6 cm (d) × 6 cm (w). The handmade box is size-wise equivalent to the commercially available Panlab Spatial Place Preference Box which we have employed for most of our studies, although it lacks the third chamber (*see* Fig. 1a, b). Whereas for rats, a CPP box measuring 63 cm (w) × 33 cm (d) × 30 cm (h), with each of the two chambers being rectangular (i.e., 25 cm (w) × 30 cm (d)) and separated by a small third

(neutral) chamber measuring 10 cm (d) × 30 cm (w) can be recommended [56, 57] (*see* Fig. 1c, d).

In the behavioral room, we use dimmed indirect light, to make the room as comfortable as possible for the animals, which helps to ensure natural exploration behavior. This can be done (depending on the size of the room) by placing up to two to four 40-W lightbulb lamps facing the corners/walls of the room. It is important to check that the light condition in the chambers of the boxes is homogenous in order to eliminate any shadowy corners that might cause a bias toward one of the CPA box chambers [54]. We use dishwasher detergent with a mild scent (such as lemon) to wash our boxes between each experimental animal. We wash floors and walls with warm water and detergent using a kitchen sponge to clean off any urine or fecal traces. We afterwash the box floors and walls with warm water to remove remaining detergent, and subsequently spray all surfaces with 70% ethanol, before wiping them dry with a paper towel or similar. This washing procedure establishes a fairly homogenous olfactory environment throughout the box and prevents olfactory-based stress/bias as a cofounding factor [58, 59].

2.2 Materials for the Sucrose Preference Test

In the two-bottle choice paradigm, we use normal filtered drinking water for the water bottles and for making a 4% (w/v) sucrose solution. These solutions are filled into two different 50 mL Falcon tubes with rubber tops and nibbles for mice, while larger standard drinking bottles are employed for rats. Importantly, each bottle type is clearly labeled: Water (W) or Sucrose (S), dependent on the condition. Water and sucrose solutions are made fresh and drinking bottles are washed with dishwasher detergent and water prior to use. We use a standard laboratory scale for weighing the bottles in order to measure the fluid consumed. Make sure to have an empty cage and an extra set of bottles, for measuring dripping bias.

2.3 Materials for the Forced Swim Test

In the forced swim test for mice we recommend a standard 2000 mL glass beaker, ca. 19 cm high, and measuring 13 cm in diameter (Pyrex®), while for rats we have used a plexiglass bowl, ca. 35 cm high and with a diameter of 50 cm. It is important that the animals cannot reach the cylinder sides or the bottom of the cylinder with their tails [33]. We use regular tap water, which can be temperature regulated, to achieve a water temperature of 25 ± 5 °C for the immediate test; water temperatures are measured using a long glass mercury thermometer. The recording of the FST is done with a standard high definition camera on a tripod, such as a Canon VIXIA HFS200 (Canon®) and analysis of the behavior is done off-line using the Porsolt test settings in the contrast-based tracking program, EthoVision XT (Noldus). When using a contrast-based tracking program for the FST, it is important to

use a brighter background for tracking black/dark rodents, and a darker background for tracking bright coated animals. The rodents are allowed to recover in clean cages with standard bedding and are dried with cotton or paper towels on a heating pad. When recording more animals in parallel a homemade plastic/cardboard space divider can be placed between the FST beakers (e.g., 20 cm (w) × 30 cm (h) for mice and 50 cm (w) × 50 cm (h) for rats), in order to prevent the animals from interfering with each other.

3 Methods

A general rule for all behavioral tests is that experimental animals should be counterbalanced to avoid environmental and time factors influencing the experimental result. Hence, animals representing different conditions (e.g., control and test) should if possible be present during each individual test session with an emphasis on distribution across all behavioral arenas used. In this way, the experimental design ensures that no eventual differences between time of day, changes in the exterior environment, behavioral arenas, or placement in a room influences the experimental outcome. All animals are kept on a regular 12-h light/dark cycle, and CPA and FST experiments are conducted during the light phase, while SPT is done during the early phase of the dark cycle. For further information, see recommendations for housing and cage cleaning in the Subheading 4.

3.1 Inflammation-Induced Conditioned Place Aversion

For a schematic overview of the conditioning procedure, please *see* Fig. 2a.

3.1.1 Day 1: Pretest

The purpose of the pretest is to get an accurate measure of the time the individual rodent spends in each of the place conditioning box chambers prior to conditioning, as this can fluctuate and illustrates distinct bias toward the box chambers. We utilize a biased conditioned place aversion protocol, described in the introduction, and hence assign each individual animal to a conditioning chamber according to their preference measured during the pretest on day 1. The chamber (left or right), which the animal prefers during the pretest, is chosen as the conditioning chamber in order to avoid reinforcing already existing aversion to the other chamber of the box.

When doing manual scoring of pre- and posttests, all experimenters should be blinded to treatment or genotype of the transgenic animals by an independent experimenter, prior to initiating the test.

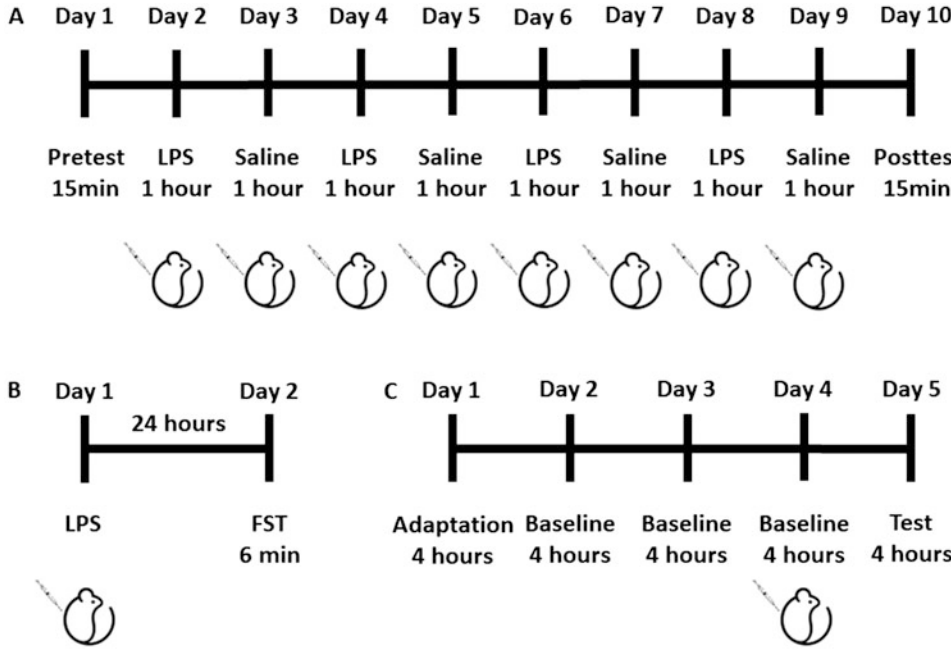

Fig. 2 Timeline overview for the conditioning procedure. (**a**) Timeline for the 10-day LPS-induced place aversion paradigm consisting of a pretest, eight consecutive training days, and a posttest. (**b**) Timeline for the LPS-induced depression model for the Forced Swim Test. (**c**) Timeline for the LPS-induced depression model in the Sucrose preference test

1. Prior to the pretest, clean the designated test box thoroughly to avoid any olfactory bias from previous experiments. Take apart all walls of the Panlab Spatial Place Preference Box, by unscrewing the eight top corner screws, using an adjustable wrench. Wipe the metal base of the box with dishwasher detergent on a wet kitchen sponge, followed by water and then 70% ethanol; all box walls, floors, and doors are washed in the same manner. Finally, all parts of the box should be dried using paper towels or clean cotton dish towels. It is important that no moisture remains in any part of the box, as it might cause bias; remember to dry underneath the base of the box as well.
2. Dim the room light prior to bringing in the rodents (*see* the Subheading 2 for appropriate light settings). Then bring the individual animal(s) to be tested into the room, while keeping the remaining experimental groups in their home cages on a trolley in an (unused) adjacent room. We never test more than a maximum of two rodents at the time (on each side of the room), in order to ensure proper separation of the animals during the test. The remaining rodents should be kept elsewhere than the CPA room, as sudden sounds from movement in the cages may interfere with test behavior or conditioning.

3. In the LPS CPA paradigm, we use a 15 min pretest. Before initiating the pretest, gently place the rodent in the corridor, which should be blocked by doors that prevents it from entering the two chambers. In the Panlab Spatial Place Preference Box, the corridor is a transparent third chamber, which makes it easy to ensure proper exploration behavior before opening the doors. If the rodent is passively still or showing other signs of anxiety (panting, stretch attend posture, etc.) wait a few minutes for it to recover before initiating the test. In our experience, most rodents return to normal exploratory behavior if given proper time to recover. In all cases, the experimenter should make sure to stay as much as possible out of sight, so the rodent can explore freely. Tips and tricks for preventing anxiety in the experimental animals can be found in the Subheading 4.
4. Initiate the pretest by gently and simultaneously, opening both doors to the chambers, and then quickly starting a 15-min countdown timer. For scoring the chamber preference, keep a stopwatch in each hand representing the individual chamber (left vs. right). The time of the individual chamber stopwatch should be started only when the rodent's field of attention is on the specific chamber. The stopwatch time is started as soon as the rodent places its head inside the chamber, looking at the chamber cues; and stopped again if it is having its head in the corridor looking out of the chamber. The corridor is the neutral zone and the time the animal spends there is not recorded!

   Write down the time spent in each chamber and save it for calculating the final preference scores. This information is also important, as it clarifies how much bias the specific cohort of animals exhibits toward the box design. We use the following exclusion criteria for the pretest: If a rodent spends longer than 600 seconds in one chamber it will be excluded due to too strong bias, and we expect each animal to exhibit minimum five crossings between the two chambers in order to ensure proper exploration and choice behavior.
5. After completing each individual pretest, wash the floors of the test box with detergent and water, followed by 70% ethanol, and spray the chamber walls with ethanol. Subsequently, everything should be dried before the next rodent is tested, and the doors placed back in place. A general rule for evaluating the cleanness of the box between each test and conditioning session is to briefly smell the box chambers and corridor, as rodent urine can be easily detected by its odor.

3.1.2 Day 2–9: Training Days

Once the conditioning chamber has been defined, CPA training starts the next day and continues over a total of eight consecutive days. Dependent on the size of the room and the number of boxes

and experimenters, the group size capacity per session may vary. We averagely condition six to eight animals at the time, using a setup with four boxes on two tables, on each side of the experimental room—that is, eight boxes overall in a room of ca. 12 m^2 with one to two experimenters.

1. On the conditioning day, bring the animals for the specific conditioning session into the experimental room in their home cages on a trolley.
2. As described in the introduction, the length of each conditioning session depends on the pharmacokinetics of the US used. For the LPS CPA paradigm, inject 10 μg/kg LPS i.p. Ten minutes prior to placing the animal in the conditioning chamber (for preparation of solutions *see* the Subheading 2). Each training session lasts 1 h to ensure proper associative learning, as the LPS induced immune response onset is sluggish and varies between 20 and 30 min post injection [60]. Gently scruff the rodent and i.p. inject the LPS or saline—this procedure should be done by an experienced experimenter as stressful handling and injection can prevent proper conditioning to aversive stimuli [61]. During the 10 min wait following the i.p. injection, keep the animals in their home cages on the trolley.
3. Then place the individual rodent into its specific conditioning chamber (i.e., the most preferred chamber during pretest). We always ensure that the same conditioned place preference box is used for the same animal during each training session. Occasionally, we find that a rodent has escaped the training chamber; if this is the case place a cage lid on top of the box chamber on the following training days to prevent future escape.
4. After 1 h, return the animals to their home cages and carefully clean the place-conditioning chambers as described in the pretest section. The cleaning between conditioning sessions is pivotal as olfactory cues can prevent proper conditioning. For instance, the scent of male urine is used for territorial demarcation [58] or sexual advertisement in the case of female mice [59].
5. Since the acute inflammation induced by LPS lasts around 4–6 h, it is not favorable to run two training sessions per day, as a spillover effect of the aversive association to the nonconditioning chamber might occur [60]. Therefore, continue the saline training, in the least preferred chamber, the very next day in the same manner as the LPS training. This alternating training procedure, where saline and LPS conditioning is done on separate days, should be continued for another 6 days completing the training phase with a final saline training session, as outlined in Fig. 2a.

3.1.3 Day 10: Posttest

On the day after the completed training, the experimental animals undergo a 15 min posttest. The posttest has to be conducted identically to the pretest:

1. chly prior to testing!
2. During the test the rodent is allowed to freely explore the entire apparatus for the same amount of time as during the pretest, that is, 15 min. Keep an eye on proper explorative behavior prior to initiating the test!
3. Remember to thoroughly clean the test box between each rodent, as described in the pretest section, and keep only the one to two rodents undergoing a test in the room.
4. Once the test is fully recorded, the time spent in the conditioning chamber versus non-conditioning chamber should be noted. The aversion score can be calculated by subtracting the time spent in the LPS-conditioned chamber during the pretest from the time spent in the LPS-conditioned during the posttest, that is, posttest time in aversion chamber (sec)—pretest time in aversion chamber (sec) = aversion score (sec). After the scores have been calculated, unblinding should be done by an independent experimenter.

3.2 The Sucrose Preference Test (SPT)

For a schematic overview of the sucrose preference test experimental procedure, please *see* Fig. 2c. Forty-eight hours to a week prior to initiating the sucrose preference protocol, animals should be single-housed to avoid stress from the changed housing conditions. Single housing is necessary for the sucrose preference test (SPT) in order to correctly determine the amount of water and sucrose solution consumed by each rodent. We conduct all phases of SPT in the home cages of the animals, during the first 4 h of the dark period of the light/dark cycle, in order to ensure active drinking.

Although different sucrose solutions have been published for the rodent SPT paradigm, we find that a 4% sucrose solution is appropriate for assessing LPS-induced anhedonia. As described in the introduction, the SPT consists of three phases: (1) adaptation, (2) baseline, and (3) test. Below you find first description of the general experimental procedure, which is roughly comparable between the three phases, followed by a description of the three individual phases of the experiment, detailing differences of each phase:

3.2.1 The Sucrose Preference Test Experimental Procedure

1. Start the preparations a few hours prior to the onset of the dark phase of the light/dark cycle of the vivarium. Each experimental animal should have two identical drinking bottles to avoid drinking bias. Wash the Falcon tubes or drinking bottles carefully with dishwasher detergent and several rounds of warm water to ensure that they are clean and soap free. Then label the

drinking tubes/bottles clearly using a permanent marker—50% of them with a "W" for water and the other 50% with an "S" for the sugar solution. Prepare the 4% sugar solution and fill half of the bottles/Falcon tubes (S); the other half should be filled with normal filtered tap water.

2. Prepare a table/trolley or other stable surface as a work station from where you can test and weigh bottles and prepare the individual rodent cages.
3. Be sure to check the bottles and sippers prior to use by tilting them upside down to observe any excessive dripping/leakage and have replacement tubes nearby. Test each bottle nibble by tabbing it with a finger until a few drops of liquid occur, to ensure that all bottles are functioning properly and not exhibiting excessive or insufficient flow.
4. Dry and place the individual tube/bottle on the tared scale in a manner that it cannot leak (e.g., inverted or balanced lying down). Note the weight of each bottle! The liquid in each bottle is measured twice per day: Once prior to placement in the cage, and then immediately after 4 h of drinking.
5. After the onset of the dark cycle, at the same time every day of all experimental phases (day 1–5), remove the standard drinking bottles from the individual rodent home cage. Carefully place in the two prepared bottles (sucrose vs. water), while avoiding any dripping. Ensure that both bottle nibbles are easily accessible. Most cage systems allow for placement of two bottles; however, check that you have a bottle system that matches your rodent home cages. Furthermore, it is a good experimental practice to prepare an empty cage, in the same manner as the experimental animal cages, to test for any liquid spill during all phases.
6. Carefully place the individual cage back into the rack, while avoiding dripping from the bottles. Then start your 4-h countdown on a timer, immediately after the first cage has received the two bottles and is placed back into the cage rack. Once all tubes and cages are in place, leave the room and allow for the test animals to exhibit natural stress-free behavior.
7. Return to the experimental room shortly before the end of the 4-h period. When the timer rings, carefully remove and weigh the bottles from each cage in the same order as they were placed, to ensure that each rodent gets the full 4 h drinking time. Remember to note the end weight of the individual bottle!
8. When the measurements are done, return each standard drinking bottle to its original position and place the animal cage back into the rack.

9. Thoroughly rinse tubes/bottles, rubber tops, and nibbles, with water, so they are ready for use the next day, make sure to use the same bottles for the same animals (label them or keep them in sequential order).

3.2.2 Overview of the Sucrose Preference Test Experimental Phases: Adaptation, Baseline, and Test

1. The adaptation phase on day 1, is the day for familiarizing the animals with the two-bottle-drinking paradigm. The weight of the bottles should not necessarily be recorded on day 1, but weighing them is good procedural training and we recommend doing so when implementing the SPT protocol.
2. During the baseline phase (day 2–4), the individual rodent baseline preference for the sucrose solution versus water is assessed. This is the phase where the animals form a drinking preference; most animals will increase their preference for the sucrose solution across the 3 days until they reach a saturation level. During these days, it is necessary to switch the positions of the sucrose and water bottles daily in order to prevent side bias!
3. Immediately after the last day of baseline drinking is completed (day 4), inject the test rodents with the high dose of LPS (830 μg/kg) i.p. and the control animals with physiological saline i.p. If LPS is injected prior to the drinking session on day 4, the rodents will experience acute systemic inflammation during the consumption of the sugar solution. This should be avoided as it may cause taste aversion, which will interfere with the interpretability of the data.
4. On the test day (day 5), the experimental procedure is repeated in the same manner as the other days, without any i.p. injections.
5. On each day, the difference in bottle weight between the two measuring points (0 and 4 h) should be calculated as the ΔWeight of each solution consumed by the rodent on a specific day. That is $\text{Weight}_{\text{time0hours}} - \text{Weight}_{\text{time4hours}} = \Delta\text{Weight}$ (sucrose or water).

   The preference for sucrose for each rodent on an individual day (days 2–5) can then be calculated as $100 \times (\Delta\text{Weightsucrose} / (\Delta\text{Weightwater} + \Delta\text{Weightsucrose})$. We then typically generate a baseline preference score from an average of the ΔWeight for the three baseline days (days 2–4). Then the averaged baseline sucrose preference can be subtracted from the sucrose preference of day 5, and the final result is expressed as a percentage change in sucrose preference. Hence in the LPS group, this calculation should yield a negative value, as the animals are expected to consume more sucrose during baseline prior to experiencing inflammation-induced anhedonia.

3.3 The Forced Swim Test

One or two days prior to the FST paradigm, we recommend habituating the animals to the experimental room (*see* Subheading 4 on stress prevention) for an hour. We administer the high dose of LPS (830 μg/kg) i.p. 24 h prior to the test, as this time allows the rodents to recover the acute phase of inflammation, while the affective component of the inflammation remains. Rodents receive saline or 830 μg/kg LPS injections i.p., according to if they are control or test animals, and are placed directly back into their home cages and housed as normal. For a schematic overview of the experimental procedure *see* Fig. 2b.

1. Make sure to prepare the experimental room prior to the test. This is done by setting up a table with the transparent cylinder (s) against a background that will ensure proper visualization of the rodent (e.g., a dark background for a white Fischer 344 rat). We do not recommend recording more than two animals at the time. In the case that you are recording more than one experimental animal, separate the two cylinders by an opaque wall, so that the animals cannot interact with each other during the test. Place up the HD camera on a tripod, in a manner ensuring the closets image possible of the complete cylinders. It is also important to prepare a recovery station, with clean cages placed on two-thirds of a heading pad; this should preferably be in a separate room from the experimental room or alternatively as far away as possible from the test arena, in order to avoid any interference between test- and recovering rodents.
2. On the test day, the animals are brought into the experimental room and left to acclimatize, we suggest to do this minimum 30 min prior to running the test.
3. Then, fill the transparent cylinders with 25 ± 0.5 °C warm water immediately before the test. Avoid any water temperature changes, as they will influence the rodents' struggling response. The water level has to be high enough to prevent the animal from reaching the bottom of the cylinder with its tail, but also low enough, to prevent the rodent from reaching the beaker's edge (i.e., ~30 cm for rats and ~14 cm for mice, *see* Subheading 2 for cylinder measures).
4. Start the video camera prior to placing the animals in the cylinders, and place up a piece of paper with rodent ID and treatment information.
5. Place the rodent in the cylinder by holding its tail and gently letting the front part of the body first reach the water surface followed by the rest of the body; this lets the rodent quickly adapt to and keep its head above the waterline. Once the rodent is floating in the water, release the tail. Take care not to block the camera view of one animal, while placing the other animal in the cylinder.

6. Keep the distance to the experiment, and stay calm, while observing that the animals are safe, and use a timer to ensure that each rodent is in the water for 6 min. We have not yet experienced an animal incapable of swimming or floating, that is, keeping its head above water within this timeframe. However, if it should happen that an animal is struggling to keep its head above the water immediately rescue it from the cylinder!
7. When the 6 min have passed stop the recording, remove the experimental animals from the water by their tails, and dry them with towels in a temporary holding cage on a heating pad, this should be done rapidly to prevent hypothermia. Once the rodents are dry and start exploring normally, return them to their home cages.
8. For analysis of the videos, we recommend using the Porsolt test settings in EthoVision XT (Noldus) to get accurate measures of mobility and immobility time. Notice, that the first 2 min should be omitted from the analysis, as this time reflects the animal's habituation to water; only the last 4 min are used for analysis.

4 Notes

The most important general advice for any rodent behavioral test is: Animals should be handled by calm and trained staff, keep the room and behavioral arenas clean, and prevent stress in housing and experimental rooms.

Stress prevention:

- Hierarchical stress among male C57BL6 mice can interfere with any behavioral assay, but it is particularly disruptive for associative learning, such as CPA. We recommend single housing the experimental animals (in clean cages) minimum 48 h prior to pretest [62].
- Avoid introducing spatial bias in the experimental room! Local differences in the ambience of the experimental room can be introduced by sounds or drafts, such as from a ventilation vent in the ceiling or by a nearby computer. Make sure to avoid placing your behavioral arenas in such a manner that these unwanted stimuli will interfere with the specific test.
- Avoid loud noises in the room and adjacent surroundings—place up clear signs that the experiment is ongoing and people should be respectful.
- Habituation to the experimental room for a day or two prior to the experiment is highly recommended. Simply let your animals stay in their (properly ventilated) cages on a trolley for an hour in

the room during similar light-, sound- and temperature settings as will be used for the experiment.

- Monitor and note the stress levels of individual animals! Freezing, hunching and cowering, and stretch-attend postures are clear signs of stress in mice and rats [63, 64]. Take preventive action (as described in the Subheaidng 3) prior to initiating the CPA test.
- On test days, if all rodents seem generally anxious, it can be beneficial to postpone the CPA test till later the same day or alternatively the next day. Sometimes general maintenance or cage change can influence the baseline stress of rodents, which likely will influence the quality of your experiment.
- Light settings in the room should be the same throughout all phases of the experiment, that is, dimmed and indirect during place conditioning, normal light conditions during the FST, and normal vivarium dark cycle conditions for the SPT procedure.
- i.p. injections should always be performed by the experienced staff! It is important to keep the injections as standardized as possible between individual subjects and to prevent unnecessary stress as a confounding factor.

Dealing with weak phenotype results:

- If the behavioral phenotype seems weak, consider changing the batch of LPS, as batch variances do occur.
- The rodent genetic background can also influence the effect of LPS; we found that C57BL/6 mice were particularly useful for CPA experiments compared to other mouse strains.
- Take notes on any changes in general baseline stress (e.g., due to alterations in sound or odor levels), as this may also influence your results.

References

1. Kronfol Z, Remick DG (2000) Cytokines and the brain: implications for clinical psychiatry. Am J Psychiatry 157(5):683–694. https://doi.org/10.1176/appi.ajp.157.5.683
2. Dantzer R, O'Connor JC, Freund GG, Johnson RW, Kelley KW (2008) From inflammation to sickness and depression: when the immune system subjugates the brain. Nat Rev Neurosci 9(1):46–56. https://doi.org/10.1038/nrn2297
3. Remus JL, Dantzer R (2016) Inflammation models of depression in rodents: relevance to psychotropic drug discovery. Int J Neuropsychopharmacol 19(9):pyw028. https://doi.org/10.1093/ijnp/pyw028
4. Reus GZ, Fries GR, Stertz L, Badawy M, Passos IC, Barichello T, Kapczinski F, Quevedo J (2015) The role of inflammation and microglial activation in the pathophysiology of psychiatric disorders. Neuroscience 300:141–154. https://doi.org/10.1016/j.neuroscience.2015.05.018
5. Kraus C, Kadriu B, Lanzenberger R, Zarate CA Jr, Kasper S (2019) Prognosis and improved outcomes in major depression: a review. Transl Psychiatry 9(1):127. https://doi.org/10.1038/s41398-019-0460-3
6. Arteaga-Henriquez G, Simon MS, Burger B, Weidinger E, Wijkhuijs A, Arolt V, Birkenhager TK, Musil R, Muller N, Drexhage HA (2019)

Low-grade inflammation as a predictor of antidepressant and anti-inflammatory therapy response in MDD patients: a systematic review of the literature in combination with an analysis of experimental data collected in the EU-MOODINFLAME consortium. Front Psych 10:458. https://doi.org/10.3389/fpsyt.2019.00458

7. Young JJ, Silber T, Bruno D, Galatzer-Levy IR, Pomara N, Marmar CR (2016) Is there progress? An overview of selecting biomarker candidates for major depressive disorder. Front Psych 7:72. https://doi.org/10.3389/fpsyt.2016.00072
8. Lee CH, Giuliani F (2019) The role of inflammation in depression and fatigue. Front Immunol 10:1696. https://doi.org/10.3389/fimmu.2019.01696
9. Dregan A, Matcham F, Harber-Aschan L, Rayner L, Brailean A, Davis K, Hatch S, Pariante C, Armstrong D, Stewart R, Hotopf M (2019) Common mental disorders within chronic inflammatory disorders: a primary care database prospective investigation. Ann Rheum Dis 78(5):688–695. https://doi.org/10.1136/annrheumdis-2018-214676
10. Kurina LM, Goldacre MJ, Yeates D, Gill LE (2001) Depression and anxiety in people with inflammatory bowel disease. J Epidemiol Community Health 55(10):716–720. https://doi.org/10.1136/jech.55.10.716
11. Waterston RH, Lander ES, Sulston JE (2002) On the sequencing of the human genome. Proc Natl Acad Sci U S A 99(6):3712–3716. https://doi.org/10.1073/pnas.042692499
12. Ramchandani VA, Umhau J, Pavon FJ, Ruiz-Velasco V, Margas W, Sun H, Damadzic R, Eskay R, Schoor M, Thorsell A, Schwandt ML, Sommer WH, George DT, Parsons LH, Herscovitch P, Hommer D, Heilig M (2011) A genetic determinant of the striatal dopamine response to alcohol in men. Mol Psychiatry 16(8):809–817. https://doi.org/10.1038/mp.2010.56
13. Eisenberger NI, Berkman ET, Inagaki TK, Rameson LT, Mashal NM, Irwin MR (2010) Inflammation-induced anhedonia: endotoxin reduces ventral striatum responses to reward. Biol Psychiatry 68(8):748–754. https://doi.org/10.1016/j.biopsych.2010.06.010
14. Martinez D, Orlowska D, Narendran R, Slifstein M, Liu F, Kumar D, Broft A, Van Heertum R, Kleber HD (2010) Dopamine type 2/3 receptor availability in the striatum and social status in human volunteers. Biol Psychiatry 67(3):275–278. https://doi.org/10.1016/j.biopsych.2009.07.037
15. Volkow ND, Fowler JS, Wang GJ, Swanson JM, Telang F (2007) Dopamine in drug abuse and addiction: results of imaging studies and treatment implications. Arch Neurol 64(11):1575–1579. https://doi.org/10.1001/archneur.64.11.1575
16. Schultz W, Romo R (1990) Dopamine neurons of the monkey midbrain: contingencies of responses to stimuli eliciting immediate behavioral reactions. J Neurophysiol 63(3):607–624. https://doi.org/10.1152/jn.1990.63.3.607
17. Tye KM, Deisseroth K (2012) Optogenetic investigation of neural circuits underlying brain disease in animal models. Nat Rev Neurosci 13(4):251–266. https://doi.org/10.1038/nrn3171
18. Bear MF, Connors BW, Paradiso MA (2007) Neuroscience: exploring the brain, 3rd edn. Lippincott Williams & Wilkins, Baltimore
19. Sanchis-Segura C, Spanagel R (2006) Behavioural assessment of drug reinforcement and addictive features in rodents: an overview. Addict Biol 11(1):2–38. https://doi.org/10.1111/j.1369-1600.2006.00012.x
20. Mueller D, de Wit H (2011) Conditioned place preference in rodents and humans. In: Raber J (ed) Animal models of behavioral analysis, Neuromethods, vol 50. Humana Press, Totowa, NJ. https://doi.org/10.1007/978-1-60761-883-6_6
21. Bardo MT, Rowlett JK, Harris MJ (1995) Conditioned place preference using opiate and stimulant drugs: a meta-analysis. Neurosci Biobehav Rev 19(1):39–51. https://doi.org/10.1016/0149-7634(94)00021-r
22. Bromberg-Martin ES, Matsumoto M, Hikosaka O (2010) Dopamine in motivational control: rewarding, aversive, and alerting. Neuron 68(5):815–834. https://doi.org/10.1016/j.neuron.2010.11.022
23. Tordoff MG (2002) Obesity by choice: the powerful influence of nutrient availability on nutrient intake. Am J Physiol Regul Integr Comp Physiol 282(5):R1536–R1539. https://doi.org/10.1152/ajpregu.00739.2001
24. American Psychiatric Association (2013) Diagnostic and statistical manual of mental disorders, 5th edn. American Psychiatric Publishing, Washington, DC

25. Hasegawa H, Tomita H (1986) Assessment of taste disorders in rats by simultaneous study of the two-bottle preference test and abnormal ingestive behavior. Auris Nasus Larynx 13 (Suppl 1):S33–S41. https://doi.org/10.1016/s0385-8146(86)80032-3
26. Willner P, Towell A, Sampson D, Sophokleous S, Muscat R (1987) Reduction of sucrose preference by chronic unpredictable mild stress, and its restoration by a tricyclic antidepressant. Psychopharmacology 93 (3):358–364. https://doi.org/10.1007/bf00187257
27. Serchov T, van Calker D, Biber K (2016) Sucrose preference test to measure anhedonic behaviour in mice. Bio-protocol 6(19):e1958. https://doi.org/10.21769/BioProtoc.1958
28. Liu MY, Yin CY, Zhu LJ, Zhu XH, Xu C, Luo CX, Chen H, Zhu DY, Zhou QG (2018) Sucrose preference test for measurement of stress-induced anhedonia in mice. Nat Protoc 13(7):1686–1698. https://doi.org/10.1038/s41596-018-0011-z
29. Ferreira MF, Castanheira L, Sebastiao AM, Telles-Correia D (2018) Depression assessment in clinical trials and pre-clinical tests: a critical review. Curr Top Med Chem 18 (19):1677–1703. https://doi.org/10.2174/1568026618666181115095920
30. Porsolt RD, Bertin A, Jalfre M (1977) Behavioral despair in mice: a primary screening test for antidepressants. Arch Int Pharmacodyn Ther 229(2):327–336
31. Porsolt RD, Le Pichon M, Jalfre M (1977) Depression: a new animal model sensitive to antidepressant treatments. Nature 266 (5604):730–732. https://doi.org/10.1038/266730a0
32. Kara NZ, Stukalin Y, Einat H (2018) Revisiting the validity of the mouse forced swim test: systematic review and meta-analysis of the effects of prototypic antidepressants. Neurosci Biobehav Rev 84:1–11. https://doi.org/10.1016/j.neubiorev.2017.11.003
33. Detke MJ, Lucki I (1996) Detection of serotonergic and noradrenergic antidepressants in the rat forced swimming test: the effects of water depth. Behav Brain Res 73(1–2):43–46. https://doi.org/10.1016/0166-4328(96)00067-8
34. Machado-Vieira R, Baumann J, Wheeler-Castillo C, Latov D, Henter ID, Salvadore G, Zarate CA (2010) The timing of antidepressant effects: a comparison of diverse pharmacological and somatic treatments. Pharmaceuticals (Basel) 3(1):19–41. https://doi.org/10.3390/ph3010019
35. Jin ZL, Chen XF, Ran YH, Li XR, Xiong J, Zheng YY, Gao NN, Li YF (2017) Mouse strain differences in SSRI sensitivity correlate with serotonin transporter binding and function. Sci Rep 7(1):8631. https://doi.org/10.1038/s41598-017-08953-4
36. Fritz M, Klawonn AM, Nilsson A, Singh AK, Zajdel J, Wilhelms DB, Lazarus M, Lofberg A, Jaarola M, Kugelberg UO, Billiar TR, Hackam DJ, Sodhi CP, Breyer MD, Jakobsson J, Schwaninger M, Schutz G, Parkitna JR, Saper CB, Blomqvist A, Engblom D (2016) Prostaglandin-dependent modulation of dopaminergic neurotransmission elicits inflammation-induced aversion in mice. J Clin Invest 126(2):695–705. https://doi.org/10.1172/JCI83844
37. Benson S, Brinkhoff A, Lueg L, Roderigo T, Kribben A, Wilde B, Witzke O, Engler H, Schedlowski M, Elsenbruch S (2017) Effects of acute systemic inflammation on the interplay between sad mood and affective cognition. Transl Psychiatry 7(12):1281. https://doi.org/10.1038/s41398-017-0043-0
38. Seemann S, Zohles F, Lupp A (2017) Comprehensive comparison of three different animal models for systemic inflammation. J Biomed Sci 24(1):60. https://doi.org/10.1186/s12929-017-0370-8
39. Saper CB, Romanovsky AA, Scammell TE (2012) Neural circuitry engaged by prostaglandins during the sickness syndrome. Nat Neurosci 15(8):1088–1095. https://doi.org/10.1038/nn.3159
40. Dantzer R (2001) Cytokine-induced sickness behavior: where do we stand? Brain Behav Immun 15(1):7–24. https://doi.org/10.1006/brbi.2000.0613
41. Teeling JL, Cunningham C, Newman TA, Perry VH (2010) The effect of non-steroidal anti-inflammatory agents on behavioural changes and cytokine production following systemic inflammation: implications for a role of COX-1. Brain Behav Immun 24 (3):409–419. https://doi.org/10.1016/j.bbi.2009.11.006
42. Biesmans S, Meert TF, Bouwknecht JA, Acton PD, Davoodi N, De Haes P, Kuijlaars J, Langlois X, Matthews LJ, Ver Donck L, Hellings N, Nuydens R (2013) Systemic immune activation leads to neuroinflammation

and sickness behavior in mice. Mediat Inflamm 2013:271359. https://doi.org/10.1155/2013/271359

43. Neurath MF (2014) Cytokines in inflammatory bowel disease. Nat Rev Immunol 14 (5):329–342. https://doi.org/10.1038/nri3661
44. Estevez J, Chen VL, Podlaha O, Li B, Le A, Vutien P, Chang ET, Rosenberg-Hasson Y, Jiang Z, Pflanz S, Ge D, Gaggar A, Nguyen MH (2017) Differential serum cytokine profiles in patients with chronic hepatitis B, C, and hepatocellular carcinoma. Sci Rep 7(1):11867. https://doi.org/10.1038/s41598-017-11975-7
45. Fritz M, Klawonn AM, Jaarola M, Engblom D (2018) Interferon- mediated signaling in the brain endothelium is critical for inflammation-induced aversion. Brain Behav Immun 67:54–58. https://doi.org/10.1016/j.bbi.2017.08.020
46. Klawonn AM, Malenka RC (2018) Nucleus accumbens modulation in reward and aversion. Cold Spring Harb Symp Quant Biol 83:119–129. https://doi.org/10.1101/sqb.2018.83.037457
47. Nilsson A, Wilhelms DB, Mirrasekhian E, Jaarola M, Blomqvist A, Engblom D (2017) Inflammation-induced anorexia and fever are elicited by distinct prostaglandin dependent mechanisms, whereas conditioned taste aversion is prostaglandin independent. Brain Behav Immun 61:236–243. https://doi.org/10.1016/j.bbi.2016.12.007
48. O'Connor JC, Lawson MA, Andre C, Moreau M, Lestage J, Castanon N, Kelley KW, Dantzer R (2009) Lipopolysaccharide-induced depressive-like behavior is mediated by indoleamine 2,3-dioxygenase activation in mice. Mol Psychiatry 14(5):511–522. https://doi.org/10.1038/sj.mp.4002148
49. Reichenberg A, Yirmiya R, Schuld A, Kraus T, Haack M, Morag A, Pollmacher T (2001) Cytokine-associated emotional and cognitive disturbances in humans. Arch Gen Psychiatry 58(5):445–452. https://doi.org/10.1001/archpsyc.58.5.445
50. Everhardt Queen A, Moerdyk-Schauwecker M, McKee LM, Leamy LJ, Huet YM (2016) Differential expression of inflammatory cytokines and stress genes in male and female mice in response to a lipopolysaccharide challenge. PLoS One 11(4):e0152289. https://doi.org/10.1371/journal.pone.0152289
51. Grota LJ, Bienen T, Felten DL (1997) Corticosterone responses of adult Lewis and Fischer rats. J Neuroimmunol 74(1–2):95–101. https://doi.org/10.1016/s0165-5728(96)00209-3
52. Stowers L, Cameron P, Keller JA (2013) Ominous odors: olfactory control of instinctive fear and aggression in mice. Curr Opin Neurobiol 23(3):339–345. https://doi.org/10.1016/j.conb.2013.01.007
53. Lorenz K (1970) Studies in animal and human behaviour 1st edn. Harvard University Press, Cambridge, MA
54. Roma PG, Riley AL (2005) Apparatus bias and the use of light and texture in place conditioning. Pharmacol Biochem Behav 82 (1):163–169. https://doi.org/10.1016/j.pbb.2005.08.004
55. Shimizu C, Oki Y, Mitani Y, Nakamura T, Nabeshima T (2015) Factors affecting ethanol-induced conditioned place preference and locomotor sensitization in mice. Biol Pharm Bull 38(12):1935–1945. https://doi.org/10.1248/bpb.b15-00626
56. Fritz M, El Rawas R, Salti A, Klement S, Bardo MT, Kemmler G, Dechant G, Saria A, Zernig G (2011) Reversal of cocaine-conditioned place preference and mesocorticolimbic Zif268 expression by social interaction in rats. Addict Biol 16(2):273–284. https://doi.org/10.1111/j.1369-1600.2010.00285.x
57. Zernig G, Pinheiro BS (2015) Dyadic social interaction inhibits cocaine-conditioned place preference and the associated activation of the accumbens corridor. Behav Pharmacol 26 (6):580–594. https://doi.org/10.1097/FBP.0000000000000167
58. Hurst JL (1990) Urine marking in populations of wild house mice mus-domesticus rutty. 2. Communication between females. Anim Behav 40:223–232. https://doi.org/10.1016/S0003-3472(05)80917-0
59. Reynolds E (1971) Urination as a social response in mice. Nature 234(5330):481. https://doi.org/10.1038/234481a0
60. Copeland S, Warren HS, Lowry SF, Calvano SE, Remick D, Inflammation, the Host Response to Injury I (2005) Acute inflammatory response to endotoxin in mice and humans. Clin Diagn Lab Immunol 12 (1):60–67. https://doi.org/10.1128/CDLI.12.1.60-67.2005
61. Cunningham CL, Gremel CM, Groblewski PA (2006) Drug-induced conditioned place

preference and aversion in mice. Nat Protoc 1 (4):1662–1670. https://doi.org/10.1038/nprot.2006.279

62. Horii Y, Nagasawa T, Sakakibara H, Takahashi A, Tanave A, Matsumoto Y, Nagayama H, Yoshimi K, Yasuda MT, Shimoi K, Koide T (2017) Hierarchy in the home cage affects behaviour and gene expression in group-housed C57BL/6 male mice. Sci Rep 7(1):6991. https://doi.org/10.1038/s41598-017-07233-5
63. Grewal SS, Shepherd JK, Bill DJ, Fletcher A, Dourish CT (1997) Behavioural and pharmacological characterisation of the canopy stretched attend posture test as a model of anxiety in mice and rats. Psychopharmacology 133(1):29–38. https://doi.org/10.1007/s002130050367
64. Blanchard DC, Griebel G, Blanchard RJ (2003) The mouse defense test battery: pharmacological and behavioral assays for anxiety and panic. Eur J Pharmacol 463 (1–3):97–116. https://doi.org/10.1016/s0014-2999(03)01276-7

Chapter 8

Behavioral Tests for Assessing Pain and Nociception: Relationship with the Brain Reward System

Marc Fakhoury, Reem Habib Mohamad Ali Ahmad, Elie D. Al-Chaer, and Nada B. Lawand

Abstract

Pain is an unpleasant sensation accompanied by an emotional experience leading to real or potential tissue damage. At the neurobiological level, the sensation of pain is mediated through the activation of nociceptors, which are biological sensory receptors that relay pain-related information to higher brain centers. Conversely, a reward can be defined as an event that produces a pleasant or positive affective experience. Although pain and reward are totally opposing processes, evidence suggests that the neural circuit of pain somewhat overlaps the neural circuit of reward. In this chapter, the relationship between the neural circuit of pain and the reward system, in particular, the mesolimbic dopaminergic system, is discussed. In addition, this chapter describes standard behavioral techniques used to study pain-related behaviors in experimental animals, including techniques that assess primary and secondary hyperalgesia in response to innocuous and noxious heat and mechanical stimulation. The full apparatus is described in detail along with the proper procedure to be followed by the experimenter.

Key words Heat hyperalgesia, Mechanical hyperalgesia, Mechanical allodynia, Nociception, Pain, Reward system

1 Introduction

1.1 Pain: Definition and Overview

The human experience of pain is multidimensional and involves sensory, affective, and cognitive components. The notion of pain, while still exceedingly elusive and complex, remains a submodality in the domain of somatosensation, which involves the process of conveying tactile, nociceptive, and proprioceptive information [1]. Similar to other sensations, pain has an aversive component exemplified by its unpleasant experience [2]. The characteristics that make pain exceptionally unique and distinct from our five basic senses have been a debatable topic since ancient times. The Greek philosopher Aristotle declared that sight, hearing, smell, taste, and touch constitute the five human senses, while he excluded the sense of pain for its lack of a specific sense organ [3]. Much like

Marc Fakhoury (ed.), *The Brain Reward System*, Neuromethods, vol. 165, https://doi.org/10.1007/978-1-0716-1146-3_8,

Plato, he incorporated pain with pleasure and described it as "passions of the soul" [1]. Today, the five-sense model still exists; however, the sense of touch refers to a group of independent senses that include pain, itching, tingling, hot, and cold.

Pain is a sensation that creates severe complications to the affected individual when it is chronic, ultimately leading to reduced quality of life and a negative emotional state [4]. This negative emotional state has been perceived as a critical factor in assessing the adequacy of strategies that aim at treating pain [5]. The sensation of pain can also be referred to as a "call for action" [1]. Similar to appetite, thirst, and the desire to rest, pain is part of the body's survival systems that collectively work to protect the organism from potential threats [1, 6]. These primordial emotions can be described by a set of sensations that signal a deviation from homeostasis and an intention to attain homeostatic balance [7]. While acute pain acts as an alarm system to prevent injury and promote healing behavior, pain, in its chronic state, evokes anxiety, fosters avoidance, and promotes adaptive behaviors that are crucial for survival.

Pain can be divided into three broad categories: nociceptive, neuropathic, and inflammatory [8]. Nociceptive pain occurs in response to potentially tissue-damaging stimuli and activation of peripheral nociceptors, which relay these injury-related stimuli through specific neural pathways to higher brain centers. Neuropathic pain is initiated by damage or pathological changes affecting the somatosensory system leading to hypersensitivity to both noxious (hyperalgesia) and innocuous (allodynia) stimuli. The main cause of neuropathic pain includes metabolic diseases such as diabetes, the experience of traumatic situations, and infection by toxins or viruses [8]. Inflammatory pain results from activation and sensitization of nociceptive pain pathways by a variety of inflammatory mediators including substance P, prostaglandins, and pro-inflammatory cytokines [8, 9].

1.2 Neural Circuit of Pain and Its Relationship with the Reward System

Despite the fact that the connection between pain and reward has been under investigation for several years, it is only recently that a direct relationship between these two processes has been found [10–12]. In particular, some studies have shown that the neural circuit of pain somewhat overlaps the neural circuit of reward and pleasure, including the mesolimbic dopaminergic system [10, 13, 14]. Investigators suggested that the circuitry of pain and reward interact inasmuch as the relief of painful stimuli could be considered rewarding [13]. For instance, stimuli that promote positive feelings (e.g., music) might have the ability to diminish pain sensation [15]. Pain may in turn decrease reward-related behaviors by reducing the motivation to obtain natural rewards such as food [16] and by promoting anhedonia, that is the inability to feel pleasure in normally pleasurable activities [17]. However, further research is

needed to explain the complex neural components that underlie the relationship between pain and reward. There appear to be complicated mechanisms regulating the harmony between pain and reward, but insufficient information on the contribution of explicit pathways or molecules is available.

In 1968, Melzack and Casey were the first to present a conceptual model of pain [18]. The model proposes that the affective and motivational aspects of pain are distinct from its sensory and discriminative aspects, implying the existence of different anatomical substrates. The partition of these components additionally inferred diverse anatomical substrates, which were proposed to include medial and lateral ascending pathways for affective/motivational and sensory/discriminative components, respectively [19]. At present, the mechanisms and neural networks underlying the aversiveness of pain sensation are still unclear. Neurons in the mesolimbic reward-related network originating from the ventral tegmental area (VTA) to the nucleus accumbens (NAc) contribute to both appetitive and aversive conditioning. Using pain avoidance tasks combined with functional magnetic resonance imaging, Roy and colleagues studied how pain expected errors were encoded in the periaqueductal gray (PAG), a brain area that is necessary for both ascending and descending nociceptive signals of pain regulation [20]. The expected error sent to the PAG emerges from the ventromedial prefrontal cortex along with relay expected error signals to prefrontal cortical areas that activate orbitofrontal, front mid-cingulate, and dorsomedial prefrontal cortices [20]. It is important to mention that the examination of the emotional characteristics of pain and aversive learning in preclinical models, and the study of the intervening circuits affecting pain sensation, are still in their early stages.

Currently, opioids are generally the most used medications for the treatment of moderate-to-severe experiences of pain. Numerous investigations have shown that the brain opioid system is particularly responsible for the emotional characteristics of pain sensation. For instance, positron emission tomography (PET) imaging studies have demonstrated the release of endogenous opioids in cortical areas of patients experiencing induced experimental pain sensation and under the effect of placebo analgesia [21, 22]. Studies have also implicated the anterior cingulate cortex (ACC) in the encoding of the aversive components of pain [23]. Rainville and colleagues used imaging procedures showing how ACC and not the somatosensory cortex, is initiated when pain sensation is exacerbated in hypnotic suggestion, demonstrating a link between frontal lobe limbic activity and pain effect [24]. On the other hand, Johansen and colleagues conducted an experiment using the conditioned place avoidance paradigm showing that excitatory amino acid microinjection into the ACC produces avoidance learning [25]. Consistent with these findings, the frontal part

of the ACC shows elevated levels of opioid receptors in humans [26], similar to the rat's cingulate cortex [27].

1.3 The Mesolimbic Dopaminergic System and Its Role in Pain Modulation

The mesolimbic dopaminergic system has been perceived to play a primordial role in motivated behaviors, reward processes, and pleasure [28]. It plays a crucial role in learning the circumstances that lead to deviation or rebuilding of homeostasis, and in this way encourages humans to maintain a strategic distance from aversive circumstances. Dopaminergic neurons may discharge different synapses and discharge at different firing patterns (tonic or phasic), and the physiological role of the co-arrival of these transmitters is being uncovered gradually. It is important to note that the mesolimbic dopaminergic system is a significant pathway that intervenes in "reward" and regulates both positive and negative feelings [29]. However, it is still vague whether the mesolimbic dopaminergic system and the molecules released in the NAc, a key area of the brain reward system, are associated with pain regulation. The mesolimbic dopaminergic system begins in the A10 region of the VTA and mostly ventures to the core part of the NAc. These neurons play a role in positive and negative reinforcement, behavioral response, decision making, working memory, motivation, and the state of positive feelings, for example, joy and happiness [30–33].

A developing body of evidence demonstrates that a hypodopaminergic state is observed under situations of chronic pain [34, 35], which is in line with the increase and decrease in the sensation of pain as observed in patients with Parkinson's disease and schizophrenia, respectively [36–38]. Furthermore, pain sensation is a regular symptom of various psychiatric diseases and conditions like major depressive disorder [39, 40]. Diminished tonic dopamine levels in the NAc leads to uncontrolled downregulation of dopamine D2 receptor signaling, which may elevate the sensation of pain, resulting in impulsivity [35, 41, 42]. Moreover, pain sensation and opioids can activate the mesolimbic dopaminergic system [2, 43], whereas exacerbated pain has the opposite effect [44].

1.4 Behavioral Tests to Assess Pain Sensation

This chapter describes the protocol for the heat hyperalgesia test, the mechanical hyperalgesia test, and the mechanical allodynia test.

2 Materials

2.1 Animals

Adult male Sprague Dawley rats (body weight between 150 and 350 g) are typically used, though a wide variety of other animal species may be used as well. All experimental procedures should be approved by the institutional animal care and use and should follow

the ethical guidelines for experimental pain on conscious animals. Upon arrival at the facility, animals are typically kept in cages at a controlled room temperature of 25 °C and exposed to 12/12 h light/dark cycle with access to water and food ad libitum.

2.2 Testing Apparatus

The apparatus for the hyperalgesia and allodynia tests include the following:

1. Ugo Basile machine (Gemonio VA, Italy; Serial number 0462 U16).
2. Ugo Basile platform with a glass plate (Gemonio VA, Italy; Length 90 cm, Width 14 cm, Height 6.5 cm).
3. Ugo Basile platform with a mesh grid (Gemonio VA, Italy; Length 90 cm, Width 14 cm, Height 10 cm).
4. Heat generator (Ugo Basile; Gemonio VA, Italy; Model 37,370–002; Serial number 046216).
5. Force actuator (Ugo Basile; Gemonio VA, Italy; Model 37,400–002).
6. Aesthesio filaments: von Frey Filament with a bending force of 2 g and 15 g (USA, Patent number 5823969–8512259).

3 Methods

3.1 Hyperalgesia Test (Plantar Test)

Heat hyperalgesia is described as increased sensitivity to a noxious heat stimulus [45–47]. Hyperalgesia at the site of tissue damage is called primary hyperalgesia, while hyperalgesia at sites surrounding the site of injury is called secondary hyperalgesia [45, 47]. The sensory attributes of primary and secondary hyperalgesia vary extensively. Although primary hyperalgesia incorporates an increased response to both mechanical and heat stimuli, secondary hyperalgesia is largely explicit for mechanical stimuli [47], though it can also be detected in response to heat stimuli [48].

The behavioral apparatus for the heat hyperalgesia test is illustrated in Fig. 1. The Ugo machine (Gemonio VA, Italy) is first turned on. After turning the machine, rats are placed individually inside a plastic cage located on top of a 3-mm thick glass plate. After 30 min of accommodation, a heat stimulus is applied to the hind paw of rats. The height of the glass plate is adjusted so that the heat stimulus applied to the plantar surface of the paw evokes a withdrawal reaction after approximately 10 s. To abstain from conditioning paw withdrawal, the heat stimulus is applied with a 5-min resting period between trials. The withdrawal latency, defined as the elapsed time, in seconds, from stimulus onset to paw withdrawal, is measured during each trial. A cut off of 20 s is imposed to prevent tissue harm. A decrease in withdrawal latency indicates the

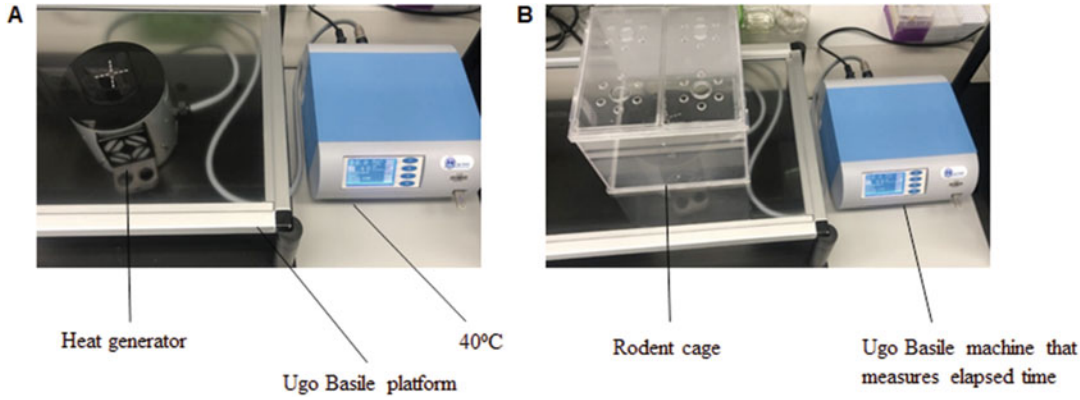

Fig. 1 Behavioral apparatus for the heat hyperalgesia test with (**a**) and without (**b**) a rodent cage. Heat hyperalgesia is assessed by measuring the paw withdrawal latency to a radiant heat stimulus applied to the plantar surface of the hind paw. The test is conducted using Ugo Basile products (Gemonio VA, Italy): the Ugo Basile machine measures the elapsed time in sec before paw withdrawal, and the Ugo Basile platform is used to hold a 3-mm thick glass plate. The heat stimulus consists of a focused infrared light source applied with a density of 40 IR (arbitrary units)

development of heat hyperalgesia, while an increase in withdrawal latency indicates an attenuation in heat hyperalgesia.

3.2 Mechanical Hyperalgesia and Allodynia Test

The behavioral apparatus for mechanical hyperalgesia and allodynia tests is illustrated in Fig. 2. Both mechanical hyperalgesia and allodynia tests are done using the same Ugo Basile product (Gemonio VA, Italy) (*see* Fig. 2b). Rats are individually placed in a transparent chamber on a metal wire mesh floor and allowed to accommodate for 30 min.

After turning the Ugo Basile machine, rats are individually placed on transparent cages and a movable force actuator is placed below the plantar surface of the hind paw (*see* Fig. 2a). The desired force preset by the examiner is applied via a von Frey-type filament until the animal withdraws its paw. In the mechanical hyperalgesia test, the paw withdrawal frequency to the application of a von Frey filament with a bending force of 15 g (noxious stimulus) to the plantar surface of the hind paw of rats is assessed. The 0.15 N power applied by the filament is known to activate mechanoreceptors and nociceptors. The tip of the filament is perpendicularly applied to the medial plantar surface from below the mesh grid. Five trials separated by 5 min time interval are usually recorded. On the other hand, in the mechanical allodynia test, the paw withdrawal frequency to the application of a von Frey filament with a bending force of 2 g (non-noxious stimulus) to the plantar surface of the hind paw of rats is assessed. Similar to the mechanical hyperalgesia test, the tip of the filament is perpendicularly applied to the medial plantar surface from below the mesh grid until the animal elicits a behavioral withdrawal reaction. Five trials separated by 5-min time

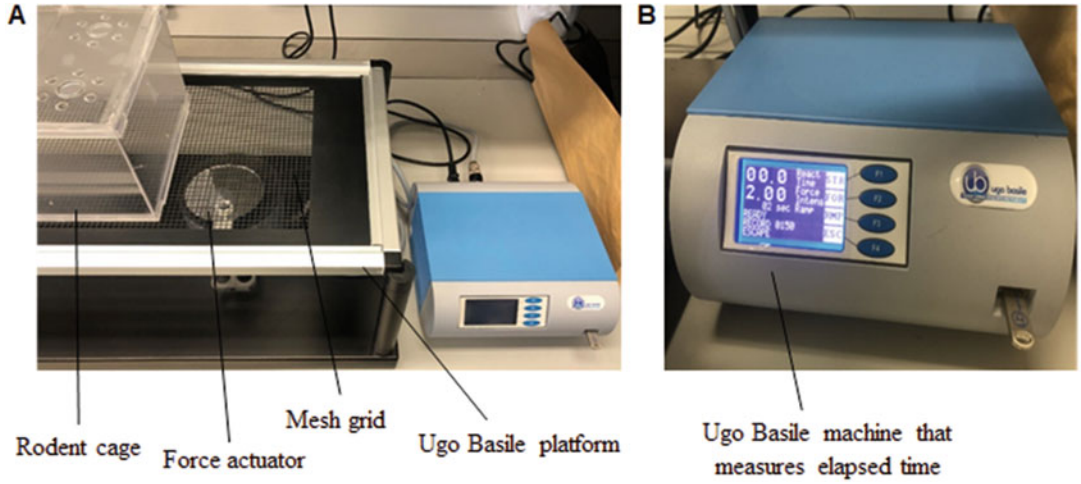

Fig. 2 Behavioral apparatus for the mechanical hyperalgesia and allodynia test. The apparatus consists of a mesh grid and a rodent cage (**a**), and a Dynamic Plantar Aesthesiometer (Ugo Basile) (Gemonio VA, Italy) (**b**). The Dynamic Plantar Aesthesiometer automatically measures the elapsed time, and the actual force at the time of the paw withdrawal reflex. A movable force actuator is placed below the plantar surface of the hind paw and the desired force is applied via a Von Frey–type filament until the animal withdraws its paw. The desired force of the filament is preset by the examiner. A 2 g force activates mechanoreceptors whereas 15 g force activates both mechanoreceptors and nociceptors. To determine the mechanical threshold for paw withdrawal, the force of filament application can be linearly increased until the animal withdraws its paw. The force recorded at the moment of foot withdrawal is considered as the threshold

interval are usually recorded. In several studies, the withdrawal threshold, defined by the bending force of the lowest strength von Frey Filament at which the animal withdrew its limb in 50% or more of the trials, is reported instead of the withdrawal frequency (*see* Fig. 3b). A decrease in withdrawal threshold indicates the development of mechanical allodynia, while an increase in withdrawal threshold indicates an attenuation in mechanical allodynia.

3.3 Interpretation of Results: Role of Glutamate Receptors in Peripheral Nociceptive Transmission

The behavioral techniques for assessing hyperalgesia and allodynia have been used by several investigators to better understand the brain circuitry involved in pain and nociceptive transmission with respect to neural pathways, brain structures, and neurotransmitter systems. In a study conducted by Lawand and colleagues, the involvement of the glutamate neurotransmitter system in peripheral nociceptive processing was assessed in a rat model of arthritis by examining the development of hyperalgesia and allodynia following injection of glutamate receptor antagonists [49]. Arthritic rats were tested for heat hyperalgesia and mechanical allodynia prior to (for baseline values) and following intra-articular injection of phosphate buffer (PB, vehicle), AP7, a non-NMDA glutamate receptor antagonist, CNQX, an AMPA glutamate receptor antagonist, and ketamine, a NMDA glutamate receptor antagonist [49]. For evaluating

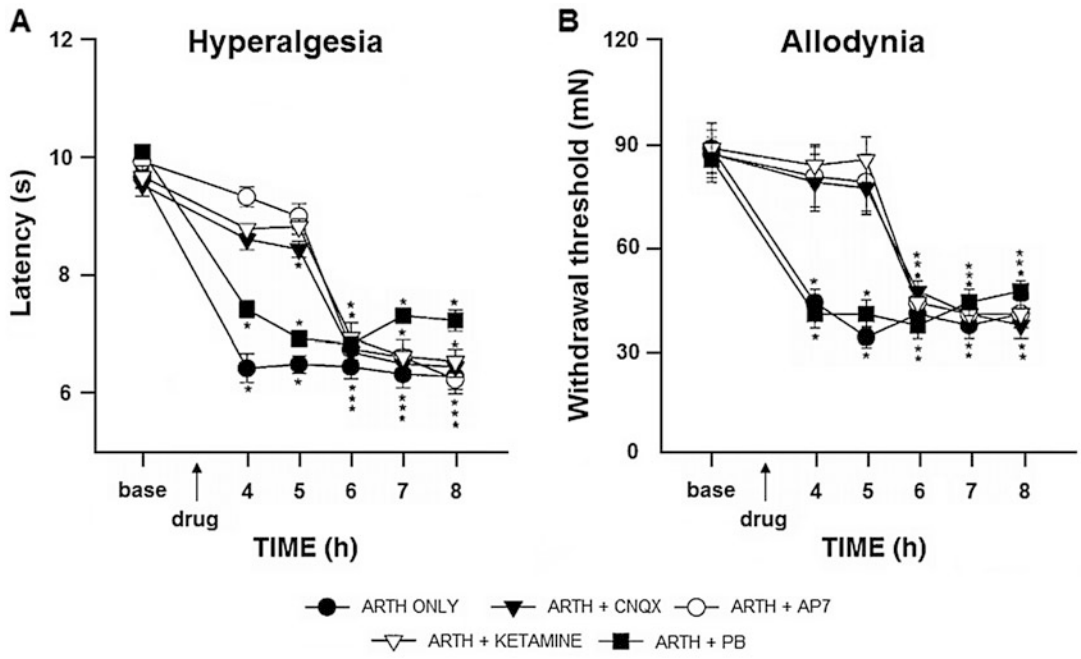

Fig. 3 (**a**) Time course of heat hyperalgesia following injection of AP7 (non-NMDA receptor antagonist), CNQX (AMPA receptor antagonist), Ketamine (NMDA receptor antagonist), and PB (Phosphate buffer; vehicle) as assessed by the mean withdrawal latency to radiant heat expressed in s. (**b**) Time course of mechanical allodynia following injection of AP7, CNQX, Ketamine, and PB as assessed by the mean withdrawal threshold to innocuous mechanical stimuli expressed in mN. Statistical significance from baseline values is indicated by * for $p < 0.05$. Adapted from (50)

the effect of intra-articular injection of glutamate receptor antagonist on heat hyperalgesia, paw withdrawal latency to a radiant heat applied to the plantar surface of the hind limb was measured prior to and up to 8 h after the injections (*see* Fig. 3a). Results show that induction of arthritis resulted in significant development of heat hyperalgesia as indicated by the decrease in paw withdrawal latency; an effect that was attenuated by AP7 and ketamine up to 2 h following the injection (*see* Fig. 3a). Investigators of the study also evaluated the effect of glutamate receptor antagonists on mechanical allodynia in arthritic rats by measuring paw withdrawal response to repeated non-noxious mechanical stimuli [49]. In their study, von Frey filaments of varying bending forces (30–100 mM) were applied to the plantar surface of the hind limb in ascending order to obtain a measure of the withdrawal threshold (i.e., bending force of the lowest strength von Frey Filament at which the animal withdrew its limb in 50% or more of the trials) [49]. Results showed that induction of arthritis resulted in significant development of mechanical allodynia as indicated by the decrease in withdrawal threshold; an effect that was attenuated by AP7, ketamine, and CNQX up to 2 h following the injection (*see* Fig. 3b).

Altogether, these findings indicate that both NMDA and non-NMDA receptors are involved in peripheral nociceptive transmission and that they could constitute a viable therapeutic target for the treatment of joint pain associated with arthritis [49].

4 Notes and Conclusion

The behavioral techniques described in this chapter for assessing hyperalgesia and allodynia are frequently utilized by investigators to assess the effect of given experimental manipulations (e.g., drug injection, surgical procedure, brain lesion, etc.) on nociceptive behaviors.

To ensure the success of these tests, it is important to consider the following points:

- Cleaning the glass table with 10% ethanol between trials is recommended to keep the testing areas clean and to ensure reliable behavioral results.
- Collection of baseline data is recommended prior to any experimental manipulation. Also, because rodents are nocturnal animals it would be ideal to perform behavioral tests during the dark cycle; however, if this is not practical, it is always better to conduct the test around the same time to avoid variability.
- Proper handling techniques should be followed to reduce the stress to animals and the experimenter. Animal handling on a regular basis prior to and after behavioral tests is crucial to habituate the animals to the experimenter and avoid agitation.
- Environmental conditions in the testing area should be consistent throughout the experiment and as quiet as possible to minimize test anxiety and control for any variable that might disturb the animal's normal physiological functions. If animals exhibit signs of anxiety (frequent urination, loose stool, agitation), they should be allowed to freely explore the cage for a few minutes before proceeding with the behavioral test.
- Depending on the study design, the animals should have free access to food and water ad libitum throughout the experiment to ensure adequate hydration and nutrient consumption.

References

1. Porreca F, Navratilova E (2017) Reward, motivation, and emotion of pain and its relief. Pain 158(Suppl 1):S43–S49. https://doi.org/10.1097/j.pain.0000000000000798
2. Fields HL (1999) Pain: an unpleasant topic. Pain Suppl 6:S61–S69. https://doi.org/10.1016/s0304-3959(99)00139-6
3. Dallenbach KM (1939) Pain: history and present status. Am J Psychol 52:331–347
4. Mingote S et al (2017) Dopamine neuron dependent behaviors mediated by glutamate cotransmission. Elife 6:e27566. https://doi.org/10.7554/eLife.27566

5. Berger A, Dukes EM, Oster G (2004) Clinical characteristics and economic costs of patients with painful neuropathic disorders. J Pain 5 (3):143–149. https://doi.org/10.1016/j.jpain.2003.12.004
6. Denton DA et al (2009) The role of primordial emotions in the evolutionary origin of consciousness. Conscious Cogn 18(2):500–514. https://doi.org/10.1016/j.concog.2008.06.009
7. Craig AD (2003) A new view of pain as a homeostatic emotion. Trends Neurosci 26 (6):303–307. https://doi.org/10.1016/s0166-2236(03)00123-1
8. Yam MF et al (2018) General pathways of pain sensation and the major neurotransmitters involved in pain regulation. Int J Mol Sci 19 (8):2164. https://doi.org/10.3390/ijms19082164
9. Linley JE et al (2010) Understanding inflammatory pain: ion channels contributing to acute and chronic nociception. Pflugers Arch 459(5):657–669. https://doi.org/10.1007/s00424-010-0784-6
10. Navratilova E, Porreca F (2014) Reward and motivation in pain and pain relief. Nat Neurosci 17(10):1304–1312. https://doi.org/10.1038/nn.3811
11. Navratilova E et al (2012) Pain relief produces negative reinforcement through activation of mesolimbic reward-valuation circuitry. Proc Natl Acad Sci U S A 109(50):20709–20713. https://doi.org/10.1073/pnas.1214605109
12. Watanabe M et al (2018) Activation of ventral tegmental area dopaminergic neurons reverses pathological allodynia resulting from nerve injury or bone cancer. Mol Pain 14:1744806918756406. https://doi.org/10.1177/1744806918756406
13. Becker S, Gandhi W, Schweinhardt P (2012) Cerebral interactions of pain and reward and their relevance for chronic pain. Neurosci Lett 520(2):182–187. https://doi.org/10.1016/j.neulet.2012.03.013
14. Leknes S, Tracey I (2008) A common neurobiology for pain and pleasure. Nat Rev Neurosci 9(4):314–320. https://doi.org/10.1038/nrn2333
15. Garza-Villarreal EA et al (2014) Music reduces pain and increases functional mobility in fibromyalgia. Front Psychol 5:90. https://doi.org/10.3389/fpsyg.2014.00090
16. Geha P et al (2014) Decreased food pleasure and disrupted satiety signals in chronic low back pain. Pain 155(4):712–722. https://doi.org/10.1016/j.pain.2013.12.027
17. Garland EL et al (2019) Anhedonia in chronic pain and prescription opioid misuse. Psychol Med 9:1–12. https://doi.org/10.1017/S0033291719002010
18. Melzack R, Casey KL (1968) Sensory, motivational, and central control determinants of pain: a new conceptual model in pain. In: Kenshalo DRG (ed) The skin senses: Proceedings. Charles C. Thomas, Springfield, IL, p 63
19. Tracey I, Mantyh PW (2007) The cerebral signature for pain perception and its modulation. Neuron 55(3):377–391. https://doi.org/10.1016/j.neuron.2007.07.012
20. Roy M et al (2014) Representation of aversive prediction errors in the human periaqueductal gray. Nat Neurosci 17(11):1607–1612. https://doi.org/10.1038/nn.3832
21. Scott DJ et al (2008) Placebo and nocebo effects are defined by opposite opioid and dopaminergic responses. Arch Gen Psychiatry 65(2):220–231. https://doi.org/10.1001/archgenpsychiatry.2007.34
22. Wager TD, Scott DJ, Zubieta JK (2007) Placebo effects on human mu-opioid activity during pain. Proc Natl Acad Sci U S A 104 (26):11056–11061. https://doi.org/10.1073/pnas.0702413104
23. Vogt BA (2005) Pain and emotion interactions in subregions of the cingulate gyrus. Nat Rev Neurosci 6(7):533–544. https://doi.org/10.1038/nrn1704
24. Rainville P et al (1997) Pain affect encoded in human anterior cingulate but not somatosensory cortex. Science 277(5328):968–971. https://doi.org/10.1126/science.277.5328.968
25. Johansen JP, Fields HL (2004) Glutamatergic activation of anterior cingulate cortex produces an aversive teaching signal. Nat Neurosci 7 (4):398–403. https://doi.org/10.1038/nn1207
26. Baumgartner U et al (2006) High opiate receptor binding potential in the human lateral pain system. NeuroImage 30(3):692–699. https://doi.org/10.1016/j.neuroimage.2005.10.033
27. Vogt LJ et al (2001) Colocalization of mu-opioid receptors and activated G-proteins in rat cingulate cortex. J Pharmacol Exp Ther 299(3):840–848
28. Watanabe M, Narita M (2018) Brain reward circuit and pain. In: Shyu BC, Tominaga M (eds) Advances in pain research: mechanisms and modulation of chronic pain, Advances in Experimental Medicine and Biology, vol 1099. Springer, Singapore
29. D'Ardenne K et al (2008) BOLD responses reflecting dopaminergic signals in the human

ventral tegmental area. Science 319 (5867):1264–1267. https://doi.org/10.1126/science.1150605

30. Adcock RA et al (2006) Reward-motivated learning: mesolimbic activation precedes memory formation. Neuron 50(3):507–517. https://doi.org/10.1016/j.neuron.2006.03.036
31. Berridge KC (2007) The debate over dopamine's role in reward: the case for incentive salience. Psychopharmacology 191 (3):391–431. https://doi.org/10.1007/s00213-006-0578-x
32. Bromberg-Martin ES, Matsumoto M, Hikosaka O (2010) Dopamine in motivational control: rewarding, aversive, and alerting. Neuron 68(5):815–834. https://doi.org/10.1016/j.neuron.2010.11.022
33. Schultz W (2007) Behavioral dopamine signals. Trends Neurosci 30(5):203–210. https://doi.org/10.1016/j.tins.2007.03.007
34. Cowan WM, Kandel E (2000) A brief history of synapses and synaptic transmission. Biology
35. Roy M, Peretz I, Rainville P (2008) Emotional valence contributes to music-induced analgesia. Pain 134(1–2):140–147. https://doi.org/10.1016/j.pain.2007.04.003
36. Blanchet PJ, Brefel-Courbon C (2018) Chronic pain and pain processing in Parkinson's disease. Prog Neuropsychopharmacol Biol Psychiatry 87(Pt B):200–206. https://doi.org/10.1016/j.pnpbp.2017.10.010
37. Mantyh P (2013) Bone cancer pain: causes, consequences, and therapeutic opportunities. Pain 154(Suppl 1):S54–S62. https://doi.org/10.1016/j.pain.2013.07.044
38. Stubbs B et al (2015) Decreased pain sensitivity among people with schizophrenia: a meta-analysis of experimental pain induction studies. Pain 156(11):2121–2131. https://doi.org/10.1097/j.pain.0000000000000304
39. Trivedi MH (2004) The link between depression and physical symptoms. Prim Care Companion J Clin Psychiatry 6(Suppl 1):12–16
40. Huyser BA, Parker JC (1999) Negative affect and pain in arthritis. Rheum Dis Clin N Am 25 (1):105–121., vi. https://doi.org/10.1016/s0889-857x(05)70057-0
41. Borsook D et al (2016) Reward deficiency and anti-reward in pain chronification. Neurosci Biobehav Rev 68:282–297. https://doi.org/10.1016/j.neubiorev.2016.05.033
42. Reboucas EC et al (2005) Effect of the blockade of mu1-opioid and 5HT2A-serotonergic/alpha1-noradrenergic receptors on sweet-substance-induced analgesia. Psychopharmacology 179(2):349–355. https://doi.org/10.1007/s00213-004-2045-x
43. Wood PB et al (2007) Reduced presynaptic dopamine activity in fibromyalgia syndrome demonstrated with positron emission tomography: a pilot study. J Pain 8(1):51–58. https://doi.org/10.1016/j.jpain.2006.05.014
44. Wood PB (2008) Role of central dopamine in pain and analgesia. Expert Rev Neurother 8 (5):781–797. https://doi.org/10.1586/14737175.8.5.781
45. Treede RD et al (1992) Peripheral and central mechanisms of cutaneous hyperalgesia. Prog Neurobiol 38(4):397–421. https://doi.org/10.1016/0301-0082(92)90027-c
46. Merskey H (1982) Pain terms: A supplementary note. Pain 14(3):205–206
47. Treede RD (2006) Chapter 1 Pain and hyperalgesia: definitions and theories. Handb Clin Neurol 81:3–10. https://doi.org/10.1016/S0072-9752(06)80005-9
48. Sumikura H, Miyazawa A, Yucel A, Anderson O, Arendt-Nielsen L (2005) Secondary heat hyperalgesia detected by radiant heat stimuli in humans: Evaluation of stimulus intensity and duration. Somatosens Mot Res 22(3):233–237. https://doi.org/10.1080/08990220500262778
49. Lawand NB, Willis WD, Westlund KN (1997) Excitatory amino acid receptor involvement in peripheral nociceptive transmission in rats. Eur J Pharmacol 324(2–3):169–177. https://doi.org/10.1016/s0014-2999(97)00072-1

Chapter 9

Chemogenetic (DREADD) Exploration of Circuits Mediating Reward-Motivated Attention

Hrishikesh Pattabhiraman and Ryan D. Ward

Abstract

The brain reward circuit is complex and it plays an important role in reward-motivated behavior and is fundamental for species survival. It is also implicated in several diseases that involve motivational deficits such as depression and schizophrenia. Due to its complex circuitry involving differential sub-neuronal populations and glia, traditional lesioning, and pharmacological manipulations have failed to differentiate the effect of these complex, intermingled circuitry. Designer receptors exclusively activated by designer drugs (DREADDs) provide a minimally invasive option to circumvent these issues. In this chapter, we address the method by which DREADD is applied in behavioral neuroscience to explore the brain reward circuit in our laboratory. We highlight the potential difficulties faced by new users of this technology and provide some of our methods to overcome them. When used properly, the DREADD system is a versatile tool to interrogate circuits and brain areas associated with reward-motivated behavior and thus is a valuable addition to any behavioral neuroscientist's methodological toolbox.

Key words Behavior, DREADD, Drug, Motivation, Reward

1 Introduction

The brain reward circuit plays a critical role in multiple aspects of an organism's survival. Stimuli that activate the brain reward circuit, such as food, water, sex, or drugs, often lead to modulation of behaviors that increase the probability of these stimuli. Reward-motivated behavior is often impaired or altered in people with disorders such as schizophrenia, depression, drug addiction, and obesity [1–4]. Therefore, understanding the role of the subregions in the reward circuit and its complex circuitry and interconnections with other brain areas and circuits is vital for understanding pathologies that involve deficits in reward-motivated behavior.

In the laboratory, reward guided behavior has been tested and measured in multiple paradigms [5]. For example, rats that are motivated to find food (by food restriction) might be provided with opportunities to obtain food rewards in pavlovian and

Marc Fakhoury (ed.), *The Brain Reward System*, Neuromethods, vol. 165, https://doi.org/10.1007/978-1-0716-1146-3_9,

operant-conditioning paradigms [6–11]. The value of a reward to an animal can be tested by progressively increasing the effort needed to obtain reward until the animal gives up. Rewards are also often used in tests of complex cognitive behavior, and assays of reward-modulated behavior have produced important insights into cognitive and decision-making processes [12, 13]. One area of research interest in our laboratory has been dissecting the circuitry involved in the motivational modulation of cognitive processes. In one paradigm, we test the ability of reward-associated signals to modulate attention. In this "signal probability-sustained attention task" (SPSA), based on the five-choice serial reaction time task, rats are exposed to a sustained attention paradigm in which cue lights signal which of two response options will be rewarded. During the ITI, a houselight signals to the rat the probability of reward for a correct response on the upcoming trial. We suggest that the signaled reward probability acts as a cognitive incentive, leading to increased discrimination accuracy on high reward-probability trials. In the past few years, we have been trying to isolate the specific areas of the brain that are responsible for this cognition-modulating effect of the reward-probability signals [13, 14].

The major neuronal circuitry involved in these reward-motivated tasks is the dorsal and ventral striatum and their complex-associated connections. Both the striatal subregions are innervated by dopaminergic afferents onto the medium spiny neurons (MSN). Major dopaminergic afferents are sourced from the ventral tegmental area (VTA) and the substantia nigra pars compacta (SNc). However, the VTA also innervates the prefrontal cortex (PFC), hippocampus (HP), and both the central (CA) and basolateral amygdala (BLA). Other than the dopaminergic innervations there are glutamatergic innervations into the nucleus accumbens (NAc) of the ventral striatum from the PFC, hippocampus, and the amygdala. The NAc is also modulated by the actions of astrocytes and the local cholinergic interneurons. Identifying the strength and relevance of this complex and intermingled reward circuitry requires a powerful tool that can selectively target and modulate these neuronal/glial activities [3, 15–21].

1.1 Methods to Study Reward Circuitry

Historically, lesions and intracranial infusions of pharmacological agents such as baclofen and muscimol have helped reveal whether certain regions of the reward circuit (like the striatum) have an impact on reward-motivated behavior [6–11]. However, lesioning and pharmacological manipulations are limited in providing a complete account of the role of these regions of interest in reward-motivated behavior. Furthermore, they are less specific in determining what kind of cells in the region of interest are responsible for the observed effects. Designer receptors exclusively activated by designer drugs (DREADD) can help in overcoming some of these issues [22–26].

DREADDs have now become a useful tool for both increasing and decreasing the likelihood of cellular firing in rodents and other laboratory animals. This is commonly done by surgically introducing a viral vector that transfects a modified human muscarinic G-protein coupled receptor (GPCR) named either hM4Di or hM3Dq on the membrane surfaces of cells of interest. These receptors are then selectively activated by an otherwise biologically inert ligand named clozapine-n-oxide (CNO). In behavioral studies, this is typically administered either orally or through intraperitoneal (IP) or subcutaneous (SC) injections in freely moving animals [22–26]. DREADDs have also been used to study the brain in vitro where the laboratory animal undergoes the aforementioned surgical procedure and the excised brain region of interest is bath applied with CNO. Other than the common DREADDs mentioned earlier, a more recent innovation involves a Gi-kappa opioid receptor (KORD) which is activated by a biologically otherwise inert salvinorin B [23, 24]. This receptor-actuator combination can be used in association with the other DREADD preparations (hM4Di or hM3Dq with CNO) to target different brain regions or cell types and to activate them at different time points [23, 24].

Electrophysiological studies have also confirmed that these DREADD receptors change the neuronal activity in the intended direction, either exciting or inhibiting cells in virally-transfected brain areas [23, 24]. With the appropriate controls, DREADD can be used in behavioral experimentation as a reliable tool without the need for electrophysiological confirmation. Therefore, one major advantage of using DREADDs is the relative lack of potentially interfering hardware during behavioral experimentation. Other common methods used to control neuronal activity require the implantation of cannulas or optic fibers for drug or light delivery and there is a potential for the hardware to interfere with the behavioral procedure. In addition, histological assessment of brains that underwent these hardware implants also shows a greater disturbance of the neuronal parenchyma, especially when used to target ventral regions of the brain. This becomes particularly problematic when a large brain region or multiple brain regions need to be targeted, or when indwelling cannulae or optic fibers are required to be in place for long periods of time [23, 24].

Furthermore, DREADD-based change in neural activity may have a physiologically more relevant neuronal activation/silencing profile [22–26]. This provides a greater level of confidence that the behavioral effects seen when using this technique are applicable to normally-behaving animals and do not reflect artificial stimulation/silencing parameters. Due to these qualities, DREADDs have been used in experiments where laboratory animals underwent continuous activation for prolonged periods of time. This feature has not been a strength using other techniques because lengthy, repeated pharmacological activation and inhibition have the potential to

cause neuronal damage in the site of injection, and in addition, the cannulae used to administer these pharmacological agents are prone to clogging over time [24].

Although there are some advantages to using this technique as discussed earlier, care needs to be taken to administer DREADDs successfully. Being aware of the nuances of the technique can help circumvent potential difficulties. The following section will address the materials and procedures used to administer DREADD based silencing and activation of the NAc core (of the striatum) and the medial orbitofrontal cortex (mOFC) of the PFC in our laboratory. We will also highlight the potential pitfalls in successfully using DREADDs along with some solutions to these potential stumbling blocks.

2 Materials

2.1 Animals

Long Evans rats were used for all behavioral procedures in our experiments. The surgical coordinates from the rat brain atlas by Paxinos and Watson were used as a guide in doing this (see Subheading 3.3 for further detail) [27].

2.2 Surgery

A Stoelting duel digital stereotaxic frame equipped with a dental drill on one stereotaxic manipulator/handle and a custom-made dental needle injector on the other was used for surgical injection of virus. This apparatus was also equipped with non-rupture ear bars to secure rats in place to prevent rupturing the tympanic membrane of the rat. A kd Scientific syringe pump (310 Plus) was also used to maintain a consistent virus injection rate and volume during the procedure. The syringe pump was attached to a 10 μL Hamilton syringe. This Hamilton syringe was connected to the dental syringe on the stereotaxic handle through polyethylene tubing.

AAV2-hSyn-HA-hM4D (Gi)-IRES-mCitrine (hM4Di) with the titre of 5.6×10^{12} particles/mL, AAV2-hSyn-HA-hM3D (Gq)-IRES-mCitrine (hM3Dq) with the titre of 2×10^{12} particles/mL and 1 μL viral injection of AAV2-hSyn-HA-EGFP (GFP) with the titre of 33×10^{12} particles/mL was used in both experimental and control groups. All viruses were purchased from the Gene therapy Centre, Vector Core of the University of North Carolina.

An E-Z systems volatile anesthetic vaporizer (EZ-7000 classic system) that supplied isoflurane to both an induction chamber and a nose cone was used to anesthetize rats during the surgical procedure and for some preparatory work (fur clipping) leading up to the surgery. The stereotaxic frame was housed in a BSC class 2, ThermoFisher safety cabinet that controlled the airflow in the surgical area.

2.3 Behavioral Procedure

In our laboratory, rats in different experimental groups underwent the behavioral procedure in parallel. The behavioral procedures were conducted in 10 operant chambers simultaneously with a mixture of experimental and control group rats undergoing their behavioral condition at a time. The CNO (dissolved in a saline vehicle) or saline (control injection) was prepared fresh daily and administered intraperitoneally 30 min before the critical behavioral procedure took place.

2.4 Perfusion Procedure

Once the behavioral procedure concluded, rats were overdosed with isoflurane and were transcardially perfused using a 10% formalin solution. Brains were extracted and placed into a container with 10% formalin for 24 h. The brains were then transferred to a container with a phosphate buffer solution (with 30% sucrose). This was custom made using sodium phosphate monobasic (i.e., $NaH_2PO_4 \times H_2O$) and sodium phosphate dibasic (i.e., $Na_2HPO_4 \times H_2O$) and sucrose.

2.5 Immunohistochemistry

In order to visualize the fluorescence, brain slices of 40 μm thickness were cut using a cryostat (Leica CM1950). A rabbit, GFP primary Polyclonal Antibody (Thermo Fisher Scientific, catalogue # A-6455) and a secondary Anti-rabbit IgG (H + L) antibody, F (ab′)2 Fragment (Alexa Fluor® 555 Conjugate) (CST, catalogue no. # 4413) were used to visualize the mCitrine with low fluorescence (see Subheading 4 for further detail).

2.6 Slice Visualization

Microscope slides were used to mount the brain slices of interest and VECTASHIELD Antifade Mounting Medium was used to slow down the fluorescence bleaching process. Slice visualizations were conducted using a ZEISS AXIO Scope.A1 microscope at 5× magnification. Photographs of the magnified images were taken using a GENOPTIK ProgRes CFcool camera that was mounted onto the microscope. The ProgRes Capture.Pro 2.8.8 program was used to determine the exposure, image capture, and storage.

3 Methods

3.1 Determining Surgical Coordinates

Long Evans rats (3 months old at delivery to the laboratory) were deeply anesthetized with isoflurane and the scalp was shaved using an electric shaver. The rats were set up on the stereotaxic frame using the non-rupture ear bars and care was taken to avoid mounting the ear bars on the temporomandibular joint as described elsewhere [28]. Once properly mounted, the rat's head tilts along the axis of the ear (external auditory canal) with little to no lateral movement and the incisors rested on an incisor bar of the stereotaxic frame. Flat skull was achieved by either raising or lowering the incisor bar and achieving the same Z plane coordinates for both the

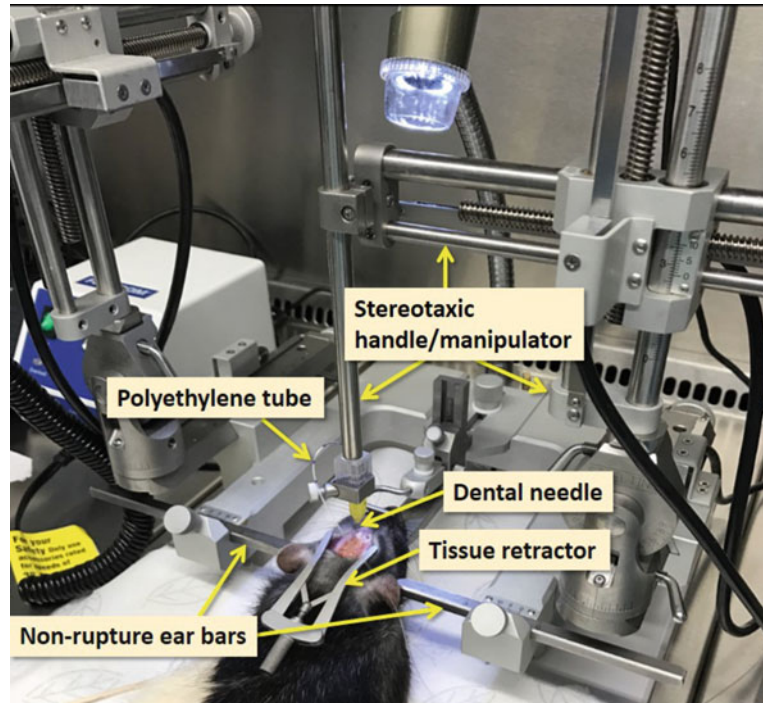

Fig. 1 Stereotaxic setup. Example photo of a rat in place in the stereotaxic surgery rig

bregma and lambda cranial suture sites (see Fig. 1 for a representative setup).

The dental needle mounted onto the second stereotaxic handle was loaded with a fast-green dye; 0.2 μL for the dye were loaded and 0.1 μL were injected bilaterally at the rate of 0.25 μL/min (taking 24 s for each injection) into the coordinates provided by the rat brain atlas. This was done to identify the epicenter of the injection. Once the desirable epicenter is identified, subsequent injections can be tested for the spread of the dye. Therefore, injection volume was increased to 1 μL (bilaterally) to test for the spread of the dye in subsequent injections. Once the desirable epicenter and spread of the dye were identified, we moved on to virus injections.

3.2 Viral Injection (Experimental Cohort)

All procedures complied with the ethical guidelines of the University of Otago, New Zealand, and all equipment was sterilized by either using 70% ethanol or was autoclaved before surgery began.

3.2.1 Anesthesia

All rats were anesthetized with isoflurane during the surgical procedure. Rats were first placed in an induction chamber for sedation before the surgical site was shaved, they were then mounted onto the stereotaxic apparatus as described earlier. During survival procedures, the stereotaxic frame was fitted with a nose cone that

supplied a combination of isoflurane and oxygen. Breathing and body temperature were monitored closely throughout the procedure and sterile saline (0.9% NaCl) was injected to compensate for dehydration due to the anesthesia.

3.2.2 Surgery

Once the rat was mounted onto the stereotaxic frame, the scalp was disinfected with 70% ethanol or surgical grade iodine. Rats were given a subcutaneous injection of lopaine (3 mg/kg) under the scalp and systemic injection of carprofen (5 mg/kg) before incision. The dental syringe suspended by the stereotaxic handle was loaded with either the adenovirus containing hM4Di (or hM3Dq) + mCitrine or GFP (control) genes. Pedal withdrawal test was performed before the procedure began.

An incision was made over the scalp along the sagittal line of the head and a tissue retractor was used to keep the open scalp apart. Any tissue between the scalp and the skull was cleared until both bregma and lambda cranial sutures were clearly visible.

Using bregma as a point of reference, the skull was bilaterally drilled at coordinates as determined from the nonsurvival procedure mentioned earlier (AP: 1.68, ML: 2.0 for NAc core and AP: 4.0, ML: 0.6 for the mOFC). Drilling was done to the bottom of the skull until the dura mater was exposed. The dental syringe was then placed on the dura mater and was slowly lowered 6.5 mm into the brain for the NAc core and 4.25 mm for the mOFC. Once the tip of the dental syringe reached the coordinates, 1.0 μL of the virus is injected at the rate of 0.25 μL/min bilaterally. Once the injection is complete, the dental syringe was left undisturbed at the injection site for 5 min. This was done to both allow enough time for the virus to spread away from the injection site and to also reduce the amount of reflux of the virus through the injection track during the removal of the needle. The dental syringe was then slowly removed from the brain (at the rate of 10 μm/min) to further minimize reflux of the virus through the needle track. The scalp incision was then sutured, and rats were removed from the stereotaxic frame for postoperative recovery.

3.3 Behavioral Procedure

Rats were provided with 3 weeks to both recover from the surgery and to allow the virus to express before being prepared for behavioral training. In our study investigating the role of mOFC all rats were injected with the hM3Dq virus where the experimental and control groups differed in whether they received CNO or saline control. However, in our most recent and updated work with the NAc core rats were split in one experimental group and three control groups.

The experimental group consisted of rats that were injected with hM4Di in the nucleus accumbens and received the chemical actuator CNO (2 mg/kg) before the critical behavioral procedure. Due to previous reports of both hM4Di and CNO having

behavioral effects independently, three other control groups were employed [19, 29, 30]. To test whether hM4Di itself had an effect in behavior, a group of rats that were injected with hM4Di were subjected to sterile saline (0.9% NaCl) solution instead of CNO. Conversely, to test whether CNO has an effect without hM4Di, a group of rats that were subjected to intercranial injection of GFP (control) virus were subjected to CNO injection. Finally, and critically, a group of rats was subjected to intercranial injection of GFP were injected with sterile saline (0.9% NaCl) to serve as a baseline for the other groups. It is therefore hypothesized that only rats from the experimental group (with the combination of hM4Di/hM3Dq and CNO) would demonstrate behavioral effects of neuronal modulation.

3.4 Results from Our Laboratory and Previous Work

We first determined whether inhibition of mOFC impacted performance on our task (Fig. 2a). For all control groups, discrimination accuracy was higher on high-probability trials than on low-probability trials. Inhibition of mOFC in the hM4Dgi group abolished the differential accuracy during high and low probability trials. Because the results showed the inhibition of mOFC abolished the ability of the signaled-reward probability to modulate attention, our next experiment assessed whether activating the mOFC could increase the acquisition of the differential significance of the reward probabilities, manifested as an increase in the rate of acquisition of the task [12, 13]. Surprisingly, results indicated that

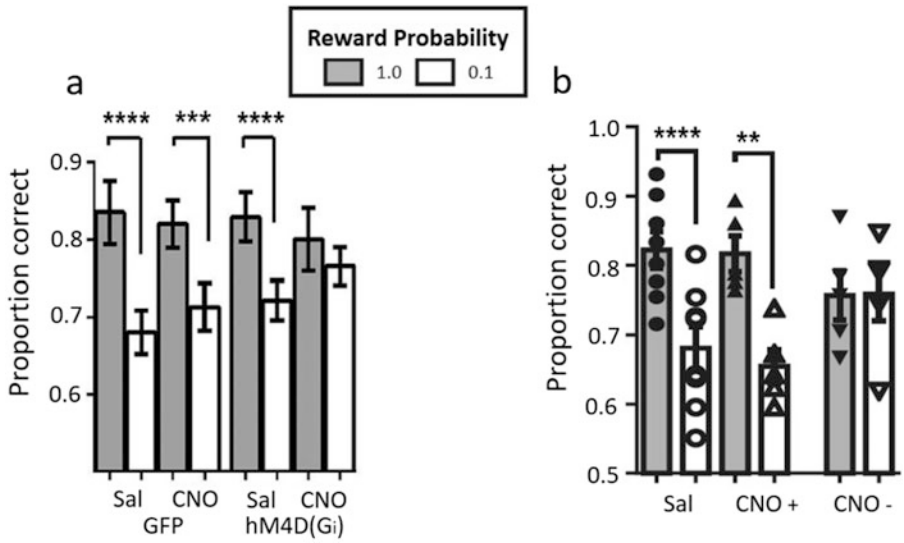

Fig. 2 DREADD interrogation of reward-modulated attention. (**a**) Results from Ward and colleagues show that the experimental group was unable to recruit greater attention for the high probability trials than the low probability trials after learning the task. All other control group animals were able to discriminate significantly (**b**) Increasing activity in the mOFC impaired learning of the SPSA as seen in the CNO group [12, 13]

neuronal activation impaired learning of the SPSA task (see Fig. 2b), although, as is evident from the figure, it did not do so across all rats.

Although neurons were specifically targeted using the human-synapsin promoter in these preparations, it is not known whether different neuronal populations in the mOFC play different roles in learning/expressing the SPSA [12, 31]. Therefore, indiscriminate activation of the local neuronal population may have led to a disruption of the local activity pattern as different neuronal populations may have opposing activity patterns. It is still possible to target sub-neuronal populations by combining transgenic technology and DREADD to tease out the role of these sub-neuronal populations [12, 13].

3.5 Rat Brain Extraction and Preparation

Once behavioral procedures were complete, rats were transcardially perfused with 10% formalin solution and the brain was extracted. These brains were submerged in a 10% formalin solution for 24 h before being transferred to a container with a phosphate buffer solution (with 30% sucrose). The extracted brain initially floats in this solution and progressively sinks to the bottom of the container, this process occurs over 48 h on average. Once the brain sinks to the bottom of the container, brain slices of 40 μm were taken using a cryostat (Leica CM1950) and were stored in phosphate buffer solution (PBS) ether before performing immunohistochemistry and/or slice visualization.

3.6 Immunohistochemistry

In our laboratory, immunohistochemistry was performed on rats that underwent hM4Di injections in the NAc core (see Subheading 4 for details). Freely floating slices were incubated in a blocking solution (10% normal goat serum in phosphate buffer/TritonX-100 solution) for 60 min before being incubated in a blocking solution containing the GFP primary Polyclonal Antibody (Thermo Fisher Scientific, catalogue # A-6455) diluted at 1:5000. The slices remained in the latter solution for 12 h at room temperature. After this period of incubation, the rat brain slices were washed out four times using a blocking solution. These slices were then submerged in a blocking solution that contained the secondary Anti-rabbit IgG (H + L) antibody, F (ab') 2 Fragment (Alexa Fluor 555 Conjugate) (CST, catalogue no. # 4413) diluted at 1:400. Slices remained in this solution for 2 h at room temperature.

3.7 Slice Visualization

Slices that were ready to be visualized were mounted onto microscope slides with an antifade solution to slow down the bleaching process. The mounted brain slices were viewed under a ZEISS AXIO Scope.A1 microscope. The mCitrine and GFP were viewed under blue illumination and the Alexa Fluor 555 Conjugate was viewed under green illumination. Photographs of these images were taken using a camera mounted onto the microscope.

4 Notes

4.1 Setting Up Dye/Viral Injection Apparatus

In our setup, a dental needle was used to inject the virus into the brain region of interest. This dental needle was attached to a polyethylene tubing that was attached to a Hamilton 10 μL Hamilton syringe on the other end. Although other setups have directly used the needle of the Hamilton syringe to inject the virus, we use the higher gauge dental needle as our previous experiments had shown increased disruption of the brain parenchyma when injecting directly with the syringe needle.

To prepare the injector, the back end of the dental needle is attached to a 25 gauge needle (or any other diameter to achieve a friction fit), this is then sealed using a silicone glue. The end of this 25 gauge needle was friction fitted with a polyethylene tubing that was attached to the Hamilton syringe (Fig. 3).

As mentioned earlier, this Hamilton syringe was attached to an injection pump that modulated the speed and the amount of injected virus. Critically, however, if the injection of the virus is done with a great amount of air between the loaded virus and the end of the Hamilton syringe, the injection rate and/or volume might be aberrant. This is because air is compressible and when the syringe pump injects the virus, it may compress the air between the virus and the head of the Hamilton syringe instead of injecting the virus into the brain. This phenomenon may even cause catastrophic damage in the local area of injection if the critical point of compression is reached to spontaneously eject the loaded virus into the brain at a high rate.

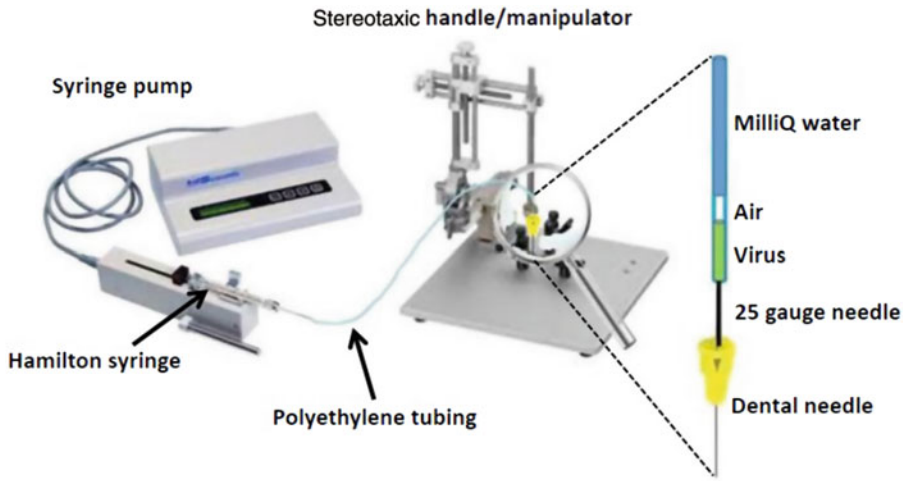

Fig. 3 Virus injection setup. Image shows the Hamilton syringe connected to the polyethylene tubing that is attached to the dental needle using a 25 gauge syringe needle. Image also schematically depicts the use of air as a medium to separate the MilliQ water from the virus

To circumvent this issue, MilliQ water was used to fill up most of the Hamilton syringe and the polyethylene tubing. A small air bubble was then drawn to separate the MilliQ water and the loaded virus (Fig. 3). This air bubble was small enough to minimize the effect of compression during injection and this size is variable depending on the size and length of the tubing used. The non-survival dye injection procedure is the best platform to test and optimize the effect of different bubble sizes on the spread and injection volume (Fig. 3).

4.2 Identifying True Bregma

We mentioned the use of bregma as a point of reference for both the drilling and for the cranial injection procedures in Subheading 3. However, it is common to find levels of variability in the shape of the cranial sutures and this may impact the location of the prospective cranial injection. Bregma is the point of intersection between the coronal and sagittal sutures where this intersection is roughly positioned in the middle of the coronal suture. One form of variability includes the skewing of the intersection toward either side of the skull and the use of this point of reference could result in a systematic error in the medial lateral (M/L) injection position. To overcome this, surgeons are able to identify bregma either through experience or through the use of lambda (the intersection of the coronal suture with the lambdoid suture). If lambdoid suture looks reasonably bisected by the sagittal suture, the M/L coordinates can be fixed using the "true lambda" of the cranial sutures and this has greatly helped reduce systematic errors in our surgical procedures (Fig. 4).

Another form of variability is when the coronal suture intersects the sagittal suture at different points. This essentially provides two potential points of bregma (as defined by the point of intersection between the sagittal and the coronal sutures) and depending on the distance between the two points of intersection, this may cause a systematic error in the anterior/posterior (A/P) coordinates. In our laboratory, early surgeons have benefitted from choosing A/P coordinates at the midway point between these two intersection points to reduce the systematic error (Fig. 4).

Finally, in our experience, we have come across multiple diagonal sagittal sutures. This is particularly difficult to tackle for early surgeons since both bregma and lambda are skewed. The most reliable method was the use of the midpoint of the sagittal suture between bregma and lambda as a marker for the M/L coordinates (Fig. 4).

4.3 Slice Visualization and Immunohistochemistry

As mentioned in Subheading 3, rat brain slices were subjected to an immunohistochemical protocol to visualize the mCitrine that was co-expressed with hM4Di. It has been reported that both mCitrine and GFP have either lost or have greatly reduced fluorescence visibility (possibly be due to the fixation procedure) in some cases [24].

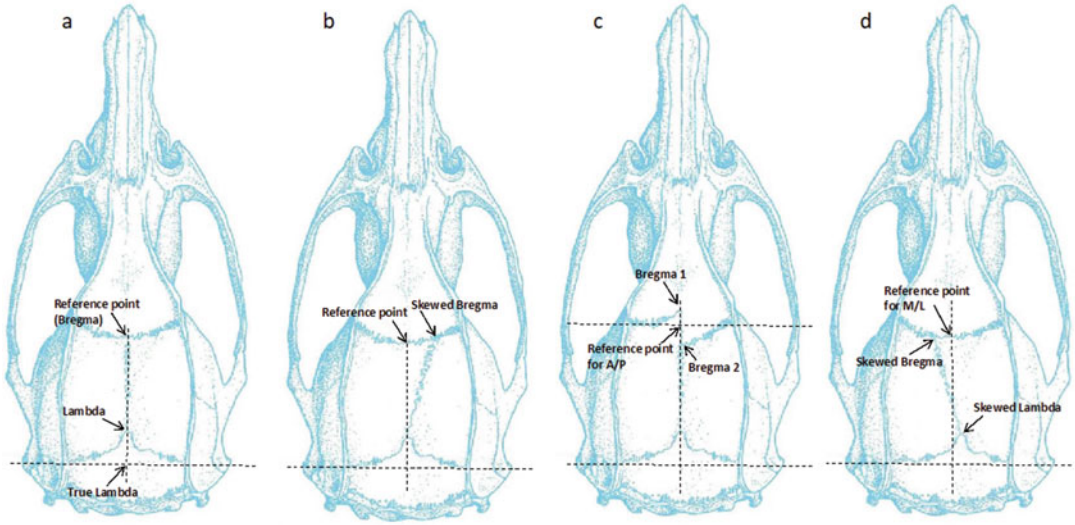

Fig. 4 Suture variations. Modified diagram from the rat brain atlas depicting the variations in sutures [27]. (**a**) Shows the standard-text book illustration of the cranial sutures in the rat skull. (**b**) Variation where the lambda conforms to the standard textbook but bregma is skewed toward one side. (**c**) Two intersections between the coronal and sagittal sutures, creating two potential points of bregma. (**d**) Both bregma and lambda skewed making the sagittal suture more diagonal

We initially encountered this hurdle when directly visualizing brain slices injected with hM4Di. Although we found little to no expression of mCitrine (as previously reported), we surprisingly found a satisfactory amount of the GFP (control) expression in the intended location NAc core. This provided us with enough confidence in the presence of the mCitrine in the group of rats that were injected with hM4Di. As mentioned earlier, a primary antibody was used to tag for the mCitrine and a secondary antibody that fluoresces in a different color was used to tag the primary antibody. We used a tag that fluoresces in a different color for the mCitrine as this would provide a greater level of confirmation that the mCitrine had indeed lost its fluorescence. By tagging the mCitrine in the same color, it would have been difficult to verify whether the observed fluorescence was a result of the immunohistochemistry. Figure 5 provides a visual representation of the fluorescence on the same brain slice under different illumination. The mCitrine is visible under blue light illumination and the Alexa Fluor® 555 Conjugate is visualized under green light.

This problem of little to no mCitrine expression is a relatively uncommon occurrence in our laboratory, therefore we advise that it is unnecessary to purchase antibodies in anticipation of this. Slices can be stored in PBS solution for months before immunohistochemistry is performed.

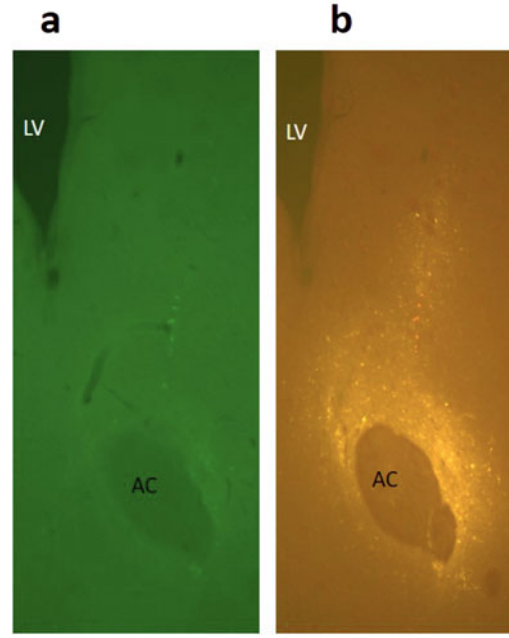

Fig. 5 Histological assessment of the mCitrine expression in the NAc core. (**a**) shows the fluorescence of the mCitrine under blue illumination. (**b**) shows the same slice under green illumination. The Lateral ventricle (LV) and the anterior commissure (AC) are labeled as points of reference. The NAc core is the immediate area surrounding the anterior commissure, projecting obliquely toward the base of the LV

5 Conclusions

DREADDs have been used in recent years in a number of paradigms to isolate and investigate the functional circuitry involved in reward processing and reward-motivated behaviors. The technology is rapidly advancing, with new DREADDs being developed which allow combinations of activation and silencing on different timescales and within different neuronal populations simultaneously. When combined with transgenic approaches and other technologies (optogenetics, electrophysiological recording), DREADDs provide useful ways to interrogate nearly any circuit of interest. With the many transgenic mice available, and increasing use of transgenic rats, we foresee that use and further development of the DREADD technique will be instrumental in elucidating the role of various brain structures and circuits involved in reward processing and modulation of behavior by reward in the future. As the behavioral paradigms employed grow ever more sophisticated, the answers gained by these investigations will shed much-needed light on the contribution of the reward system to adaptive functioning and will provide information on how it goes wrong in psychiatric disease.

References

1. Russo SJ, Nestler EJ (2013) The brain reward circuitry in mood disorders. Nat Rev Neurosci 14:609–625
2. Dichter GS, Damiano CA, Allen JA (2012) Reward circuitry dysfunction in psychiatric and neurodevelopmental disorders and genetic syndromes: animal models and clinical findings. J Neurodev Disord. https://doi.org/10.1186/1866-1955-4-19
3. Kelley AE, Berridge KC (2002) The neuroscience of natural rewards: relevance to addictive drugs. J Neurosci 22:3306–3311
4. Cooper S, Robison AJ, Mazei-Robison MS (2017) Reward Circuitry in Addiction. Neurotherapeutics 14:687–697
5. Simpson EH, Balsam PD (2016) Behavioral neuroscience of motivation. Springer, Switzerland
6. Balleine B, Killcross S (1994) Effects of ibotenic acid lesions of the nucleus accumbens on instrumental action. Behav Brain Res 65:181–193
7. Balleine BW, Delgado MR, Hikosaka O (2007) The role of the dorsal striatum in reward and decision-making. J Neurosci 27:8161–8165
8. Blaiss CA, Janak PH (2009) The nucleus accumbens core and shell are critical for the expression, but not the consolidation, of Pavlovian conditioned approach. Behav Brain Res 200:22–32
9. Cassataro D et al (2013) Reverse pharmacogenetic modulation of the nucleus accumbens reduces ethanol consumption in a limited access paradigm. Neuropsychopharmacology 39:283–290
10. Hernandez PJ, Sadeghian K, Kelley AE (2002) Early consolidation of instrumental learning requires protein synthesis in the nucleus accumbens. Nat Neurosci 5:1327–1331
11. Parkinson JA et al (1999) Dissociation in effects of lesions of the nucleus accumbens core and shell on appetitive pavlovian approach behavior and the potentiation of conditioned reinforcement and locomotor activity byd-amphetamine. J Neurosci 19:2401–2411
12. Ward RD et al (2015) Orbitofrontal cortex mediates the differential impact of signaled-reward probability on discrimination accuracy. Front Neurosci 9:230. https://doi.org/10.3389/fnins.2015.00230
13. Hall-McMaster S et al (2017) Medial orbitofrontal cortex modulates associative learning between environmental cues and reward probability. Behav Neurosci 131:1–10
14. Robbins T (2002) The 5-choice serial reaction time task: behavioural pharmacology and functional neurochemistry. Psychopharmacology 163:362–380
15. Kelley AE et al (2005) Corticostriatal-hypothalamic circuitry and food motivation: integration of energy, action and reward. Physiol Behav 86:773–795
16. Cox J, Witten IB (2019) Striatal circuits for reward learning and decision-making. Nat Rev Neurosci 1:482–494
17. Bressan RA, Crippa JA (2005) The role of dopamine in reward and pleasure behaviour--review of data from preclinical research. Acta Psychiatr Scand 111:14–21
18. Sesack SR, Grace AA (2010) Cortico-basal ganglia reward network: microcircuitry. Neuropsychopharmacology 35:27–47
19. Simon NW, Moghaddam B (2015) Neural processing of reward in adolescent rodents. Dev Cogn Neurosci 11:145–154
20. Robbins TW, Everitt BJ (1996) Neurobehavioural mechanisms of reward and motivation. Curr Opin Neurobiol 6:228–236
21. Kelley AE (2004) Ventral striatal control of appetitive motivation: role in ingestive behavior and reward-related learning. Neurosci Biobehav Rev 27:765–776
22. Armbruster BN et al (2007) Evolving the lock to fit the key to create a family of G protein-coupled receptors potently activated by an inert ligand. PNAS 104:5163–5168
23. Campbell EJ, Marchant NJ (2018) The use of chemogenetics in behavioural neuroscience: receptor variants, targeting approaches and caveats. Br J Pharmacol 175:994–1003
24. Smith KS et al (2016) DREADDS: use and application in behavioral neuroscience. Behav Neurosci 130:137–155
25. Roth BL (2016) DREADDs for neuroscientists. Neuron 89:683–694
26. Zhu H, Roth BL (2014) Silencing synapses with DREADDs. Neuron 82:723–725
27. Paxinos G, Watson C (2006) The rat brain in stereotaxic coordinates: hard cover edition. Elsevier
28. Cetin A et al (2006) Stereotaxic gene delivery in the rodent brain. Nat Protoc 1:3166–3173
29. Manvich DF et al (2018) The DREADD agonist clozapine N-oxide (CNO) is reverse-metabolized to clozapine and produces clozapine-like interoceptive stimulus effects in rats and mice. Sci Rep 8:3840. https://doi.org/10.1038/s41598-018-22116-z

30. MacLaren DA et al (2016) Clozapine N-oxide administration produces behavioral effects in Long-Evans rats: implications for designing DREADD experiments. eNeuro. https://doi.org/10.1523/ENEURO.0219-16.2016

31. Kügler S, Kilic E, Bähr M (2003) Human synapsin 1 gene promoter confers highly neuron-specific long-term transgene expression from an adenoviral vector in the adult rat brain depending on the transduced area. Gene Ther 10:337–347

Part III

Techniques for Assessing the Effect of Drugs of Abuse

Chapter 10

Intracranial Self-Stimulation: Using the Curve-Shift Paradigm to Assess the Abuse Potential of Drugs

Ritchy Hodebourg

Abstract

Intracranial self-stimulation (ICSS) is an operant conditioning procedure used to quantify the brain reward function. Thus, this procedure allows us to study the effects of behavioral, pharmacological, or molecular manipulations on the reward circuit. In the context of drug abuse and addiction, ICSS is generally used to test the abuse potential of drugs and to evaluate the aversive effect induced by withdrawal from chronic drug exposure. There are two main methods to assess the effect of a drug on brain stimulation reward: the discrete trial current intensity paradigm and the frequency-rate curve-shift paradigm. However, this chapter describes specifically the frequency-rate curve-shift paradigm in rats. The purpose of this section is to provide the reader with how to perform the frequency-rate curve-shift paradigm with several types of drug exposure.

Key words Addiction, Brain stimulation reward, Drugs of abuse, Intracranial self-stimulation, Frequency-rate curve-shift paradigm

1 Introduction

Intracranial self-stimulation (ICSS) was accidentally discovered in the earlier 1950s by James Olds and Peter Milner at McGill University, Montreal [1]. Indeed, Olds and Milner were studying the effect of electrical stimulation on the reticular formation in freely moving rats. They found that most rats avoided the place associated with the electrical stimulation except one that developed an appetitive behavior, such as sniffing and searching, during the stimulation. After checking they noticed that the electrode was placed near the anterior hypothalamus instead of the reticular formation [2]. James Olds then built his own Skinner box and noted that his rat had rapidly learned to press the lever to self-administer the electrical stimulation; it was the first model of ICSS [1, 2].

Thus, ICSS is an operant conditioning protocol in which experimental subjects are implanted with an electrode targeting a specific site of the brain reward pathway and are trained to perform an

Marc Fakhoury (ed.), *The Brain Reward System*, Neuromethods, vol. 165, https://doi.org/10.1007/978-1-0716-1146-3_10,

operant response (e.g., lever press or nosepoke) to self-stimulate. Since its discovery, ICSS has been extensively used to map the brain reward pathway [3, 4]. It is also a powerful tool for assessing the hedonic state of an animal, especially in the preclinical model of major depressive disorder [5–7]. In the field of addiction, ICSS is used to determine the abuse potential of substances [8, 9]. One of the major advantages of this procedure is that it accurately quantifies the rewarding or aversive effect of a drug.

Several methods have been developed to assess the effects of drugs on brain stimulation reward, sometimes making it difficult to interpret data between different studies in a reader unfamiliar with ICSS. This chapter describes one of the most commonly used protocols, namely the frequency-rate curve-shift paradigm.

1.1 The Frequency-Rate Curve-Shift Paradigm

Edmonds and Gallistel (1974) developed the frequency-rate curve-shift paradigm (or just the curve-shift paradigm) in a runway model of ICSS, to assess the effect of an independent variable, such as a drug, on the reward signal induced by electrical stimulation [10]. Thereafter, Miliaressis et al. (1986) adapted the procedure to a Skinner box [11]. This protocol is widely inspired by the dose–response curves in pharmacology. However, instead of varying the concentration of a pharmacological agent, they varied frequencies of electrical stimulation. Like dose–response curves, frequency–response (F/R) curves assume a sigmoidal function. A reward threshold (M50) was inferred from the F/R curve and corresponds to the frequency that supports a response rate equal to 50% of the maximum response. When a pharmacological treatment induces a leftward shift of the F/R curve, there is a decrease in M50 corresponding to an increase of the brain stimulation reward (Fig. 1a). In other words, this treatment amplifies the reward signal

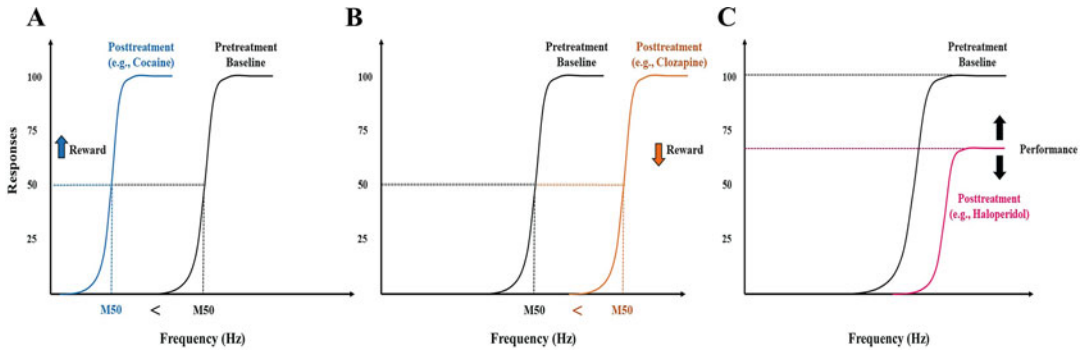

Fig. 1 Curve-shift paradigm. (**a**) Injection of a psychostimulant drug (e.g., cocaine) induces a leftward shift of the F/R curve, implying an increase in brain stimulation reward. (**b**) Injection of an atypical antipsychotic (e.g., clozapine) induces a rightward shift of the F/R curve, implying a decrease in brain stimulation reward. (**c**) Injection of a typical antipsychotics (e.g., haloperidol) induces a downward shift of the F/R curve, implying a change in the animal's ability to produce an operant response

induced by the electrical stimulation because it takes lower frequencies to produce an operant response. Thus, a leftward shift of the F/R curve is considered as an abuse-related effect of the treatment [9]. In contrast, when a treatment induces a rightward shift of the F/R curve there is an increase in M50 corresponding to a decrease of the brain stimulation reward (Fig. 1b). So, higher frequencies are required to produce a reward signal and thus an operant response. The rightward shift is interpreted as an aversive effect of the treatment [7]. Another important parameter in the curve-shift paradigm is the maximum response. The maximum response is an index of the animal's ability to produce an operant response (Fig. 1c).

1.2 General Procedure

The curve-shift paradigm breaks down into four stages namely: (I) surgery, (II) training, (III) F/R curves, and (IV) the testing. The three first stages are common to all of the experiments, however, the testing stage could vary depending on the kind of drug used, the route of drug administration and the effect to be studied (e.g., the abuse potential or withdrawal from drug administration). During the surgery, a stimulation electrode is stereotaxically implanted in a brain site supporting self-stimulation. The brain sites most often used are the medial forebrain bundle at the level of the lateral hypothalamus and the VTA. Then, rats are trained to perform an operant response (e.g., lever press or nosepoke) to self-administer an electrical stimulation. Once the self-stimulation behavior is acquired, rats are trained to respond under the F/R curve schedule of reinforcement, and reward thresholds (M50) are calculated. At this stage, the current intensity is adjusted to obtain an approximately equal M50 value between each rat. Following the establishment of stable M50 value, the effects of drugs of abuse on the brain stimulation reward can be studied during the testing stage.

2 Material

2.1 Electrodes

Monopolar stimulation electrodes are made with a stainless steel wire (0.27 mm in diameter) insulated with epoxy, except at the tip, connected to a male Amphenol plug. These electrodes are the cathodes. The anodes are made with a male Amphenol plug linked to uninsulated stainless steel wire and are wrapped around stainless steel screws that are threaded into the skull, to serve as the ground (Fig. 2) (*see* **Note 1**). Flexible leads coated with plastic and connected to female Amphenol plugs are used to conduct the current from the swivel commutator to stimulations electrodes.

2.2 Apparatus

ICSS experiments are conducted in an operant chamber equipped with a lever (it can also be a nosepoke hole or a wheel manipulandum). A constant current stimulator (PHM-152/2, Med

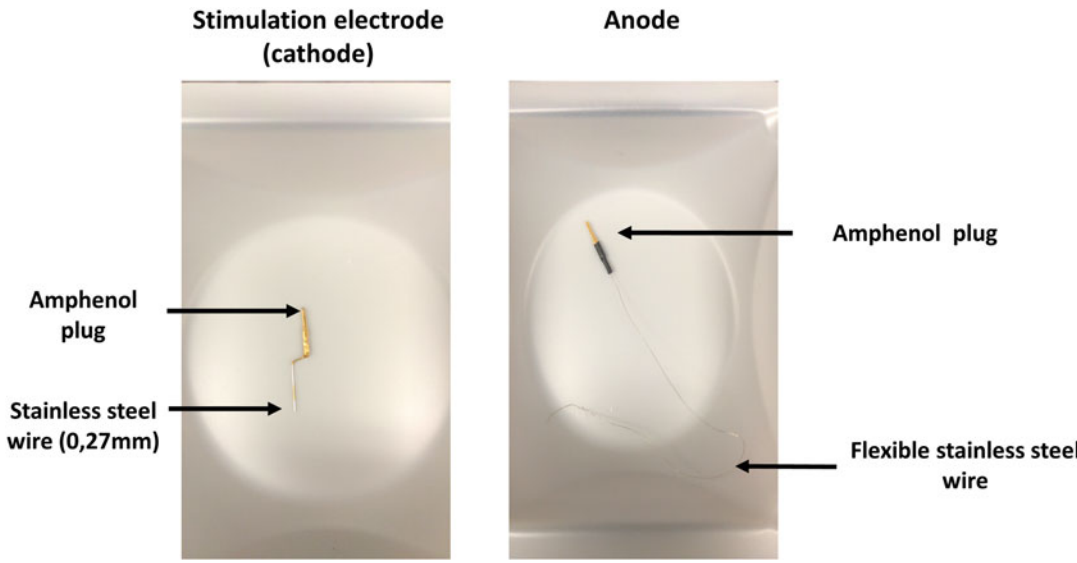

Fig. 2 Stimulation electrode and Amphenol plug used in ICSS. The stimulation electrode is made of a stainless steel wire of 0.27 mm connected to an Amphenol plug and serves to transit the cathodal current (left panel). The anodal current is transmitted through a flexible stainless steel wire connected to an Amphenol plug (right panel)

Associates Inc., St Albans, VT, USA) is used to generate the current and an oscilloscope is used to monitor the electrical stimulation of each rat (Fig. 3).

2.3 Parameters

To conduct an ICSS experiment, several parameters must be defined:

- Current intensity measured in μA.
- Current frequency measured in Hz.
- Duration of stimulation train measured in milliseconds.
- Pulse duration measured in milliseconds.
- Number of trials.
- Trial duration measured in seconds.
- Numbers of primes.
- Timeout period measured in milliseconds.
- Intertrial interval measured in seconds.

3 Methods

3.1 Training

After the surgery and recovery period, rats are trained to press a lever to self-administer an electrical stimulation under a fixed ratio 1 (FR1) schedule of reinforcement. To this end, the following

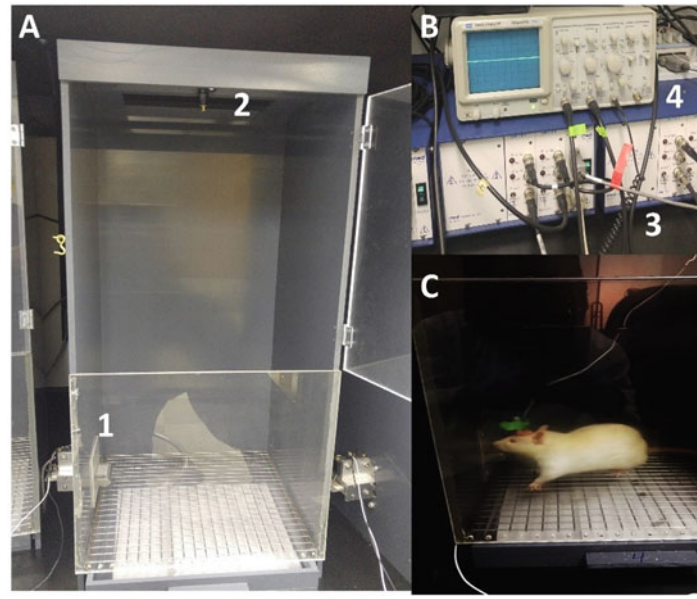

Fig. 3 The intracranial self-stimulation setup. (**a**) The operant chamber is equipped with (*1*) a lever and (*2*) a swivel commutator. (**b**) The stimulation apparatus is composed of (*3*) a constant current stimulator and (*4*) an oscilloscope. (**c**) A rat is connected to the swivel commutator via a flexible lead

parameters should be set before the beginning of the training. The duration of the stimulation train is set at 400 ms, the pulse duration at 0.1 ms, and the timeout period at 600 ms. The number of primes is set at 5. All these parameters should remain constant throughout the experience.

The first step of the training allows rats to self-stimulate during a 1-hour session separated into four trials of 15 min. For this purpose, the number of trials is set at 4 and the trial duration at 900 s with an intertrial interval of 15 s. Then, the current intensity and the current frequency are set at 250 μA and 250 Hz, respectively. The beginning of each trial is signaled by five trains of noncontingent stimulation. Usually, after the noncontingent stimulation, rats will develop an appetitive behavior and start to explore the operant box (*see* **Note 2**). At this stage, each time a rat is near the lever, a noncontingent stimulation will be given by the experimenter until the rat starts to press the lever to self-administer the electrical stimulation. The current intensity will be increased from 50 to 100 μA (up to 1000 μA) in rats that do not respond to the initial parameters. It is also possible to adjust the frequency. Thus, for each rat, the experimenter will determine what will be the intensity and the frequency of the current necessary to achieve an operant response. Once the operant response is acquired, rats are allowed to self-stimulate for at least two days under these parameters.

In the second step of the training, rats are trained to self-stimulate with the same parameters of stimulation (intensity and frequency), but during 55 s discrete trials followed by 15 s intertrial interval. To this end, the trial duration is set at 55 s and the number of passes at 15.

3.2 Frequency–Response Curve

In order to obtain an F/R curve, the frequency is decreased by approximately 0.1 $\log_{10}$ after each trial. A single session of self-stimulation is composed of four F/R curves and each F/R curve will consist of 12 trials of 55 s with stimulation frequencies ranging from 90 to 23 Hz (*see* **Note 3**). The first F/R curve is considered as a warm-up and is excluded from data analysis. To achieve this, the number of trials should be set at 12 and the number of passes at 4. The stimulation frequencies are set at: 90, 80, 70, 62, 54, 48, 42, 37, 33, 29, 26, and 23 Hz. At this stage, the beginning of each F/R curve is signaled by five trains of noncontingent stimulation at 90 Hz and rats are allowed to self-stimulate at 90 Hz during 55 s. Then, after 15 s of the timeout period, rats receive five trains of stimulation at 80 Hz and rats are allowed to self-stimulate at this frequency during 55 s, and so on until the last trial at 23 Hz (Fig. 4). At the end of the session, the reward threshold (M50) is calculated for the last three F/R curves, and an average is computed. The experimenter will then have to adjust the current intensity for each rat, to generate an M50 approximately equal to 50 Hz (e.g., between 47.5 and 57.5 Hz). There is an inverse relationship between the current intensity and the M50. For example, to increase the M50, it is necessary to decrease the current intensity.

3.3 Testing

3.3.1 Effect of an Acute Injection of a Drug

After at least three days with a stable reward threshold (M50 ≈ 50 Hz), the testing step can begin. Each test day is constituted by two ISCC sessions: a pretreatment session (baseline) composed by four F/R curves, and a posttreatment session also composed of four F/R curves (*see* **Note 4**). Immediately after the

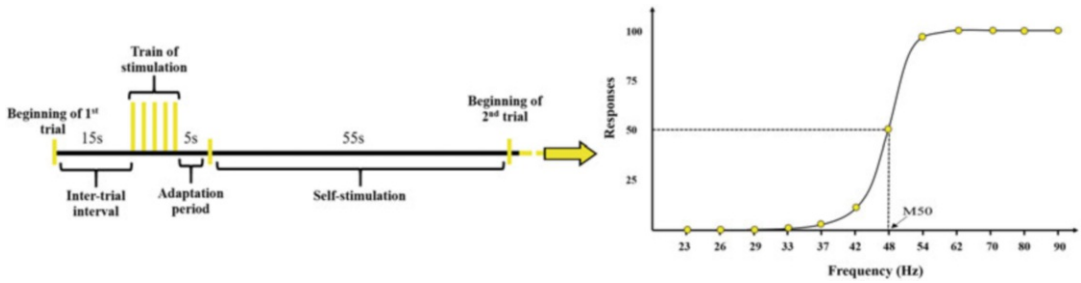

Fig. 4 ICSS protocol and the frequency/response curve. Each trial of ICSS typically begins with an intertrial interval of 15 s, followed by the delivery of 5 trains of noncontingent stimulation, a 5 s adaptation period, and a 55 s period during which the animal is allowed to freely self-stimulate. The trial is repeated many times with different frequencies to generate F/R curves that correlate the operant response rate with the frequency of stimulation

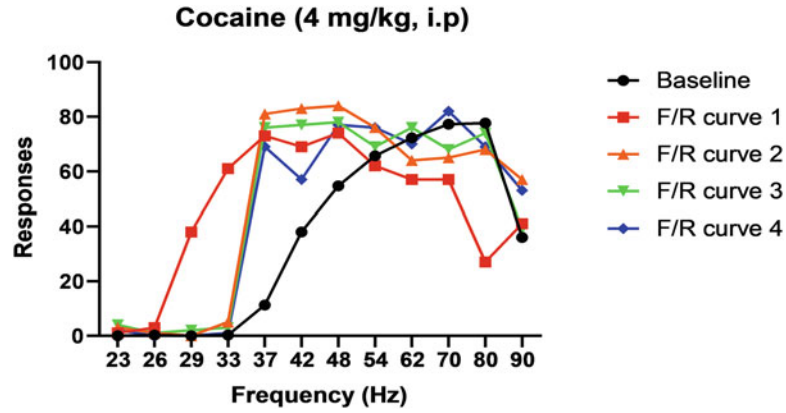

Fig. 5 F/R curve following injection of cocaine. Injection of cocaine (4 mg/kg, i.p.) induces a leftward shift in the F/R curve, implying an increase in brain stimulation reward. The effect is the highest 15 min after the injection (curve 1) and lasts 60 min after the injection (curve 4)

pretreatment session, rats received an injection of the drug of interest or its vehicle (e.g., an i.p injection of cocaine 4 mg/kg, Fig. 5). The posttreatment session begins immediately after the injection (*see* **Note 5**). In a within-subject paradigm, it is important to counterbalance the injections of the drug of interest and its vehicle, especially if you use different drugs or different doses. To avoid potential effects of tolerance and/or sensitization, each test day must be separated by at least 4 days without a test. Another possibility is to separate each test day by at least four days of ICSS session without any drugs.

3.3.2 Data Analysis

During the baseline session, the first F/R is always treated as a warm-up curve and is discarded from data analysis. Thus, the M50 and the maximum response is measured for each of the last three curves and an average is calculated. However, during the posttreatment session, the M50 and the maximum rate is calculated for all F/R curves. Data are then expressed as a percentage of the baseline (Fig. 6).

3.3.3 Effect of Chronic Injection of a Drug

To study the effect of chronic drug treatment, the experimenter should first determine a pre-manipulation baseline threshold. To this end, after establishing a stable M50, an average of the M50 and the maximum response is calculated over at least the last three days of the F/R curve training (Subheading 3.2). Then, there are several possibilities to perform chronic treatment. For example, the experimenter can inject the drug daily. For this purpose, the M50 and the maximum response are measured before and after each injection using the protocol described in Subheading 3.3.1. Another possibility is to use osmotic minipumps. After the establishment of the pre-manipulation baseline, an osmotic minipump (e.g., model

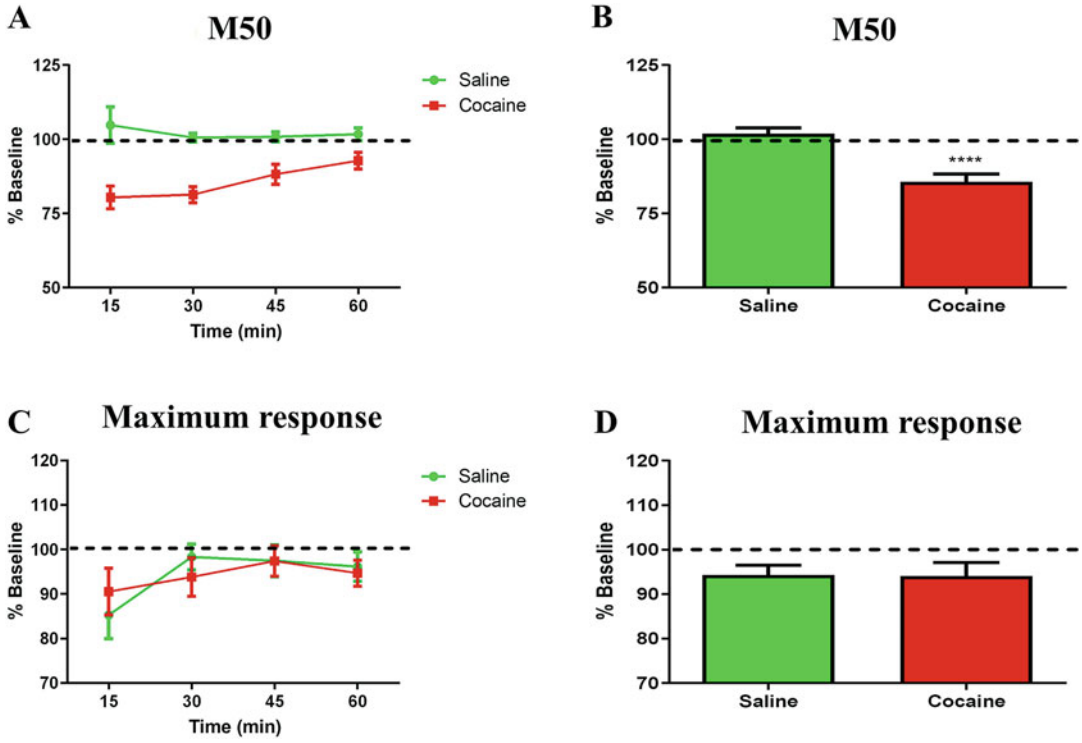

Fig. 6 Changes in M50 and the maximum response following cocaine injection (4 mg/kg, i.p.). (**a**) Changes in M50 following cocaine injection at each trial of ICSS. (**b**) Average changes in M50 following cocaine injection and compared to the baseline value. (**c**) Changes in maximum response rate following cocaine injection at each trial of ICSS. (**d**) Average changes in maximum response rate following cocaine injection and compared to the baseline value

2ML2, 5 μL/h flow rate, Alzet, Cupertino, CA, USA) beforehand filled with the drug or its vehicle is implanted subcutaneously in the midscapular region [12]. At least after a recovery day, the M50 and the maximum response can be calculated daily during the treatment and at different times after the pump removal.

4 Notes

1. It is possible to make the cathode and anode with female Amphenol plugs. In this case, the flexible lead used to connect the rat to the swivel commutator must be made with male Amphenol plugs. A monopolar stimulation electrode can be moveable along the dorsal–ventral axis [13]. Although this kind of electrode is primarily used to map the brain reward pathway [14], it is can be useful when a rat fails to self-stimulate. Indeed, the experimenter can go down the tip of the electrode and try to train the rat. In the curve-shift

paradigm literature, monopolar electrodes have mainly been used [15]. However, stimulation electrodes can also be bipolar. A bipolar electrode is made with two insulated stainless-steel wires, except at the tips, twisted together [16]. The advantage is that two poles of the electrode (cathode and anode) are located near the brain site and can be interchanged. However, the diameter of a bipolar electrode is usually larger than a monopolar electrode and cause more damage to the brain [8, 9, 16].

2. In some cases, rats fail to acquire the operant response. This problem can have multiple causes. First, it is necessary to check on the oscilloscope if the rat receives the electrical stimulation. When the oscilloscope does not show current, it is important to check if the rat is correctly connected to the stimulator via the flexible lead. For example, reversing the polarity of the lead (i.e., by plugging the cathode instead of the anode) blocks the current. If the problem persists when the rat is properly connected, it is possible to change the lead and test the stimulation again. If the issue is not related to the lead, the electrode and/or anode may be compromised. In this case, the rat should be excluded from the study. When the electrode is misplaced, the stimulation can be aversive and/or induce the motor effect. It is then necessary to reduce the intensity of the current. If this solution does not work, the rat should be removed from the study.
3. The number of trials and frequencies have been provided as a guide. It is completely possible to vary the number of trials between 10 and 15 [8, 9]. The most important thing is to have enough frequencies to monitor the leftward or rightward shift of the F/R curve. The range of frequencies can also be changed as well as the way to lower the stimulation. Some laboratories decrease the stimulation frequency by 0.1 $\log_{10}$ and other by 0.05 $\log_{10}$ [17, 18]. The M50 will be chosen according to the range of frequencies and the number of trials used by the experimenter. Ideally, the M50 should be approximately equal to the frequency at half the number of trials. For example, if the F/R curve contains 12 trials, the M50 should be close to the sixth trial.
4. The number of F/R curves during the posttreatment session can vary between four and seven [17, 19].
5. It is possible to assess the time course of the drug of interest. To this end, it is necessary to add different delays between the injection and the start of the posttreatment session. For example, the posttreatment session can start after 10, 30, 100, or 300 min [18, 20].

References

1. Olds J, Milner P (1954) Positive reinforcement produced by electrical stimulation of septal area and other regions of rat brain. J Comp Physiol Psychol 47(6):419–427
2. Milner PM (1989) The discovery of self-stimulation and other stories. Neurosci Biobehav Rev 13(2–3):61–67
3. Rolls ET (1975) The neural basis of brain-stimulation reward. Prog Neurobiol 3:73–160
4. Rompre PP, Boye S (1989) Localization of reward-relevant neurons in the pontine tegmentum: a moveable electrode mapping study. Brain Res 496(1–2):295–302. https://doi.org/10.1016/0006-8993(89)91076-7
5. Bechtholt-Gompf AJ, Walther HV, Adams MA, Carlezon WA Jr, Ongur D, Cohen BM (2010) Blockade of astrocytic glutamate uptake in rats induces signs of anhedonia and impaired spatial memory. Neuropsychopharmacology 35(10):2049–2059. https://doi.org/10.1038/npp.2010.74
6. John CS, Smith KL, Van't Veer A, Gompf HS, Carlezon WA Jr, Cohen BM, Ongur D, Bechtholt-Gompf AJ (2012) Blockade of astrocytic glutamate uptake in the prefrontal cortex induces anhedonia. Neuropsychopharmacology 37(11):2467–2475. https://doi.org/10.1038/npp.2012.105
7. Slattery DA, Markou A, Cryan JF (2007) Evaluation of reward processes in an animal model of depression. Psychopharmacology 190 (4):555–568. https://doi.org/10.1007/s00213-006-0630-x
8. Carlezon WA Jr, Chartoff EH (2007) Intracranial self-stimulation (ICSS) in rodents to study the neurobiology of motivation. Nat Protoc 2:2987. https://doi.org/10.1038/nprot.2007.441. https://www.nature.com/articles/nprot.2007.441#supplementary-information
9. Negus SS, Miller LL (2014) Intracranial self-stimulation to evaluate abuse potential of drugs. Pharmacol Rev 66(3):869–917. https://doi.org/10.1124/pr.112.007419
10. Edmonds DE, Gallistel CR (1974) Parametric analysis of brain stimulation reward in the rat: III. Effect of performance variables on the reward summation function. J Comp Physiol Psychol 87(5):876–883
11. Miliaressis E, Rompré P-P, Laviolette P, Philippe L, Coulombe D (1986) The curve-shift paradigm in self-stimulation. Physiol Behav 37:85–91
12. Bauer CT, Banks ML, Negus SS (2014) The effect of chronic amphetamine treatment on cocaine-induced facilitation of intracranial self-stimulation in rats. Psychopharmacology 231(12):2461–2470. https://doi.org/10.1007/s00213-013-3405-1
13. Miliaressis E (1981) A miniature, moveable electrode for brain stimulation in small animals. Brain Res Bull 6:715–718
14. Miliaressis E, Rompré PP, Durivage A (1982) Psychophysical method for mapping behavioral substrates using a moveable electrode. Brain Res Bull 8(6):693–701. https://doi.org/10.1016/0361-9230(82)90097-1
15. Vlachou S, Markou A (2011) Intracranial Self-Stimulation. In: Olmstead MC (ed) Animal Models of Drug Addiction. Humana Press, Totowa, NJ, pp 3–56. https://doi.org/10.1007/978-1-60761-934-5_1
16. Desai SJ, Bharne AP, Upadhya MA, Somalwar AR, Subhedar NK, Kokare DM (2014) A simple and economical method of electrode fabrication for brain self-stimulation in rats. J Pharmacol Toxicol Methods 69(2):141–149. https://doi.org/10.1016/j.vascn.2013.12.006
17. Bergeron S, Rompré P-P (2013) Blockade of ventral midbrain NMDA receptors enhances brain stimulation reward: A preferential role for GluN2A subunits. Eur Neuropsychopharmacol 23:1623–1635
18. Bonano JS, Glennon RA, De Felice LJ, Banks ML, Negus SS (2014) Abuse-related and abuse-limiting effects of methcathinone and the synthetic "bath salts" cathinone analogs methylenedioxypyrovalerone (MDPV), methylone and mephedrone on intracranial self-stimulation in rats. Psychopharmacology 231 (1):199–207. https://doi.org/10.1007/s00213-013-3223-5
19. Gallo A, Lapointe S, Stip E, Potvin S, Rompre PP (2010) Quetiapine blocks cocaine-induced enhancement of brain stimulation reward. Behav Brain Res 208(1):163–168. https://doi.org/10.1016/j.bbr.2009.11.029
20. Bauer CT, Banks ML, Blough BE, Negus SS (2013) Use of intracranial self-stimulation to evaluate abuse-related and abuse-limiting effects of monoamine releasers in rats. Br J Pharmacol 168(4):850–862. https://doi.org/10.1111/j.1476-5381.2012.02214.x

Chapter 11

Drug Self-Administration as a Model to Study the Reward System

Florence Allain and Anne-Noël Samaha

Abstract

Laboratory animals voluntarily self-administer almost all drugs of abuse humans do. Laboratory animals also develop patterns of drug-taking and seeking that are relevant to addiction. This makes drug self-administration models powerful tools to study drug-induced changes in neurobiological, psychological, and behavioral functions that are thought to contribute to the transition to addiction. We describe here the basic procedures used in drug self-administration studies carried out in laboratory animals. Mice, rats, cats, dogs, and primates used in the laboratory can self-administer drugs of abuse, but we describe methods appropriate for female and male rats, as we have long-standing expertise in carrying out such studies. Drug self-administration studies can also use the oral, inhaled, or intravenous routes to deliver drugs, but here we focus on the intravenous route, as it is the most commonly used. Thus, we describe procedures for intravenous catheter construction, catheter implantation into the jugular vein, and catheter maintenance to promote catheter patency over the course of a typical drug self-administration study. We also describe the hardware and software needed to carry out such studies. We also include visual illustrations as support for these descriptions.

Key words Intravenous drug self-administration, Rat, Catheter, Jugular vein, Operant box, Reward system, Cocaine, Locomotor activity, Psychomotor sensitization, Dopamine

1 Introduction

In 1940, S.D.S. Spragg discovered that morphine-deprived chimpanzees could demonstrate abstinence symptoms and could also work to obtain a dose of drug (select a key and open a box containing a loaded syringe [1]). This study challenged the assumption that only humans voluntarily take psychoactive drugs. It became potentially feasible then, to model behavioral and psychological symptoms of drug addiction in laboratory animals, as this would be of great interest for the treatment of this human brain disorder [2]. Modeling drug addiction in animals is key in understanding how drugs act in the brain and how they change the reward system to produce pathological drug use [3]. The brain reward system which is activated by rewards necessary for survival, such as food,

Marc Fakhoury (ed.), *The Brain Reward System*, Neuromethods, vol. 165, https://doi.org/10.1007/978-1-0716-1146-3_11,

water, safety, and a reproductive partner, is also the common target of drugs of abuse [4]. With repeated drug exposure, the brain reward system can change, leading to the transition to pathological patterns of drug-seeking and taking that characterize drug addiction. Understanding how this transition occurs is a critical first step toward the development of treatment strategies [5, 6]. To adequately study this transition, it is essential for animals to voluntarily take a drug, rather than to passively receive drug injections. In preclinical studies, this is achieved using the intravenous drug self-administration procedure.

Both intracranial self-stimulation (see Chapter 1 of the present book for more details) and drug self-administration procedures provide animals with a choice: to perform an action to obtain reward or not to perform such an action [7, 8]. In both procedures, animals thus voluntarily consume drug/electrical brain stimulation. In drug self-administration studies, this volitional aspect is clinically relevant because human drug users also choose to perform actions to voluntarily consume drug. Thus, drug self-administration studies mimic the human condition, where drug-seeking and taking are volitional. However, the behavior that leads to drug consumption is much more complex in humans than in laboratory animals. While humans must—for example—hustle to get money, find a drug dealer, and buy drug; laboratory animals are generally only required to perform an instrumental response, such as pressing a lever or introducing their snout into a recessed hole to obtain a drug dose. As stated by Olds [9] following intracranial self-stimulation observations in rats, "by putting the animal in the 'do-it-yourself situation' (i.e., pressing a lever to stimulate its own brain) we could translate the animal's strength of 'desire' into response frequency, which can be seen and measured." Similarly, studies using drug self-administration paradigms are also "do-it-yourself" situations, where the experimenter can analyze the animal's strength of "desire" for a drug.

Self-administration procedures can involve different routes of drug administration. Drugs can be administered intraperitoneally [10, 11], intracerebrally [12–14], via inhalation [15, 16], orally [17, 18], or intravenously [8]. The route of administration is generally selected according to the drug to be studied. For example, the oral route is mainly used for alcohol self-administration, but it is not very good for self-administration of other drugs, as the slow pharmacokinetics of oral administration reduces reinforcing efficacy [19–21]. In contrast, with intravenous administration, a drug has immediate access to the venous bloodstream which bypasses any absorption process or first-pass metabolism, and yields excellent drug bioavailability, such that drugs are quickly distributed to the brain and the reward system [22, 23]. The i.v. route is also relatively practical. For these reasons, the i.v. route of administration is commonly used in preclinical research on drug addiction [24].

In the present chapter, we focus on intravenous drug self-administration procedures and some applications of this technique in studying the mammalian reward system. Of note, while voluntary drug self-administration can be studied in many animal species, the procedures we outline here are specific for the rat.

2 Materials and Methods

2.1 Preparing Catheters for Intravenous Drug Self-Administration in the Adult Female or Male Rat

2.1.1 Materials for Catheter Preparation

The materials needed to build a catheter for intravenous implantation are illustrated in Fig. 1a

- Cannula (C313G-5UP; Stainless-Steel; 5-mm upward projection; 11-mm length; 22 Gauge; Plastics1).
- Silastic tubing (Inner ∅ = 0.51 mm; Outer ∅ = 0.94 mm; Dow Corning, CAT. NO. 508-002).
- Polyolefin heat-shrink tubing (Inner ∅ = 1.17 mm; Recovered ∅ = 0.58 mm; Alpha Wire, FIT 221 3/64).
- Nylon mesh (Bard® Mesh, Monofilament polypropylene mesh, REF. NO. 0112660).
- 100–200 μL pipette tips
- Soldering iron.
- Chloroform.
- Dental cement.
- Silicone.
- Razor blade, scissors, marker pen.
- Tygon® (Polymers) tubing (Inner ∅ = 0.51 mm; Outer ∅ = 1.52 mm; Cole-Parmer® REF. NO. 06419-01).

2.1.2 Methods for Catheter Preparation

The steps to build a catheter are summarized in Fig. 1b, c

- The cannula should be bent to a 135° angle (Fig. 1b).
- The silastic tubing is cut to produce a ~15 cm piece of tubing for adult male rats and a ~13.5 cm piece for adult female rats (this can be adapted depending upon the strain and the weight of male and female rats). One end of the tubing is cut at a beveled angle, as illustrated in Fig. 1b and two lines are drawn with a marker pen; the first at ~3 cm or ~2.4 cm from the beveled end (for male and female rats, respectively) and the second, 1.7 cm above the first line (same distance for both sexes).
- The non-beveled end of the silastic tubing is immersed in chloroform for a few seconds to distend the tubing. The angled tip of the cannula is then inserted into the distended tubing. Wait a few seconds for the tubing to air dry and to naturally constrict around the cannula.

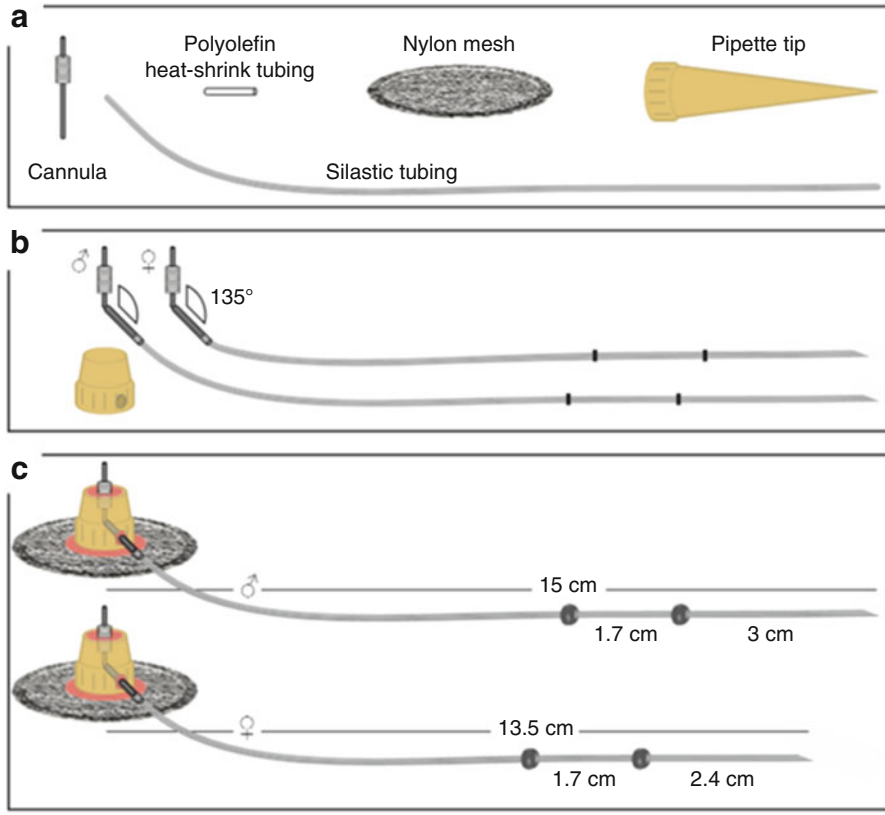

Fig. 1 How to build an intravenous catheter. (**a**) Materials needed to build a catheter. (**b**) The cannula is curved to a 135° angle and the curved extremity of the cannula is attached to a piece a silastic tubing. (**c**) The curved cannula linked to the silastic tubing is inserted in a pipette tip previously cut and fixed on a piece of nylon mesh with dental cement. Silicone bubbles are shaped on the silastic tubing

- A piece of polyolefin heat-shrink tubing (~1.3–1.5 cm) is cut to cover the cannula. The silastic tubing attached to the cannula is inserted into the piece of heat-shrink tubing. With the soldering iron, apply heat to the polyolefin tubing around the cannula. This shrinks the polyolefin tubing around the silastic tubing and the cannula, as represented in Fig. 1b. This step serves to protect that silastic tubing from rupture, thus consolidating the catheter.
- With a razor blade, the 100 or 200 μL pipette tip is cut as illustrated in Fig. 1b. With the soldering iron, a hole is made at the base of the tip to create an exit for the cannula. If necessary, to avoid eventual discomfort for animals, the tip's asperities can be melted with the soldering iron.
- The cannula consolidated with the tubing (silastic tubing and polyolefin tubing) is inserted into the pipette tip through the hole.

- The pipette tip is filled with dental cement to consolidate the system.
- Dental cement is placed at the base of the pipette tip and a circular piece of nylon mesh is quickly placed on the dental cement to be held in place. Another layer of dental cement (more liquid than the previous one) is put on the other side of the nylon mesh to consolidate the system. Wait ~1 h for the dental cement to solidify completely.

  **Note that the skin in females is thinner than in males. To avoid any discomfort, the circular piece of mesh can be made smaller in females than in males. The mesh used to build the catheter can also be of a more flexible type in females than in males. The size/type of mesh used can also be adjusted based on the weight of rats used for the experiment.*
- At the two lines previously drawn on the silastic tubing, two silicone bubbles are shaped around the tubing (Fig. 1c). Wait 2 days for the silicone to dry.
- To seal cannulae tips, bouts (~1 cm) of Tygon tubing are heated at one extremity and closed at that extremity by applying pressure. The other end of the tubing will be used as a cap to seal the catheter's cannulae after implantation into the animal.

2.2 Implantation of the Catheter into the Jugular Vein

Typically, upon arrival to our laboratory, male Wistar rats weigh 225–250 g and female Wistar rats weigh 175–225 g (these windows of weight can vary depending on the aims of the study—catheter's length can also change according to rats' weight). Rats are left undisturbed during at least 3 days after their arrival for habituation to the animal colony. Food and water are available ad libitum during this time. During self-administration training and testing, rats are often food restricted. Note that some but not all laboratories use food restriction. Drastic food restriction (e.g., 10 g of standard lab chow/day, in adult male rats) can cause rats to lose weight over time and can also increase the reinforcing efficacy of many drugs of abuse [25]. In our laboratory, food restriction is moderate (20 g standard lab chow/day for females and 25 g/day for males, see [26]) and approximates 75–85% of free-feeding body weight [26–30]. Food restriction is used to facilitate the acquisition of operant responses required to self-administer drug and to also reduce the total amount of drug used. Food restriction can also help improve the health of laboratory animals [31]. On the days surrounding the implantation of the catheter into the jugular vein, more food is given to help recovery from surgery (35 g/day in male rats and 30 g/day in female rats).

2.2.1 Materials for Catheter Implantation into the Jugular Vein

- Prior to surgery, catheters are submerged in a bath containing a solution of Cidex OPA for disinfection.
- 70% Ethanol
- Chlorhexidine.
- 0.9% Saline solution
- Anesthesia (e.g., isoflurane).
- Medicine.
  - Analgesic Carprofen (Rimadyl, 50 mg/mL, 0.03 mL/rat).
  - Penicillin antibiotic (Derapen, 300 mg/mL, 0.3 mL/rat).
  - Heparin (0.2 mg/mL) + Baytril (2 mg/mL) diluted in saline.
  - Ophthalmic ointment.
  - Antibacterial cream (e.g., Flamazine, silver sulfadiazine cream).
- Syringes for medicine injections.
- Gauze sponges and Q-tips.
- Razor.
- Surgical instruments:
  - Scissors, large and smaller.
  - Surgical forceps.
  - Straight and curved hemostats.
  - Straight and curved probes.

    **Note that surgical instruments are put in autoclave prior the surgery.*
- A Z-shaped needle (22G × 1½ in., 0.7 mm × 40 mm) is attached to a Q-tip (Fig. 2a). The Q-tip handle makes the needle easier to manipulate to make a hole in the vein.
- Beakers.
- For nonabsorbable surgical sutures.
  - Circular suturing needles.
  - 5-0 USP (1.0 metric) thread (Ref. No. SP115)—for internal sutures (to attach the catheter to the vein and the chest muscle)
  - 3-0 USP (2.0 metric) thread (Ref. No. SP117)—for external sutures (to close the wounds).

2.2.2 Methods for Catheter Implantation into the Jugular Vein

Surgery to implant a catheter into the jugular vein is illustrated in Fig. 2.

- The rat is anesthetized under isoflurane (5% for induction, 2–3% for maintenance).

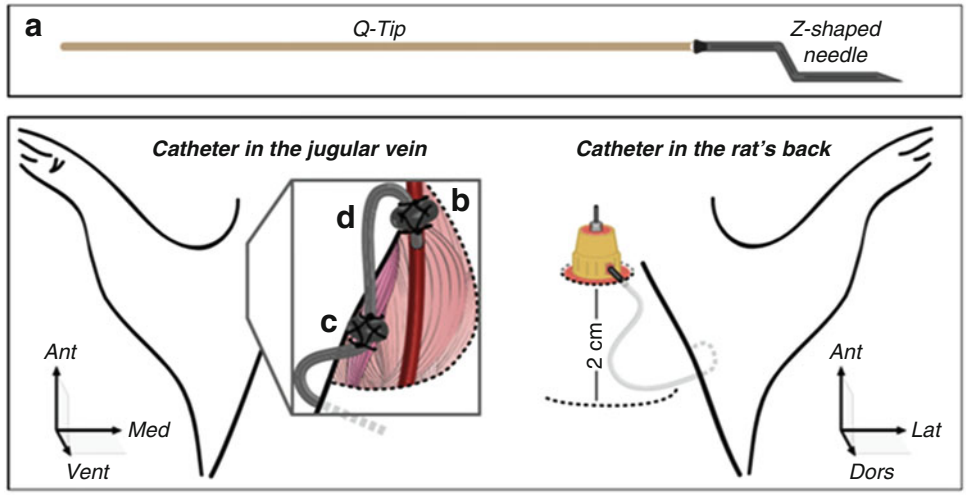

Fig. 2 Surgical implantation of a catheter into the jugular vein. (**a**) Needle needed to make a hole in the jugular vein. (**b**–**d**) The silastic tubing part of the catheter is inserted into the jugular vein and (i) attached to the vein with suturing thread tied around the first silicone bubble and (ii) attached to the chest muscle with suturing thread tied around the second silicone bubble. (**e**) The nylon mesh of the catheter is positioned under the skin in the rat's back

- Incision areas on the rat's back and the skin above the jugular vein are shaved. Catheters can be implanted into either the right or left jugular veins.

  **Note that in case of difficulties during the surgery, the experimenter can implant the catheter into the second jugular vein (this is a very rare occurrence in experienced experimenters).*

- During the surgery, a source of heat is provided to the rat for body temperature regulation (e.g., a heating disc under the rat). Put a pad between the source of heat and the rat to avoid any discomfort or skin burns.
- The rat is injected with analgesic and antibiotic, and lubricating ointment is applied to both eyes to avoid damage to the cornea, as eyes stay open during surgery.
- Incision areas are disinfected—first with 70% ethanol and then with chlorhexidine. The procedure is repeated three times.
- All surgical instruments are placed in a beaker containing a solution of 70% ethanol. Before using an instrument, it is rinsed in another beaker containing a 0.9% saline solution and returned to the 70% ethanol beaker once it has been used. Same for the threads: bouts of threads are immersed in 70% ethanol and rinsed in saline before being in contact with the rat.
- On the rat's back
  - A first incision is made under the neck.

  - A bigger incision is made ~2 cm below that first incision.
  - In the space under the skin between the two incisions, a straight hemostat is inserted and opened and closed two to three times. This helps to loosen connective tissue between the two holes for subsequent insertion of the catheter.
- Above the jugular vein
  - The surgeon can locate the vein by observing the skin, as the vein's rhythmic beating is visible on the skin's surface. A first incision is made on the skin where this rhythmic beating occurs. A deeper incision is made on the second layer of skin to open the muscle protecting the vein. This will serve to reveal the vein.
  - The jugular vein is separated from the surrounding tissue and fat using curved probe and forceps.
  - A piece of thin tread (5.0 USP) is placed under the isolated vein.
- Back port for the catheter
  - The Cidex around the catheter is first rinsed with tap water and the catheter is filled with saline and connected to a 1-mL syringe filled with saline.
  - A curved hemostat is inserted under the skin at the level of the vein area incision and carefully brought to the big hole on the rat's back. Then, the silastic tubing of the catheter is picked up between the two silicone bubbles with the curved hemostat and threaded back—still under the skin, but on the opposite way—toward the isolated jugular vein.
  - Saline can be flushed through the catheter to check its good condition (i.e., no ruptures).
- Inserting the catheter into the jugular vein
  - The vein is clamped (as high as possible toward the animal's head) with a straight hemostat, taking care not to clamp the vein too tightly.
  - The vein is held up away from the body using the straight clamp and the straight probe—both surgical instruments are held in the nondominant hand like chopsticks.
  - With the dominant hand, the vein is pierced with the Z-shaped needle placed on a Q-tip (see Fig. 2a). With the needle, up and down movements are gently made within the vein to distend it. The needle is then removed, and the location of the hole previously made on the vein, which is only barely visible, is mentally noted to be able to insert the catheter into the vein.
  - The catheter is brought with forceps in the dominant hand (the nondominant hand is holding the vein up and away from

the body) and inserted into the vein up until the first silicone bubble (if the vein appears dry, apply saline to facilitate the insertion of the catheter).

- Some blood is slowly aspirated into the catheter to confirm it is correctly placed in the vein and then saline is pushed back through the catheter.

- Fastening the catheter to the jugular vein and to the chest muscle
  - The piece of thin thread previously placed under the vein is tied above the silicone bubble. A second piece of thin thread is tied under the vein below the silicone bubble. Then, the two pieces of thread are tied together. This secures the catheter inside the vein (Fig. 2b).
  - The same strategy is used to fasten the second bubble of silicone to the chest muscle (Fig. 2c).
  - Between each knot, catheter good position and fluidity are checked by pulling/pushing blood/saline through the catheter.

    **Note that if at any moment, there is no blood appearing in the catheter when the syringe plunger is pulled, then either knots have to be removed and retied more loosely or the position of the catheter has to be readjusted. It is also possible that when pulling blood into the catheter, the surgeon feels suction such that blood is not aspired into the catheter. In this case, even if some blood can be seen through the catheter, it is recommended to adjust the knots or to change the orientation of the catheter's loop* (Fig. 2d).
  - When the catheter is anchored to the chest muscle and placed in a naturally resting position below the skin (i.e., with no kinks)—then close the incision with the thick threads (3.0 USP).

- On the rat's back, the cannula with the nylon mesh (the back port) is next transferred, under the skin, from the big hole to the little one (Fig. 2e). This allows the cannula to be located in between the rat's scapulae to minimize the risk that the rat will scratch it and damage it.
- The nylon mesh is carefully flattened under the skin to avoid possible discomfort to the rat.
- To confirm that the silastic tubing is well positioned under the skin, catheter position, and fluidity are checked the last time by aspirating blood into the catheter.
- The catheter is flushed with heparin followed by saline (0.1 mL of each).
- For protection and to avoid venous reflux, a cap (see Subheading 2.1.2) is placed on the cannula.

- Sutures are made to close the big hole in the back's rat with thick threads.
- The skin is cleaned with chlorhexidine to remove any blood and antibacterial ointment is applied on the incisions. If the rat has bled during the surgery (a very rare occurrence), 1 mL of saline can be injected subcutaneously.
- The isoflurane vaporizer is turned off and the rat is kept only on oxygen until it starts to move. Then, the rat is transferred to its home cage under observation until recovery.
- Between rats, surgical instruments are cleaned and dried before being sterilized using a Germinator 500. Beakers containing 70% ethanol and saline are changed every three to five rats or before if solutions are considered too dirty.

2.2.3 Postoperative Care

- On each of the 3 days following the surgery, wounds are cleaned with chlorhexidine and antibacterial ointment is applied.
- Sutures are checked daily for a week post-surgery. If sutures become undone, rats are re-anesthetized, and sutures are redone.
- Throughout the experiment, catheters are flushed each day with a saline solution and every other day with a heparinized saline solution. This avoids blood clots in the catheters.
- During catheter implantation surgery, it is possible to trim the rats' front claws to prevent scratching. We have observed that if the catheter is placed correctly in between the rat's scapulae, rats do not have easy access to the catheter, and so it is not always necessary to trim the claws.
- Intravenous drug self-administration generally starts 5–7 days after the surgery. This can vary depending on how well rats recover from surgery. The recovery period can be decided based upon visual inspection of the animal and the incisions. Female rats or younger rats can require more recovery days than male rats, as they have more delicate skin.

2.3 Intravenous Drug Self-Administration

2.3.1 Materials for Intravenous Drug Self-administration

Here we describe the apparatus used for drug self-administration in rats ([8, 32, 33]; also described in [34]). This apparatus is also illustrated in Fig. 3.

- Standard operant boxes (e.g., 31.8 cm × 25.4 cm × 26.7 cm; Med Associates Inc.)
  - Some laboratories keep their operant boxes in a testing room different from the room where rats are housed. Other laboratories house the rats in the operant boxes during experiments.

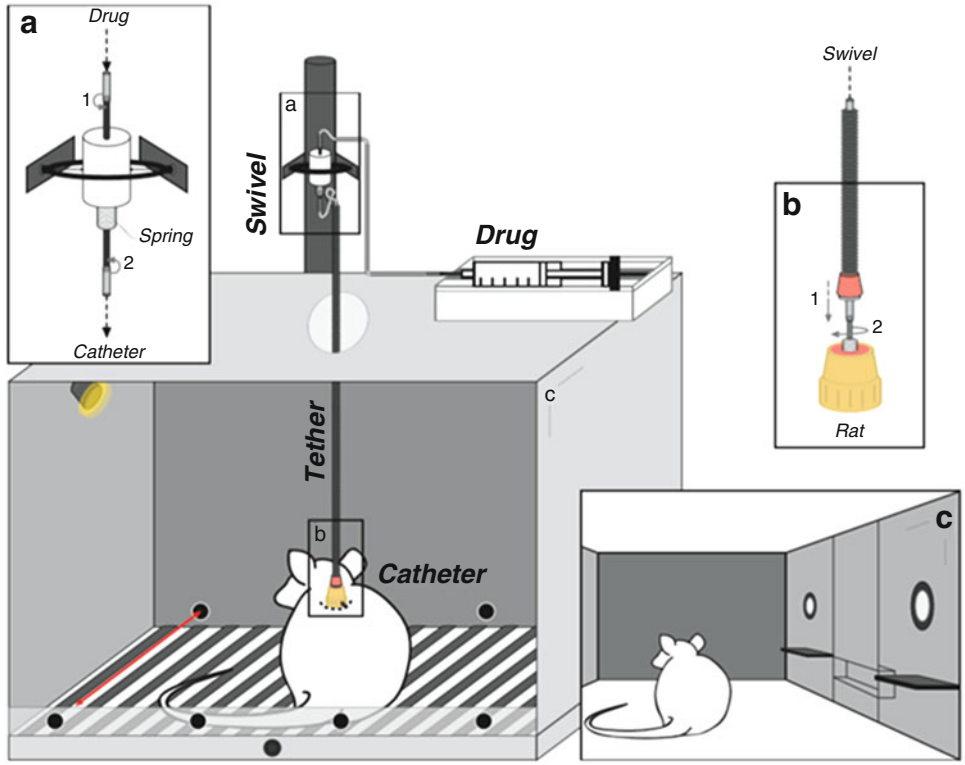

Fig. 3 An operant cage for intravenous drug self-administration. (**a**) The swivel connects the drug-filled syringe to (**b**) the animal's intrajugular catheter. (**c**) The rat can press a lever to trigger the delivery of one drug injection. Alternatively, the operant response can be nose poking into a recessed magazine (not shown on figure)

  - Each standard operant box is equipped with a metal grid floor.
  - To avoid external noise, each standard operant box is placed in a larger sound-attenuating cubicle equipped with a fan.
- Swivel and tether apparatus (Fig. 3a).
  - A swivel (22G, RSP1) is used to permit free movement of the rat, all the while enabling drug infusions via tubing. The swivel is mounted on a counterbalanced arm.
  - The tether can be a metal (steel) spring—resistant and durable (30.7 cm length). The metal spring is an important piece of equipment in self-administration studies because it shields against rat's bites and avoids damage to the infusion tubing.
  - The end of the tether is attached to a plastic cap using dental cement. This cap allows the tether to be screwed onto the cannula on the rat's back (Fig. 3b).
- Automated syringe pumps equipped with a motor that rotates to deliver the drug of interest. The number of rotations per minute

(RPM) will determine the speed of drug delivery and the volume of drug to inject.

- A syringe filled with the drug of interest that fits onto the syringe pump.
  - Drug solution. Depending on the drug, the pH might have to be adjusted, and the solution filtered.
  - The size of the syringe (e.g., 10 mL or 20 mL) can be adjusted according to the protocol used and the drug of interest—If large amounts of drugs are likely to be self-administered, then high-capacity syringes are preferred. In some cases, the syringe has to be refilled during a self-administration session.
- A computer with, for example, Med-PC (Med-Associates) software to control drug delivery (syringe pump) and presentation of discrete, drug-associated cues (operant boxes).
- Tygon (Polymers) Tubing (Inner ∅ = 0.51 mm; Outer ∅ = 1.52 mm; Cole-Parmer Ref. No. 06419-01).
  - A piece of Tygon tubing is connected to the upper part of the swivel and linked to the syringe filled with the drug of interest (Fig. 3a). Rats do not have access to this part of the tubing. As such, there is no need to protect it with a spring (Fig. 3a).
  - Another piece of Tygon tubing is connected to the bottom part of the swivel and inserted into the tether system (spring) connected to the cannula. The tubing is inserted on the cannula and the tether system is screwed around the cannula to consolidate the system (Fig. 3a, b). Thus, via the swivel and tether apparatus, the drug of interest can be delivered to the vein via the in-dwelling catheter (Fig. 3).

    **Note that before connecting the rat to the tether apparatus and starting a self-administration session, it is important to manually push the syringe pump in order to entirely fill the Tygon tubing with drug. After this, there would be no dead volume in the Tygon tubing, but there would still be a dead volume in the in-dwelling catheter. As such, the first self-administered infusion will likely deliver an incomplete dose to the rat.*
- Manipulanda and other stimuli in the operant boxes (Fig. 3c).
  - A house light, generally situated on the top of the back wall.
  - On the opposite wall: two 4-cm wide levers. A distance of 12 cm separates the two levers. One lever is associated with the drug: it is called the active lever. When a rat presses this lever, this is reinforced by an intravenous infusion of drug. The other lever can be non-reinforced to evaluate nonspecific behavior: in this case, it is called the inactive lever. When a rat presses the inactive lever, there are no programmed

consequences. The two levers can be retractable or not. Retractable levers can be used to indicate the period of drug access and can be used as cues for drug delivery [35]. Note that intravenous self-administration studies can be performed using nose pokes instead of lever presses, where rats insert their snouts in a hole to trigger drug delivery [36].

- A cue light is located above each lever. These lights can be used as drug-associated cues (e.g., the light above the active lever can be turned ON when the rat is self-administering drug).
- A food magazine is placed between the two levers. In the case where the reward is food, active lever presses order the delivery of food into the receptacle. The apparatus to deliver food pellets is located outside the operant box and not represented in Fig. 3.
- Infrared photocells can be installed horizontally to measure locomotor activity during drug self-administration sessions ([37], Fig. 3, See Subheading 2.3.3 for applications).

**Note that these materials and their location in the operant boxes can differ between laboratories. Other equipment in the operant boxes can also be used depending on the measured behavior. Here, we only describe the basic procedure for intravenous drug self-administration in rats.*

2.3.2 Methods for Intravenous Drug Self-Administration in Rats

- Food training
  - Food training is not a necessary step for intravenous drug self-administration, but it can accelerate the acquisition of the operant response.
  - Rats self-administering food do not need to be catheterized thus food training procedure can start either before or after the catheter implantation surgery.
  - During food training, food restriction is adjusted to 15 g/day in adult male rats and 13 g/day in adult female rats [26].
  - Rats can press the active lever to obtain a food pellet (45-mg banana-flavored grain-based pellets; VWR, Town of Mount-Royal, QC) directly delivered into the food receptacle in between the two levers (Fig. 3c).
  - Most rats quickly learn to self-administer food (one to two sessions). Each session can last 1 h/day but most rats take less than 1 h to self-administer 100 pellets, thus the session can stop earlier. If after two sessions, there is no reliable food self-administration behavior (<10 pellets self-administered on the two sessions), rats can be put in the operant box overnight (this is a rare occurrence).

  - Even though some rats might not show reliable food self-administration behavior, they can still later reliably self-administer drugs. Thus, no rats should be excluded from subsequent drug self-administration testing due to poor performance during food self-administration.

- Acquisition of intravenous drug self-administration
  - After food training (if this is used), catheterization, and recovery, rats are connected to the tether apparatus (Fig. 3b).
  - At the beginning of the session, the house light is turned ON and the two levers are inserted into the operant box (if using retractable levers).
  - Many studies use fixed-ratio (FR) schedules of drug self-administration [38] meaning that rats have to press a fixed number of times on the active lever to get one injection of drug (e.g., FR1, one active-lever press is required to get one intravenous drug injection). Under FR, the dose–response curve follows an inverted U-shaped curve [39–41]. In this context, both an increase and a decrease in the rate of lever-responding can reflect an increase in the reinforcing efficacy of a drug [42]. This can lead problems in interpretation data when studying drug-reinforcing efficacy [42]. In contrast, under a progressive ratio (PR) schedule of drug reinforcement, the dose–response curve is linear, at least for psychostimulant drugs [43]. Under a PR schedule, the number of lever presses needed to get each successive drug injection increases exponentially [42, 44, 45]. Thus, the drug becomes harder and harder to get, until rats cease earning injections. The last ratio reached before this point is termed "breakpoint," and the breakpoint is an index of the motivation to take the drug.

    **Note that it is important to adjust the behavioral measure used depending on the class of drug studied. As an example, PR responding for stimulants and opiates is different* [42].

    ***Note that other schedules of reinforcement exist. This includes variable ratio and variable interval schedules* [38]. *These schedules are less commonly used in drug self-administration studies in the rat.*
  - consider that rats acquired reliable drug self-administration, we use different criteria: (i) The number of presses on the active lever should be at least twice the number of lever presses on the inactive lever; (ii) The pattern of drug intake should be regularly distributed across the session, rather than taken in "bursts"; (iii) Rats should take a minimum number of drug injections within the session. These criteria have to be met for at least two successive sessions of drug self-administration. Criteria (ii) and (iii) are illustrated in Fig. 4

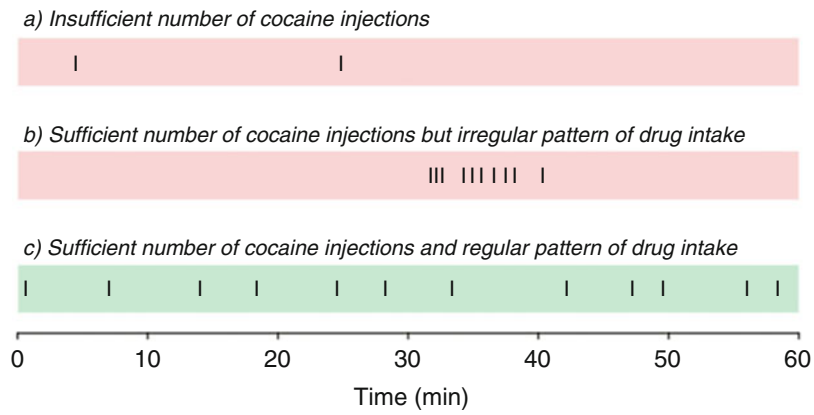

Fig. 4 Criteria for reliable drug self-administration. In this example, a rat is given a 1-h session with access to 0.25 mg/kg/injection of cocaine. Each tick mark represents a self-administered infusion. (**a, b**) These patterns of intake suggest that drug self-administration has not been acquired. (**c**) This pattern of intake, characterized by regular intake over the session, indicates reliable acquisition of cocaine self-administration behavior. It is recommended that rats show reliable drug intake on at least two consecutive sessions before proceeding to the next experimental steps

with an example where rats could self-administer cocaine (0.25 mg/kg/injection; 1-h sessions).

**Note that if there is a food training step before drug self-administration, data from the first drug self-administration session could be disregarded, because of potential carryover effects from past food self-administration sessions.*

**Note also that criterion* (iii) *for intravenous drug self-administration acquisition can vary depending on the class of drug tested but also on the dose used. Indeed, under FR, the dose–response function tends to follow an inverted U-shaped curve* [39–41].

– Rats typically self-administer most drugs humans consume [8, 24].

- From the acquisition of intravenous drug self-administration to the development of an addiction-like phenotype.

  In humans, taking a drug is not tantamount to being addicted to this drug. Many people experiment with potentially addictive drugs, but only a few will lose control over their drug use and develop a substance use disorder or addiction [46]. This is also the case in rats; a rat that reliably self-administers a drug is not necessarily a "drug-addicted" rat [47]. This is the reason why drug self-administration procedures have been developed to promote the development of addiction-like features, based on diagnostic criteria listed in the DSM [47–53]. Different variables can influence the development of addiction-like behavioral features in rats:

- **Drug dose**. For instance, in cocaine self-administration studies in rats, drug dose can influence the likelihood of seeing escalated drug intake [54–56].
- **Length of the self-administration session**. Generally, daily 1 or 2 h sessions are sufficient for rats to reliably self-administer a drug. However, to increase cumulative drug exposure, rats can be switched from short-access sessions (ShA; 1–2 h/day) to long-access sessions (LgA; 6+ h/day), where under both conditions, drug is continuously available to the rats [57]. Compared to ShA, LgA sessions promote an escalation in drug intake over time, and this effect has been observed with different classes of drugs—from opiates to stimulants ([56–59], but not with nicotine [60]). Compared to ShA, LgA drug intake can also promote the development of behavioral features of drug addiction [57, 59–61]. However, escalation of drug use over time is not necessary for rats to show such features [50, 62].

  **Note that the development of escalation also depends upon the drug* [60]*, the drug dose* [55]*, and the speed of intravenous drug delivery* [36, 63].
- **The pattern of drug use.** The temporal pattern of drug intake within each self-administration session is also decisive in predicting the development of addiction-relevant behavioral features [39, 50]. For instance, experienced cocaine users take their cocaine in an intermittent pattern within a bout of intoxication, achieving spikes and troughs in brain cocaine concentrations [64]. A recent self-administration procedure models this in rats, using an intermittent access (IntA) procedure. During an IntA session, rats have intermittent access to the drug-taking lever within each 6-h session (twelve 5–6 min ON periods intercalated with 25–26 min OFF periods; [35, 37, 65]). Just like rats given LgA sessions, rats given IntA sessions also escalate their cocaine use, but while LgA rats consume much more cocaine than IntA rats do, IntA rats develop more robust signs of drug addiction [35, 50, 62, 66–68]. Interestingly, even limited exposure to intermittent cocaine self-administration (2 h/day) is sufficient *to promote the development of addiction-relevant features* [69]. IntA and LgA cocaine intake also produces different, sometimes opposite changes in the brain, where IntA promotes a *hyper*dopaminergic response to cocaine, whereas LgA promotes a *hypo*dopaminergic response [68, 70, 71].
- **The speed of drug delivery**. Cocaine can be administered via different routes of administration (orally, intranasally, via inhalation or intravenously). Inhalation and intravenous injection are the two fastest methods of getting cocaine to

the brain, and the risk of addiction is also greatest with these two methods [72]. To study the effects of variation in the speed of drug delivery in a drug self-administration study, the experimenter can manipulate the speed of intravenous drug delivery by using different syringe pump motors in the operant cage (Fig. 3). As an example, to model rapid routes of cocaine administration (intravenous injection or via inhalation), each injection can be delivered rapidly (e.g., over 1–5 s using a syringe pump motor with 3.33 rotations per minute). Similarly, to model slower routes of cocaine administration (intranasal or oral route), each injection can be delivered over longer periods using a slower syringe pump motor (e.g., 0.1 RPM).

**Note that the volume of drug injected with the two motors differs. A 3.33 RPM motor delivers ~ 151 μL of liquid over 5 s while a 0.1 RPM motor delivers ~ 77 μL of liquid over 90 s* [37]. *Thus, in order to keep a similar concentration of cocaine delivered per injection, the drug solution to be used must be adjusted under each condition.*

Rats that take faster intravenous cocaine injections (e.g., injected over 5 s) develop more robust behavioral features of cocaine addiction compared to rats taking slower injections (e.g., 90 s), and this is the case regardless of whether rats are given LgA or IntA self-administration sessions [36, 37, 73, 74].

- Catheter patency should be verified at the end of an experiment. One way to do this is to give rats a passive intravenous injection of sodium thiopental solution (20 mg/mL in sterile water; CDMV, St Hyacinthe, Qc) or propofol (1 mg per 0.1 mL, CDMV, St-Hyacinthe, QC). Rats that do not become ataxic within 10 s of the injection should be excluded from data analysis because this suggests a compromised intravenous catheter.

  **Note that catheter patency can be checked during the experiment if there is doubt about catheter function. For example, if a rat does not acquire drug self-administration after several sessions, catheter patency can be checked. Under certain conditions, a new catheter can be implanted into the alternate vein.*

2.3.3 Studying the Reward System Using Intravenous Drug Self-Administration Procedures

Drugs of abuse from all classes interact with the brain's reward system [75, 76]. In its most reduced version, this system includes dopaminergic projections from the ventral tegmental area to the nucleus accumbens or ventral striatum ([75], also see Chapter 1 of the present book). Drugs of abuse increase dopamine neurotransmission in the nucleus accumbens, and one resulting effect is an increase in psychomotor activity, which includes horizontal and vertical exploratory behaviors, and also stereotypy [4]. Drug-

induced increases in psychomotor activity involve many neurotransmitter systems, but they are most tightly linked to drug-induced increases in dopamine neurotransmission ([4, 77, 78]; note, however, that drug-induced psychomotor activity can peak earlier than drug-induced dopamine concentrations [79–82]).

- Changes in drug-induced psychomotor activity with *acute* drug intake.

  Combining intravenous drug self-administration with a technique that can detect neurotransmitter levels in real time is an ideal way to study how drug taking influences dopamine neurotransmission in a given brain region [83–85]. Such techniques include in vivo fast-scan cyclic voltammetry, microdialysis, and selective biosensors. A complementary approach is to study how drug taking influences drug-induced psychomotor activity, as this is a more accessible and less invasive approach than quantitative neurochemical techniques. Measuring drug-induced psychomotor activity is of interest because, in particular for cocaine, brain concentrations of cocaine and dopamine and psychomotor activity follow similar time courses and are tightly linked. As an example, using a mathematical model to estimate brain cocaine concentrations [35, 37, 62, 65, 69, 70, 78, 86–90] during an intravenous cocaine self-administration session, we can show that estimated fluctuations in brain drug concentrations map tightly onto fluctuations in psychomotor activity (Fig. 5, red vs. black curve; also see [78, 83, 84, 90–92]). Thus, changes in psychomotor activity levels during cocaine self-

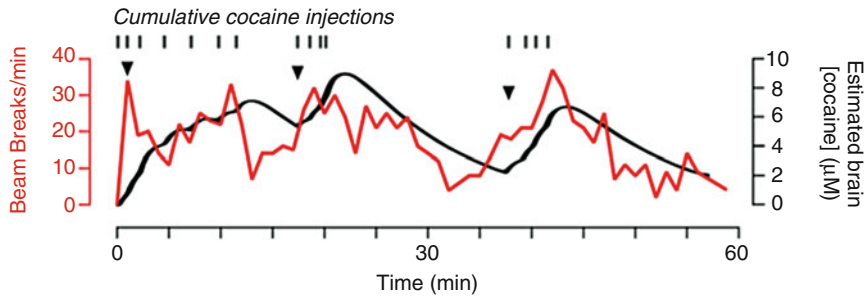

Fig. 5 During a cocaine self-administration session, estimated brain cocaine concentrations and locomotor activity are tightly coupled. In this example, a rat is lever pressing for 0.25 mg/kg/injection of cocaine during a 1-h session. The tick marks at the top represent self-administered infusions during the session. The red curve represents locomotor activity during the session (left Y-axis). Locomotion was measured with infrared photocells placed horizontally in the operant box (see Fig. 3). The black curve shows estimated brain cocaine concentrations during the session (right Y-axis). This curve was generated using a well-established pharmacokinetic model [88]. When the rat starts to self-administer cocaine, both brain cocaine concentrations and locomotor activity increase. The two variables follow a similar time course over the session, with three "spikes" in brain cocaine concentrations/locomotion following the initiation of three distinct bouts of cocaine intake (arrows)

administration could reflect changes in brain dopamine concentrations [77–79, 90, 93].

- Changes in drug-induced psychomotor activity with *chronic* drug intake.

  Chronic and intermittent exposure to a drug can potentiate the psychomotor activating effects of that drug and this is termed psychomotor sensitization [76, 94]. Psychomotor sensitization can be induced by *chronic drug self-administration* [26, 37, 69, 95–97]. The implication is that chronic drug intake can produce sensitization to both the psychomotor activating and reward-associated effects of a drug, in particular within the dopamine system [26, 37, 70, 71, 98]. Such findings support the view that the development of psychomotor sensitization and the development of drug addiction share common neural substrates [4, 76, 94]. As stated by Terry E. Robinson and Kent C. Berridge in their incentive salience theory of drug addiction, "The psychological process responsible for 'reward-related' psychomotor activation is the attribution of incentive salience. Although incentive salience may lead to locomotion and approach, because this psychological process makes stimuli in the environment more salient, attractive and 'wanted', these functions may be separable. [. . .] Increased psychomotor activation is just a correlate of sensitized incentive salience" [76]. Thus, an increase in drug-induced psychomotor activity over drug self-administration sessions can be an *indicator* of the development of increased incentive motivation for the drug. Indeed, the extend of psychomotor sensitization to self-administered cocaine positively correlates with the extent of incentive motivation for the drug, as measured by responding under a progressive ratio schedule of reinforcement [26, 37].

3 Conclusion

In this chapter, we described a useful technique to study the reinforcing effects of drugs of abuse. Many people take drugs but, fortunately, only a minority of drug users will develop a substance use disorder [46, 99–101]. Similarly, nonhuman laboratory animals readily take drugs, and under certain conditions we describe above, these animals can also show behavioral features that reflect some of the addiction diagnostic criteria described in the Diagnosis and Statistical Manual of Mental Disorders (DSM; [49]). Thus, the intravenous drug self-administration procedure can be used to effectively model these features in rats [39, 48, 50, 51, 102] and this holds great promise for understanding the behavioral, psychological, and neurobiological changes that mediate the transition to addiction in women and men.

References

1. Spragg SDS (1940) Morphine addiction in chimpanzees. Comp Psychol Monogr 15:1–132
2. Spanagel R (2017) Animal models of addiction. Dialogues Clin Neurosci 19 (3):247–258
3. Olmstead MC (2006) Animal models of drug addiction: where do we go from here? Q J Exp Psychol (Hove) 59(4):625–653. https://doi.org/10.1080/17470210500356308
4. Wise RA, Bozarth MA (1987) A psychomotor stimulant theory of addiction. Psychol Rev 94 (4):469–492
5. Volkow ND, Fowler JS, Wang GJ (2004) The addicted human brain viewed in the light of imaging studies: brain circuits and treatment strategies. Neuropharmacology 47(Suppl 1):3–13. https://doi.org/10.1016/j.neuropharm.2004.07.019
6. Negus SS, Henningfield J (2015) Agonist medications for the treatment of cocaine use disorder. Neuropsychopharmacology 40 (8):1815–1825. https://doi.org/10.1038/npp.2014.322
7. Olds J, Milner P (1954) Positive reinforcement produced by electrical stimulation of septal area and other regions of rat brain. J Comp Physiol Psychol 47(6):419–427. https://doi.org/10.1037/h0058775
8. Weeks JR (1962) Experimental morphine addiction: method for automatic intravenous injections in unrestrained rats. Science 138 (3537):143–144
9. Olds J (1956) Pleasure centers in the brain. Sci Am 195:105–116
10. Davis WM, Nichols JR (1963) A technique for self-injection of drugs in the study of reinforcement. J Exp Anal Behav 6:233–235. https://doi.org/10.1901/jeab.1963.6-233
11. Headlee CP, Coppock HW, Hichols JR (1955) Apparatus and technique involved in a laboratory method of detecting the addictiveness of drugs. J Am Pharm Assoc Am Pharm Assoc 44(4):229–231
12. Bozarth MA, Wise RA (1981) Intracranial self-administration of morphine into the ventral tegmental area in rats. Life Sci 28 (5):551–555. https://doi.org/10.1016/0024-3205(81)90148-x
13. Phillips AG, Mora F, Rolls ET (1981) Intracerebral self-administration of amphetamine by rhesus monkeys. Neurosci Lett 24 (1):81–86. https://doi.org/10.1016/0304-3940(81)90363-3
14. Goeders NE, Smith JE (1993) Intracranial cocaine self-administration into the medial prefrontal cortex increases dopamine turnover in the nucleus accumbens. J Pharmacol Exp Ther 265(2):592–600
15. Jarvik ME (1967) Tobacco smoking in monkeys. Ann NY Acad Sci 142:280–294
16. Carroll ME et al (1990) Cocaine-base smoking in rhesus monkeys: reinforcing and physiological effects. Psychopharmacology 102 (4):443–450. https://doi.org/10.1007/bf02247123
17. Myers RD, Carey R (1961) Preference factors in experimental alcoholism. Science 134 (3477):469–470
18. Grant KA, Samson HH (1985) Oral self administration of ethanol in free feeding rats. Alcohol 2(2):317–321
19. Bell SM et al (1993) Water deprivation-induced oral self-administration of cocaine in the Lewis rat: evidence for locomotor effects but not reinforcement. Pharmacol Biochem Behav 45(3):749–754
20. Bell SM et al (1995) The failure of cocaine to serve as an orally self-administered reinforcer in Lewis rats. Behav Pharmacol 6(4):366–374
21. Meisch RA (2001) Oral drug self-administration: an overview of laboratory animal studies. Alcohol 24(2):117–128
22. Gibaldi M, Levy G (1976) Pharmacokinetics in clinical practice I. Concepts. JAMA 235 (17):1864–1867
23. Jenkins AJ, Cone EJ (1998) Pharmacokinetics: drug absorption, distribution, and elimination. In: Karch SB (ed) Drug abuse handbook. CRC Press LLC., pp 165–215
24. Schuster CR, Thompson T (1969) Self administration of and behavioral dependence on drugs. Annu Rev Pharmacol 9:483–502. https://doi.org/10.1146/annurev.pa.09.040169.002411
25. Cabeza de Vaca S, Carr KD (1998) Food restriction enhances the central rewarding effect of abused drugs. J Neurosci 18 (18):7502–7510
26. Algallal H et al (2019) Sex differences in cocaine self-administration behaviour under long access versus intermittent access conditions. Addict Biol. https://doi.org/10.1111/adb.12809
27. Bongiovanni M, See RE (2008) A comparison of the effects of different operant training experiences and dietary restriction on the reinstatement of cocaine-seeking in rats. Pharmacol Biochem Behav 89(2):227–233.

https://doi.org/10.1016/j.pbb.2007.12.019

28. Ferrario CR et al (2005) Neural and behavioral plasticity associated with the transition from controlled to escalated cocaine use. Biol Psychiatry 58(9):751–759. https://doi.org/10.1016/j.biopsych.2005.04.046
29. Figueroa-Guzman Y et al (2011) Oral administration of levo-tetrahydropalmatine attenuates reinstatement of extinguished cocaine seeking by cocaine, stress or drug-associated cues in rats. Drug Alcohol Depend 116 (1–3):72–79. https://doi.org/10.1016/j.drugalcdep.2010.11.023
30. McFarland K, Lapish CC, Kalivas PW (2003) Prefrontal glutamate release into the core of the nucleus accumbens mediates cocaine-induced reinstatement of drug-seeking behavior. J Neurosci 23(8):3531–3537
31. Rowland NE (2007) Food or fluid restriction in common laboratory animals: balancing welfare considerations with scientific inquiry. Comp Med 57(2):149–160
32. Davis JD (1966) A method for chronic intravenous infusion in freely moving rats. J Exp Anal Behav 9(4):385–387. https://doi.org/10.1901/jeab.1966.9-385
33. Weeks JR, Davis JD (1964) Chronic Intravenous Cannulas for Rats. J Appl Physiol 19:540–541
34. Samaha AN, Minogianis EA, Nachar W (2011) Cues paired with either rapid or slower self-administered cocaine injections acquire similar conditioned rewarding properties. PLoS One 6(10):e26481. https://doi.org/10.1371/journal.pone.0026481
35. Zimmer BA, Oleson EB, Roberts DC (2012) The motivation to self-administer is increased after a history of spiking brain levels of cocaine. Neuropsychopharmacology 37 (8):1901–1910. https://doi.org/10.1038/npp.2012.37
36. Wakabayashi KT et al (2010) Rats markedly escalate their intake and show a persistent susceptibility to reinstatement only when cocaine is injected rapidly. J Neurosci 30 (34):11346–11355. https://doi.org/10.1523/JNEUROSCI.2524-10.2010
37. Allain F et al (2017) Intermittent intake of rapid cocaine injections promotes robust psychomotor sensitization, increased incentive motivation for the drug and mGlu2/3 receptor dysregulation. Neuropharmacology 117:227–237. https://doi.org/10.1016/j.neuropharm.2017.01.026
38. Spealman RD, Goldberg SR (1978) Drug self-administration by laboratory animals: control by schedules of reinforcement. Annu Rev Pharmacol Toxicol 18:313–339. https://doi.org/10.1146/annurev.pa.18.040178.001525
39. Allain F et al (2015) How fast and how often: the pharmacokinetics of drug use are decisive in addiction. Neurosci Biobehav Rev 56:166–179. https://doi.org/10.1016/j.neubiorev.2015.06.012
40. Oleson EB, Roberts DC (2009) Behavioral economic assessment of price and cocaine consumption following self-administration histories that produce escalation of either final ratios or intake. Neuropsychopharmacology 34(3):796–804. https://doi.org/10.1038/npp.2008.195
41. Sizemore GM et al (1997) Dose-effect functions for cocaine self-administration: effects of schedule and dosing procedure. Pharmacol Biochem Behav 57(3):523–531
42. Arnold JM, Roberts DC (1997) A critique of fixed and progressive ratio schedules used to examine the neural substrates of drug reinforcement. Pharmacol Biochem Behav 57 (3):441–447
43. French ED et al (1995) A comparison of the reinforcing efficacy of PCP, the PCP derivatives TCP and BTCP, and cocaine using a progressive ratio schedule in the rat. Behav Pharmacol 6(3):223–228
44. Hodos W (1961) Progressive ratio as a measure of reward strength. Science 134 (3483):943–944
45. Richardson NR, Roberts DC (1996) Progressive ratio schedules in drug self-administration studies in rats: a method to evaluate reinforcing efficacy. J Neurosci Methods 66(1):1–11
46. Anthony JC, Warner LA, Kessler RC (1994) Comparative epidemiology of dependence on tobacco, alcohol, controlled substances, and inhalants: basic findings from the national comorbidity survey. Exp Clin Psychopharmacol 2:244–268
47. Deroche-Gamonet V, Belin D, Piazza PV (2004) Evidence for addiction-like behavior in the rat. Science 305(5686):1014–1017. https://doi.org/10.1126/science.1099020
48. Ahmed SH (2012) The science of making drug-addicted animals. Neuroscience 211:107–125. https://doi.org/10.1016/j.neuroscience.2011.08.014
49. APA (2013) DSM V Diagnostic and statistical manual of mental disorders. American Psychiatric Association
50. Kawa AB et al (2019) The transition to cocaine addiction: the importance of

pharmacokinetics for preclinical models. Psychopharmacology 236(4). https://doi.org/10.1007/s00213-019-5164-0

51. Roberts DC, Morgan D, Liu Y (2007) How to make a rat addicted to cocaine. Prog Neuro-Psychopharmacol Biol Psychiatry 31 (8):1614–1624. https://doi.org/10.1016/j.pnpbp.2007.08.028
52. Everitt BJ, Giuliano C, Belin D (2018) Addictive behaviour in experimental animals: prospects for translation. Philos Trans R Soc Lond Ser B Biol Sci 373(1742). https://doi.org/10.1098/rstb.2017.0027
53. Lynch WJ (2018) Modeling the development of drug addiction in male and female animals. Pharmacol Biochem Behav 164:50–61. https://doi.org/10.1016/j.pbb.2017.06.006
54. Mantsch JR et al (2001) Predictable individual differences in the initiation of cocaine self-administration by rats under extended-access conditions are dose-dependent. Psychopharmacology 157(1):31–39
55. Mantsch JR et al (2004) Effects of extended access to high versus low cocaine doses on self-administration, cocaine-induced reinstatement and brain mRNA levels in rats. Psychopharmacology 175(1):26–36. https://doi.org/10.1007/s00213-004-1778-x
56. Kitamura O et al (2006) Escalation of methamphetamine self-administration in rats: a dose-effect function. Psychopharmacology 186(1):48–53. https://doi.org/10.1007/s00213-006-0353-z
57. Ahmed SH, Koob GF (1998) Transition from moderate to excessive drug intake: change in hedonic set point. Science 282 (5387):298–300
58. Ahmed SH, Koob GF (1999) Long-lasting increase in the set point for cocaine self-administration after escalation in rats. Psychopharmacology 146(3):303–312
59. Ahmed SH, Walker JR, Koob GF (2000) Persistent increase in the motivation to take heroin in rats with a history of drug escalation. Neuropsychopharmacology 22(4):413–421. https://doi.org/10.1016/S0893-133X(99)00133-5
60. Paterson NE, Markou A (2004) Prolonged nicotine dependence associated with extended access to nicotine self-administration in rats. Psychopharmacology 173(1–2):64–72. https://doi.org/10.1007/s00213-003-1692-7
61. Paterson NE, Markou A (2003) Increased motivation for self-administered cocaine after escalated cocaine intake. Neuroreport 14 (17):2229–2232. https://doi.org/10.1097/01.wnr.0000091685.94870.ba
62. Allain F, Bouayad-Gervais K, Samaha AN (2018) High and escalating levels of cocaine intake are dissociable from subsequent incentive motivation for the drug in rats. Psychopharmacology 235(1):317–328. https://doi.org/10.1007/s00213-017-4773-8
63. Bouayad-Gervais K et al (2014) The self-administration of rapidly delivered cocaine promotes increased motivation to take the drug: contributions of prior levels of operant responding and cocaine intake. Psychopharmacology 231(21):4241–4252. https://doi.org/10.1007/s00213-014-3576-4
64. Beveridge TJR et al (2012) Analyzing human cocaine use patterns to inform animal addiction model development. Published abstract for the College on Problems of Drug Dependence Annual Meeting, Palm Springs, CA
65. Zimmer BA, Dobrin CV, Roberts DC (2011) Brain-cocaine concentrations determine the dose self-administered by rats on a novel behaviorally dependent dosing schedule. Neuropsychopharmacology 36 (13):2741–2749. https://doi.org/10.1038/npp.2011.165
66. James MH et al (2019) Increased number and activity of a lateral subpopulation of hypothalamic orexin/hypocretin neurons underlies the expression of an addicted state in rats. Biol Psychiatry 85(11):925–935. https://doi.org/10.1016/j.biopsych.2018.07.022
67. Kawa AB, Bentzley BS, Robinson TE (2016) Less is more: prolonged intermittent access cocaine self-administration produces incentive-sensitization and addiction-like behavior. Psychopharmacology 233 (19–20):3587–3602. https://doi.org/10.1007/s00213-016-4393-8
68. Kawa AB, Valenta AC, Kennedy RT, Robinson TE (2019) Incentive and dopamine sensitization produced by intermittent but not long access cocaine self-administration. Eur J Neurosci. 50(4):2663–2682
69. Allain F, Samaha AN (2018) Revisiting long-access versus short-access cocaine self-administration in rats: intermittent intake promotes addiction symptoms independent of session length. Addict Biol 24 (4):641–651. https://doi.org/10.1111/adb.12629
70. Calipari ES et al (2014) Intermittent cocaine self-administration produces sensitization of stimulant effects at the dopamine transporter. J Pharmacol Exp Ther 349(2):192–198. https://doi.org/10.1124/jpet.114.212993

71. Calipari ES et al (2013) Temporal pattern of cocaine intake determines tolerance vs sensitization of cocaine effects at the dopamine transporter. Neuropsychopharmacology 38 (12):2385–2392. https://doi.org/10.1038/npp.2013.136
72. Hatsukami DK, Fischman MW (1996) Crack cocaine and cocaine hydrochloride. Are the differences myth or reality? JAMA 276 (19):1580–1588
73. Gueye AB, Allain F, Samaha AN (2019) Intermittent intake of rapid cocaine injections promotes the risk of relapse and increases mesocorticolimbic BDNF levels during abstinence. Neuropsychopharmacology 44 (6):1027–1035. https://doi.org/10.1038/s41386-018-0249-8
74. Minogianis EA, Levesque D, Samaha AN (2013) The speed of cocaine delivery determines the subsequent motivation to self-administer the drug. Neuropsychopharmacology 38(13):2644–2656. https://doi.org/10.1038/npp.2013.173
75. Koob GF, Nestler EJ (1997) The neurobiology of drug addiction. J Neuropsychiatry Clin Neurosci 9(3):482–497. https://doi.org/10.1176/jnp.9.3.482
76. Robinson TE, Berridge KC (1993) The neural basis of drug craving: an incentive-sensitization theory of addiction. Brain Res Brain Res Rev 18(3):247–291
77. Nicolaysen LC, Pan HT, Justice JB Jr (1988) Extracellular cocaine and dopamine concentrations are linearly related in rat striatum. Brain Res 456(2):317–323
78. Shou M et al (2006) Monitoring dopamine in vivo by microdialysis sampling and on-line CE-laser-induced fluorescence. Anal Chem 78(19):6717–6725. https://doi.org/10.1021/ac0608218
79. Minogianis EA et al (2018) Varying the rate of intravenous cocaine infusion influences the temporal dynamics of both drug and dopamine concentrations in the striatum. Eur J Neurosci, ePub: doi:https://doi.org/10.1111/ejn.13941
80. Kalivas PW, Duffy P (1990) Effect of acute and daily cocaine treatment on extracellular dopamine in the nucleus accumbens. Synapse 5(1):48–58. https://doi.org/10.1002/syn.890050104
81. Gerasimov MR et al (2000) Comparison between intraperitoneal and oral methylphenidate administration: a micradialysis and locomotor activity study. J Pharmacol Exp Ther 295(1):51–57
82. Benwell ME, Balfour DJ (1992) The effects of acute and repeated nicotine treatment on nucleus accumbens dopamine and locomotor activity. Br J Pharmacol 105(4):849–856. https://doi.org/10.1111/j.1476-5381.1992.tb09067.x
83. Pettit HO, Justice JB Jr (1989) Dopamine in the nucleus accumbens during cocaine self-administration as studied by in vivo microdialysis. Pharmacol Biochem Behav 34 (4):899–904
84. Pettit HO, Justice JB Jr (1991) Effect of dose on cocaine self-administration behavior and dopamine levels in the nucleus accumbens. Brain Res 539(1):94–102
85. Phillips PE et al (2003) Subsecond dopamine release promotes cocaine seeking. Nature 422 (6932):614–618. https://doi.org/10.1038/nature01476
86. Martin-Garcia E et al (2014) Frequency of cocaine self-administration influences drug seeking in the rat: optogenetic evidence for a role of the prelimbic cortex. Neuropsychopharmacology 39(10):2317–2330. https://doi.org/10.1038/npp.2014.66
87. Nicola SM, Deadwyler SA (2000) Firing rate of nucleus accumbens neurons is dopamine-dependent and reflects the timing of cocaine-seeking behavior in rats on a progressive ratio schedule of reinforcement. J Neurosci 20 (14):5526–5537
88. Pan HT, Menacherry S, Justice JB Jr (1991) Differences in the pharmacokinetics of cocaine in naive and cocaine-experienced rats. J Neurochem 56(4):1299–1306
89. Samaha AN, Li Y, Robinson TE (2002) The rate of intravenous cocaine administration determines susceptibility to sensitization. J Neurosci 22(8):3244–3250. doi:20026273
90. Wise RA et al (1995) Fluctuations in nucleus accumbens dopamine concentration during intravenous cocaine self-administration in rats. Psychopharmacology 120(1):10–20
91. Church WH, Justice JB Jr, Byrd LD (1987) Extracellular dopamine in rat striatum following uptake inhibition by cocaine, nomifensine and benztropine. Eur J Pharmacol 139 (3):345–348
92. Di Chiara G, Imperato A (1988) Drugs abused by humans preferentially increase synaptic dopamine concentrations in the mesolimbic system of freely moving rats. Proc Natl Acad Sci U S A 85(14):5274–5278
93. Hurd YL, Kehr J, Ungerstedt U (1988) In vivo microdialysis as a technique to monitor drug transport: correlation of extracellular

cocaine levels and dopamine overflow in the rat brain. J Neurochem 51(4):1314–1316

94. Robinson TE, Berridge KC (2000) The psychology and neurobiology of addiction: an incentive-sensitization view. Addiction 95 (Suppl 2):S91–S117
95. Hooks MS et al (1994) Behavioral and neurochemical sensitization following cocaine self-administration. Psychopharmacology 115 (1–2):265–272
96. Phillips AG, Di Ciano P (1996) Behavioral sensitization is induced by intravenous self-administration of cocaine by rats. Psychopharmacology 124(3):279–281
97. Minogianis EA et al (2019) Role of the orbitofrontal cortex and the dorsal striatum in incentive motivation for cocaine. Behav Brain Res 372:112026. https://doi.org/10.1016/j.bbr.2019.112026
98. Calipari ES et al (2015) Brief intermittent cocaine self-administration and abstinence sensitizes cocaine effects on the dopamine transporter and increases drug seeking. Neuropsychopharmacology 40(3):728–735. https://doi.org/10.1038/npp.2014.238
99. UNODC (2017) United Nations Office on Drugs and Crime World Drug Report 2017
100. Goldstein A, Kalant H (1990) Drug policy: striking the right balance. Science 249 (4976):1513–1521
101. Nutt D et al (2007) Development of a rational scale to assess the harm of drugs of potential misuse. Lancet 369(9566):1047–1053. https://doi.org/10.1016/S0140-6736(07)60464-4
102. Lynch WJ et al (2010) Animal models of substance abuse and addiction: implications for science, animal welfare, and society. Comp Med 60(3):177–188

Chapter 12

Viral Vectors for Studying Drug-Seeking Behavior

Arlene Martínez-Rivera, Caitlin E. Burgdorf, and Anjali M. Rajadhyaksha

Abstract

Addiction to drugs of abuse represents a significant public health concern worldwide. After decades of studies, clinical treatments are lacking. The understanding of mechanisms within the reward pathway modified by drugs of abuse has made a breakthrough in recent years with the development of various techniques. In particular, many of the latest advances in preclinical research investigating drugs of abuse are largely due to the use of different viral vectors strategies. Using viral vector strategies in transgenic mice, investigators can manipulate genes at the level of neuronal cell types and brain-specific circuits. In addition, techniques that depend on viral vector approaches, such as opto- and chemo-genetics, have provided a better understanding of circuits recruited during drug-related behaviors. In this chapter, we describe the advantages and disadvantages of different viral vector tools and the method by which these viral vectors can be used in conjunction with transgenic mouse lines for the study of drug-seeking behavior. Next, we focus on different techniques using viral vectors for functional manipulation such as genetic manipulation, chemogenetics, and optogenetics. Then, we discuss various techniques that can be used to observe natural neuronal activity during drug-related behaviors such as two-photon microscopy, one-photon microscopy, and fiber photometry. We bring the chapter to a close with a brief discussion of newly developed techniques that can be used to study molecular mechanisms underlying drug-seeking behavior and discuss the success and challenges of using viral vectors for clinical treatments and therapies.

Key words Adenovirus, Adeno-associated virus, DREADDs, Herpes simplex virus, In vivo calcium imaging, Optogenetics, Retrovirus, Rodent brain

1 Introduction

The discovery that numerous brain disorders, including addiction, involve changes in gene expression within complex neural networks has placed an emphasis on determining the brain regions, cell types, and circuits by which these genes drive behaviors. The ability to manipulate and study the brain at genetic levels in combination with behavioral testing has contributed enormously to our current understanding of the neurobiology of addiction and brain mechanisms that enable different aspects of drug-seeking behaviors. These

Arlene Martínez-Rivera and Caitlin E. Burgdorf contributed equally to this work.

Marc Fakhoury (ed.), *The Brain Reward System*, Neuromethods, vol. 165, https://doi.org/10.1007/978-1-0716-1146-3_12,

studies have been primarily possible through the use of viral vectors which are genetically modified tools designed for the delivery of genetic material into cells.

In the 1960s, the ability of retroviruses to insert their DNA into a host cell was discovered independently by Howard Temin and David Baltimore. Later in the mid-1970s, Varmus and Bishop's meticulous study resulted in the discovery that retroviruses can incorporate an oncogene into the chromosomes of infected cells and reengineer the cellular processes [1]. This was the first step for the use of retroviruses for genetic engineering. At the same time, Paul Baerg developed a technique to join DNA from a monkey tumor virus with DNA from bacterial virus [2], giving rise to what is known today as recombinant DNA technology. Since then, different viral vectors have been developed to manipulate and study the role of genes for the understanding of normal brain function as well as disease pathophysiology, with recent studies examining this at the cell type and circuit-specific level.

The development of viral vectors has greatly benefitted behavioral neuroscience studies because of the ability to manipulate genes in a cell type, circuit, and temporal manner. Additionally, techniques such as optogenetics, chemogenetics, and fiber photometry utilize viral vectors to manipulate specific brain regions, cell-type populations, and distinct neuronal circuitry to deepen the scientific understanding of different neuropsychiatric disorders including drug-seeking behavior. Our understanding of the mechanisms underlying drug-seeking behavior that is associated with substance use disorders would have been impossible without the development and use of viral vectors.

In this chapter, we emphasize viral vector technology used to study genes involved in drug-seeking behavior in order to better understand substance use disorder. First, we describe the different types of viral vectors used in the field of neuroscience and the method used for the delivery of these viral vectors into the mouse brain. In addition, we provide a brief description of two commonly used behavioral protocols to study drug-seeking behavior in animal models. In the next section, we focus on different vectors strategies for gene manipulation, and we discuss how viral vectors can be used to manipulate cells and circuits during drug-seeking behavior.

Next, we discuss different behavioral applications using viral vectors for functional manipulation during drug-seeking behavior followed by a section of how viral vectors have been beneficial to study natural neural activity during drug-seeking behavior using in vivo calcium imaging. Furthermore, we address emerging techniques that can be used to investigate neuronal mechanisms underlying drug-seeking behavior. Lastly, we provide examples of viral techniques currently being used in clinical trials.

2 Materials

2.1 Types of Viral Vectors

Viral vectors can be utilized to manipulate genes in a brain region and cell type-specific manner in order to silence or overexpress a gene or can be used as a tool to manipulate or monitor neuronal activity in a region, cell type, or circuit-specific manner. Each viral vector that has been developed and optimized has its advantages and disadvantages [3, 4], which should be carefully considered to best fit the research needs of the scientific question. First, the type of vector is selected based on the individual needs of the experiment. In preclinical research, the most commonly used viral vectors are adenovirus, adeno-associated virus (AAV), herpes simplex virus (HSV), and retrovirus (most commonly lentivirus). For gene therapy in clinical research trials, the most commonly used viral vectors were historically retrovirus vectors. However, more recently, AAV has been gaining preference due to its lower immunogenicity [5–8]. In addition, each viral construct differs in transduction efficiency, onset and duration of expression, tropism (preference of expression in particular cell types of tissue), transgene size limitations, and ability to express in the presence of a particular promoter (outlined in Table 1).

2.1.1 Adenovirus

Adenoviruses carry double-stranded DNA with a capacity to express a transgene up to 8 kb in size and infect both dividing and nondividing cells with extremely high efficacy. Since the virus enters the cell via the coxsackie/adenovirus receptor (CAR), adenoviruses have a broad tropism, allowing for infection in a large range of tissues and cell types with a fast expression profile within a day following injection. Adenoviruses are easily purified and can be produced in high titers with a packaging capacity larger than other adeno-associated viruses (discussed below). However, the biggest limitation of adenoviruses is the high immune response following infection which has the potential to decrease vector-mediated transgene expression. In addition, the immune response limits expression to 2–3 weeks following injection. Due to the potential probability of producing replication-competent adenovirus, additional biosafety cautions must be used when handling this virus in the laboratory.

2.1.2 Adeno-Associated Virus (AAV)

AAV-mediated gene transfer has developed into the most popular viral vector due to its efficient and persistent expression in a wide range of cell types including neurons and glial cells in the brain [33]. In addition, AAV vectors have minimal pathogenicity and low immunogenicity and have begun to be used in clinical applications. AAVs package single-stranded linear DNA and the viral genome does not integrate into the host genome in the rodent brain [14]. The AAV reaches maximal expression 3–4 weeks after

Table 1
Characteristics of viral vector types

Characteristic	Adenovirus	AAV	Retrovirus	HSV
Genetic material of wild-type virus	Double-stranded linear DNA (36 kb)	Single-stranded DNA (4.7 kb)	Diploid positive strand RNA (9.2 kb)	Double-stranded linear DNA (152 kb)
Insert capacity	<7.5 kb	<4.7 kb	8 kb	>30 kb
Onset of in vivo expression	1 day–1 week	1–3 weeks	1–2 weeks	1–2 days
Duration of in vivo expression in brain	10 days to 6 months	>6 months	>6 months	1–2 weeks
Integration of genetic material	No	No	Yes	No
Achievable titer	High	High	Low	High
Viral tropism	Diving and nondividing cells (cell type depends on serotype)	Diving and nondividing cells (cell type depends on serotype)	Dividing cells only (murine vectors)/diving and nondividing cells (lentiviral vectors)	Diving and nondividing cells
Promoter flexibility	Yes	Yes	Yes	Yes
Safety issues	Immune and inflammatory response (biosafety level 2)	Low cloning capacity	Insertional mutagenesis and instability of vectors	Immune and inflammatory response Possible toxicities and recombination risk
References	[9–13]	[14–20]	[21–26]	[27–32]

injection and can last in the brain for several months to years [34, 35]. Although AAV vectors are often the preferred tool to target transgene expression, the vector size is limited to 4.7 kb [4], hindering it as a means to express genes greater than this size. However, the diversity of serotypes which differ in tropism and viral spread in the brain allows greater selection for particular cell types or tissue [36].

AAVs have become the most widely used tool in neuroscience to study gene function (e.g., using the Cre–Lox system) and cell- and circuit-level function (opto- and chemo-genetic strategies), including their use in models of drug reward and drug-seeking behaviors [37–39] as discussed below.

2.1.3 Retrovirus

The retrovirus was the first method by which gene transfer was performed. Viruses of the retrovirus family are formed of single-stranded RNA that reverse-transcribe their genetic material into double-stranded viral DNA and integrate transgenes up to 8 kb into the host genome to allow for highly efficient, long-term, stable gene expression, [33, 40]. Retroviral vectors are composed of "split-vector systems" that separate viral genes and transgene expression across different plasmids. However, retroviruses can randomly integrate into the host genome [3].

Retroviruses can be classified as simple or complex and differ on whether they transduce dividing or nondividing cells, respectively, an important consideration in the brain. For example, Gammaretrovirus is the most commonly used simple retroviruses in cancer stem cell research, but its expression is limited to dividing cells [3]. As a result, Gammaretroviruses have been most used in the brain with neural stem cells such as in the case of neurogenesis due to the presence of dividing neurons. Gammaretroviruses can be used to express a gene of interest or express RNA interference (RNAi) to silence a gene and can be used in combination with Cre–Lox technology or CRISPR technology. A more commonly used retrovirus in the brain is lentiviruses. Lentiviral vectors, derived from the human immunodeficient virus (HIV), are used to infect nondividing cells such as mature neurons [40]. Lentivirus vectors are an effective tool to both overexpress a transgene or for expression of small interfering RNA (siRNA)/short-hairpin RNA (shRNA) to assess the function of that gene in a brain region [41]. In addition, with the use of inducible lentiviral vectors, the effect of the transgene expression can be examined within the same animal or across groups using doxycycline-on or -off states [41].

2.1.4 Herpes Simplex Virus (HSV)

HSV-1 is an enveloped double-stranded DNA virus that preferentially infects neurons for local modification of gene expression. Although HSV does not integrate into the genome, the virus causes latent infection of transgenes up to 150 kbp in size [42], allowing

for incorporation of large genes. A key characteristic of HSV-derived vectors is the quick and transient transgene expression of 2–5 days in vivo following injection [35]. Although transgene expression in the brain is temporally limited, this can also act as an advantage by allowing researchers to test the effect of transgene expression before and after manipulation. In this way, investigators can examine whether behavioral changes parallel fluctuations in transgene expression and if this results in long-lasting changes in behavior [43].

3 Methods

3.1 Vector Preparation and Resources

Many frequently used viral vectors are commercially available for purchase from viral vector cores at academic institutions or other commercial sources. If a new viral vector must be designed, one can design the vector within the laboratory (for brief instructions, see [44]) or order a new virus from a viral vector core after providing them with the viral sequence and vector type of interest. Based on the requirements of the experiment and scientific question, a viral vector type is chosen from those described above. Other considerations include choice of serotype that dictates tropism and spread, promoter-specific expression for cell-type specificity, and fluorescent tags. In addition to considering known viral vector characteristics, some techniques such as optogenetics or chemogenetics have historically only used AAVs to express the transgene required for the technique, which should be considered when choosing the viral vector.

3.2 Stereotaxic Surgery

3.2.1 Viral Vector Injection

Stereotaxic brain surgery is a well-established technique used in behavioral neuroscience to microinject viral vectors into distinct rodent brain regions of anesthetized animals to obtain temporal- and region-specific control [45]. Stereotaxic surgery is also used for the implantation of hardware such as guide cannulas and optical fibers for optogenetic or fiber photometry applications. Briefly, mice are anesthetized with the desired anesthetic (i.e., isoflurane, pentobarbital, ketamine), and the head of the mice is shaved and disinfected. Then, the mouse is placed in the stereotaxic apparatus in order to restrain its head in a stable position, and it is locally injected with an anesthetic (i.e., lidocaine), followed by an anterior to posterior incision to expose the skull. Once the head is aligned and flattened using bregma and lambda as a reference, the investigator obtains the coordinates for bregma; anterior posterior (AP), medial lateral (ML), and dorsal ventral (DV). Using the bregma coordinates as a reference, the investigator locates the desired brain region with known coordinates of that region [46]. For viral injection, small holes are drilled in the skull of the mouse, and a microinfusion needle is lowered into the desired area.

The volume of virus to be injected depends on various factors such as the type of virus, virus serotype, and promoter selection [35, 47], as well as some intrinsic factors such as the brain region of interest and the cell type to be targeted [35]. For example, a common amount of AAV injected in different brain regions within the reward pathway fluctuates between 200 and 500 nL [48–50], at an infusion rate of 0.1–0.2 μL/min [51], and a titer of 10^{12}–10^{13} vg/mL [51]. HSV usually requires a higher volume infusion, when compared with AAVs [35]. After virus infusion, the microinfusion needle is retracted, and the exposed skull is covered and sealed by tissue sutures or tissue glue. Animals are allowed to recover before any behavioral test. The timing of behavioral testing is coordinated to the time course and peak expression of the virus used.

3.2.2 Instrument Implantation

For implantation of instruments such as optic fibers or cannulas, preparation of the animal for stereotaxic surgery is the same as that discussed above. In this case, once the desired brain region is located using known coordinates, the investigator proceeds to drill unilateral or bilateral holes. The instrument is implanted in these coordinates, and the depth of the instrument is carefully chosen based on the type of instrument. For example, in a recent publication from our laboratory [50], following injection of the virus, an optic fiber is implanted unilaterally 0.1 mm (DV) above the desired brain region and is secured with adhesive cement material.

3.3 Behavioral Models to Study cocaine Reward and Drug-Seeking Behavior

The use of different preclinical models in behavioral neuroscience has been imperative for the neurobiological understanding of drug addiction. Different behavioral paradigms (contingent and non-contingent) have been well established for the study of drug-seeking behavior in rodents. Using viral vectors, investigators can study different phases of the drug-seeking behavior such as acquisition, extinction, and reinstatement of drug-seeking behavior. The operant drug self-administration paradigm is the most common behavioral paradigm and its origin hails from the studies of B.F. Skinner. In this paradigm, animals are trained in a box to self-administer the drug by an operant behavior such as a lever press or a nose poke. The delivery of the drug is usually paired with an environmental cue (discriminative stimuli) that triggers an association between the rewarding (or reinforcing) effects of the drug and the environmental cue.

Although the drug self-administration paradigm is the most translational behavioral paradigm, other noncontingent paradigms have also shed light on the reinforcing effects of several drugs. One of the most common noncontingent protocol, in which the experimenter administers the drug to the animals, is conditioned place preference (CPP). The CPP behavioral model, in which an unconditioned stimulus (drug effect) is paired with a conditioned

stimulus (specific environment) is a model of a Pavlovian conditioning. In this kind of conditioning, a preference is developed for a specific environment based on the learned association with the rewarding effects of the drug. The animal learns to associate a certain environment with an investigator-administered drug treatment and then learns to associate another environment with the absence of the drug or investigator-administered vehicle treatment. After several training days, the animal acquires a preference (or aversion) for the drug treatment effects.

In our studies of drug-seeking behavior using CPP, we use a three-chamber apparatus (Med Associates, Inc.). Each chamber is divided by sliding doors and is wired with photo-beams that connects to a computer to track and record the animal location. Each chamber has different colors and floor texture. The middle chamber is gray with a smooth surface floor, while each preference chamber is black or white, with a floor comprised of either a metal grid or metal rods [52].

4 Viral Vector Strategies for Gene Manipulation in Rodent Brain

Behavioral neuroscience research has taken advantage of viral vector-mediated manipulation of genes in combination with behavioral testing to address the specific role of a gene in a particular brain region, population of neurons, or circuit in various aspects of drug-seeking behaviors. The use of viral vectors overcome limitations of traditional knockout or transgenic animals including lack of brain region specificity or lack of temporal control [7, 53]. Only within the past few decades, the emergence of novel viral vector techniques has allowed researchers to manipulate cellular activity with region, cell type, and projection specificity in awake, behaving mice. As behavior is a key component of drug-motivated behavior, these technologies have been instrumental in determining genetic, cellular, and pathway-specific contributions to addiction.

4.1 Cre–Lox Brain-Region–Specific Conditional Gene Knockout

Viral vectors can be utilized to manipulate genes through various mechanisms. One of the most widely used strategies to test gene function in selected brain regions or cell types is via conditional gene inactivation using the DNA recombinase Cre and its ability to recognize LoxP sites (Fig. 1a). The Cre–Lox approaches can be utilized to study the region-specific, cell type specific, and projection-specific roles of a transgene. For example, in a recent study from our laboratory that examined the role of the $Ca_v1.2$ L-type calcium channel in hippocampal subregions [48], floxed mice that had the *cacna1c* gene encoding $Ca_v1.2$ flanked by two LoxP sites were injected with AAV–Cre into the dorsal hippocampus or the ventral hippocampus in order to delete $Ca_v1.2$ from either subregion. Following viral expression, mice were trained and tested

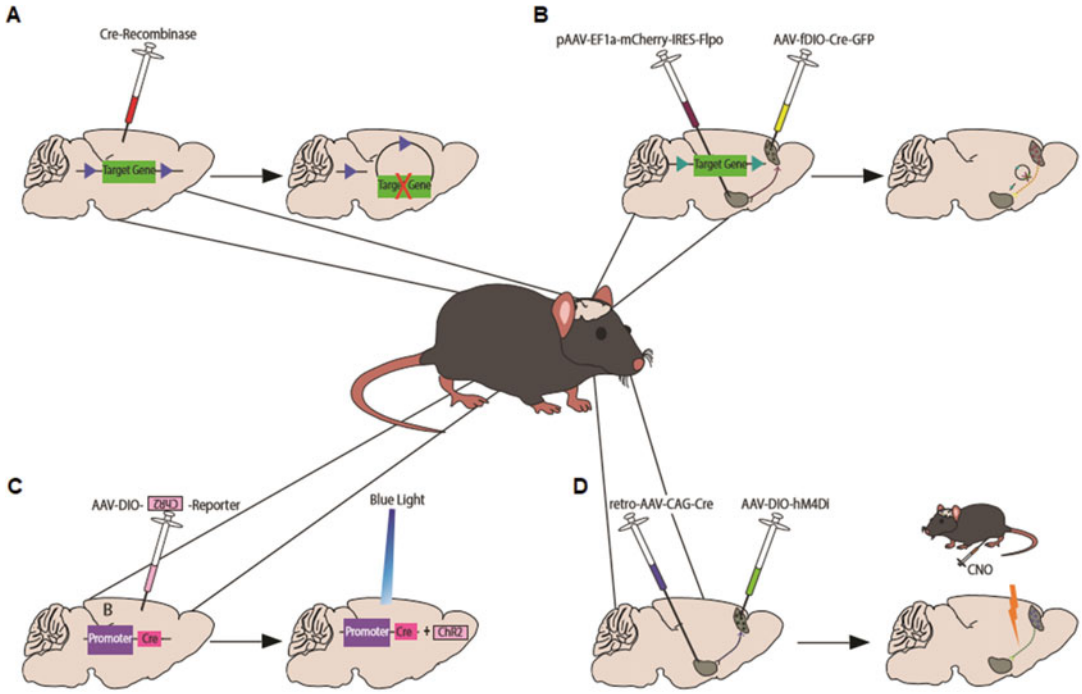

Fig. 1 Cre-recombinase strategies in rodents. (**a**) Deletion of a gene in brain region- or cell type–specific manner using floxed mice. Triangle represents LoxP sites. (**b**) FLP–FRT strategy to delete a gene in a pathway-specific manner using floxed mice. (**c**) Expression of optogenetically controlled proteins such as channelrhodopsin (ChR2) in a cell type-specific manner using mouse driver lines expressing Cre recombinase under the control of specific promoters and activation of ChR2 using blue light. (**d**) Circuit-specific expression of DREADD such as the inhibitory DREADD hM4Di using a retrograde AAV and Cre-dependent viruses. Further manipulation of these DREADDs can be achieved by systemically injection of CNO

in cocaine-conditioned place preference (CPP) and were subsequently run through extinction training. Mice that had $Ca_v1.2$ deleted in the dorsal hippocampus, but not ventral hippocampus, were unable to extinguish the cocaine CPP, demonstrating a role of $Ca_v1.2$ within the dorsal hippocampus for cocaine extinction (Fig. 2a, b, d, e). A similar strategy was also used to show that $Ca_v1.2$ deletion in either hippocampal subregion had no effect on the maintenance of cocaine CPP (Fig. 2c, f).

In addition, using Cre–Lox technology, viral vectors can be engineered to selectively knockdown expression of a gene in a particular cell type through promoter-specific Cre expression. For example, to examine the role of $Ca_v1.2$ in a specific cell type, we injected an AAV expressing Cre under the control of the CaM Kinase 2 promoter that largely targets excitatory cells, into the dorsal dentate gyrus (dDG) of floxed mice that had *cacna1c* flanked by two LoxP sites [54]. As a result, $Ca_v1.2$ was deleted in excitatory cells of the dDG in these mice. When trained in acquisition and extinction of cocaine CPP, these mice-acquired CPP but were

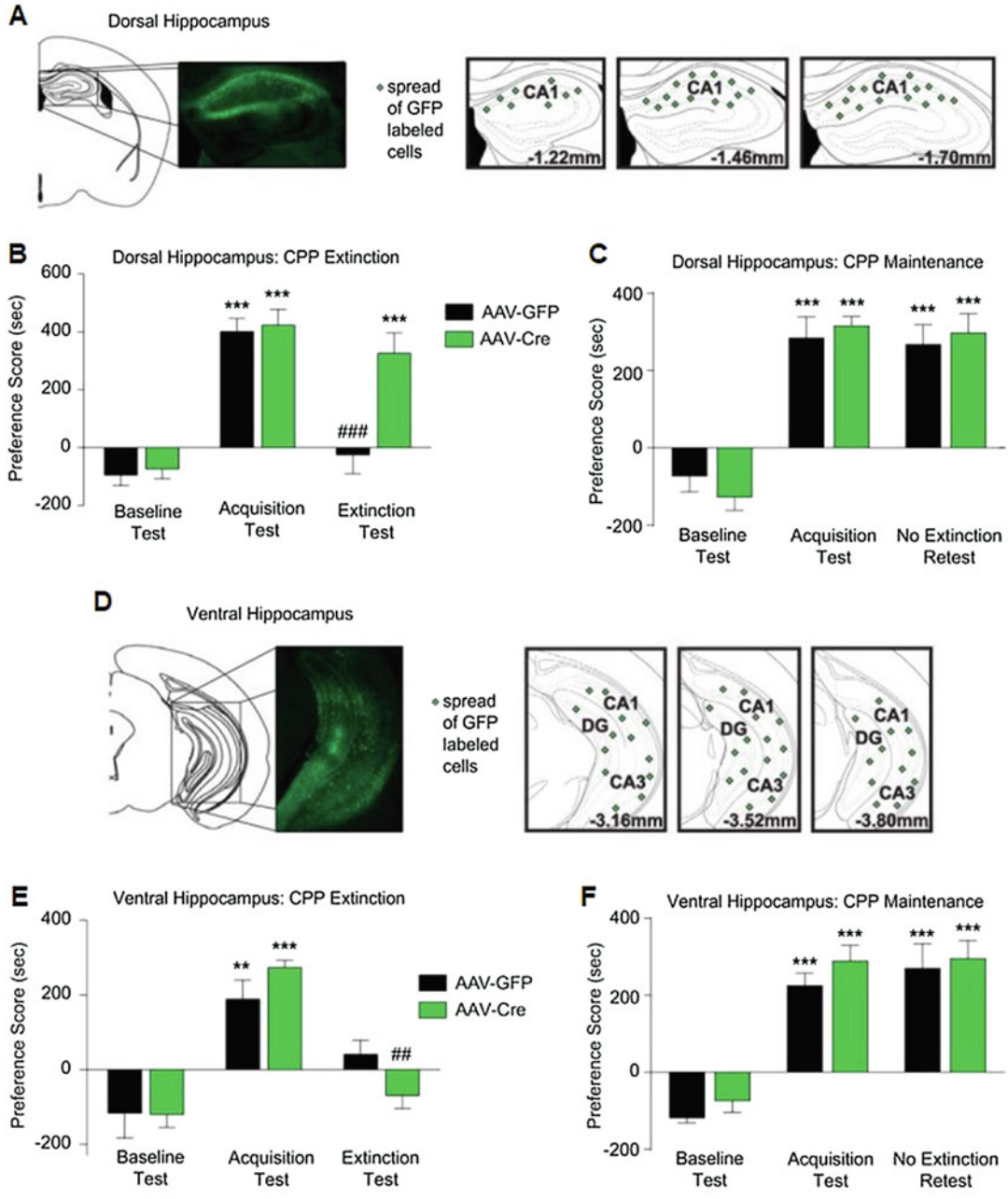

Fig. 2 Focal deletion of $Ca_v1.2$ in the dorsal hippocampus induces a deficit in extinction of cocaine CPP. (**a**, **d**) Representative images of green fluorescent protein (GFP)-positive cells and representations of coronal sections showing spread of AAV expression, as indicated by green symbol labeling, resulting from AAV bilaterally microinjected into dorsal hippocampus (**a**) or ventral hippocampus (**d**) of *cacna1c*$^{fl/fl}$ mice. (**b**) Deletion of $Ca_v1.2$ in the dorsal hippocampus had no effect on acquisition of cocaine CPP, but attenuated extinction significantly compared with mice injected with AAV–GFP. (**c**) Deletion of $Ca_v1.2$ in the dorsal hippocampus had no effect on maintenance of cocaine CPP when tested 4 days after the acquisition test. (**e**) Deletion of $Ca_v1.2$ in the ventral hippocampus had no effect on acquisition or extinction of cocaine CPP. (**f**)

unable to extinguish their cocaine preference, demonstrating a role of $Ca_v1.2$ channels within excitatory cells of the dDG for cocaine extinction (Fig. 3). The same manipulation in the CA1 subregion of the dorsal hippocampus had no effect on acquisition or extinction of cocaine CPP (Fig. 3).

4.2 shRNA Gene Knockout/Silencing

To manipulate genes in other species or situations when a floxed mouse expressing LoxP sites around the target gene of interest (for gene manipulation) is not available, viral vectors expressing short/small hairpin RNA (shRNA) can be employed. shRNAs are artificial RNA molecules that are used to mediate gene silencing. This artificial RNA is integrated into a viral vector and can then be delivered into the animal in a brain- and cell type-specific manner through stereotaxic surgery [49, 55–57]. The shRNA is transcribed in the nucleus. The resulting mRNA is cleaved by a silencing complex, ultimately leading to silencing of that gene in the targeted brain region or cell type [55]. We have successfully utilized this strategy to knockdown $Ca_v1.3$ channels in the VTA to demonstrate the necessity of these channels in cocaine-induced behavioral sensitization [57] and cocaine CPP ([49]; Fig. 4).

4.3 Retrogradely Transported Cre Recombinase: Brain Circuit Manipulation

With the growing discovery of the involvement of brain circuits in drug-seeking behavior, retrograde transport of viral vectors can be used to interrogate neuronal circuit function and target projection-specific manipulations of the genome (described in next section). More specifically, retrograde transport of viral vectors allows researchers to understand how large-scale networks contribute to drug-seeking behavior by monitoring or manipulating projection-specific activity or repairing pathological mutations [58]. These approaches take advantage of Cre recombinase to produce specific brain circuit manipulations (by expression, e.g., of optogenetic or chemogenetic tools) in wild-type mice. Similar manipulations can also be used in genetic knockout or mutant animals to examine the ability to reverse behavioral phenotypes as we have recently shown using $Ca_v1.2$ knockout mice and reinstatement of cocaine CPP [50]. A Cre-dependent viral construct with a double-floxed inverse orientation (DiO) can be delivered into a desired brain region, and a retrograde viral vector expressing the Cre recombinase enzyme can be delivered into an output brain region. In this manner, virus retrogradely travels through neurons that send projections to the output region. The projection neurons that have incorporated the Cre-dependent virus construct, through stereotaxic infusion of the Cre-dependent (DiO-expressing) virus in that region, in addition

Fig. 2 (continued) Deletion of $Ca_v1.2$ in the ventral hippocampus had no effect on maintenance of cocaine CPP. $^{***}p < 0.001$ compared with baseline test; $^{\#}p < 0.05$, $^{\#\#\#}p < 0.001$ compared with acquisition test. Data are presented as mean ± SEM. Taken from Ref. [48]

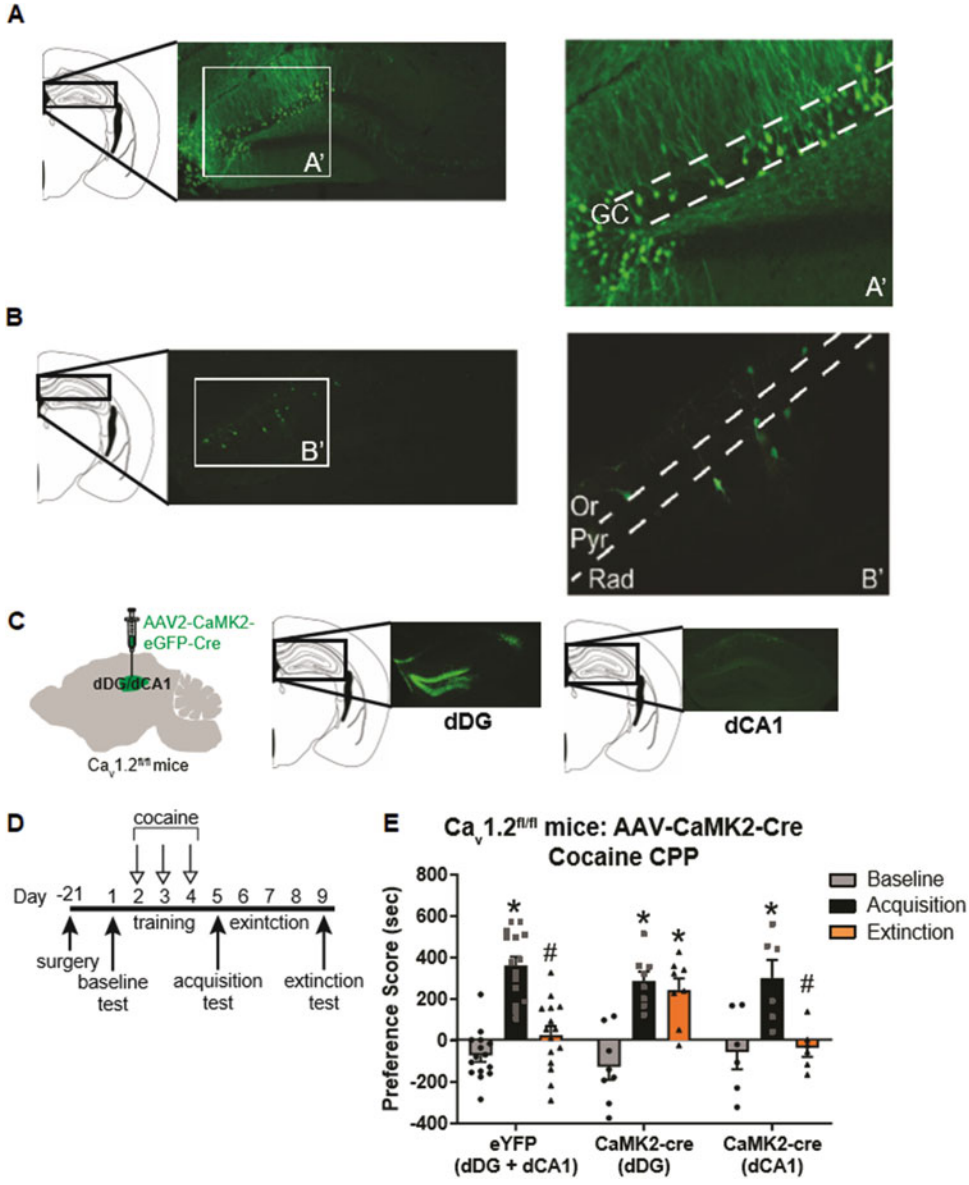

Fig. 3 Focal knockout of $Ca_v1.2$ channels in excitatory cells of the dDG results in a cocaine extinction deficit. (**a**) Representative images of brain sections from $D1^{cre}$, $Ca_v1.2^{fl/fl}$ mice displaying mCitrine-positive D1R-expressing cells in the dDG. Labeled cells are expressed most densely in the granule cell (GC) layer of the dDG and display morphological characteristics of principal excitatory cells (A′). (**b**) Representative images of brain sections from $D1^{cre}$, $Ca_v1.2^{fl/fl}$ mice displaying mCitrine-positive D1R-expressing cells in the dCA1. Labeled cells are sparsely expressed throughout the stratum radiatum (Rad) and stratum oriens (Or) with almost a complete lack of expression in the stratum pyramidale (Pyr) (B′). Labeled cells display morphological characteristics of inhibitory neurons. (**c**) Left, $Ca_v1.2^{fl/fl}$ mice were injected with an AAV expressing Cre under the CaMK2 promoter into either bilateral dDG or bilateral dCA1 in order to selectively delete $Ca_v1.2$ in excitatory cells of these subregions. Right, Representative images of brain sections from $Ca_v1.2^{fl/fl}$ mice displaying eGFP-positive cells expressing AAV2-CaMK2-eGFP-cre in either the dDG or dCA1. (**d**) Experimental timeline of surgery and the CPP extinction protocol. (**e**) Control mice (eYFP (dDG + dCA1); $n = 15$) acquired

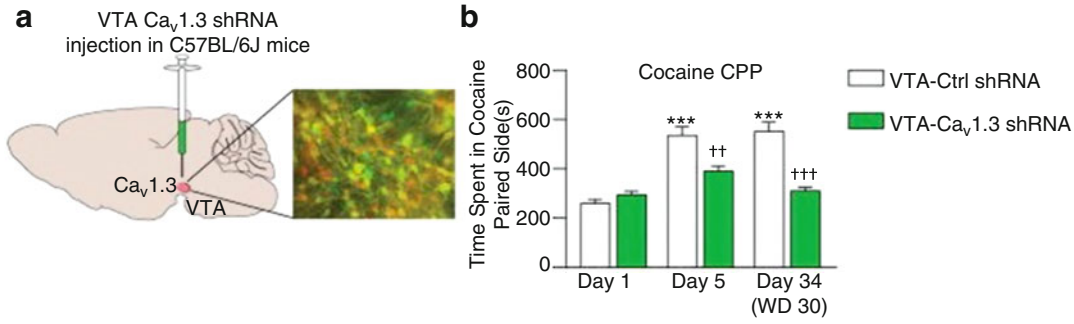

Fig. 4 Inhibition of VTA $Ca_v1.3$ channels via shRNA counteract cocaine induce CPP. (**a**) Inset, image shows green fluorescent protein (GFP-green), tyrosine hydroxylase (TH-red), and dual-labeled (yellow) cells. (**b**) Intra-VTA stereotaxic delivery of $Ca_v1.3$ shRNA (21 days before the start of CPP) attenuated the expression of CPP tested on day 5 and 34 (two-way ANOVA (VTA injection × day, $F(2, 51) = 14.09$, $P < 0.0011$); Bonferroni post hoc test: Ctrl shRNA: Day 1 vs. Day 5 $^{***}P < 0.001$, Ctrl shRNA Day 1 vs. Day 34 $^{***}P < 0.001$, Day 5: Ctrl shRNA vs. $Ca_v1.3$ shRNA $^{\dagger\dagger}P < 0.01$, Day 34: Ctrl shRNA vs. $Ca_v1.3$ shRNA $^{\dagger\dagger\dagger}P < 0.001$. Ctrl shRNA $n = 10$, $Ca_v1.3$ shRNA $n = 9$). Taken and adapted from Ref. [49]

to the retrogradely transported Cre enzyme will express the full viral construct (Fig. 1b, d).

Recently, two retrogradely transported Cre-expressing viruses have been used in conjunction with Cre-dependent viral vectors to target projections between two brain regions of interest. Canine adenovirus type 2 (CAV-2), which has high preference for neuronal transduction, modest distribution via axonal transport, and long duration of expression [59], and retrograde AAV, which has robust axonal internalization and retrograde transmission with minimal toxicity [58], have been widely used to access projection neurons. These retroviral strategies have been successfully used to manipulate circuits using optogenetic and chemogenetic tools [38, 60, 61] as well as reversing behavioral phenotypes in genetic knockout animals as we have recently published for stress- and cocaine-induced reinstatement of cocaine CPP [50].

4.4 FLP–FRT System: Brain Circuit-Specific Gene Knockout

Given the discovery of the role of brain circuits in addiction-related behavior, it has become necessary to probe gene function at the level of neuronal pathways. Circuit-specific manipulation of genes can be achieved using the FLP–FRT system. The FLP system works in a similar manner to the Cre system. FLP recombinase has the

Fig. 3 (continued) ($^{*}p < 0.0001$, Bonferroni post hoc baseline vs. acquisition) and extinguished ($^{\#}p < 0.0001$, Bonferroni post hoc acquisition vs. extinction) cocaine CPP. Mice with $Ca_v1.2$ deleted in excitatory cells of the dDG ($n = 8$) acquired ($^{*}p < 0.0001$, Bonferroni post hoc baseline vs. acquisition) but did not extinguish ($^{*}p < 0.0001$, Bonferroni post hoc baseline vs. extinction) cocaine CPP. Mice with $Ca_v1.2$ deleted in excitatory cells of the dCA1 ($n = 6$) acquired ($^{*}p < 0.001$, Bonferroni post hoc baseline vs. acquisition) and extinguished ($^{\#}p < 0.001$, Bonferroni post hoc acquisition vs. extinction) cocaine CPP. Taken from Ref. [54]

ability to invert a gene of interest that is flanked by FRT sites. FLP recombinase recognizes FRT sites and initiates gene recombination between these sites (Fig. 1b). By combining retro AAV expressing FLP recombinase and FLP-dependent Cre recombinase expression in floxed mice, it is possible to induce gene knockout in a pathway-specific manner. Recently, our group has successfully used this strategy to generate knockout of the *cacna1c* gene in prelimbic (PrL) neurons projecting to the nucleus accumbens core (NAcC) in mice to test a projection-specific role of *cacan1c* in cocaine-conditioned place preference [50] (Fig. 5). To perform this, *cacna1c* floxed mice were injected with an AAV expressing FLP-dependent Cre recombinase (i.e., AAV-fDIO-Cre-GFP) in the PrL and a retrograde AAV expressing FLP recombinase (i.e., AAV-EF1a-mCherry-IRES-Flpo) in the NAcC. Using this technique, we demonstrated that $Ca_v1.2$ channels in the PrL–NAcC pathway are necessary for stress- and cocaine-induced reinstatement of cocaine CPP (SPR and CPR, respectively) and has no role in acquisition or extinction of cocaine CPP [50].

4.5 CRISPR

The genome can also be modified through emerging gene-editing technologies such as CRISPR/Cas9 [58]. Using this approach, genomic double-stranded DNA breaks are created at specific gene loci, inducing nonhomologous end joining or homologous recombination to generate genome editing. This editing can result in gene knockout, deletion, correction, or addition [62]. The CRISPR/Cas9 complex can be introduced into the organism (i.e., mouse) via different delivery approaches [63], among them viral vectors [64]. The delivery of the complex via viral vectors has been beneficial for in vivo genome editing in animals, through different routes of administration including stereotaxic brain infusions [65].

To knockout/knockdown a particular gene, viral vectors can deliver Cas9 protein and single-guide RNA (sgRNA) to the brain region of interest [66] to cause a double-strand break surrounding the particular gene, resulting in nonhomologous end joining. To knockin a gene, Cas9, sgRNA, and a donor DNA containing the sequence of interest can be injected into a specific brain region using viral vectors [67], allowing for the incorporation of the homologous recombinant repair template.

4.6 Use of Transient Viral Vector Tools to Evaluate Gene Function

Viral vectors that overexpress a transgene allows investigators to compare the effect of transgene expression before and after expression in the same animal. For example, a recent study took advantage of the transient transgene expression of HSV-derived vectors to determine the effect of overexpression of histone dimethyltransferase G9a within the NAc on cocaine self-administration behavior [68]. In this study, rats received intra-NAc infusions of HSV-G9a after being trained in cocaine self-administration. Three days after

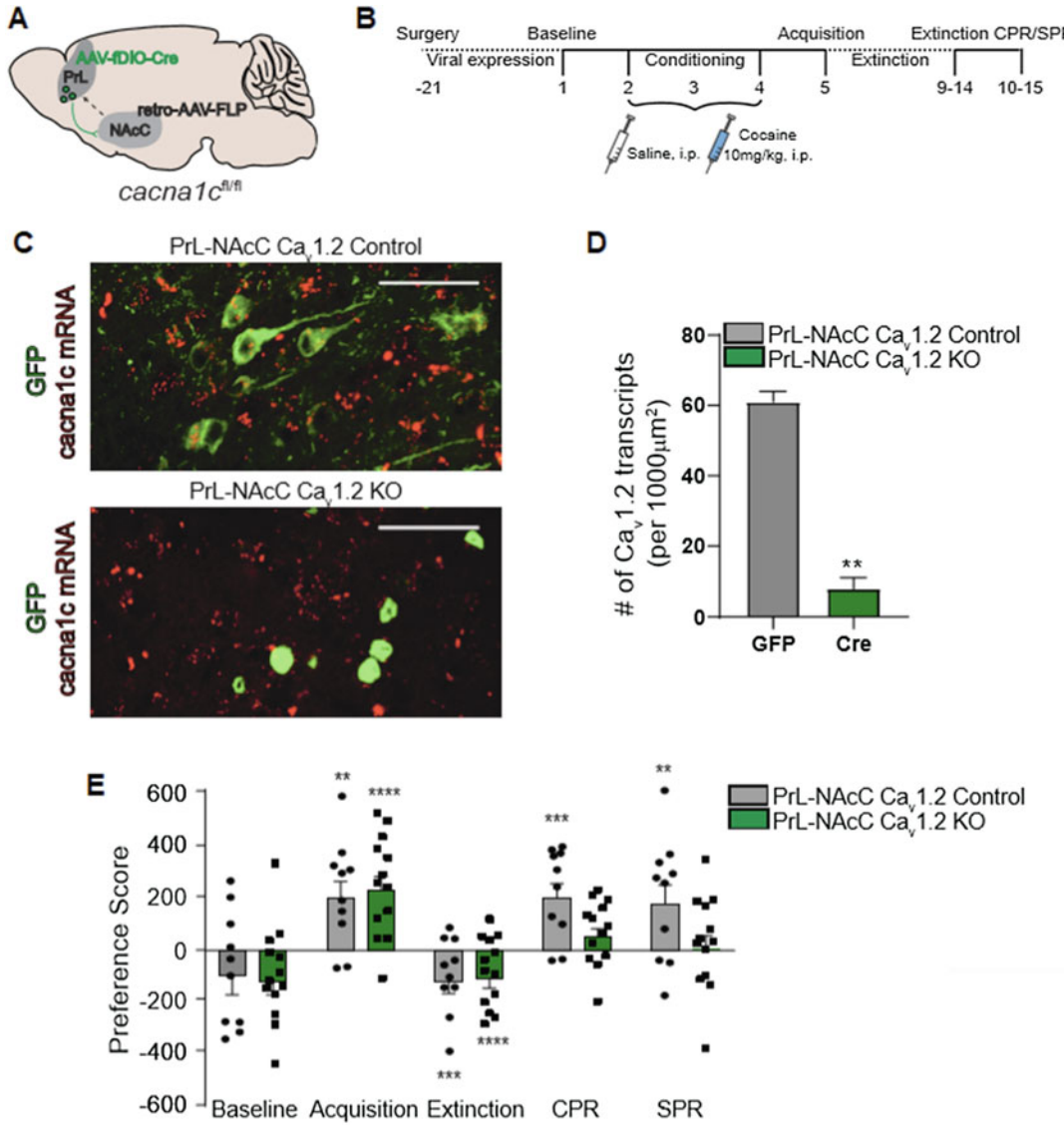

Fig. 5 $Ca_v1.2$ within the PrL → NAcC projection is required for reinstatement. (**a**) cacan1c-floxed mice were injected with an Flp-dependent AAV expressing Cre recombinase (AAV-fDIO-Cre-GFP) into bilateral PrL and a retrograde AAV expressing Flp (retro-AAV-Flp) into bilateral NAcC to knockdown cacna1c expression selectively in PrL → NAcC cells. (**b**) Experimental timeline for surgery and behavioral experiments. (**c**) Representative images of RNAscope in situ hybridization showing cacna1c mRNA (red) and GFP-tagged cells (green) in the PrL of control mice injected with AAV–GFP (Top-PrL-NAcC $Ca_v1.2$ control) and experimental cacna1c-floxed mice injected with AAV-fDIO-Cre-GFP into the PrL and retro-AAV-Flp into the NAcC (bottom-PrL-NAcC $Ca_v1.2$ KO). Scale bar = 50 μm. (**d**) Quantitative analysis of cacna1c mRNA transcripts. Mice with $Ca_v1.2$ knocked out in PrL cells projecting to the NAcC have significantly less cacna1c mRNA in GFP + cells in the PrL compared with controls (**$p < 0.01$, unpaired *t*-test; GFP, $n = 2$ mice, 26–30 cells/mouse, Cre, $n = 3$ mice, 30 cells/mouse). (**e**) Control mice (PrL-NAcC $Ca_v1.2$ Control) and mice with knockdown of $Ca_v1.2$ within the PrL → NAcC projection (PrL-NAcC $Ca_v1.2$ KO) acquired (****$p < 0.0001$, **$p < 0.01$) and extinguished (****$p < 0.0001$, ***$p < 0.001$) cocaine CPP. CPR significantly increased preference score in PrL-NAcC $Ca_v1.2$ control mice (***$p < 0.001$, $n = 10$) but not in PrL-NAcC $Ca_v1.2$ KO mice ($n = 13$). Similarly, SPR significantly increased preference score in PrL-NAcC $Ca_v1.2$ control mice (**$p < 0.01$) but not in PrL-NAcC $Ca_v1.2$ KO mice. Data are presented as mean + SEM. Taken from Ref. [50]

infusion, during peak HSV-mediated expression, rats that received HSV-G9a were more sensitive to maintenance of cocaine self-administration. This enhanced cocaine-self administration persisted a week later even after HSV-G9a expression subsided, suggesting that transgene expression of G9a was sufficient to induce long-lasting changes in cocaine self-administration behavior. In another study, rats received intra-NAc infusions of HSV-mediated expression of GluA1 accessory protein, SAP97 microRNA (HSV-SAP97) following training and extinction of cocaine self-administration [69]. Rats with HSV-SAP97 microRNA-mediated knockdown of SAP97 demonstrated decreased reinstatement behavior 4 days following infusion, but behaved similar to control animals 1 week following infusion, indicating that the behavioral change as a result of SAP97 knockdown was transient. These studies demonstrate that HSV-mediated vectors can be used to manipulate genes to test drug-seeking behavior on shorter time scales.

Lentiviral vectors system have also been utilized to overexpress or silence genes such as a study that examined the role of alpha-synuclein in cocaine self-administration in rats [70]. Overexpression of alpha-synuclein in the NAc throughout the training period and initial testing period enhanced cocaine self-administration. Furthermore, silencing of alpha-synuclein in the NAc (using lentivirus expressing siRNAs specific for alpha-synuclein), decreased cocaine self-administration.

5 Behavioral Applications Using Viral Vectors

5.1 Viral Vectors for Functional Manipulation During Drug-Seeking Behavior

Viral vector strategies can also be used to study the function of specific cell types or projections. Recent advancements in the field of viral vector technology and the development of promoter-specific Cre recombinase mouse lines allow for the manipulation of cells and circuits using several approaches. For cell-type specific manipulation, Cre recombinase-dependent viral vectors are injected into transgenic Cre mouse lines. These mice have the Cre recombinase gene under the regulatory control of a specific promoter, allowing promoter-specific Cre expression. To allow for projection-specific manipulation, viral vectors are injected in a wild-type mouse along with a retrogradely-transported Cre recombinase as discussed above (Subheading 4.3) [38, 50, 58–61]. These viral strategies have been most beneficial for optogenetic (Fig. 1c) and chemogenetic (Fig. 1d) activation or inactivation of a specific cell type in a brain region of interest or specific neural circuit, as described below.

5.1.1 Chemogenetics

Chemogenetics has recently offered a powerful tool for neuroscientists to manipulate both cell type and projection-specific activity in a behaving mouse. The most common chemogenetic technique is a

technology called designer receptors exclusively activated by designer drugs (DREADDs) which relies on a modified structure of the muscarinic receptor [71]. In this modified state, the receptor can only bind clozapine-N-oxide (CNO), an otherwise inert substrate, to either activate or inhibit neuronal activity through a coupling of either Gq or Gi-triggered activity in the cell, respectively.

As DREADD technology continues to develop, researchers have been expressing the AAV-DREADD construct in cell types of interest with the use of cell-type specific promoters. In addition, as DREADDs can also be expressed in a Cre-dependent manner, this viral vector can be combined with retrograde expression of Cre, allowing for DREADD expression solely in the targeted pathway (Fig. 1d). CNO can be injected systemically or intra-brain to stimulate cells in a cell-type specific as we have recently demonstrated in [54] or a projection-specific manner (described below). DREADDs can be used to either activate or inhibit cellular activity over a period of 30–120 min [72, 73], allowing for manipulation of specific cells over the entire duration of a behavioral training or testing period. Furthermore, this technique is advantageous because unlike manipulation of genes discussed above, DREADD manipulation is targeted to a short time period and can selectively test the function of cells or circuits during one particular phase of drug-seeking behavior, eliminating possible chance of compensation during earlier phases of training.

For example, in a recent publication from our laboratory [50], we employed chemogenetics to manipulate the activity of NAc-projecting PrL cells during cocaine and stress-primed reinstatement of cocaine CPP. By injecting retro-AAV-CAG-Cre into the bilateral NAc and a cre-dependent AAV expressing hM4Di excitatory DREADD into the PrL, NAc-projecting PrL cells could be inhibited during reinstatement testing of cocaine CPP. Inhibition of NAc-projecting PrL cells attenuated reinstatement, providing evidence that this projection was required for reinstatement of cocaine CPP.

5.1.2 *Optogenetics*

Optogenetics represents a vital technology to the field of neuroscience to investigate causal relationships between genetically defined populations of neurons. In addition, optogenetics provides a specific advantage to studying drug-seeking behavior due to its temporal precision in changing neuronal activity. This technique requires the expression of exogenous photosensitive ion channels using viral vectors in order to control the activity of cells in response to light and time locks this cellular function to behavioral activity [74] (Fig. 1c). To achieve brain region-, cell type-, or projection-specific activation of cells, the light-sensitive channelrhodopsin (ChR2) is injected into a brain region followed by implantation

with a laser instrument. Upon stimulation with blue light, the ChR2 channels open and cause depolarization, and thus activation of the cell. In contrast, to achieve brain region-, cell type-, or projection-specific inhibition of cells, viruses expressing the light-sensitive halorhodopsin (NpHR) are used. These light-sensitive channels can be engineered with specific promoters or Cre-dependent expression strategies in order to express ChR2 or NpHR in particular cell types or neural circuits. These optogenetic manipulations can be paired with in vivo behavioral testing to further dissect mechanisms underlying addiction-related behaviors.

Viral vector-mediated optogenetic manipulation of VTA dopamine (DA) neurons has established the involvement of these cells in reward [75–77] such as cocaine [78] and heroin's reinforcing effects [79]. In the heroin study, the VTA of dopamine transporter (DAT)–Cre mice was injected with AAV5-DIO-hChR2-eYFP to transfect DA cells for optogenetic self-stimulation in the presence of increasing concentrations of heroin. The study found that heroin exposure dose-dependently decreased the amount of VTA DA neuron self-stimulations when compared with baseline levels [79].

As mentioned before, these techniques have also brought insight in the identification of neurocircuits involved in drug-seeking behaviors. For example, activation via AAV-expressing channelrhodopsins of glutamatergic inputs to the NAc from the mPFC, hippocampus, and/or amygdala has been shown to induce cocaine CPP [38]. While on the other hand, inhibition of prelimbic projections to the NAc core via AAV-expressing halorhodopsin reduced cocaine-primed and cue-induced reinstatement [38].

Another application for viral-expressing optogenetic methods is for silencing neurons activated in drug-paired environments. This approach has been used to examine the contribution of hippocampal place cells to spatial representations of a drug-associated environment [80]. To label and manipulate the specific neurons that were recruited during exploration of a drug-associated environment, c-Fos-tTA transgeneic mice were injected with a viral construct expressing TRE3G-ArchT-GFP in the CA1 subregion of the hippocampus. Active neurons during cocaine place preference were tagged with ArchT, a molecule that silences neuronal activity upon optogenetic stimulation of light. Using this method, by silencing neurons active in the cocaine-paired environment, cocaine place preference was lost. In this manner, viral vector tools can be used to manipulate behaviorally tagged neurons to directly link cell populations to drug-seeking behavior.

5.2 Viral Vectors to Examine Natural Neuronal Activity During Drug-Seeking Behavior

Neural activity has been traditionally assessed through electrophysiology recordings. However, recent advances in calcium imaging techniques allow neuroscientists to measures intracellular calcium changes, providing an alternative means to measure neuronal activity. With the use of viral vectors, genetically encoded fluorescent calcium indicators can be delivered into rodents brain through

stereotaxic surgeries. There are different types of calcium indicators that serve different needs; therefore, the experiment should be carefully evaluated to determine which calcium indicator is best suited for the experimental requirements [7].

In vivo calcium imaging allows for the visualization and measurement of calcium dynamics through fluorescent signal as a representation of neuronal activity [81] and can occur through three different techniques: (1) Two-photon calcium imaging, (2) single-photon calcium imaging/mini-epifluorescence microscope (miniscope), and (3) fiber photometry. Two-photon imaging provides the best subcellular resolution, but the animal's head is immobilized. However, newly developed virtual reality behavioral protocols may overcome the head-fixed limitation of two-photon imaging (see below). One photon calcium imaging with miniscope and fiber photometry allows for visualization of in vivo calcium imaging in behaving animals [82] and thus, the ability to easily measure calcium signal during drug-seeking behavior. However, the cellular resolution with one photon calcium imaging and fiber photometry is compromised when compared to two-photon calcium imaging [83].

5.2.1 Two-Photon Microscopy

This technique allows for the measurement of neural activity with in vivo calcium imaging at a high resolution. First, the viral vector containing the calcium indicator is delivered into the mouse brain as described before. Following this infusion, different surgical preparations can be performed to obtain access to the desired brain regions for imaging [84]. A glass-covered cranial window can be implanted in the mouse following removal of a piece of the skull. Alternatively, a thinned skull cranial window can be implanted in the mouse which requires drilling through the skull to eliminate bone layers prior to implanting a cover glass [85]. Following either preparation, the lens (i.e., gradient index (GRIN)) needs to be implanted to image neural activity from deep brain structures.

One of the limitations of two-photon in vivo calcium imaging is that the head of the animal is immobilized, and the animal is not freely moving. However, with the use of an air-supported styrofoam ball, some adaptations have been made to this technique to allow animals to be mobile [86]. One of the most recent advances using this styrofoam ball and the two-photon microscopies was the development of a virtual CPP [87]. As with the usual two-photon microscopy, the head of the animal was immobilized. However, researchers were able to develop a virtual reality CPP (VR-CPP) to simulate the behavioral testing environment. In this study, investigators exposed mice to different room environments through a projector. Upon presentation of a reward (water or morphine), mice were able to develop a preference for the reward-associated project-displayed environment. Using two-photon microscopy,

they measured the neuronal activity of the dorsal hippocampus CA1 during conditioning, acquisition testing, and extinction training of VR-CPP in response to a natural reward (water) or morphine. The neuronal activity of the dorsal CA1 was higher in the VR water-paired environment compared to the VR non-water-paired environment, but this activity was eliminated during extinction training. Although animals acquired a preference for the morphine-paired environment, activity of dorsal CA1 neurons in response to the morphine-paired context compared to the non-morphine-paired environment was not increased in these mice. These data suggest that the neuronal encoding for natural rewards differs from the neuronal encoding for morphine-induce reward.

5.2.2 Fiber Photometry In Vivo Calcium Imaging

Fiber photometry has emerged over the past several years as a calcium imaging technique that measures neuronal activity in freely moving animals. Through the use of genetically encoded calcium indicators (i.e., GCaMP), this technique can detect naturally occurring neural activity of genetically modified neurons through an optic fiber. First, a stereotaxic surgery is performed for the delivery of a viral vector expressing the genetically encoded calcium indicator, GCaMP. During the same surgery, an optic fiber is implanted unilaterally above the desired brain region, and it is secured with the adhesive cement material. The implantation of this optic fiber permits repeated and long-term neuronal activity recording of the same population of cells during different behavioral tasks. Briefly, excitation light passes through an optical patch cord and is delivered to the mouse brain through the optic fiber in order to excite the calcium indicator, producing fluorescence. The emitted fluorescence returns through the same patch cord until it reaches the photodetector that converts the fluorescence signal into an analog signal. Since this technique can be performed in behaviorally active mice, a transitor–transitor logic (TTL) pulse can be delivered to the computer concurrently with the fluorescent signal to denote the start of a behavioral task. Therefore, this signal is transmitted to the processor in real time allowing for alignment of calcium recordings to behavioral measures. Different adaptations have been developed with fiber photometry, which allows for activity measurements not only through one, but multiple optic fibers to simultaneously study different brain regions [88, 89].

Understanding the effects of drugs of abuse on neural activity and neural circuits is imperative for the development of new therapeutic treatments. Using fiber photometry during cocaine CPP, Calipari et al. (2016) demonstrated that chronic cocaine exposure dysregulates D1 receptor-containing neurons in the NAc core which facilitates the reinstatement of drug-seeking behavior [90]. First, using fiber photometry, they evaluated in vivo NAc neuronal activity during the cocaine CPP acquisition test. The

NAc showed increased activity during the acquisition test immediately before entering into the cocaine paired chamber. In order to parse out NAc cell type activity during the distinct phases of cocaine CPP, they injected mice that expressed Cre recombinase under the expression of the D1 or D2 promoter with a Cre-dependent GCaMP virus. With this viral vector strategy, they were able to determine that D1-containing cells were driving NAc activity immediately before entering into the cocaine-paired chamber during the acquisition test as well as during reinstatement of cocaine-seeking behavior.

In a more recent publication from our lab [50], we used fiber photometry to assess in vivo neural activity of a specific neural circuit during cocaine- and stress-induced reinstatement of cocaine CPP. In order to assess the activity within a particular neural circuit during reinstatement behavior, we delivered a Cre-dependent virus expressing the GCaMP indicator into the PrL and a retrograde virus expressing the Cre-recombinase enzyme into the NAc core. Using fiber photometry, we found that the projection from the PrL to the NAc core is recruited during cocaine- and stress-induced reinstatement. To further dissect molecular mechanisms, fiber photometry experiments measured the neuronal activity of projections from the PrL to the NAc in mice injected with an inhibitor of LTCCs, which we have shown to be required for cocaine reinstatement behavior [50]. Mice that had LTCCs pharmacologically inhibited during reinstatement denoted altered neuronal activity in the PrL–NAc projection, demonstrating that LTCCs are involved in the neuronal activity patterns within this circuit during reinstatement.

5.2.3 Single Photon: Mini-Epifluorescence Microscope (Miniscope)

As with fiber photometry, the development of the miniaturized fluorescence microscope (miniscope) allows for in vivo calcium imaging technique with freely behaving animals. First, a modified viral vector containing a calcium indicator is delivered into the desired brain region. In addition, a microendoscopic lens such as a GRIN lens is implanted above the region of interest, along with a baseplate which sits on the skull and serves as an interface with the miniscope. The baseplate allows for further visualization of the fluorescent calcium indicator through the miniscope.

Using in vivo calcium imaging through the miniscope technique, dorsal CA1 hippocampus neuronal activity was found to be associated with the acquisition and expression of nicotine CPP [91]. Specifically, researchers noticed that cells activated during training of the nicotine CPP sessions had higher Ca^{2+} frequency than cells activated during training of the saline CPP sessions. These findings suggest that neurons within the CA1 play a role in contextual association with nicotine reward.

5.3 Viral Vector Strategies to Study Molecular Mechanisms Underlying Drug-Seeking Behavior

5.3.1 Drugs Acutely Restricted by Tethering (DART)

Research in drug addiction has focused on identifying molecular pathways that can be targeted for the treatment of substance use disorders. However, research continues to underscore the region- and cell type-specific mechanisms that may be contributing to behavioral components of addiction. Recently, a technique named DART (drugs acutely restricted by tethering) was developed to deliver pharmacological agents to genetically defined cell types. DART relies on a bacterial enzyme called HaloTag, which can be injected into the brain using a Cre-dependent viral vector, to capture and tether pharmacological agents to select cell types in the brain [92]. When injected into Cre-expressing animals, HaloTag will express only in cells within that brain region that express Cre. A HaloTag ligand can be engineered such that it is fused to a pharmacological agent of interest, including receptor and channel antagonists and agonists. This technique has been used to examine the contribution of glutamate AMPAR activity within D1R- and D2R-expressing cells in the striatum to locomotor activity deficits seen in mouse models of Parkinson's disease [92], however, has not been tested in drug-seeking behavior. This technique holds great promise for the field of addiction research for acute, cell type-specific effects on endogenous receptors involved in drug-seeking behavior.

5.3.2 Translating Ribosome Affinity Purification (TRAP)

Activation of gene expression is highly involved in mediating the long-lasting effects of drugs of abuse and underlies drug-seeking behavior observed in animal models [93, 94]. Given the growing knowledge of the cell type- and circuit-level mechanisms in various aspects of drug-seeking behavior, the need to examine changes in gene expression within genetically defined cell populations and circuits is becoming necessary. Recently, a viral vector-based TRAP (vTRAP) technique has allowed researchers to isolate actively translating mRNA within select cell types in a brain region of interest [95]. Following injection of a Cre-dependent AAV expressing the ribosomal protein L10a fused to GFP in Cre-drive mouse lines, immunoprecipitation using brain tissue homogenate and GFP antibody allows access to translating mRNAs from the cell population tagged with the virus.

vTRAP has additionally been modified to isolate translating mRNAs from projection-specific cell types. For selective profiling of projection neurons, Cre-driver mouse lines are injected with an AAV engineered to express a modified L10-GFP fusion protein (NBL10) in brain region of interest and a retro-AAV in the target region [96]. Taking it one step further, new TRAP technologies are able to isolate neuronal sub-compartments such as axonal projections or synaptosomal fractionations through Axon-TRAP [97] and SynapTRAP [98], respectively. These advances provide an optimal tool for the use of TRAP to profile cell type-specific,

projection-specific, and neuronal compartment-restricted changes in drug-seeking behavior in future studies [99].

5.4 Clinical Use of Viral Techniques in Drug Addiction

In 1990, Stephen Rosenberg was the first to successfully insert foreign genes into humans with the use of retrovirus [100], while French Anderson was the first to successfully perform a retroviral-mediated gene therapy for a congenital disease [101]. However, after three decades, these viral techniques still have made limited progress in the clinical sector. Currently only four FDA-approved gene therapy approaches exist for non-neurological conditions (LUXTURNA and ZOLGENSMA use AAV; KYMRIAH uses lentiviral vector; IMLYGIC uses HSV) [102]. In order to perform effective gene therapy in clinical populations using viral vectors, several critical issues need to be carefully considered. One of the main concerns lies in the inherent characteristics of the original virus. As a result, the virus can invade the human immune system and cause health problems in the individual. A safety mechanism is needed to ensure the delivery of this vector to the target cells. Otherwise, the off-target effects can result in harmful consequence to the host [5]. Conversely, the immune system can recognize the viral vector as a foreign agent and destroy it, eliminating the therapeutic effect.

In the case of gene therapy for the treatment of neurological and neuropsychiatric disorders, the delivery of the viral vectors to the intended target is even more complicated because the virus needs to be capable of crossing the blood–brain barrier. From all the gene therapy clinical trials available, $<3\%$ of trials were intended to target the central nervous system (CNS) [6]. The trials targeting the CNS are mainly for the treatment of a neurological or an autosomal disorder [5, 6, 103], using AAV for in vivo gene transfer [6, 104, 105] and lentivirus for ex vivo gene transfer [104].

The development of any long-term pharmacology effective treatment for neuropsychiatric disorders, especially addiction, has been challenging. Nonetheless, gene therapy as a treatment in itself is an even more challenging task. In the past years, the possibility of immunopharmacotherapy for the treatment of cocaine abuse has made great advances. The efficacy of a vaccine that counteracts the rewarding effects of cocaine and prevents relapse has been validated in nonhuman primates [106, 107] and is currently at a clinical trial level [108]. The anti-cocaine vaccine, dAd5GNE, was developed using a disrupted adenovirus. The vaccine induces high titers of cocaine antibodies to target cocaine in the bloodstream and prevent it from reaching the CNS. If results are promising, it might represent the first clinical treatment to prevent cocaine relapse, one of the biggest challenges of drug addiction.

6 Conclusion

Use of viral vectors has dramatically expanded techniques that can be used in research investigating drug-seeking behavior. Although viral vector strategies rely on ectopic transgene expression, the viral strategy limits expression to a desired length of time and avoids issues of developmental effects that can be observed with transgenic animals. From gene therapy, to manipulating neuronal activity, to recording naturally occurring neuronal activity, these tools have allowed investigators to dissect detailed mechanisms involved in reward behavior. In addition, the ability to restrict viral expression to subregions of the brain, specific cell-types, and single projections has demonstrated the wide diversity of genes, cell types, and projections that contribute to processes underlying drug-seeking behavior. Further advances should be focused on dissecting the specific mechanisms that can be brought to the clinical sphere. Efforts to expand viral vector-mediated technologies will continue to deepen our understanding of brain mechanisms that contribute to drug-seeking behavior and allow for potential clinical therapeutics for the treatment of addiction.

References

1. Duesberg PH, Vogt PK (1970) Differences between the ribonucleic acids of transforming and nontransforming avian tumor viruses. Proc Natl Acad Sci U S A 67(4):1673–1680. https://doi.org/10.1073/pnas.67.4.1673
2. Jackson DA, Symons RH, Berg P (1972) Biochemical method for inserting new genetic information into DNA of Simian Virus 40: circular SV40 DNA molecules containing lambda phage genes and the galactose operon of Escherichia coli. Proc Natl Acad Sci U S A 69(10):2904–2909. https://doi.org/10.1073/pnas.69.10.2904
3. Walther W, Stein U (2000) Viral vectors for gene transfer: a review of their use in the treatment of human diseases. Drugs 60 (2):249–271. https://doi.org/10.2165/00003495-200060020-00002
4. Papale A, Cerovic M, Brambilla R (2009) Viral vector approaches to modify gene expression in the brain. J Neurosci Methods 185(1):1–14. https://doi.org/10.1016/j.jneumeth.2009.08.013
5. Bouard D, Alazard-Dany D, Cosset FL (2009) Viral vectors: from virology to transgene expression. Brit J Pharmacol 157 (2):153–165. https://doi.org/10.1038/bjp.2008.349
6. Gray SJ, Woodard KT, Samulski RJ (2010) Viral vectors and delivery strategies for CNS gene therapy. Ther Del 1(4):517–534
7. Wang Y et al (2018) Viral vectors as a novel tool for clinical and neuropsychiatric research applications. General Psychiatry 31(2): e000015. https://doi.org/10.1136/gpsych-2018-000015
8. Lundstrom K (2018) Viral vectors in gene therapy. Diseases (Basel, Switzerland) 6(2). https://doi.org/10.3390/diseases6020042
9. Schiedner G et al (1998) Genomic DNA transfer with a high-capacity adenovirus vector results in improved in vivo gene expression and decreased toxicity. Nat Genet 18 (2):180–183. https://doi.org/10.1038/ng0298-180
10. Wang F et al (2012) Biodistribution and safety assessment of bladder cancer specific recombinant oncolytic adenovirus in subcutaneous xenografts tumor model in nude mice. Curr Gene Therapy 12(2):67–76. https://doi.org/10.2174/156652312800099599
11. Wei Q et al (2017) Engineering the Rapid Adenovirus Production and Amplification (RAPA) cell line to expedite the generation of recombinant adenoviruses. Cell Physiol Biochem 41(6):2383–2398. https://doi.org/10.1159/000475909

12. Nicklin SA, Baker AH (2002) Tropism-modified adenoviral and adeno-associated viral vectors for gene therapy. Curr Gene Therapy 2(3):273–293. https://doi.org/10.2174/1566523023347797
13. Wold WS, Toth K (2013) Adenovirus vectors for gene therapy, vaccination and cancer gene therapy. Curr Gene Therapy 13(6):421–433. https://doi.org/10.2174/1566523213666131125095046
14. Samulski RJ, Muzyczka N (2014) AAV-Mediated gene therapy for research and therapeutic purposes. Annu Rev Virol 1 (1):427–451. https://doi.org/10.1146/annurev-virology-031413-085355
15. Park K et al (2008) Cancer gene therapy using adeno-associated virus vectors. Front Biosci 13:2653–2659. https://doi.org/10.2741/2872
16. Mingozzi F, High KA (2013) Immune responses to AAV vectors: overcoming barriers to successful gene therapy. Blood 122 (1):23–36. https://doi.org/10.1182/blood-2013-01-306647
17. Grieger JC, Samulski RJ (2005) Packaging capacity of adeno-associated virus serotypes: impact of larger genomes on infectivity and postentry steps. J Virol 79(15):9933–9944. https://doi.org/10.1128/jvi.79.15.9933-9944.2005
18. Kwon I, Schaffer DV (2008) Designer gene delivery vectors: molecular engineering and evolution of adeno-associated viral vectors for enhanced gene transfer. Pharm Res 25 (3):489–499. https://doi.org/10.1007/s11095-007-9431-0
19. Vandenberghe LH, Wilson JM, Gao G (2009) Tailoring the AAV vector capsid for gene therapy. Gene Ther 16(3):311–319. https://doi.org/10.1038/gt.2008.170
20. Smith RH (2008) Adeno-associated virus integration: virus versus vector. Gene Ther 15(11):817–822. https://doi.org/10.1038/gt.2008.55
21. Schambach A, Morgan M (2016) Retroviral vectors for cancer gene therapy. Recent Results Cancer Res 209:17–35. https://doi.org/10.1007/978-3-319-42934-2_2
22. Hu WS, Pathak VK (2000) Design of retroviral vectors and helper cells for gene therapy. Pharmacol Rev 52(4):493–511
23. Vigna E, Naldini L (2000) Lentiviral vectors: excellent tools for experimental gene transfer and promising candidates for gene therapy. J Gene Med 2(5):308–316. https://doi.org/10.1002/1521-2254(200009/10)2:5<308::aid-jgm131>3.0.co;2-3
24. Kay MA, Glorioso JC, Naldini L (2001) Viral vectors for gene therapy: the art of turning infectious agents into vehicles of therapeutics. Nat Med 7(1):33–40. https://doi.org/10.1038/83324
25. Cronin J, Zhang XY, Reiser J (2005) Altering the tropism of lentiviral vectors through pseudotyping. Curr Gene Therapy 5(4):387–398. https://doi.org/10.2174/1566523054546224
26. Lundberg C et al (2008) Applications of lentiviral vectors for biology and gene therapy of neurological disorders. Curr Gene Therapy 8 (6):461–473. https://doi.org/10.2174/156652308786847996
27. Epstein AL et al (2005) HSV-1-derived recombinant and amplicon vectors for gene transfer and gene therapy. Curr Gene Therapy 5(5):445–458. https://doi.org/10.2174/156652305774329285
28. Holmes KD et al (2000) A multi-mutant herpes simplex virus vector has minimal cytotoxic effects on the distribution of filamentous actin, alpha-actinin 2 and a glutamate receptor in differentiated PC12 cells. J Neurovirol 6 (1):33–45. https://doi.org/10.3109/13550280009006380
29. Neve RL (2012) Overview of gene delivery into cells using HSV-1-based vectors. Curr Protoc Neurosci Chapter 4:Unit 4.12. https://doi.org/10.1002/0471142301.ns0412s61
30. Neve RL et al (2005) Use of herpes virus amplicon vectors to study brain disorders. BioTechniques 39(3):381–391. https://doi.org/10.2144/05393ps01
31. Cuchet D et al (2007) HSV-1 amplicon vectors: a promising and versatile tool for gene delivery. Expert Opin Biol Therapy 7 (7):975–995. https://doi.org/10.1517/14712598.7.7.975
32. Berges BK, Wolfe JH, Fraser NW (2007) Transduction of brain by herpes simplex virus vectors. Mol Therapy 15(1):20–29. https://doi.org/10.1038/sj.mt.6300018
33. Lentz TB, Gray SJ, Samulski RJ (2012) Viral vectors for gene delivery to the central nervous system. Neurobiol Dis 48(2):179–188. https://doi.org/10.1016/j.nbd.2011.09.014
34. Reimsnider S et al (2007) Time course of transgene expression after intrastriatal pseudotyped rAAV2/1, rAAV2/2, rAAV2/5, and rAAV2/8 transduction in the rat. Mol Ther 15(8):1504–1511. https://doi.org/10.1038/sj.mt.6300227

35. Penrod RD et al (2015) Use of adeno-associated and herpes simplex viral vectors for in vivo neuronal expression in mice. Curr Protoc Neurosci 73:4.37.31–34.37.31. https://doi.org/10.1002/0471142301.ns0437s73
36. Watakabe A et al (2015) Comparative analyses of adeno-associated viral vector serotypes 1, 2, 5, 8 and 9 in marmoset, mouse and macaque cerebral cortex. Neurosci Res 93:144–157. https://doi.org/10.1016/j.neures.2014.09.002
37. Cardozo Pinto DF, Lammel S (2018) Viral vector strategies for investigating midbrain dopamine circuits underlying motivated behaviors. Pharmacol Biochem Behav 174:23–32. https://doi.org/10.1016/j.pbb.2017.02.006
38. Garcia AF, Nakata KG, Ferguson SM (2018) Viral strategies for targeting cortical circuits that control cocaine-taking and cocaine-seeking in rodents. Pharmacol Biochem Behav 174:33–41. https://doi.org/10.1016/j.pbb.2017.05.009
39. Muller Ewald VA, LaLumiere RT (2018) Neural systems mediating the inhibition of cocaine-seeking behaviors. Pharmacol Biochem Behav 174:53–63. https://doi.org/10.1016/j.pbb.2017.07.006
40. Parr-Brownlie LC et al (2015) Lentiviral vectors as tools to understand central nervous system biology in mammalian model organisms. Front Mol Neurosci 8:14. https://doi.org/10.3389/fnmol.2015.00014
41. Dreyer JL (2010) Lentiviral vector-mediated gene transfer and RNA silencing technology in neuronal dysfunctions. Methods Mol Biol (Clifton, NJ) 614:3–35. https://doi.org/10.1007/978-1-60761-533-0_1
42. Epstein AL (2009) HSV-1-derived amplicon vectors: recent technological improvements and remaining difficulties—a review. Memorias do Instituto Oswaldo Cruz 104 (3):399–410. https://doi.org/10.1590/s0074-02762009000300002
43. Neve RL, Lim F (2013) Generation of high-titer defective HSV-1 vectors. Curr Protoc Neurosci Chapter 4:Unit 4.13. https://doi.org/10.1002/0471142301.ns0413s62
44. Challis RC et al (2019) Systemic AAV vectors for widespread and targeted gene delivery in rodents. Nat Protoc 14(2):379–414. https://doi.org/10.1038/s41596-018-0097-3
45. Schierberl KC, Rajadhyaksha AM (2013) Stereotaxic microinjection of viral vectors expressing Cre recombinase to study the role of target genes in cocaine conditioned place preference. JoVE 77. https://doi.org/10.3791/50600
46. Paxinos G, Franklin KBJ (2004) The mouse brain in stereotaxic coordinates. Elsevier Academic, San Diego, CA
47. Gholizadeh S et al (2013) Transduction of the central nervous system after intracerebroventricular injection of adeno-associated viral vectors in neonatal and juvenile mice. Hum Gene Therapy Methods 24(4):205–213. https://doi.org/10.1089/hgtb.2013.076
48. Burgdorf CE et al (2017) Extinction of contextual cocaine memories requires $Ca_v1.2$ within D1R-expressing cells and recruits hippocampal $Ca_v1.2$-dependent signaling mechanisms. J Neurosci 37 (49):11894–11911. https://doi.org/10.1523/jneurosci.2397-17.2017
49. Martinez-Rivera A et al (2017) Enhancing VTA $Ca_v1.3$ L-type Ca(2+) channel activity promotes cocaine and mood-related behaviors via overlapping AMPA receptor mechanisms in the nucleus accumbens. Mol Psychiatry 22(12):1735–1745. https://doi.org/10.1038/mp.2017.9
50. Bavley CC et al (2019) Cocaine- and stress-primed reinstatement of drug-associated memories elicit differential behavioral and frontostriatal circuit activity patterns via recruitment of L-type Ca(2+) channels. Mol Psychiatry. https://doi.org/10.1038/s41380-019-0513-2
51. Stoica L et al (2013) Gene transfer to the CNS using recombinant adeno-associated virus. Curr Protoc Microbiol Chapter 14: Unit14D.15. https://doi.org/10.1002/9780471729259.mc14d05s29
52. Tropea TF, Kosofsky BE, Rajadhyaksha AM (2008) Enhanced CREB and DARPP-32 phosphorylation in the nucleus accumbens and CREB, ERK, and GluR1 phosphorylation in the dorsal hippocampus is associated with cocaine-conditioned place preference behavior. J Neurochem 106(4):1780–1790. https://doi.org/10.1111/j.1471-4159.2008.05518.x
53. Blum K et al (2015) Neurogenetics and gene therapy for reward deficiency syndrome: are we going to the promised land? Expert Opin Biol Therapy 15(7):973–985. https://doi.org/10.1517/14712598.2015.1045871
54. Burgdorf CE, Bavley CC, Fischer DK, Walsh A, Martínez-Rivera A, Hackett JE, Zallar LJ, Ireton K, Hofmann F, Hell J, Huganir R, Rajadhyaksha AM (2020) Contribution of D1R-expressing neurons of the dorsal dentate gyrus and $Ca_v1.2$ channels in extinction of cocaine conditioned place

preference. Neuropsychopharmacology 45 (9):1506–1517. https://doi.org/10.1038/s41386-019-0597-z

55. Rao MK, Wilkinson MF (2006) Tissue-specific and cell type-specific RNA interference in vivo. Nat Protoc 1(3):1494–1501. https://doi.org/10.1038/nprot.2006.260
56. Arango-Lievano M et al (2014) Cell-type specific expression of p11 controls cocaine reward. Biol Psychiatry 76(10):794–801. https://doi.org/10.1016/j.biopsych.2014.02.012
57. Schierberl K et al (2011) $Ca_v1.2$ L-type Ca(2)(+) channels mediate cocaine-induced GluA1 trafficking in the nucleus accumbens, a long-term adaptation dependent on ventral tegmental area Ca(v)1.3 channels. J Neurosci 31(38):13562–13575. https://doi.org/10.1523/jneurosci.2315-11.2011
58. Tervo DG et al (2016) A designer AAV variant permits efficient retrograde access to projection neurons. Neuron 92(2):372–382. https://doi.org/10.1016/j.neuron.2016.09.021
59. Junyent F, Kremer EJ (2015) CAV-2--why a canine virus is a neurobiologist's best friend. Curr Opin Pharmacol 24:86–93. https://doi.org/10.1016/j.coph.2015.08.004
60. Han MH, Friedman AK (2012) Virogenetic and optogenetic mechanisms to define potential therapeutic targets in psychiatric disorders. Neuropharmacology 62(1):89–100. https://doi.org/10.1016/j.neuropharm.2011.09.009
61. Sarno E, Robison AJ (2018) Emerging role of viral vectors for circuit-specific gene interrogation and manipulation in rodent brain. Pharmacol Biochem Behav 174:2–8. https://doi.org/10.1016/j.pbb.2018.04.008
62. Lino CA et al (2018) Delivering CRISPR: a review of the challenges and approaches. Drug Del 25(1):1234–1257. https://doi.org/10.1080/10717544.2018.1474964
63. Liu C et al (2017) Delivery strategies of the CRISPR-Cas9 gene-editing system for therapeutic applications. J Control Release 266:17–26. https://doi.org/10.1016/j.jconrel.2017.09.012
64. Xu CL et al (2019) Viral delivery systems for CRISPR. Viruses 11(1). https://doi.org/10.3390/v11010028
65. Lau CH, Suh Y (2017) In vivo genome editing in animals using AAV-CRISPR system: applications to translational research of human disease. F1000Res 6:2153. https://doi.org/10.12688/f1000research.11243.1
66. Swiech L et al (2015) In vivo interrogation of gene function in the mammalian brain using CRISPR-Cas9. Nat Biotechnol 33 (1):102–106. https://doi.org/10.1038/nbt.3055
67. Nishiyama J, Mikuni T, Yasuda R (2017) Virus-mediated genome editing via homology-directed repair in mitotic and post-mitotic cells in mammalian brain. Neuron 96 (4):755–768.e755. https://doi.org/10.1016/j.neuron.2017.10.004
68. Anderson EM et al (2018) Overexpression of the histone dimethyltransferase G9a in nucleus accumbens shell increases cocaine self-administration, stress-induced reinstatement, and anxiety. J Neurosci 38 (4):803–813. https://doi.org/10.1523/jneurosci.1657-17.2017
69. White SL et al (2016) A critical role for the glua1 accessory protein, SAP97, in cocaine seeking. Neuropsychopharmacology 41 (3):736–750. https://doi.org/10.1038/npp.2015.199
70. Boyer F, Dreyer JL (2007) Alpha-synuclein in the nucleus accumbens induces changes in cocaine behaviour in rats. Eur J Neurosci 26 (10):2764–2776. https://doi.org/10.1111/j.1460-9568.2007.05878.x
71. Sternson SM, Roth BL (2014) Chemogenetic tools to interrogate brain functions. Annu Rev Neurosci 37:387–407. https://doi.org/10.1146/annurev-neuro-071013-014048
72. Mahler SV, Aston-Jones G (2018) CNO Evil? Considerations for the use of DREADDs in behavioral neuroscience. Neuropsychopharmacology 43(5):934–936. https://doi.org/10.1038/npp.2017.299
73. Gomez JL et al (2017) Chemogenetics revealed: DREADD occupancy and activation via converted clozapine. Science (New York, NY) 357(6350):503–507. https://doi.org/10.1126/science.aan2475
74. Stamatakis AM, Stuber GD (2012) Optogenetic strategies to dissect the neural circuits that underlie reward and addiction. Cold Spring Harbor Perspect Med 2(11). https://doi.org/10.1101/cshperspect.a011924
75. Tsai HC et al (2009) Phasic firing in dopaminergic neurons is sufficient for behavioral conditioning. Science (New York, NY) 324 (5930):1080–1084. https://doi.org/10.1126/science.1168878
76. Witten IB et al (2011) Recombinase-driver rat lines: tools, techniques, and optogenetic application to dopamine-mediated reinforcement. Neuron 72(5):721–733. https://doi.org/10.1016/j.neuron.2011.10.028

77. Ilango A et al (2014) Similar roles of substantia nigra and ventral tegmental dopamine neurons in reward and aversion. J Neurosci 34 (3):817–822. https://doi.org/10.1523/jneurosci.1703-13.2014
78. Pascoli V et al (2015) Sufficiency of mesolimbic dopamine neuron stimulation for the progression to addiction. Neuron 88 (5):1054–1066. https://doi.org/10.1016/j.neuron.2015.10.017
79. Corre J et al (2018) Dopamine neurons projecting to medial shell of the nucleus accumbens drive heroin reinforcement. elife 7. https://doi.org/10.7554/eLife.39945
80. Trouche S et al (2016) Recoding a cocaine-place memory engram to a neutral engram in the hippocampus. Nature Neurosci 19 (4):564–567. https://doi.org/10.1038/nn.4250
81. Hamel EJ et al (2015) Cellular level brain imaging in behaving mammals: an engineering approach. Neuron 86(1):140–159. https://doi.org/10.1016/j.neuron.2015.03.055
82. Resendez SL, Stuber GD (2015) In vivo calcium imaging to illuminate neurocircuit activity dynamics underlying naturalistic behavior. Neuropsychopharmacology 40(1):238–239. https://doi.org/10.1038/npp.2014.206
83. Girven KS, Sparta DR (2017) Probing deep brain circuitry: new advances in in vivo calcium measurement strategies. ACS Chem Neurosci 8(2):243–251. https://doi.org/10.1021/acschemneuro.6b00307
84. Mostany R et al (2015) Two-photon excitation microscopy and its applications in neuroscience. Methods Mol Biol (Clifton, NJ) 1251:25–42. https://doi.org/10.1007/978-1-4939-2080-8_2
85. Marker DF et al (2010) A thin-skull window technique for chronic two-photon in vivo imaging of murine microglia in models of neuroinflammation. JoVE (43):2059. https://doi.org/10.3791/2059
86. Helmchen F (2009) Frontiers in neuroscience two-photon functional imaging of neuronal activity. In: Frostig RD (ed) In vivo optical imaging of brain function. CRC Press/Taylor & Francis, Taylor & Francis Group, LLC, Boca Raton, FL
87. Williams SB et al (2019) Hippocampal activity dynamics during contextual reward association in virtual reality place conditioning. bioRxiv:545608. https://doi.org/10.1101/545608
88. Guo Q et al (2015) Multi-channel fiber photometry for population neuronal activity recording. Biomed Optics Express 6 (10):3919–3931. https://doi.org/10.1364/boe.6.003919
89. Sych Y et al (2019) High-density multi-fiber photometry for studying large-scale brain circuit dynamics. Nat Methods 16(6):553–560. https://doi.org/10.1038/s41592-019-0400-4
90. Calipari ES et al (2016) In vivo imaging identifies temporal signature of D1 and D2 medium spiny neurons in cocaine reward. Proc Natl Acad Sci U S A 113 (10):2726–2731. https://doi.org/10.1073/pnas.1521238113
91. Xia L et al (2017) Dorsal-CA1 hippocampal neuronal ensembles encode nicotine-reward contextual associations. Cell Rep 19 (10):2143–2156. https://doi.org/10.1016/j.celrep.2017.05.047
92. Shields BC et al (2017) Deconstructing behavioral neuropharmacology with cellular specificity. Science (New York, NY) 356 (6333). https://doi.org/10.1126/science.aaj2161
93. Nestler EJ, Luscher C (2019) The molecular basis of drug addiction: linking epigenetic to synaptic and circuit mechanisms. Neuron 102 (1):48–59. https://doi.org/10.1016/j.neuron.2019.01.016
94. Bali P, Kenny PJ (2019) Transcriptional mechanisms of drug addiction. Dialogues Clin Neurosci 21(4):379–387. https://doi.org/10.31887/DCNS.2019.21.4/pkenny
95. Nectow AR et al (2017) Rapid molecular profiling of defined cell types using viral TRAP. Cell Rep 19(3):655–667. https://doi.org/10.1016/j.celrep.2017.03.048
96. Nectow AR, Ekstrand MI, Friedman JM (2015) Molecular characterization of neuronal cell types based on patterns of projection with Retro-TRAP. Nat Protoc 10 (9):1319–1327. https://doi.org/10.1038/nprot.2015.087
97. Shigeoka T et al (2016) Dynamic axonal translation in developing and mature visual circuits. Cell 166(1):181–192. https://doi.org/10.1016/j.cell.2016.05.029
98. Ouwenga R et al (2017) Transcriptomic analysis of ribosome-bound mRNA in cortical neurites in vivo. J Neurosci 37 (36):8688–8705. https://doi.org/10.1523/jneurosci.3044-16.2017
99. Logrip ML (2019) Molecular tools to elucidate factors regulating alcohol use. Alcohol (Fayetteville, NY) 74:3–9. https://doi.org/10.1016/j.alcohol.2018.03.006

100. Rosenberg SA et al (1990) Gene transfer into humans--immunotherapy of patients with advanced melanoma, using tumor-infiltrating lymphocytes modified by retroviral gene transduction. N Engl J Med 323 (9):570–578. https://doi.org/10.1056/nejm199008303230904
101. Blaese RM et al (1995) T lymphocyte-directed gene therapy for ADA- SCID: initial trial results after 4 years. Science (New York, NY) 270(5235):475–480. https://doi.org/10.1126/science.270.5235.475
102. Approved Cellular and Gene Therapy Products. (2019)
103. Hocquemiller M et al (2016) Adeno-associated virus-based gene therapy for CNS diseases. Hum Gene Therapy 27 (7):478–496. https://doi.org/10.1089/hum.2016.087
104. Kantor B et al (2014) Clinical applications involving CNS gene transfer. Adv Genet 87:71–124. https://doi.org/10.1016/b978-0-12-800149-3.00002-0
105. Deverman BE et al (2018) Gene therapy for neurological disorders: progress and prospects. Nat Rev Drug Discov 17(10):767. https://doi.org/10.1038/nrd.2018.158
106. Maoz A et al (2013) Adenovirus capsid-based anti-cocaine vaccine prevents cocaine from binding to the nonhuman primate CNS dopamine transporter. Neuropsychopharmacology 38(11):2170–2178. https://doi.org/10.1038/npp.2013.114
107. Evans SM et al (2016) Efficacy of an adenovirus-based anti-cocaine vaccine to reduce cocaine self-administration and reacqusition using a choice procedure in rhesus macaques. Pharmacol Biochem Behav 150–151:76–86. https://doi.org/10.1016/j.pbb.2016.09.008
108. Havlicek D, De B, Rosenber J, Pagovich O, Sondhi D, Kaminsky S, Crystal R (2016) Translation of an adenovirus-based cocaine vaccine dAd5GNE to a clinical trial. Mol Ther 24(Suppl. 1):S16

Chapter 13

Conditioned Place Preference Test for Assessing the Rewarding Effects of Drugs of Abuse

Todd Hillhouse and Adam Prus

Abstract

The conditioned place preference (CPP) procedure is used for assessing the rewarding effects of drugs. This is demonstrated when a novel environment becomes associated with a drug's effects, to the extent that an organism, when given the choice, will prefer to be in that environment. The procedure has been used across numerous drug classes and species. This chapter reviews the approaches to conducting CPP studies, including considerations on equipment setups, training procedures, data analyses, pharmacological manipulations, conditioned place aversion, and other features of place conditioning. The chapter serves as a primer for using this procedure for the study of drugs that produce rewarding or aversive effects.

Key words Conditioned place preference, Drug, Motivation, Reward

1 Introduction: Conditioned Place Preference

The conditioned place preference (CPP) procedure is used to determine if a drug exhibits rewarding effects capable of developing associations with environmental stimuli. The general approach for this procedure consists of an organism experiencing the effects of a drug while situated in an environment that is markedly different from an environment where the organism experiences none of the drug's effects. CPP readily occurs after multiple pairings with a drug that displays rewarding effects, such as morphine or cocaine. The preference for the drug-associated environment comes after conditioning sessions have been conducted. During a test session that follows a series of conditioning sessions, the organism is provided free range in the experimental chamber to access both the drug and nondrug conditioning environments, and a CPP is shown if significantly more time is spent in the drug-paired environment.

The procedure also is used to evaluate a drug's aversive effects. For this approach, an organism spends significantly more time in the nondrug paired environment. When this is observed, the

Marc Fakhoury (ed.), *The Brain Reward System*, Neuromethods, vol. 165, https://doi.org/10.1007/978-1-0716-1146-3_13,

finding is referred to as a *conditioned place aversion (CPA)*. CPA studies have been used for drugs that exhibit unpleasant effects as well as for withdrawal effects from a chronically-administered substance. Because this conditioning procedure might result in preference or aversion, the procedure has also been referred to more generally as *place conditioning*.

CPP studies yield findings applicable to models of drug addiction, thereby making this procedure useful for basic studies on abused substances. Addiction models and supportive evidence have well-established the role of drug-associated environmental stimuli toward motivating drug seeking, maintenance use, and relapse. As CPP procedures demonstrate that environmental stimuli, through associations with rewarding drug states, become themselves sufficiently rewarding to engage an organism to seek them out, the inherent demonstration of these effects lends themselves to understanding the role of drug-associated stimuli in addiction. A noted feature of addiction, for example, is incentive salience, the act of drug-associated stimuli attracting the attention of a current user or former user that can trigger a "wanting" for the substance. If a drug readily produces CPP through associating the drug's rewarding effects with the contextual stimuli, then this same drug is likely capable of leading to incentivized stimuli through repeated use. Another example comes from the failure of tolerance studies reported by Shepard Siegel [1]. Siegel's work demonstrated that overdose among experienced users occurred as a failure of tolerance in situations where environmental stimuli that otherwise would have induced the necessary physiological state that normally counters the drug's effects were not present. Since CPP depends entirely on the strength of stimulus-drug associations, CPP studies have value in understanding features of drug addiction for known or novel substances.

This chapter provides an overview of the methodological approaches for CPP (or CPA), species studied, and adherence of findings to basic pharmacological principles. Coverage includes how to interpret results and advantages and disadvantages to using this procedure compared to other procedures.

2 Methodological Approaches

2.1 Subjects

CPP experiments are most commonly conducted in male C57BL/6 mice and Sprague Dawley rats that are at least eight weeks old. Although C57BL/6 mice and Sprague Dawley rats are the most commonly used strains/species, it is possible to conduct CPP in female mice, different strains, and transgenic animals. For the remainder of the chapter, we will use the term mice (or mouse), however, the methods using rats are normally the same.

2.2 CPP Apparatus

When determining the CPP chamber for your experimental design, there are several options to consider. That is, two chambers versus three chambers and commercial or lab-built equipment. For rodents, CPP chambers are normally configured as a shuttle box with compartments arranged completely side by side, although other designs are not uncommon. This section will discuss the advantage and disadvantages of the different experimental apparatus designs.

A common rodent shuttle box used for CPP studies consist of three side-by-side chambers, closed off from each other by a guillotine door (Fig. 1a, b). This provides for conditioning sessions using the outermost compartments, and for preconditioning sessions, which may be used for habituation and/or to assess for any initial preferences for a compartment before conditioning, a "neutral" compartment separating the conditioning compartments. Thus, for a preconditioning session, a mouse can be placed in the neutral compartment as a starting area for exploring the chamber. During test sessions, where time spent in either of the conditioning chambers is assessed, the mouse can start the session in the neutral chamber. Doing so prevents a potential confound of selecting a conditioning chamber as a starting chamber during a test. For example, if a mouse were placed in the drug-paired side for a test session and then failed to leave the chamber, it would be unclear if a preference was demonstrated or if some other factor, such as anxiety, prevented the mouse from venturing beyond the chamber it was placed in. Thus, placing a mouse in a neutral chamber can largely address this issue as a potential confound. One disadvantage to using a three-chamber design, however, is that on preconditioning and test days, some of the time spent on the drug- or saline-paired side, which is the primary dependent variable, is "lost" when animals spend time in the neutral zone. Generally, some number of mice in every group will spend a substantial amount of the test session time in the neutral zone, making it difficult to determine if a true preference for a drug-paired compartment was demonstrated even when there was significantly more time spent in a drug-paired versus vehicle-paired condition.

The two-chamber design has two distinct chambers that are separated by a guillotine door (Fig. 1c, d). As an apparatus with two chambers, one side serves as the drug-associated compartment and the opposite side serves as the vehicle-associated compartment. During any assessments that allow animals to pass back and forth between the two compartments, an animal must first be placed in either of the compartments. This requirement can result in increased time on that side if an animal does not readily leave the chamber it was initially placed in. Due to this, a potential confound can occur and must be addressed by counterbalancing the start position across animals. Unlike the three-chamber designs, the two-chamber design creates a forced choice situation for the

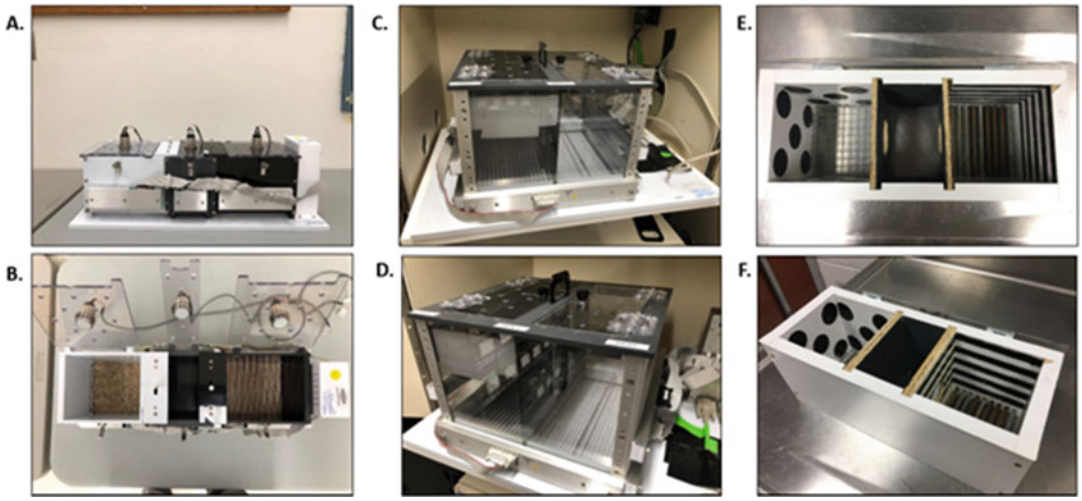

Fig. 1 Selected types of place conditioning equipment. (**a** and **b**): A standard three-compartment shuttle box for mice (top view **a** and side view **b**) includes two distinctly different left and right compartments and a middle compartment. This is a commercially built chamber (Med-Associates, Inc.) typically used for place conditioning studies. (**c** and **d**): For laboratories that use open field equipment, inserts can be added to allow use for place conditioning studies. The inserts for this open field provides for two compartments. Pictured is a commercially-built open field with place conditioning inserts provided by the manufacturer (Med-Associates, Inc.). (**e** and **f**): A three-compartment shuttle box constructed from laminated particleboard, transparent acrylic lid, and metal bars or grids for floors. This is a lab-built unit built to similar dimensions as commercially build mouse chambers. Panel **e** shows the apparatus with the doors "open" (a circular opening cut with a hole saw) and panel F shows the apparatus with the doors "shut" (a panel pressed against each opening. Sessions using these chambers are recorded by an overhead camera (not shown). Photos **a**, **b**, **e**, and **f** taken by the chapter authors; photos **c** & **d** generously provided by Joseph Porter. The apparatus shown in **e** and **f** was built by Lindsey Galbo

animals, which avoids losing time to a neutral chamber, as in a three-chamber apparatus.

As the apparatus is relatively simple, it is common and acceptable for researchers to either use a commercially built apparatus or a lab-built apparatus for CPP procedures. Regardless of the origin of the equipment, the two conditioning compartments must have unique visual, tactile, and/or olfactory stimuli to establish distinct environments to serve as cues for pairing and test sessions. The arrangement and choice of stimuli create extensive variety across laboratories, which largely precludes a specific standard set up. However, laboratories should arrange stimuli so that one compartment is not innately preferred to animals over another. For example, a common set up includes having one compartment with white walls and another compartment with black walls. If a sufficient degree of illumination is not provided to each compartment, then the side with black walls will likely provide the darkest, and therefore, the most attractive location for mice or rats. This, of

course, would provide an element of bias into the study, which may compromise an interpretation of test data.

As noted, a common laboratory arrangement consists of having one compartment with white walls and another compartment with either black walls or black stripes. Tactile stimuli are also common as an additional set of stimuli, and for rodent studies, these stimuli typically consist of a horizontal bar floor in one chamber and a grid floor in another chamber. Many studies also use olfactory stimuli as a third type, which can be achieved by adding an odor to the bedding pan beneath the grid floor. In addition, using different types of bedding for each chamber (e.g., wood shavings vs. corn cob bedding) may be sufficient to provide different olfactory stimuli.

One commercial company that provides shuttle box chambers for CPP experiments is Med-Associates Inc. (St. Albans, VT USA). Med-Associates manufactures a two- and three-chamber stand-alone system that comes equipped with a white chamber that has a grid floor and a black chamber that has a bar floor. There is a house light located at the top of each chamber to produce equal lighting on either side, which precludes the black-walled chamber from having darker illumination than the white-wall chamber (Fig. 1a, b). These systems can be equipped with manual or automated guillotine doors, and generally come equipped with several photobeams generators and receivers within each chamber. Alternatively, a tilting grid floor can be used to register entry into a chamber, but this is restricted to a two-chamber arrangement.

Med-Associates has a third system that inserts into their open-field arena (Fig. 1c, d). The CPP insert is a two-chamber system that is equipped with a wire floor and bar floor; however, the walls are clear. To make the walls distinct, dark, white, or pattern paper can be fixed to the outside of the transparent walls of the chambers.

San Diego Instruments Inc. (San Diego, CA) manufactures a two- and three-chamber CPP apparatus that provides more flexibility to the researcher. Their chambers have clear walls, which allows the researcher to provide distinct visual cues by fixing them to the outside of the walls. The chambers also have a reversible floor that features both a rough and smooth side. Activity in the apparatus is recorded via a photobeam array. In general, most small laboratory animal behavior testing equipment suppliers offer an apparatus for conducting CPP studies, and they tend to be similar in set up, although the size will differ between mice and rats.

Due to the simplicity of the CPP design, another option is to build a CPP unit in the lab. Lab-built units need to be constructed out of a nonporous material (e.g., plexiglass, high-density polyethylene, etc.) and should conform to the dimensions normally used for mice or rats (Fig. 1e, f). Researchers can refer to published CPP papers to review the dimensions of equipment used or they can review the dimensions of commercial CPP chambers. As mentioned

earlier, these chambers should at least have distinct visual cues and tactile flooring cues. The lab-built units are far less expensive than commercial units, but adding automation, for either operating the chamber or tracking behavior, to the lab-built units requires a degree of technical know-how.

As noted earlier, the Med-Associates Inc. and San Diego Instruments Inc. systems use automated methods for tracking movement, which normally consists of photobeam arrays. These photobeam systems can track time spent in each chamber, number of entries into each chamber, ambulatory activity, stereotypic behaviors, and so on. Tilting grid floors are available from Med-Associates, as well, but these can only inform the researcher about entries and time spent in a chamber. In addition, animals sitting near the entry of a compartment may not have crossed far enough in to tilt the floor and mark an entry into the compartment. There are several top-view video-tracking systems (e.g., EthoVision, TopScan, etc.) that can record the same data as the photobeam systems, however, they also have the capability for more detailed measures such as average speed and grooming.

All of these systems are appropriate for the CPP assay for the primary dependent variable needed for a CPP procedure (i.e., time spent in a compartment), and most provide a means for assessing ambulatory activity. The most cost-effective approach involves building an apparatus and video recording sessions from an overhead camera. Afterward, researchers can view the video and use timers to record time spent in the compartments. In this arrangement, multiple experimentally blind observers should be used to score these measures, and comparisons between the observers should be conducted to ensure accuracy.

3 Research Design for CPP Procedures

CPP experiments consist of three main phases: (1) preconditioning sessions (e.g., a bias test), (2) conditioning sessions, and (3) test sessions.

3.1 Preconditioning Sessions

Preconditioning sessions provide a means to habituate animals to the CPP chambers and can be used to assess for natural biases toward any of the chambers. Researchers typically use one or two preconditioning sessions before moving on to conditioning sessions. From an associative learning standpoint, too many preconditioning sessions may impair the development of CPP for a drug as the environmental stimuli lose their novelty the longer animals are given in the environment prior to conditioning.

When a preconditioning session is used to determine if animals have an unconditioned preference for any of the chambers, this is referred to as a bias test session. For test bias sessions, mice are

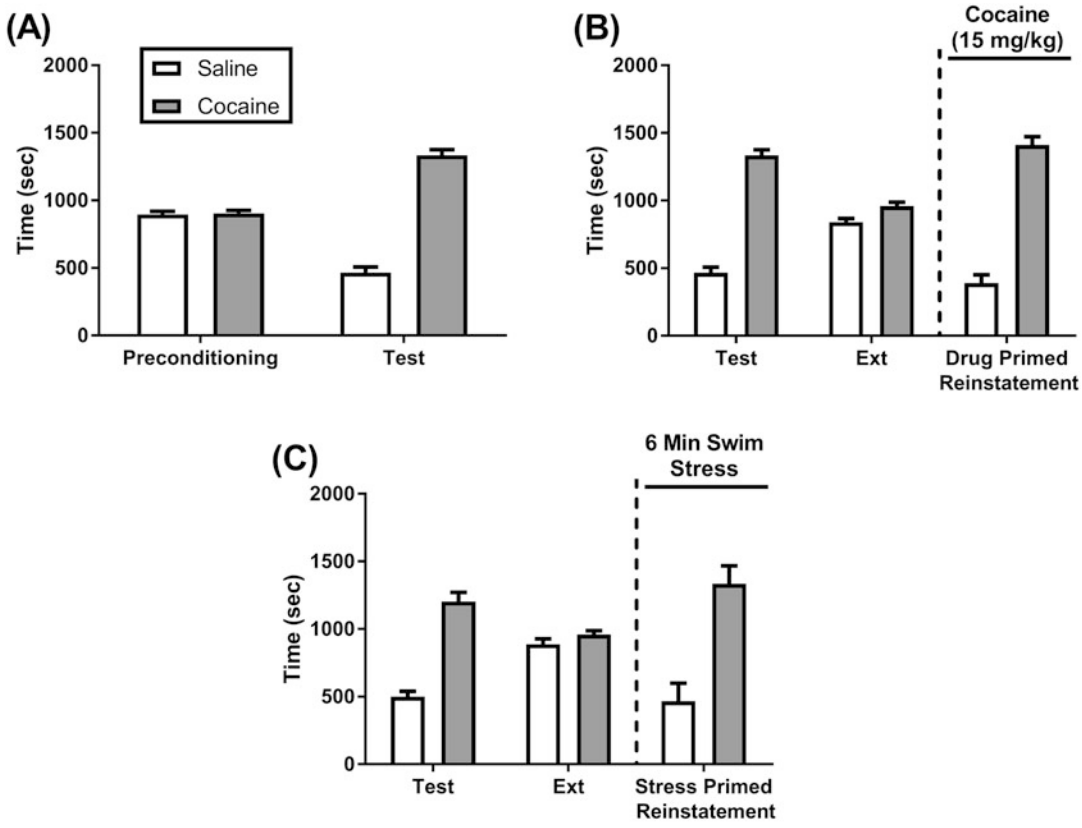

Fig. 2 Effects of 15 mg/kg cocaine on conditioned placed preference using time on drug and saline paired sides as the dependent variable. Unbiased counterbalanced conditioning designed was used as mice did not have a preference for one side during the preconditioning phase. Mice were conditioned in two-chamber Med-associates CPP chambers. (**a**–**c**) After 2 days of cocaine pairing, cocaine significantly increases the time spent on the drug paired side. (**b**, **c**) Following several extinction pairings (i.e., no drugs were administered), mice successfully met extinction criteria (i.e., 50% reduction in cocaine preference). (**b**) For cocaine primed reinstatement, mice were administered a single cocaine dose (15 mg/kg) prior to the start of the session. The pretreatment of cocaine elicited a significant increase in the time spent on the cocaine pair side (i.e., cocaine reinstatement). (**c**) For stress-primed reinstatement, mice experienced a single 6-min swim and placed into the CPP chambers immediately after being towel dried. The swim stress produced a significant increase in the time spent on the drug side. Data are expressed as mean ± standard error of the mean. Data were generously provided by John Traynor at the University of Michigan

placed in the CPP apparatus with all interchamber doors opened, which allows free exploration of the apparatus. The session length can vary from 15 to 45 min; however, the final preference test day (given after conditioning sessions) must be the same duration as the bias test session. Time spent on each side is recorded, and an unconditioned preference each mouse demonstrates between the conditioning chambers can be identified (Fig. 2a).

The information gained for assessing unconditioned preferences facilitates either of two approaches for CPP conditioning

and testing. The first approach is referred to as *biased testing*. For biased testing, the assignment of a chamber for *drug conditioning will consist of the least-preferred side* (e.g., [2–4]). For example, if a mouse has a preference for the black chamber then the drug conditioning will occur in the white chamber. By using this approach, test session data can be interpreted by how much the preference for the least-preferred side shifted from the most-preferred side. Although the bias design provides a greater "window" to establish a drug preference because they spent less time on this side during the preconditioning phase, there is a concern that some of this drug preference can be attributed to the mouse becoming neutral to the two sides of the CPP apparatus. That is, there may be a lack of preference shown during a CPP test in terms of total time spent in each chamber, although a neutral preference may represent a statistically significant shift in preference from the least-preferred to the most-preferred side.

The second approach is referred to as an *unbiased* testing design for CPP. In this approach, the chamber used for drug conditioning is either randomly assigned or assigned in a counterbalanced manner across subjects (e.g., [5–7]). For example, approximately half the mice will have drug-paired on the side in which they had a preference and the other half will have saline-paired on the side in which they had a preference. Unconditioned assessments are conducted to determine which animals have a strong preference for one side and could, therefore, confound the study results. Many laboratories remove mice from a study if >70% of the time spent on one side is shown during the bias test session. Bardo et al. [8] conducted an excellent meta-analysis on how methodological variables can influence CPP, which includes biased versus unbiased designs.

Generally, one bias test session is conducted; however, some laboratories conduct two bias sessions. When using two bias session, you have the option to use the first bias session as a "habituation" day, in which you will not record the time spent on either side [4, 9]. The second option is to record the time spent on each side for both bias sessions and take the average [5, 10]. It is possible that a mouse might show a preference on bias day 1, but not bias day 2. In this case, fewer mice will be eliminated from the study.

3.2 Conditioning Sessions

During the conditioning phase, mice will be administered the drug of interest or saline and confined to one side of the CPP apparatus. There are a number of options for conducting the conditioning phase which include the number of pairings (2–5 pairings), the time between drug and saline pairings (same day or 24 h apart), and duration of conditioning session (20–45 min). The drug or drug class can determine many of these factors. For example,

buprenorphine requires a 24-h period between drug and saline conditioning sessions [11–13]; whereas, the conditioning session for nicotine and cocaine can occur on the same day with 4–6 h between injections [4, 14, 15].

3.3 Preference Test

The preference test session will be conducted identically to the preconditioning session. Mice are free to explore both sides of the CPP box for the same duration as the bias test session. Time spent on each side will be recorded for the test session. See the data analysis section for dependent variable calculations.

3.4 Using CPP for Reinstatement Testing

CPP procedures also can be used to assess reinstatement. For self-administration studies, reinstatement tests are conducted after numerous extinction sessions have led to little or no self-administration responses. During reinstatement testing, a cue associated with drug administration is activated and drug administration responded is assessed. If an appreciable level of responding occurs, then the cue is noted as having reinstated self-administration responding. In CPP, procedures analogous to reinstatement in self-administration studies have been used.

Extinction Training. As in self-administration studies, extinction sessions are conducted following the determination of CPP for a drug. Following the CPP test, mice receive daily extinction sessions. For extinction sessions, mice do not receive an injection and are free to explore both sides of the CPP box for the same duration as bias and test sessions. Time spent on each side is recorded. Extinction training continues until the preference for the drug-paired side is reduced by 50% of the initial test preference.

Another option is to evaluate the group of animals as a whole in which extinction is defined as no significant difference between the extinction session and bias test session [2, 6, 9, 16]. One issue with this method is that not all mice will meet the extinction criteria, and thus you are not measuring reinstatement in all of the animals. Mice that do not show extinction after a number of sessions, such as 40 extinction sessions, are eliminated from assessments for reinstatement sessions.

Reinstatement Testing. Once mice meet the extinction criteria, mice can be subject to drug-primed or stress-primed reinstatement. For *drug-primed reinstatement*, mice are administered the drug of interest (either the drug used during conditioning or another substance with similar effects) and placed immediately in the CPP apparatus (Figs. 2b and 3a). Time spent on each side is recorded. Another option is to subject the mice to one cycle of conditioning (one drug pairing and one saline pairing), which is insufficient to produce CPP in naive mice. Reinstatement will be examined 24 h after the single cycle of conditioning [2].

For *stressed-primed reinstatement*, mice are subjected to a stressor prior to being placed in the CPP apparatus. One example

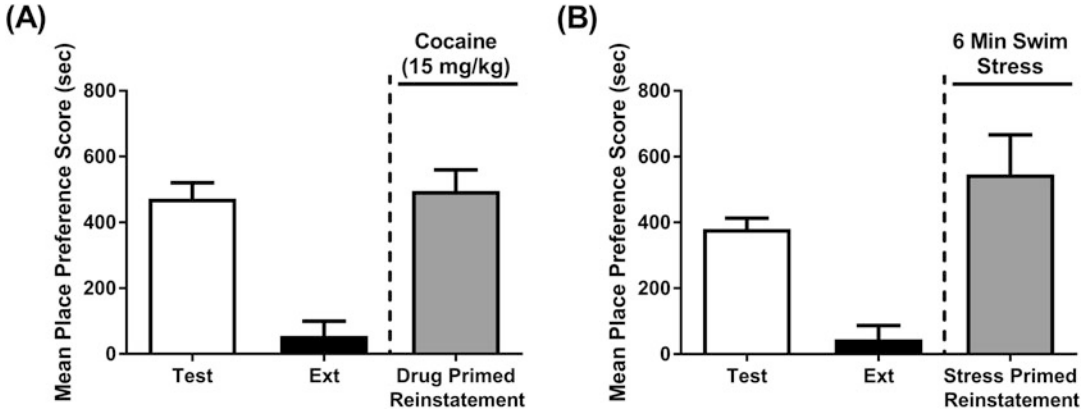

Fig. 3 Effects of 15 mg/kg cocaine on conditioned placed preference using cocaine preference scores as the dependent variable. Conditioning procedures are identical to Fig. 1. (**a**, **b**) After 2 days of cocaine pairing, cocaine significantly increases in the cocaine preference score (**b**, **c**) Mice successfully met extinction criteria. (**a**) A single cocaine injection (15 mg/kg) significantly increase in the cocaine preference score indicating drug primed reinstatement. (**b**) Exposure to a single 6-min swim elicited a significant increase cocaine preference score indicating stress primed reinstatement. Data are expressed as mean ± standard error of the mean. Data were generously provided by John Traynor at the University of Michigan

of this is swim-stress. Swim-stress consists of placing mice in a glass cylinder (18 cm tall × 14 cm in diameter) filled with 30 °C water to a depth of 14 cm for 6 min [2, 3]. Swim–stress has been shown to produce a significant reinstatement effect for CPP (Figs. 2c and 3b).

3.5 Data Analysis

There are a number of approaches for analyzing data in a CPP procedure. The approaches used depend partly on whether a biased or unbiased CPP design is used for the study. In an unbiased design, a simple approach consists of statistically comparing the time spent in the drug-paired side versus the vehicle-paired side (Fig. 2). For a study utilizing a three-compartment chamber for the purpose of having a neutral compartment, time spent across all compartments might also be analyzed. Essentially, this factors in a "no preference" condition into the analysis. Alternatively, preference for a drug-paired versus vehicle-paired side when using a neutral condition can also be expressed as a percentage of total time spent on each side. The percentage calculation might also be calculated out of the sum of time spent in the drug-paired and vehicle-paired sides. This later calculation can provide an analysis focused on only drug or vehicle. However, if a substantial amount of time was actually spent in the neutral condition, then only displaying percentage data for the drug- and vehicle-paired side would mislead readers into seeing a stronger preference that was actually found.

Biased designs provide an additional approach for analyzing CPP data. Given that baseline preference data are available in a

biased design, analyses can include a comparison between the preference test session and the baseline preference assessment session (s). In this analysis, researchers consider whether conditioning led to a shift in preference, rather than simply assessing for a difference between drug and vehicle side preferences from the preference test. This approach for a biased design determines a *place preference score*. A place preference score is calculated by subtracting the time spent on the drug-paired side on the baseline preference assessment session from the time spent on the drug-paired side on the preference day (Fig. 3). Again, when using a three-compartment chamber that allows for a neutral position, preferences might also be assessed as percentages of time spent in only the vehicle and drug paired sides. While a biased design requires the use of place preference scores, an unbiased design can also use the score to display and analyze the results (Fig. 3).

Another measure used during CPP procedures is the locomotor activity within a compartment. Locomotor activity assessments do not convey place preferences, but they do offer measures of nonspecific motor effects. These measures can be especially helpful for assessing drugs that may have stimulant or sedative effects as these measures assist in verifying that doses are behaviorally active. Locomotor assessments also provide a means for collecting data during training conditions. This may be of interest in assessing certain classes of drugs, such as psychostimulant, which may produce sensitization across training sessions. The measure of locomotor activity nearly always includes an automated recording method, such as photobeam breaks or path length tracking from an overhead camera.

4 Conditioned Place Aversion

The approach to using place conditioning to examine CPA follows the same procedures as CPP. Typically, researchers randomly assign compartments across animals for the aversive condition (unbiased design). If a bias design were used, then the aversive would be assigned to each animal's preferred side.

Antagonist precipitated CPA following repeated administration of drugs of abuse: One way to evaluate the negative effects of drug withdrawal to first repeatedly administer a drug of abuse to achieve dependence, and then conduct place conditioning with the drug's antagonist, which creates conditioning with a withdrawal state. This procedure will readily produce a CPA. For example, to evaluate the withdrawal (CPA) effects of morphine, mice are administered with repeated doses of morphine over 4–5 days. Following the final morphine treatment, mice are administered naloxone to precipitate withdrawal and confined to one side of the CPP apparatus. Naloxone produces a robust CPA in rodents previously treated

with morphine. However, naloxone does not produce a CPA in the control animals that received repeated treatment with saline [17, 18]. Similar methods have been used to study the withdrawal effects of nicotine [19].

Lithium Chloride (LiCl) CPA design: The Ossenkopp research group has demonstrated that several doses LiCl (32, 95, and 127 mg/kg) produce CPA that lasts for up to 5 days [20–22]. To accomplish this CPA, these studies conducted two "conditioning cycles" that were separated by 72 h. Each conditioning cycle consisted of two LiCl and two saline pairings that were separated by 24 h (i.e., LiCl, NaCl, LiCl, NaCl). The conditioning cycle was repeated 72 h after the last conditioning session of the first conditioning cycle. Two research groups have demonstrated that LiCl CPA can be achieved with less conditioning sessions. For example, Buffalari et al. [23] produced LiCl CPA after two LiCl and two saline pairings over four consecutive days. These conditioning sessions were separated by 24 h. Bagdas et al. [24, 25], found that LiCl (150 mg/kg) produces a significant CPA score with twice a day conditioning session over three conditioning days. In these studies, mice received both LiCl and saline conditioning sessions on the same day.

Acetic acid CPA design: CPA has been used to evaluate the aversive effects of acute pain states in rodents. The goal of this protocol is to evaluate the analgesic effects of novel compounds. Bagdas et al. [24] used a 3-day unbiased design which consisted of one preconditioning day, one conditioning day, and one test day. On the conditioning day, animals received saline or acetic acid (0.32–1.0%) and were confined to one side for 40 min. Saline and acetic acid conditioning were separated by at least 4 h. Acetic acid produced a concentration dependent aversion score with 1.0% acetic acid producing the greatest aversion. Pretreatment with the nonsteroidal anti-inflammatory drug ketoprofen, mu-agonist morphine, and nonselective nicotinic agonist nicotine on the conditioning day attenuated the expression of CPA [24, 25].

5 Pharmacological Assessments Using the Conditioned Place Preference Procedure

The conditioned place preference procedure, when used for pharmacological procedures, generally adheres to basic pharmacological principles. That is, CPP is subject to such things as a drug's time of onset, elimination rate, metabolic considerations, and counteractions at the site of action (e.g., administration of a receptor antagonist). Dose-dependency may not always be demonstrated as drugs that demonstrate a statistically significant CPP to reach a maximum effect, precluding assessing dose-dependent effects. Along these lines, the difficulty in producing dose response curves for conditioned place preference preclude studies to assess tolerance

or sensitization in this procedure. These factors do not come into play during the procedure's test session, which is conducted in a drug-free state. This section considers these issues and highlights the study findings to serve as examples.

As in any pharmacological investigation, a drug's pretreatment time must be determined so that a drug has time to reach its site of action and generate pharmacological effects. In CPP, the considerations must involve placing an animal in the drug-paired compartment at a time when a sufficient magnitude of drug effects, if not peak drug effects, are present. For a relatively short pretreatment time (approximately 5 min), animals might be placed immediately in the conditioning chamber, whereas a drug with a longer pretreatment time might be kept in the homecage for a duration of time while the drug takes effect. For example, Itzhak and Martin [26] assessed CPP for 15 mg/kg (ip) cocaine in mice, which consisted of injecting the mice and then placing them immediately in the appropriate compartment for a 30-min session. The onset of cocaine's effects that presumably were weak at the beginning of the session but quickly grew to adequate intensity was sufficient for establishing a CPP for cocaine for the course of four pairings.

As noted earlier, dose response curves may be difficult to produce for CPP since low doses of a drug tend to reach near-maximum levels of preference that also is shown for higher drug doses. However, Barr et al. [27] demonstrated that dose dependency is shown when a reference reinforcing compound is used in place of the vehicle. In this study, CPP was assessed for morphine (0.1, 0.3, 3.0, and 5.0 mg/kg) CPP versus a 1.0 mg/kg dose of morphine. The results found that rats spent more time in the 1.0 mg/kg compartment compared to lower doses and less time in the 1.0 mg/kg compartment compared to higher doses. The degree of preference began low for the 0.1 mg/kg dose and reached a place preference of approximately 70% (vs. 1.0 mg/kg) for the 3.0 and 5.0 mg/kg doses. In this way, they demonstrated incremental increases in preference for morphine as doses were increased.

For some compounds, moderate doses may lead to CPP while higher doses may fail to exhibit CPP. For example, in a study by Kota, Martin, and Damaj [28], adolescent female mice were assessed for CPP using either a 0.1, 0.5, 0.7, or 1.0 mg/kg dose of nicotine. A CPP was observed for the 0.5 mg/kg dose, but neither a CPP nor CPA was shown for the higher doses or lower dose tested. This study also tested adult female mice, finding CPP for a 0.7 and 1.0 mg/kg dose, but no effect for lower doses. In another study from this group, male adolescent mice exhibited CPP for a 0.05, 0.1, and 0.5 mg/kg dose of nicotine, but not for higher doses. Adult mice only exhibited CPP for a 0.5 mg/kg dose, whereas no effects were observed for lower or higher doses [29].

Conditioning in these procedures is subject to extinction and can be reinstated. Extinction occurs following repeated exposures to the drug-conditioned compartment without the effects of drug present. Itzhak and Martin [26], for example, established a CPP for cocaine in mice following eight conditioning sessions (four per condition). Then they gave eight subsequent sessions of only vehicle administration paired with each compartment. A test session following these vehicle sessions did not reveal a preference for either compartment. This study also demonstrated reinstatement by conducting another test session following the administration of the conditioning dose of cocaine. During a cocaine drug state, mice spent significantly more time in the cocaine-associated compartment. In a similar demonstration, Parker and Mcdonald [30] reported extinction and reinstatement for a morphine CPP and a LiCl CPA.

Antagonist effects can be shown in this procedure, normally at doses that alone do not cause a change in place conditioning. Studies using the D_1 receptor antagonist SCH23390 serve as a common example of this. Administration of SCH23390 alone does not induce either a CPA or CPP, yet the compound is capable of counteracting CPP to number compounds that induce reinforcing effects. For example, in a study by Acquas et al. [31] conditioning trials that pretreated rats with SCH23390 before morphine, nicotine, or diazepam administration prevented CPP for these compounds. An effect by SCH23390 alone was not found. However, the opioid antagonist naloxone induces CPA. In this same study, CPA was demonstrated by naloxone, phencyclidine, and the convulsant picrotoxin. Here too, pretreatment with SCH23390 prevented CPA by these compounds.

6 Conclusions

Place conditioning serves as a robust behavioral paradigm for assessing rewarding or aversive states. Rewarding states, such as those generated by abused substances, engender a preference for the side that drug conditioning occurred on, and aversive states demonstrate the opposite preference. The majority of CPP studies use mice, but a wide variety of species have been used. Equipment typically consists of a two- or three-compartment shuttle box, and each apparatus has unique advantages and disadvantages. Quality studies can be conducted using either commercially built chambers or lab-built chambers, provided there is a means for recording preference data. The procedure is sensitive to pharmacological manipulations, although dose-effect curves are difficult to generate.

Acknowledgments

The authors wish to thank Joseph Porter (Virginia Commonwealth University) for providing images of his place conditioning equipment (Fig. 1) and John Traynor (University of Michigan) for providing unpublished data for CPP (Figs. 2 and 3).

References

1. Siegal S et al (1982) Heroin "overdose" death: Contribution of drug-associated environmental cues. Science 216:436–437
2. Carey AN et al (2007) Reinstatement of cocaine place-conditioning prevented by the peptide kappa-opioid receptor antagonist arodyn. Eur J Pharmacol 569:84–89
3. McLaughlin JP, Marton-Popovici M, Chavkin C (2003) κ opioid receptor antagonism and prodynorphin gene disruption block stress-induced behavioral responses. J Neurosci 23:5674–5683
4. Shin EJ et al (2005) The dextromethorphan analog dimemorfan attenuates kainate-induced seizures via σ1 receptor activation: comparison with the effects of dextromethorphan. Br J Pharmacol 144:908–918
5. Anand JP et al (2016) The behavioral effects of a mixed efficacy antinociceptive peptide, VRP26, following chronic administration in mice. Psychopharmacol 233:2479–2487
6. Brabant C, Quertemont E, Tirelli E (2005) Influence of the dose and the number of drug-context pairings on the magnitude and the long-lasting retention of cocaine-induced conditioned place preference in C57BL/6J mice. Psychopharmacol 180:33–40
7. Suzuki T et al (1992) The role of mu-and kappa-opioid receptors in cocaine-induced conditioned place preference. Japanese J Pharmacol 58:435–442
8. Bardo MT, Bevins RA (2000) Conditioned place preference: what does it add to our preclinical understanding of drug reward? Psychopharmacol 153:31–43
9. Szumlinski KK et al (2002) Unconditioned and conditioned factors contribute to the 'reinstatement'of cocaine place conditioning following extinction in C57BL/6 mice. Behavioural Brain Res 136:151–160
10. Anand JP et al (2018) In vivo effects of μ-opioid receptor agonist/δ-opioid receptor antagonist peptidomimetics following acute and repeated administration. Br J Pharmacol 175:2013–2027
11. Cordery SF et al (2014) A non-rewarding, non-aversive buprenorphine/naltrexone combination attenuates drug-primed reinstatement to cocaine and morphine in rats in a conditioned place preference paradigm. Addiction Bio 19:575–586
12. Marquez P et al (2007) The mu opioid receptor is involved in buprenorphine-induced locomotor stimulation and conditioned place preference. Neuropharmacology 52:1336–1341
13. Marquez P et al (2008) The endogenous OFQ/N/ORL-1 receptor system regulates the rewarding effects of acute cocaine. Neuropharmacology 54:564–568
14. Brunzell DH et al (2009) Nucleus accumbens CREB activity is necessary for nicotine conditioned place preference. Neuropsychopharmacology 34:1993
15. Walters CL et al (2006) The β2 but not α7 subunit of the nicotinic acetylcholine receptor is required for nicotine-conditioned place preference in mice. Psychopharmacol 184:339–344
16. Paris JJ, Fenwick J, McLaughlin JP (2014) Estrous cycle and HIV-1 Tat protein influence cocaine-conditioned place preference and induced locomotion of female mice. Curr HIV Res 12:388–396
17. García-Carmona J-A et al (2015) Sex differences between CRF1 receptor deficient mice following naloxone-precipitated morphine withdrawal in a conditioned place aversion paradigm: implication of HPA axis. PLoS One 10 (4):e0121125–e0121125
18. Yu H et al (2012) Effects of exogenous cholecystokinin octapeptide on acquisition of naloxone precipitated withdrawal induced conditioned place aversion in rats. PLoS One 7:e41860–e41860
19. Bowers, MS et al (20160 N-acetylcysteine decreased nicotine reward-like properties and withdrawal in mice. Psychopharmacology (Berl) 233:995–1003
20. Cloutier CJ, Kavaliers M, Ossenkopp KP (2018) Lipopolysaccharide (LPS) induced

sickness in adolescent female rats alters the acute-phase response and lithium chloride (LiCl)-induced impairment of conditioned place avoidance/aversion learning, following a homotypic LPS challenge in adulthood. Behavioural Br Res 351:121–130

21. Tenk CM, Kavaliers M, Ossenkopp KP (2005) Dose response effects of lithium chloride on conditioned place aversions and locomotor activity in rats. Eur J Pharmacol 515:117–127
22. Tenk CM, Kavaliers M, Ossenkopp KP (2006) The effects of acute corticosterone on lithium chloride-induced conditioned place aversion and locomotor activity in rats. Life Sci 79:1069–1080
23. Buffalari DM (2016) Nicotine Enhances Footshock- and Lithium Chloride-Conditioned Place Avoidance in Male Rats. Nicotine & tobacco research: official journal of the Society for Research on Nicotine and Tobacco 18:1920–1923
24. Bagdas D et al (2016) Expression and pharmacological modulation of visceral pain-induced conditioned place aversion in mice. Neuropharmacology 102:236–243
25. Bagdas D et al (2018) Effect of nicotine and alpha-7 nicotinic modulators on visceral pain-induced conditioned place aversion in mice. Eur J Pain 22:1419–1427
26. Itzhak Y, Martin JL (2002) Cocaine-induced conditioned place preference in mice: induction, extinction and reinstatement by related psychostimulants. Neuropsychopharmacology 26:130
27. Barr GA, Paredes W, Bridger WH (1985) Place conditioning with morphine and phencyclidine: dose dependent effects. Life Sci 36:363–368
28. Kota D, Martin BR, Damaj MI (2008) Age-dependent differences in nicotine reward and withdrawal in female mice. Psychopharmacol 198:201–210
29. Kota D et al (2007) Nicotine dependence and reward differ between adolescent and adult male mice. J Pharmacol Exp Ther 322:399–407
30. Parker LA, Mcdonald RV (2000) Reinstatement of both a conditioned place preference and a conditioned place aversion with drug primes. Pharmaco Biochem Behav 66:559–561
31. Acquas E et al (1989) SCH 23390 blocks drug-conditioned place-preference and place-aversion: anhedonia (lack of reward) or apathy (lack of motivation) after dopamine-receptor blockade? Psychopharmacol 99:151–155

Part IV

Imaging and Electrophysiological Techniques

Chapter 14

Positron Emission Tomography of the Reward System

Diego Romero-Miguel, Nicolás Lamanna-Rama, Marta Casquero-Veiga, Vanessa Gómez-Rangel, Manuel Desco, and María Luisa Soto-Montenegro

Abstract

Recently, great efforts have been focused on understanding and treating reward-related dysfunction in psychiatric disorders. This has led to preclinical and clinical advances in understanding the neurobiology of the reward system, highlighting the case of the field of neuroimaging. In this respect, neuroimaging has an unprecedented potential to unravel the neurobiology of different pathologies, covering a wide spectrum, from structural plasticity in gray and white matter to evoked neuronal responses, neuronal network dynamics, global and regional perfusion and metabolism, receptor-binding studies, or neurotransmitter release. Among the different medical imaging techniques, positron emission tomography (PET), single-photon emission computed tomography (SPECT), or functional magnetic resonance imaging (fMRI) have been extensively applied to study different aspects of mental and psychiatric disorders. Therefore, this chapter focused on molecular neuroimaging of the dopamine reward system by means of PET technique.

Key words Positron emission tomography, PET, Dopamine, Reward system

1 Introduction

The reward system is a group of brain structures and neural pathways, which are activated by a reinforcing stimulus. Thus, when exposed to rewarding stimuli, such as addictive drugs, the brain responds by increasing the release of the neurotransmitter dopamine, producing a feeling of pleasure. In this sense, the reward system is found among the major dopaminergic pathways in the brain, which mainly involves the cortico-basal ganglia-thalamocortical loop. In this respect, two big players are relevant in the circuitry of the reward system: the mesolimbic dopaminergic pathway, which connects the ventral tegmental area (VTA) with the nucleus accumbens, and the mesocortical dopaminergic pathway, which connects the VTA to the cerebral cortex (Fig. 1).

Diego Romero-Miguel and Nicolás Lamanna-Rama contributed equally to this work.

Marc Fakhoury (ed.), *The Brain Reward System*, Neuromethods, vol. 165, https://doi.org/10.1007/978-1-0716-1146-3_14,

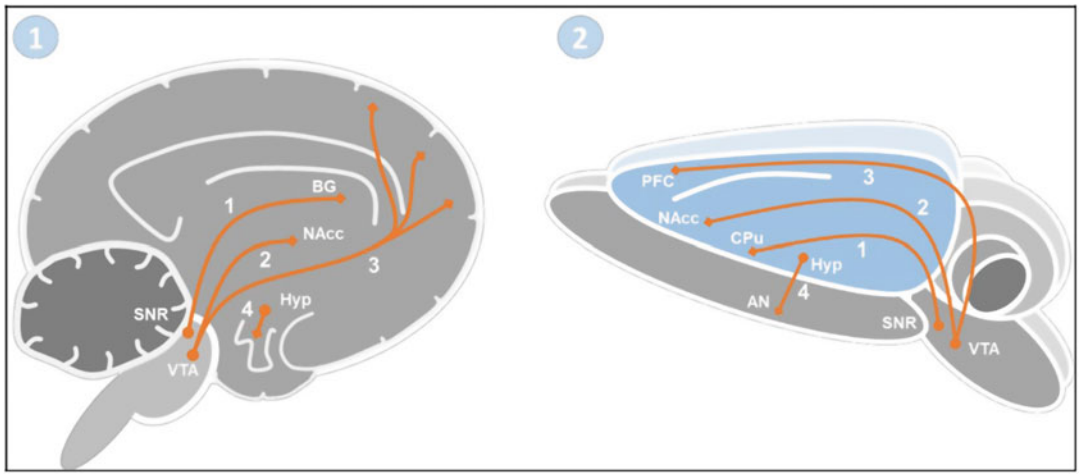

Fig. 1 Dopamine pathways in the (1) human and (2) rat brain: (*1*) nigrostriatal pathway, (*2*) mesolimbic pathway, (*3*) mesocortical pathway, and (*4*) tuberoinfundibular pathway. (*PFC* prefrontal cortex, *BG* basal ganglia, *NAcc* nucleus accumbens, *Hyp* hypothalamus, *CPu* caudate–putamen, *AN* arcuate nucleus, *SNR* subtantia nigra, *VTA* ventral tegmental area)

Recently, great efforts have been focused on understanding and treating reward-related dysfunction in psychiatric disorders. This has led to preclinical and clinical advances in understanding the neurobiology of the reward system, highlighting the case of the field of neuroimaging. In this respect, neuroimaging has an unprecedented potential to unravel the neurobiology of different pathologies, covering a wide spectrum, from structural plasticity in gray and white matter to evoked neuronal responses, neuronal network dynamics, global and regional perfusion and metabolism, receptor binding studies, or neurotransmitter release. Among the different medical imaging techniques, positron emission tomography (PET), single-photon emission computed tomography (SPECT), or functional magnetic resonance imaging (fMRI) have been extensively applied to study different aspects of mental and psychiatric disorders [1, 2]. Also, the development of new biomedical molecular imaging technologies for preclinical research has allowed to perform in vivo functional imaging studies in small animals for a better understanding of physiological and pathological processes [3–9]. Nowadays, preclinical imaging devices have become indispensable in basic science and drug development, providing noninvasive images with morphological and functional information, and allowing the monitoring of disease progression and response to therapy in different models of disease [10–13]. Therefore, this chapter focused on molecular neuroimaging of the dopamine reward system by means of PET technique.

2 Materials and Methods

2.1 How Does PET Work?

PET is a functional medical imaging technology, as it provides tridimensional tomographic information on the functioning or metabolism of different biological systems, being complementary to morphological techniques. It is based on the capacity of bio-distribution of a radioactive labeled molecule (radiotracer) into the bloodstream traveling to its biological target. The result is the accumulation of the radioactivity in the tissue that can be visualized as an image. The physical principle of PET involves the use of positron-emitting radioisotopes. The annihilation of the positron emitted from the radiotracer and an electron from the living tissue, resulting in two gamma rays (511 KeV each, also known as photons) that travel in opposite directions (180°) and are detected by a pair of detectors in a ring-like pattern. Thus, only photons that reach opposite detectors are considered for the creation of the final PET image. Figure 2 shows the principles of in vivo imaging tissue function with PET [14]. One characteristic of these PET tracers is that they are radiolabeled with a high-specific activity that allows a very low amount of tracer to be injected, thus minimizing any pharmacological effect. These concerns are essential in preclinical studies using microPET scanners, where there must be a balance between the injected radioactivity in rodents (compatible

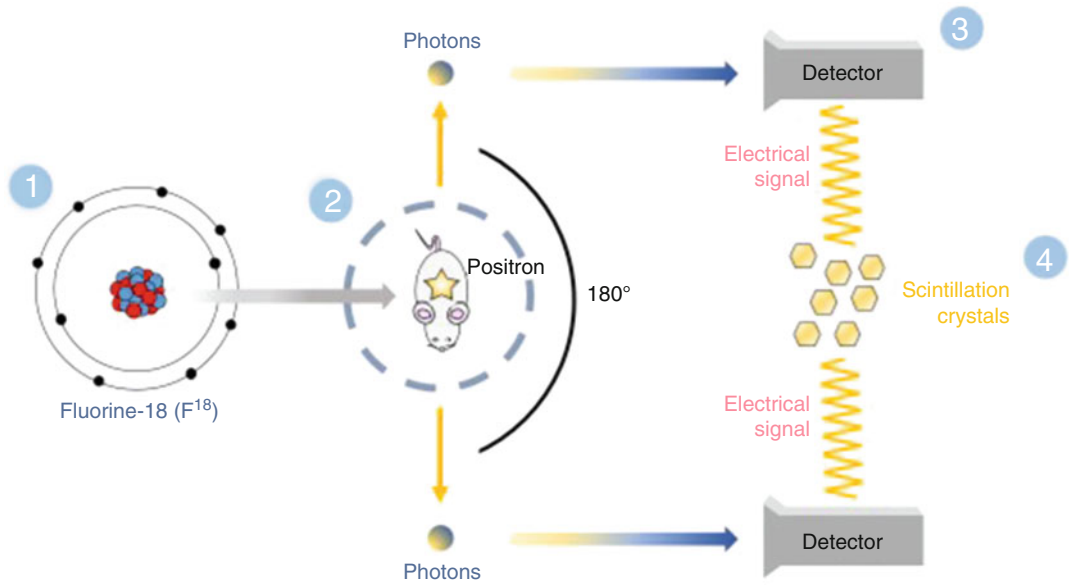

Fig. 2 How does PET work? First, (*1*) a positron (positive electron or antimatter particle) is emitted by the nucleus of the isotope. (*2*) When the positron interacts with an electron in the tissue results in the annihilation of both particles and the emission of two gamma rays or photons. Then, (*3*) the photons are detected by photomultiplier–scintillation detectors located around the subject in PET cameras. Finally, (*4*) the photomultipliers convert and amplify the photons to electrical signals

with the PET sensitivity) and the highest specific activity that must reach the brain, in order to minimize the degree of occupancy in the case of specific radiotracers [15]. Additional advantages of PET are: (a) its high sensitivity due to the use of short-lived positron-emitting isotopes, (b) the use of isotopes of elements often included in physiological compounds (nitrogen, oxygen, carbon), and (c) the accurate quantification of regional tracer activity [15].

Therefore, PET imaging requires: (1) a PET scanner, (2) a radiotracer, and (3) the subject:

(a) Radiotracer: A radiotracer is a molecule in which one atom of its structure is replaced by a radioisotope. The administration of this radiotracer will allow the visualization of biochemical and metabolic reactions in the body. The isotopes used for labeling PET radiotracers or radiopharmaceuticals include ^{11}C, ^{13}N, ^{15}O, ^{18}F, ^{64}Cu, ^{62}Cu, ^{124}I, ^{76}Br, ^{82}Rb, and ^{68}Ga; being the ^{18}F the most clinically used due to its long half-life of 109 min and wide availability. Radiotracers are usually intravenously injected through a catheter.

(b) PET scanner: Clinical PET scanner or preclinical PET scanner for small animals is commonly combined with computerized tomography (CT) or magnetic resonance imaging (MRI) for further evaluation of morphological or anatomical changes (Fig. 3). This multimodality imaging approach is also common with patients and is becoming a standard clinical practice. The procedure can be done using a hybrid scanner or by employing a posteriori co-registration software.

(c) Subjects: humans, for clinical PET studies, or animals (mainly rodents), for preclinical PET studies.

2.2 Radiotracers

Along with the development of PET instrumentation, there is a parallel development of radiotracers. This is of great importance since depending on the radiotracer used, it is possible to study different biological processes. Nowadays, brain imaging techniques allow to display brain neurotransmitters at three locations: the presynaptic neuron, the postsynaptic neuron, and the intraneuronal metabolism [16]. In addition, among the different neurotransmitter systems, the dopaminergic, serotonergic, cholinergic, and peptidergic systems are the ones which can be currently explored by PET imaging. This is of great interest since the interactions between transporters/receptors and neurotransmitters play a role in the diagnosis and treatment of, not only reward system-related disorders, but also psychiatric and neurodegenerative pathologies [17–26].

The selection of the tracer is critically important to maximize sensitivity to competitive binding to the ligand. This is of great importance when there are several tracers available for one

Fig. 3 Preclinical PET/CT scanner (Super Argus, SEDECAL, Madrid, Spain) at the Medical Imaging Laboratory (LIM) at the Gregorio Marañón Health Research Institute (Spain). The scanner is connected to an animal monitoring system (VisionPET, RGB, Madrid, Spain) that measures multiple physiological parameters (temperature, electrocardiogram and respiration, and optionally, oxygen saturation, blood pressure, and exhaled CO_2). Picture is courtesy of the head of LIM, Dr. Manuel Desco

particular target. Thus, the selection of a target for nuclear imaging must be determined by: (a) the understanding of the disease process; (b) the high target affinity, allowing a clear image visualization; (c) the high selectivity for the target, reducing to the minimum the visualization of off-target processes; (d) the low nonspecific or non-displaceable binding of the tracer, reducing the background of the image; (e) the capacity of the radiotracer to cross the blood–brain barrier, and (f) the tracer metabolism knowledge to avoid or take into account possible radiometabolites that can affect the PET image.

Focusing on the dopamine neurotransmitter, this has been one of the most extensively studied neurotransmitters of the brain and was also the first neurotransmitter to be evaluated in the living human brain using both PET and SPECT techniques [27]. As it was mentioned before, dopamine system is involved in the regulation of brain regions that control the reward system. Disruptions of the dopamine function are associated with neurological [28] and psychiatric diseases including addictions [29, 30] as well as on some of the deficits associated with aging [31, 32]. This has made the

dopamine system an important molecular target for drug development in research in both neuroscience and neuroimaging. Table 1 shows some dopamine radiotracers of clinical utility.

In the following sections, we review several radiotracers that allow the study of the reward system.

2.2.1 Dopamine Synthesis

In the early 1970s, major efforts were initially focused on the radiosynthesis of the dopamine synthesis tracer [^{18}F]-labeled 3,4-dihydroxyphenyl-L-alanine (FDOPA) and other analogs [33]. This tracer crosses the blood–brain barrier by diffusion and is decarboxylated to [^{18}F] 6-DOPA, which is trapped within vesicles of presynaptic dopamine neurons. Despite the degradation products formed after FDOPA metabolism, which may hamper PET images interpretation, it is worldwide used for diagnostic imaging studies in Parkinson's disease (PD) [34] and movement disorders [35], since it is useful to quantify the loss of nigrostriatal dopamine terminal function. Thus, a reduction in the ratio between the striatum and the cerebellum is indicative of nigrostriatal degeneration. By using [^{18}F] 6-DOPA and fMRI techniques, it has been shown that the dopamine system is particularly vulnerable to aging, occurring an age-dependent dopaminergic tuning mechanism for cortical reward processing in healthy aging [36]. PD patients show disruptions in the mesocorticolimbic pathway, as it is shown in [^{18}F] 6-DOPA-PET studies, with tracer reductions in the prefrontal cortex [37] and the anterior cingulate cortex [38]. In contrast, early PD patients without dementia and non-medicated showed increased [^{18}F] 6-DOPA uptake in the dorsolateral prefrontal cortex, anterior cingulate, and medial frontal cortex [39]. Besides its capacity of diagnosis, it also allows to monitor disease severity and progression, detect disease stages, and differentiate idiopathic PD from other parkinsonian syndromes [40]. Nowadays, new tracers are been studied in an attempt to reduce the interferences produced by the presence of [^{18}F] 6-DOPA metabolites [41, 42].

Studies in drug abusers have shown lower dopamine synthesis capacity in (1) nicotine-dependent smokers, which appears to normalize with abstinence [43] and (2) alcoholic patients who appear to be linked to high levels of craving [44]. Dopaminergic modulation of neural learning signals is also disrupted in alcohol dependence in proportion to long-term alcohol intake of patients [45]. Impulse control disorders such as pathological gambling (PG) and binge-eating disorders (BEDs) have been described in patients with PD when they are treated with dopamine agonist therapy for their motor symptoms [46]. In relation to this, several studies have shown that BEDs are associated with reductions in striatal [^{18}F] 6-DOPA, while PG was associated with no changes in this brain area. In addition, [^{18}F] 6-DOPA uptake is 20% lower in BED compared with PG and controls, highlighting the heterogeneity underlying the subtypes of addiction [46, 47].

Table 1
Some of the PET radiotracers available for targeting dopaminergic neurotransmission and applications

Targeting	Tracer	Chemical name	Clinical studies (references)
Dopamine synthesis	^{18}F-DOPA	L-3,4-dihydroxy-6-[^{18}F]-fluorophenylalanine	PD [34, 37–39], movement disorder [35, 55], aging [36], ADHD [27], schizophrenia [49, 50], drug challenge [33], drug addiction [43–47]
Dopamine transporter	^{11}C-CFT	[^{11}C]-2 β -carbomethoxy-3 β -Itropane	Aging [135]
	^{11}C-altropane	2 β -carbomethoxy-3 β -(4-fluorophenyl)-N-((E)-3-iodo-prop-2-enyl)tropane	ADHD [148]
	^{11}C-cocaine	[N-11C-methyl]-cocaine	Drug challenge [104], drug abuse [105]
	^{11}C-MP	^{11}C-methylphenidate	Aging and PD [138], drug challenge [142]
	^{18}F-β-CIT-FE or ^{11}C-β-CIT-FE	N-(2-fluoroethyl)-2 beta-carbomethoxy-3 beta-(4-iodophenyl)nortropane labelled with ^{18}F or ^{11}C	Aging [127, 135, 136], PD [137], drug abuse [102, 141, 147], ADHD [149]
	^{18}F-FE-PE2	[18F](E)-N-(3-iodoprop-2-enyl)-2b-carbofluoroethoxy-3b-(4′-methyl-phenyl) nortropane	PD [143]
D1 Receptors	^{11}C-NNC 112	(+)-5-(7-Benzofuranyl)-8-chloro-7-hydroxy-3-methyl-2,3,4,5-tetrahydro-1H-3-benzazepine	Cocaine dependence [82], Schizophrenia [71]
	^{11}C-SCH 23390	(RH+)-8-Chloro-2,3,4,5-tetrahydro-3-[^{11}C]methyl-5-phenyl-1 H-3-benzazepin-7-ol	Schizophrenia [84, 85]
D2/D3 Receptors	^{11}C-Raclopride	3,5-dichloro-N-{[(2S)-1-ethylpyrrolidin-2-yl]methyl}-2-hydroxy-6-[^{11}C]methoxybenzamide	Aging [68, 69], drug abuse [75, 76, 79, 81], antipsychotic challenge [86], ADHD [89, 150]
	^{11}C- NMSP	^{11}C- methylspiperone	Movement disorders [73, 74], Schizophrenia [84]
	^{18}F-Falypride	(S)-N-[(1 allyl-2-pyrrolidinyl)methyl]-5-(3[^{18}F] fluoropropyl)-2,3-dimethoxybenzamide	Aging [70, 71, 212], schizophrenia [87, 88, 213, 214], cocaine abuse [77, 215], drug abuse [78, 80, 216, 217], ADHD [218]
VMAT-2	^{11}C-DTBZ	(±)- α -[^{11}C]dihydrotetrabenazine	PD [155], AD [156], other movement disorders [157], drug challenge [158], schizophrenia [151, 159]

In schizophrenia, imaging data with [^{18}F] 6-DOPA suggest an abnormal striatal DA transmission at the presynaptic level, showing a 10–30% increased striatal synthesis rates during psychosis, while reductions in striatal [^{18}F] 6-DOPA during symptomatic remission of positive symptoms have been described [48]. In addition, [^{18}F] 6-DOPA uptake is useful as an index of severity of presynaptic dopamine dysfunction in response to antipsychotic treatment [49].

2.2.2 Dopamine Receptors

Dopamine receptors are located at both pre- and postsynaptic dopaminergic neurons and have been the main targets in the treatment of psychosis and extrapyramidal motor symptoms in patients with PD [50]. There are five subtypes of dopamine receptors, D1–D5, but only D1 and D2/D3 have currently specific PET ligands. D2 and D3 receptors are expressed in high abundance in the striatum and ventral midbrain and lower levels of certain limbic and cortical regions. Other efforts have been made to develop specific D3 antagonist ligands [51] and probes for the low abundance of D4 receptors [52, 53].

In the late 1980s, it was developed the first radiopharmaceutical for imaging dopamine receptors, [^{11}C]3-N-methylspirone, a dopamine D2-like receptor antagonist radiotracer, which also has a high binding predisposition to serotonin receptors. Later, two D1 PET ligands were developed and are currently used at clinic, [^{11}C]-NNC 112 [54, 55] and [^{11}C]-SCH23390 [56–58]. However, both of them have not appeared to be sensitive to acute changes in extracellular dopamine concentrations, probably due to (1) low affinity to D1R, (2) existence of D1R in the low-affinity state, or (3) localization of D1R extrasynaptically [59]. This deficiency impulses the continued development of more specific dopamine receptor imaging tracers.

In 1985, it was developed a benzamide radiotracer: [^{11}C]raclopride. This tracer is a nonselective dopamine D2/D3 antagonist, being the more used in the clinical field, as it allows to display D2 receptors [60]. Another nonselective D2/D3 PET antagonists [61] are [^{18}F]Fallypride and [^{11}C]FLB457, with lower level of nonspecific binding and higher signal-to-background uptake in extrastriatal regions than [^{11}C]raclopride [62]. Both of them are used to investigate extrastriatal brain regions, where the density of D2R is much lower than in the striatum. In an attempt to increase sensitivity of radioligand binding, nonselective D2/D3 agonists were developed such as [^{11}C]-(+)-PHNO [63], [^{11}C]-NPA [64], [^{11}C]-MNPA [65], and [^{11}C]-MCL-524 [66]. The main advantage of agonist tracers over the antagonist is the supposed capacity of discrimination between the low- and high-affinity states of the receptor; although in the last years the existence of two distinct affinity states in vivo is in question [67].

Radioligands for D1 and D2 receptors have been used in aging, psychiatric, and neurological disorders. Aging has been associated with decreased availability of dopamine receptors and transporters, but without changes in synthesis capacity [68]. These reductions are mainly focused on the striatum and frontal cortex and ranged between 6 and 16% per decade of life [69, 70]. Also, DRD2/3 availability declined with age [71]. Studies with patients with Parkinson's disease have shown no differences in D2 receptor concentrations. However, imaging with D2 receptors is still in use to predict responsiveness to treatment in patients with movement disorders [72]. Furthermore, Huntington's disease, another movement disorder, has also shown significant reductions in striatal D2 [73] and striatal and prefrontal cortical D1 [74] receptors.

As previously highlighted, drug addiction research has been usually linked to dopamine system. Particularly, PET research has mainly focused on the D2/D3 receptor, showing significant reductions in D2 availability in cocaine, amphetamine, or methamphetamine users [75–77], nicotine [78], alcohol dependence [79, 80], and videogame playing [81]. D1 receptor availability has also been studied recently in patients with cocaine addiction, showing that low D1 availability in the ventral striatum is associated with the choice to self-administer cocaine and the risk of relapse in cocaine dependence [82].

Schizophrenia patients show salient abnormalities in the brain reward system measured by fMRI that are linked to psychotic symptoms, probably due to a dysfunction of the dopamine in striatal regions [83]. Moreover, schizophrenia is associated with decreased prefrontal D1 receptors [84, 85]. In addition, dopamine receptors have been used to evaluate receptor occupancy by antipsychotic drugs. It has been estimated that 70–80% of the D2 receptors need to be occupied for therapeutic efficacy and that higher occupancies (80–90%) are associated with side effects for the typical antipsychotic drugs [86]. In contrast, the average D2 occupancy is lower (20–67%) for atypical antipsychotic drugs, indicating that D2 receptors are the main target for typical but not for atypical antipsychotic drugs [86]. And finally, overlapping decreases in extrastriatal dopamine D2/D3-receptor availability and glucose metabolism have been reported in subjects with schizophrenia [87, 88].

2.2.3 *Dopamine Transporters*

The dopamine transporter (DAT) is a plasmatic membrane protein localized on the presynaptic terminal of the dopaminergic neurons. In addition to reward responses, it is also involved in the regulation of another important brain functions such as locomotor activity and cognition. Several radioligands for DAT have been developed, such as ^{11}C-PE2I [89], ^{11}C-CFT [90–94], ^{11}C-altropane [95–99], ^{11}C-cocaine [100–106], ^{11}C-methylphenidate [107–114], ^{18}F--

CIT or ^{11}C--CIT [115–126], ^{11}C--CIT-FE or ^{18}F--CIT-FE [127], ^{18}F-FECNT, and ^{11}C-nomifensine [128–133]. These tracers differ in their affinity and specificity for the DAT, their kinetics, and their specific–nonspecific binding ratios, being its uptake approximately 7–10% of the injected dose. Of note, both CFT and -CIT show affinities for DAT of 10 and 100 times higher, respectively, than those of cocaine. Second-generation ^{18}F-radioligands for DAT are LTB-999 and fluoroethyl-PE2I; however, none of them have been applied to humans yet [134].

Therefore, preclinical and clinical studies have shown that the most desirable properties for a DAT radioligand include high affinity to DAT and a high specific-to-nonspecific binding ratio. This is the case of -CIT and ^{11}C-altropane. The rest of DAT radioligands is able to bind DAT but have some disadvantages, such as binding to other transporters (i.e., ^{11}C-nomifensine binds also to the norepinephrine transporter) or lower kinetics limiting the statistical quality of PET images.

DAT radioligands have been mainly used in aging [36, 135–138], addictions [75, 102, 104, 139–142], Parkinson's disease (PD) [36, 135–138], other movement disorders [143–145], and attention-deficit hyperactivity disorder (ADHD) [89, 98, 106]. Aging has been associated with deficits in DAT availability with a 6–8% decline of DAT per decade together with a deterioration in episodic memory and executive functioning at advanced age [127]. PET and SPECT have shown that an approximately 50% loss of dopamine terminals is required for the onset of PD symptoms. Nowadays, great efforts are being made to identify individuals at risk for PD before the onset of motor symptoms by combining dopaminergic imaging, early clinical signs, and known genetic mutations for PD [146]. In this respect, DAT radioligands, such as -CIT and -CIT-FE, are able to discriminate PD from normal aging, particularly when DAT availability in the putamen is evaluated [143].

Studies in drug abusers have shown increases in DAT shortly after cocaine withdrawal and decreases or no changes with protracted withdrawal [105]. Increases of DAT have been also shown in violent alcoholic subjects [147]. DAT imaging has also been used in the study of psychiatric disorders. Studies in ADHD patients have shown contradictory results, with increased [148] or no changes, or rather reduced [149] striatal DAT availability. In ADHD, DAT availability is also reduced in the midbrain, suggesting that substantia nigra is also involved in the dopamine dysfunction [89], as well as the caudate and the nucleus accumbens [150].

2.2.4 Vesicular Monoamine Transporter Type-2

The vesicular monoamine transporter type-2 (VMAT2) is a presynaptic protein responsible for transporting monoamine neurotransmitters (dopamine, norepinephrine, or serotonin) from cytosol into

synaptic vesicles for subsequent storage and release. In the striatum, more than 95% of the specific binding of VMAT2 is associated with dopaminergic terminals and linearly reflects the concentration of dopamine in the striatum [151, 152]. As VMAT-2 abnormalities have been involved in a variety of neurodegenerative and psychiatric disorders, great efforts have been made toward the development of VMAT-2 radiotracers [153]. Two tracers based on dihydrotetrabenazine (DTBZ) derivatives are at the clinic, the 9-^{11}C-DTBZ and the 9-^{18}F-FE-DTBZ with good striatum-to-cerebellum ratio [154].

Studies in PD have shown that 9-^{11}C-DTBZ has an excellent accuracy for differentiating idiopathic PD from other disorders [155], and dementia with Lewy bodies from both PD and Alzheimer's disease (AD) in a single neuroimaging study [156]. Patients with Huntington's disease show decreased striatal monoaminergic terminals [157]. Studies in drug addiction have shown increased striatal 9-^{11}C-DTBZ binding in some chronic methamphetamine users during early drug abstinence, reflecting a possible loss of vesicular DA [158]. Patients with schizophrenia show no differences in VMAT-2 uptake compared to controls, suggesting that there is no difference in the dopamine terminal density [151]. However, another study in schizophrenia patients showed increased dopamine terminal density [159]. Also, a comparative study in patients with bipolar disorder type I with history of mania with psychosis and schizophrenia showed both similarities and differences in regional VMAT2 binding, reflecting anomalies in serotonin to dopamine regulation, common to both disorders [159].

2.2.5 Dopamine Metabolism

Dopamine is metabolized by monoamine oxidase (MAO) subtype A or B. The major medical interest in MAO comes from the neurophysiological effects of MAO inhibitors as antidepressant drugs. Thus, radiolabeled inhibitors of MAO were explored extensively in clinical PET research. Early work was focused on irreversible binding ligands, such as [^{11}C]-D2-clorgyline for MAO-A and [^{11}C]L-deprenyl and [^{11}C]L-deprenyl-D2 for MAO-B [160]. Deprenyl is a drug that has been given as an adjuvant therapy in the treatment of PD [161]. It has been labeled with ^{11}C and used in PET studies to image the distribution of available MAO-B in the brain in aging [162], PD [163], AD [164–166], or drug addiction [167–169]. Newer generation tracers have reversible binding, making them more accessible for clinical research, such as [^{11}C]-harmine and [^{11}C]-SL2511.88 for MAO-A and MAO-B, respectively. These tracers have been used for imaging mood disorders and the effect of new antidepressant treatment [170], and psychiatric disorders, such as antisocial personality disorder [171] and borderline personality disorder [172]. Thus, low levels of MAO-A in the PFC are associated with aggression, while high levels are

associated with major depressive disorder (MDD) and also risk for recurrence of depressive episodes [173]. Higher MAO-A binding is clinically associated with an adaptive personality facet [173]. Studies in MDD have shown elevated MAO-A levels throughout the gray matter of the brain, including prefrontal, temporal and cingulate cortex, thalamus, caudate, putamen, hippocampus, and midbrain in medication-free major depressive episode secondary to early-onset MDD [174]. Since MAO-A metabolizes several monoamines, elevations in MAO-A levels, would be expected to drive down the levels of these monoamines. In MDD, depletion of monoamines particularly in the PFC and anterior cingulate cortex (ACC) leads to depressed mood.

Also, dopamine can be metabolized by catechol-O-methyltransferase (COMT). The product of dopamine metabolism by COMT represents an index of dopamine release, being COMT an important molecular target in the development of drugs to treat PD [175]. However, PET studies in baboons using a potent inhibitor of COMT, showed a negligible uptake in the brain, demonstrating the potential to research peripheral but not central activity [176].

2.2.6 Regional Brain Glucose Metabolism

Glucose brain metabolism is in close relation with functional activity and it may provide an alternative way to explore the functional changes associated with drugs that are able to modify the dopaminergic system [8, 175]. In 1976, it was developed a glucose analog labeled with fluorine, ^{18}F-fluorodeoxyglucose (^{18}F-FDG). This tracer is used as a marker of cerebral glucose consumption resulting from neuronal entrapment and accumulation of ^{18}F-FDG-6-PO4, which indicates neuronal activity [7]. It is by far the most common radiotracer in clinical and preclinical fields. ^{18}F-FDG is a broad-spectrum tracer since its uptake in the brain is produced by all existing cell types, independently of the neurotransmission system involved [8]. This could represent a disadvantage with respect to specific dopamine tracers. However, the visualization of metabolic changes throughout the entire nervous system makes possible the identification of complex neuronal networks that may be evaluated in response to a pharmacological manipulation, helping in the study of the dopaminergic system [8, 177, 178]. Definitely, the main advantage of this tracer is its wider availability (as compared to more specific dopaminergic tracers) making it more likely to become useful in clinical medicine and animal research [8].

^{18}F-FDG has been used to study the effect of drugs that increase dopamine concentrations when given acutely, such as cocaine or amphetamine. These studies have shown that these abuse drugs produced a widespread decrease in brain glucose metabolism [179, 180]. Studies in schizophrenia have shown its association with extensive cerebral dysfunction and neurochemical

alterations, including serotonin and dopamine neurotransmitter systems [181–183]. Specifically, ^{18}F-FDG PET studies in patients with schizophrenia treated with D2 receptor antagonist reported increases in striatal metabolism and decreases in glucose metabolism in the whole brain [184]; more specifically in cortical areas [185–188], thalamic nuclei [189], and hippocampus [190]. Furthermore, the acute administration of haloperidol, a neuroleptic, decreased brain metabolism in frontal and limbic cortices, thalamus, and caudate in normal subjects [191] while no changes or minimal changes are shown in schizophrenia patients [192]. However, care must be taken when interpreting these findings since changes in metabolism could also respond to changes in dopamine levels and adaptation processes [192].

2.3 PET Imaging Acquisition

2.3.1 Clinical

The procedures described below follow the European Association of Nuclear Medicine (EANM) procedure guidelines for brain neurotransmission [193, 194] and brain metabolism [195].

(a) Patient preparation and information
- Prior to the scanning, patients should avoid taking any medication or drugs of abuse which could influence the posterior visual and quantitative analysis [194]. In the case of DAT-binding ligands, a withdrawal period of at least five times the drug's biological half-life is recommended [193]. In the case of ^{18}F-FDG PET studies, a fasting period of at least 6 h is required before the administration of ^{18}F-FDG in order to avoid competition between the radiotracer and the blood glucose.
- A knowledge of the patient's history and current medication is required.
- Patients are informed about all the procedures. Whether sedation is necessary, it should be given at the earliest 1 h prior to the imaging acquisition. Doses of sedative medication should be reduced in elderly patients.

(b) Administration of the radiotracer

No anesthesia is required. The radiotracer is injected using an intravenous catheter inserted in the arm over approximately 20 s. Later, saline is administered to flush the intravenous line. The time from injection to the beginning of the data acquisition will vary according to the isotope and molecule (e.g., for [^{11}C]Raclopride, between 30 and 60 min, for [^{18}F]Fallypride between 2.5 and 3 h and for ^{18}F-FDG between 60 and 90 min). It is recommended to fix the time between the injection and the start of data acquisition to ensure intraindividual follow-up studies and make data comparable between subjects.

(c) Setup for data acquisition

Patients are asked to lie down on the scanner bed and get positioned for maximum comfort. Patients must avoid voluntary movements.

2.3.2 Preclinical

The following steps are necessary to scan rodents in a dedicated PET scanner [3, 6, 7, 12, 196–198]:

(a) Animal preparation
- Animals are weighted since the amount of radiotracer to be injected depends on their weight. Total activity of the syringe is recorded before the injection.

(b) Administration of the radiotracer
- Animals are anesthetized using inhalant anesthesia (sevoflurane: 4.5% induction, 2.5% maintenance in 100% O_2; or isoflurane: 3.5% induction, 1.5% maintenance in 100% O_2).
- The tail of the animal is warmed in order to facilitate the visualization of the vein, by using warm water or a red heat lamp. Once the vein is localized, a cannula is inserted into the tail vein. The administration of the radiotracer is performed through this catheter.
- In case of metabolic studies, an arterial catheterization is desirable for blood sampling. It could be in the tail or the femoral artery. The amount of blood to collect depends on the species and size of the animal. The basic principles that underlie the regulation of animal research are very similar in all countries. This is regulated by the European Communities Council Directive 2010/63/EU in Europe [199, 200], by the Canadian Council or Animal Care in Canada or by the Institutional Animal Care and Use Committees (IACUCs) created by the Animal Welfare Act in the United States.

(c) Setup for data acquisition
- In a static scan, the radiotracer is administered through the tail vein and then, the animal is placed back into its cage for an uptake period that will vary according to the radiotracer (similarly to the clinics). This scan provides information about the radiotracer concentration after this time of uptake. Of note, this protocol is not recommended for studies with short half-life radioisotopes, given that it would imply to lose important binding information as not enough signal would be emitted, and hence detected, after the uptake period.
- In a dynamic scan, the animal is moved to the PET scanner bed and the radiotracer is injected simultaneously with the PET scan beginning. This scan measures the tracer uptake

over an extended time and allows the recording of the whole uptake process, providing enough data for full quantitative kinetic analyses of the PET study.

- Animals are monitored (body temperature, respiration rate, pressure, pulse oximetry, etc.) during the scan. It is very important to maintain body temperature by using a heat blanket as the anesthesia tends to decrease it. A small drop in temperature can have fatal consequences for the image.
- Once the PET image acquisition has finished, the catheter is removed and the animal is placed back to its cage. Since the PET camera is usually combined with a CT scanner, a CT scan could be acquired for anatomical information at the end of the PET scan.
- In the case of biodistribution studies, at the end of the scan or after the administration of the tracer, the animal is sacrificed. The brain is removed and dissected into different brain areas of interest which are then measured in a gamma-counter.

2.4 PET Data Analysis

The data analysis is similar for both preclinical and clinical studies. Detailed PET data analysis requires an independent chapter. Here, we focus on basic quantitative analysis used for the PET data analysis.

2.4.1 Visual Interpretation

Visual assessment gives an idea whether binding is normal, elevated, or reduced as well as whether the image acquisition has been successfully performed (e.g., without voluntary body movements). Also, it provides information about right to left asymmetry and about the most affected structures (i.e., striatal subregions).

Data evaluation must take into account the age of the subject as well as relevant anatomical information (CT, MRI). Attention should be paid to those structures used as reference regions for semiquantitative analysis.

2.4.2 Quantification

The quantitative assessment of brain changes could include two approaches:

(a) Semiquantitative analysis

For glucose metabolism, the most well-known method is the standardized uptake value (SUV), which measures the relative concentration of the radiotracer in the volume of interest. The calculation of SUV takes into account the tissue activity in a specific time, the injected activity, and the subject's body weight. These parameters are necessary for the reproducibility of the data, enabling the comparison of images obtained from different scanners or acquisition/processing protocols [201, 202]. SUV analysis requires the identification

(segmentation) of regions of interest (ROI) based on manual, semiautomatic, or fully automatic segmentation [178]. If possible, ROI analysis should be based on individual morphology as obtained by image fusion with CT or MRI. Alternatively, standardized ROIs can be obtained using atlas templates [203, 204].

For DAT and receptors, the reference tissue model is widely used. This model implies the existence of a reference tissue without specific binding of the ligand, assuming that the level of nonspecific binding is the same in the tissue of interest and reference. The clear advantage of this method is the nonnecessity of arterial cannulation and blood sampling, reducing the complexity of the scanning protocol and posterior data analysis. This method estimates the parameter of interest, the potential (BPND), which provides information on the ratio of specifically bound radiotracer to its free concentration [205]. In the last years, this method has been simplified using three parameters, such as in the simplified reference tissue model (SRTM) or two parameters, such as in the multilinear reference tissue model (MRTM) [206].

Interpretation of semiquantitative results is based on the comparison of specific metabolic or binding values obtained by ROI techniques with those of age-matched normal controls.

(b) Quantitative analysis

The quantitative analysis involves a kinetic model, which is the most accurate method of PET data analysis. However, this method requires arterial cannulation and blood sampling, thus increasing the complexity of the scanning protocol. The pharmacokinetics and pharmacodynamics of the injected radiotracer have been mathematically modeled as compartmental models, which depend on the nature of the tracer. A compartment could refer to both the physical location of the radiotracer and its chemical state. In this respect, there exist one-, two-, or three-compartment models which have been used for different tracers and pathological conditions. Detailed kinetic modeling approach can be found elsewhere [207–211].

3 Conclusions

The present chapter presents basic principles of PET methodology for the understanding of the reward system. The development of PET technology along with the advances in the chemistry field, leading to new specific radiotracers for the dopaminergic system, have become indispensable tools in both clinical and preclinical research. These facts have greatly contributed to the advance of

knowledge in those psychiatric and neurological disorders in which the reward system is involved. Of note, an interesting feature of preclinical PET imaging is summarized in the word "translational," since the gap between preclinical science and clinical applications in human patients may be shortened. The translational applicability of this technique makes the PET one of the most appreciated upcoming imaging technologies.

Acknowledgments

Acknowledgments to the Ministerio de Ciencia, Innovación y Universidades, Instituto de Salud Carlos III (PI17/01766) co-funded by European Regional Development Fund (ERDF), "A way of making Europe," CIBERSAM, Delegación del Gobierno para el Plan Nacional sobre Drogas (2017/085), Fundación Alicia Koplowitz, Consejería de Educación e Investigación, Comunidad de Madrid, co-funded by European Social Fund "Investing in your future" (PEJD-2018-PRE/BMD-7899, PEJ-2017-TL/BMD-7385) and Fundación Tatiana Pérez de Guzmán el Bueno.

References

1. Abi-Dargham A, Horga G (2016) The search for imaging biomarkers in psychiatric disorders. Nat Med 22(11):1248–1255
2. Newberg AB et al (2011) Positron emission tomography in psychiatric disorders. Ann N Y Acad Sci 1228:E13–E25
3. Gasull-Camos J et al (2017) Differential patterns of subcortical activity evoked by glial GLT-1 blockade in prelimbic and infralimbic cortex: relationship to antidepressant-like effects in rats. Int J Neuropsychopharmacol 20(12):988–993
4. Green MV et al (2001) High resolution PET, SPECT and projection imaging in small animals. Comput Med Imaging Graph 25 (2):79–86
5. Pascau J et al (2009) Automated method for small-animal PET image registration with intrinsic validation. Mol Imaging Biol 11 (2):107–113
6. Ravasi L et al (2011) Use of [^{18}F]fluorodeoxyglucose and the ATLAS small animal PET scanner to examine cerebral functional activation by whisker stimulation in unanesthetized rats. Nucl Med Commun 32(5):336–342
7. Shimoji K et al (2004) Measurement of cerebral glucose metabolic rates in the anesthetized rat by dynamic scanning with ^{18}F-FDG, the ATLAS small animal PET scanner, and arterial blood sampling. J Nucl Med 45(4):665–672
8. Soto-Montenegro ML et al (2015) Functional neuroimaging of amphetamine-induced striatal neurotoxicity in the pleiotrophin knockout mouse model. Neurosci Lett 591:132–137
9. Vaquero JJ et al (2014) In-line high resolution PET and 3T MRI hybrid device for preclinical multimodal imaging. EJNMMI Phys 1(Suppl 1):A7
10. Higuera-Matas A et al (2011) Chronic cannabinoid administration to periadolescent rats modulates the metabolic response to acute cocaine in the adult brain. Mol Imaging Biol 13(3):411–415
11. Lauber DT et al (2017) State of the art in vivo imaging techniques for laboratory animals. Lab Anim 51(5):465–478
12. Soto-Montenegro ML et al (2009) Detection of visual activation in the rat brain using 2-deoxy-2-[(18)F]fluoro-D: -glucose and statistical parametric mapping (SPM). Mol Imaging Biol 11(2):94–99
13. Thanos PK et al (2008) Differences in response to food stimuli in a rat model of obesity: in-vivo assessment of brain glucose metabolism. Int J Obes 32(7):1171–1179

14. Berger A (2003) How does it work? Positron emission tomography. BMJ 326(7404):1449
15. Lancelot S, Zimmer L (2010) Small-animal positron emission tomography as a tool for neuropharmacology. Trends Pharmacol Sci 31(9):411–417
16. Heiss WD, Herholz K (2006) Brain receptor imaging. J Nucl Med 47(2):302–312
17. Arlicot N et al (2012) Initial evaluation in healthy humans of [^{18}F]DPA-714, a potential PET biomarker for neuroinflammation. Nucl Med Biol 39(4):570–578
18. Cerami C, Iaccarino L, Perani D (2017) Molecular imaging of neuroinflammation in neurodegenerative dementias: the role of in vivo PET imaging. Int J Mol Sci 18(5):993
19. Cho H et al (2016) Tau PET in Alzheimer disease and mild cognitive impairment. Neurology 87(4):375–383
20. Crawshaw AA, Robertson NP (2017) The role of TSPO PET in assessing neuroinflammation. J Neurol 264(8):1825–1827
21. Hagens M, van Berckel B, Barkhof F (2016) Novel MRI and PET markers of neuroinflammation in multiple sclerosis. Curr Opin Neurol 29(3):229–236
22. Lagarde J, Sarazin M, Bottlaender M (2018) In vivo PET imaging of neuroinflammation in Alzheimer's disease. J Neural Transm (Vienna) 125(5):847–867
23. Payer DE et al (2016) D3 dopamine receptor-preferring [^{11}C]PHNO PET imaging in Parkinson patients with dyskinesia. Neurology 86 (3):224–230
24. Peng S et al (2013) Dopamine: PET imaging and Parkinson disease. PET Clin 8 (4):469–485
25. Wood H (2014) Parkinson disease: ^{18}F-DTBZ PET tracks dopaminergic degeneration in patients with Parkinson disease. Nat Rev Neurol 10(6):305
26. Xia C et al (2017) Association of in vivo [^{18}F] AV-1451 Tau PET imaging results with cortical atrophy and symptoms in typical and atypical Alzheimer disease. JAMA Neurol 74 (4):427–436
27. Laruelle M (1995) et al, SPECT imaging of striatal dopamine release after amphetamine challenge. J Nucl Med 36(7):1182–1190
28. Klein MO et al (2019) Dopamine: functions, signaling, and association with neurological diseases. Cell Mol Neurobiol 39(1):31–59
29. Koob GF, Volkow ND (2010) Neurocircuitry of addiction. Neuropsychopharmacology 35 (1):217–238
30. Stepnicki P, Kondej M, Kaczor AA (2018) Current concepts and treatments of Schizophrenia. Molecules 23(8):2087
31. Walsh JP, Akopian G (2019) Physiological aging at striatal synapses. J Neurosci Res 97 (12):1720–1727
32. Zhang S, Wang R, Wang G (2019) Impact of dopamine oxidation on dopaminergic neurodegeneration. ACS Chem Neurosci 10 (2):945–953
33. Vernaleken I et al (2006) Modulation of [^{18}F] fluorodopa (FDOPA) kinetics in the brain of healthy volunteers after acute haloperidol challenge. NeuroImage 30(4):1332–1339
34. Sioka C, Fotopoulos A, Kyritsis AP (2010) Recent advances in PET imaging for evaluation of Parkinson's disease. Eur J Nucl Med Mol Imaging 37(8):1594–1603
35. Criswell SR et al (2018) [(18)F]FDOPA positron emission tomography in manganese-exposed workers. Neurotoxicology 64:43–49
36. Dreher JC et al (2008) Age-related changes in midbrain dopaminergic regulation of the human reward system. Proc Natl Acad Sci U S A 105(39):15106–15111
37. Ruottinen HM et al (2000) An FDOPA PET study in patients with periodic limb movement disorder and restless legs syndrome. Neurology 54(2):502–504
38. Ito K et al (2002) Striatal and extrastriatal dysfunction in Parkinson's disease with dementia: a 6-[^{18}F]fluoro-L-dopa PET study. Brain 125(Pt 6):1358–1365
39. Bruck A et al (2005) Cortical 6-[^{18}F]fluoro-L-dopa uptake and frontal cognitive functions in early Parkinson's disease. Neurobiol Aging 26(6):891–898
40. Cropley VL et al (2006) Molecular imaging of the dopaminergic system and its association with human cognitive function. Biol Psychiatry 59(10):898–907
41. Becker G et al (2017) Comparative assessment of 6-[(18)F]fluoro-L-m-tyrosine and 6-[(18) F]fluoro-L-dopa to evaluate dopaminergic presynaptic integrity in a Parkinson's disease rat model. J Neurochem 141 (4):626–635
42. Kanazawa M et al (2016) Evaluation of 6-^{11}C-Methyl-m-Tyrosine as a PET probe for presynaptic dopaminergic activity: a comparison PET study with beta-^{11}C-l-DOPA and ^{18}F-FDOPA in Parkinson Disease Monkeys. J Nucl Med 57(2):303–308
43. Rademacher L et al (2016) Effects of smoking cessation on presynaptic dopamine function of addicted male smokers. Biol Psychiatry 80 (3):198–206

44. Heinz A et al (2005) Correlation of alcohol craving with striatal dopamine synthesis capacity and D2/3 receptor availability: a combined [^{18}F]DOPA and [^{18}F]DMFP PET study in detoxified alcoholic patients. Am J Psychiatry 162(8):1515–1520
45. Deserno L et al (2015) Chronic alcohol intake abolishes the relationship between dopamine synthesis capacity and learning signals in the ventral striatum. Eur J Neurosci 41 (4):477–486
46. Napier TC et al (2015) Linking neuroscience with modern concepts of impulse control disorders in Parkinson's disease. Mov Disord 30 (2):141–149
47. Majuri J et al (2017) Dopamine and opioid neurotransmission in behavioral addictions: a comparative PET study in pathological gambling and binge eating. Neuropsychopharmacology 42(5):1169–1177
48. Avram M et al (2019) Reduced striatal dopamine synthesis capacity in patients with schizophrenia during remission of positive symptoms. Brain 142(6):1813–1826
49. Demjaha A et al (2012) Dopamine synthesis capacity in patients with treatment-resistant schizophrenia. Am J Psychiatry 169 (11):1203–1210
50. Seeman P (2013) Schizophrenia and dopamine receptors. Eur Neuropsychopharmacol 23(9):999–1009
51. Doot RK et al (2019) Selectivity of probes for PET imaging of dopamine D3 receptors. Neurosci Lett 691:18–25
52. Banerjee A et al (2013) Click chemistry based synthesis of dopamine D4 selective receptor ligands for the selection of potential PET tracers. Bioorg Med Chem Lett 23 (22):6079–6082
53. Lacivita E et al (2014) Design, synthesis, lipophilic properties, and binding affinities of potential ligands in positron emission tomography (PET) for visualization of brain dopamine D4 receptors. Chem Biodivers 11 (2):299–310
54. Halldin C et al (1998) Carbon-11-NNC 112: a radioligand for PET examination of striatal and neocortial D1-dopamine receptors. J Nucl Med 39(12):2061–2068
55. Cropley VL et al (2008) Pre- and post-synaptic dopamine imaging and its relation with frontostriatal cognitive function in Parkinson disease: PET studies with [^{11}C]NNC 112 and [^{18}F]FDOPA. Psychiatry Res 163 (2):171–182
56. Leung K (2004) (R)-(+)-8-Chloro-2,3,4,5-tetrahydro-3-[(11)C]methyl-5-phenyl-1H-3-benzazepin-7-ol ([(11)C]SCH 23390). In: Molecular Imaging and Contrast Agent Database (MICAD). National Center for Biotechnology Information, Bethesda, MD
57. Matheson GJ et al (2017) Reliability of volumetric and surface-based normalisation and smoothing techniques for PET analysis of the cortex: a test-retest analysis using [(11) C]SCH-23390. NeuroImage 155:344–353
58. Ram S, Ehrenkaufer RE, Spicer LD (1989) Synthesis of the labeled D1 receptor antagonist SCH 23390 using [^{11}C]carbon dioxide. Int J Rad Appl Instrum A 40(5):425–427
59. Finnema SJ et al (2015) Application of cross-species PET imaging to assess neurotransmitter release in brain. Psychopharmacology 232 (21–22):4129–4157
60. Farde L et al (1985) Substituted benzamides as ligands for visualization of dopamine receptor binding in the human brain by positron emission tomography. Proc Natl Acad Sci U S A 82(11):3863–3867
61. Mukherjee J et al (2002) Brain imaging of ^{18}F-fallypride in normal volunteers: blood analysis, distribution, test-retest studies, and preliminary assessment of sensitivity to aging effects on dopamine D-2/D-3 receptors. Synapse 46(3):170–188
62. Halldin C et al (1995) Carbon-11-FLB 457: a radioligand for extrastriatal D2 dopamine receptors. J Nucl Med 36(7):1275–1281
63. Willeit M et al (2006) High-affinity states of human brain dopamine D2/3 receptors imaged by the agonist [^{11}C]-(+)-PHNO. Biol Psychiatry 59(5):389–394
64. Hwang DR, Kegeles LS, Laruelle M (2000) (−)-N-[(11)C]propyl-norapomorphine: a positron-labeled dopamine agonist for PET imaging of D(2) receptors. Nucl Med Biol 27(6):533–539
65. Finnema SJ et al (2005) A preliminary PET evaluation of the new dopamine D2 receptor agonist [^{11}C]MNPA in cynomolgus monkey. Nucl Med Biol 32(4):353–360
66. Finnema SJ et al (2014) (18)F-MCL-524, an (18)F-Labeled dopamine D2 and D3 receptor agonist sensitive to dopamine: a preliminary PET Study. J Nucl Med 55(7):1164–1170
67. Finnema SJ et al (2010) Current state of agonist radioligands for imaging of brain dopamine D2/D3 receptors in vivo with positron emission tomography. Curr Top Med Chem 10(15):1477–1498
68. Karrer TM et al (2017) Reduced dopamine receptors and transporters but not synthesis capacity in normal aging adults: a meta-analysis. Neurobiol Aging 57:36–46

69. Antonini A, Leenders KL (1993) Dopamine D2 receptors in normal human brain: effect of age measured by positron emission tomography (PET) and [^{11}C]-raclopride. Ann N Y Acad Sci 695:81–85
70. Seaman KL et al (2019) Differential regional decline in dopamine receptor availability across adulthood: linear and nonlinear effects of age. Hum Brain Mapp 40(10):3125–3138
71. Dang LC et al (2016) Associations between dopamine D2 receptor availability and BMI depend on age. NeuroImage 138:176–183
72. Schwarz J et al (1993) 123I-iodobenzamide-SPECT in 83 patients with de novo parkinsonism. Neurology 43(12 Suppl 6):S17–S20
73. Brandt J et al (1990) D2 receptors in Huntington's disease: positron emission tomography findings and clinical correlates. J Neuropsychiatry Clin Neurosci 2(1):20–27
74. Sedvall G et al (1994) Dopamine D1 receptor number—a sensitive PET marker for early brain degeneration in Huntington's disease. Eur Arch Psychiatry Clin Neurosci 243 (5):249–255
75. Volkow ND et al (1990) Effects of chronic cocaine abuse on postsynaptic dopamine receptors. Am J Psychiatry 147(6):719–724
76. Ashok AH et al (2017) Association of stimulant use with dopaminergic alterations in users of cocaine, amphetamine, or methamphetamine: a systematic review and meta-analysis. JAMA Psychiat 74(5):511–519
77. Fotros A et al (2013) Cocaine cue-induced dopamine release in amygdala and hippocampus: a high-resolution PET [(1)(8)F]fallypride study in cocaine dependent participants. Neuropsychopharmacology 38 (9):1780–1788
78. Naylor JE et al (2017) Positron emission tomography (PET) imaging of nicotine-induced dopamine release in squirrel monkeys using [(18)F]Fallypride. Drug Alcohol Depend 179:254–259
79. Hietala J et al (1994) Striatal D2 dopamine receptor binding characteristics in vivo in patients with alcohol dependence. Psychopharmacology 116(3):285–290
80. Rominger A et al (2012) [^{18}F]Fallypride PET measurement of striatal and extrastriatal dopamine D 2/3 receptor availability in recently abstinent alcoholics. Addict Biol 17 (2):490–503
81. Egerton A et al (2009) The dopaminergic basis of human behaviors: a review of molecular imaging studies. Neurosci Biobehav Rev 33(7):1109–1132
82. Martinez D et al (2009) Dopamine D1 receptors in cocaine dependence measured with PET and the choice to self-administer cocaine. Neuropsychopharmacology 34 (7):1774–1782
83. Wulff S et al (2019) The relation between dopamine D2 receptor blockade and the brain reward system: a longitudinal study of first-episode schizophrenia patients. Psychol Med 2019:1–9
84. Okubo Y et al (1997) Decreased prefrontal dopamine D1 receptors in schizophrenia revealed by PET. Nature 385(6617):634–636
85. Poels EM et al (2013) In vivo binding of the dopamine-1 receptor PET tracers [(1)(1)C] NNC112 and [(1)(1)C]SCH23390: a comparison study in individuals with schizophrenia. Psychopharmacology 228(1):167–174
86. Caravaggio F et al (2019) What proportion of striatal D2 receptors are occupied by endogenous dopamine at baseline? A meta-analysis with implications for understanding antipsychotic occupancy. Neuropharmacology 163:107591
87. Mitelman SA et al (2019) Positive association between cerebral grey matter metabolism and dopamine D2/D3 receptor availability in healthy and schizophrenia subjects: an (18) F-fluorodeoxyglucose and (18)F-fallypride positron emission tomography study. World J Biol Psychiatry 2019:1–15
88. Mitelman SA et al (2020) Dopamine receptor density and white matter integrity: (18)F-fallypride positron emission tomography and diffusion tensor imaging study in healthy and schizophrenia subjects. Brain Imaging Behav 14(3):736–752
89. Jucaite A et al (2005) Reduced midbrain dopamine transporter binding in male adolescents with attention-deficit/hyperactivity disorder: association between striatal dopamine markers and motor hyperactivity. Biol Psychiatry 57(3):229–238
90. Hantraye P et al (1992) Dopamine fiber detection by [^{11}C]-CFT and PET in a primate model of parkinsonism. Neuroreport 3 (3):265–268
91. Huang T et al (2012) The influence of residual nor-beta-CFT in ^{11}C CFT injection on the Parkinson disease diagnosis: a ^{11}C CFT PET study. Clin Nucl Med 37(8):743–747
92. Rinne JO et al (2004) Unchanged striatal dopamine transporter availability in narcolepsy: a PET study with [^{11}C]-CFT. Acta Neurol Scand 109(1):52–55
93. Sun X et al (2019) Quantitative research of (11)C-CFT and (18)F-FDG PET in

Parkinson's disease: a Pilot Study with NeuroQ software. Front Neurosci 13:299

94. Wu L et al (2018) ^{11}C-CFT-PET in Presymptomatic FTDP-17: a potential biomarker predicting onset. J Alzheimers Dis 61 (2):613–618
95. Pizzagalli DA et al (2019) Assessment of striatal dopamine transporter binding in individuals with major depressive disorder: in vivo positron emission tomography and postmortem evidence. JAMA Psychiatry 76 (8):854–861
96. Rieckmann A et al (2015) Putamen-midbrain functional connectivity is related to striatal dopamine transporter availability in patients with Lewy body diseases. Neuroimage Clin 8:554–559
97. Shirvan J et al (2019) Neuropathologic correlates of amyloid and dopamine transporter imaging in Lewy body disease. Neurology 93 (5):e476–e484
98. Spencer TJ et al (2013) Functional genomics of attention-deficit/hyperactivity disorder (ADHD) risk alleles on dopamine transporter binding in ADHD and healthy control subjects. Biol Psychiatry 74(2):84–89
99. Spencer TJ et al (2010) A PET study examining pharmacokinetics and dopamine transporter occupancy of two long-acting formulations of methylphenidate in adults. Int J Mol Med 25(2):261–265
100. Benveniste H et al (2005) Maternal and fetal ^{11}C-cocaine uptake and kinetics measured in vivo by combined PET and MRI in pregnant nonhuman primates. J Nucl Med 46 (2):312–320
101. Fowler JS et al (1989) Mapping cocaine binding sites in human and baboon brain in vivo. Synapse 4(4):371–377
102. Volkow ND et al (1995) Long-lasting inhibition of in vivo cocaine binding to dopamine transporters by 3 beta-(4-iodophenyl)tropane-2-carboxylic acid methyl ester: RTI-55 or beta CIT. Synapse 19(3):206–211
103. Volkow ND et al (2000) Effects of route of administration on cocaine induced dopamine transporter blockade in the human brain. Life Sci 67(12):1507–1515
104. Volkow ND et al (1998) Dopamine transporter occupancies in the human brain induced by therapeutic doses of oral methylphenidate. Am J Psychiatry 155 (10):1325–1331
105. Volkow ND et al (1996) Cocaine uptake is decreased in the brain of detoxified cocaine abusers. Neuropsychopharmacology 14 (3):159–168
106. Volkow ND et al (2007) Brain dopamine transporter levels in treatment and drug naive adults with ADHD. NeuroImage 34 (3):1182–1190
107. Albin RL et al (2009) Striatal [^{11}C]dihydrotetrabenazine and [^{11}C]methylphenidate binding in Tourette syndrome. Neurology 72(16):1390–1396
108. Fischer K et al (2012) In vivo quantification of dopamine transporters in mice with unilateral 6-OHDA lesions using [^{11}C]methylphenidate and PET. NeuroImage 59 (3):2413–2422
109. Gatley SJ et al (1995) Binding of d-threo-[^{11}C]methylphenidate to the dopamine transporter in vivo: insensitivity to synaptic dopamine. Eur J Pharmacol 281(2):141–149
110. Johanson CE et al (2006) Cognitive function and nigrostriatal markers in abstinent methamphetamine abusers. Psychopharmacology 185(3):327–338
111. Sossi V et al (2012) In vivo dopamine transporter imaging in a unilateral 6-hydroxydopamine rat model of Parkinson disease using ^{11}C-methylphenidate PET. J Nucl Med 53(5):813–822
112. Sossi V et al (2010) Levodopa and pramipexole effects on presynaptic dopamine PET markers and estimated dopamine release. Eur J Nucl Med Mol Imaging 37(12):2364–2370
113. Sossi V et al (2000) Analysis of four dopaminergic tracers kinetics using two different tissue input function methods. J Cereb Blood Flow Metab 20(4):653–660
114. Volkow ND et al (1995) Is methylphenidate like cocaine? Studies on their pharmacokinetics and distribution in the human brain. Arch Gen Psychiatry 52(6):456–463
115. Farde L et al (1994) PET study of [^{11}C]beta-CIT binding to monoamine transporters in the monkey and human brain. Synapse 16 (2):93–103
116. Ginovart N et al (1997) PET study of the pre- and post-synaptic dopaminergic markers for the neurodegenerative process in Huntington's disease. Brain 120(Pt 3):503–514
117. Halldin C et al (1996) [^{11}C]beta-CIT-FE, a radioligand for quantitation of the dopamine transporter in the living brain using positron emission tomography. Synapse 22 (4):386–390
118. Laihinen AO et al (1995) PET studies on brain monoamine transporters with carbon-11-beta-CIT in Parkinson's disease. J Nucl Med 36(7):1263–1267
119. Lundkvist C et al (1997) [^{18}F] beta-CIT-FP is superior to [^{11}C] beta-CIT-FP for

quantitation of the dopamine transporter. Nucl Med Biol 24(7):621–627

120. Suhara T et al (1996) Effects of cocaine on [^{11}C]norepinephrine and [^{11}C] beta-CIT uptake in the primate peripheral organs measured by PET. Ann Nucl Med 10 (1):85–88
121. Ko JH, Lee CS, Eidelberg D (2017) Metabolic network expression in parkinsonism: clinical and dopaminergic correlations. J Cereb Blood Flow Metab 37(2):683–693
122. Leung K (2004) N-4-[(18)F]Fluorobut-2-yn-1-yl-2beta-carbomethoxy-3beta-phenyltropane. In: Molecular Imaging and Contrast Agent Database (MICAD). National Center for Biotechnology Information, Bethesda, MD
123. Leung K (2004) N-4-Fluorobut-2-yn-1-yl-2beta-carbo-[(11)C]methoxy-3beta-phenyltropane. In: Molecular Imaging and Contrast Agent Database (MICAD). National Center for Biotechnology Information, Bethesda, MD
124. Niethammer M et al (2013) Parkinson's disease cognitive network correlates with caudate dopamine. NeuroImage 78:204–209
125. Pagano G, Niccolini F, Politis M (2016) Current status of PET imaging in Huntington's disease. Eur J Nucl Med Mol Imaging 43 (6):1171–1182
126. Voon V et al (2014) Impulse control disorders in Parkinson's disease: decreased striatal dopamine transporter levels. J Neurol Neurosurg Psychiatry 85(2):148–152
127. Erixon-Lindroth N et al (2005) The role of the striatal dopamine transporter in cognitive aging. Psychiatry Res 138(1):1–12
128. Aquilonius SM (1991) What has PET told us about Parkinson's disease? Acta Neurol Scand Suppl 136:37–39
129. Edling C et al (1997) Do organic solvents induce changes in the dopaminergic system? Positron emission tomography studies of occupationally exposed subjects. Int Arch Occup Environ Health 70(3):180–186
130. Edling C et al (1997) Positron emission tomography studies of healthy volunteers--no effects on the dopamine terminals and synthesis after short-term exposure to toluene. Hum Exp Toxicol 16(3):171–176
131. Pike VW et al (1990) Labelled agents for PET studies of the dopaminergic system--some quality assurance methods, experience and issues. Int J Rad Appl Instrum A 41 (5):483–492
132. Tedroff J et al (1992) Cerebral uptake and utilization of therapeutic [beta-^{11}C]-L-DOPA in Parkinson's disease measured by positron emission tomography. Relations to motor response. Acta Neurol Scand 85 (2):95–102
133. Tedroff J et al (1990) Striatal kinetics of [^{11}C]-(+)-nomifensine and 6-[^{18}F]fluoro-L-dopa in Parkinson's disease measured with positron emission tomography. Acta Neurol Scand 81(1):24–30
134. Varrone A, Halldin C (2010) Molecular imaging of the dopamine transporter. J Nucl Med 51(9):1331–1334
135. Kawamura K, Oda K, Ishiwata K (2003) Age-related changes of the [^{11}C]CFT binding to the striatal dopamine transporters in the Fischer 344 rats: a PET study. Ann Nucl Med 17(3):249–253
136. Larsson M et al (2009) Age-related loss of olfactory sensitivity: association to dopamine transporter binding in putamen. Neuroscience 161(2):422–426
137. Oh M et al (2012) Subregional patterns of preferential striatal dopamine transporter loss differ in Parkinson disease, progressive supranuclear palsy, and multiple-system atrophy. J Nucl Med 53(3):399–406
138. Troiano AR et al (2010) Dopamine transporter PET in normal aging: dopamine transporter decline and its possible role in preservation of motor function. Synapse 64 (2):146–151
139. Lambert G, Karila L, Lowenstein W (2008) Neuroimaging and cocaine: mapping dependence? Presse Med 37(4 Pt 2):679–688
140. Le Foll B et al (2009) Baseline expression of alpha4beta2* nicotinic acetylcholine receptors predicts motivation to self-administer nicotine. Biol Psychiatry 65(8):714–716
141. Narendran R, Martinez D (2008) Cocaine abuse and sensitization of striatal dopamine transmission: a critical review of the preclinical and clinical imaging literature. Synapse 62 (11):851–869
142. Spencer TJ et al (2006) PET study examining pharmacokinetics, detection and likeability, and dopamine transporter receptor occupancy of short- and long-acting oral methylphenidate. Am J Psychiatry 163(3):387–395
143. Fazio P et al (2018) Nigrostriatal dopamine transporter availability in early Parkinson's disease. Mov Disord 33(4):592–599
144. Gerasimou GP et al (2006) Molecular imaging (SPECT and PET) in the evaluation of patients with movement disorders. Nucl Med Rev Cent East Eur 9(2):147–153
145. Saeed U et al (2017) Imaging biomarkers in Parkinson's disease and Parkinsonian

syndromes: current and emerging concepts. Transl Neurodegener 6:8

146. Marek K, Jennings D (2009) Can we image premotor Parkinson disease? Neurology 72 (7 Suppl):S21–S26
147. Tiihonen J et al (1995) Altered striatal dopamine re-uptake site densities in habitually violent and non-violent alcoholics. Nat Med 1 (7):654–657
148. Spencer TJ et al (2007) Further evidence of dopamine transporter dysregulation in ADHD: a controlled PET imaging study using altropane. Biol Psychiatry 62 (9):1059–1061
149. Hesse S et al (2009) Dopamine transporter imaging in adult patients with attention-deficit/hyperactivity disorder. Psychiatry Res 171 (2):120–128
150. Volkow ND et al (2009) Evaluating dopamine reward pathway in ADHD: clinical implications. JAMA 302(10):1084–1091
151. Taylor SF et al (2000) In vivo measurement of the vesicular monoamine transporter in schizophrenia. Neuropsychopharmacology 23(6):667–675
152. Chang L et al (2007) Structural and metabolic brain changes in the striatum associated with methamphetamine abuse. Addiction 102 (Suppl 1):16–32
153. Frey KA, Koeppe RA, Kilbourn MR (2001) Imaging the vesicular monoamine transporter. Adv Neurol 86:237–247
154. Huang ZR et al (2016) A novel potential positron emission tomography imaging agent for vesicular monoamine transporter type 2. PLoS One 11(9):e0161295
155. Perez-Lohman C et al (2018) Diagnostic utility of [^{11}C]DTBZ positron emission tomography in clinically uncertain parkinsonism: experience of a single tertiary center. Rev Investig Clin 70(6):285–290
156. Koeppe RA et al (2008) Differentiating Alzheimer's disease from dementia with Lewy bodies and Parkinson's disease with (+)-[^{11}C]dihydrotetrabenazine positron emission tomography. Alzheimers Dement 4(1 Suppl 1):S67–S76
157. Bohnen NI et al (2000) Decreased striatal monoaminergic terminals in Huntington disease. Neurology 54(9):1753–1759
158. Boileau I et al (2010) Influence of a low dose of amphetamine on vesicular monoamine transporter binding: a PET (+)[^{11}C]DTBZ study in humans. Synapse 64(6):417–420
159. Zubieta JK et al (2001) Vesicular monoamine transporter concentrations in bipolar disorder type I, schizophrenia, and healthy subjects. Biol Psychiatry 49(2):110–116
160. Hirvonen J et al (2009) Assessment of MAO-B occupancy in the brain with PET and [^{11}C]-L-deprenyl-D2: a dose-finding study with a novel MAO-B inhibitor, EVT 301. Clin Pharmacol Ther 85(5):506–512
161. Deleu D, Northway MG, Hanssens Y (2002) Clinical pharmacokinetic and pharmacodynamic properties of drugs used in the treatment of Parkinson's disease. Clin Pharmacokinet 41(4):261–309
162. Fowler JS et al (1997) Age-related increases in brain monoamine oxidase B in living healthy human subjects. Neurobiol Aging 18 (4):431–435
163. Fowler JS et al (1993) Monoamine oxidase B (MAO B) inhibitor therapy in Parkinson's disease: the degree and reversibility of human brain MAO B inhibition by Ro 19 6327. Neurology 43(10):1984–1992
164. Carter SF et al (2019) Longitudinal association between astrocyte function and glucose metabolism in autosomal dominant Alzheimer's disease. Eur J Nucl Med Mol Imaging 46(2):348–356
165. Olsen M et al (2018) Astroglial responses to amyloid-beta progression in a mouse model of Alzheimer's disease. Mol Imaging Biol 20 (4):605–614
166. Rodriguez-Vieitez E et al (2016) Comparison of early-phase ^{11}C-Deuterium-l-deprenyl and ^{11}C-Pittsburgh compound B PET for assessing brain perfusion in Alzheimer disease. J Nucl Med 57(7):1071–1077
167. Fowler JS et al (1998) An acute dose of nicotine does not inhibit MAO B in baboon brain in vivo. Life Sci 63(2):PL19–PL23
168. Fowler JS et al (1998) Neuropharmacological actions of cigarette smoke: brain monoamine oxidase B (MAO B) inhibition. J Addict Dis 17(1):23–34
169. Kilbourn MR et al (1996) Effects of dopaminergic drug treatments on in vivo radioligand binding to brain vesicular monoamine transporters. Nucl Med Biol 23(4):467–471
170. Zanderigo F et al (2018) [(11)C]Harmine binding to brain monoamine oxidase A: test-retest properties and noninvasive quantification. Mol Imaging Biol 20(4):667–681
171. Kolla NJ et al (2015) Lower monoamine oxidase-A total distribution volume in impulsive and violent male offenders with antisocial personality disorder and high psychopathic traits: an [(11)C] harmine positron emission tomography study. Neuropsychopharmacology 40(11):2596–2603

172. Kolla NJ et al (2016) Elevated monoamine oxidase-A distribution volume in borderline personality disorder is associated with severity across mood symptoms, suicidality, and cognition. Biol Psychiatry 79(2):117–126
173. Soliman A et al (2011) Relationship of monoamine oxidase A binding to adaptive and maladaptive personality traits. Psychol Med 41 (5):1051–1060
174. Meyer JH (2017) Neuroprogression and immune activation in major depressive disorder. Mod Trends Pharmacopsychiatry 31:27–36
175. Volkow ND et al (1996) PET evaluation of the dopamine system of the human brain. J Nucl Med 37(7):1242–1256
176. Ding YS et al (1996) Mapping catechol-O-methyltransferase in vivo: initial studies with [^{18}F]Ro41-0960. Life Sci 58(3):195–208
177. Higuera-Matas A et al (2008) Augmented acquisition of cocaine self-administration and altered brain glucose metabolism in adult female but not male rats exposed to a cannabinoid agonist during adolescence. Neuropsychopharmacology 33(4):806–813
178. Soto-Montenegro ML et al (2007) Effects of MDMA on blood glucose levels and brain glucose metabolism. Eur J Nucl Med Mol Imaging 34(6):916–925
179. Wolkin A et al (1987) Effects of amphetamine on local cerebral metabolism in normal and schizophrenic subjects as determined by positron emission tomography. Psychopharmacology 92(2):241–246
180. London ED et al (1990) Cocaine-induced reduction of glucose utilization in human brain. A study using positron emission tomography and [fluorine 18]-fluorodeoxyglucose. Arch Gen Psychiatry 47(6):567–574
181. Dean B (2012) Neurochemistry of schizophrenia: the contribution of neuroimaging postmortem pathology and neurochemistry in schizophrenia. Curr Top Med Chem 12 (21):2375–2392
182. Frankle WG et al (2005) Serotonin transporter availability in patients with schizophrenia: a positron emission tomography imaging study with [^{11}C]DASB. Biol Psychiatry 57 (12):1510–1516
183. Kim JH et al (2015) Serotonin transporter availability in thalamic subregions in schizophrenia: a study using 7.0-T MRI with [(11) C]DASB high-resolution PET. Psychiatry Res 231(1):50–57
184. Volkow ND et al (1987) Phenomenological correlates of metabolic activity in 18 patients with chronic schizophrenia. Am J Psychiatry 144(2):151–158
185. Bralet MC et al (2016) FDG-PET scans in patients with Kraepelinian and non-Kraepelinian schizophrenia. Eur Arch Psychiatry Clin Neurosci 266(6):481–494
186. Buchsbaum MS et al (1998) MRI white matter diffusion anisotropy and PET metabolic rate in schizophrenia. Neuroreport 9 (3):425–430
187. Buchsbaum MS et al (2002) Differential metabolic rates in prefrontal and temporal Brodmann areas in schizophrenia and schizotypal personality disorder. Schizophr Res 54 (1-2):141–150
188. Fujimoto T et al (2007) Abnormal glucose metabolism in the anterior cingulate cortex in patients with schizophrenia. Psychiatry Res 154(1):49–58
189. Hazlett EA et al (2004) Abnormal glucose metabolism in the mediodorsal nucleus of the thalamus in schizophrenia. Am J Psychiatry 161(2):305–314
190. Tamminga CA et al (1992) Limbic system abnormalities identified in schizophrenia using positron emission tomography with fluorodeoxyglucose and neocortical alterations with deficit syndrome. Arch Gen Psychiatry 49(7):522–530
191. Bartlett EJ et al (1994) Effects of haloperidol challenge on regional cerebral glucose utilization in normal human subjects. Am J Psychiatry 151(5):681–686
192. Volkow ND et al (1986) Brain metabolism in patients with schizophrenia before and after acute neuroleptic administration. J Neurol Neurosurg Psychiatry 49(10):1199–1202
193. Darcourt J et al (2010) EANM procedure guidelines for brain neurotransmission SPECT using (123)I-labelled dopamine transporter ligands, version 2. Eur J Nucl Med Mol Imaging 37(2):443–450
194. Van Laere K et al (2010) EANM procedure guidelines for brain neurotransmission SPECT/PET using dopamine D2 receptor ligands, version 2. Eur J Nucl Med Mol Imaging 37(2):434–442
195. Varrone A et al (2009) EANM procedure guidelines for PET brain imaging using [^{18}F]FDG, version 2. Eur J Nucl Med Mol Imaging 36(12):2103–2110
196. Casquero-Veiga M et al (2018) Understanding deep brain stimulation: in vivo metabolic consequences of the electrode insertional effect. Biomed Res Int 2018:8560232
197. Casquero-Veiga M et al (2019) Risperidone administered during adolescence induced

metabolic, anatomical and inflammatory/oxidative changes in adult brain: a PET and MRI study in the maternal immune stimulation animal model. Eur Neuropsychopharmacol 29(7):880–896

198. Soto-Montenegro ML, Pascau J, Desco M (2014) Response to deep brain stimulation in the lateral hypothalamic area in a rat model of obesity: in vivo assessment of brain glucose metabolism. Mol Imaging Biol 16 (6):830–837
199. Hartung T (2010) Comparative analysis of the revised Directive 2010/63/EU for the protection of laboratory animals with its predecessor 86/609/EEC—a t4 report. ALTEX 27(4):285–303
200. Wells DJ (2011) Animal welfare and the 3Rs in European biomedical research. Ann N Y Acad Sci 1245:14–16
201. Schiffer WK, Mirrione MM, Dewey SL (2007) Optimizing experimental protocols for quantitative behavioral imaging with ^{18}F-FDG in rodents. J Nucl Med 48 (2):277–287
202. Prando S et al (2019) Comparison of different quantification methods for ^{18}F-fluorodeoxyglucose-positron emission tomography studies in rat brains. Clinics (Sao Paulo) 74: e1273
203. Calvini P et al (2007) The basal ganglia matching tools package for striatal uptake semi-quantification: description and validation. Eur J Nucl Med Mol Imaging 34 (8):1240–1253
204. Valdes-Hernandez PA et al (2011) An in vivo MRI template set for morphometry, tissue segmentation, and fMRI localization in rats. Front Neuroinform 5:26
205. Lammertsma AA, Hume SP (1996) Simplified reference tissue model for PET receptor studies. NeuroImage 4(3 Pt 1):153–158
206. Ichise M et al (2003) Linearized reference tissue parametric imaging methods: application to [^{11}C]DASB positron emission tomography studies of the serotonin transporter in human brain. J Cereb Blood Flow Metab 23 (9):1096–1112
207. Ben Bouallegue F, Vauchot F, Mariano-Goulart D (2019) Comparative assessment of linear least-squares, nonlinear least-squares, and Patlak graphical method for regional and local quantitative tracer kinetic modeling in cerebral dynamic (18) F-FDG PET. Med Phys 46(3):1260–1271
208. Bentourkia M (2006) Kinetic modeling of PET-FDG in the brain without blood sampling. Comput Med Imaging Graph 30 (8):447–451
209. Bentourkia M, Zaidi H (2007) Tracer kinetic modeling in PET. PET Clin 2(2):267–277
210. Endres CJ et al (1997) Kinetic modeling of [^{11}C]raclopride: combined PET-microdialysis studies. J Cereb Blood Flow Metab 17 (9):932–942
211. Pan L et al (2017) Machine learning-based kinetic modeling: a robust and reproducible solution for quantitative analysis of dynamic PET data. Phys Med Biol 62(9):3566–3581
212. Juarez EJ et al (2019) Reproducibility of the correlative triad among aging, dopamine receptor availability, and cognition. Psychol Aging 34(7):921–932
213. Veselinovic T et al (2018) The role of striatal dopamine D2/3 receptors in cognitive performance in drug-free patients with schizophrenia. Psychopharmacology 235 (8):2221–2232
214. Vyas NS et al (2018) D2/D3 dopamine receptor binding with [F-18]fallypride correlates of executive function in medication-naive patients with schizophrenia. Schizophr Res 192:442–456
215. Milella MS et al (2016) Cocaine cue-induced dopamine release in the human prefrontal cortex. J Psychiatry Neurosci 41(5):322–330
216. Leurquin-Sterk G et al (2018) Cerebral dopaminergic and glutamatergic transmission relate to different subjective responses of acute alcohol intake: an in vivo multimodal imaging study. Addict Biol 23(3):931–944
217. Pfeifer P et al (2017) Acute effect of intravenously applied alcohol in the human striatal and extrastriatal D2 /D3 dopamine system. Addict Biol 22(5):1449–1458
218. Barlow RL et al (2018) Ventral striatal D2/3 receptor availability is associated with impulsive choice behavior as well as limbic corticostriatal connectivity. Int J Neuropsychopharmacol 21(7):705–707

Chapter 15

In Vivo Electrophysiology for Reward Anticipation and Processing

Laura A. Alba, Elizabeth Baker, and Katherine K. M. Stavropoulos

Abstract

One of the humans' most adaptive functions is the brain's ability to predict future outcomes, especially regarding the ability to secure rewards. Neuroscience research studies in both healthy and psychiatric populations have provided important insights into the brain activity associated with both reward anticipation and processing. One effective method to measure reward-related brain activity is electroencephalography (EEG), a neuroimaging method with precise temporal resolution. This chapter highlights current research using electrophysiology to examine reward processing and anticipation in humans. We first review three event-related potential (ERP) components that are commonly associated with reward processes: the stimulus preceding negativity (SPN), the reward positivity (RewP), and the P300. Common paradigms designed to elicit the aforementioned ERP components are also reviewed. Such paradigms include gambling tasks, time estimation tasks, monetary incentive delay tasks, and delay discounting tasks. Next, we review previous literature using these paradigms to measure reward anticipation and processing in neurotypical adults. Finally, we briefly review previous research with psychiatric populations (e.g., individuals with attention deficit/hyperactivity disorder, schizophrenia, substance abuse, and depression).

Key words Electrophysiology, RewP, FRN, SPN, Reward

1 Introduction

One of the humans' most adaptive functions for survival stems from the brain's ability to predict future outcomes, especially regarding the ability to secure rewards [1, 2]. The ability to adaptively process and seek out rewards reinforces certain behaviors and lessens others that do not result in rewards, such that human behavior is shaped by what we recognize, implicitly or explicitly, as being rewarding [3]. Understanding how we process information after receiving positive or negative feedback to subsequently alter behavior is crucial for learning, behavior modification, and maximizing future rewards [4]. In particular, the magnitude of reward is often a critical predictor for influencing behavior [5]. Moreover, the value of

Marc Fakhoury (ed.), *The Brain Reward System*, Neuromethods, vol. 165, https://doi.org/10.1007/978-1-0716-1146-3_15,

reward serves as a tool for measuring approaching or anticipating positive outcomes and avoiding punishments [6].

Motivated by advances in neuroimaging methods, research studies in both healthy and psychiatric populations have provided evidence of the neural circuitry responsible for both anticipating and processing rewards. Previous work by Schultz and colleagues [2, 7, 8] suggests that reward prediction errors are encoded in midbrain dopamine neurons. Midbrain regions recruited for reward anticipation and processing include the ventral striatum (VS), medial orbitofrontal cortex (OFC), ventromedial prefrontal cortex (vPFC), amygdala, and the anterior cingulate cortex (ACC) [2, 9, 10]. Dopamine neurons in these brain regions are more active when an individual has better outcomes than expected compared to poor outcomes, during which decreased activity in dopamine neurons is observed [2].

One effective method used to measure reward is electroencephalography (EEG), a neuroimaging method with precise temporal resolution (see [11] for a description of spatial and temporal resolution in EEG). EEG allows for the study of event-related potentials (ERPs), the brain's response to stimuli in the environment [12, 13]. On the human scalp, the ERP waveform is continuous and shows positive and negative deflections that vary in duration and amplitude [12]. ERP components are used to provide meaningful information about neural, cognitive, and psychological processes [12]. ERP components are described as a change in scalp-recorded voltage that reflects a specific neural process [12]. Furthermore, ERPs reflect voltage fluctuations that are time-locked to a specific event, such as anticipating or processing a stimulus [13]. Given the superior temporal resolution of EEG recordings compared to techniques such as functional magnetic resonance imaging (fMRI), researchers are able to investigate the process of neural circuitry within milliseconds, thus allowing for the examination of the brain's immediate response to an event [14].

The goal of this chapter is to highlight current research using electrophysiology to examine reward processing and anticipation in human adults. Specifically, this chapter is focused on human studies using ERP components to discover brain processes related to reward. Furthermore, this chapter aims to develop a foundation for how to interpret and understand ERP components in reward processing and anticipation broadly in the domains of brain and behavior.

2 ERP Components

Measuring reward anticipation and processing is heterogeneous in nature, such that anticipating a reward and receiving feedback elicits different ERP components, which depend on the nature of

the specifications of stimuli presentation. Before reviewing the recent ERP literature measuring reward-related brain activity, it is prudent to highlight the most widely validated ERP components for investigating the reward system. The following sections focus on core ERP components that have been identified as related to the reward system. In addition, examples of commonly used reward anticipation and processing tasks are presented.

2.1 Feedback Related Negativity/ Reward Positivity

Over the past two decades, researchers have examined the differences between positive and negative feedback in order to understand reward processing. The feedback error-related negativity, FRN or fERN [15, 16] is a component with a negative deflection peaking between 200 and 400 ms after the presentation of a feedback stimulus [16]. Note that in recent literature, the FRN is distinguished from the error-related negativity (ERN). The ERN is typically measured as a response-locked component and is elicited when participants make an error (and are aware of having made the error) [17, 18]. The ERN is often observed in tasks where participants are aware of correct and incorrect responses but may make errors due to trying to respond quickly (e.g., Stroop color tasks, Go/No-Go tasks).

The FRN, in contrast, is a feedback locked component that occurs after participants receive feedback indicating whether their response is correct or incorrect. However, some previous literature does not differentiate between the two components and refers to the negative deflection observed in response to receiving negative feedback as the ERN (e.g. [19]). Studies examining source localization suggest that the FRN component is generated by activity in the ACC, which is located in the frontal portion of the cingulate cortex and is associated with reward [2, 16, 20, 21]. The FRN is postulated to be related to processing a wrong decision or receiving negative feedback [12, 15]. The FRN is influenced by feedback valence (e.g., whether feedback indicates that the participant is correct or incorrect), reward magnitude, and by the context in which the reward is presented [22, 23]. Typically, the FRN is conceptualized as a difference wave calculated by subtracting brain activity in response to positive feedback from brain activity in response to negative feedback, which results in negativity [15, 16].

The FRN was originally hypothesized to represent an error signal when encountering negative outcomes [15, 24, 25]. However, recent findings suggest that the FRN might be driven by a *lack* of positive ERP deflection after negative feedback rather than by an *increase* in negative ERP deflection after negative feedback. That is, a relative positivity in the ERP signal following positive feedback (e.g., feedback indicating a correct response) may be absent for negative feedback [26–29]. Therefore, recent literature has noted that the FRN may be calculated as a positive waveform called the

reward positivity (RewP) [26]. The RewP is calculated by subtracting the response to negative feedback (e.g., a "loss") from response to positive feedback (e.g., a "win") [26, 30]. As the RewP is often conceptualized as the inverse of the FRN (as the calculation for one is the inverse of the calculation for the other), it also peaks 200–300 ms after reward stimuli are presented and are generated by activity in the ACC [26, 30, 31].

2.2 P300

The feedback-locked P300 is a slow wave component that peaks approximately 300 ms after a stimulus and shows positive polarity [32, 33]. The P300 evidences a larger positive peak for feedback than for no feedback [32, 33]. Several studies have argued that the P300 may be sensitive to feedback valence, reward probability, and reward magnitude [34–38]. The P300 component is not only modulated by brain regions associated with reward but also by regions associated with attentional control [39]. For instance, Krebs and colleagues [39] suggested that the P300 likely reflects both increased attention during reward prediction and task-related effort. In regard to scalp distribution, the P300 is elicited in the parieto-occipital regions of the scalp [39].

2.3 Stimulus-Preceding Negativity

Another component often used to examine reward and one that is hypothesized to reflect activity in the dopaminergic reward system is the stimulus-preceding negativity (SPN) [40, 41]. The SPN is a slow cortical potential that reflects anticipation before reward-related stimuli are presented [42]. The amplitude of the SPN component is increased when an individual anticipates unpredictable stimuli [43] or unexpected rewards [44] relative to expected feedback. Moreover, a larger SPN amplitude is observed when a participant perceives that a reward has an actual consequence than when no perceived consequence is anticipated [45–48]. That is, a larger SPN is observed when participants perceive themselves as having control over a task outcome than when they do not perceive having control [45, 46].

3 Reward Tasks

Several tasks have been developed to evaluate reward anticipation and processing, which we review below. Modifications and adaptations to these tasks may be needed for specific populations.

3.1 Gambling Tasks

The most widely used tasks to measure reward anticipation and processing are gambling tasks. Gambling tasks allow researchers to measure valence (e.g., reward/gain vs. punishment/loss), correctness (e.g., whether the participant responded correctly or incorrectly), and reward/punishment magnitude (e.g., the size of the gain or loss on a given trial) [16]. In a basic gambling task,

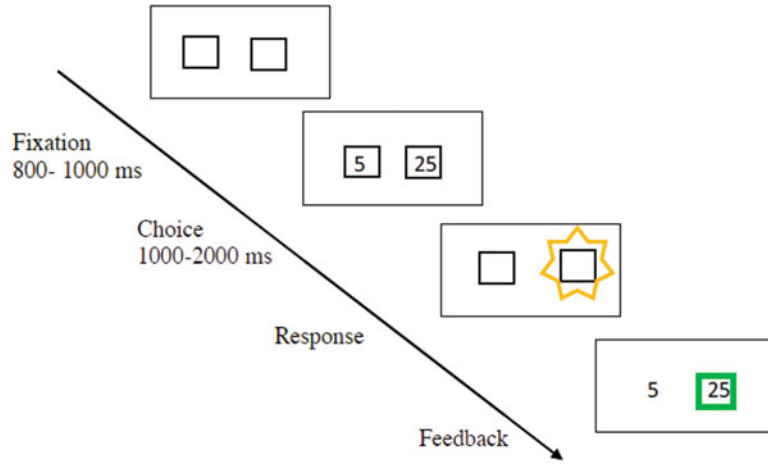

Fig. 1 Gambling task. A schematic of a gambling task. After viewing a central fixation image Fixation), participants are presented with two options (Choice). Participants provide a response and receive feedback about whether or not their choice was correct. In this example, green is associated with a win

participants start off with a set of points or money and are then instructed to gain as many points or as much money as possible. For example, two options are provided to participants with a specific monetary value, and participants are instructed to make a choice (e.g. [16]). Once a choice is made, feedback about whether the choice was correct or incorrect is provided. Within the gambling task, set probabilities for losses and gains are computed into task parameters [16]. A schematic of a gambling task is shown in Fig. 1.

3.2 Time Estimation Tasks

Time estimation tasks are also used to study reward and share some elements in common with the gambling tasks described above [49, 50]. In a time estimation task, participants are required to estimate a time interval (e.g., 1 s) as accurately as possible via a button press. After participants have made their estimation, they are presented with feedback about their accuracy. Correct and incorrect trials are either randomized (e.g., chosen randomly by a computer) or based on participant performance such that the criterion becomes stricter with better performance and more relaxed with poorer performance (e.g. [49, 50]). A schematic of a time estimation task is shown in Fig. 2.

3.3 Delayed Discounting Tasks

Delayed discounting tasks are a third commonly used paradigm to measure reward. In a delayed discounting task, participants are presented with a hypothetical or real choice with two options (e.g., "would you prefer $100 right now or $1000 in a month?"), such that immediate rewards may be valued more strongly relative to future rewards (e.g. [51, 52]). Across paradigms, the magnitude of the reward for the two options varies, however, the design of the

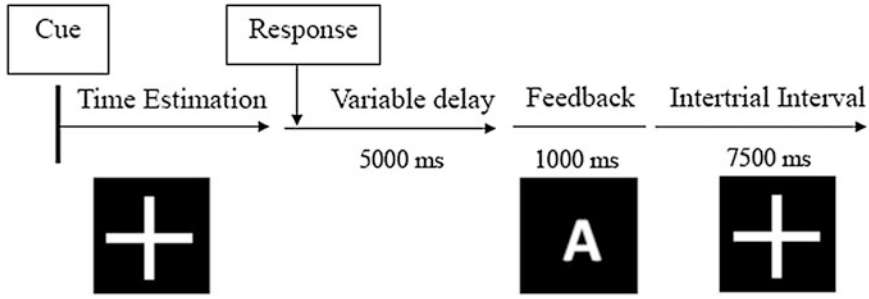

Fig. 2 Time estimation task. A schematic of a time estimation task. In this example, participants are asked to accurately estimate a time interval (Time Estimation). After the participant provides their estimation (Response), there is a variable delay (Variable Delay) prior to the presentation of feedback (Feedback)

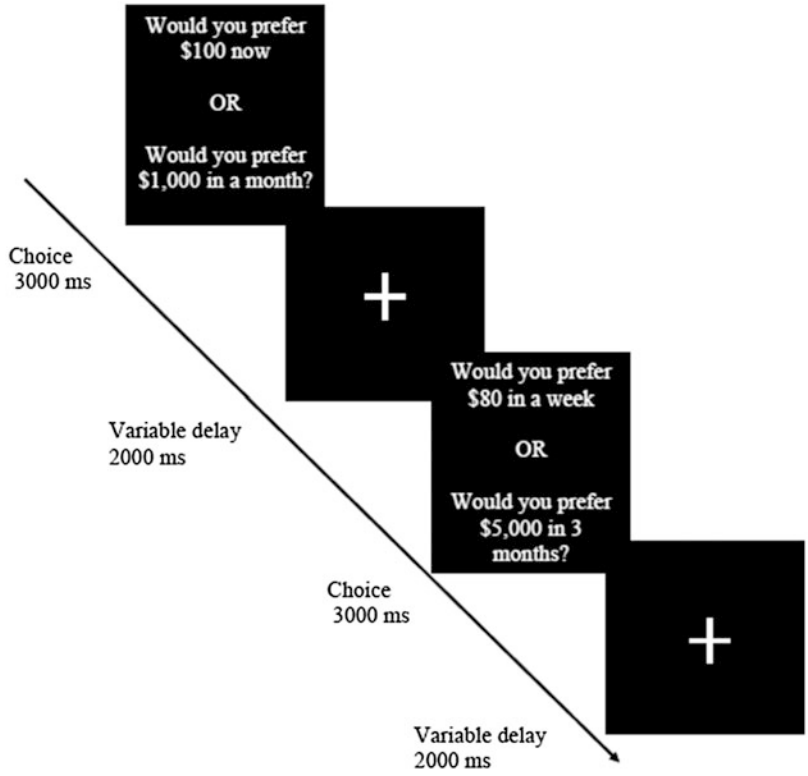

Fig. 3 Delayed discounting task. A schematic of a delayed discounting task. In this example, participants are asked to choose between a smaller reward obtained sooner or a larger reward received later. After participants make a choice, they are presented with a variable delay and then more choice trials

task remains the same. The delayed discounting task is commonly used to examine impulsive behavior, such as in individuals with attention-deficit hyperactivity disorder (ADHD) or substance dependency [53]. A schematic of a delayed discounting task is shown in Fig. 3.

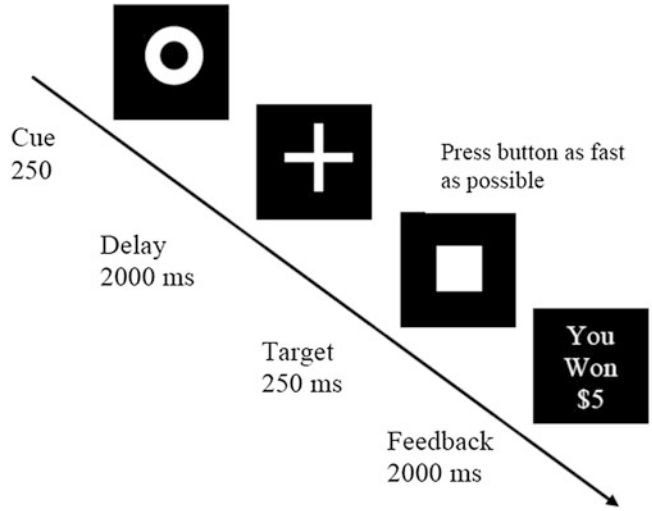

Fig. 4 Monetary incentive delay task. A schematic of a monetary incentive delay task. The circle (Cue) represents the trial type (either a small or large gain trial), followed by a delay. The participant then presses a button as fast as possible in response to a target and is provided with feedback

3.4 Monetary Incentive Delay Tasks

Another commonly used task is the monetary incentive delay (MID) paradigm. In MID paradigms, participants are presented with pretrial information about reward and posttrial information about valence. For example, participants are shown a visual cue which informs them about the reward on the current trial (e.g., an image of money if accurate performance on that trial would result in a monetary gain, or a blank image if accurate performance on a given trial will not result in any reward), wait for a variable amount of time, and then respond as quickly as possible via button press to a stimulus. Participants are subsequently shown feedback to indicate whether they won or lost based on response time. The MID can be used to evaluate both reward anticipation and processing (e.g. [54]). A schematic of a MID task is shown in Fig. 4.

4 Reward Processing and Anticipation in Neurotypical Adults

In the past decade, many studies have used electrophysiology to examine reward anticipation and processing in neurotypical adults. The following sections highlight and briefly review selected studies that have utilized the FRN/RewP, P300, and/or SPN components. A combination of the described ERP components is often examined together or independently across studies.

4.1 FRN/RewP

The extant literature indicates that the FRN is sensitive to reward prediction errors. Specifically, a more robust FRN is elicited for negative feedback (e.g., feedback indicating a "loss"), than for

positive feedback, such as a monetary gain [55, 56]. In addition, the magnitude of the FRN may be modulated by reward probability [57]. For example, Cohen et al. [57] observed that FRN magnitude was modulated by the probability of reward versus loss—but only in "win" trials [57]. That is, the FRN was significantly larger in "win" trials during which the probability of winning was low (e.g., 25% or 50%) compared to "win" trials in which the probability was higher (e.g., 75%). Interestingly, FRN magnitude was not modulated by probability during "loss" trials [57]. Similarly, Yaple and colleagues [58] used a risky decision-making task in which participants made a choice between risky or safe decisions in a blocked design containing *gain* and *loss* blocks [58]. In gain blocks, safe decisions resulted in a 100% probability of a small reward, and risky decisions resulted in a 50% chance of receiving a large reward (and 50% chance of receiving nothing). In loss blocks, safe decisions resulted in a 100% chance of a small loss, and risky decisions resulted in a 50% of a large loss (and 50% chance of losing nothing). The authors observed larger magnitude FRN amplitudes during the *gain* blocks in response to no-win trials (e.g., when participants won nothing) compared to both win trials during the gain blocks and trials during the loss blocks [57]. These findings were consistent with those from Cohen et al. [57], as no significant differences were found between trial types during the *loss* blocks [57].

Meadows and colleagues [59] used a MID task to examine the effects of valence and reward magnitude on both FRN and RewP components [59]. Participants were instructed that faster reaction times increased the likelihood of both earning a monetary reward and earning larger sums of money. That is, participants with faster reaction times were both more likely to win money *and* more likely to win a larger sum of money compared to participants with slower reaction times. In contrast with the commonly-used method of subtracting average brain activity for "win" trials from "loss" trials to calculate the FRN, and the converse (e.g., subtracting brain activity from "loss" trials from "win" trials to calculate the RewP), the authors used brain activity from "win" trials to calculate the RewP and brain activity from "loss" trials to calculate the FRN. This allowed for a direct investigation of whether the RewP and/or FRN were sensitive to reward magnitude. Results indicated that reward magnitude had a significant effect on the RewP, but not on the FRN, such that a larger RewP was associated with larger reward magnitudes relative to smaller rewards [57]. Overall, findings from the FRN and RewP suggest that this component is sensitive to feedback valance, although it is still debatable whether this component is driven by increased negative deflection in response to loss (e.g., FRN) or whether it is characterized by a positive deflection in response to gain, which is absent in response to loss (e.g., RewP).

4.2 P300

Several studies have simultaneously investigated FRN and P300 components to explore each component's sensitivity to reward magnitude, reward probability, and feedback valance [22, 36, 60, 61]. The question of whether the P300 is sensitive to valence has mixed support in the literature [37]. Wu and Zhou [36] measured both the FRN and P300 components and their sensitivity to valence, magnitude, and probability using a cued gambling task [36]. Results suggest that the P300 is modulated by both reward/loss magnitude and feedback valence, as the P300 was enhanced for large versus small feedback magnitude and was larger for positive versus negative outcomes. Interestingly, P300 modulation in response to large versus small magnitude feedback was only observed when feedback was expected. This modulation was not observed for unexpected feedback. Similarly, the effect of valence (e.g., larger P300 amplitude for positive vs. negative feedback) was enhanced in the expected compared to the unexpected condition. Increased FRN amplitudes were found to be modulated by feedback valence such that losing money elicited a more negative deflection relative to gaining money. FRN amplitude was also modulated by expectation (with larger FRNs being observed when feedback was unexpected compared to when it was expected) and magnitude such that the FRN was larger when the reward magnitude was small compared to when it was large [36].

Pfabigan et al. [61] investigated the sensitivity of FRN and P300 amplitudes to feedback valence and expectancy using a probabilistic gambling task [61]. Findings indicated that the FRN was modulated by both expectancy and feedback valence. Increased FRN amplitudes were observed for negative valence feedback when compared to positive valence, and the FRN was larger after unexpected compared to expected feedback. The P300 was not modulated by feedback valence but was larger for unexpected versus expected feedback [61]. Taken together, the above studies suggest that the P300 is modulated by feedback expectancy and reward/loss magnitude but may not be sensitive to feedback valance.

4.3 SPN

It has been well-documented that the SPN component is sensitive to whether task feedback is meaningful [46, 47]. That is, the SPN is larger when anticipating feedback that is designated as highly informative [45, 46, 62]. For example, Masaki, Tamazaki, and Hackley [46] used a gambling task in which there were choice and no-choice trials. For choice trials, participants gained money for correct choices [46]. In the no-choice trials, participants were told that feedback would be random and not tied to their responses. The SPN amplitude was larger in the choice versus the no-choice condition, suggesting that the SPN amplitude is sensitive to whether or not participants are anticipating meaningful feedback [46]. Similarly, Mühlberger et al. [45] observed a larger SPN amplitude in a

condition in which participants perceived themselves as having high levels of control over whether rewards were received relative to a condition in which participants perceived themselves as having less control over reward outcomes [45].

SPN amplitude appears to be modulated by reward magnitude but not by contextual valence [63]. Zheng et al. [63] investigated the effects of both contextual valence and reward magnitude on the SPN using a two-choice gambling task with a sample of 37 undergraduate students [63]. Participants completed the gambling task during two different contexts: a gain condition during which they attempted to maximize gains and a loss context where they tried to minimize losses. In both the gain and loss contexts, the magnitude of gains and losses varied between trials. Results suggest that the SPN was not sensitive to context (e.g., no difference in SPN amplitude was observed for loss vs. gain contexts). However, the SPN was sensitive to feedback magnitude and was larger when participants were faced with either losing or winning more money compared to losing or winning less money [63]. Overall, the SPN appears sensitive to both upcoming reward magnitude and whether participants perceive high versus low levels of control over task outcomes. However, in contrast to the FRN/RewP and P300, the SPN does not appear to be modulated by contextual valence.

5 Reward Processing and Anticipation in Psychiatric Populations

Altered reward processing is a hallmark feature of several psychiatric disorders. Differences in the reward system have been implicated in major depressive disorder (MDD) [64–66] and addiction [60, 67, 68]. The following sections briefly review the literature on reward in individuals with psychiatric diagnoses.

5.1 Depression and Reward

Previous studies suggest that ERP components involved in reward anticipation and processing may serve as potential biomarkers for depression [26, 69, 70]. Notably, reduced RewP amplitude is associated with depression in adults [26, 65] and may predict the onset of depression symptoms [30]. In addition, when individuals with depression or those who have increased syndromes of depression participate in tasks which require them to make a rewarding choice (e.g., a gambling task), they exhibit slower response times, are more conservative when making choices, and lack flexibility for switching between rewards [26, 65, 70].

Foti and Hajcak [65] examined the association between depressive symptoms and both the FRN and P300 using a gambling task in a sample of 85 undergraduate students [65]. Results indicated that reduced FRN was associated with higher levels of depression. The FRN appears to be specifically associated with depressive symptoms, as FRN amplitude was inversely correlated with depression

and stress but not related to anxiety symptoms. Monetary losses elicited a larger P300 compared to gains, and significant negative correlations were found between P300 amplitude on reward trials and scores on measures of both depression and anxiety [65]. Similarly, Santesso et al. [71] examined the role of negative affect on performance monitoring in 30 neurotypical adults using a delay discounting task [71]. Participants reported on symptoms of depression and both positive and negative affect using the *Positive and Negative Affect Schedule* (PANAS) [72]. Increased negative emotionality on the PANAS was associated with increased FRN amplitude in the loss condition [71]. Taken together, the above findings provide evidence for the utility of the FRN and P300 as potential markers for symptoms of depression in neurotypical populations.

Although findings on neurotypical populations with high scores on measures of depression provide insight about reward and related ERPs, in populations with clinical depression alterations in reward sensitivity are more pronounced [73]. Experiencing anhedonia (e.g., a loss of pleasure in previously enjoyed activities), may be associated with reward-processing difficulties which in turn increase the risk of depression [74–76]. Specifically, research suggests that reduced sensitivity to rewards is associated with depression (see [77] for a review). Moreover, brain regions responsible for reward processing show reduced functioning and blunted ERP components among populations with depression [65, 78–81]. Liu et al. [81] used a gambling task in a sample of 27 participants with and 27 without depression [81]. Results showed that participants with depression exhibited a blunted FRN relative to control participants. When separating losses and gains, participants with depression had smaller FRN amplitudes in response to gains compared to control participants. In control participants, symptoms of anhedonia were negatively associated with FRN amplitude.

Overall, the reward system appears to play a critical role in both depressive symptoms and the neurophysiology of individuals with clinical depression. In particular, reduced reward-related brain activity is reduced among individuals with depression and is associated with anhedonia (e.g., loss of pleasure), which is a core symptom of major depressive disorder [82].

5.2 Addiction and Reward

Addiction manifests itself when an individual compulsively uses a substance or engages in a harmful activity despite the substance or activity causing harm [82]. Individuals with addiction disorders show differences in both reward anticipation and processing compared to controls (e.g. [67, 68, 83]). Hewig et al. (2009) used an online version of Blackjack with participants with and without gambling problems [83]. Participants were instructed to try to get as close as possible to a score of 21 without going over. At a score of 16, participants chose whether they wanted another card

(i.e., a high-risk decision) or to not take another card (i.e., a low-risk decision). Participants with gambling problems were both more likely to make risky decisions and evidenced neural hypersensitivity to risky decisions which did not result in a loss. In particular, individuals with gambling problems evidenced larger P300 amplitudes during trials in which they made risky decisions and did not lose (e.g., when they took another card at a score of 16 and it did not result in a "bust") versus controls, but did not evidence brain activity differences in response to risky decisions which resulted in a loss (e.g., when taking another card at a score of 16 resulted in a "bust") [83]. This pattern of hypersensitivity to unexpected rewards after risk-taking behavior has direct implications for neural circuitry that may underlie both high-risk behavior itself and the "rush" of positive feelings which occur for problem gamblers when they win.

Kamarajan et al. [67] measured the P300 during a gambling task in a sample of participants with and without alcoholism [67]. The authors found a smaller P300 amplitude for all conditions in those with alcoholism relative to the control group, indicating neural hyposensitivity to rewards in this population [67]. Parvaz and colleagues [68], measured both the FRN and P300 in controls compared to those with cocaine use disorder (CUD) who were current users (e.g., tested positive for cocaine within the previous 72 h; CUD+) and those who used cocaine less frequently (e.g., did not test positive within the previous 72 h; CUD−) [68]. Findings indicated that the CUD group overall evidenced reduced FRN amplitudes in response to loss compared to the control group. Interestingly, individuals in the CUD− group evidenced reduced sensitivity to positive reward valence (e.g., "wins") compared to both the CUD+ group and controls. No differences in P300 amplitude were observed between groups [68]. This finding has important implications for the cycle of reward hyposensitivity that may drive individuals with drug addiction to continue using the drug, and for the increased pleasure and reward response that individuals experience after using the drug.

5.3 Other Psychiatric Disorders and Reward

In line with findings related to both depression and addiction, other disorders such as ADHD (see [84] for a review), schizophrenia [85, 86], bipolar disorder [86], and autism spectrum disorder (ASD) show evidence of differences in reward-related brain activity. The following sections provide a brief overview of relevant studies examining reward and related ERPs for ADHD, schizophrenia, bipolar disorders, and autism spectrum disorder (ASD). For the sake of brevity, only these disorders were described given the vast literature on reward and psychiatric conditions.

Due to the symptoms of increased risk-taking behavior, impulsivity, and hyperactivity in ADHD, studies have measured reward-related brain activity in this population. Neuroscience studies

provide evidence that children with ADHD evidence a blunted FRN to both negative and positive feedback when compared to control participants [87], though the literature is mixed (e.g [88]. observed *hyper*responsivity to social rewards and *hypo*sensitivity to monetary rewards in individuals with ADHD compared to neurotypical controls using fMRI). In adults with ADHD, there is evidence of reduced sensitivity to feedback valance—but intact sensitivity to reward magnitude—compared to controls [89]. In addition, reduced P300 amplitudes have been observed in adults and children with ADHD [87, 89]. Taken together, findings related to ADHD and reward sensitivity appear to vary based on both age and specific reward task. Longitudinal research in this population using a variety of reward tasks would further clarify age and task-related differences in reward sensitivity in those with ADHD compared to their neurotypical peers.

Reward-related differences have also been observed in individuals with schizophrenia. In particular, there is evidence for decreased reward sensitivity in this population, for example [85, 86, 90], though the literature is mixed (e.g. [91]). Individuals with schizophrenia who exhibit negative symptoms (e.g., anhedonia, withdrawal) appear to have specific deficits in reward anticipation as measured by self-report (e.g. [92]). ERP studies support these behavioral findings. For example, Wynn et al. [93] measured the SPN component among a sample of individuals with and without schizophrenia [93]. Participants with schizophrenia evidenced reduced SPN amplitudes while anticipating forthcoming images compared to control participants. Consistent with previous behavioral research, patients with schizophrenia also reported feeling less anticipatory pleasure than individuals without schizophrenia [93]. Taken together, both behavioral and neuroscience research suggests hyposensitivity toward reward anticipation in this population.

In a two-choice gambling task, Ibanez et al. [89] measured the P300 and FRN (referred to as the feedback error-related negativity in the manuscript) in adults with bipolar disorder (BD), those with ADHD, and neurotypical controls [89]. Compared to neurotypical adults, individuals with BD evidenced reduced fERN/FRN modulation to feedback valance. That is, in neurotypical control adults, the fERN/FRN was modulated by feedback valence, whereas it was not for those with BD. Interestingly, for the P300, individuals with BD evidenced hypersensitivity to reward magnitude. Differences in P300 amplitude between large and small magnitude rewards were almost two times larger for those with BD compared to neurotypical controls [89]. These findings suggest both hypo and hypersensitivity to rewards in individuals with BD, which may have implications for the cyclical nature of the disorder (e.g., individuals with BD experience both depression and mania).

Finally, recent findings have observed alterations in the neural reward system in individuals with ASD (e.g. [88, 94–97]). particularly when it comes to social rewards [98]. It has been hypothesized that core social deficits in ASD may stem from aberrant sensitivity to social rewards (e.g [99]. for an overview). Kohls and colleagues [95] measured the P300 component in response to social versus monetary rewards using a modified go/no-go task in children and adolescents with and without ASD [95]. Results indicated that participants with ASD had smaller P300 amplitudes when anticipating social rewards relative to monetary rewards. Interestingly, in children with ASD, the P300 amplitude was not modulated based on whether rewards were present or absent. That is, unlike neurotypical controls, no differences were found in the P300 amplitude for the reward conditions relative to the non-reward condition in the ASD group—suggesting overall reward hyposensitivity in this population. Subsequently, Stavropoulos and Carver [98] measured the SPN and FRN components in children with and without ASD [98]. Compared to their neurotypical peers, children with ASD evidenced reduced SPN amplitudes when anticipating a social reward versus a non-social reward, and a mixed pattern of insensitivity to feedback. Though findings of what particular reward-related processes differ in children with and without ASD are mixed, findings provide evidence that the reward system is likely implicated in the underlying pathophysiology of ASD.

Results from the above studies highlight the role of the neural reward system in psychiatric disorder symptomatology. Information about reward sensitivity in those with psychiatric diagnoses informs our understanding of neural mechanisms underlying disorders as well as providing useful treatment targets. Importantly, neuroscience can serve as an objective outcome measure of intervention, which allows researchers to explore whether behavioral and/or medical interventions alter neural circuitry.

6 Conclusions

This chapter highlights recent ERP research on reward anticipation and processing. EEG studies have identified specific ERP components, including the FRN/RewP and P300 that are elicited during reward processing, and the SPN which is elicited during reward anticipation. Specifically, the FRN/RewP is a negative/positive deflection that is sensitive to both feedback valence, reward magnitude, and reward probability. The P300, which is a positive deflection, is sensitive to whether or not feedback is present, but does not appear to be modulated by reward magnitude or probability. The SPN is a slow negative deflection which is sensitive to reward probability, magnitude, and the subjects' perceived control over task outcomes. Along with reviewing relevant ERP components

for reward anticipation and processing, paradigms used to test reward anticipation and processing were reviewed. These paradigms include gambling tasks, delayed discounting tasks, time estimation tasks, and monetary incentive tasks. Using these well-known and validated tasks allow research to further explore reward sensitivity among both neurotypical and psychiatric populations.

Building our understanding of the specific ERP components elicited for reward anticipation and processing in neurotypical populations can clarify the clinical relevance of alterations observed in both individuals with subclinical symptoms of psychiatric disorders and those with clinical diagnoses. Given the importance of reward anticipation and processing for learning, motivation, and adapting behaviors to increase positive outcomes, understanding when, how, and why alterations in the reward system occur in psychiatric populations is critical for informing therapeutic efforts.

References

1. Gottfried JA, O'Doherty J, Dolan RJ (2003) Encoding predictive reward value in human amygdala and orbitofrontal cortex. Science 301:1104–1107. https://doi.org/10.1126/science.1087919
2. Schultz W, Dayan P, Montague PR (1997) A neural substrate of prediction and reward. Science 275:1593–1599. https://doi.org/10.1126/science.275.5306.1593
3. McClure SM, York MK, Montague PR (2004) The neural substrates of reward processing in humans: the modern role of FMRI. Neuroscientist 10:260–268. https://doi.org/10.1177/1073858404263526
4. Barto AG, Sutton RS (1997) Reinforcement learning in artificial intelligence. In: Donahoe JW, Packard Dorsel V (eds) Advances in psychology. North-Holland, pp 358–386
5. Bromberg-Martin ES, Matsumoto M, Hikosaka O (2010) Dopamine in motivational control: rewarding, aversive, and alerting. Neuron 68:815–834. https://doi.org/10.1016/j.neuron.2010.11.022
6. Kahnt T, Park SQ, Haynes J-D, Tobler PN (2014) Disentangling neural representations of value and salience in the human brain. PNAS 111:5000–5005. https://doi.org/10.1073/pnas.1320189111
7. Schultz W (2002) Getting formal with dopamine and reward. Neuron 36:241–263. https://doi.org/10.1016/S0896-6273(02)00967-4
8. Schultz W (2004) Neural coding of basic reward terms of animal learning theory, game theory, microeconomics and behavioural ecology. Curr Opin Neurobiol 14:139–147. https://doi.org/10.1016/j.conb.2004.03.017
9. Haber SN, Knutson B (2010) The reward circuit: linking primate anatomy and human imaging. Neuropsychopharmacology 35:4–26. https://doi.org/10.1038/npp.2009.129
10. Lesage E, Stein EA (2016) Networks associated with reward. In: Pfaff DW, Volkow ND (eds) Neuroscience in the 21st century. Springer, New York, NY, pp 1–27
11. Burle B, Spieser L, Roger C, Casini L, Hasbroucq T, Vidal F (2015) Spatial and temporal resolutions of EEG: is it really black and white? A scalp current density view. Int J Psychophysiol 97:210–220. https://doi.org/10.1016/j.ijpsycho.2015.05.004
12. Coles MGH, Rugg MD (1995) Event-related brain potentials: an introduction. In: Electrophysiology of mind: event-related brain potentials and cognition. Oxford University Press, New York, NY, pp 1–26
13. Coles MGH, Gratton G, Fabiani M (1990) Event-related brain potentials. In: Principles of psychophysiology: Physical, social, and inferential elements. Cambridge University Press, New York, NY, pp 413–455
14. Regan D (1989) Human brain electrophysiology. Evoked potentials and evoked magnetic fields in science and medicine
15. Miltner WH, Braun CH, Coles MG (1997) Event-related brain potentials following incorrect feedback in a time-estimation task: evidence for a "generic" neural system for error

detection. J Cogn Neurosci 9:788–798. https://doi.org/10.1162/jocn.1997.9.6.788

16. Gehring WJ, Willoughby AR (2002) The medial frontal cortex and the rapid processing of monetary gains and losses. Science 295:2279–2282. https://doi.org/10.1126/science.1066893
17. Falkenstein M, Hohnsbein J, Hoormann J, Blanke L (1991) Effects of crossmodal divided attention on late ERP components. II. Error processing in choice reaction tasks. Electroencephalogr Clin Neurophysiol 78:447–455. https://doi.org/10.1016/0013-4694(91)90062-9
18. Gehring WJ, Goss B, Coles MGH, Meyer DE, Donchin E (1993) A neural system for error detection and compensation. Psychol Sci 4:385–390. https://doi.org/10.1111/j.1467-9280.1993.tb00586.x
19. Holroyd CB, Coles MGH (2002) The neural basis of human error processing: reinforcement learning, dopamine, and the error-related negativity. Psychol Rev 109:679–709. https://doi.org/10.1037/0033-295X.109.4.679
20. Luu P, Tucker DM, Derryberry D, Reed M, Poulsen C (2003) Electrophysiological responses to errors and feedback in the process of action regulation. Psychol Sci 14:47–53. https://doi.org/10.1111/1467-9280.01417
21. Yu R, Zhou W, Zhou X (2011) Rapid processing of both reward probability and reward uncertainty in the human anterior cingulate cortex. PLoS One 6:e29633. https://doi.org/10.1371/journal.pone.0029633
22. Bellebaum C, Polezzi D, Daum I (2010) It is less than you expected: the feedback-related negativity reflects violations of reward magnitude expectations. Neuropsychologia 48:3343–3350. https://doi.org/10.1016/j.neuropsychologia.2010.07.023
23. Holroyd CB, Larsen JT, Cohen JD (2004) Context dependence of the event-related brain potential associated with reward and punishment. Psychophysiology 41:245–253. https://doi.org/10.1111/j.1469-8986.2004.00152.x
24. Hajcak G, Simons RF (2002) Error-related brain activity in obsessive-compulsive undergraduates. Psychiatry Res 110:63–72. https://doi.org/10.1016/s0165-1781(02)00034-3
25. Hajcak G, Moser JS, Holroyd CB, Simons RF (2006) The feedback-related negativity reflects the binary evaluation of good versus bad outcomes. Biol Psychol 71:148–154. https://doi.org/10.1016/j.biopsycho.2005.04.001
26. Proudfit GH (2015) The reward positivity: From basic research on reward to a biomarker for depression. Psychophysiology 52:449–459. https://doi.org/10.1111/psyp.12370
27. Carlson JM, Foti D, Mujica-Parodi LR, Harmon-Jones E, Hajcak G (2011) Ventral striatal and medial prefrontal BOLD activation is correlated with reward-related electrocortical activity: a combined ERP and fMRI study. NeuroImage 57:1608–1616. https://doi.org/10.1016/j.neuroimage.2011.05.037
28. Kujawa A, Smith E, Luhmann C, Hajcak G (2013) The feedback negativity reflects favorable compared to nonfavorable outcomes based on global, not local, alternatives. Psychophysiology 50:134–138. https://doi.org/10.1111/psyp.12002
29. Holroyd CB, Pakzad-Vaezi KL, Krigolson OE (2008) The feedback correct-related positivity: sensitivity of the event-related brain potential to unexpected positive feedback. Psychophysiology 45:688–697. https://doi.org/10.1111/j.1469-8986.2008.00668.x
30. Bress JN, Smith E, Foti D, Klein DN, Hajcak G (2012) Neural response to reward and depressive symptoms in late childhood to early adolescence. Biol Psychol 89:156–162. https://doi.org/10.1016/j.biopsycho.2011.10.004
31. Foti D, Weinberg A, Dien J, Hajcak G (2011) Event-related potential activity in the basal ganglia differentiates rewards from nonrewards: temporospatial principal components analysis and source localization of the feedback negativity. Hum Brain Mapp 32:2207–2216. https://doi.org/10.1002/hbm.21182
32. Sutton S, Tueting P, Hammer M, Hakerem G (1978) Evoked potentials and feedback. In: Otto DA (ed) Multidisciplinary perspectives in event-related brain potential research. Government Printing Office, Washington, DC, pp 184–188
33. Johnston VS (1979) Stimuli with biological significance. In: Begleiter H (ed) Evoked brain potentials and behavior. Springer, Boston, MA, pp 1–12
34. Hajcak G, Moser JS, Yeung N, Simons RF (2005) On the ERN and the significance of errors. Psychophysiology 42:151–160. https://doi.org/10.1111/j.1469-8986.2005.00270.x
35. Leng Y, Zhou X (2010) Modulation of the brain activity in outcome evaluation by interpersonal relationship: an ERP study. Neuropsychologia 48:448–455. https://doi.org/10.1016/j.neuropsychologia.2009.10.002
36. Wu Y, Zhou X (2009) The P300 and reward valence, magnitude, and expectancy in outcome evaluation. Brain Res 1286:114–122.

https://doi.org/10.1016/j.brainres.2009.06.032

37. Yeung N, Sanfey AG (2004) Independent coding of reward magnitude and valence in the human brain. J Neurosci 24:6258–6264. https://doi.org/10.1523/JNEUROSCI.4537-03.2004
38. Zhou Z, Yu R, Zhou X (2010) To do or not to do? Action enlarges the FRN and P300 effects in outcome evaluation. Neuropsychologia 48:3606–3613. https://doi.org/10.1016/j.neuropsychologia.2010.08.010
39. Krebs RM, Boehler CN, Appelbaum LG, Woldorff MG (2013) Reward associations reduce behavioral interference by changing the temporal dynamics of conflict processing. PLoS One 8:e53894. https://doi.org/10.1371/journal.pone.0053894
40. Brunia CHM (1988) Movement and stimulus preceding negativity. Biol Psychol 26:165–178. https://doi.org/10.1016/0301-0511(88)90018-X
41. Brunia CH, Damen EJ (1988) Distribution of slow brain potentials related to motor preparation and stimulus anticipation in a time estimation task. Electroencephalogr Clin Neurophysiol 69:234–243. https://doi.org/10.1016/0013-4694(88)90132-0
42. Brunia CHM, Hackley SA, van Boxtel GJM, Kotani Y, Ohgami Y (2011) Waiting to perceive: reward or punishment? Clin Neurophysiol 122:858–868. https://doi.org/10.1016/j.clinph.2010.12.039
43. Catena A, Perales JC, Megías A, Cándido A, Jara E, Maldonado A (2012) The brain network of expectancy and uncertainty processing. PLoS One 7. https://doi.org/10.1371/journal.pone.0040252
44. Fuentemilla L, Cucurell D, Marco-Pallarés J, Guitart-Masip M, Morís J, Rodríguez-Fornells A (2013) Electrophysiological correlates of anticipating improbable but desired events. NeuroImage 78:135–144. https://doi.org/10.1016/j.neuroimage.2013.03.062
45. Mühlberger C, Angus DJ, Jonas E, Harmon-Jones C, Harmon-Jones E (2017) Perceived control increases the reward positivity and stimulus preceding negativity. Psychophysiology 54:310–322. https://doi.org/10.1111/psyp.12786
46. Masaki H, Yamazaki K, Hackley SA (2010) Stimulus-preceding negativity is modulated by action-outcome contingency. Neuroreport 21:277–281. https://doi.org/10.1097/WNR.0b013e3283360bc3
47. Kotani Y, Kishida S, Hiraku S, Suda K, Ishii M, Aihara Y (2003) Effects of information and reward on stimulus-preceding negativity prior to feedback stimuli. Psychophysiology 40:818–826. https://doi.org/10.1111/1469-8986.00082
48. Kotani Y, Ohgami Y, Yoshida N, Kiryu S, Inoue Y (2017) Anticipation process of the human brain measured by stimulus-preceding negativity (SPN). JPFSM 6:7–14. https://doi.org/10.7600/jpfsm.6.7
49. Becker MPI, Nitsch AM, Miltner WHR, Straube T (2014) A single-trial estimation of the feedback-related negativity and its relation to BOLD responses in a time-estimation task. J Neurosci 34:3005–3012. https://doi.org/10.1523/JNEUROSCI.3684-13.2014
50. Holroyd CB, Krigolson OE (2007) Reward prediction error signals associated with a modified time estimation task. Psychophysiology 44:913–917. https://doi.org/10.1111/j.1469-8986.2007.00561.x
51. Hyten C, Madden GJ, Field DP (1994) Exchange delays and impulsive choice in adult humans. J Exp Anal Behav 62:225–233. https://doi.org/10.1901/jeab.1994.62-225
52. Lane SD, Cherek DR, Rhodes HM, Pietras CJ, Tcheremissine OV (2003) Relationships among laboratory and psychometric measures of impulsivity: implications in substance abuse and dependence. Addict Disord Treat 2:33–40. https://doi.org/10.1097/00132576-200302020-00001
53. Madden GJ, Petry NM, Badger GJ, Bickel WK (1997) Impulsive and self-control choices in opioid-dependent patients and non-drug-using control patients: drug and monetary rewards. Exp Clin Psychopharmacol 5:256–262. https://doi.org/10.1037/1064-1297.5.3.256
54. Knutson B, Fong GW, Adams CM, Varner JL, Hommer D (2001) Dissociation of reward anticipation and outcome with event-related fMRI. Neuroreport 12:3683–3687. https://doi.org/10.1097/00001756-200112040-00016
55. Hajcak G, Moser JS, Holroyd CB, Simons RF (2007) It's worse than you thought: the feedback negativity and violations of reward prediction in gambling tasks. Psychophysiology 44:905–912. https://doi.org/10.1111/j.1469-8986.2007.00567.x
56. Hajihosseini A, Holroyd CB (2013) Frontal midline theta and N200 amplitude reflect complementary information about expectancy and outcome evaluation. Psychophysiology 50:550–562. https://doi.org/10.1111/psyp.12040

57. Cohen MX, Elger CE, Ranganath C (2007) Reward expectation modulates feedback-related negativity and EEG spectra. NeuroImage 35:968–978. https://doi.org/10.1016/j.neuroimage.2006.11.056
58. Yaple Z, Shestakova A, Klucharev V (2018) Feedback-related negativity reflects omission of monetary gains: evidence from ERP gambling study. Neurosci Lett 686:145–149. https://doi.org/10.1016/j.neulet.2018.09.007
59. Meadows CC, Gable PA, Lohse KR, Miller MW (2016) The effects of reward magnitude on reward processing: an averaged and single trial event-related potential study. Biol Psychol 118:154–160. https://doi.org/10.1016/j.biopsycho.2016.06.002
60. Kreussel L, Hewig J, Kretschmer N, Hecht H, Coles MGH, Miltner WHR (2012) The influence of the magnitude, probability, and valence of potential wins and losses on the amplitude of the feedback negativity. Psychophysiology 49:207–219. https://doi.org/10.1111/j.1469-8986.2011.01291.x
61. Pfabigan DM, Alexopoulos J, Bauer H, Sailer U (2011) Manipulation of feedback expectancy and valence induces negative and positive reward prediction error signals manifest in event-related brain potentials. Psychophysiology 48:656–664. https://doi.org/10.1111/j.1469-8986.2010.01136.x
62. Zheng L, Grove R, Eapen V (2019) Spectrum or subtypes? A latent profile analysis of restricted and repetitive behaviours in autism. Res Autism Spectr Disord 57:46–54. https://doi.org/10.1016/j.rasd.2018.10.003
63. Zheng Y, Li Q, Zhang Y, Li Q, Shen H, Gao Q, Zhou S (2017) Reward processing in gain versus loss context: an ERP study. Psychophysiology 54:1040–1053. https://doi.org/10.1111/psyp.12855
64. Baskin-Sommers AR, Foti D (2015) Abnormal reward functioning across substance use disorders and major depressive disorder: considering reward as a transdiagnostic mechanism. Int J Psychophysiol 98:227–239. https://doi.org/10.1016/j.ijpsycho.2015.01.011
65. Foti D, Hajcak G (2009) Depression and reduced sensitivity to non-rewards versus rewards: Evidence from event-related potentials. Biol Psychol 81:1–8. https://doi.org/10.1016/j.biopsycho.2008.12.004
66. Proudfit GH, Bress JN, Foti D, Kujawa A, Klein DN (2015) Depression and event-related potentials: Emotional disengagement and reward insensitivity. Curr Opin Psychol 4:110–113. https://doi.org/10.1016/j.copsyc.2014.12.018
67. Kamarajan C, Rangaswamy M, Tang Y, Chorlian DB, Pandey AK, Roopesh BN, Manz N, Saunders R, Stimus AT, Porjesz B (2010) Dysfunctional reward processing in male alcoholics: an ERP study during a gambling task. J Psychiatr Res 44:576–590. https://doi.org/10.1016/j.jpsychires.2009.11.019
68. Parvaz MA, Konova AB, Proudfit GH, Dunning JP, Malaker P, Moeller SJ, Maloney T, Alia-Klein N, Goldstein RZ (2015) Impaired neural response to negative prediction errors in cocaine addiction. J Neurosci 35:1872–1879. https://doi.org/10.1523/JNEUROSCI.2777-14.2015
69. Nelson BD, Shankman SA, Proudfit GH (2014) Intolerance of uncertainty mediates reduced reward anticipation in major depressive disorder. J Affect Disord 158:108–113. https://doi.org/10.1016/j.jad.2014.02.014
70. Shankman SA, Klein DN, Tenke CE, Bruder GE (2007) Reward sensitivity in depression: a biobehavioral study. J Abnorm Psychol 116:95–104. https://doi.org/10.1037/0021-843X.116.1.95
71. Santesso DL, Bogdan R, Birk JL, Goetz EL, Holmes AJ, Pizzagalli DA (2012) Neural responses to negative feedback are related to negative emotionality in healthy adults. Soc Cogn Affect Neurosci 7:794–803. https://doi.org/10.1093/scan/nsr054
72. Watson D, Clark LA, Tellegen A (1988) Development and validation of brief measures of positive and negative affect: the PANAS scales. J Pers Soc Psychol 54:1063–1070. https://doi.org/10.1037/0022-3514.54.6.1063
73. Treadway MT, Zald DH (2013) Parsing anhedonia: translational models of reward-processing deficits in psychopathology. Curr Dir Psychol Sci 22:244–249. https://doi.org/10.1177/0963721412474460
74. Eshel N, Roiser JP (2010) Reward and punishment processing in depression. Biol Psychiatry 68:118–124. https://doi.org/10.1016/j.biopsych.2010.01.027
75. Nestler EJ, Carlezon WA (2006) The mesolimbic dopamine reward circuit in depression. Biol Psychiatry 59:1151–1159. https://doi.org/10.1016/j.biopsych.2005.09.018
76. Der-Avakian A, Markou A (2012) The neurobiology of anhedonia and other reward-related deficits. Trends Neurosci 35:68–77. https://doi.org/10.1016/j.tins.2011.11.005
77. Fitzgerald PB, Laird AR, Maller J, Daskalakis ZJ (2008) A meta-analytic study of changes in brain activation in depression. Hum Brain Mapp 29:683–695. https://doi.org/10.1002/hbm.20426

78. Forbes EE (2009) Where's the fun in that? Broadening the focus on reward function in depression. Biol Psychiatry 66:199–200. https://doi.org/10.1016/j.biopsych.2009.05.001
79. Pizzagalli DA, Holmes AJ, Dillon DG, Goetz EL, Birk JL, Bogdan R, Dougherty DD, Iosifescu DV, Rauch SL, Fava M (2009) Reduced caudate and nucleus accumbens response to rewards in unmedicated individuals with major depressive disorder. Am J Psychiatry 166:702–710. https://doi.org/10.1176/appi.ajp.2008.08081201
80. Steele JD, Kumar P, Ebmeier KP (2007) Blunted response to feedback information in depressive illness. Brain 130:2367–2374. https://doi.org/10.1093/brain/awm150
81. Liu W, Wang L, Shang H, Shen Y, Li Z, Cheung EFC, Chan RCK (2014) The influence of anhedonia on feedback negativity in major depressive disorder. Neuropsychologia 53:213–220. https://doi.org/10.1016/j.neuropsychologia.2013.11.023
82. American Psychiatric Association (2013) Diagnostic and statistical manual of mental disorders, 5th edn. American Psychiatric Publishing, Washington, D.C.
83. Hewig J, Kretschmer N, Trippe RH, Hecht H, Coles MGH, Holroyd CB, Miltner WHR (2010) Hypersensitivity to reward in problem gamblers. Biol Psychiatry 67:781–783. https://doi.org/10.1016/j.biopsych.2009.11.009
84. Luman M, Tripp G, Scheres A (2010) Identifying the neurobiology of altered reinforcement sensitivity in ADHD: a review and research agenda. Neurosci Biobehav Rev 34:744–754. https://doi.org/10.1016/j.neubiorev.2009.11.021
85. Vignapiano A, Mucci A, Ford J, Montefusco V, Plescia GM, Bucci P, Galderisi S (2016) Reward anticipation and trait anhedonia: An electrophysiological investigation in subjects with schizophrenia. Clin Neurophysiol 127:2149–2160. https://doi.org/10.1016/j.clinph.2016.01.006
86. Whitton AE, Treadway MT, Pizzagalli DA (2015) Reward processing dysfunction in major depression, bipolar disorder and schizophrenia. Curr Opini Psychiatry 28:7–12. https://doi.org/10.1097/YCO.0000000000000122
87. van Meel CS, Heslenfeld DJ, Oosterlaan J, Luman M, Sergeant JA (2011) ERPs associated with monitoring and evaluation of monetary reward and punishment in children with ADHD. J Child Psychol Psychiatry 52:942–953. https://doi.org/10.1111/j.1469-7610.2010.02352.x
88. Kohls G, Thönessen H, Bartley GK, Grossheinrich N, Fink GR, Herpertz-Dahlmann B, Konrad K (2014) Differentiating neural reward responsiveness in autism versus ADHD. Dev Cogn Neurosci 10:104–116. https://doi.org/10.1016/j.dcn.2014.08.003
89. Ibanez A, Cetkovich M, Petroni A, Urquina H, Baez S, Gonzalez-Gadea ML, Kamienkowski JE, Torralva T, Torrente F, Strejilevich S, Teitelbaum J, Hurtado E, Guex R, Melloni M, Lischinsky A, Sigman M, Manes F (2012) The neural basis of decision-making and reward processing in adults with euthymic bipolar disorder or attention-deficit/hyperactivity disorder (ADHD). PLoS One 7:e37306. https://doi.org/10.1371/journal.pone.0037306
90. Morris SE, Heerey EA, Gold JM, Holroyd CB (2008) Learning-related changes in brain activity following errors and performance feedback in schizophrenia. Schizophr Res 99:274–285. https://doi.org/10.1016/j.schres.2007.08.027
91. Horan WP, Foti D, Hajcak G, Wynn JK, Green MF (2012) Impaired neural response to internal but not external feedback in schizophrenia. Psychol Med 42:1637–1647. https://doi.org/10.1017/S0033291711002819
92. Gard DE, Kring AM, Gard MG, Horan WP, Green MF (2007) Anhedonia in schizophrenia: distinctions between anticipatory and consummatory pleasure. Schizophr Res 93:253–260. https://doi.org/10.1016/j.schres.2007.03.008
93. Wynn JK, Horan WP, Kring AM, Simons RF, Green MF (2010) Impaired anticipatory event-related potentials in schizophrenia. Int J Psychophysiol 77:141–149. https://doi.org/10.1016/j.ijpsycho.2010.05.009
94. Gonzalez-Gadea M, Sigman M, Rattazzi A et al (2016) Neural markers of social and monetary rewards in children with Attention-Deficit/Hyperactivity Disorder and Autism Spectrum Disorder. Sci Rep 6:30588. https://doi.org/10.1038/srep30588
95. Kohls G, Peltzer J, Schulte-Rüther M, Kamp-Becker I, Remschmidt H, Herpertz-Dahlmann B, Konrad K (2011) Atypical brain responses to reward cues in autism as revealed by event-related potentials. J Autism Dev Disord 41:1523–1533. https://doi.org/10.1007/s10803-011-1177-1
96. Schultz RT (2005) Developmental deficits in social perception in autism: the role of the amygdala and fusiform face area. Int J Dev

Neurosci 23:125–141. https://doi.org/10.1016/j.ijdevneu.2004.12.012

97. Schmitz N, Rubia K, van Amelsvoort T, Daly E, Smith A, Murphy DGM (2008) Neural correlates of reward in autism. Br J Psychiatry 192:19–24. https://doi.org/10.1192/bjp.bp.107.036921
98. Stavropoulos KKM, Carver LJ (2014) Reward anticipation and processing of social versus nonsocial stimuli in children with and without autism spectrum disorders. J Child Psychol Psychiatry 55:1398–1408. https://doi.org/10.1111/jcpp.12270
99. Dawson G, Webb SJ, McPartland J (2005) Understanding the nature of face processing impairment in autism: insights from behavioral and electrophysiological studies. Dev Neuropsychol 27:403–424. https://doi.org/10.1207/s15326942dn2703_6

Chapter 16

Fiber Photometry of Neural Activity in Specific Neural Circuit

Jinsong Yu, Yue Li, Mona N. Hussein, Zhongchao Wang, Jinxia Dai, and Gang Cao

Abstract

Fiber photometry is a powerful technique to monitor neural activity dynamics of a particular population of neurons in living animal brains for the functional study. With the help of retrograde viral-based tracing, a specific neural circuit can be labeled with genetically encoded calcium indicators (GECIs) to facilitate in vivo activity measurement based on calcium imaging via fiber photometry. Here, we provided a simple and feasible protocol for fiber photometry of virus labeled specific neural circuitry in mice. The detailed protocol included virus injection, optic fiber implantation, Ca^{2+} signal detection, histology, imaging, and data analysis. Furthermore, we applied this protocol to label paraventricular thalamus (PVT) projection neurons targeting to the paraventricular nucleus of the hypothalamus (PVN), to specifically monitor neural activity of PVT–PVN circuit. Finally, we discussed the key points of the protocol, which should be concerned during fiber photometry of a specific neural circuit. In summary, this protocol is highly efficient and feasible and may contribute to the functional study of neural circuits.

Key words Fiber photometry, Calcium imaging, Neural circuit, Retrograde tracing virus

1 Introduction

The mammalian brain is a highly complex neural network connected by a huge number of neurons [1, 2]. Resolving the function of certain neural circuits is pivotal for understating specific brain functions including sensation, movement, learning, and memory, and so on. For the functional study of the brain, in vivo calcium imaging has been extensively applied for neural activity measurement. Fiber photometry has increasingly become popular as a viable tool for in vivo calcium recording of certain neurons in living and behaving animals [3, 4]. It is the simple, low cost and sensitive approach for assessment of neuronal functions at in vivo level in freely moving mice [5–7]. With the aid of fiber photometry, the functions of specific neural circuits and brain regions have been explored including feeding circuits [5], basal ganglia [8], dopamine

Marc Fakhoury (ed.), *The Brain Reward System*, Neuromethods, vol. 165, https://doi.org/10.1007/978-1-0716-1146-3_16,

reward system [9], basal forebrain [10], as well as sensory and motor cortices [6, 11–15]. Calcium is considered as the most important intracellular indicator of neuronal activity as its concentration elevates during neuronal activity from 10 to 100 times higher than that at the resting stage (50–100 nM) [16]. Thus, calcium imaging is widely used to explore neural activity and function. Calcium imaging in the living brain has been greatly facilitated by genetically encoded calcium indicators (GECIs) [17]. New generations of GECIs, including GCaMP6 and jGCaMP7 family members, displaying similar ultra-sensitivity and kinetics to conventional dyes, are more suitable for neuronal activity detection at in vivo level with higher temporal resolution [18–20]. With the aid of viral tracers, GECIs can be genetically delivered to the specific neural circuit and monitor the neural activity at both cellular and subcellular (dendrites, spines, axonal boutons) resolution via in vivo calcium imaging of anesthetized and freely behaving mice [7].

For in vivo calcium imaging, several imaging techniques have been introduced. Two-photon microscopy is a useful method for long-term calcium imaging in the living brain with a high spatial resolution [21–23]. However, due to light scattering and aberrations originating from tissue, the penetration depth of two-photon imaging is usually limited to the upper cortical layer of mice [24]. Besides, calcium imaging with two-photon microscopy requests animal head been fixed. For calcium imaging of deeper brain neurons for long-term neural activity measurement in freely moving animals, miniscope implementation is promising but is accompanied by more tissue damage [25]. Recent investigations have improved the two-photon imaging to reach the deeper layers of the cerebral cortex with individual cell resolution not only in anesthetized mice but also in freely waking mice through the labeling with the red-shifted fluorescent calcium indicator Cal-590 and ultrashort laser pulses [26]. Moreover, two-photon calcium imaging with a novel light source based on a semiconductor laser has reached a more deeper brain region involving the hippocampus [27]. Yet, it is still impossible to reach deeper brain regions such as the hypothalamus. As a comparison, the fiber photometry is an ideal method for recording population neurons activities in the deep nucleus in freely moving animals with low cost [28].

There are several methods for fiber photometry, including single, dual, and multiple channel modes. Those methods would help record neural activities in different brain nucleus within the same mouse and different interacting mice [3]. Because a single stimulus may cause excitation to neurons existing in different brain areas, it is important to use dual and triple channel modes in fiber photometry [29, 30]. In addition, the multiple channels of fiber photometry are necessary for studying neurons function in

different brain areas in the same mice or different animals at the same time [3].

In this chapter, we will introduce a detailed protocol for fiber photometry of virus-labeled neural circuits in anesthetized mice, including virus injection, optic fiber implantation, Ca^{2+} signal detection, histology, imaging, and data analysis. This protocol was applied to detect in vivo calcium activity of projection neurons targeting the paraventricular nucleus of the hypothalamus (PVN) in the paraventricular thalamus (PVT), to specifically explore the neural activity of PVT–PVN circuit. We will also discuss the key points of the protocol during fiber photometry of certain neural circuits.

2 Materials

2.1 Reagents

Mice: Two-month-old male C57BL/6 mice were purchased from the experimental animal center of Huazhong agricultural university. All the experimental procedures in mice were following the Research Ethics Committee rules.

Sterile saline: 0.9% NaCl.

Anesthetics: Mixed anesthetics (7.5 g urethane (U2500-100 g, Sigma), 3 g chloral hydrate (Tianjin Damao Chemical Reagent Factory, China) and 75 mg xylazine (X1251-5 g, Sigma) in 100 mL ddH_2O); 1% Isoflurane (R510-22, RWD life science, China) in medical oxygen (Wuhan Shuanglonghe, China).

Dental cement kit (Super-Bond C&B of Sun Medica, Japan): The kit contains monomer, polymer (L-type Clear), catalyst V, spoon, and ceramic disc (Fig. 1a).

Virus: The rRV-ΔG-GCaMP6s-DsRed, of which the glycoprotein (G) was deleted to eliminate trans-synapse spreading ability, was prepared and stored at −80 °C. For microinjection, 10^9 infectious particles per mL of rRV-ΔG-GCaMP6s-DsRed were used. Viral amplification was performed in accordance with the Biosafety Guidelines of the Huazhong Agricultural University Administrative Biosafety Committee on Laboratory.

Mineral oil and Hot-melt adhesive

PBS and 4% paraformaldehyde (PFA) (#BL539A, biosharp, China).

2.2 Equipment

Injection syringe: 10 μL microinjection syringes (0.7 mm tip diameter) were purchased from Shanghai Gaoge industrial and trade, China (Fig. 1b). Borosilicate glass capillary with filament (O.D. 1.5 mm, I.D. 0.86 mm, #BF150-86-10) was from Sutter, USA (Fig. 1b).

Surgical tools: Vana's scissors (S11037-08, RWD life science, China), fine forceps (F1102-11, RWD life science, China), fiber stub holders (Convergence Technology, China), blade, sleeve

Fig. 1 Materials and Equipments for Surgical Operation during Virus Injection and Fiber Stubs Insertion. (**a**, **b**) Surgical tools and materials. A1, Fine forceps; A2, Surgical scissors; A3, vanas scissors; A4, blade for mouse hair shaving; A5, wrenches for holders; A6, fiber stubs for recording; A7, catalyst V for dental cement; A8, spoon for dental cement polymer; A9, ceramic disk for cement mixing; A10, the monomer for dental cement and L-type polymer; A11, monomer for dental cement; A12 fiber stubs holders; (**b**), Virus microinjection needle made by pulled glass capillary fused with 10 μL microsyringe by hot-melt adhesive. (**c**) Puller PC-10 for making Virus microinjection needle. (**d**) Instruments for Ca^{2+} signal recording. (**e**) Equipments for

(Convergence Technology, China), hexagon bar wrenches (Convergence Technology, China), thick fiber stubs (ø200 μm, NA.0.37 for Ca^{2+} signal detection, Convergence Technology, China) (Fig. 1a).

Animal surgical pad (#80098, RWD life science, China).

Stereomicroscope (#77001, RWD life science, China) (Fig. 1e).

Mouse/neonatal rat adaptor (#68030, RWD life science, China) (Fig. 1e).

Desktop digital stereotaxic instruments: (#68025, RWD life science, China) (Fig. 1e).

Temperature controller (#69001, RWD life science, China) (Fig. 1e).

High-speed dental drill and 0.5 mm diameter drill bits (#78001 and #78012, RWD life science, China) (Fig. 1e).

Puller PC-10 (DL Naturegene Life Sciences, USA) (Fig. 1c).

KDS Legato™130*micro* – *pump*(*KDScientific*, *USA*)(*Fig*.1*e*).

Fiber photometry: Fiber photometry recording was performed with a commercialized fiber photometry system (Thinker Tech Nanjing Biotech Limited Co.), and the data were exported as MATLAB. Mat files from Spike2 software (supplied by Nanjing ThinkerTech) for further analysis (Fig. 1d).

1 mL syringe with needle.

3 Methods

3.1 Stereotaxic Microinjection of Tracing Virus in Adult Mice Brain

3.1.1 Anesthesia

The mice were anesthetized by intraperitoneal (i.p.) injection of mixed anesthetics with a dose of 900 μL per 100 g body weight. Then mice were fastened in the stereotaxic apparatus after squeezing the hind limb to ensure its deep anesthesia (Fig. 2a). The fur of the mouse scalp was shaved by a blade. The head skin was removed to expose the skull for dental cement adhesion. Finally, the mice were fastened on a stereotaxic apparatus (Fig. 2a). We covered both eyes of mice with lubricant ophthalmic gel to avoid keratitis during surgery.

3.1.2 Mouse Skull Horizontal Calibration

The horizontal calibration of the mouse skull was performed before virus injection to ensure the accuracy of the injection site and the fiber stub embedding site. First, the bregma point was set as the origin of anterior to posterior (AP: 0.00), medial to lateral (ML:

Fig. 1 (continued) microinjection. E1, KDS Legato™ 130 micro-pump; E2, high-speed dental drill; E3, desktop digital stereotaxic instruments; E4, mouse adaptor; E5, Stereomicroscope; E6, temperature controller; E7, small animal anesthesia machine (The images of E1–7 are from RWD website which was approved by the company)

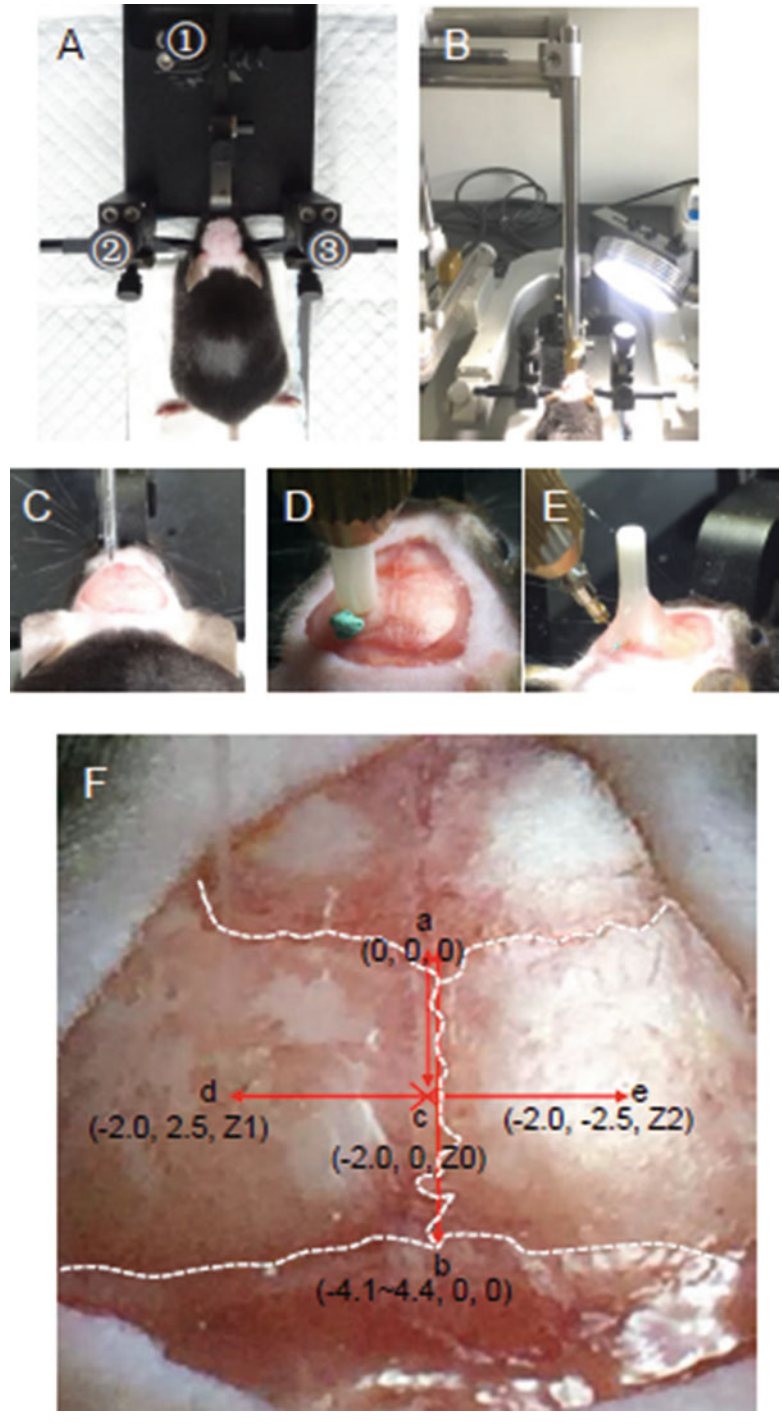

Fig. 2 Stereotaxic microinjection of virus and implantation of fiber stub. (**a**) Anesthetized mouse is fastened on the adaptor after shaving. ① Screws for adjusting the incisor adaptor to calibrate horizontal plane along bregma–lambda axis; ② and ③ Screws for adjusting the level of two ear bars to calibrate

0.00), and dorsal to ventral (DV: 0.00). The distance between lambda and bregma is 4.10–4.40 mm, depending on the age and individual differences of the mice. For anteroposterior alignment, the coordinates of the lambda in the DV direction should be adjusted to the same as that of the bregma to get final coordinates at AP: −4.10 to −4.40 mm. ML: 0.00 mm, DV: 0.00 mm. Next, the alignment of the medial to the lateral axis was performed. A center point (AP: −2.00 mm, ML: 0.00 mm, DV: 0.00 mm) on the bregma–lambda axis was marked (Fig. 2f). Starting from this center point, we marked one point on the left (AP: −2.00 mm, ML: 2.50 mm, DV: $Z1$ mm, Z is the value on the skull) and the other on the right (AP: −2.00 mm, ML: −2.50 mm, DV: $Z2$ mm) hemisphere at a distance of 2.50 mm (Fig. 2f). $Z1$ and $Z2$ were adjusted to the same value ($Z1 = Z2$) to align medial to the lateral axis. The level of the bregma–lambda axis should be checked again after the medial to lateral axis alignment. An error of 0.03 mm during the calibration process is acceptable.

3.1.3 Virus Injection

Locate the injection site, and gently drill a small hole at 0.5 mm diameter in the skull to expose the meninges. The hole in the skull should be covered with sterile saline to keep it moist. Fix the injector on the micro-drive arm of the micropump (KDS Legato™ 130 micro-pump), and load 300 nL of RV-ΔG-GCaMP6s-DsRed into the injector through direct sucking or sucking by micropump. To make an injector, a microelectrode pulled by Puller PC-10 is fused with 10 μL microsyringe through hot-melt adhesive and filled it with mineral oil. Inject RV-ΔG-GCaMP6s-DsRed virus into PVN (AP: 0.2 mm, ML: −0.8 mm, DV: 4.75 mm). The saline on the skull surface should be cleaned before loading the injector to the target site and added again after the injector loading. At the end of virus injection, leave the needle in the injection site for 5 min to avoid virus backflow (Fig. 2b).

3.2 Optic Fiber Implantation

Locate the brain site for Ca^{2+} signal detection, and drill a small hole in the skull and cover it with sterile saline. Replace the micro-drive arm of micropump with a stub holder, then remove the saline and dry the skull with a sponge or cotton swab. After that, a thick fiber stub was inserted from the meninges into the target nuclei

Fig. 2 (continued) horizontal plane along the medial–lateral axis. (**b**) Inserting needle to the target coordinate and injecting virus. (**c**) Replacing the micro-drive for injector by fiber stub holder. (**d**, **e**) Loading the fiber stub to target coordinates and fixing it with dental cement. (**f**) Horizontal plane calibration strategy. a, coordinates of bregma; b, coordinates of lambda, the attitude of a and b (Z value) should be the same; c, coordinates of reference point; d and e, the symmetry point coordinates of the head skull. When Z1 = Z2, the medial–lateral axis is in a horizontal plane. Adapted from Li et al. (2018)

paraventricular thalamus (PVT) (AP: 0.1 mm, ML: −1.60 mm, DV: 3.0 mm) (Fig. 2c). Add four drop monomer, one drop catalyst, and one small flat spoon polymer to the precooled ceramic disc and mix them thoroughly with a sterile toothpick. Cover the entire skull with the mixed dental cement so that the fiber stub could be well secured to the skull (Fig. 2d). An additional 5 min later, carefully scrape off the excess dental cement on the skull with fine scissors. After another 5 min, the fiber stub was released from the stent after the dental cement has completely solidified (Fig. 2e). During the operation, keep the body temperature of the mouse with a heater. After fiber stub embedding, the mouse was transferred into a 37 °C controller till to wake up.

3.3 Ca^{2+} Signal Detection

The surgical mice should be kept for 1–2 weeks to ensure that RV-ΔG-GCaMP6s-DsRed virus expresses GCaMP6s protein before Ca^{2+} signal detection by fiber photometry. The dual-color fiber photometry system (Nanjing ThinkerTech) used in our study contains both red and green fluorescent channels, which can simultaneously record the green fluorescence of the calcium signal (GCaMP6s) and the red fluorescence of the baseline reference (DsRed) through the same fiber. The system has a minimum effective detectable power of 0.6 pW and a low-pass filter cutoff frequency of 35 Hz. It is recommended to use a fiber with a numerical aperture of 0.37 and above, and a fiber-optic connector as a standard FC–PC. The fiber photometry software used for recording is provided by the company (Nanjing ThinkerTech), and the recording rate can be determined according to experimental requirements.

3.4 Histology and Imaging

It is necessary to confirm the accuracy of virus injection and fiber stub insertion according to the fluorescence protein expression in the injection area and position of stubs. After fiber optics recording, the anesthetized mice were transcardially rinsed with 30 mL 1 × PBS containing 20 mg/mL heparin and perfused with 40 mL 4% PFA in 1 × PBS containing 20 mg/mL heparin. All the perfusion solutions were pre-warmed to 37 °C. After perfusion, the mouse brain was dissected out carefully, and postfixed in 4% PFA/1 × PBS overnight. Then the mouse brain was embedded in 5% agar in 1 × PBS and sectioned into 30 μm thick slices with a vibratome (Leica VT1200S). Brain slices were imaged by an autostaged fluorescent microscope (Olympus, BX63).

3.5 Data Analysis

The software TDMS Viewer can be utilized to view the collected data and convert the data into a CSV file. Note that the recording rate of the software should be consistent with the fiber photometry software. The data analysis software OpSignal was used to analyze calcium signal data. After comparing the calcium signals of paraventricular thalamus (PVT) with or without virus labeling, we

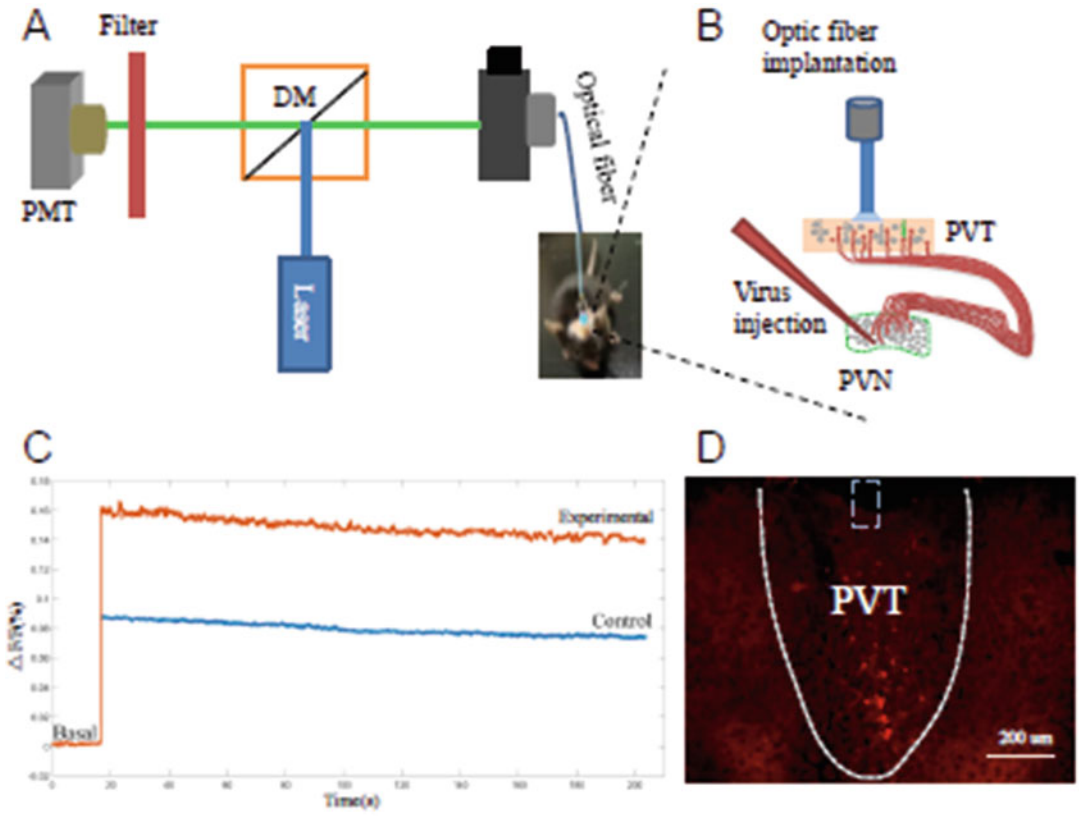

Fig. 3 Ca^{2+} recording of PVT neurons in PVT–PVN circuit by fiber photometry in freely moving mice. (**a**) Schematic diagram for in vivo Ca^{2+} recording by fiber photometry. (**b**) Diagram of virus injection and fiber insertion for PVT–PVN neuron activity detection. (**c**) The trace of Ca^{2+} dynamics in PVT–PVN neurons recorded by fiber photometry. Basal trace is fiber photometry data acquired under ambient light. Experimental trace is the recording data in PVT neurons with viruses labeling. Control trace is the data recorded in PVT neurons without virus injection. (**d**) Confirmation of virus injection and fiber insertion
PMT photomultiplier tube, *DM* dichroic mirror, *PVN* paraventricular nucleus of the hypothalamus, *PVT* paraventricular thalamus

found a significant difference between the two groups, supporting that the signals detected through our protocol were reliable (Fig. 3c).

4 Notes and Conclusion

In summary, the calcium dynamics of PVT–PVN circuit were successfully recorded by our method of fiber photometry, as no signal was detected in the circuit without virus injection. Of note, there are some critical points during the fiber photometry experiment by our protocol. First, the determination of accurate coordinates for virus injection into a specific brain nucleus is a primary key step,

which mainly depends on the correct verification of bregma and lambda. Upon opening head skin, sagittal suture is clear on the moist skull and can be clearly seen through gentle pressing on the skull by fine forceps. The intersection of superior coronal sinus and the sagittal suture is bregma point. It is necessary to determine the coordinates with the dye before the formal injection of the tracing virus. The coordinates may vary slightly depending on the individual's experience. Secondly, it is necessary to re-anesthetize the mice during long-term surgery. When a mouse beard shakes fast, it is the time to add extra anesthetics. The additional anesthetics are 0.05 mL of mixed anesthetics per 20 g body weight. Finally, the mice with fiber stub should be carefully housed in a 37 °C incubator for a while and fed with jelly to avoid frequent heads-ups.

Fiber photometry for calcium recording in freely moving mice provides a powerful tool for neuroscientists to study the dynamics of population neurons at in vivo level. Combined with retrograde viral tracers, the calcium signals can be recorded in a specific neural circuit. Here, we present a detailed, simple, and piratical method for fiber recording of a specific neural circuitry, which may contribute to dissect and elucidate the functional neural circuit.

Acknowledgments

This research was supported by the National Natural Science Foundation of China (Grant No. 31371106, 91632110, 31700934).

References

1. Katz LC, Iarovici DM Green fluorescent latex microspheres: a new retrograde tracer. Neuroscience 34(2):511–520
2. Ugolini G Advances in viral transneuronal tracing. J Neurosci Methods 194(1):2–20
3. Guo Q et al (2015) Multi-channel fiber photometry for population neuronal activity recording. Biomed Optics Express 6(10):3919
4. Arbuthnott GWGW (2000) Fundamental neuroscience. In: Zigmond MJ, Bloom FE, Landis SC, Roberts JL, Squire LR (Eds.) Trends in neurosciences 23(1): 41–42
5. Yiming C et al (2015) Sensory detection of food rapidly modulates arcuate feeding circuits. Cell 160(5):829–841
6. Lütcke H et al (2010) Optical recording of neuronal activity with a genetically-encoded calcium indicator in anesthetized and freely moving mice. Front Neural Circuits 4(3):9
7. Li L et al (2017) In vivo fiber photometry of neural activity in response to optogenetically manipulated inputs in freely moving mice. J Innov Opt Health Sci 10(05):1743001
8. Cui G et al (2013) Concurrent activation of striatal direct and indirect pathways during action initiation. Nature 494(7436):238–242
9. Gunaydin LA et al (2014) Natural neural projection dynamics underlying social behavior. Cell 157(7):1535–1551
10. Fuhrmann F et al (2015) Locomotion, theta oscillations, and the speed-correlated firing of hippocampal neurons are controlled by a medial septal glutamatergic circuit. Neuron 86(5):1253–1264
11. Helmuth A, Olga G, Arthur K (2005) Cortical calcium waves in resting newborn mice. Nat Neurosci 8(8):988–990
12. Christine G et al (2012) Sound-evoked network calcium transients in mouse auditory cortex in vivo. J Physiol 590(4):899–918
13. Stroh A et al (2013) Making waves: initiation and propagation of corticothalamic Ca^{2+} waves invivo. Neuron 77(6):1136–1150

14. Adelsberger H et al (2014, 2014) In vivo calcium recordings and Channelrhodopsin-2-activation through an optical fiber. Cold Spring Harbor Protoc (10) pdb.prot084145
15. Helmuth A et al (2014) Local domains of motor cortical activity revealed by fiber-optic calcium recordings in behaving nonhuman primates. Proc Natl Acad Sci U S A 111 (1):463–468
16. Berridge MJ, Lipp P, ., Bootman MD (2000) The versatility and universality of calcium signalling. Nat Rev Mol Cell Biol 1 (1):11
17. Chen T-W et al (2013) Ultrasensitive fluorescent proteins for imaging neuronal activity. Nature 499:295. https://doi.org/10.1038/nature12354. https://www.nature.com/articles/nature12354#supplementary-information
18. Barnett L, Hughes T, Drobizhev M (2017) Deciphering the molecular mechanism responsible for GCaMP6m's Ca^{2+}-dependent change in fluorescence. PLoS One 12:e0170934. https://doi.org/10.1371/journal.pone.0170934
19. Shen Y et al (2019) Correction to: A genetically encoded Ca^{2+} indicator based on circularly permutated sea anemone red fluorescent protein eqFP578. BMC Biol 17. https://doi.org/10.1186/s12915-019-0707-8
20. Ohkura M et al (2012) Genetically encoded green fluorescent Ca^{2+} indicators with improved detectability for neuronal Ca^{2+} signals. PLoS One 7:e51286. https://doi.org/10.1371/journal.pone.0051286
21. Stosiek C et al (2003) In vivo two-photon calcium imaging of neuronal networks. Proc Natl Acad Sci U S A 100(12):7319–7324. https://doi.org/10.1073/pnas.1232232100
22. Camiré O, Topolnik L (2018) Two-photon calcium imaging in neuronal dendrites in brain slices. JoVE (133):e56776. https://doi.org/10.3791/56776
23. Sadakane O et al (2015) Long-term two-photon calcium imaging of neuronal populations with subcellular resolution in adult non-human primates. Cell Rep 13. https://doi.org/10.1016/j.celrep.2015.10.050
24. Ebina T et al (2018) Two-photon imaging of neuronal activity in motor cortex of marmosets during upper-limb movement tasks. Nat Commun 9(1):1879. https://doi.org/10.1038/s41467-018-04286-6
25. Ghosh KK et al (2013) Miniaturized integration of a fluorescence microscope. Nat Methods 8(10):871–878
26. Birkner A, Tischbirek CH, Konnerth A (2017) Improved deep two-photon calcium imaging in vivo. Cell Calcium 64:29–35
27. Nemoto T Development of novel two-photon microscopy for living brain and neuron. Microscopy 63(Suppl 1):i7–i8
28. Guohong C et al (2014) Deep brain optical measurements of cell type-specific neural activity in behaving mice. Nature Protoc 9(6):1213
29. Betley JN, Xu S, Cao ZF, Gong R, Magnus CJ, Yu Y, Sternson SM (2015) Neurons for hunger and thirst transmit a negative-valence teaching signal. Nature 521(7551):180
30. Cohen JY et al (2012) Neuron-type-specific signals for reward and punishment in the ventral tegmental area. Nature 482(7383):85–88

Chapter 17

Two-Photon Microscopy for Studying Reward Circuits of the Brain

Rafiq Huda, Leena Ali Ibrahim, and Bernard Bloem

Abstract

The intrinsic ability of an animal to adapt its behavior and achieve reward is fundamental to survival. Reward-guided behaviors elicit distributed activity across the brain, recruiting cortical and subcortical brain structures such as the prefrontal cortex (PFC), striatum, ventral tegmental area (VTA), and others. Recent advances in techniques for optical physiology have been transformative in our understanding of the brain's reward system. The ability to measure and manipulate the activity of specific neurons during reward-guided behavior is beginning to shed light on the functional roles for genetically and/or anatomically defined neuronal populations. Here, we first provide an overview of imaging techniques enabling such studies, with an emphasis on measuring cellular and subcellular neuronal signals with two-photon microscopy using genetically encoded sensors for calcium and neurotransmitters like dopamine. We then describe how recent studies have applied these techniques to subcortical (dopamine system and striatum) and cortical (prefrontal cortex) systems of reward processing. Although this chapter is not meant as an exhaustive review of the literature, we highlight areas of inquiries where novel optical tools have provided important new data that have been used to both test old hypotheses and generate novel insights about the circuit organization of the brain reward system.

Key words Two-photon microscopy, Dopamine, Striatum, Prefrontal cortex, Reward

1 Introduction

Reward brain circuits are highly complex and dynamic. Traditionally, electrophysiological methods have been employed to record neuronal activity with millisecond resolution. While electrophysiology has generated invaluable information about the role of individual and populations of neurons in reward processing and behavior, some challenges remain including high-throughput recordings and establishing the identity of the neuron types being recorded. Innovations such as multiple single-unit recordings using high-density silicon probes (e.g., neuropixel probes [1] have overcome some of

Rafiq Huda and Leena Ali Ibrahim contributed equally to this work.

Marc Fakhoury (ed.), *The Brain Reward System*, Neuromethods, vol. 165, https://doi.org/10.1007/978-1-0716-1146-3_17,

these limitations). Moreover, combining electrophysiology with optogenetics in transgenic mouse or rat lines has also allowed recordings from genetically and/or anatomically specified cell types using the opto-tagging technique [2–6]. However, simultaneously recording from large populations of identified neurons involved in different brain functions, along with measuring the activity of subcellular compartments such as axons or dendrites, remains a significant challenge with electrophysiology.

Recently, two-photon microscopy and calcium imaging have emerged as a powerful complementary technology to address some of the limitations of electrophysiology. This technique allows recording/imaging of neuronal activity using a calcium-sensitive fluorescent indicator, typically at rates of 30 Hz or higher, depending on the configuration of the microscope and the resolution desired. Action potentials activate voltage-gated calcium conductances, leading to calcium influx that roughly correlates with the level of neuronal activity. Calcium imaging relies on visualizing changes in fluorescence due to calcium influx and its optical nature makes it advantageous for not only recording the activity of hundreds of neurons at a time but also tracking the same neurons over days or even months [7–9]. There are at least three main advantages of two-photon (2P) imaging compared to electrophysiology: (1) 2P imaging allows taking advantage of the full plethora of genetic/viral tools available for mice, including intersectional tools for simultaneously labeling multiple genetically and/or projection-defined cell types [10, 11]; (2) the high spatial resolution of 2P microscopy allows recordings at subcellular level (axons/boutons/spines/dendrites) to visualize compartment specific structural changes and functional activity [12–14]; and (3) electrophysiology only allows measuring membrane voltage or spikes, but 2P microscopy allows imaging anything that can be fluorescently encoded; e.g., neuromodulator release, localization/trafficking of various proteins, intracellular messengers like cAMP, or biochemical events like transcription [15–18]. A unique advantage of electrophysiology is its high temporal resolution that allows measuring neuronal events at the time scale of single-action potentials, synaptic transmission, and even single ion channel activity. However, technologies for fast optical imaging of voltage, both at the level of sensor probes and microscopy solutions, are being developed [19–24] and hold the promise of closing this temporal resolution gap.

Many neuronal processes occur deep within the brain. The light-scattering properties of brain tissue limit the effectiveness of single-photon microscopy for real-time imaging in behaving animals (e.g., confocal microscopy). Moreover, one-photon excitation light also suffers from limited depth penetration due to light absorption by naturally occurring molecules in the tissue. Similar issues also apply to the one-photon light emitted by fluorophores.

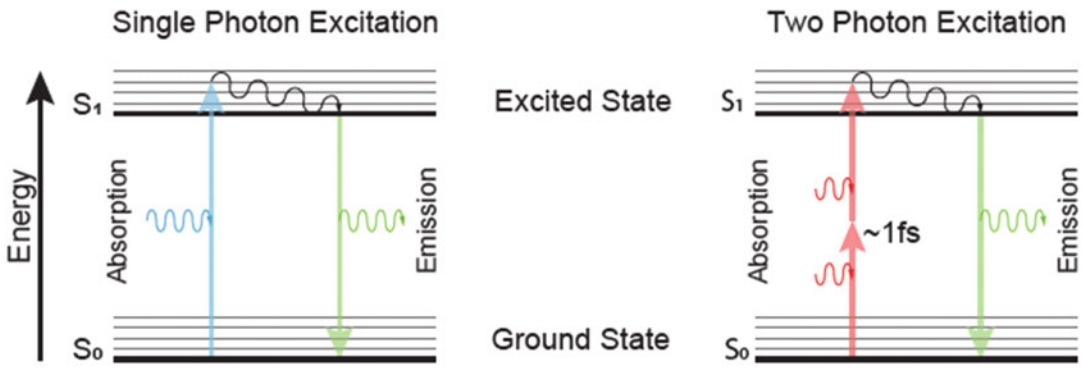

Fig. 1 Jablonski diagram illustrating difference between single-photon excitation (left) and two-photon excitation (right) of a fluorophore. In the case of two-photon excitation, two photons of double the wavelength (red) have to reach within ~1 fs in order to excite the fluorophore from the ground state S_0 to excited state S_1. Once the molecule is in the S_1, a process of internal conversion brings it down to a lower energy state. The molecule then emits light of a lower energy (longer wavelength) resulting in fluorescence emission (green), as it returns to its S_0

Techniques like confocal microscopy compound this problem by excluding emitted light with the pinhole, leading to low-intensity signals. Hence, both light scatter and penetration are fundamental issues in imaging any thick tissue. Absorption and the scattering of light are wavelength dependent; at longer wavelengths, there is less scattering (scattering scales with wavelength as $\sim\lambda - 4$; Rayleigh scattering). Hence, imaging at wavelengths near-infrared minimizes both scattering and absorption. How can one then image regular fluorophores at near infrared wavelengths?

In traditional one-photon microscopy, a fluorescent dye is excited using a single photon of a specific wavelength that brings the fluorophore into an excited state from its ground state (lowest energy state). This then results in a process of internal conversion whereby the excited molecule relaxes, giving off energy (of a longer wavelength) before coming back to its ground state. This phenomenon is called fluorescence and beautifully depicted by the famous Jablonski Energy diagram (Fig. 1). Most fluorophores are excited by wavelengths of light in the visible spectrum but these wavelengths do not penetrate deep into the tissue due to scattering and absorption, as discussed above. One solution is to use fluorophores that are excited by infrared wavelengths, however, these are very limited. Another strategy is to use the existing variety of fluorophores but excite them in a different way. 2P microscopy utilizes two photons of double the wavelength (and hence half the energy) to near-simultaneously excite a fluorophore within ~1 fs. The additive effect of two half-energy photons is enough to bring the fluorophore from its ground state to an excited state. Importantly, the process of two photons exciting a fluorophore simultaneously is a very low probability event and scales with the

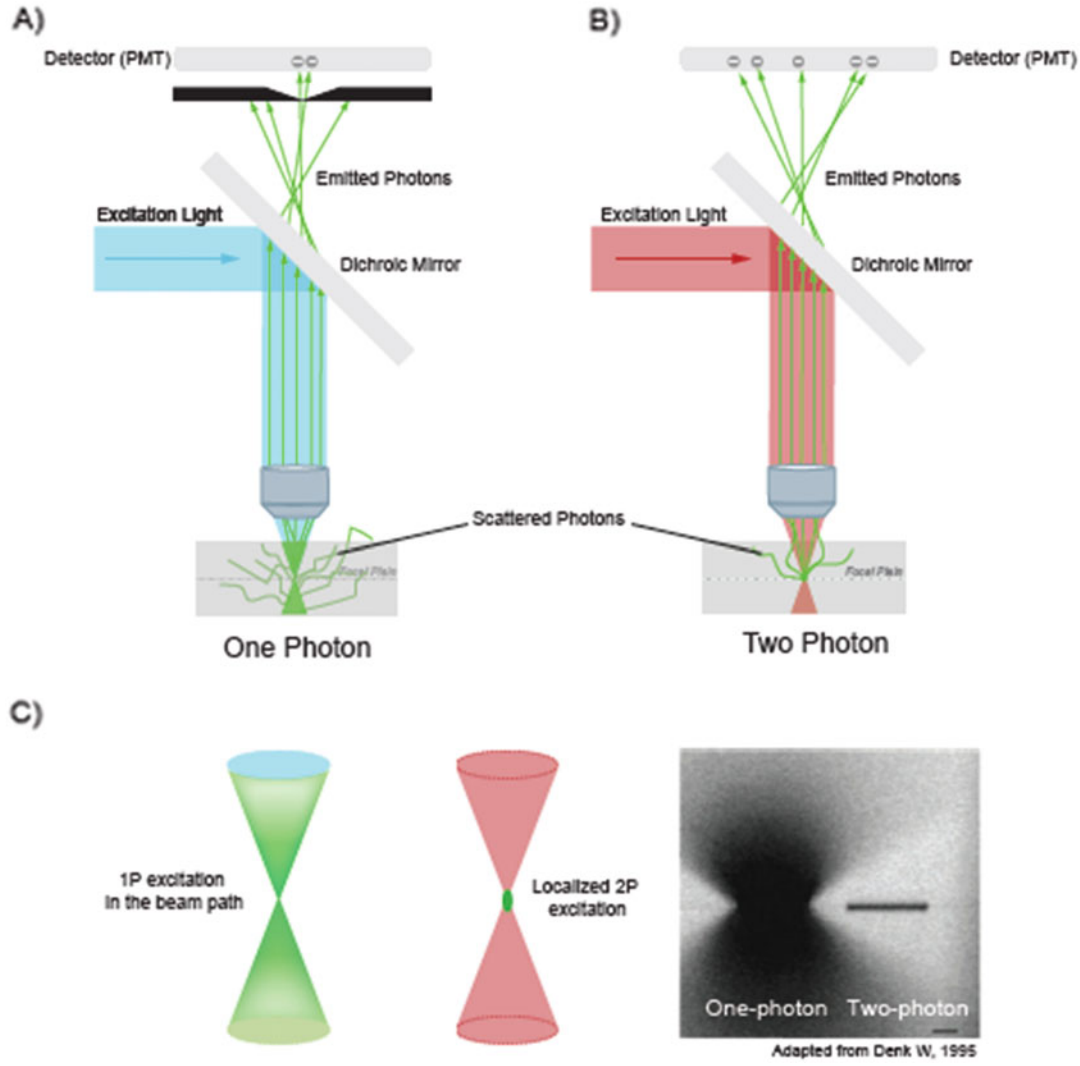

Fig. 2 Difference between one-photon and two-photon excitation at the focus. (**a**) In the case of one-photon (1P) excitation, many in focus emitted photons fail to reach the detector (PMT) because of the small pinhole used to eliminate out of focus fluorescence. This results in a lower signal. (**b**) In two-photon (2P) excitation, all the photons emitted from the focus are detected by the PMT. (**c**) Illustration of the illumination path in the sample. Left, conical-shaped excitation from 1P results in out of focus excitation, whereas in 2P excitation (center), a localized spot of excitation eliminates the need of a pinhole. Right, a bleaching experiment illustrating the difference between 1P and 2P excitation in the sample

square of the incident laser intensity. Because of this nonlinearity, 2P provides a means of localized excitation. Basically, the only region where a fluorescent molecule is excited is in the exact focal point, without any out of focus excitation occurring that commonly occurs with 1P excitation (Fig. 2). This has proven to be advantageous and provides optical sectioning with similar resolution as a confocal, without the requirement of a pinhole thereby

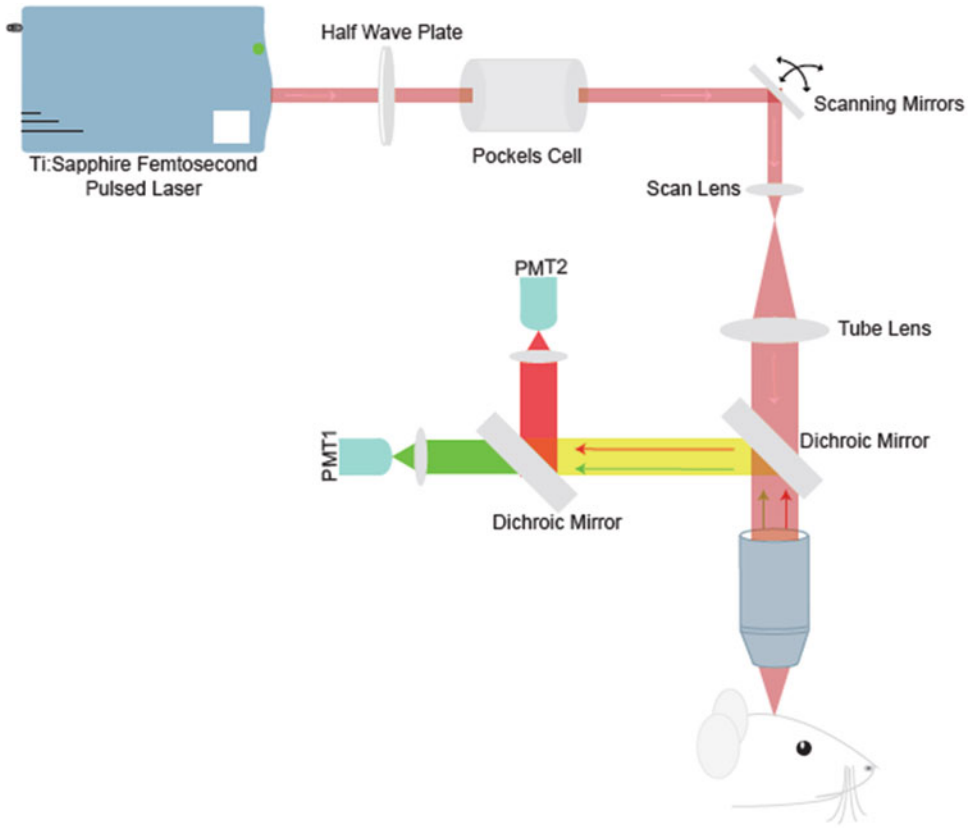

Fig. 3 A simple two-photon microscope setup. Excitation light from a pulsed laser source (Ti:Sapphire) is modulated (in power) using a half-wave plate and/or a pockels cell. The excitation beam then reaches the scan head. The scanning mirrors steer the beam in *x* and *y* positions (for scanning across the sample). The beam is expanded and made coherent using a scan lens and tube lens assembly. This is then relayed via a dichroic mirror that reflects the light to the brain region of interest through the objective. The emitted light is then collected by the PMTs. In this case, two channels, red and green, are split using another dichroic into its individual wavelength components, detected by two PMTs, one for each channel

allowing all emitted signals to be collected. Since 2P provides a confined excitation spot, almost all the emitted light is guaranteed to come from that spot, hence there is no need to exclude the "out of focus" fluorescence and can capture all scattered light (as much as the objective allows).

Below, we briefly describe the simplest version of a 2P microscope (Fig. 3), followed by latest developments of genetically encoded sensor probes for measuring calcium activity and neurotransmitter release, transgenic and viral technologies for expressing these probes in specific neuronal populations, and surgical techniques for preparing mice for two-photon imaging. We end by providing a brief review of the literature on the role of the dopamine system and the prefrontal cortex in reward-guided behaviors to highlight areas of inquiries tackled by recent work using the optical techniques described herein.

2 Basic Components of a 2P Microscope

Laser: The most important component of a 2P microscope is the laser. Typically, a Titanium Sapphire (Ti:S) laser is used, so named because it uses a crystal of sapphire doped with titanium as the lasing medium. This laser produces tunable wavelengths in the red-near infrared (NIR) range (700–1000 nm) by adjusting the internal optics in the laser. It is a pulsed femtosecond laser, producing intense ultrashort pulses at a megahertz (MHz) repetition rate (~80–100 fs at 80 MHz, with 12.5 ns between pulses). In those ultrashort pulses of intense light, the peak energy is extremely high, increasing the probability $\left(\text{peak power} = \frac{\text{average power}}{\text{pulse width} \times \text{rep rate}}\right)$ of 2P absorption while keeping the average energy low. Typically, the average power is about 1 W (coming straight out of the laser); however, the peak power is at least 100,000 times more. The most commonly used tunable 2P lasers are the Mai Tai laser from Spectra Physics Inc. and the Chameleon laser from Coherent Inc.

Optical components: The laser beam going into the microscope is routed and aligned using various mirrors and other components that are laid out on the vibration isolation table (Newport). Half-wave plate ($\lambda/2$) is used as a light intensity controller; dielectric mirrors that ensure more than 99% reflectance and periscope mirrors that allow the laser beam to reach the scan head in an upright microscope are used. Additionally, a pockels cell (Conoptics), a crystal polarizer that changes orientation with voltage, allows for rapid modulation of the laser power with a high dynamic range and high temporal resolution to control the light intensity entering the brain.

Scan head: A set of XY scanning mirrors are used to steer the laser beam and scan across the sample. Generally, the imaging field of view (FOV) is broken up into multiple lines that are raster scanned sequentially. The x mirror scans across lines, whereas the y mirror is used to switch the beam between lines. The scanning mirrors are linked to a scan lens and a tube lens (part of the microscope) to form a telescope that collimates the beam going to the objective. The beam is reflected downwards toward the objective using a dichroic mirror. Some commercial systems offer two modes of scanning (e.g., the Bruker 2P plus), while others offer either both or an option between the two. Galvo-galvo scanning uses galvanometer scanners for both x and y movement. High spatial resolution imaging is an advantage of galvo-galvo scanning since it allows users to specify a dwell time for pixels within a line scan. Increasing the dwell time generally increases the signal generated. Moreover, galvo-galvo allows scanning of arbitrary geometric patterns, including line scans, spiral scans, and scanning over user-defined regions of interest (ROI). However, galvo-galvo

scanning suffers from a low temporal resolution. Another option is galvo-resonant scanning, in which the *x* scanning mirror is a resonant scanner that scans at a high frequency (8 or 12 kHz), with a *y* galvo mirror used for raster scanning between lines. Depending on the spatial resolution, galvo-resonant scanners can provide frame rates of up to 90 Hz; a temporal resolution of 30 Hz at a FOV pixel size of 512 × 512 is common.

Detectors: The detector assembly is placed close to the objective in order to collect as much light as possible, increasing the detection efficiency. Since a pinhole and a descanned path are not required (optical sectioning is achieved by the mere nature of the excitation itself), the detectors can be placed right after the objective. In this regard, the detection path is simpler than a confocal microscope. The detectors are either alkali or GaASP photomultiplier tubes (PMTs, from Hamamatsu), with GaASP PMTs providing more sensitive detection. Multiple PMTs can be used to detect different emission wavelengths using filter cubes with a dichroic mirror and band-pass filters that only allow certain wavelengths to pass through. An IR filter is placed in front of the PMT to block excitation light from reaching the PMTs. The signal from the PMT is then fed to a current amplifier and eventually into a data acquisition board. Because the PMT is a highly light-sensitive device, experimental setups requiring visual stimulation or other light sources need to be properly designed to prevent leakage of extraneous light into the PMTs.

3 Indicators/Sensors to Study Neuronal Function

Calcium indicators: Calcium is one of the most essential intracellular messengers in neurons. During electrical activity in neurons, the concentration of calcium increases by about a 100-fold inside neurons [25, 26]. A balance between calcium influx, efflux, exchange with intracellular stores as well as buffering by calcium-binding proteins determines the calcium dynamics within the cells [26]. Oregon Green Bapta (OGB1) and Fura2 are commonly used chemical calcium indicators that fluoresce upon calcium binding. These fluorophores are conjugated as AM ester dyes to facilitate cellular uptake and allow bulk loading into live tissue. Esterases expressed by healthy cells cleave the AM ester group, freeing the fluorophore intracellularly [27]. However, a limitation is that these fluorophores enter all cells without any specificity. On the other hand, genetically encoded calcium indicators (GECIs) can be expressed with cell-type specificity (as discussed below). A prime member of the GECIs is the GCaMP family. They primarily consist of a circularly permuted enhanced green fluorescent protein (EGFP), flanked by calmodulin, a calcium-binding protein; and on the other side by the calmodulin-binding peptide M13. In the

presence of calcium, calmodulin–M13 interactions cause a conformational change in the fluorophore, thereby increasing the fluorescence [28]. The GCaMP family of proteins is continuously being improved to increase signal-to-noise ratio, dynamic range, and response kinetics. Recently, GCaMP7 has been developed through a series of incremental improvements. The latest GCaMPs are very fast, with optimal basal fluorescence and fast kinetics capable of tracking single action potentials in neurons [29]. Additionally, GCaMPs have been linked to compartment-specific proteins, such as GAP43, that localize the calcium sensor to axons, allowing for better compartment-specific imaging of neuronal activity [14]. In addition to these GFP-based sensors, RFP-based sensors (e.g., RCaMP1h and jRGeCO) also exist allowing for dual-channel imaging of intermingled neuronal populations.

Indicators for imaging neuromodulator release: Neuromodulators play very important roles such as in attention (acetylcholine) and during reward (dopamine) in the brain. However, studying their transmission and cell-specific roles have been challenging due to lack of methods to monitor their activity. Recently, sensors for neuromodulator release have been developed. For example, cholinergic sensors, such as GACh, a G-protein coupled receptor, have recently been developed and imaged using 2P microscopy [30]. The development of genetically encoded GPCR-activation-based DA sensors like GRABDA and dlight has enabled the measurement of dopamine dynamics in model organisms while performing complex behaviors [31]. They exhibit large fluorescence increases with subcellular resolution, fast kinetics, nanomolar affinities, and high molecular specificity [15]. These sensors are continuously being improved to achieve even better kinetics and resolution.

4 Transgenic Lines for Cell Type–Specific Investigation

Cell type–specific transgenic mouse lines have enabled neuroscientists to investigate the role of the diverse neuron types in various brain functions. Local microcircuits are composed of excitatory and inhibitory neurons, which are distinct in their morphology, electrophysiological properties, and the molecular markers that they express, thereby imparting special functions to the different neuron subtypes [32, 33]. Moreover, cells in major neuromodulatory nuclei of the brain, such as dopaminergic, cholinergic, serotonergic, and noradrenergic, as well as other functionally specialized cell types can be defined based on expression of specific molecular and genetic markers. Many cell types additionally express specific markers at certain time points during development, allowing the use of birthdating techniques to further define specific cells based on developmental trajectories [34–36]. Neuroscientists have taken

advantage of the diversity of unique molecular profiles and developed cell type–specific Cre and Flp (DNA site-specific recombinases) transgenic lines [37] that enable the expression of various neuronal effectors in order to either manipulate a specific neuron type or visualize its morphology and function. In combination with GECIs, these transgenic lines have proven useful to study the activity of a large group of neurons that perform similar functions. Typically, adeno-associated viruses (AAVs) are used to deliver the GECIs in a specific region of the brain using stereotaxic injections (see Surgical Procedures below). In addition to viral delivery of GECIs, transgenic mouse lines that encode calcium sensors are widely being used to eliminate the process of virus injections. The expression of the sensor in these transgenics is dependent on the presence of Cre or Flp. Expression of GECIs in this way results in the sensor being expressed in every cell that expresses the Cre recombinase. Care must be taken however in using this approach as there have been reports of spontaneous aberrant activity in some of these mice lines [38]. Moreover, transient expression of the transgene during development (but not in adulthood) can cause loss of specificity [39]. Additionally, since inhibitory neurons tend to be directly driven by neuromodulators, utilizing Cre driver lines for inhibitory neurons (such as PV, SOM, VIP, and L1) in combination with the neuromodulatory sensors described above, one can really begin dissecting the roles of these diverse interneuron types in reward-related processes in the brain. Similarly, by allowing targeting of specific cell types in neuromodulatory nuclei, these techniques hold the promise for elaborating how specific circuits contribute to various reward-guided behaviors.

5 Viral Vectors for Labeling Neurons Based on Anatomical Connectivity

Recent advances in viral vector technology have made it possible to label specific neuron types based on the pattern of their afferent and efferent connectivity. Several options are now available for retrograde expression of transgenes, including modified rabies viruses [11, 40, 41], canine adenovirus type-2 (CAV-2) [42], and retrogradely traveling AAV viruses [43]. Using modified rabies viruses for monosynaptic tracing has proven especially useful for identifying the presynaptic partners of molecularly defined neurons [44]. A general strategy is to inject retrograde viruses expressing the Cre (or Flp) recombinase in the output area. Injecting Cre-dependent AAV viruses in an upstream area of interest results in the expression of the desired genetic payload in specific projection neurons. This strategy can be used to introduce structural markers such as fluorophores, various genetically encoded activity sensors, or opsins of

interest based on output connectivity. By making recombinase expression contingent on the presence of another recombinase (e.g., a Cre-dependent Flp recombinase), these retrograde viral vectors can be combined with transgenic lines to label further refined subpopulations of neurons based on both molecular genetic identity and projection pattern.

6 Surgical Procedures

6.1 List of Materials

For Anesthesia:
O_2 tank.

Isoflurane USP.

Isoflurane Setup (Parkland Scientific).

For Surgery:
Local anesthetic such as bupivacaine.

Analgesic such as meloxicam or buprenorphine.

Dexamethasone for reducing brain swelling.

Stereotaxic frame (e.g., Kopf or Stoelting).

Heat pad with temperature control and feedback (e.g., Stoelting).

Sterile gloves.

Eye lubricant such as Systane.

Razor blade to shave the head.

Sterile gauze.

70% Ethanol pads

Betadine scrub.

Sterile surgical grade tools such as forceps, scissors, scalpel, etc.

1× PBS

0.9% Saline

Sterile absorbent sponges or triangles (e.g., GELFOAM or absorption spears, F.S.T.)

3 mm glass coverslip and 5 mm glass coverslip (or GRIN lens/imaging cannula) glued together with UV curable glue (Norland 61)

3 mm biopsy punch (e.g., Acuderm)

Surgical/dental drill.

Drill bit (Fine Science Tools).

Blunt needle syringe coupled to a vacuum source.

Kwisksil (World Precision Instruments).

Dental cement such as Metabond (Parkell).

Metal headbar.

Vetbond glue.

Loctite 409 glue.

For Virus Injections:
AAV virus-carrying transgene of interest.

Pulled glass capillaries.

Fast green dye.

NanoInjector such as NanoInject III.

Most steps of the surgical procedures are the same, with alternative steps marked by * or **. *Approval from the appropriate institutional regulatory bodies should be obtained before performing these experimental procedures on mice.*

Anesthesia. The mouse is placed in a Plexiglas box through which a mixture of oxygen and 3% isoflurane is perfused. After the mouse is deeply anesthetized, as evidenced by slowed breathing rate and lack of locomotion, it is transferred to the stereotaxic apparatus, equipped with a closed ventilation nose piece (Kopf Instruments, Inc.). The isoflurane anesthesia setup (Parkland Instruments, Inc.) is adjusted to provide a constant 1–2% level of the anesthetic, which is adjusted as needed throughout the surgery. Surgery begins only after the animal has reached a surgical plane of anesthesia, as assessed by the absence of paw withdrawal in response to a toe or tail pinch. Body temperature is maintained at 37 °C using a small animal warmer (Stoelting) or another similar device. The depth of anesthesia is monitored continuously, ensuring that there is no limb withdrawal, movement other than respiration, change in heart rate or breathing during a toe or tail pinch.

Surgery. Surgery is performed using the "no-touch" sterile procedure with all tools and surgical materials (gauze pads, etc.) sterilized by autoclaving. The eyes are protected by a drop of lubricant eye ointment (Systane). Fur is removed from the scalp by shaving with surgical clippers or using a depilatory cream. The surgical site is treated with the antiseptic and bactericide Betadine (Betadine scrub, containing povidone iodine) starting with the head and moving toward the neck, and then wiped with 70% ethanol. This is repeated three times, followed by an application of Betadine solution, which is left on to dry. Bupivacaine (Marcaine) is injected subcutaneously in the surgical area prior to cutting the skin (the commercially available 0.25% solution is diluted hundredfold to yield 0.025 mg/mL and 0.2 mL of the diluted solution is used per 100 g body weight). Corticosteroids may also be injected at this time to minimize both intraoperative brain swelling and postoperative inflammation and gliosis around injection site. These include dexamethasone 0.5 mg/kg IP or methylprednisolone 30 mg/kg IP. A midsagittal incision is made in the scalp using

a sterile scalpel and a patch of the scalp above the surgical site is removed. The skin is retracted and the surface of the skull is exposed and cleared of periosteum using the back side of a scalpel blade. A sterilized piece of gauze with a slit in the center is used to isolate the surgical area from the skin. The skull is then scored with a scalpel to make the surface rough for optimal adherence of the dental cement used to attach the headbar. Any bleeding at the surface of the skull is promptly resolved. A 3 mm biopsy punch is used to mark the site of the craniotomy at the site of interest. A circular craniotomy is drilled with a dental drill and sterile tip above the intended brain region. After enough drilling (and sometimes etching with a scribe) the skull gets soft enough around the perimeter and can be easily pierced. A slightly blunt scalpel blade is used at a shallow angle to lift off the piece of skull and expose the underlying cortex with minimal damage and bleeding. The exposed cortex is covered with small pieces of gel foam sponge soaked in 1× PBS to prevent the drying of the brain tissue.

AAV injections. Depending on the experiment, viruses can be injected during the craniotomy surgery or in a previous surgical procedure. AAV virus carrying GCaMP or other sensors (1012 or 1013 titer) is mixed with fast green (for visualization of the injected solution) and loaded into a fine glass pipette pulled to have a tip size of ~10–20 μm. After piercing the dura, 50–500 μL of the virus solution is pressure injected into the target brain area based on stereotaxic coordinates using a Drummond Nanoinject III apparatus (or any other nanoinjection device). The virus is injected at a rate of 50–100 nL/s. After injection, the pipette is held in place for at least 10 min before removal to allow diffusion of viral particles into the nearby tissue.

**For 2P imaging of cortical surface*: After removal of the pipette, a round glass window is carefully placed above the cortex and positioned such that it fits nicely within the craniotomy. Using forceps, the window is pressed gently and Vetbond (a biocompatible glue) is applied to the edges to secure the window in place and prevent it from popping out. Finally, a head bar is placed on the skull using Loctite 409 (gel-based glue), and then the entire skull together with the glass window and the metal headbar are further secured using a strong dental cement such as Metabond (Parkell, Inc.). This is required for head fixing the animal under the 2P microscope.

**For 2P cortical imaging over the midline*: The mouse anterior cingulate cortex (ACC) is a prefrontal cortical region that has been widely implicated in reward and other behavioral processes. In the mouse, the caudo-dorsal aspects of the ACC are amenable to 2P imaging. We have successfully made two-photon recordings from this area previously [45] and describe here key details for the success of this preparation. A significant challenge is that the ACC

is located on the midline, requiring careful craniotomy procedures to avoid rupturing the underlying sagittal sinus. The mouse is prepared for surgery as described above. A 3 mm biopsy punch is centered on the midline at 0.5–0.8 mm anterior to bregma and gently pressed down to create an outline for the craniotomy. A dental drill with a small drill bit (~0.5 mm, Fine Science Tools) is set to medium speed and used to slowly create the craniotomy. Drops of saline are added periodically to dissipate the heat created by the drilling. In our hands, the best strategy is to continue drilling until the deepest layer of the bone has cracks in it without fully breaking. Special care must be taken when drilling the bone overlying the sinus; yet, the bone in these regions still needs to be cracked. To determine if the craniotomy has been drilled enough, a drop of saline is added to the skull and the bone flap is tapped gently with a pair of forceps. The bone flap is ready to be removed if it moves slightly when tapped. Place a piece of saline-soaked surgical gelfoam sponge besides the bone flap. To remove the bone flap, first identify an area devoid of large blood vessels, ideally in the posterior portion of the craniotomy. Slowly lift the bone flap using a pair of fine forceps. As you start lifting, you may notice the dura attached to the underside of the bone flap. Lift the flap a little bit at a time so as not to tug the dura too hard, which can result in rupturing of the sinus and major, life-threatening bleeding. In some instances, a little bleeding from the sinus can occur upon removal of the bone flap. In this case, move the gelfoam onto the bleeding spot, then gently press an absorbent triangle against the gelfoam, allowing the saline to be absorbed through capillary action. In our experience, this technique usually resolves small bleeds from the sinus. A similar strategy can be taken to resolve small bleeds occurring elsewhere. Flush the cortical surface with sterile saline or PBS. Remove any shards of bone that may not have come off cleanly during the bone flap removal. This is especially important for animals meant for long-term experiments; bone can regrow underneath the implanted chronic window if small shards are not removed, compromising the clarity of the imaging window.

The skull, especially in the anterior half of the craniotomy, is relatively thick, requiring additional steps to adequately dampen brain movement and prevent artifacts in the imaging data. The craniotomy is fitted with a "double" chronic window plug, which is assembled by adhering two 3 mm and one 5 mm #0 coverslips (World precision instruments) together with UV curable glue (Norland 61). Importantly, the skull in the perimeter of the craniotomy is thinned using the dental drill so that its thickness is about the height of the two stacked 3 mm coverslip (Fig. 4; note that thinning should be done before the boneflap is removed). This ensures that the 3 mm part of the window touches and provides slight downward pressure on the brain. The double window is held in place above the craniotomy using a blunt needle syringe

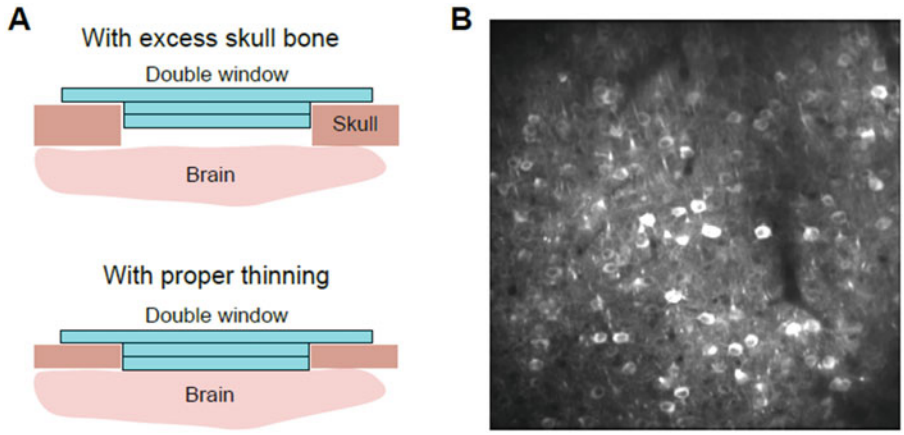

Fig. 4 Imaging in the anterior cingulate cortex (ACC) with a chronic imaging window. (**a**) Schematics illustrating fit of the double chronic window with (top) and without (bottom) adequate bone thinning around the perimeters of the craniotomy. (**b**) GCaMP6s-expressing ACC neurons imaging with a two-photon microscope

connected to a vacuum source and mounted on the stereotaxic arm of the surgery setup. A drop of saline is placed on the brain and the window is lowered slowly onto the brain through the saline drop. An absorption triangle (Fine Science Tools) is used to wipe up excess saline by placing it against the side of the 5 mm coverslip. It is critical that saline is removed from underneath the 5 mm coverslip, but a thin layer remains on the brain. This way, the metabond used to adhere the window to the skull can flow underneath the 5 mm coverslip without going onto the brain. The vacuum feeding the blunt needle syringe is turned off before applying the metabond. The metabond should be allowed to fully dry before removing the needle. As the last step, a headbar is attached to the skull using metabond before returning the animal to its cage to recover from the surgery.

* *For deep 2P imaging*: Gradient Index (GRIN) lens can be used for imaging deep structures such as the ventral tegmental area (VTA) or deep layers of the medial prefrontal cortex (mPFC). A cannula window can be used for dorsal striatum imaging.

** *GRIN lens implantation*: Part of the cortex is aspirated using an aspiration needle connected to a vacuum pump, while slowly irrigating prewarmed (37 °C) aCSF. Aspiration is performed gradually until the desired brain region is reached, usually visible by changes in density of the different brain regions. Bleeding is expected due to vessel rupture during the aspiration procedure, continuous aCSF irrigation is recommended until bleeding stops and the vessels are sealed. The needle is then withdrawn and irrigation stopped. A disinfected (using 70% ethanol) 1 mm GRIN lens is lowered carefully into the hole surrounded by aCSF and avoiding bubbles. Agarose is then applied to seal the area between the skull

and the GRIN lens. Finally, Metabond is applied at the edges of the lens and the exposed skull.

*******Dorsal striatum imaging through imaging cannula*: It is recommended that virus be injected 1–2 weeks before the imaging cannula surgery. The imaging cannula is assembled by adhering a 2.7 mm glass coverslip to the end of a custom-sized stainless steel metal tube (1.7 mm long, 2.7 mm diameter). Mice are water restricted for a week before the cannula surgery. Bregma and lambda are aligned horizontally and craniotomy coordinates are marked. The skull is titled and rolled by 5° to make it horizontal at the cannula implant site. A dental drill is used to make a 2.7 mm diameter craniotomy. The cortical tissue is gently aspirated with gentle suction under constant perfusion with cooled autoclaved 0.01 M phosphate-buffered saline (PBS) until the underlying white matter appears. A small layer of the white matter is removed and covered with a thin layer of Kwisksil (World Precision Instruments) before inserting the cannula into the cavity. The cannula, as well as a custom headplate, is attached to the skull using metabond (Parkell).

Recovery. At the end of the surgery, a long-acting pain killer such as buprenorphine, (Buprenex) (0.05 mg/kg), or Meloxicam is injected which provides analgesia for 6–10 h. This is followed by an injection of the drug for an additional 2 days. The animal is transferred to a heated postoperative chamber using a heating pad placed under the cage. The animal is allowed to recover until it moves freely and normal behaviors are resumed. After this, it is returned to its home cage and is monitored daily until full recovery.

7 Function of the Dopamine System in Learning

The neuromodulator dopamine has long been associated with reward learning, movement, and motivation [46]. How the dopamine system fulfills these related but distinct functions remain a subject of active investigation, with new optical tools providing important new data that are being used to both test old hypotheses and generate novel insights. Midbrain dopamine producing neurons of the ventral tegmental area (VTA) and the substantia nigra par compacta (SNc) send dense outputs to multiple forebrain targets, including the striatum and nucleus accumbens and the medial prefrontal cortex [47–49]. Studies examining the activity of dopamine neurons in reward-guided behaviors provide strong evidence that dopamine neurons encode a reward prediction error, which signals the difference between obtained and expected rewards [50–52]. Dopamine neurons show transient, phasic responses to unexpected rewards, but respond minimally to expected rewards. Moreover, omission of expected rewards leads to a decrease in the tonic activity of dopamine neurons. Hence, dopamine neurons increase

firing in response to unexpected rewards and decrease firing to omission of expected rewards, thereby encoding a positive RPE when outcomes are better than expected, and a negative RPE when they are worse. Importantly, during associative learning, dopamine responses to reward transfer to the reward-predictive cue.

In early stages of training, reward is unexpected and elicits strong phasic dopamine neuron firing. As the associated sensory cue comes to predict the reward with learning, no activity modulation is observed at the time of reward delivery. Instead, dopamine neuron activity increases around the time of the predictive cue. Such RPE encoding by dopamine neurons is a widespread phenomenon that has been observed in multiple species, including humans [53–60]. Yet, such signaling does not capture the full extent of dopamine neuron activity, with some neurons also signaling salient and aversive events [61, 62], as well as movement initiation [63, 64] (also see below).

In theories of associative learning, the RPE acts as a teaching signal that allows learning about the relationship between rewards and states and/or actions that are associated with them [65–67]. Optogenetics, the ability to control neuronal activity with light with a high temporal resolution [68, 69], in combination with transgenic rat and mouse lines that enable selective targeting of dopamine neurons, has allowed direct test of the hypothesis that activity in DA neurons drives learning. In an elegant study, TH-Cre rats were used to selectively express the optogenetic actuator ChR2 in dopaminergic neurons of the VTA and a blocking associative learning paradigm was used to test the relationship between DA neuron firing, RPEs, and learning [70]. In blocking experiments, learning the association between a sensory cue and reward is impaired if that cue is presented simultaneously with another cue, which was previously paired with reward [71]. Generally, animals are first trained to associate a sensory cue (cue A) with rewards like sucrose. Performance is measured by quantifying behavioral responding to the cue, such as time spent in the reward port. Training proceeds until high levels of behavioral responses are achieved, indicating that animals are using the sensory cue to predict the availability of reward. This is followed by a compound cue training phase during which cue A is simultaneously presented with a novel cue B to signal reward availability. Even though cue B is paired with reward during this phase, its presentation alone in a subsequent test phase fails to elicit significant behavioral responding. Hence, compounding cue B with cue A blocks learning that cue B predicts reward. This blocking illustrates the crucial role RPEs play in driving learning. During the compound training phase, the reward is fully predicted because of its prior association with cue A. Because the expected and obtained rewards are equivalent in this condition, no RPE is generated and hence no learning

occurs. If RPE encoding by DA neurons is related to learning, then activating these neurons at the time of reward during compound cue training should create an artificial RPE that mimics a learning signal in the brain and produce behavioral responding to cue B in the test phase. Remarkably, this is exactly what happens with optogenetic activation of DA neurons [70]. This work, along with other recent studies [72–77], suggests a strong causal relationship between DA neuron activity and learning from rewards. Although dopamine effects on learning are most clearly understood with cue-based learning paradigms, considerable evidence shows that dopamine also plays a critical role in learning the values of actions, particularly in SNc–dorsal striatum circuits [72, 78, 79].

8 The Dopamine System and Movement

In addition to its involvement in cue-reward learning, the dopamine system is also strongly implicated in movement and motivation [46, 63, 80, 81]. Indeed, degeneration of dopamine-producing cells in the SNc results in severe movement phenotypes characteristic of Parkinson's disease [82, 83]. Specifically, dopamine is thought to invigorate behavior, in addition to modulating other motivational processes [84]. In classic accounts, the phasic activity of dopamine neurons is mostly related to reward signaling but not to movement. However, several studies challenge this view. In head-fixed mice running on a wheel, movement initiation is associated with phasic activation of a subset of dopamine neurons, which were identified via juxtacellular labeling and post hoc immunohistochemical analysis [85]. Recent studies have also used the opto-tagging technique to make recordings from identified dopamine neurons in freely moving mice during self-paced movements [86]. Dopamine neurons in the SNc were found to be transiently active before movement initiation. Moreover, the level of dopamine neuron activation positively correlated with the acceleration of movement bouts, suggesting that this activity is related to the vigor of movements [86]. Similar to dopamine neuron firing, dopamine release in downstream structures is also modulated by movement. Dopamine release in the nucleus accumbens in response to reward predicting cues is attenuated when getting rewards requires no movement, compared to when movement is required [87]. Similarly, other studies have reported dopamine signals to movement initiation which also scale with the speed of a motor response [88], as well as prolonged dopamine signaling that scales with spatial distance to rewards [89].

9 Interrogation of Specific Dopamine Circuits Using Optical Techniques

With the advent of optical techniques for measuring calcium activity of neurons and release of neurotransmitters like dopamine, combined with transgenic and viral technologies, we can begin to unravel the dichotomous role of dopamine in reward learning and movement. Recent studies have begun addressing this question by leveraging two-photon calcium imaging to simultaneously record from large populations of identified dopamine neurons [90]. Dopamine neurons were selectively labeled via conditional expression of GCaMP6 in DAT-Cre (dopamine transporter) mice and imaged via a GRIN lens implanted over the VTA, similar to as we describe above. Importantly, mice were trained on a decision-making task in virtual reality that incorporated multiple behavioral functions that have been ascribed to dopamine. As mice navigated the central stem of a virtual T-maze, discrete visual cues appeared on the left and right side of the stem. Mice were rewarded if they turned to the side with more cues at the end of central stem. A regression-based encoding model showed that, as a population, dopamine neurons represent multiple variables during the cue period of the task, including cues, movement kinematics, and choice accuracy, in addition to most neurons responding to rewards during the outcome period. While individual neurons encoded multiple non-reward variables, there were functional clusters of cells that preferentially encoded specific task components. The cellular resolution of two-photon imaging further allowed the authors to determine that dopamine neurons with similar encoding properties cluster together spatially. Since the topographical organization of VTA dopamine neurons depends on their projection targets [48], this finding suggests that encoding of non-reward variables by dopamine neurons, including movement, is specialized based on downstream targets.

One strategy for measuring target-specific signals is to take advantage of the high spatial resolution afforded by two-photon microscopy to directly visualize calcium influx into axons, which correlates with neurotransmitter release. Howe and Dombeck took this approach to directly assess the activity of dopamine axons in the dorsal striatum during self-initiated locomotion in head-fixed mice. Locomotion onsets were preceded by increases in dopamine axon calcium activity. Importantly, these signals seem to causally contribute to movement since optogenetic activation of dopaminergic axons to the striatum triggered locomotion. Measuring the activity of axons emanating from distinct midbrain dopamine nuclei showed that VTA axons responded predominantly to unexpected rewards, whereas SNc axons were active around movement bouts [64]. This suggests that functional heterogeneity of dopamine signaling in the striatum is potentially due to distinct sources of

dopamine axons. Axonal measurements are also possible using fiber photometry, which allows bulk recording of fluorescent signals [91, 92]. This technique has allowed comparison of movement and reward encoding by dopamine terminals in dorsal striatum and nucleus accumbens, revealing functional heterogeneities based on the projection target [93].

Ultimately, the effect of dopamine neuron activity on downstream circuits depends on the release of dopamine from terminals. It has long been appreciated that locally specialized mechanisms potently modulate release from dopamine terminals [94–97], potentially decoupling dopamine cell firing from release. Indeed, direct measurements of dopamine release using microdialysis or fast-scan cyclic voltammetry reveal local dopamine signals that are not observed in the firing activity of dopamine neurons [48, 98]. While these techniques have produced a wealth of information on dopamine dynamics in local circuits, they lack adequate resolution to determine the fine spatiotemporal profile of dopamine release. Recently, genetically encoded sensors for neuromodulators, including for dopamine, have become available [15]. In combination with high-resolution imaging technologies like two-photon microscopy, these novel sensors hold the promise for elucidating when and where dopamine is released during specific behavioral events.

Whereas the influence of dopamine on the striatum has been studied extensively, the striatum also directly innervates dopamine neurons [99, 100]. The striatum can be divided into neurochemically distinct matrix and striosome (patch) compartments [101], the latter of which sends strong inhibitory projections to dopamine neurons in the SNc. Although specific transgenic mouse lines allow for the visualization of striosome compartments in the striatum, many tend to be unselective and exhibit sparse striosome labeling. We recently combined two-photon imaging with a birth dating technique to label striosome neurons based on developmental time points. This allowed us to measure responses from visually identified striosomes and demonstrate a role for this compartment in encoding of reward predicting cues [36]. Whether and how this striosome activity affects dopamine signaling and function in reward-based behaviors remains to be discovered and is an exciting future endeavor.

10 Cortical Circuits for Reward-Based Learning

Reward-guided behaviors are complex processes that require communication between not only subcortical structures as discussed above but also interactions between cortical and subcortical areas. The prefrontal cortex (PFC) is perhaps the cortical structure most widely associated with reward processing. Activity in the PFC can

exert bidirectional control over reward-seeking behaviors via complex interactions with its downstream targets [102–104]. For example, optogenetically inducing asynchronous activity in populations of PFC neurons can suppress reward-seeking behaviors by modulating interactions between subcortical structures like the midbrain dopaminergic nuclei and the striatum [103].

Recent application of optical techniques to the study of anatomically defined neuronal populations has started to elucidate the organizational principles for how specific long-range cortical circuits modulate reward seeking. In a recent study, two-photon imaging through a GRIN lens was used to gain optical access to the dorsomedial prefrontal cortex [104]. Retrograde viral vectors were used to selectively express GCaMP in cortical neurons projecting to the nucleus accumbens or the thalamus and a Pavlovian conditioning task was used to study their responses during task performance. Remarkably, corticostriatal and corticothalamic neurons responded to reward-predictive cues with increases and decreases in activity, respectively. In agreement, optogenetic manipulations showed that corticostriatal and corticothalamic pathways promote and suppress conditioned reward seeking, respectively [104]. Hence, the prefrontal cortex can both promote and suppress reward-seeking behaviors depending on the specific output circuits engaged.

11 Concluding Remarks

We have presented here a brief overview of the role of subcortical and cortical structures in reward-guided behaviors while highlighting how application of novel imaging techniques such as two-photon microscopy coupled with neuronal activity sensors has disentangled the role of dopamine in specific reward-based processes. Given the wide breadth of experimental cell type–specific manipulations possible with these techniques, some of which we have discussed here, we expect that optical methods will continue to revolutionize our understanding of the neural circuits underlying reward-based learning and behavior.

Acknowledgments

RH is supported by funds from the National Institute of Mental Health (R00 MH112855). LAI is supported by the Hearst Foundation Postdoctoral Fellowship.

References

1. Jun JJ, Steinmetz NA, Siegle JH, Denman DJ, Bauza M, Barbarits B, Lee AK, Anastassiou CA, Andrei A, Aydın Ç et al (2017) Fully integrated silicon probes for high-density recording of neural activity. Nature 551:232–236
2. Lima SQ, Hromadka T, Znamenskiy P, Zador AM (2009) PINP: a new method of tagging neuronal populations for identification during in vivo electrophysiological recording. PLoS One 4:e6099
3. Kvitsiani D, Ranade S, Hangya B, Taniguchi H, Huang JZ, Kepecs A (2013) Distinct behavioural and network correlates of two interneuron types in prefrontal cortex. Nature 498:363–366
4. Breton-Provencher V, Sur M (2019) Active control of arousal by a locus coeruleus GABAergic circuit. Nat Neurosci 22:218–228
5. Allsop SA, Wichmann R, Mills F, Burgos-Robles A, Chang CJ, Felix-Ortiz AC, Vienne A, Beyeler A, Izadmehr EM, Glober G et al (2018) Corticoamygdala transfer of socially derived information gates observational learning. Cell 173:1329–1342. e18
6. Kravitz AV, Owen SF, Kreitzer AC (2013) Optogenetic identification of striatal projection neuron subtypes during in vivo recordings. Brain Res 1511:21–32
7. Driscoll LN, Pettit NL, Minderer M, Chettih SN, Harvey CD (2017) Dynamic reorganization of neuronal activity patterns in parietal cortex. Cell 170:986–999. e16
8. Margolis DJ, Lütcke H, Schulz K, Haiss F, Weber B, Kügler S, Hasan MT, Helmchen F (2012) Reorganization of cortical population activity imaged throughout long-term sensory deprivation. Nat Neurosci 15:1539–1546
9. Rose T, Jaepel J, Hübener M, Bonhoeffer T (2016) Cell-specific restoration of stimulus preference after monocular deprivation in the visual cortex. Science 352:1319–1322
10. Madisen L, Garner AR, Shimaoka D, Chuong AS, Klapoetke NC, Li L, Van Der Bourg A, Niino Y, Egolf L, Monetti C et al (2015) Transgenic mice for intersectional targeting of neural sensors and effectors with high specificity and performance. Neuron 85:942–958
11. Chatterjee S, Sullivan HA, Maclennan BJ, Xu R, Hou Y, Lavin TK, Lea NE, Michalski JE, Babcock KR, Dietrich S et al (2018) Nontoxic, double- deletion-mutant rabies viral vectors for retrograde targeting of projection neurons. Nat Neurosci 21:638–646
12. El-Boustani S, Ip JPK, Breton-Provencher V, Knott GW, Okuno H, Bito H, Sur M (2018) Locally coordinated synaptic plasticity of visual cortex neurons in vivo. Science 360:1349–1354
13. Glickfeld LL, Andermann ML, Bonin V, Reid RC (2013) Cortico-cortical projections in mouse visual cortex are functionally target specific. Nat Neurosci 16:219–226
14. Broussard GJ, Liang Y, Fridman M, Unger EK, Meng G, Xiao X, Ji N, Petreanu L, Tian L (2018) In vivo measurement of afferent activity with axon- specific calcium imaging. Nat Neurosci 21:1272–1280
15. Sun F, Zeng J, Jing M, Zhou J, Feng J, Owen SF, Luo Y, Li F, Wang H, Yamaguchi T et al (2018) A genetically encoded fluorescent sensor enables rapid and specific detection of dopamine in flies, fish, and mice. Cell 174:481–496. e19
16. Roth RH, Zhang Y, Huganir RL (2017) Dynamic imaging of AMPA receptor trafficking in vitro and in vivo. Curr Opin Neurobiol 45:51–58
17. Hackley CR, Mazzoni EO, Blau J (2018) cAMPr: a single-wavelength fluorescent sensor for cyclic AMP. Sci Signal 11
18. Das S, Moon HC, Singer RH, Park HY (2018) A transgenic mouse for imaging activity-dependent dynamics of endogenous Arc mRNA in live neurons. Sci Adv 4: eaar3448
19. Akemann W, Sasaki M, Mutoh H, Imamura T, Honkura N, Knöpfel T (2013) Two-photon voltage imaging using a genetically encoded voltage indicator. Sci Rep 3:2231
20. Chamberland S, Yang HH, Pan MM, Evans SW, Guan S, Chavarha M, Yang Y, Salesse C, Wu H, Wu JC et al (2017) Fast two-photon imaging of subcellular voltage dynamics in neuronal tissue with genetically encoded indicators. elife:6
21. Tian L, Looger LL (2008) Genetically encoded fluorescent sensors for studying healthy and diseased nervous systems. Drug Discov Today Dis Models 5:27–35
22. Abdelfattah AS, Kawashima T, Singh A, Novak O, Liu H, Shuai Y, Huang YC, Campagnola L, Seeman SC, Yu J et al (2019) Bright and photostable chemigenetic indicators for extended in vivo voltage imaging. Science 365:699–704

23. Adam Y, Kim JJ, Lou S, Zhao Y, Xie ME, Brinks D, Wu H, Mostajo-Radji MA, Kheifets S, Parot V et al (2019) Voltage imaging and optogenetics reveal behaviour-dependent changes in hippocampal dynamics. Nature 569:413–417
24. Piatkevich KD, Bensussen S, Tseng HA, Shroff SN, Lopez-Huerta VG, Park D, Jung EE, Shemesh OA, Straub C, Gritton HJ et al (2019) Population imaging of neural activity in awake behaving mice. Nature 574:413–417
25. Berridge MJ, Lipp P, Bootman MD (2000) The versatility and universality of calcium signalling. Nat Rev Mol Cell Biol 1:11–21
26. Grienberger C, Konnerth A (2012) Imaging calcium in neurons. Neuron 73:862–885
27. Dawitz J, Kroon T, Hjorth JJ, Meredith RM (2011) Functional calcium imaging in developing cortical networks. J Vis Exp (56):3550. https://doi.org/10.3791/3550
28. Tian L, Hires SA, Mao T, Huber D, Chiappe ME, Chalasani SH, Petreanu L, Akerboom J, Mckinney SA, Schreiter ER et al (2009) Imaging neural activity in worms, flies and mice with improved GCaMP calcium indicators. Nat Methods 6:875–881
29. Dana H, Sun Y, Mohar B, Hulse BK, Kerlin AM, Hasseman JP, Tsegaye G, Tsang A, Wong A, Patel R et al (2019) High-performance calcium sensors for imaging activity in neuronal populations and microcompartments. Nat Methods 16:649–657
30. Jing M, Zhang P, Wang G, Feng J, Mesik L, Zeng J, Jiang H, Wang S, Looby JC, Guagliardo NA et al (2018) A genetically encoded fluorescent acetylcholine indicator for in vitro and in vivo studies. Nat Biotechnol 36:726–737
31. Patriarchi T, Cho JR, Merten K, Howe MW, Marley A, Xiong WH, Folk RW, Broussard GJ, Liang R, Jang MJ et al (2018) Ultrafast neuronal imaging of dopamine dynamics with designed genetically encoded sensors. Science 360(6396):eaat4422. https://doi.org/10.1126/science.aat4422
32. Petilla Interneuron Nomenclature G, Ascoli GA, Alonso-Nanclares L, Anderson SA, Barrionuevo G, Benavides-Piccione R, Burkhalter A, Buzsaki G, Cauli B, Defelipe J et al (2008) Petilla terminology: nomenclature of features of GABAergic interneurons of the cerebral cortex. Nat Rev Neurosci 9:557–568
33. Tasic B, Yao Z, Graybuck LT, Smith KA, Nguyen TN, Bertagnolli D, Goldy J, Garren E, Economo MN, Viswanathan S et al (2018) Shared and distinct transcriptomic cell types across neocortical areas. Nature 563:72–78
34. Donato F, Chowdhury A, Lahr M, Caroni P (2015) Early- and late-born parvalbumin basket cell subpopulations exhibiting distinct regulation and roles in learning. Neuron 85:770–786
35. Kelly SM, Raudales R, He M, Lee JH, Kim Y, Gibb LG, Wu P, Matho K, Osten P, Graybiel AM et al (2018) Radial glial lineage progression and differential intermediate progenitor amplification underlie striatal compartments and circuit organization. Neuron 99:345–361. e4
36. Bloem B, Huda R, Sur M, Graybiel AM (2017) Two-photon imaging in mice shows striosomes and matrix have overlapping but differential reinforcement-related responses. elife 6:e32353. https://doi.org/10.7554/eLife.32353
37. Taniguchi H, He M, Wu P, Kim S, Paik R, Sugino K, Kvitsiani D, Fu Y, Lu J, Lin Y et al (2011) A resource of Cre driver lines for genetic targeting of GABAergic neurons in cerebral cortex. Neuron 71:995–1013
38. Steinmetz NA, Buetfering C, Lecoq J, Lee CR, Peters AJ, Jacobs EAK, Coen P, Ollerenshaw DR, Valley MT, De Vries SEJ et al (2017) Aberrant cortical activity in multiple GCaMP6-expressing transgenic mouse lines. eNeuro 4(5):ENEURO.0207–E-NEURO.0217. https://doi.org/10.1523/ENEURO.0207-17.2017
39. Gong S, Doughty M, Harbaugh CR, Cummins A, Hatten ME, Heintz N, Gerfen CR (2007) Targeting Cre recombinase to specific neuron populations with bacterial artificial chromosome constructs. J Neurosci 27:9817–9823
40. Callaway EM, Luo L (2015) Monosynaptic circuit tracing with glycoprotein-deleted rabies viruses. J Neurosci 35:8979–8985
41. Reardon TR, Murray AJ, Turi GF, Wirblich C, Croce KR, Schnell MJ, Jessell TM, Losonczy A (2016) Rabies virus CVS-N2c(ΔG) strain enhances retrograde synaptic transfer and neuronal viability. Neuron 89:711–724
42. Del Rio D, Beucher B, Lavigne M, Wehbi A, Gonzalez Dopeso-Reyes I, Saggio I, Kremer EJ (2019) CAV-2 Vector development and gene transfer in the central and peripheral nervous systems. Front Mol Neurosci 12:71
43. Tervo DG, Hwang BY, Viswanathan S, Gaj T, Lavzin M, Ritola KD, Lindo S, Michael S, Kuleshova E, Ojala D et al (2016) A Designer

AAV variant permits efficient retrograde access to projection neurons. Neuron 92:372–382

44. Wall NR, Wickersham IR, Cetin A, De La Parra M, Callaway EM (2010) Monosynaptic circuit tracing in vivo through Cre-dependent targeting and complementation of modified rabies virus. Proc Natl Acad Sci 107:21848
45. Huda R, Sipe GO, Adam E, Breton-Provencher V, Pho G, Gunter L, Wickersham IR, Sur M (2018) Bidirectional control of goal-oriented action selection by distinct prefrontal cortex circuits. bioRxiv:307009
46. Berke JD (2018) What does dopamine mean? Nat Neurosci 21:787–793
47. Lerner TN, Shilyansky C, Davidson TJ, Evans KE, Beier KT, Zalocusky KA, Crow AK, Malenka RC, Luo L, Tomer R et al (2015) Intact-brain analyses reveal distinct information carried by SNc dopamine subcircuits. Cell 162:635–647
48. Beier KT, Steinberg EE, Deloach KE, Xie S, Miyamichi K, Schwarz L, Gao XJ, Kremer EJ, Malenka RC, Luo L (2015) Circuit architecture of VTA dopamine neurons revealed by systematic input–output mapping. Cell 162:622–634
49. Beier KT, Gao XJ, Xie S, Deloach KE, Malenka RC, Luo L (2019) Topological organization of ventral tegmental area connectivity revealed by viral-genetic dissection of input-output relations. Cell Rep 26:159–167. e6
50. Keiflin R, Janak PH (2015) Dopamine prediction errors in reward learning and addiction: from theory to neural circuitry. Neuron 88:247–263
51. Schultz W (1994) Behavior-related activity of primate dopamine neurons. Rev Neurol (Paris) 150:634–639
52. Schultz W (1998) Predictive reward signal of dopamine neurons. J Neurophysiol 80:1–27
53. Zaghloul KA, Blanco JA, Weidemann CT, Mcgill K, Jaggi JL, Baltuch GH, Kahana MJ (2009) Human substantia nigra neurons encode unexpected financial rewards. Science 323:1496–1499
54. D'ardenne K, Mcclure SM, Nystrom LE, Cohen JD (2008) BOLD responses reflecting dopaminergic signals in the human ventral tegmental area. Science 319:1264–1267
55. Cohen JY, Haesler S, Vong L, Lowell BB, Uchida N (2012) Neuron-type- specific signals for reward and punishment in the ventral tegmental area. Nature 482:85–88
56. Bayer HM, Glimcher PW (2005) Midbrain dopamine neurons encode a quantitative reward prediction error signal. Neuron 47:129–141
57. Krigolson OE, Hassall CD, Handy TC (2014) How we learn to make decisions: rapid propagation of reinforcement learning prediction errors in humans. J Cogn Neurosci 26:635–644
58. Eshel N, Tian J, Bukwich M, Uchida N (2016) Dopamine neurons share common response function for reward prediction error. Nat Neurosci 19:479–486
59. Matsumoto M, Hikosaka O (2009) Two types of dopamine neuron distinctly convey positive and negative motivational signals. Nature 459:837–841
60. Pan WX, Schmidt R, Wickens JR, Hyland BI (2005) Dopamine cells respond to predicted events during classical conditioning: evidence for eligibility traces in the reward-learning network. J Neurosci 25:6235–6242
61. Menegas W, Akiti K, Amo R, Uchida N, Watabe-Uchida M (2018) Dopamine neurons projecting to the posterior striatum reinforce avoidance of threatening stimuli. Nat Neurosci 21:1421–1430
62. Fiorillo CD (2013) Two dimensions of value: dopamine neurons represent reward but not aversiveness. Science 341:546–549
63. Coddington LT, Dudman JT (2019) Learning from action: reconsidering movement signaling in midbrain dopamine neuron activity. Neuron 104:63–77
64. Howe MW, Dombeck DA (2016) Rapid signalling in distinct dopaminergic axons during locomotion and reward. Nature 535:505–510
65. Nasser HM, Calu DJ, Schoenbaum G, Sharpe MJ (2017) The dopamine prediction error: contributions to associative models of reward learning. Front Psychol 8:244
66. Schultz W, Dayan P, Montague PR (1997) A neural substrate of prediction and reward. Science 275:1593–1599
67. Waelti P, Dickinson A, Schultz W (2001) Dopamine responses comply with basic assumptions of formal learning theory. Nature 412:43–48
68. Boyden ES, Zhang F, Bamberg E, Nagel G, Deisseroth K (2005) Millisecond- timescale, genetically targeted optical control of neural activity. Nat Neurosci 8:1263–1268
69. Zhang F, Tsai HC, Airan RD, Stuber GD, Adamantidis AR, De Lecea L, Bonci A, Deisseroth K (2015) Optogenetics in freely moving mammals: dopamine and reward. Cold Spring Harb Protoc 2015:715–724

70. Steinberg EE, Keiflin R, Boivin JR, Witten IB, Deisseroth K, Janak PH (2013) A causal link between prediction errors, dopamine neurons and learning. Nat Neurosci 16:966–973
71. Rescorla RA, Holland PC (1982) Behavioral studies of associative learning in animals. Annu Rev Psychol 33:265–308
72. Hamid AA, Pettibone JR, Mabrouk OS, Hetrick VL, Schmidt R, Vander Weele CM, Kennedy RT, Aragona BJ, Berke JD (2016) Mesolimbic dopamine signals the value of work. Nat Neurosci 19:117–126
73. Kim KM, Baratta MV, Yang A, Lee D, Boyden ES, Fiorillo CD (2012) Optogenetic mimicry of the transient activation of dopamine neurons by natural reward is sufficient for operant reinforcement. PLoS One 7:e33612
74. Lak A, Okun M, Moss MM, Gurnani H, Farrell K, Wells MJ, Reddy CB, Kepecs A, Harris KD, Carandini M (2020) Dopaminergic and prefrontal basis of learning from sensory confidence and reward value. Neuron 105:700–711. e6
75. Stauffer WR, Lak A, Yang A, Borel M, Paulsen O, Boyden ES, Schultz W (2016) Dopamine neuron-specific optogenetic stimulation in rhesus macaques. Cell 166:1564–1571. e6
76. Chang CY, Esber GR, Marrero-Garcia Y, Yau HJ, Bonci A, Schoenbaum G (2016) Brief optogenetic inhibition of dopamine neurons mimics endogenous negative reward prediction errors. Nat Neurosci 19:111–116
77. Saunders BT, Richard JM, Margolis EB, Janak PH (2018) Dopamine neurons create Pavlovian conditioned stimuli with circuit-defined motivational properties. Nat Neurosci 21:1072–1083
78. Yttri EA, Dudman JT (2016) Opponent and bidirectional control of movement velocity in the basal ganglia. Nature 533:402–406
79. Tai LH, Lee AM, Benavidez N, Bonci A, Wilbrecht L (2012) Transient stimulation of distinct subpopulations of striatal neurons mimics changes in action value. Nat Neurosci 15:1281–1289
80. Wickens JR, Horvitz JC, Costa RM, Killcross S (2007) Dopaminergic mechanisms in actions and habits. J Neurosci 27:8181–8183
81. Palmiter RD (2008) Dopamine signaling in the dorsal striatum is essential for motivated behaviors: lessons from dopamine-deficient mice. Ann N Y Acad Sci 1129:35
82. German DC, Manaye K, Smith WK, Woodward DJ, Saper CB (1989) Midbrain dopaminergic cell loss in Parkinson's disease: computer visualization. Ann Neurol 26:507–514
83. Chinaglia G, Alvarez FJ, Probst A, Palacios JM (1992) Mesostriatal and mesolimbic dopamine uptake binding sites are reduced in Parkinson's disease and progressive supranuclear palsy: a quantitative autoradiographic study using [3H]mazindol. Neuroscience 49:317–327
84. Salamone JD, Correa M (2012) The mysterious motivational functions of mesolimbic dopamine. Neuron 76:470–485
85. Dodson PD, Dreyer JK, Jennings KA, Syed ECJ, Wade-Martins R, Cragg SJ, Bolam JP, Magill PJ (2016) Representation of spontaneous movement by dopaminergic neurons is cell-type selective and disrupted in parkinsonism. Proc Natl Acad Sci 113:E2180
86. Da Silva JA, Tecuapetla F, Paixão V, Costa RM (2018) Dopamine neuron activity before action initiation gates and invigorates future movements. Nature 554:244–248
87. Syed EC, Grima LL, Magill PJ, Bogacz R, Brown P, Walton ME (2016) Action initiation shapes mesolimbic dopamine encoding of future rewards. Nat Neurosci 19:34–36
88. Wassum KM, Ostlund SB, Maidment NT (2012) Phasic mesolimbic dopamine signaling precedes and predicts performance of a self-initiated action sequence task. Biol Psychiatry 71:846–854
89. Howe MW, Tierney PL, Sandberg SG, Phillips PE, Graybiel AM (2013) Prolonged dopamine signalling in striatum signals proximity and value of distant rewards. Nature 500:575–579
90. Engelhard B, Finkelstein J, Cox J, Fleming W, Jang HJ, Ornelas S, Koay SA, Thiberge SY, Daw ND, Tank DW et al (2019) Specialized coding of sensory, motor and cognitive variables in VTA dopamine neurons. Nature 570:509–513
91. Guo Q, Zhou J, Feng Q, Lin R, Gong H, Luo Q, Zeng S, Luo M, Fu L (2015) Multichannel fiber photometry for population neuronal activity recording. Biomed Opt Express 6:3919–3931
92. Gunaydin LA, Grosenick L, Finkelstein JC, Kauvar IV, Fenno LE, Adhikari A, Lammel S, Mirzabekov JJ, Airan RD, Zalocusky KA et al (2014) Natural neural projection dynamics underlying social behavior. Cell 157:1535–1551
93. Parker NF, Cameron CM, Taliaferro JP, Lee J, Choi JY, Davidson TJ, Daw ND, Witten IB (2016) Reward and choice encoding in

terminals of midbrain dopamine neurons depends on striatal target. Nat Neurosci 19:845–854

94. Zhou FM, Liang Y, Dani JA (2001) Endogenous nicotinic cholinergic activity regulates dopamine release in the striatum. Nat Neurosci 4:1224–1229
95. Sulzer D, Cragg SJ, Rice ME (2016) Striatal dopamine neurotransmission: regulation of release and uptake. Basal Ganglia 6:123–148
96. Cover KK, Gyawali U, Kerkhoff WG, Patton MH, Mu C, White MG, Marquardt AE, Roberts BM, Cheer JF, Mathur BN (2019) Activation of the rostral intralaminar thalamus drives reinforcement through striatal dopamine release. Cell Rep 26:1389–1398. e3
97. Threlfell S, Lalic T, Platt NJ, Jennings KA, Deisseroth K, Cragg SJ (2012) Striatal dopamine release is triggered by synchronized activity in cholinergic interneurons. Neuron 75:58–64
98. Mohebi A, Pettibone JR, Hamid AA, Wong JT, Vinson LT, Patriarchi T, Tian L, Kennedy RT, Berke JD (2019) Dissociable dopamine dynamics for learning and motivation. Nature 570:65–70
99. Crittenden JR, Tillberg PW, Riad MH, Shima Y, Gerfen CR, Curry J, Housman DE, Nelson SB, Boyden ES, Graybiel AM (2016) Striosome- dendron bouquets highlight a unique striatonigral circuit targeting dopamine- containing neurons. Proc Natl Acad Sci U S A 113:11318–11323
100. Mcgregor MM, Mckinsey GL, Girasole AE, Bair-Marshall CJ, Rubenstein JLR, Nelson AB (2019) Functionally distinct connectivity of developmentally targeted striosome neurons. Cell Rep 29:1419–1428. e5
101. Graybiel AM, Ragsdale CW Jr (1978) Histochemically distinct compartments in the striatum of human, monkeys, and cat demonstrated by acetylthiocholinesterase staining. Proc Natl Acad Sci U S A 75:5723–5726
102. Kim CK, Ye L, Jennings JH, Pichamoorthy N, Tang DD, Yoo A-CW, Ramakrishnan C, Deisseroth K (2017) Molecular and circuit-dynamical identification of top-down neural mechanisms for restraint of reward seeking. Cell 170:1013–1027. e14
103. Ferenczi EA, Zalocusky KA, Liston C, Grosenick L, Warden MR, Amatya D, Katovich K, Mehta H, Patenaude B, Ramakrishnan C et al (2016) Prefrontal cortical regulation of brainwide circuit dynamics and reward-related behavior. Science 351: aac9698
104. Otis JM, Namboodiri VMK, Matan AM, Voets ES, Mohorn EP, Kosyk O, Mchenry JA, Robinson JE, Resendez SL, Rossi MA et al (2017) Prefrontal cortex output circuits guide reward seeking through divergent cue encoding. Nature 543:103–107

INDEX

A

Addictions 181, 200, 209, 210, 223–227, 233, 239, 240, 254–256, 264, 285, 289–291, 316–318
Adeno-associated virus (AAV) 235–237, 239, 241, 242, 244–247, 249, 254, 255, 347, 349, 350
Adenovirus 187, 235, 236, 245, 255, 347
Adult neurogensis 77–81
Amperometry 32, 33, 37
Anhedonia 145–163, 170, 317, 319
Aversions 21, 22, 24, 28, 32, 145–163, 240, 264, 274

B

Basal ganglia 55, 125, 327
Behaviors 3–7, 13, 14, 16, 21–25, 28, 33, 35–39, 52, 53, 57, 60, 68, 70, 79, 97, 106, 107, 109, 117, 125, 128, 130, 147–152, 156, 157, 159, 170, 171, 176, 181, 182, 193, 199, 201, 203, 233–256, 267, 268, 307, 308, 312, 318, 321, 339, 343, 346, 347, 349, 353, 355, 357, 358
Brain microdialysis 32
Brain stimulation reward 4–6, 13, 15, 16, 39, 200, 201, 205

C

Calcium imaging 36, 37, 250–253, 328, 340, 356
Carbon-fiber microelectrode 94, 98, 100, 102, 103, 105, 106, 109
Catheters 211–217, 219, 220, 225
Cocaine 33, 35, 38, 39, 132, 200, 205, 206, 223–227, 239, 241–250, 252, 253, 255, 263, 269, 271, 272, 275, 276, 284, 289, 290, 292–295, 318
Conditioned place aversion (CPA) 148, 151–157, 162, 163, 264, 273–276
Conditioned place preference (CPP) 57, 148, 152, 157, 239–247, 249–253, 263–277

D

Dentate gyrus (DG) 77, 78, 81, 83–86, 241
Depression 8, 37, 79, 146, 155, 181, 316–319
Designer Receptors Exclusively Activated by Designer Drugs (DREADDs) 35, 100, 112, 182–184, 193, 249
Despair 145–163
Dopamine (DA) 22–24, 28, 31–39, 52–54, 60, 65, 93, 95, 97, 125–142, 146, 171, 222, 226, 227, 250, 281, 282, 285, 286, 288–293, 308, 327, 343, 346, 349–358
Drugs 8, 11–15, 23–25, 31–39, 57, 86, 100, 112, 176, 181, 183, 199–207, 209–212, 215, 219–227, 234, 237, 239, 240, 248–250, 252, 254, 255, 263, 264, 266, 269–276, 281, 282, 285, 286, 289–293, 318, 353
Drugs of abuse 16, 201, 210, 212, 222, 226, 252, 254, 263–277, 293

E

Electrical self-stimulation 33, 35
Electrochemistry 97–100, 114
Electrophysiology 65, 70, 94, 111, 250, 307–313, 339, 340
Excitotoxins 54, 58, 66, 67

F

Feedback-error related negativity 309
Fiber photometry 32, 33, 36, 37, 234, 238, 251–253, 327–329, 331, 334–336, 357
Forced swim test (FST) 149–152, 154, 155, 161–163
Frequency-rate curve-shift paradigm 200, 201

H

Heat hyperalgesia 171, 173–176
Herpes simplex virus (HSV) 235–237, 239, 255
Hippocampus 6, 28, 55, 68, 77, 79, 82, 182, 240–243, 250, 252, 253, 292, 293, 328

Marc Fakhoury (ed.), *The Brain Reward System*, Neuromethods, vol. 165, https://doi.org/10.1007/978-1-0716-1146-3,

I

Immune-to-brain signaling 145–163
Intracranial self-stimulation (ICSS) 3–11, 13–16, 39, 199–206, 210
Intravenous drug self-administration 210–212, 215–227
In vivo calcium imaging 234, 251–253, 327, 328

J

Jugular veins 212–218

L

Lesions 6, 7, 11–15, 51–71, 109, 176, 182
Lipopolysaccharide (LPS) 150–152, 156, 157, 159, 161, 163
Locomotor activity 14, 149, 221, 226, 254, 273, 289

M

Mechanical allodynia 171, 174–176
Mechanical hyperalgesia 171, 174, 175
Microelectrodes 38, 39, 93–95, 98–100, 104, 105, 107, 110–113, 115, 117, 118, 129, 132
Motivation 22, 53, 55–57, 65, 146, 170, 171, 222, 227, 321, 349, 355

N

Neural circuits 6, 24, 170, 171, 248, 250, 252, 253, 327–336, 358
Neurochemicals 21, 22, 31, 65, 93–118, 126, 128, 130, 133, 226, 292
Nociception 169–177
Nucleus accumbens (NAs) 6, 22, 27, 28, 32, 33, 35–38, 54, 56, 58, 106, 109, 110, 146, 171, 182, 187, 222, 246, 281, 290, 349, 355, 357, 358

O

Operant boxes 203, 215, 219–222, 226
Optogenetics 6, 16, 23–25, 32, 33, 35, 36, 38, 65, 68, 100, 112, 193, 234, 238, 241, 245, 248–250, 340, 354–356, 358

P

Pain 22, 26, 57, 169–177, 274, 353
Positron emission tomography (PET) 171, 282–285, 287–297
Prefrontal cortex (PFC) 6, 22, 28, 54, 58, 146, 171, 182, 184, 282, 285, 291, 292, 308, 343, 349, 352, 357, 358
Psychomotor sensitization 227

R

Reinforcement 4, 9, 12, 23, 37, 39, 52, 93, 148, 171, 201, 202, 222, 227
Retrovirus 235–237, 255
Reward positivity (RewP) 309, 310, 313, 314, 316, 319
Rewards 4, 7, 9–13, 15, 16, 21–25, 28, 32–41, 51–58, 60, 62, 63, 65, 68–71, 113, 128, 145–163, 170, 171, 181–184, 188, 193, 199–201, 203, 206, 209, 210, 221, 237, 239, 250–253, 256, 284, 285, 289, 307–321, 339–358
Reward systems 3–16, 21–41, 169–177, 193, 209–228, 281–297, 309, 310, 316, 317, 320, 321, 327
Rodent brain 25, 38, 130, 235, 238, 240–248

S

Stem/progenitor cells 77, 81, 84–86
Stereology 81
Stereotaxic ..... vii, 8, 9, 21–40, 56–59, 67, 69, 94, 96, 105, 107, 108, 132, 137, 138, 142, 184–187, 201, 238–239, 243, 245, 246, 251, 252, 331, 332, 347–350, 352
Stimulus-preceding negativity (SPN) 310, 313, 315, 316, 319, 320
Striatum 22, 28, 34, 37–39, 53–56, 58, 61, 70, 105, 107, 112, 125, 130, 182, 184, 222, 254, 285, 288, 289, 291, 308, 349, 352, 353, 355–358
Sucrose preference test (SPT) 149, 151, 152, 154, 155, 157–159, 163
Systemic inflammation 145, 146, 150, 151, 159

T

Two-photon microscopy 251, 328, 340, 357

V

Voltammetry 32, 33, 37, 93–118, 126, 226, 357